

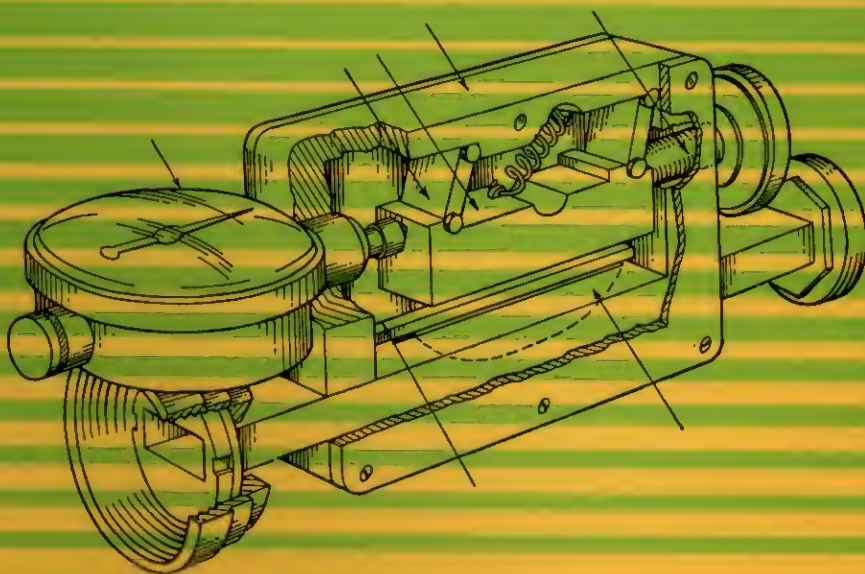
£1.50 net  
IN UK ONLY

# TECHNIQUE OF MICROWAVE MEASUREMENTS

EDITED BY  
CAROL G. MONTGOMERY

IN TWO VOLUMES

VOLUME II



TECHNIQUE OF  
MICROWAVE MEASUREMENTS

VOLUME II

DOVER

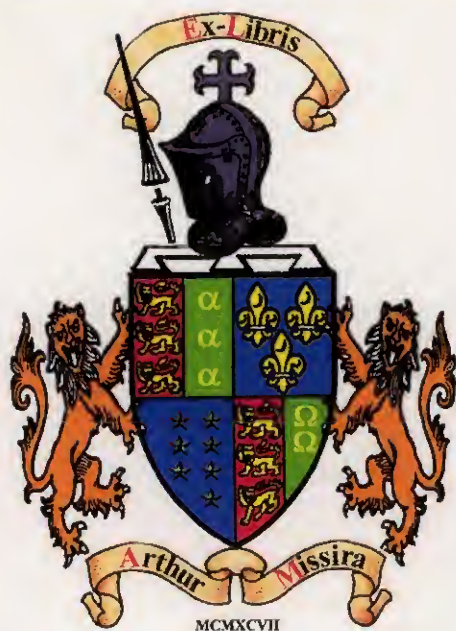
S1596

MONTGOMERY

# DOVER BOOKS ON ENGINEERING AND ENGINEERING PHYSICS

- Theory of Wing Sections, Ira H. Abbott and Albert E. von Doenhoff. \$3.25  
De Re Metallica, Georgius Agricola. Clothbound \$10.00  
Charles Babbage and His Calculating Engines, edited by Philip Morrison and Emily Morrison. \$2.00  
Treatise on Hydrodynamics, A. B. Basset. Two volume set \$3.50  
Traveling Waves on Transmission Systems, L. V. Bewley. \$3.00  
Two-Dimensional Fields in Electrical Engineering, L. V. Bewley. \$1.50  
Flux Linkages and Electromagnetic Induction, L. V. Bewley. \$1.25  
The Measurement of Power Spectra from the Point of View of Communications Engineering, Ralph B. Blackman and John W. Tukey. \$1.85  
Theory of Ship Motions, S. N. Blagoveshchensky. Two volume set \$4.00  
The Thermodynamics of Electrical Phenomena in Metals, and A Condensed Collection of Thermodynamic Formulas, Percy W. Bridgman. \$1.75  
Analytical Mechanics of Gears, Earle Buckingham. \$2.75  
Piezoelectricity, Walter G. Cady. Two volume set \$5.00  
Mathematical Tables and Formulas, Robert D. Carmichael and Edwin R. Smith. \$1.00  
Operational Methods in Applied Mathematics, H. S. Carslaw and John C. Jaeger. \$2.25  
Gaseous Conductors: Theory and Engineering Applications, James D. Cobine. \$2.95  
Applied Optics and Optical Design, A. E. Conrady. Two volume set \$5.90  
Electrical Theory on the Giorgi System, P. Cornelius. Clothbound \$6.00  
Mechanics of the Gyroscope: Dynamics of Rotation, Richard F. Deimel. \$1.65  
Mechanics, J. P. Den Hartog. \$2.25  
Strength of Materials, J. P. Den Hartog. \$2.00  
Teach Yourself Heat Engines, E. De Ville. Clothbound \$2.00  
A Diderot Pictorial Encyclopedia of Trades and Industry: Manufacturing and the Technical Arts in Plates Selected from L'Encyclopédie ou Dictionnaire Raisonné des Sciences, des Arts, et des Métiers, edited by Charles Gillispie. Clothbound. Two volume set \$18.50  
Hydrodynamics, Hugh L. Dryden, Francis D. Murnaghan, and Harry Bateman. \$2.75  
A Guide to Operational Research, Eric Duckworth. Clothbound \$3.50  
Aerodynamic Theory, William F. Durand, editor-in-chief. Clothbound. Three volume set \$17.50

(continued on back flap)



# TECHNIQUE OF MICROWAVE MEASUREMENTS

*Edited by*  
CAROL G. MONTGOMERY

*in two volumes*  
*Volume II*

NEW YORK  
DOVER PUBLICATIONS, INC.



Published in Canada by General Publishing Company, Ltd., 30 Lesmill Road, Don Mills, Toronto, Ontario.

Published in the United Kingdom by Constable and Company, Ltd., 10 Orange Street, London W. C. 2. .

This Dover edition, first published in 1966, is an unabridged and unaltered republication of the work first published by McGraw-Hill Book Company, Inc., in 1947. It is made available through the kind cooperation of McGraw-Hill Book Company, Inc.

This book was originally published as volume 11 in the Massachusetts Institute of Technology Radiation Laboratory Series.

For convenience in handling, the present edition has been divided into two volumes. Volume I contains pages 1 through 470; Volume II, pages 471 through 927.

*Library of Congress Catalog Card Number 66-17128*

Manufactured in the United States of America  
Dover Publications Inc.  
180 Varick Street  
New York, N. Y. 10014

# *TECHNIQUE OF MICROWAVE MEASUREMENTS*

## *EDITORIAL STAFF*

C. G. MONTGOMERY

D. D. MONTGOMERY

CATHERINE F. SCOTT

## *CONTRIBUTING AUTHORS*

R. BERINGER

R. N. GRIESHEIMER

D. HAMILTON

R. A. HOWARD

G. N. KAMM

S. KATZ

R. L. KYHL

C. G. MONTGOMERY

R. V. POUND

E. M. PURCELL

R. M. REDHEFFER

E. WEBER

H. R. WORTHINGTON

L. B. YOUNG

# Contents

## Volume II

### PART III. THE MEASUREMENT OF IMPEDANCE AND STANDING WAVES

CHAP. 8. MEASUREMENTS OF STANDING WAVES. . . . .	473
8-1. Fundamental Relations . . . . .	475
8-2. The Slotted Section and Traveling Probe. . . . .	478
8-3. The Properties of the Slotted Line. . . . .	480
8-4. The Properties of the Probe . . . . .	483
8-5. The Design of Slotted Sections and Probes. . . . .	488
8-6. Detectors and Amplifiers. . . . .	496
8-7. Matched Loads and Other Accessories. . . . .	503
8-8. Measurement of High Standing-wave Ratios . . . . .	505
8-9. The Squeeze Section. . . . .	507
8-10. Standing-wave Measurements at High Power. . . . .	510
8-11. Continuously Indicating Standing-wave Detectors. . . . .	511
8-12. Measurements on Lossless Devices . . . . .	512
CHAP. 9. IMPEDANCE BRIDGES . . . . .	515
BRIDGE ELEMENTS . . . . .	516
9-1. The Side-outlet T. . . . .	516
9-2. Analysis of the Operation and Properties of Side-outlet T's . . . . .	517
9-3. Analysis of the Directional Coupler as a Bridge Element . . . . .	522
9-4. T-construction . . . . .	524
9-5. Matching Techniques for T's. . . . .	525
9-6. Ring Networks and Coaxial T's. . . . .	527
BASIC MEASURING TECHNIQUES. . . . .	530
9-7. The Single-frequency Bridge . . . . .	530
9-8. T-asymmetry. . . . .	532
9-9. Bridge Balance and the Sliding Match. . . . .	534
9-10. Magic-T Alignment. . . . .	535
9-11. The Measurement of Large Reflections. . . . .	536
9-12. Methods Which Provide Simultaneous Indications at Several Frequencies . . . . .	537
9-13. Line Components. . . . .	540
IMPEDANCE BRIDGES UTILIZING MODULATION-FREQUENCY DISCRIMINATION. . . . .	543
9-14. Microwave Sources . . . . .	543
9-15. Line Components. . . . .	544
9-16. Selective Amplifiers . . . . .	545
9-17. Range of Measurement . . . . .	547

IMPEDANCE BRIDGES THAT EMPLOY PULSE MODULATION . . . . .	548
9-18. Microwave Sources . . . . .	548
9-19. Line Components. . . . .	549
9-20. Pulse Amplifier. . . . .	550
9-21. Range of Measurement . . . . .	551
IMPEDANCE BRIDGES UTILIZING PANORAMIC RECEIVERS . . . . .	552
9-22. Microwave Sources and Local Oscillators. . . . .	552
9-23. Line Components. . . . .	554
9-24. Receiver. . . . .	555
9-25. Range of Measurement . . . . .	556
CALIBRATING DEVICES AND SOURCES OF ERROR . . . . .	556
9-26. Adjustable Reference Mismatches. . . . .	557
9-27. Fixed Mismatches and Calibrated Attenuators . . . . .	557
9-28. Built-in Calibrators. . . . .	558
9-29. Sources of Error . . . . .	559
CHAP. 10. THE MEASUREMENT OF DIELECTRIC CONSTANTS . . . . .	561
INTRODUCTION . . . . .	561
10-1. Derivation of Relations for Proceeding from Data to Results . . . . .	562
10-2. General Considerations Influencing Choice of Method. . . . .	568
METHODS DEPENDING ON TRANSMISSION IN GUIDE . . . . .	570
10-3. Techniques for Phase Measurement. . . . .	570
10-4. Techniques for Amplitude Measurement. . . . .	577
10-5. Details of Computation . . . . .	584
10-6. Uses. . . . .	591
MEASUREMENT BY TRANSMISSION IN FREE SPACE . . . . .	591
10-7. Experimental Procedure for Normal Incidence . . . . .	593
10-8. Computations for Normal Incidence. . . . .	597
10-9. Arbitrary Incidence. . . . .	599
10-10. Comparison with Optical Methods . . . . .	604
10-11. Uses. . . . .	605
GENERAL METHODS DEPENDING ON REFLECTION . . . . .	606
10-12. Interface Reflection. . . . .	606
10-13. Reflection Measurement in Free Space. . . . .	612
10-14. Change of Termination . . . . .	616
10-15. Short Circuit, Zero Reflection at Interface . . . . .	620
THE SHORT-CIRCUITED-LINE METHOD . . . . .	625
10-16. Theory . . . . .	625
10-17. Measurement Procedure. . . . .	633
10-18. A Few Sources of Error . . . . .	640
10-19. Modified Procedure for Low Power . . . . .	644
10-20. Uses. . . . .	654
CONCLUSION . . . . .	656
10-21. Resonant-cavity Methods . . . . .	657
10-22. Summary. Methods Tabulated. . . . .	666
BIBLIOGRAPHY . . . . .	672

## PART IV. ATTENUATORS AND RADIATION MEASUREMENTS

CHAP. 11. MICROWAVE ATTENUATORS. CUTOFF ATTENUATORS . . . . .	679
INTRODUCTION . . . . .	679
11-1. Definitions of Attenuation . . . . .	679
11-2. General Design Considerations . . . . .	682
CUTOFF ATTENUATORS. . . . .	685
11-3. Principles of Cutoff Attenuators . . . . .	685
11-4. Purity of Useful Mode. . . . .	687
11-5. Separation of Undesirable Modes . . . . .	689
11-6. Principle of Mode Filtering. . . . .	693
11-7. Variation of Input Impedance with Close Coupling . . . . .	696
11-8. Impedance-matching Techniques . . . . .	700
11-9. Examples of Waveguide Attenuators for 3000 Mc/sec . . . . .	707
11-10. A Waveguide Attenuator for 9000 Mc/sec . . . . .	715
11-11. An Attenuator for 24,000 Mc/sec. . . . .	716
11-12. The Design of Cutoff Attenuators Using the $TM_{01}$ -mode. . . . .	719
CHAP. 12. MICROWAVE ATTENUATORS. RESISTIVE ATTENUATORS . . . . .	720
MATCHED TRANSMISSION-LINE TERMINATIONS. . . . .	720
12-1. Low-power Coaxial-line Terminations . . . . .	722
12-2. Low-power Waveguide Terminations with Polyiron . . . . .	726
12-3. Low-power Waveguide Terminations Which Use Other Lossy Materials . . . . .	728
12-4. Low-power Terminations Using Metalized Glass . . . . .	731
12-5. High-power Coaxial-line Loads . . . . .	732
12-6. High-power Waveguide Loads . . . . .	735
GENERAL LABORATORY ATTENUATORS . . . . .	743
12-7. Cables as Coaxial Attenuators . . . . .	743
12-8. Fixed Coaxial Pads . . . . .	745
12-9. Fixed Waveguide Attenuators . . . . .	747
12-10. Variable Waveguide Attenuators . . . . .	748
PRECISION METALIZED-GLASS ATTENUATORS . . . . .	751
12-11. Electrical Design of Coaxial-pad Inserts . . . . .	752
12-12. Construction of Coaxial Fixed Pads. . . . .	757
12-13. Performance Characteristics of Fixed Coaxial Pads . . . . .	763
12-14. Variable Metalized-glass Coaxial Attenuators. . . . .	769
12-15. Design of Elements for Waveguide Attenuators. . . . .	774
12-16. Waveguide Pads of Fixed Values . . . . .	781
12-17. Construction of Variable Waveguide Attenuators . . . . .	784
12-18. Performance Characteristics of Variable Waveguide Attenuators . . . . .	790
POWER DIVIDERS AS ATTENUATORS . . . . .	799
12-19. Calibrated Pickup Probe . . . . .	799
12-20. Directional Couplers. . . . .	800
12-21. Bifurcated Lines . . . . .	801
12-22. Branched Lines. . . . .	803
CHAP. 13. THE MEASUREMENT OF ATTENUATION . . . . .	804



13-1.	Direct Measurement of Power Ratio. . . . .	805
13-2.	Substitution Methods . . . . .	808
13-3.	Measurement of Attenuation by Standing-wave Effects . . . . .	816
13-4.	Measurement of Very Small Attenuation Values . . . . .	821
13-5.	Common Sources of Errors in Attenuation Measurements . . . . .	824
13-6.	Calibration of Attenuation Standards . . . . .	832
13-7.	Calibration with Absolute Power Measurement. . . . .	838
13-8.	Calibration of Secondary Standards by the Substitution Method . . . . .	841
13-9.	Production Calibration . . . . .	848
CHAP. 14.	DIRECTIONAL COUPLERS. . . . .	854
14-1.	Introduction . . . . .	854
14-2.	Equivalent Circuit of a Directional Coupler . . . . .	855
14-3.	The Bethe-hole Coupler . . . . .	858
14-4.	Branched-guide Couplers. . . . .	866
14-5.	Two-hole Couplers . . . . .	873
14-6.	Multiple-path Couplers . . . . .	879
14-7.	Reverse-coupling Types . . . . .	883
14-8.	Long-slot Couplers . . . . .	885
14-9.	Resistive-loop Couplers . . . . .	891
14-10.	General Theoretical Considerations . . . . .	891
14-11.	Measurements of the Properties of Directional Couplers . . . . .	894
14-12.	The Reflectometer . . . . .	896
CHAP. 15.	R-F PHASE AND PATTERN MEASUREMENTS . . . . .	898
15-1.	Terminology and Definitions. . . . .	898
15-2.	Pattern Intensity Measurements . . . . .	900
15-3.	The Measurement of Antenna Gain. . . . .	907
15-4.	Effect of Antenna Scattering in Gain Measurements. . . . .	909
15-5.	The Mirror Method of Gain Determination . . . . .	911
15-6.	Gain Determination by Pattern Integration . . . . .	914
15-7.	R-f Phase Measurements. . . . .	915
15-8.	Phase Apparatus for Point Sources . . . . .	916
15-9.	Frequency Sensitivity of Phase. . . . .	917
15-10.	Phase Apparatus for Line Sources. . . . .	918
15-11.	Phase-modulation Method. . . . .	919
APPENDIX.	MANUFACTURERS OF MICROWAVE EQUIPMENT . . . . .	923
1.	R-f Cables and Connectors . . . . .	923
2.	Waveguide and Rigid Coaxial Line and Connectors . . . . .	923
3.	Amplifiers and Power Supplies . . . . .	924
4.	Crystal Rectifiers . . . . .	924
5.	Oscillator Tubes. . . . .	924
6.	Power Measurements . . . . .	924
7.	Attenuators. . . . .	925
8.	Spectrum Analyzers . . . . .	925
9.	R-f Components. . . . .	925
10.	Wavemeters . . . . .	925
MANUFACTURERS	. . . . .	925
INDEX.	. . . . .	929

**PART III**

**THE MEASUREMENT OF  
IMPEDANCE AND STANDING  
WAVES**

## CHAPTER 8

### MEASUREMENTS OF STANDING WAVES

By E. M. PURCELL

If a uniform transmission line is excited by a generator at a frequency that is not too high, the steady state can be described by saying that there are two waves on the line, one running in each direction. The amplitude of each of these waves can be associated with some quantity characteristic of the electromagnetic field, such as the electric field strength at some arbitrarily selected location on a cross section of the transmission line. With this understanding, the amplitude of the waves may be formally described, at any point along the line and at any time, by complex numbers  $A$  and  $B$ , which refer to the wave running from the generator and the wave running toward the generator, respectively. If the positive  $x$  direction is pointed away from the generator,

$$\begin{aligned} A &= A_0 e^{j\omega t - \gamma x}, \\ B &= B_0 e^{j\omega t + \gamma x}. \end{aligned} \tag{1}$$

The instantaneous magnitude of the electromagnetic field quantity to which the amplitude refers is understood to be the real part of  $A$ , or of  $B$ . The numbers  $A_0$  and  $B_0$  depend on choice of the zero points for the measurement of time and distance. The quantity  $\gamma$  is called the propagation constant of the wave; it depends upon the properties of the transmission line, and upon the frequency. It is customary to denote the real and imaginary parts of  $\gamma$  by  $\alpha$  and  $\beta$ , that is,

$$\gamma = \alpha + j\beta. \tag{2}$$

If the transmission line is lossless,  $\alpha = 0$ , and  $\beta = 2\pi f/v$ , where  $v$  is the phase velocity of a wave on the line at frequency  $f$ . If attenuation along the line must be reckoned with,  $\alpha > 0$ ; there is then an exponential decrease of the absolute magnitude of  $A$ , and a corresponding increase of the absolute magnitude of  $B$ , as  $x$  increases.

The total amplitude,  $A + B$ , at some point along the line, is the quantity of interest and more particularly the time average of some function of  $|A + B|$ , for the instruments are not, as a rule, capable of following the rapid variations at frequency  $f$ . Suppose for definiteness that something proportional to the time average of  $|A + B|^2$  can be measured, the result of one such measurement being a single real number

which will be called  $P_s$  and which will be a function of  $x$ , although not, of course, a function of  $t$ . Then,

$$P_s \propto |A_0 e^{-\gamma x} + B_0 e^{+\gamma x}|^2. \quad (3)$$

In general,  $P_s$  will display maxima and minima as  $x$  is varied; it may be said that there are *standing waves* on the line. From the variation of  $P_s$  with  $x$  it is possible to deduce the ratio of  $A_0$  to  $B_0$ , which is a complex number, and also  $\gamma$ , if necessary. This is the object of all standing-wave measurements. Such measurements are useful because knowledge of  $A_0/B_0$ , together with  $\gamma$ , suffices to determine completely the properties of the termination of the transmission line at the prevailing frequency.

In most microwave measurements it is permissible to neglect the attenuation in the transmission line itself and to assume that

$$\gamma = j\beta = j2\pi f/v.$$

This may seem at first rather surprising if one is accustomed to associate high losses with high frequencies, in consequence of the decrease of skin depth with increasing frequency. The significant quantity, however, is the attenuation per wavelength and for transmission lines of a *given size* this decreases, with increasing frequency, as  $1/\sqrt{f}$ . Microwave transmission lines are not much smaller in cross section than lines used at much lower frequencies, as a rule, and hence the approximation made by neglecting the attenuation is much better than it would be at low frequencies. As the high-frequency end of the microwave spectrum is approached, however, transmission lines (which in most cases take the form of hollow waveguides) must be made smaller to avoid the possibility of propagation in higher modes, and the attenuation per wavelength increases, approximately as  $\sqrt{f}$ . But even at 30,000 Mc/sec the ratio of  $\alpha$  to  $\beta$  is usually less than  $10^{-3}$ . The effect of line attenuation upon standing-wave measurements will be considered briefly later; in most of what follows it will be neglected.

It has already been suggested that, if the frequency is too high or the transmission line too large in cross section, propagation of energy in more than one mode may be possible. In that case the two waves of Eq. (1) do not suffice to describe conditions within the line, and other waves must be included. For an introduction to this special problem which will not be treated here, the reader is referred to Chap. 10 of Vol. 8.

It will be assumed throughout the chapter that the electromagnetic fields under examination correspond to a steady state, which is equivalent to the assumption that a single sharply defined frequency is involved. Nevertheless, the results can be applied, in many cases, to a modulated signal. This is allowable when the modulation frequencies concerned

are much lower than the carrier frequency, as is almost always true in the microwave region.

**8.1. Fundamental Relations.**—If  $\gamma$  is known in advance, the result of a measurement of the standing-wave pattern on a line at a fixed frequency with a given load can be expressed by a single complex number, the ratio of  $B$  to  $A$ , the amplitudes appearing in Eq. (1), at some selected point on the line. From this number the ratio of  $B$  to  $A$  at any other point can be computed from Eq. (1). In particular, the value of  $B/A$  at the load can be found, which is, by definition, the complex reflection coefficient  $\Gamma_L$  of the load,

$$\Gamma_L = \left( \frac{B}{A} \right)_L. \quad (4)$$

More generally  $B/A$  at any point  $x$  on the line can be called the reflection coefficient of the remainder of the line terminating in the load.

The form of the standing-wave pattern, that is, the curve of  $P_s$  as a function of distance  $x$  along the line, can be derived at once from Eq. (2). For simplicity let the origin of  $x$  be taken at a point where  $B/A$  is the positive real number  $\Gamma_0$ . Then,

$$\begin{aligned} P_s &= \text{constant} \times [(1 + \Gamma_0)^2 \cos^2 \beta x + (1 - \Gamma_0)^2 \sin^2 \beta x] \\ &= \text{constant} \times (1 + \Gamma_0 + 2\Gamma_0 \cos 2\beta x). \end{aligned} \quad (5)$$

The curves in Fig. 8-1 show how  $P_s$  varies with  $x$  for certain values of  $\Gamma_0$ . No significance is ordinarily attached to the absolute magnitude of  $P_s$  in a standing wave, but the *relative* magnitudes of the waves of Fig. 8-1 are correct for the case of a matched generator. That is to say, the "constant" in Eq. (5) is the same for all the curves of Fig. 8-1, corresponding to constant amplitude of the wave running *from* the generator.

It must be remembered that the form of the standing-wave pattern actually observed will resemble a  $P_s$  curve only if the indication is proportional to the square of the total amplitude of the waves. The discussion in this chapter will be based on this special case, for the most part, both because the analysis is simpler, and because the detectors that are actually used can, with certain precautions, be made to approximate this response law very closely.

The features of the standing-wave pattern which are most easily

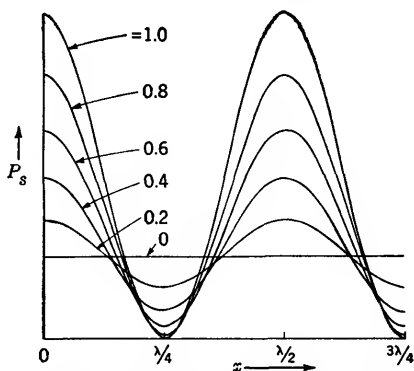


FIG. 8-1.—Variation of probe power  $P_s$  with position of probe. The parameter is  $\Gamma_0$ .



measured are the ratio of the maximum to the minimum reading,  $P_{s\max}/P_{s\min}$ , and the position of a maximum or a minimum along the line. The ratio,  $P_{s\max}/P_{s\min}$ , is called the power standing-wave ratio, whereas  $\sqrt{P_{s\max}/P_{s\min}}$  is called the voltage standing-wave ratio, sometimes abbreviated VSWR, and denoted by the letter  $r$ ,

$$r = \sqrt{\frac{P_{s\max}}{P_{s\min}}} = \frac{|A| + |B|}{|A| - |B|}. \quad (6)$$

The connection between  $r$  and  $|\Gamma|$  is particularly simple; it is at once evident from Eq. (5) that

$$r = \frac{1 + |\Gamma|}{1 - |\Gamma|}; \quad |\Gamma| = \frac{r - 1}{r + 1}. \quad (7)$$

The phase angle of the reflection coefficient of the load can be determined by observing the distance between the load and the nearest *minimum* in  $P_s$ . If this distance is denoted by  $x_{\min}$  and if the reflection coefficient of the load is written  $\Gamma = |\Gamma|e^{j\theta}$ , then

$$\theta = 2\beta x_{\min} \pm \pi. \quad (8)$$

It is often convenient to describe the load by its impedance  $Z_L$  or its admittance  $Y_L$  measured, respectively, in units of the characteristic impedance or the characteristic admittance of the line. The relation between these dimensionless quantities and  $\Gamma$  is

$$\Gamma_L = \frac{Z_L - 1}{Z_L + 1} = \frac{1 - Y_L}{1 + Y_L}. \quad (9)$$

If the dimensions of the transmission line and the load are small compared to a wavelength, the quantity  $Z_L$  appearing in Eq. (9) is the ratio of two impedances, that of the load and that of the line, which are uniquely defined in terms of voltage and current. Equation (9) can be derived by applying the boundary conditions on voltage and current which the load imposes. In a waveguide transmission line or circuit, voltage and current cannot be given a unique and universally useful definition. Equation (9) is to be regarded as *defining*  $Y$  and  $Z$  in terms of  $\Gamma$ . The introduction of the impedance concept does not increase the amount of information made available by a standing-wave measurement, but it does facilitate the comparison of the system under investigation with equivalent circuits composed of transmission lines and lumped impedances, the analysis of which, in turn, is readily carried out by familiar methods.

It is helpful to adopt a method of plotting the results of a series of standing-wave measurements which displays all of the information obtained. A natural way to do this is to plot the quantity  $\Gamma = |\Gamma|e^{j\theta}$  in

the complex plane, with  $\Gamma$  the reflection coefficient at some selected reference point on the line. Often it is convenient to choose as this reference point the termination of the line. All values of  $\Gamma$  will fall on or within the unit circle, at least for passive terminations, and the diagrams take the form of Fig. 8-2a. Through the relations between  $|\Gamma|$  and  $r$ ,

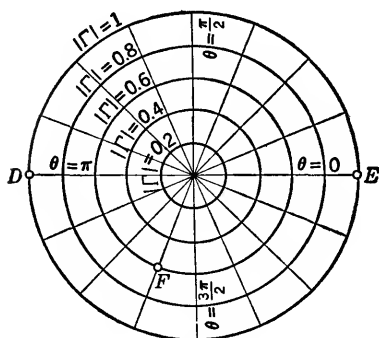
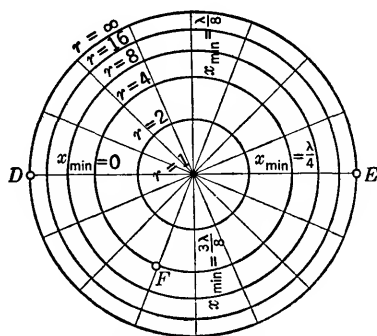
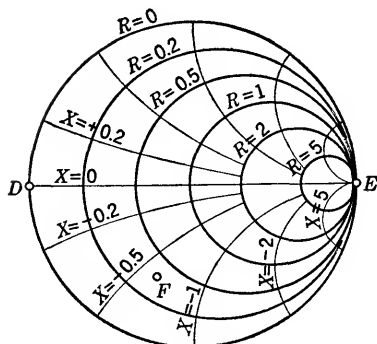
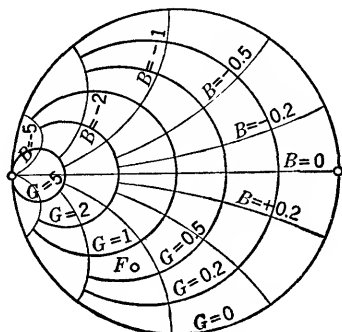
(a)  $\Gamma = |\Gamma|e^{j\theta}$ (b)  $r = \frac{1+|\Gamma|}{1-|\Gamma|}$      $x_{\min} = \frac{\lambda}{4\pi} (\theta \pm \pi)$ (c)  $Z = R + jX = \frac{1+\Gamma}{1-\Gamma}$ (d)  $Y = G + jB = \frac{1-\Gamma}{1+\Gamma}$ 

FIG. 8-2.—Representation of properties of the load by points in the complex plane; (a) reflection coefficient, (b) standing-wave ratio and minimum position, (c) impedance, (d) admittance.

and between  $\theta$  and  $x_{\min}$ , another set of lines and circles can be drawn in the same complex plane from which  $r$  and  $x_{\min}$  can be read directly. This new grid is shown in Fig. 8-2b. The quantity  $x_{\min}$  is understood to be positive when it represents the distance between the reference point on the line and a minimum in  $P$ , located between the reference point and the generator. The location of a point in the  $\Gamma$ -plane can also be described in terms of the impedance  $Z$ , or the admittance  $Y$ , seen at the

reference point in the line, by imposing on the  $\Gamma$ -plane the curves of Fig. 8-2c or Fig. 8-2d.

For example, the points  $D$ ,  $E$ , and  $F$  which appear in each of the plots may be considered. The point  $D$ , in each plot, corresponds to a short circuit,  $\Gamma = -1$ , at the reference position, hence to a zero in  $P_s$  at that point, with  $r = \infty$ . The same point in Figs. 8-2c and d is to be interpreted as zero impedance and infinite admittance, respectively. The point  $E$  represents an open circuit at the reference position, giving  $r = \infty$ , with  $x_m = \lambda/4$ ,  $Z = \infty$ ,  $Y = 0$ . For the point  $F$ , for which

$\Gamma = 0.6e^{j\frac{11\pi}{8}}$ , the minimum in  $P_s$  occurs  $\frac{13}{32}\lambda$  from the reference position, measured toward the generator,  $r = 4$ ,  $Z = 0.35 - j0.61$  and

$$Y = 0.76 + j1.31.$$

The diagrams of Fig. 8-2c and d are the so-called "Smith charts"<sup>1</sup> for impedance and admittance, respectively. They have proved to be very useful in microwave work because, being based on a plot in the  $\Gamma$ -plane, they permit line-length transformations to be effected by simply rotating the whole diagram. The reader may have noted that one additional convention has been introduced without warning, which is that the quantity  $P_s$  refers to the transverse electric field in the line. This convention is established when it is stated that  $P_s = 0$  at a short circuit. It is consistent with the use of electric antennas, or probes, projecting in through the wall of the guide to pick up the signal eventually indicated as  $P_s$ . As will be seen in the following sections, a probe of this type is almost universally favored in microwave measurements, and therefore the convention adopted is natural and convenient.

**8-2. The Slotted Section and Traveling Probe.**—The instrument that has been most widely used for the measurement of standing waves consists of a section of transmission line or waveguide into which a small antenna, or *probe*, can be introduced through a slot. The probe extracts a small fraction of the power flowing in the transmission line, and is connected to an external circuit containing a rectifier, sometimes an amplifier, and a meter. By moving the probe along the slot, which is parallel to the axis of the line, the field in the interior of the line is explored and a curve similar to those of Fig. 8-1 is obtained. The simplified diagrams in Fig. 8-3 show the arrangement of the probe and the slot in a coaxial-line standing-wave instrument and in a waveguide instrument.

The slot is cut so that it runs parallel to the lines of surface current flow associated with the electromagnetic field in an unslotted line or guide, and its presence modifies the original field configuration only to a minor extent. The current flow in a coaxial line in the principal mode is,

<sup>1</sup> Phillip H Smith, *Electronics*, January, 1939, and January, 1944.

of course, directed exclusively parallel to the axis, and a longitudinal slot anywhere on the periphery is allowable. In a rectangular waveguide carrying the dominant mode ( $TE_{10}$ ) the slot must be located at the center of either of the two broad walls of the guide, as is at once evident from a consideration of the electromagnetic field configuration for this mode.

The slot should be long enough to permit observation of at least one maximum and one minimum in  $P_z$  regardless of the position of the standing-wave pattern relative to the slot. Reference to Fig. 8-1 shows that the minimum probe travel thus required is half a wavelength. In

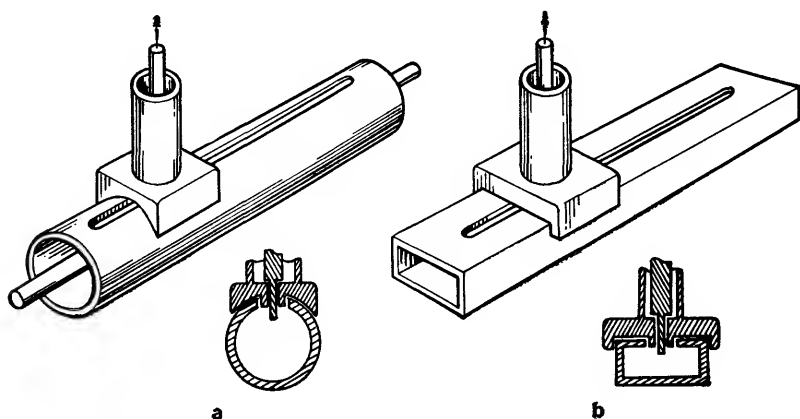


FIG. 8-3.—Slotted section with probe (a) coaxial line, (b) waveguide.

practice, a considerably longer probe travel is advantageous, for the observation of several maxima and minima affords a useful check on the instrument and allows a more accurate determination of the wavelength in the slotted section. It is usually easy to provide this additional length, and most microwave slotted sections permit a probe travel of  $1\frac{1}{2}$  to 3 wavelengths.

The probes shown in Fig. 8-3 are called electric probes because the power that is withdrawn to the indicating circuit depends on the intensity of the electric field at the probe. A magnetic probe, consisting of a small loop antenna could be used instead, and has occasionally been used. The construction of a very small loop that responds only to the magnetic component of the field within the transmission line is difficult, however, if the line leading from the probe out to the detector is a *coaxial* line. There are practical reasons for preferring the coaxial line (rather than a shielded pair, for example) for this function, and the magnetic probe is thereby ruled out in most cases.

Little has been said about the indicating circuit itself, the function

of which is to detect the power picked up by the probe, perhaps to amplify it, and to provide a meter indication proportional to  $|A + B|^2$  or to some other known function of  $|A + B|$ . This part of the instrument will be considered in a later section. For the present, the probe will be regarded simply as a load on the main transmission line, and it will be assumed that the ultimate meter reading is proportional to the power absorbed by this load.

The slotted-section technique is based on two assumptions: first, that the slotted line itself can be treated as a uniform lossless transmission line; second, that the presence of the probe does not seriously modify the electromagnetic field in the line. The validity of these assumptions is restricted by several factors which must be carefully examined if the best use is to be made of such an instrument, and which must be taken into account in the design of slotted sections and probes. The disturbing influences to be reckoned with are of two kinds: those which cannot be avoided so long as the probe and slot are of finite size and a finite amount of power is required to actuate the indicator, and those which can be blamed on accidental mechanical irregularities, departures from perfect symmetry, and so on. In the following sections effects of the first sort will be examined.

**8-3. The Properties of the Slotted Line.**—The effect of a longitudinal slot in the outer conductor of a coaxial line is to change the characteristic impedance of the line slightly, and to introduce a finite, but usually negligible, loss. The change in impedance can be understood by recalling that the characteristic impedance of a line consisting of two parallel cylinders, which need be neither circular in cross section nor coaxial, is uniquely determined by the capacitance of the line per unit length.<sup>1</sup> The creation of the slot reduces slightly the capacitance per unit length. The magnitude of the effect is given approximately by the following formula which was derived for the case of an infinitely thick outer conductor as in Fig. 8-4a.

$$\frac{\Delta Z_0}{Z_0} = \frac{1}{4\pi^2} \frac{w^2}{R_2^2 - R_1^2} \quad (10)$$

Here  $\Delta Z_0$  is the change in characteristic impedance,  $R_1$  and  $R_2$  are the radii of the inner and outer conductors, respectively, and  $w$  is the width of the slot. For a wall of finite thickness the effect will be only slightly larger. The only significant consequence of a change in characteristic impedance is that a small reflection of the waves in the line will occur where the slot begins and again where it ends. The reflection coefficient will be, in absolute value,  $\frac{1}{2}\Delta Z_0/Z_0$  from Eq. (10). For very precise work the effect might prove troublesome. It can be avoided, if neces-

<sup>1</sup> It is assumed that the magnetic permeability of the intervening medium is fixed.



sary, by compensating the change in impedance caused by the slot by an increase in the diameter of the inner conductor.

In a waveguide slotted section, the presence of the slot affects the propagation constant of the line, as well as the characteristic impedance. The guide wavelength  $\lambda'_g$  in a slotted guide differs slightly from the guide

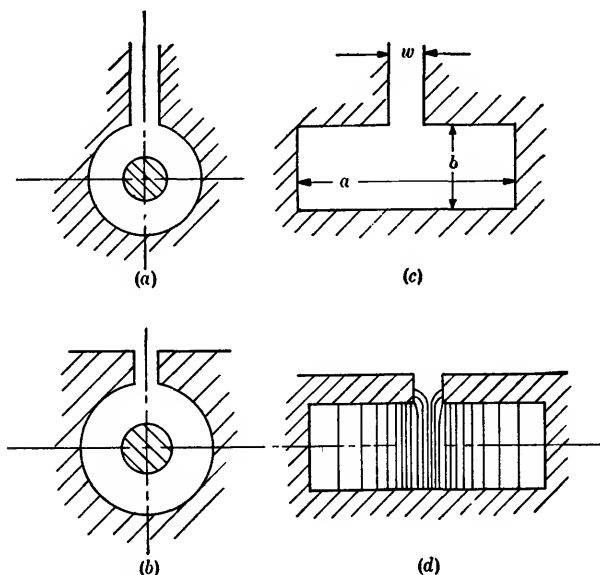


FIG. 8-4.—Cross section of slotted coaxial line and slotted guide.

wavelength  $\lambda_g$  in a guide of the same cross section but without a slot. The magnitude of the effect for a rectangular guide of width  $a$ , height  $b$ , and slot of width  $w$ , (see Fig. 8-4) is given approximately by

$$\lambda'_g = \lambda_g \left( 1 + \frac{w^2 \lambda_g^2}{8\pi b a^3} \right). \quad (11)$$

Expressed in another way, the slotted guide of width  $a$  acts like an ordinary guide of width

$$\left( a - \frac{w^2}{2\pi b} \right).$$

Equation (11) was derived for a guide of infinite wall thickness, but can be used without significant error when the thickness is of the order of magnitude of the slot width, as is usually the case. The change in  $\lambda_g$  for most slotted sections amounts to less than 1 per cent. It causes no difficulty because the guide wavelength in a slotted section can and should be determined by direct measurement, where high accuracy is required. The wave-impedance of the guide will be increased by the

same factor  $\left(1 + \frac{w^2 \lambda_g^2}{8\pi b a^3}\right)$ ; as a consequence a small reflection may be expected at the beginning and at the end of the slot, as in the case of the coaxial slotted section.

The electric field will penetrate the slot to some extent and unless the wall is infinitely thick the field will extend into the exterior region

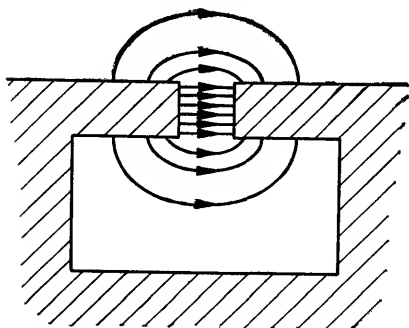


Fig. 8-5.—Electric field in a slot wave.

with consequent loss of power by radiation. This effect, however, is ordinarily immeasurably small, for when the wall thickness is comparable with the slot width, the slot acts as a waveguide far beyond cutoff for the penetrating field, which may be thought of as a  $TM$ -wave in the parallel-plate transmission line formed by the sides of the slot. The attenuation of this wave in a direction normal to the axis of the line or guide

is so rapid that the coupling to the exterior region is of no practical importance. The actual field configuration must resemble that sketched in Fig. 8-4*d*.

The slotted waveguide has another property that occasionally makes itself evident. A new mode of propagation is made possible by the presence of the slot. The field configuration of this mode is sketched in Fig. 8-5. It will be noted that the symmetry of the field is such that it cannot be excited by a wave incident in the  $TM_{01}$ -mode unless the cross section of the guide departs in some way from perfect symmetry, as, for example, if the slot is slightly off center. The possibility of departures from symmetry cannot be ignored in practice. Even weak excitation of the mode of Fig. 8-5 may have a disturbing effect upon the standing-wave measurement through a resonance effect like that which can occur in a waveguide section carrying several modes, one of which cannot be propagated in the sections immediately preceding and following. That is to say, the *slot waves*, as the oscillations in this mode will be called, are totally reflected at each end of the slot, and although energy is lost by radiation, to some extent, a pronounced resonance reaction upon the primary  $TE_{10}$ -wave is sometimes observed when the length of the slot is an integral multiple of half the guide wavelength for this mode. Moreover, the slot is divided into two sections by the probe and carriage (see Fig. 8-3). As the probe travels, the lengths of these sections vary, allowing full opportunity for a slot-wave resonance if the slot wave is excited.

The cutoff wavelength for the slot wave can be calculated by an application of formulas derived for the series waveguide T. If the thickness of the waveguide wall is  $t$ , and if  $w$  denotes the slot width with  $a$  and  $b$  as the waveguide dimensions, the cutoff wavelength  $\lambda_c$  for the slot wave is given implicitly by the relation

$$\cot\left(\frac{\pi a}{\lambda_c}\right) = \frac{2b}{\lambda_c} \left[ 2 \ln\left(\frac{0.372b\lambda_c}{w^2}\right) + \frac{2}{\sqrt{1 - \left(\frac{2b}{\lambda_c}\right)^2}} + \frac{2\pi t}{w} \right]. \quad (12)$$

For typical guide and slot dimensions, Eq. (12) is satisfied by a value of  $\lambda_c$  which is considerably larger than  $2a$ . That is, the guide wavelength of the slot mode is shorter than the guide wavelength of the  $TE_{10}$ -mode in the guide. For example, the dimensions  $a = 0.84\lambda_0$ ,  $b = 0.34\lambda_0$ ,  $t = w = 0.08\lambda_0$  lead to  $\lambda_c = 6.0\lambda_0$ . The slot-wave resonance, in this case of a relatively wide slot, is damped by radiation to the extent that the associated  $Q$  is about 7.<sup>1</sup>

Slot-wave resonances are not excluded from coaxial-line slotted sections even though, in the absence of the slot, only the principal mode is allowed. The Formula (12) applies approximately in this case, if  $a$  represents the mean circumference and  $b$  the distance between inner and outer conductors.

In all cases, of course, perfect geometrical symmetry of the slotted section and the probe will prevent excitation of the slot mode and will ensure that the slotted section behaves as a uniform, nearly lossless transmission line supporting only one mode of propagation.

**8.4. The Properties of the Probe.**—An ideal probe would be one whose presence in no way altered the fields within the transmission line and which, nevertheless, provided an indication of the intensity of the electric field within the line. The ideal is unattainable, and in fact for rough measurements only is it permissible to neglect the effect of the probe upon the line. Fortunately it is not difficult to analyze the action of the probe if two assumptions are made: (1) The probe and any associated high-frequency circuit components can be included in the complete microwave circuit of generator, transmission line, and load without introducing nonlinear circuit elements. This means that the line which connects the probe antenna to the external detecting circuit presents, as seen from the probe, an impedance which is independent of the amplitude

<sup>1</sup> The formulas used in deriving the properties of the slot wave were taken from *The Waveguide Handbook*, Vol. 10 of the Series, Sec. 10-4a. The slot is treated as the perpendicular branch of an  $E$ -plane T terminating in a transition to an infinite guide of infinite height. The loading referred to is also derived from this model and is given approximately by  $Q = \lambda_c^2/2\pi^2ab$ .

of excitation. (2) The dimensions of the probe in a direction parallel to the slot are small compared with a wavelength.

The first assumption is not, as might at first be supposed, incompatible with the use of a crystal detector to rectify the signal picked up by the probe. The signal is required to be very weak for other reasons, and the detector then appears to the *microwave line* as a linear load. The second assumption is very well fulfilled also in most instruments.

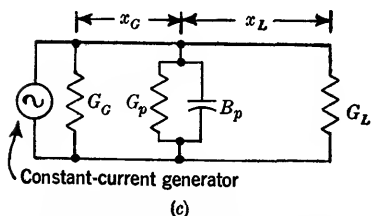
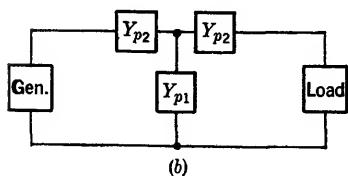
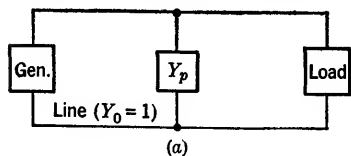


FIG. 8-6.—Equivalent circuit for the probe; in (a) and (c) the probe is represented as a simple shunt admittance  $Y_p = G_p + jB_p$ .

The representation of the probe as a *shunt* element is not the only possibility, but it is convenient because of the convention already adopted that the probe reading refers to the transverse electric field, that is, that the probe is actually an electric antenna.

The influence of the probe upon the observed standing-wave pattern can now be analyzed by expressing the power dissipated in the conductance  $G_p$  as a function of the position of the probe on the line, the load admittance  $Y_L$ , and the generator admittance  $Y_L$ . The case  $Y_L = 1$ , that of a *matched* generator, will be considered first. The distance between generator and probe will be denoted by  $x_G$  and the distance between probe and load by  $x_L$ . It will suffice to consider  $Y_L$  as real, writing it as  $G_L$ , since any load of complex admittance will give rise to the same standing-wave pattern as some real load, except for a

As a direct consequence of assumptions (1) and (2), the probe can be represented as a simple shunt admittance connected across the transmission line or waveguide, and the complete equivalent circuit takes the form shown in Fig. 8-6a. Had assumption (2) not been made, it would have been necessary to adopt a more complicated equivalent circuit for the probe, such as the T-network of Fig. 8-6b.

In Fig. 8-6c, the probe admittance  $Y_p$  is separated into a conductance  $G_p$  and a susceptance  $B_p$ . The power extracted by the probe is that dissipated in  $G_p$  and although this power, in the actual probe, may not all reach the detector because of ohmic loss in the probe circuit, it may still be assumed that the final indication  $P_s$  is proportional to  $e_p^2 G_p$  where  $e_p$  is the voltage across the line at the probe position.

shift of the pattern along the line. Alternatively, it may be said that  $x_L$  is measured between the probe and a point on the line at which the admittance of the remainder of the line, terminating in the load, is real and of magnitude  $G_L$ .

A straightforward application of the transmission-line relations now leads to an expression for the power absorbed in  $G_p$ , which apart from an irrelevant constant factor involving the generator current, the efficiency of the detector, and so forth can be identified with  $P_s$ , the probe reading.

$$P_s \propto \frac{G_p(1 + G_L^2 \tan^2 \theta)^2}{[1 + G_L + G_p + G_L(1 + G_L + G_p G_L) \tan^2 \theta]^2 + [B_p + (1 - G_L^2) \tan \theta + B_p G_L^2 \tan^2 \theta]^2}. \quad (13)$$

The angle  $\theta$  has been written in place of  $2\pi x_L/\lambda_g$ . That  $P_s$  does not depend on  $x_G$  is the result of assuming a matched generator.

Consider first the case  $G_L = 0$ . Eq. (13) becomes

$$P_s \propto \frac{G_p}{(1 + G_p)^2 + (B_p + \tan \theta)^2}. \quad (14)$$

The standing-wave pattern displays zeros for  $\tan \theta = \infty$ , a condition that does not involve  $B_p$  and  $G_p$ . In other words, the zeros in the standing-wave pattern appear just where they would if the probe were ideally infinitesimal. The *maxima*, however, are shifted, since they are located by the condition  $\tan \theta = -B_p$ , rather than  $\tan \theta = 0$ , and the pattern as a whole is distorted compared to that which would be observed with an infinitesimal probe. Figure 8-7 displays a rather extreme case of such distortion, observed with a probe for which  $B_p$  was about 0.5. The circles are experimental points.

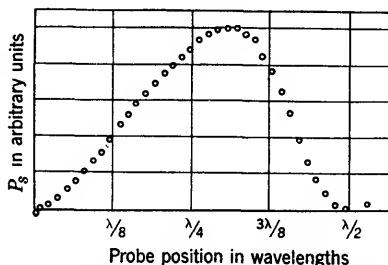


FIG. 8-7.—Observed standing-wave pattern showing distortion by probe susceptance. Circles are experimental points.

The shift in the maximum affords a direct measure of  $B_p$ . The maxima will be shifted toward the load if  $B_p$  is positive. The degree of asymmetry can also be specified by comparing values of  $P_s$  measured at two points  $\lambda/8$  to either side of a minimum, where  $\tan \theta = +1$  and  $-1$ , respectively. The ratio  $\rho$  of the two readings will be

$$\rho = \frac{(1 + G_p)^2 + (B_p - 1)^2}{(1 + G_p)^2 + (B_p + 1)^2},$$



or approximately, if  $G_p$  and  $B_p$  are small,

$$\rho = 1 - 2B_p.$$

If  $G_L$  is not zero, the probe admittance may be expected to affect the measured standing-wave ratio  $r_m$ , as well as the positions of maxima and minima. The shifts in maxima and minima can be computed from Eq. (13). The shift of the minimum from the "true" position, that is, from the position where a minimum would be found with an infinitesimal probe, may be denoted by  $\delta_{\min}$  and the shift of the maximum by  $\delta_{\max}$ .

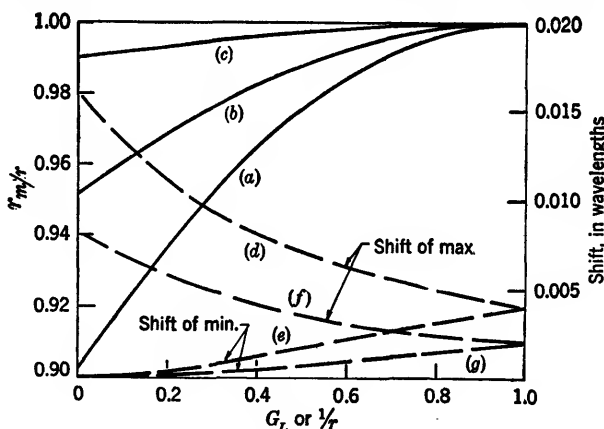


FIG. 8-8.—Solid curves show effect of probe conductance  $G_p$  on measured standing-wave ratio  $r_m$  as a function of  $G_L$ , with  $B_p = 0$ . Curves (a), (b), (c) are for  $G_p = 0.1$ , 0.05, and 0.01, respectively. Dashed curves show effect of  $B_p$  in shifting maximum and minimum. Curves (d) and (e) are for  $B = 0.1$ ; curves (f) and (g) for  $B = 0.05$ .

If  $B_p$  and  $G_p$  are both small, by differentiation of Eq. (13) the following formulas for the case  $G_L \leq 1$  are obtained,

$$\frac{\delta_{\min}}{\lambda_g} = \frac{G_L^2 B_p}{(1 + G_L)^2}, \quad (15)$$

$$\frac{\delta_{\max}}{\lambda_g} = \frac{B_p}{(1 + G_L)^2}. \quad (16)$$

These relations are plotted in Fig. 8-8. For  $G_L \geq 1$  the subscripts *min* and *max* need only be interchanged, or, what amounts to the same thing,  $G_L$  be replaced by  $1/G_L$ . Thus, the shift of the minimum is in general less than the shift of the maximum, and when the standing-wave ratio is large ( $G_L \ll 1$  or  $G_L \gg 1$ ), the shift of the minimum is very small indeed. Moreover, to the first order, the minimum shift and the maximum shift depend only on  $B_p$ . It is in fact readily shown from Eq. (13) that if  $B_p = 0$ , both shifts are zero, no matter how large  $G_p$ . It is obvious from these results that a large value of  $B_p$  is undesirable and that in any case the

location of the *minimum*, rather than the *maximum*, should be used to establish the phase of the reflection coefficient of the load in a standing-wave measurement.

It must also be expected that the measured standing-wave ratio  $r_m$  will differ somewhat from the value  $r$  which would be observed with an infinitesimal probe. This effect is due both to  $G_p$  and  $B_p$ , and if  $G_p$  and  $B_p$  are of the same order of magnitude, the analysis is tedious and the result rather complicated. Only the case of  $B_p = 0$  will be discussed. It has been pointed out that it is desirable to reduce  $B_p$  and in most cases this can be done by a tuning adjustment in the probe circuit. If  $B_p = 0$ , Eq. (13) yields immediately

$$\frac{r_m}{r} = \frac{1 + G_L + G_p G_L}{1 + G_L + G_p} \quad (17)$$

for  $G_L \leq 1$ . Since  $r = 1/G_L$  when  $G_L \leq 1$ , the result can also be written

$$\frac{r_m}{r} = \frac{1 + r + G_p}{1 + r + rG_p} \quad (18)$$

The observed standing-wave ratio is always less than the true standing-wave ratio if  $B_p = 0$ . The solid curve in Fig. 8-8 is a plot of the formula just given.

The quantity  $G_p$  is a particularly significant parameter, for it determines the amount of power extracted by the probe. For example, if the load is matched ( $G_L = 1$ ) and if  $G_p \ll 1$ ,  $G_p$  is identical with the fraction of the power flowing toward the load which is diverted by the probe to the measuring circuit. It is therefore appropriate to call  $G_p$  the *coupling coefficient* of the probe. Every standing-wave measurement poses the problem of a compromise between a very small coupling coefficient, which would make severe demands on the sensitivity of the indicating circuit or upon the output power of the generator, and a larger coupling coefficient necessarily accompanied by larger discrepancies between the measured and the true standing-wave ratio. Where the compromise is to be struck depends, of course, on the circumstances—the degree of accuracy sought, the power available, and so forth. The point that must be emphasized here is that a compromise cannot be avoided; both the power extracted and the error in  $r_m$  depend directly on  $G_p$ . It is not possible to construct a probe that has a coupling coefficient of 0.05 without introducing across the line a conductance  $G_p = 0.05$ .

Two probes that are adjusted to have the same  $G_p$  can differ only in the value of  $B_p$ , no matter how dissimilar their physical appearance; if  $B_p$  can be tuned to zero for each, the probes will be electrically identical. These conclusions, of course, hold only if the probe can be considered a simple shunt circuit; this is allowable in nearly all practical cases because the

dimensions of the probe, in a direction parallel to the slot, are small compared to a wavelength.

If the generator is not matched ( $G_g \neq 1$ ), the formula for the power dissipated in the probe conductance necessarily becomes very complicated, involving  $G_g$ ,  $B_g$ ,  $G_p$ ,  $B_p$ ,  $G_L$ , and both  $x_g$  and  $x_L$ .  $B_g$  could of course be eliminated by a suitable choice of the point to which  $x_g$  is measured. Only a special case will be considered, that of a matched load  $G_L = 1$ , and a probe of zero susceptance  $B_p = 0$ . As the probe is moved, maxima and minima will be observed in  $P_s$ , despite the fact that  $G_L = 1$ , because a change in  $x_g$  changes the load on the generator. The apparent standing-wave ratio  $r_a$  is

$$r_a = \frac{1 + G_g + G_p}{1 + G_g + G_p G_g}, \quad \text{for } G_g < 1. \quad (19)$$

Thus, for  $G_p = 0.1$ ,  $G_g = 0.5$ , an apparent standing-wave ratio of 1.03 would be observed. The error due to a mismatched generator decreases as  $G_p$ , the probe coupling, is decreased. The example just discussed shows how the degree of mismatch might be found, if  $G_p$  were known, or conversely how  $G_p$  might be measured if  $G_g$  were known; in both cases a matched load is utilized.

An exhaustive analysis of more general cases which cannot be treated here, together with abundant experimental data, has been given by Redheffer and Dowker.<sup>1</sup>

**8-5. The Design of Slotted Sections and Probes.**—The most important requirements that must be satisfied in designing a slotted section and traveling probe can be stated in this way: (1) A cross section of the guide and probe assembly, at the plane containing the probe, should display perfect symmetry about the axis of the probe over all regions accessible to the electromagnetic field associated with the guide. (2) The cross-section view must not be altered in any way as the probe travels along the slot. A cross section of a typical instrument is shown in Fig. 8-9, with certain details omitted which are of no concern in this discussion. The requirements stated apply to the region below line A-A including the gap between the guide and probe carriage.

The effect of any specified departure from symmetry and uniformity is easily understood in a qualitative way. In general, lack of symmetry causes excitation of the slot wave described in Sec. 8-3. A change in the depth of penetration of the probe, or of the dimensions of the guide near the probe, as the probe moves, results in a variation in the probe admittance  $Y_p$ . It is not unusual to discover a small systematic effect of this sort, a gradual and uniform increase or decrease of  $G_p$  with distance along

<sup>1</sup> Y. Dowker and R. M. Redheffer, "An Investigation of RF Probes," RL Report 483-14, Feb. 6, 1946.

the slot, for which faulty alignment of the ways upon which the probe carriage moves is often to blame. In a coaxial slotted section such a "slope effect" may be observed if the axes of the inner and outer conductor and the path of the probe are not everywhere parallel.<sup>1</sup>

Thus good *mechanical* design is extremely important. The method of construction should be one which lends itself to the maintenance of close tolerances on all critical dimensions not easily adjustable.

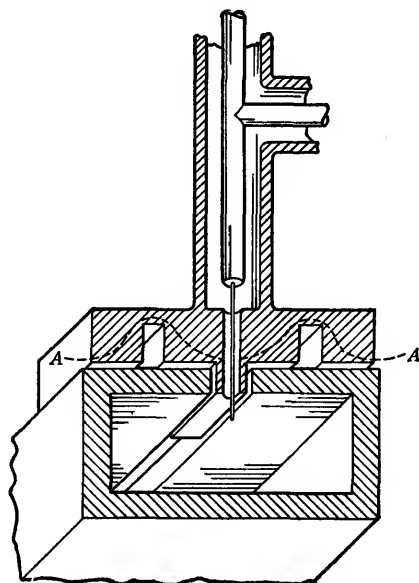


FIG. 8-9.—Shielded probe in slot.

The means for guiding and moving the probe require more careful attention than might at first be supposed. It should be possible to move the probe easily and rapidly over the whole length of the slot, and immediately thereafter to set the probe very precisely at some position. The position of the probe, in accurate work, should be indicated directly and legibly with an error of not more than a few thousandths of a wavelength. The way in which this problem is solved varies widely with the accuracy sought, the wavelength range for which the instrument is intended, and with the inclination and ingenuity of the designer. Only a few general remarks can be made here on the subject.

<sup>1</sup> If the probe penetration is not too small, it has been found empirically that it is more important to maintain a uniform distance between the end of the probe and the inner conductor than to maintain uniform penetration in the event that inner and outer conductor are not parallel. It is difficult, however, to make general statements about a problem in which so many parameters are involved.

At wavelengths of 10 cm or greater, no elaborate driving mechanism is required, as a rule. The probe carriage can be moved by hand, directly, and its position read with sufficient accuracy on a vernier scale. Likewise the tolerances on dimensions are not beyond normal machining practice with the possible exception of the dimension that controls the depth of penetration of the probe in a coaxial instrument. Instruments designed for shorter wavelengths usually embody a reduction in the driving mecha-

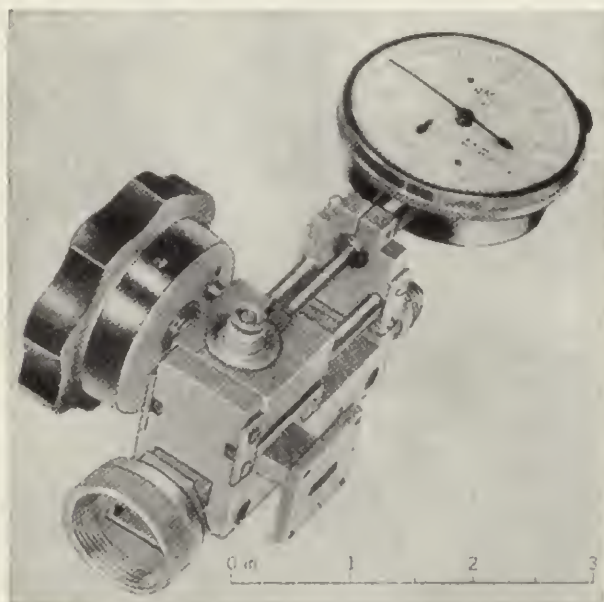


FIG. 8-10.—Standing-wave detector for 1.25 cm. The detector which connects to the square flange is not shown.

nism, and for wavelengths shorter than 3 or 4 cm, amplification of the position reading is almost necessary. A simple screw reduction is not suitable for it does not allow rapid traversal of the entire slot. In several instances a rack and pinion drive, with separate means for registering the probe position, has been satisfactory. In the standing-wave detector for use at 1.25-cm wavelength, shown in Fig. 8-10, a setting and reading accuracy of 0.001 in. is attained without sacrificing the possibility of rapid motion. A friction drive kinematically equivalent to a rack and pinion, but free from backlash,<sup>1</sup> is used; the position of the carriage is indicated by a commercial dial gauge permitting a travel of one inch and reading directly in thousandths of an inch.

<sup>1</sup> Backlash in the drive would not affect the accuracy of position measurement, but it could be a minor annoyance in setting the probe on a sharp minimum.

Instruments of recent design are provided with accurate ways that define the path of the probe carriage. In general, the tendency has been toward a more massive construction, similar to that of other precision instruments. This tendency reflects the increasing interest in, and usefulness of accurate impedance measurements, as well as the progress to higher frequencies.

The requirement of symmetry can be made less stringent by certain modifications in the design of the probe and probe carriage. Indeed experience has shown that these modifications are necessary at short wavelengths in order to achieve a reliable instrument at reasonable cost. Of the features referred to, all of which are visible in Fig. 8-9, the most important is the probe *shield*. The probe shield is the tongue of metal, integral with the probe carriage, which projects into the slot; its lower surface is level with the inner wall of the waveguide. The probe wire runs through a small hole in this shield. The presence of the shield greatly reduces the chance of exciting slot waves through lack of symmetry in the probe. The length of slot filled by the tongue is usually made half a wavelength to minimize the effect of reflections at the ends of the tongue.

It will be noted that no part of the probe carriage in Fig. 8-9 touches the slot or the top of the guide. A positive clearance is maintained on both sides of the shielding tongue and beneath the carriage. It is easier to maintain this clearance with a tolerance of a few thousandths of an inch than to assure intimate but freely sliding contact everywhere between the carriage and shield, and the guide. If such an attempt were made, the location of the *actual* point of bearing, and hence of electrical contact, would depend on minute irregularities, and the electrical symmetry of the system would be jeopardized.

If the two modifications mentioned are introduced, the narrow gap on either side of the probe shield will be excited to a slight extent by the primary wave in the guide. The excitation can be thought of as arising from the current which tends to flow across the narrow gap between the guide and the probe shield. If the probe wire were withdrawn, the current would be merely that required to charge the lower surface of the probe shield. To this must be added, when the probe is inserted, the input current to the probe line. The effect of this current ordinarily predominates. A rough calculation indicates that the probe current exceeds the shield current in a typical case if  $G_p > 0.005$ . Thus, two impedance elements, corresponding to the impedance of the two gaps, one on either side of the probe shield, are in effect connected in series with the probe; if these impedances vary, the probe power will change. To avoid any such effect, the "transmission line" represented by the continuation of the gap into the space beneath the probe carriage is

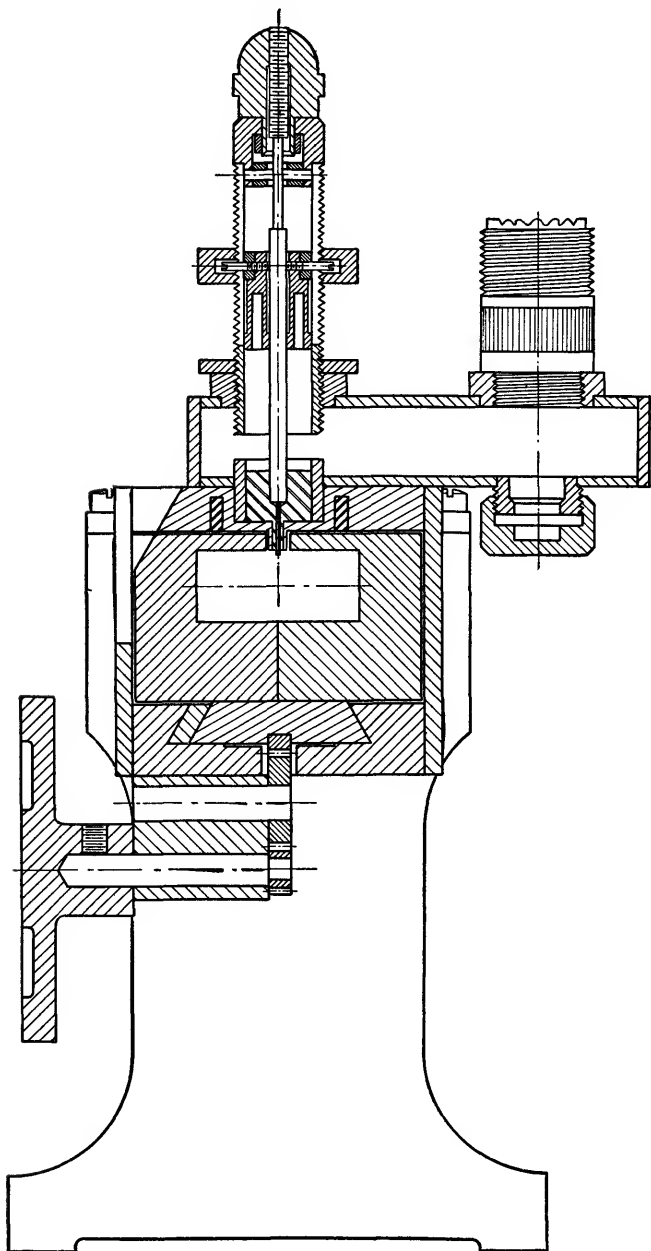


FIG. 8-11.—Cross section of standing-wave detector for 3.2-cm wavelength

terminated in an open circuit approximately  $\frac{1}{4}\lambda$  from the gap, which results in a very *low* impedance at the gap itself. The open-circuit termination is provided by a quarter-wave trap consisting of a longitudinal groove in the bottom of the probe carriage. In the instrument shown in Fig. 8-11 the groove is filled with dielectric to save space; the depth is  $(\lambda/4)(1/\sqrt{k_e})$ . The distance between the mouth of the groove and the lower edge of the shield, which is nominally  $\lambda/4$ , is not critical, as the characteristic impedance of the transmission line is very small.<sup>1</sup>

The probe is ordinarily adjustable in its penetration; this is the easiest way to vary the probe coupling, or probe conductance  $G_p$ . In general,  $B_p$  will be found to change as the probe penetration is varied, and provision must be made for an additional adjustment which will allow  $B_p$  to be made small at any setting of the probe depth. The cross section of a 3-cm standing-wave instrument, Fig. 8-11, shows such a tuning device, in this case a coaxial stub on the probe line with a movable plunger. The probe itself is the projecting end of a thin central rod which can be extended or withdrawn by the screw adjustment at the top of the coaxial stub. It should be clear from the discussion in Sec. 8-4 that any further adjustments would be redundant; the characteristics of the probe are entirely determined by  $G_p$  and  $B_p$ .

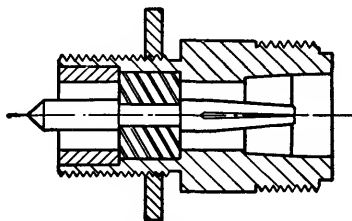


FIG. 8-12.—Attachment for standing-wave detector shown in Fig. 8-11 to allow r-f power from the probe to be sent through a cable.

Certain other features of the instrument of Fig. 8-11 are worth noting. The carriage moves on dovetail ways and is driven by a rack and pinion with an intermediate idler gear whose chief function is to make the sense of the motion the natural one. The short auxiliary guide to which the probe couples is provided with a mount for a cartridge crystal rectifier; an interchangeable fitting allows r-f power to be led off through a suitable cable to a remote rectifier or mixer, if desired. The attachment for this purpose is shown in Fig. 8-12. Finally, the slotted guide itself is made of two blocks joined together; these blocks can be cut from the same milled section, which ensures a highly symmetrical guide and slot. A photograph of the complete instrument is shown in Fig. 8-13.

Figure 8-14 shows in cross section the probe assembly belonging to a 10-cm coaxial slotted section. The probe was designed for the measure-

<sup>1</sup> The basic wavelength is the *free-space* wavelength, where excitation of the gap by the probe current is concerned, because the mode excited in the gap transmission line corresponds nearly to the dominant mode in a parallel-plate transmission line with open sides.



ment of very small reflections in a line of unusually small diameter ( $\frac{5}{16}$  in.); it therefore had to meet exacting requirements.

The internal dimensions of the guide in a waveguide slotted section are usually determined in advance by the existence of standard guide dimensions for the frequency range to be covered. In any case the limitations are identical with those which apply to waveguide in general, namely, the dimensions must be small enough to exclude the possibility of propagation by higher modes at the short-wavelength end of the range, and yet

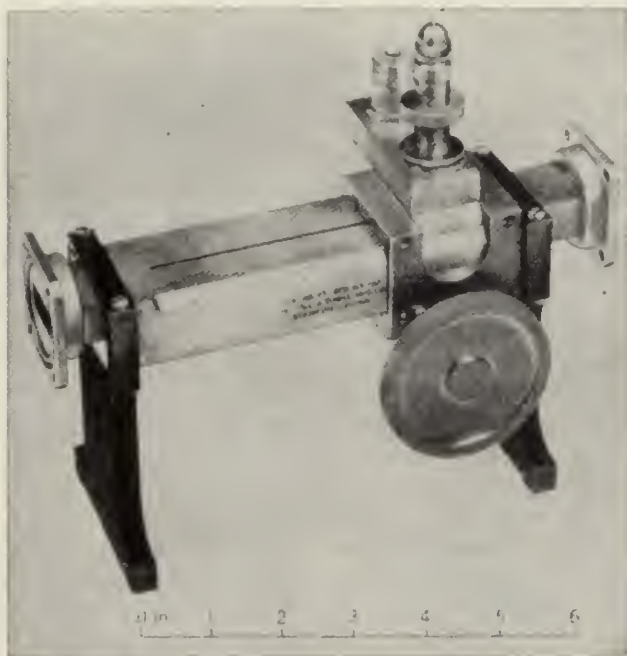


FIG. 8-13.—Standing-wave detector for 3.2-cm wavelength.

large enough to be comfortably far from cutoff for the longest wavelength. In coaxial slotted sections the upper limit of size is set by the occurrence of the lowest mode other than the principal coaxial mode. This next higher mode must be guarded against more carefully in slotted coaxial line than in an ordinary unslotted line, for the presence of the slot represents a departure from axial symmetry favorable for the excitation of the mode in question. The cutoff wavelength for the mode is approximately equal to the mean circumference of the line,  $\pi(R_1 + R_2)$ , where  $R_1$  and  $R_2$  are the radii of the inner and outer conductor. The true value of  $\lambda_c$  differs from  $\pi(R_1 + R_2)$  by less than 3 per cent for  $1 \leq R_2/R_1 \leq 15$ .

The support of the inner conductor in a coaxial slotted section poses a

problem which is already familiar to the microwave engineer but which is particularly acute here since, as has been seen, the accuracy of the standing-wave measurements depends to a large degree on the uniformity of the cross section. Three methods of support for the inner conductor should be mentioned: (a) support by low-reflection beads, or insulators at either end of the section; (b) support by  $\lambda/4$  stubs; (c) support by the device under test, or "cantilever" support. In every case the requirements of low reflection are most severe at the *load* end of the line; as has been shown in Sec. 8.4, the effect of a mismatched *generator*, which would be equivalent to a reflecting support at the generator end, is small.

Method (c) is a rough-and-ready method suitable for measurement of low precision. Quarter-wave stubs provide rigid support if the line diameter is not too small compared to the stub length. Broadband stubs (see Vol. 9 Sec. 4.4) are used in most cases; the frequency sensitivity of an uncompensated  $\lambda/4$  line would be objectionable. The 10-cm instrument in Fig. 8.15 has a stub-supported center conductor, and is provided in addition with an adjustable two-stub transformer by means of which residual reflections between slotted section and load can be matched out. Less use has been made of reflectionless insulators, which, beginning with a simple half-wave bead, can be elaborated, with varying degrees of frequency compensation.

Finally, attention must be paid to the junction between the slotted section and the device under test. The limit of accuracy in the measurement of standing-wave ratios near unity is often set by the small reflection from an imperfect junction. For extremely precise work in waveguides, a tightly clamped butt joint between ground flat surfaces, with some positive means for alignment, is probably the best solution. For most

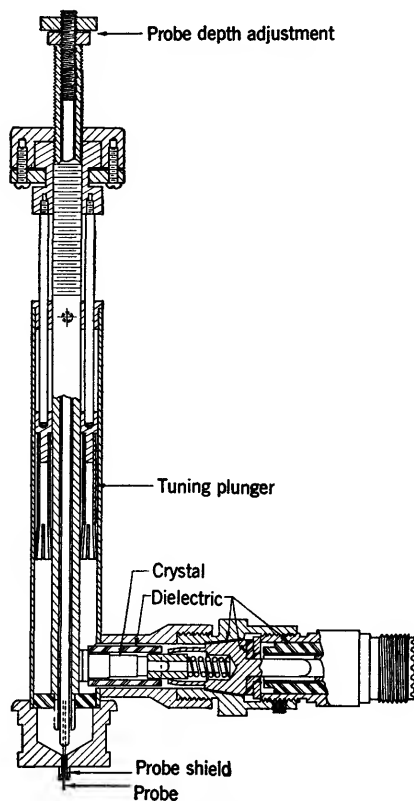


FIG. 8.14.—Cross section of 10-cm probe.

measurements the standard guide coupling, whatever it may be, is of course preferred, for convenience.

**8-6. Detectors and Amplifiers.**—The power that is diverted from the slotted line by the probe ultimately causes deflection of a meter or an oscilloscope trace. The important characteristics of the apparatus by which the conversion from r-f power to meter deflection is accomplished are (1) the over-all *sensitivity* of the detecting system, and (2) the *response law*, that is, the nature of the function that connects probe power with meter reading. The problem is not the same as that of r-f power measure-

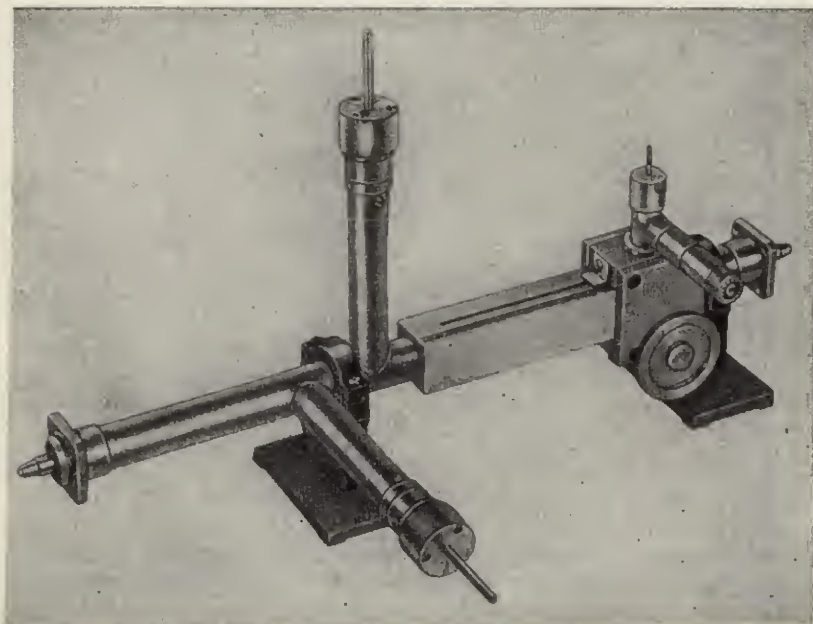


FIG. 8-15.—Coaxial standing-wave detector for 10-cm wavelength.

ment although in principle any of the methods for absolute power measurement described in Chap. 3 are applicable. The difference is that relative power measurements only are required and these must be made rapidly and conveniently.

High sensitivity is an advantage that can be utilized in several ways. Obviously, the output power required of the generator depends inversely on the sensitivity of the detecting system. But even if the output power of the generator seems adequate, it may be desirable to isolate the generator from the line by attenuating pads in order to avoid frequency changes caused by a changing load, or to satisfy the condition  $G_a = 1$ , or both. Also, the errors attributable to the presence of the probe in the line rapidly

become smaller as  $G_p$ , and hence the power available from the probe, are reduced. Finally, the measurement of large standing-wave ratios taxes the sensitivity of the system because the amplitude of the field in the line near a voltage minimum is very small compared to the amplitude observed with the same generator power when the load is matched.

Whatever the form of the function connecting the probe power with the meter indication, the standing-wave patterns obtained with the system can be interpreted if the system has been calibrated over the range of probe power covered by the measurements. A calibration can be obtained, for example, by terminating the slotted section in a short circuit and recording the meter reading as a function of probe position. The variation of probe power with distance is especially simple in this case; it is described by  $\sin^2(2\pi x_p/\lambda_g)$ , if  $G_p$  can be neglected, or, in the next higher approximation by

$$P_s \approx \sin^2 \frac{2\pi x}{g} \left( 1 - 2G_p \sin^2 \frac{2\pi x}{\lambda_g} \right). \quad (20)$$

In each case  $B_p$  has been assumed to be zero. It is then a straightforward procedure to construct a calibration curve by which subsequent measurements can be reduced to some selected basis.

The question of the response law is thus one of convenience only. Nevertheless, the inconvenience of the procedure just outlined is formidable, particularly if the calibration has to be repeated for different ranges of probe power, and repeated again after any significant alteration in the detecting and amplifying system such as replacement of a crystal detector. Most workers have therefore preferred detectors, or detector-amplifier combinations, for which the response, if not accurately proportional to the probe power, is at least a simple function of the probe power over a wide range. For example, it may be possible to represent the final meter deflection  $D$  fairly accurately over some range by a simple power law, such as

$$D = k|A + B|^\mu, \quad (21)$$

where  $A$  and  $B$  represent the amplitudes of the waves in the line, as in Sec. 8-1, and  $\mu$  is a constant. If  $\mu$  is very nearly 2, the response is said to be approximately *square law* in the range in question. Even if the square law is only approximately obeyed, it may be permissible to assume  $\mu = 2$  when dealing with standing-wave ratios near unity. It is easy to see that the error made in supposing that  $\mu = 2$  when the response, in fact, should be represented by  $\mu = 2.3$ , for example, increases rapidly as the standing-wave ratio  $r$  increases.

Detector and amplifier systems that have found general use in microwave standing-wave measurements can be grouped in three categories, more or less in order of increasing sensitivity and complexity.

1. Unmodulated source; crystal detector followed by d-c meter or d-c amplifier and meter.
2. Modulated source; crystal detector or bolometer, followed by a narrow-band amplifier at the modulation frequency.
3. Unmodulated source; superheterodyne receiver employing crystal mixer, local oscillator, and second detector.

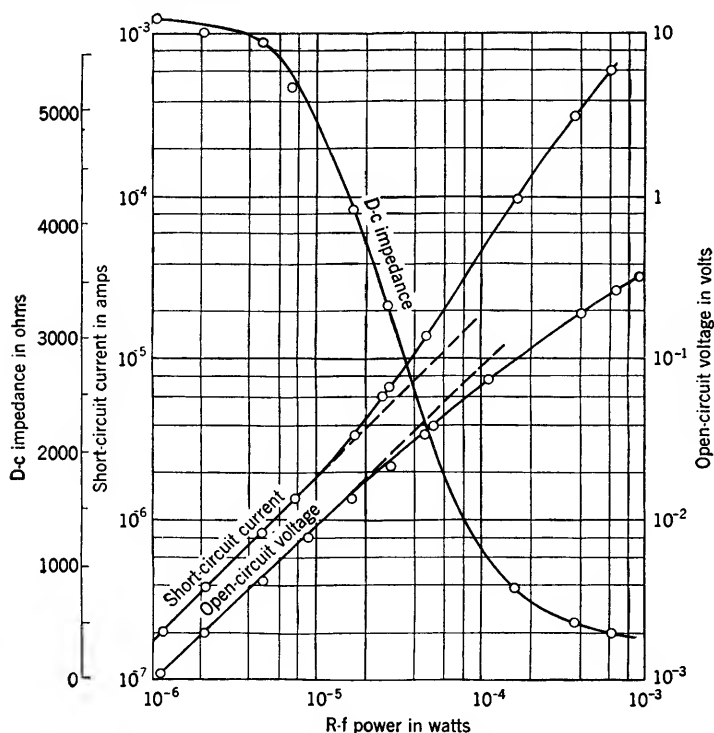


FIG. 8-16.—The rectification properties of a silicon crystal at 3300 Mc/sec.

A crystal rectifier connected to a suitable meter is perhaps the simplest indicating device. The sensitivity that can be achieved with standard microwave crystals is of the order of  $1 \mu\text{a}$  of rectified current (into a low-impedance load) for  $1 \mu\text{w}$  of r-f power absorbed in the crystal. The rectified current is in most cases very nearly proportional to the power absorbed for powers not greater than a few microwatts, but the response law of a new crystal should be checked before accurate measurements are undertaken. The r-f impedance of the crystal is substantially independent of the power level below a few microwatts, and it may be assumed that the response law is not affected by tuning the r-f parts of the probe circuit.

Figure 8-16 is a graph of the characteristics of a silicon crystal rectifier at 3300 Mc/sec. It will be observed that the response is nearly square-law below  $10 \mu\text{w}$ . The sensitivity of this particular sample is however not typical of the best obtainable since it is considerably less than 1 amp/watt. The crystal types which are preferable as detectors are those selected for this property: types 1N27 and 1N32 for 10 cm, types 1N30 and 1N31 for 3 cm.

The meter that measures the rectified current should have a sensitivity of 10  $\mu\text{a}$  for full-scale deflection, or better, not more than a few hundred

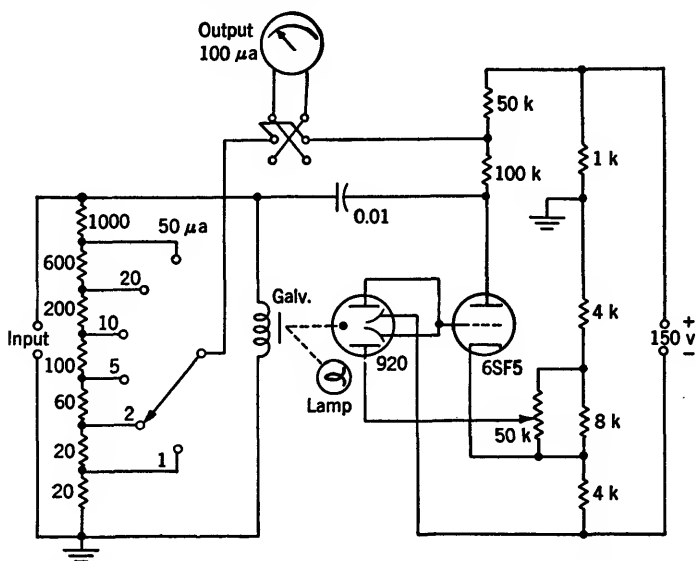


Fig. 8-17.—A galvanometer-amplifier; in effect, a microammeter of very low input resistance.

ohms resistance, and a reasonably short period. Galvanometers of the taut-suspension type which satisfy these requirements are available commercially. A sensitivity of 1  $\mu$ a full scale, with a period of about 3 sec, can be obtained in an instrument rugged enough for general laboratory use.

Much higher *current* sensitivity could be provided by a conventional d-c amplifier, but the crystal is not a constant-current source. Reference to Fig. 8-16 shows that the maximum open-circuit voltage obtainable under the power limitation imposed is only a few millivolts. Little is to be gained therefore by using a direct-coupled d-c amplifier.

A device that avoids the well-known limitations of the conventional amplifier is the galvanometer-amplifier, the circuit of which is shown in Fig. 8-17. The input current, in this case the rectified current from the

crystal, tends to deflect the mirror of the galvanometer that is connected across the input terminals. Deflection of the mirror alters the light distribution on the double photo-cell, which displaces the grid potential of the amplifier tube. The output current of the tube is connected back in such a way as to restore the galvanometer to its zero position. The negative feedback is so strong that the current through the galvanometer remains negligibly small at all times. Very nearly all of the input current, therefore, flows through the tapped resistance at the left; the potential difference between the input terminals is practically zero, and the input and output currents are related by a constant factor depending only on fixed resistances. An additional capacitive feedback path of higher gain is provided to eliminate hunting in the servo system. The device is, in effect, a microammeter of high sensitivity and zero resistance. The response time is that of the output meter; the natural period of the galvanometer plays no role whatever. A discussion of the galvanometer-amplifier, and modifications thereof, can be found in Vol. 18 Sec. 12-16.

Modulation of the r-f source makes it possible to use a-c amplification of the signal from the probe. How modulation can be applied to a microwave oscillator has already been explained in Chap. 2. For standing-wave measurements the percentage of amplitude modulation should be large, but frequency modulation is to be avoided, for a frequency change displaces the standing-wave pattern along the line. Therefore "on-off" modulation, with a square modulation envelope, is preferred. The modulation frequencies ordinarily used are in the audio-frequency range. The difference in frequency between the resulting modulation sidebands and the carrier is entirely negligible, in contrast to frequency differences of many megacycles per second which may arise from changes in the applied potentials of the oscillator during operation.

Demodulation of the signal picked up by the probe can be effected in various ways. A *crystal* detector can be used, connected directly to a tuned audio-frequency amplifier. A *bolometer* can also be used if the response time is not too long compared to the modulation period. A suitable type is the fine-wire *barretter* described at length in Chap. 3. A voltage is applied to the barretter from a d-c source; the temperature changes caused by the absorption of r-f power in the barretter wire are manifested as periodic changes in resistance, and consequently the current through the wire has a component at the modulation frequency. If the temperature change during each cycle is small, the response is accurately square-law, which is one of the principal advantages of the barretter over the crystal. In addition to this advantage, the barretter is less vulnerable to burnout by high pulse power, and is therefore always to be preferred to the crystal when the modulation has the form of short, widely spaced pulses.

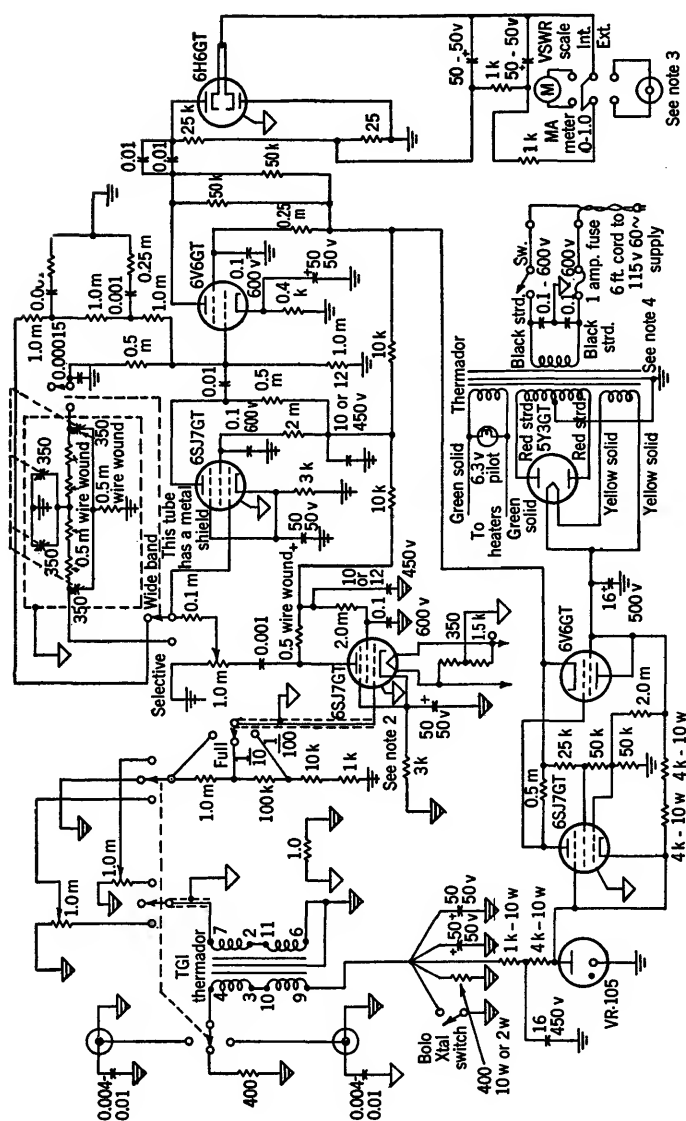


FIG. 8-18.—TWT amplifier. Notes: (1) Transformer and input connectors insulated from chassis and grounded to a common point with wire. (2) This tube has metal shield and is cushion-mounted. (3) This connector must be insulated from chassis. (4) Transformer spaced from chassis by 1-in. bakelite plate. Case connected to ground system through only one mounting screw.



A tuned amplifier that has been used successfully in conjunction with both crystals and bolometers is shown in Fig. 8-18. The tuning has two advantages; it not only eliminates much extraneous interference, but reduces the effect of any frequency modulation that may occur during the rise and fall of the modulating square wave. If neither the rise nor the fall of the modulating voltage that is applied to the source occurs instantaneously, a brief period of oscillation at a frequency other than that prevailing during the main portion of the *on* period may sometimes be observed during the rise, and again during the fall. This spurious signal, after demodulation, will have its strongest component at *twice* the modulation frequency, if the on and off periods have equal length, and will be suppressed, relative to the fundamental, in the tuned amplifier. The frequency selectivity of the amplifier of Fig. 8-17 is provided by a twin-T feedback network applied to the second stage. For a discussion of the principles governing the design of twin-T feedback amplifiers, the reader is referred to Vol. 18, Chap. 11. The circuit of Fig. 8-18 has been carefully designed to avoid ground currents that might result from indiscriminate grounding of points nominally at ground potential.

Sensitivity far exceeding that of the methods so far discussed can be achieved with a "double detection" system, that is, a microwave superheterodyne receiver consisting of a crystal mixer, local oscillator, i-f amplifier, second detector, and some form of indication. The *spectrum analyzer* described in Chap. 7, which is basically just such a receiver, is ideal for the purpose. At least up to the second detector the response of the system is accurately proportional to the input signal power. The excellent power sensitivity, however, (of the order of  $10^{-18}$  watt ultimate sensitivity) allows the problem of the response law to be avoided, or, more precisely, to be transferred to an r-f attenuator. The power picked up by the probe is transmitted through an adjustable attenuator to the input terminals of the spectrum analyzer. A reading is taken by adjusting the attenuator to bring the final output indication to some chosen reference level. A standing-wave ratio is thus determined directly by the difference between two settings of the attenuator. A wide range, in decibels, is available, and consequently high standing-wave ratios can be measured reliably. The attenuator is usually of the waveguide-beyond-cutoff type (see Chap. 11) and requires no calibration. It is the rather high minimum attenuation of such *absolute* attenuators which restricts the application of the method to systems of high sensitivity.

It is characteristic of the spectrum analyzer that the frequency of the local oscillator is continually swept over a range of many megacycles per second. In the application under discussion, this feature makes accurate tuning of source to receiver, or vice versa, unnecessary, and provides incidentally a continual check on the spectral purity of the source.

The methods so far described are not the only ones which have been or could be used, for, as mentioned at the beginning of this section, the only essential requirement is the measurement of relative power at microwave frequencies. For example, the thermistor bridge discussed in Chap. 3 is well suited for standing-wave measurement in some circumstances. The task of reviewing each of the power-measurement methods discussed in Chap. 3, with a view toward their application in standing-wave measurement is, however, left to the reader.

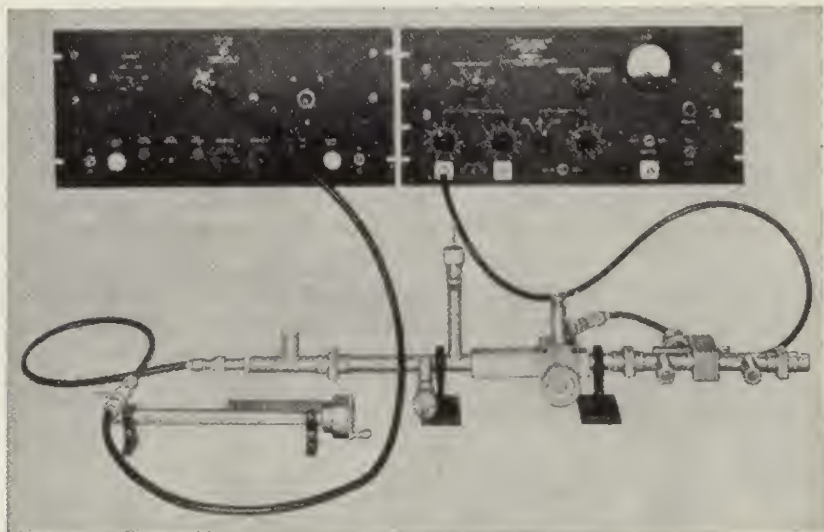


FIG. 8-19.—Assembled apparatus for standing-wave measurement at 10-cm wavelength. The amplifier is the twin-T amplifier whose circuit diagram appears in Fig. 8-18.

A typical assembly of equipment for standing-wave measurement in coaxial line is shown in Fig. 8-19. The unit at the upper left provides square-wave-modulated r-f power from a 10-cm klystron. The power is transmitted by cable to a coaxial wavemeter and thence to the slotted section. The tuning stubs in the slotted section are used here to match the generator to the line. The device under test appears at the right. The rectified crystal current is led to the twin-T amplifier at the upper right.

**8-7. Matched Loads and Other Accessories.**—As in many other experiments it is helpful and sometimes necessary to check the standing-wave instrument, and the technique, against a standard. The calibration of a crystal by means of a short-circuit termination has been mentioned in the preceding section. A somewhat similar procedure was suggested in Sec. 8-4 as a means by which the magnitude of the probe susceptance

$B_p$  could be found. In each case a short-circuit termination, ideally one without loss, is required. If, as in those two cases, the termination need not be movable, a short length of guide or coaxial line closed by a soldered end-cap is adequate. In other cases a movable short circuit, that is, a plunger, is needed. For example, the generator admittance  $Y_G$  can be

measured by determining the height of the maximum in  $P_r$  for several positions of a terminating plunger.

The design of a plunger that is easily movable and yet produces a practically total reflection is not a simple matter. The problem of the design of a plunger is discussed at length elsewhere (Vol. 9 Chap. 8). The most successful waveguide plungers have been those in which actual mechanical contact

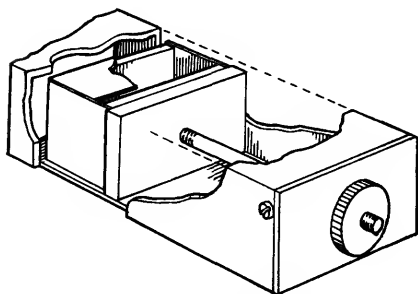


FIG. 8-20.—A short-circuiting plunger with a choke trap consisting of an anti-resonant box.

between plunger and guide walls, where r-f currents are to flow, is avoided by the use of chokes, or traps. In other words, there are no sliding electrical contacts. A plunger of this type is shown in Fig. 8-20. Many other designs have been tried and it is not easy to select the best.

A *calibrated* plunger provides a short circuit whose position is accurately measurable and which can be used to establish a reference position with respect to which the equivalent line length between the probe and some other unknown load can be determined. The reflection from a noncontact plunger may occur as if it were from a conducting plane slightly displaced from the actual plunger face. For very accurate work the difference must be taken into account.

A *matched load* is the standard of reference when standing-wave ratios near unity are being measured. At microwavelengths, fortunately, a tapered absorber is not inconveniently long. A tapered load that has a very small reflection coefficient can be fashioned from almost any lossy material, such as wood, hard rubber, or any of the special materials developed for microwave absorbers if the taper is made several wavelengths long and the onset of the absorption at the input end of the absorber is very gradual. If somewhat more care is taken the over-all length of the absorber can be reduced (see Chap. 12).

The reflection coefficient of the absorbing load is easily measured if the absorber can slide along within a uniform guide or line. This is easily arranged in the case of the tapered loads mentioned. With a fixed probe, and constant generator power, variations in probe power which are observed as the load alone is moved can only be caused by a reflection

from the load. Thus, small reflections from connections, from the end of the slot, or other irregularities cannot mask the small reflection from the load itself, and it is possible by repeating this test after judicious alterations in the shape of the tapered load to arrive at a very well-matched condition with the reflection coefficient of the load less than 0.01. Such a load can then be used to check the uniformity of probe coupling along the slot, the reflection from connectors, and other disturbances which may interfere with the measurement of very small reflection coefficients.

**8-8. Measurement of High Standing-wave Ratios.**—The standing-wave ratio  $r$  increases rapidly as the reflection coefficient of the load approaches one. If  $|\Gamma| = 0.9$ ,  $r = 19$  and  $r^2$ , the ratio of maximum to minimum probe power, is almost 400. To measure  $r^2$  directly by any of the methods previously described, other than the one that makes use of a spectrum analyzer and an r-f attenuator, is almost out of the question. The range over which the detector would be required to respond according to an accurately determined law is too great. There is, however, another procedure by which  $r^2$  can be determined from measurements in a restricted power range. The procedure, in short, consists in examining the standing-wave pattern in the immediate neighborhood of a voltage minimum.

In the neighborhood of a minimum, if  $G_L < 1$ ,  $\tan \theta$  in Eq. (13) can be replaced by  $1/(\pi/2) - \theta$ . If the angle  $(\pi/2) - \theta$  is denoted by  $\phi$ ,  $P_s$  after substitution is

$$P_s \propto \frac{G_p(G_L^2 + \phi^2)^2}{[\phi^2(1 + G_L + G_p) + G_L(1 + G_L + G_p G_L)]^2 + [\phi^2 B_+ + (1 - G_L^2)\phi + B_p G_L^2]^2} \quad (22)$$

To consider the simplest case first, suppose that  $B_p = 0$ ,  $G_L \ll 1$ ,  $G_p \ll 1$ , and take only terms of the lowest order in  $G_L$ ,  $G_p$ , and  $\phi$ . Equation (22) then becomes simply

$$P_s \propto G_L^2 + \phi^2. \quad (23)$$

The curve of  $P_s$  versus probe displacement (measured by  $\phi$ ) is a parabola, the solid curve in Fig. 8-21. Measurement of  $P_s$  at three positions suffices to determine the parabola. A method that is often used is to measure  $P_s$  at the minimum, that is,  $P_1$  in Fig. 8-21, then to determine the width

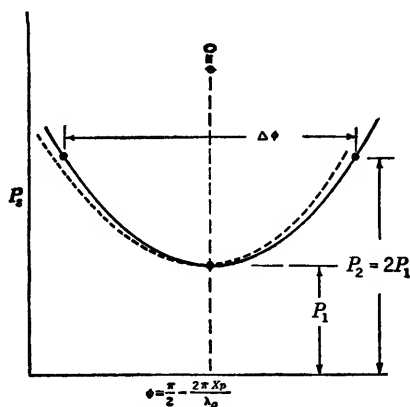


FIG. 8-21.—Variation of probe power in the neighborhood of a minimum.

of the curves  $\Delta\phi$  between points of twice the minimum height. In this case, Eq. (23) yields directly

$$G_L = \frac{1}{r} = \frac{\Delta\phi}{2}. \quad (24)$$

In terms of the directly measured probe displacement  $\Delta x_p$  between points of twice minimum value

$$G_L = \frac{1}{r} = \frac{\pi\Delta x_p}{\lambda_p}. \quad (25)$$

For example, if the separation so measured is  $0.01\lambda_p$ ,  $r = 32$  is obtained.

The inclusion of higher-order terms modifies Eq. (23) only slightly, as does the effect of finite probe susceptance, which will be considered first. If  $B_p$  is no longer neglected, the following is derived from Eq. (22), instead of Eq. (23);

$$P_s \propto (G_L^2 + \phi^2) \left( 1 - \frac{2B_p G_L^2 \phi}{G_L^2 + \phi^2} \right). \quad (26)$$

For the range of  $\phi$  involved in the twice-minimum procedure,  $|\phi| \leq G_L$ . The correction term  $2B_p G_L^2 \phi / (G_L^2 + \phi^2)$ , therefore, does not exceed  $B_p G_L$ . Moreover, this correction term is an odd function of  $\phi$  and the effect is merely to distort the pattern as indicated by the dotted curve in Fig. 8-21, without changing (except in a still higher approximation) the separation of the twice-minimum points. Thus, the effect of probe susceptance upon the measurement of  $r$  by this method is, in practice, negligible, even though  $B_p$  may be as large as unity.

The correction for terms of higher order in  $G_L$  and  $G_p$  is also small. A calculation based on Eq. (22) shows that a determination of  $G_L$  by the twice-minimum procedure using Eq. (24) leads to a result which is too large by the factor  $[1 + G_L^2(\frac{1}{2} + G_p)]$ . The error in  $G_L$ , or in  $r$ , is, therefore, less than 1 per cent for  $G_L < 0.14$  ( $r > 7$ ) if  $G_p \ll 1$ . It may be noted at this point that the error made in replacing  $\tan \theta$  by  $1/\phi$  is also less than 1 per cent for  $r > 7$  and is in the direction to make the measured value of  $G_L$  too small.

Since the correction term  $G_L^2(1 + G_p)$  is not significantly larger if  $G_p$  is made fairly large, *strong probe coupling* is permissible. This makes the demands on the sensitivity of the detector less severe. In fact, a condition as extreme as  $G_p = 1$ ,  $B_p = 1$  is not objectionable.

By the procedure just outlined, the necessity of measuring the probe power at widely different power levels is avoided. On the other hand, the method requires accurate measurement of small probe displacements. If many measurements of this type are contemplated, it may be worth while to construct a special slotted section equipped with a micrometer drive operating over a short distance.

In the measurement of high standing-wave ratios it is not always permissible to neglect, as has been done so far in this chapter, the attenuation in the guide or line between the probe and the load. The effect is easily taken into account. Suppose that a wave traveling from the probe to the load is attenuated in amplitude by the factor  $f$ , which can be computed readily if the properties of the line are known. If  $\Gamma'_L$  is the measured reflection coefficient of the load, the true reflection coefficient of the load  $\Gamma$  is clearly

$$\Gamma = \frac{\Gamma'}{f^2}. \quad (27)$$

Similarly, the measured standing-wave ratio  $r_m$  is related to the standing-wave ratio  $r$ , which would be observed if the line were lossless, by

$$r_m = \frac{r + 1 + f^2(r - 1)}{r + 1 - f^2(r - 1)}. \quad (28)$$

A totally reflecting termination ( $r = \infty$ ) at the end of a line causing attenuation will give rise to a standing-wave ratio

$$r_m = \frac{1 + f^2}{1 - f^2}. \quad (29)$$

Thus the attenuation in a line or guide can be found by measuring the standing-wave ratio at the entrance to a section of the line which is terminated in a short circuit. The method described in this section is well suited to this particular problem. Similar problems arise in the investigation of dielectrics at microwave frequencies (see Chap. 10).

**8.9. The Squeeze Section.**—If the generator is matched ( $Y_G = 1$ ), the probe power depends not upon  $X_G$ , the distance between generator and probe, but only upon  $X_L$ , the distance between probe and load (Sec. 8.1). For that reason, it is possible to ignore the change in  $X_G$  which accompanies the change in  $X_L$  as the probe is moved. Obviously, then, the same variation in probe power would be observed if  $X_L$  were changed without changing  $X_G$ , that is, if the length of line between the load and a *fixed* probe were varied. A coaxial transmission line of variable length is a rather cumbersome affair involving telescoping joints. In waveguide, however, the dependence of phase velocity upon the width of the guide makes it possible to achieve an equivalent result by very simple means. A small change in the width of the guide changes also the *electrical* length.

A guide of variable width can be made by cutting a long narrow slot in each of the broad sides of an ordinary rectangular waveguide. The width is varied by squeezing the split guide, and the device is usually called a *squeeze section*. The change in width is not the same at all points of course, but is greatest at the midpoint of the section where the squeezing

constraint is applied and decreases toward either end of the slot. This effects a very gradually tapered transition, and is just what is needed to avoid reflections. In every cross section taken through the squeezed guide the slots will be centrally located, if they were so originally; hence the loss of power through the slot will be negligibly small as explained in Sec. 8-3. Thus the squeeze section, simple as it is, fulfills the requirements of an ideal line stretcher in all respects but one—the relation between the squeezing displacement and the resulting change in electrical length is only approximately linear, and cannot be easily computed with great accuracy as it depends on the shape assumed by the stressed guide.

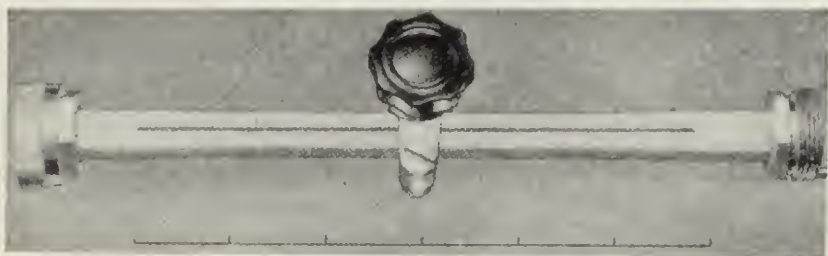


FIG. 8-22.—Squeeze section for 1.25-cm wavelength. The scale marks are inches.

A squeeze section designed for 1.25-cm wavelength is shown in Fig. 8-22. The squeezing is accomplished by links through which passes an eccentric shaft with a knob. The mechanism ensures that the guide will neither be squeezed nor dilated beyond fixed limits, but of course introduces further nonlinearity in the connection between the motion introduced by the operator and the change in electrical length thereby effected. Other examples use a screw drive, which is better adapted to calibration; in the simplest of these the elasticity of the guide itself is relied upon to expand the guide as the screw pressure is relaxed.

Standard 1.25-cm guide (0.420 in. inside width) is so wide that a relatively large change in width is needed to produce a considerable change in  $\lambda_g$ . For this reason, the section shown in Fig. 8-22, although made from standard guide, is actually reduced in width, even in its relaxed condition, over most of the slot length. This is accomplished in manufacture by cutting preliminary slots, then annealing the guide near the ends of the slots and squeezing the slots shut irreversibly by forces applied near the ends. The slots are then milled out to a final width of  $\frac{1}{8}$  in. If it is important to conserve length, as in this case, the internal width of the squeeze section, in its relaxed condition, should be  $0.70$  to  $0.75\lambda_0$ , as a general rule.

For the purpose of preliminary design the electrical length of a squeezed guide can be estimated roughly by assuming that over the length of the slot it is equivalent to a uniform guide whose width is the arithmetic

average of the actual widths at the center and at the end of the slot, respectively. A squeeze section made from standard 1.25-cm guide (not "pre-squeezed" as was the one in Fig. 8-22) with 0.0625-in. slots 10 in. in length changed in electrical length by 5.24 radians when squeezed shut at the center. This figure is the result of a direct measurement at  $\lambda_0 = 1.25$  cm. The approximate method of calculation recommended above predicts a change of 4.65 radians.

For the use of the squeeze section in standing-wave measurements, the section is connected between the load and the probe shown in the diagram of Fig. 8-23. The probe is fixed and usually consists merely of a small hole coupling to a branch guide that is soldered to the main guide and terminated in the detector. The admittance of a probe of this type is adjustable only by tuning the branch guide; usually no provision is made for such tuning. More elaborate coupling circuits could be used instead; the hole has the advantage of simplicity and of a predictable admittance. With the generator matched the ratio of maximum to minimum probe power, observed as the electrical length of the squeeze section is varied, is the standing-wave ratio  $r$ .

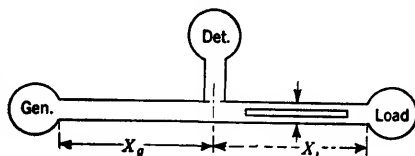


FIG. 8-23.—A diagram illustrating the use of a squeeze section.

The *phase angle* of the reflection coefficient of the load is not so easy to find. Perhaps the most direct method is the following: Adjust the squeeze section to minimize the probe power. Then replace the load with a plunger, and move the plunger to reduce the probe power to zero. The plunger is now an integral number of half wavelengths from the probe, and the distance between the plunger face and the former position of the load is equivalent to  $X_{\min}$  in the traveling-probe type of measurement.

It must be emphasized that the requirement of a matched generator is much more stringent here than in the traveling-probe method. There the load in the generator changed as the probe moved only because of a finite probe admittance  $Y_p$ . Here the distance between the generator and the load  $Y_L$  is changing and the error caused by a mismatched generator vanishes only as  $Y_L \rightarrow 1$ . The method is for that reason best suited to the examination of nearly matched loads, as in routine testing of components that must satisfy some specification of maximum allowable standing-wave ratio.

The squeeze-section method has been highly refined by N. I. Korman<sup>1</sup> and applied to the measurement of very small reflection coefficients. The reader is referred to his report for further analysis of the method and

<sup>1</sup> N. I. Korman, "A Precision Standing-wave Detector for Waveguides," RCA Report TR-12-C, Nov. 27, 1942.



for important variations in the method, including the use of a squeeze section on either side of the probe.

**8.10. Standing-wave Measurements at High Power.**—In testing pulsed microwave transmitters and also in testing many microwave transmission systems during actual operation, or under conditions resembling actual operation, it becomes necessary to measure the standing-wave ratio in a line in which the pulse power is very high. Certain problems which arise deserve mention in this chapter.

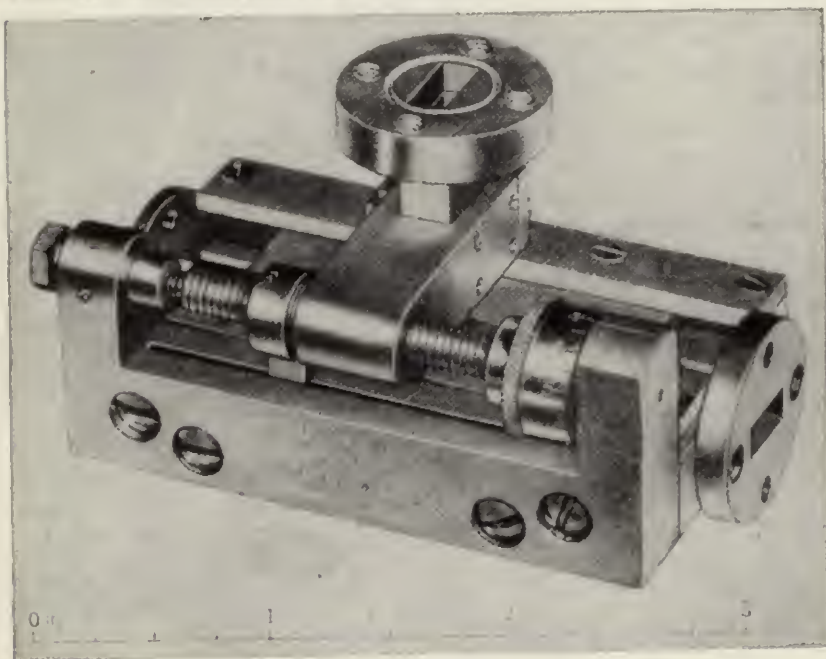


FIG. 8-24.—High-power standing-wave detector.

In the first place it is clear that the requirements on the detecting system are now rather different. Extreme sensitivity is not needed. Instead a detector is required which will withstand relatively high pulse power but will show adequate response to much lower *average* power. A bolometer or a thermistor bridge may be used, for example, coupled in either case very loosely to the line ( $G_p \ll 1$ ) and perhaps protected additionally by an attenuating pad in the probe circuit.

The purpose of the test usually forbids the use of an attenuating pad at the generator end of the line. Therefore, the errors which may be caused by a mismatched generator must be guarded against.

The chief difficulty, however, is voltage breakdown, or sparking, at the probe or slot. The conventional probe is a fine wire projecting slightly

into the guide at a point where the electric field is most intense; there is also a concentration of the field at the inner corners of the slot and at the ends of the probe shield. The usual slotted section, in other words, is not designed to transmit high power, and will break down electrically at a power level considerably lower than that which regular transmission-line components will withstand.

The only steps which can be taken to raise the breakdown limit, as long as the conventional design is adhered to, are the obvious ones of enlarging the dimensions and rounding the corners of any necessary projections, rounding the edges of the slot, and so on. If these precautions are not enough it may be necessary to devise a traveling probe of different type.

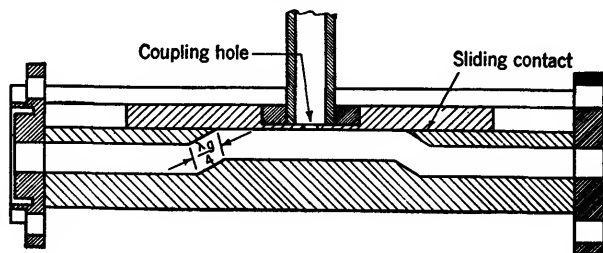


FIG. 8-25.—Cross section of high-power standing-wave detector.

One such design has been worked out with notable success by A. Nordsieck of the Columbia Radiation Laboratory.

Nordsieck's instrument, shown in Fig. 8-24, is a radical departure from previous methods in this respect: the part that travels includes the whole top surface of the waveguide. The probe is merely a small hole in this surface connecting to a branch guide and thence to a detector. In order to bring the inner surface of the guide up to a level accessible to this "cover plate" (see Fig. 8-25) the guide makes two jogs. Each jog is designed to be reflectionless, or nearly so, by spacing successive bends  $\lambda_g/4$  apart.

The crucial problem raised in this design is that of electrical contact, for now the sliding part makes contact with the main body of the guide at a point where the current flow is large. This problem was solved by providing hard, smooth, extremely flat surfaces on the contact members. The surfaces were ground, chromium plated, and lapped, to a tolerance of 0.0002 in. in flatness. It was found possible to obtain a smoothly sliding joint that displayed no sparking at powers up to 100 kw and behaved in other respects as a perfect electrical contact.

**8-11. Continuously Indicating Standing-wave Detectors.**—It would often be helpful to the experimenter if he could see the entire standing-wave pattern at a glance, without the necessity of successive measurements of probe power. If, for instance, he is trying to match the

terminating device by means of tuning adjustments, after each adjustment a new measurement of  $r$  must be made. It does not suffice merely to set the probe at a minimum and then maximize the meter reading by tuning adjustments (although an adjustment in that direction is a good first step) because the adjustments will in general alter the phase as well as the magnitude of the reflection coefficient of the load. There is, therefore, some reason to desire what might be called an *automatic*, or perhaps better, a *continuously indicating* standing-wave detector. There are several more or less obvious ways to build such a device, which will be briefly described.

A standing-wave detector employing a continuously and rapidly movable probe was designed at the Telecommunications Research Establishment. The slotted portion of the main guide followed a semicircular arc, the plane of the circle lying in the plane of the electric field in the guide. The slot was in the inner face and continued a short way beyond the ends of the semicircular arc. This allowed a probe mounted on an arm extending from the center of the arc to move into the slot at one end, travel around the semicircular arc, and emerge from the slot at the other. The probe arm revolved continuously and the rectified crystal current was led to an ordinary oscilloscope upon which the standing-wave pattern was displayed.

A device designed by G. E. Mueller, of the Bell Telephone Laboratories employed a long squeeze section bent into a hairpin shape and vibrated rapidly by a cam arrangement. Again the detector output voltage could be displayed on an oscilloscope.

H. E. Kallmann of the Radiation Laboratory has described an automatic standing-wave detector<sup>1</sup> in which rapid "line stretching" was accomplished by a rotating dielectric disk which dipped into the waveguide through a slot. The waveguide was bent into a circular arc, permitting a considerable length of the periphery of the disk to be used. This instrument included a special peak-voltmeter circuit, the output voltage of which depended on the difference between maximum and minimum probe power. A single meter was calibrated to read  $r$  directly after a preliminary normalizing procedure.

**8-12. Measurements on Lossless Devices.**—Many microwave circuit elements can be treated as lossless devices that serve to connect together two or more uniform waveguides or transmission lines. A junction of waveguides, for example a waveguide T, is such a device. A transition between a waveguide and a coaxial line, a tuning post, an inductive iris, the series-parallel T described in Chap. 9, are other examples. Each of these is equivalent to an electrical network having  $n$  pairs of terminals

<sup>1</sup> H. E. Kallmann, "Matchmeter," RL Report 705, Apr. 9, 1945.

when  $n$  is the number of transmission lines or waveguides connected together by the device.<sup>1</sup> It has been found possible, and convenient, to describe the electrical properties of such a device at a single frequency by an *equivalent circuit*, an  $n$ -terminal-pair network made up of lumped impedance elements. The representation of a lossless device will of course contain reactive elements only. In many cases the *form* of an appropriate equivalent circuit can be deduced from general theoretical considerations but the magnitude of the elements usually cannot be found without solving a complicated electromagnetic boundary-value problem. Then arises the problem of determining the value of the equivalent-circuit parameters experimentally by suitable measurements. It is the purpose of this section to call attention to a method which is especially well suited to the purpose.

A representation of some given device will contain a limited number of parameters. A lossless two-terminal-pair device (sometimes called a *four-terminal device*) requires for its description three parameters, which might be the elements of an equivalent T-, or those of an equivalent  $\pi$ -network; other representations are possible, also, but in every case *three* quantities have to be determined by measurement. A way in which this might be done is to find the input impedance at one terminal pair by means of a standing-wave measurement for each of three arbitrarily selected terminating impedances. The information obtained would suffice to fix the circuit parameters with an accuracy which would depend on the accuracy of the standing-wave measurement, and upon the way in which the various values of the terminating impedance were chosen.

Now the device itself is lossless, and advantage can be taken of this circumstance by making the terminating impedance a pure reactance in each case. The input impedance is necessarily a pure reactance also, the standing-wave ratio is infinite, and the standing-wave measurement consists merely in locating the *minimum position*. When the standing-wave ratio is high, it is easy to locate the minimum with precision, and the true minimum position coincides with the apparent minimum position even for strong probe coupling (Sec. 8-8). The response law of the detector, which is the chief source of uncertainty in the measurement of finite standing-wave ratios, has no influence on the measurement. Also it should be noted that the reactive termination of the circuit under test is the easiest sort of known, variable termination to provide. All that is needed is a calibrated plunger (Sec. 8-7).

When the circuit possesses more than two terminal pairs, the procedure is to terminate all but two of these in plungers which for the time being are left fixed. The resulting two-terminal-pair device is then examined by

<sup>1</sup> It is assumed here that in each of the lines or guides only one propagating mode can exist. A guide carrying two modes must be counted as two terminal pairs.

the method already described, and from these measurements three numbers, in general, are derived. The process is repeated for other settings of the plungers that terminate the remaining pipes until enough information has been acquired to fix the values of all equivalent-circuit parameters.

The deduction of the circuit parameters from the measurements of minimum position *vs* plunger setting deserves more attention than can be allotted to it in this chapter, which is concerned only with standing-wave measurements. Of the numerous procedures that might be followed, one or two are superior in affording not only maximum accuracy and convenience, but a thorough check on the internal consistency of the data.

## CHAPTER 9

### IMPEDANCE BRIDGES

BY LOUIS B. YOUNG<sup>1</sup>

A multifrequency impedance bridge provides simultaneous indications of the power reflected from some test piece at three or more frequencies. Such a device is extremely useful in the development of r-f components which must be well matched over a wide range of frequencies. For example, power detectors such as thermistors are not exactly reproducible in their r-f characteristics and so are mounted in holders that have two or three tuning adjustments. When a slotted section is used in the matching procedure, the mount is tuned for an optimum midband match, and then is checked at the band extremes. If the match is not acceptable at one extreme, it is difficult to make an improvement without adversely affecting the match at the opposite extreme. Another measurement is necessary to check this effect, and the procedure becomes one of successive approximations. On the other hand, when an impedance bridge is used, an optimum match across the band is readily achieved since the effects of tuning may be visualized simultaneously at three or more frequencies.

An impedance bridge consists of three groups of components: r-f sources, the bridge element, and the detector-indicator. Of these, the bridge element is the most interesting since it must couple to the detector only that power which is reflected from the test piece. Although both side-outlet T's and directional couplers can satisfy this requirement, the T is preferred because its selective properties result from symmetry and hence are not frequency-sensitive, an important consideration for multifrequency bridges. In addition to the discrimination requirement, the bridge element must be matched looking back from the test piece, and the coupling to the detector must be independent of the phase of the wave reflected from the test piece. In the case of the side-outlet T, techniques that match it over a wide frequency range also tend to introduce asymmetry and hence impair discrimination. Accordingly, the design of practical impedance bridges often effects a compromise between the errors resulting from asymmetry and mismatch.

<sup>1</sup> The author is indebted to W. E. Waller for assistance in preparing the material that describes bridge elements and basic measuring techniques.

## BRIDGE ELEMENTS

**9-1. The Side-outlet T.**—The waveguide side-outlet T consists of an *E*-plane T and an *H*-plane T arranged as shown in Fig. 9-1. By virtue of the symmetrical construction, a wave coupled into arm 3 will divide between arms 1 and 2, but will not cross-couple into arm 4 if all arms are coupled to matched generators or matched loads. This property may be shown qualitatively by coupling coherent generators of arbitrary phase to arms 1 and 2. The waves that they excite in the waveguide are indicated

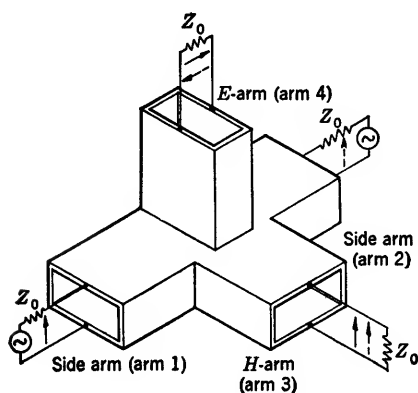


FIG. 9-1.—Side-outlet T.

by the solid and dashed vectors, respectively. The orientation of the vectors is unchanged in the process of coupling into the *H*-arm, and the resultant wave amplitude is  $\sqrt{2}$  times the original amplitude of the input waves (since even power split at a T-junction corresponds to a voltage split by a factor  $\sqrt{2}/2$ ). When the input waves are coupled from the side arms into the *E*-arm, the vectors swing around the corners to produce two waves of equal amplitude but opposite phase. Hence, there

is no resultant wave in the *E*-arm. Now, by reciprocity, if a wave of relative amplitude equal to  $\sqrt{2}$  is coupled into the *H*-arm, equal waves of unit amplitude and equal phase will be propagated in the side arms, but no wave will be propagated in the *E*-arm.

By reversing the phase of the generator coupled to arm 2, a similar argument will show that when power is coupled into the *E*-arm, it divides between the side arms with no cross-coupling to the *H*-arm. It should be noted that the waves propagated in the side arms are of opposite phase.

By coupling arbitrary generators to the *E*- and *H*-arms, the same method of argument can be employed to show that there is no cross-coupling between the two side arms. This is an important property since it means the impedance seen looking into either side arm is a function of the *E*- and *H*-arms and is independent of the load on the opposite side arm.

In a bridge element, power is coupled into arm 3 or 4 from the r-f sources, and out of arm 4 or 3 to the detector. A matched termination is placed on arm 2 and it becomes the reference arm. The test piece is coupled to arm 1 and it becomes the test arm. Since there is no cross-coupling between arms 3 and 4, and since no power is reflected from the

reference termination, the only power coupled to the detector is that reflected from the test piece. When the test piece is matched, the bridge is balanced and no power reaches the detector.

However, the simple side-outlet T fails in one respect. Even with matched loads on all arms, the impedance seen looking into the test arm is not a match. Consequently, when the test piece is not matched, interaction between the T and test piece makes the power delivered to the detector dependent on the phase of the test-piece reflection coefficient. This trouble can be alleviated by tuning the *E*- and *H*-arms so that a match is seen looking into the test arm. Unfortunately, this procedure does not necessarily result in matches looking into the *E*- and *H*-arms, a highly desirable property when the T is used with variable attenuators that are calibrated for use in a matched line.

Consequently, it is wise to tune the *E*- and *H*-arms for matches looking into them. It is a property of the T that such a matching procedure automatically results in matches seen looking into the side arms. If the resultant T is matched looking into all arms, it is referred to as a magic T.

### 9.2. Analysis of the Operation and Properties of Side-outlet T's.—

The side-outlet T may be regarded as an eight-terminal network in which the four terminal pairs represent the four waveguide arms. The amplitude of the wave out of any terminal pair may be related to the amplitudes of the waves coupled into all pairs by a simple linear combination of these input amplitudes, each being multiplied by an appropriate proportionality constant. For example,

$$E_{o1} = S_{11}E_{i1} + S_{12}E_{i2} + S_{13}E_{i3} + S_{14}E_{i4},$$

where  $E_{o1}$  is proportional to the amplitude of the wave out of the test arm,  $E_{i1}$  is proportional to the amplitude of the wave incident on the test arm (reflected from the test piece),  $S_{11}$  is the complex reflection coefficient seen looking into the test arm,  $E_{i2}$  is proportional to the amplitude of the wave incident on the reference arm (reflected from an imperfect reference termination),  $S_{12}$  is the complex amplitude transfer coefficient between the test and reference arms, and so on for the other coefficients. The  $E$ 's are proportional to wave amplitudes by a constant which is chosen so that  $|E|^2$  is equal to the incident or reflected power. Similar equations can be written for the other three arms, and the like-numbered  $S$ 's are reflection coefficients whereas the unlike-numbered  $S$ 's indicate coupling between two arms. Again it is assumed that all arms are coupled to matched generators or loads when the proportionality constants are defined. The constants from the output amplitude equations may be arranged to form the so-called *scattering matrix*. Before writing the matrix, however, it is useful to examine the effects of sym-



metry and reciprocity. From symmetry,

$$\begin{aligned} S_{11} &= S_{22}, \\ S_{13} &= -S_{23}, \end{aligned}$$

and

$$S_{14} = S_{24}.$$

From reciprocity, if all lines have the same characteristic impedance,

$$\begin{aligned} S_{12} &= S_{21}, \\ S_{13} &= S_{31}, \\ S_{14} &= S_{41}, \\ S_{23} &= S_{32}, \\ S_{24} &= S_{42}, \end{aligned}$$

and

$$S_{34} = S_{43}.$$

Accordingly, the scattering matrix is written

$$\begin{pmatrix} S_{11} & S_{12} & S_{13} & S_{14} \\ S_{12} & S_{11} & -S_{13} & S_{14} \\ S_{13} & -S_{13} & S_{33} & S_{34} \\ S_{14} & S_{14} & S_{34} & S_{44} \end{pmatrix}. \quad (1)$$

This is a unitary matrix of which two theorems are true:

Theorem I. The sum of the squares of the absolute magnitudes of any row or column is equal to unity.

Theorem II. For any pair of rows (or columns), the sum of the products of each  $S$  in one row (or column) with the conjugate of the corresponding  $S$  in the other row (or column) is equal to zero.

These two theorems may be applied to the scattering matrix to prove six statements that are important for impedance-bridge design.

Statement I: If a T is matched looking into arms 3 and 4, there is an equal power split between arms 3 and 4 for power reflected toward the T from a test piece on arm 1. That is, if

$$S_{33} = S_{34} = 0,$$

then

$$|S_{14}| = |S_{13}|.$$

This statement is proved by applying Theorem I to columns 3 and 4 of Matrix (1).

Statement II: Even if the  $E$ - and  $H$ -arms do not appear matched looking into the T, there is no cross-coupling between the  $E$ - and  $H$ -arms. That is, even if

$$S_{33} \neq 0$$

and

$$S_{44} \neq 0,$$

still

$$S_{34} = 0.$$

This statement is proved by applying Theorem II to columns 3 and 4 of Matrix (1).

Statement III: If the *E*- and *H*-arms appear matched looking into the T, there is no cross-coupling between the side arms, and the side arms appear matched looking into the T. That is, if

$$S_{33} = S_{44} = 0,$$

then

$$S_{12} = 0,$$

$$S_{11} = 0,$$

and

$$S_{22} = 0.$$

This statement is proved by applying Statement II to Matrix (1) to give

$$\begin{pmatrix} S_{11} & S_{12} & S_{13} & S_{14} \\ S_{12} & S_{22} & -S_{13} & S_{14} \\ S_{13} & -S_{13} & S_{33} & 0 \\ S_{14} & S_{14} & 0 & S_{44} \end{pmatrix}. \quad (2)$$

Application of Statement I and Theorem I to columns 1 and 4 will prove that  $S_{12} = 0$  and  $S_{11} = 0$ . Application of Theorem I to rows 1 and 2 will prove that  $|S_{11}| = |S_{22}|$  so that  $S_{22} = 0$ .

Statement IV: If a T is matched looking into the side arms, the VSWR's looking into the *E*- and *H*-arms are equal, but not necessarily unity. That is, if

$$S_{11} = S_{22} = 0,$$

then

$$|S_{33}| = |S_{44}|.$$

This statement is proved by applying Theorem I to columns 3 and 4 of Matrix (2).

Statement V: If a T is matched looking into the side arms, there is an even power split between arms 3 and 4 for power reflected toward the T from a test piece on arm 1. That is, if

$$S_{11} = S_{22} = 0,$$

then

$$|S_{13}| = |S_{14}|.$$

This statement is proved by applying Theorem I to columns 1 and 2 of Matrix (2).

Statement VI: If the T is matched looking into the side arms, but not matched looking into the *E*- and *H*-arms, there can be cross-coupling

between the side arms. That is, if

$$S_{11} = S_{22} = 0,$$

but

$$S_{33} \neq 0$$

and

$$S_{44} \neq 0,$$

then

$$S_{12} \neq 0.$$

This statement is proved by applying Theorem I and Statement V to Matrix (2) and  $|S_{12}| = |S_{33}|$ .

When a T is used as a bridge element, it is convenient to assume that a matched generator supplies a wave of unit amplitude incident on arm 3, that is,  $E_{i3} = 1$ , and that a matched detector is coupled to arm 4, that is,  $E_{i4} = 0$ . If the reference match has a reflection coefficient  $\Gamma_m$  and is coupled to arm 2, then

$$E_{i2} = \Gamma_m E_{o2}.$$

If the test piece has a reflection coefficient  $\Gamma_t$  and is coupled to arm 1, then

$$E_{i1} = \Gamma_t E_{o1}.$$

When these values are substituted in the equations defined by Matrix (2), the solution of the equations gives the wave amplitude delivered to the detector as

$$E_{o4} = \frac{S_{13}S_{14}(\Gamma_m - S_{11}\Gamma_m\Gamma_t + S_{12}\Gamma_m\Gamma_t - \Gamma_t)}{(1 - S_{12}\Gamma_m)(1 - S_{11}\Gamma_t) - S_{12}^2\Gamma_m\Gamma_t}. \quad (3)$$

If the reference match is perfect,  $\Gamma_m = 0$ , and Eq. (3) becomes

$$|E_{o4}| = \frac{|S_{13}| \cdot |S_{14}| \cdot |\Gamma_t|}{|1 - S_{11}\Gamma_t|}. \quad (4)$$

Application of Theorem I to columns 3 and 4 of Matrix (2) gives

$$|S_{13}| = \left( \frac{1 - |S_{33}|^2}{2} \right)^{1/2},$$

and

$$|S_{14}| = \left( \frac{1 - |S_{44}|^2}{2} \right)^{1/2}.$$

Substitution in Eq. (4) gives the maximum and minimum values for the power delivered to the detector, that is,

$$P = \frac{1}{4} (1 - |S_{33}|^2)(1 - |S_{44}|^2) \frac{|\Gamma_t|^2}{1 \pm |S_{11}\Gamma_t|^2}. \quad (5)$$

The terms involving  $S_{33}$  and  $S_{44}$  are not important since they merely represent inefficient power transfer if the T is not matched to the generator and detector. The power delivered to the detector is seen to be proportional to the fractional power reflection,  $|\Gamma_t|^2$ , from the test piece. If the T is not matched looking into the test arm, however, there will be interaction between the T and test piece so that the power to the detector is not independent of the phase of the reflection from the test piece. This "phase error" is represented by the term involving  $|S_{11}\Gamma_t|$  and is illustrated by Fig. 9-2.

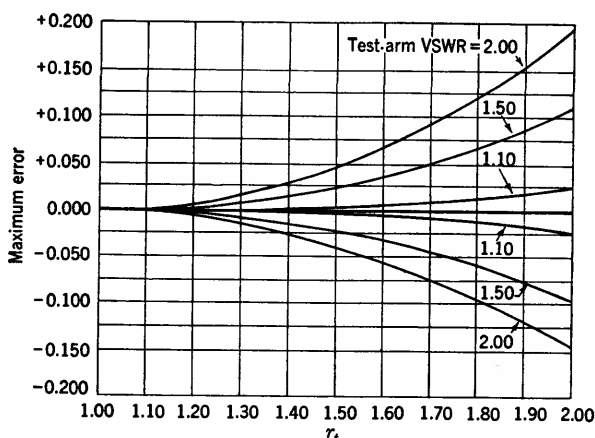


FIG. 9-2.—Effect of T-mismatch on the measurement of  $r_t$ .

If the reference match is imperfect ( $\Gamma_m \neq 0$ ), matters are not so simple. The effect of the imperfect reference match can be seen by considering a magic T for which  $S_{11}$ ,  $S_{22}$ ,  $S_{33}$ ,  $S_{44}$  and  $S_{12}$  are zero. In this case Eq. (3) becomes

$$E_{o4} = \frac{1}{2}(\Gamma_m - \Gamma_t),$$

and the maximum and minimum values of power to the detector are given by

$$P = \frac{1}{4}(|\Gamma_t| \pm |\Gamma_m|)^2.$$

If the reference-match VSWR is less than 1.02, and if the VSWR of the test piece does not exceed 2, then  $|\Gamma_t| \cdot |\Gamma_m| \ll 1$ . Accordingly, the apparent standing-wave ratio of the test piece lies between  $r_t/r_m$  and  $r_t/r_m$ .

If the T is not magic, this is still a good approximation for the apparent VSWR since the cross-coupling between the side arms and secondary reflections from the reference match are small if  $r_m$  is less than 1.02. It should be noted that, since the phase error results from the mismatch

seen looking into the side arms, in practice this error may be increased if the generator and detector are not matched to the line.

**9.3. Analysis of the Directional Coupler as a Bridge Element.**—A directional coupler may be represented as an eight-terminal network as shown in Fig. 9-3. The amplitude transfer coefficient between the two lines is defined as

$$K = \frac{E_{o3}}{E_{i1}} = \frac{E_{o4}}{E_{i2}},$$

with all lines coupled to matched generators or loads. The directive property of the coupler is defined as

$$d = \frac{E_{o4}}{E_{o3}}$$

when the generator is coupled to pair 1. The reflection coefficient of

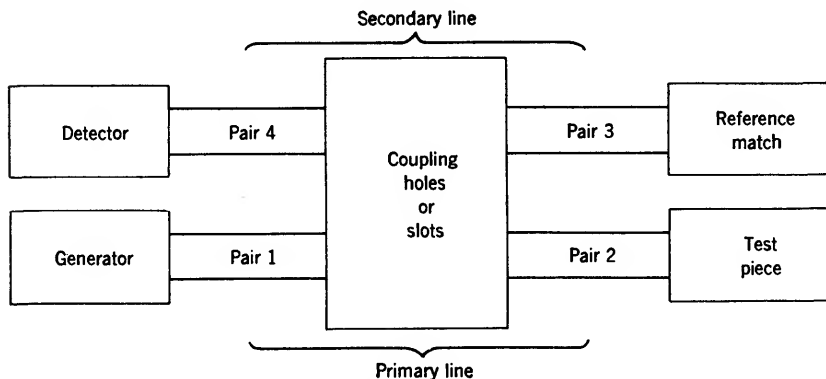


FIG. 9-3.—Directional coupler as a bridge element.

the slots is  $\Gamma_c$ ; that of the reference match,  $\Gamma_m$ ; and that of the test piece,  $\Gamma_t$ . If the generator and detector are matched to the line,

$$E_{o3} = K(E_{i1} + dE_{i2}).$$

Since

$$E_{i3} = \Gamma_m E_{o3},$$

substitution for  $E_{o3}$  gives

$$E_{i3} = \Gamma_m K(E_{i1} + dE_{i2}).$$

This wave is incident in the direction of the detector, but is reduced by coupling to the primary line and reflection by the slots. If small secondary reflections and couplings are ignored,

$$E_{o4} = \beta E_{i3} + K E_{i2} + K d E_{i1},$$

where

$$|\beta|^2 = 1 - |K|^2 - |\Gamma_c|^2$$

for conservation of energy. Also,

$$E_{o2} = \beta E_{i1} + \Gamma_c E_{i2}.$$

Since

$$E_{i2} = \Gamma_t E_{o2},$$

substitution for  $E_{o2}$  gives

$$E_{i2} = \frac{\Gamma_t \beta E_{i1}}{1 - \Gamma_c \Gamma_t}.$$

Substitution for  $E_{i2}$  gives

$$E_{o4} = \beta \Gamma_m K E_{i1} + \frac{\beta \Gamma_m K d \Gamma_t (1 - K) E_{i1}}{1 - \Gamma_c \Gamma_t} + \frac{K \Gamma_t \beta E_{i1}}{1 - \Gamma_c \Gamma_t} + K d E_{i1}.$$

Since the second term is smaller than all others by factors  $\Gamma_t d$ ,  $\Gamma_m d$  or  $\Gamma_m \Gamma_t$ , the equation for  $E_{o4}$  may be approximated by

$$E_{o4} = K E_{i1} \left( \Gamma_m \beta + \frac{\Gamma_t \beta}{1 - \Gamma_c \Gamma_t} + d \right).$$

Accordingly, the maximum and minimum values of the voltage to the detector are given by

$$|E_{o4}| = |K| \cdot |E_{i1}| \left( \frac{|\beta| \cdot |\Gamma_t|}{1 \pm \Gamma_c \Gamma_t} \mp |\beta| \cdot |\Gamma_m| \mp |d| \right).$$

Since  $|\beta|$  is very nearly unity, the phase error and imperfect-reference-match error enter in the same way as in the case of the T. Although  $\Gamma_c$  is much smaller than  $S_{11}$  for an unmatched (not magic) T, a T can usually be matched so that the phase error is as small as in the case of a coupler. The important factor is the term  $d$ , which makes the coupler undesirable as a bridge element.

A good directional coupler has a directivity that is 30 to 35 db over a narrow band. Over a wide band, however, the directivity often is as low as 15 or 20 db for part of the band. This corresponds to  $|d| > 0.1$ , and the maximum error in measuring  $r_t$  can be a factor of 1.22. Even if the directivity is 35 db, the error can be as large as a factor of 1.04. That the error is frequency-sensitive is an intrinsic property of the directional coupler. This error in the case of a coupler results from direct-coupling between the generator and the detector. In a T, an analogous error enters if the T is asymmetrical and there is cross-coupling between the  $E$ - and  $H$ -arms. Since the effect results only from asymmetry, however, it is not frequency sensitive, and T's can be constructed commercially so that the error from asymmetry does not exceed a factor of 1.01. This corresponds to a directivity of 52 db for a directional coupler.

**9-4. T-construction.**—Four fundamental processes have been used to manufacture waveguide T's. They are (1) fabrication from rectangular tubing, (2) electroforming, (3) die-casting, and (4) milling channels in a block of metal split into two halves.

Figure 9-4 shows a T fabricated from 1- by  $\frac{1}{2}$ -in. rectangular tubing. Since the characteristic impedance of the lines depends on the dimensions, 6-in. lengths of tubing are broached to tolerances of  $+0.002$  and  $-0.000$  in. The positive tolerance results from the outward bowing of the tubing after broaching. The three pieces are jigged and soldered, and extreme



FIG. 9-4.—T fabricated from broached tubing.

care is taken not to warp the tubing during soldering. In order to avoid introducing asymmetry no matching irises or posts are used. This type of construction is well suited for large waveguide,  $1\frac{1}{2}$  by 3 in., for example, but is not precise enough for  $\frac{1}{4}$ - by  $\frac{1}{2}$ -in. waveguide.

It was hoped that electroforming would facilitate the manufacture of small waveguide T's, but this was not the case. If a removable matrix is used, it must be made from three pieces whose assembly is subject to asymmetry. If the matrix is made as one piece and is dissolved after electroforming, a new matrix is necessary for each T and production costs are increased. Also, it is difficult to "throw" metal into the sharp corners of the T, and the resultant structure is mechanically weak.

Die-casting is a satisfactory solution for quantity production. The finished product is as good as the die, and slots may be cast into which matching irises may be driven. Irises are usually placed so close to the

T-junction that they introduce some asymmetry, which varies from T to T. Measurements indicate, however, that the error in measuring  $r_i$  can be as small as a factor of 1.005.

In small quantities, satisfactory T's can be made by milling channels in a block as shown in Fig. 9-5. It is difficult to insert matching irises, and r-f leakage and alignment are additional problems. Nevertheless, T's have been made whose  $r_i$ -error from asymmetry did not exceed a factor of 1.01.

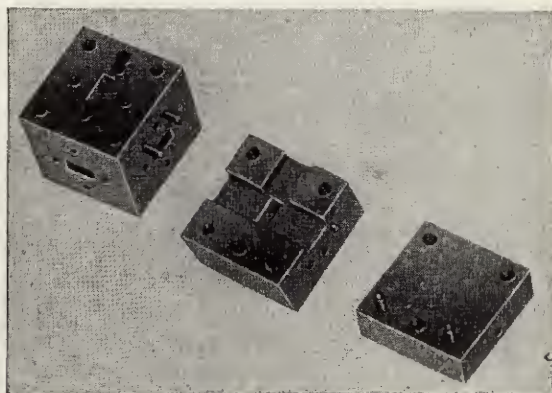


FIG. 9-5.—T made by milling channels in a block.

**9-5. Matching Techniques for T's.**—A T that appears matched looking into all arms is called a “magic” T. It is desirable to make a magic T in order to avoid three sources of error in measuring the voltage standing-wave ratio of a test piece. There is cross-coupling between the side arms of an unmatched T and interaction between the T and the test piece. Also, if a variable, calibrated attenuator is coupled to the  $E$ - or  $H$ -arms, interaction with the T will change the effective attenuation. Although it is desirable to match a T, the problem is not simple. To match a T over a wide band requires that the matching elements be placed as close as possible to the T-junction. If elements are placed in or near the junction, asymmetry is often introduced and this new source of error may overshadow those eliminated by matching the T.

Figure 9-6 indicates the success with which a post and iris may be used to match a T made from  $1\frac{1}{2}$ - by 3-in. waveguide. The dimensions and positions of the matching elements are shown in Fig. 9-7. The post is 0.375 in. in diameter and 1.750 in. high. The iris is made from 0.032-in. stock.

Figures 9-8 and 9-9 indicate the post-and-iris scheme as applied to a  $\frac{1}{2}$ - by 1-in. waveguide T. The post is 0.125 in. in diameter and 0.650 in. high. The iris is made from 0.032-in. stock.



T's made of  $\frac{1}{4}$ - by  $\frac{1}{2}$ -in. waveguide have been matched by using two irises. Figures 9-10 and 9-11 indicate the dimensions and success of matching. The irises are made from 0.020-in. stock.

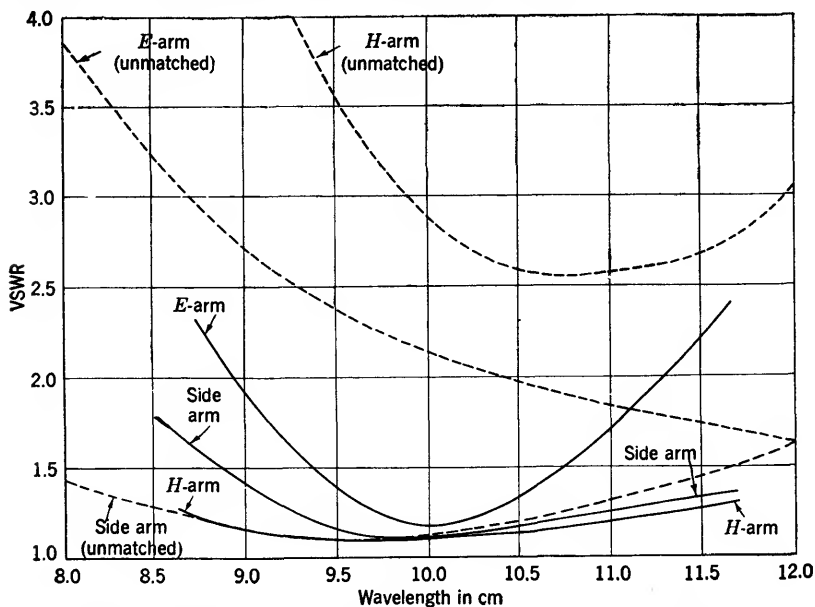


FIG. 9-6.—Effects of a post and iris for matching a  $1\frac{1}{2}$ - by 3-in. waveguide T.

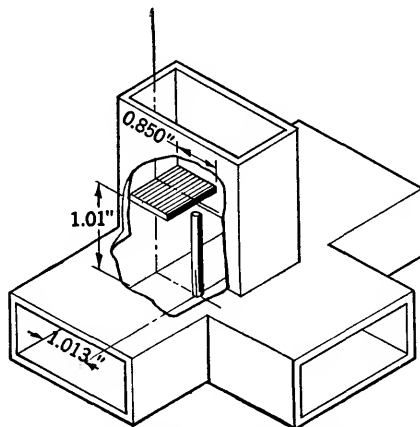


FIG. 9-7.—Positions of post and iris for matching a  $1\frac{1}{2}$ - by 3-in. waveguide T.

A British scheme for matching T's is shown in Fig. 9-12. Both side arms and the H-arm have the narrow dimension reduced by a factor of two through one-quarter-wavelength transformers. A circular block

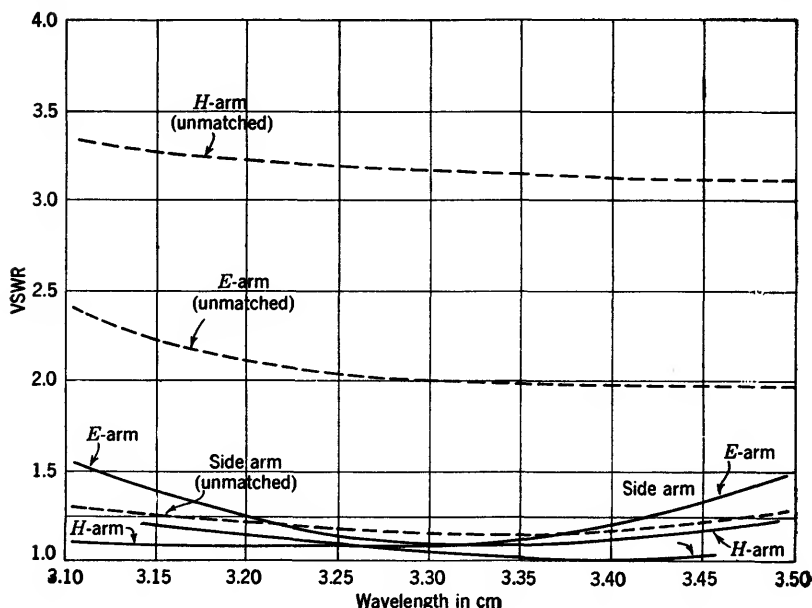


FIG. 9-8.—Effects of a post and iris for matching a  $1\frac{1}{2}$ -by 1-in. waveguide T.

and post are mounted so that the post projects into the *E*-arm. All arms have VSWR's not exceeding 1.07 from 3.1 to 3.3 cm when the terminals are  $\frac{1}{2}$ -by 1-in. waveguide. Although no additional data are available, the technique would seem to be equally applicable to other sizes of waveguide.

When a post is employed as a matching element, it can also be used to correct asymmetry. If the post is fastened to the waveguide by means of a pin which allows it to rotate eccentrically, this movement may be used to compensate asymmetry and to eliminate cross-coupling without appreciably affecting the impedance match.

#### 9-6. Ring Networks and Coaxial

**T's.**—Figure 9-13 illustrates both waveguide and coaxial ring networks that are analogous to T's and may be used as bridge elements. Their selective properties result from the spacings of the arms and hence are frequency sensitive. However, it is easy to match the devices over a wide range of frequencies.

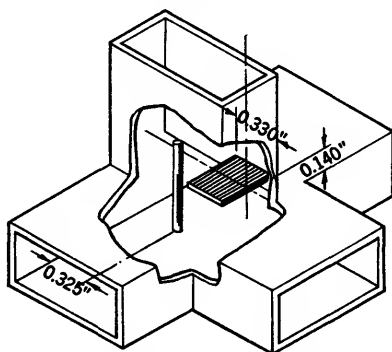


FIG. 9-9.—Positions of post and iris for matching a  $\frac{1}{2}$ -by 1-in. waveguide T.

For example, the waveguide ring network consists of *E*-plane T's, with the result that the impedance looking into a junction from a side arm is the sum of the impedances seen looking both ways into the ring

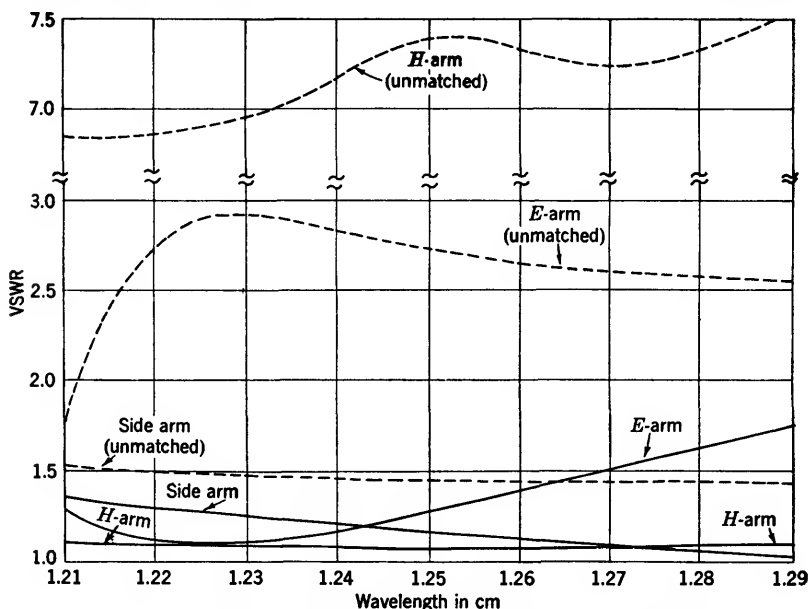


FIG. 9-10.—Effect of irises for matching a  $\frac{1}{4}$ - by  $\frac{1}{2}$ -in. waveguide T.

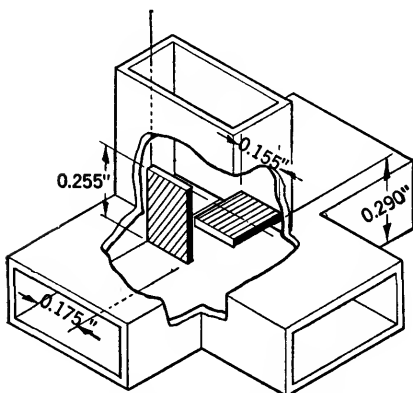


FIG. 9-11.—Positions of matching irises for  $\frac{1}{4}$ - by  $\frac{1}{2}$ -in. waveguide T.

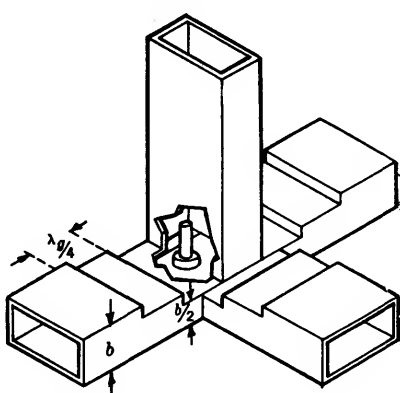


FIG. 9-12.—British method for matching waveguide T's.

from the junction. If power is coupled into arm 1, no power is coupled out of arm 3 since wave interference effectively short-circuits junction 3. Consequently, junctions 2 and 4 see an open circuit when looking toward

junction 3, and only the side arms determine the impedances of junctions 2 and 4. Looking into junction 1 from its side arm, there appear, in series, the characteristic impedances of arms 2 and 4 transformed through

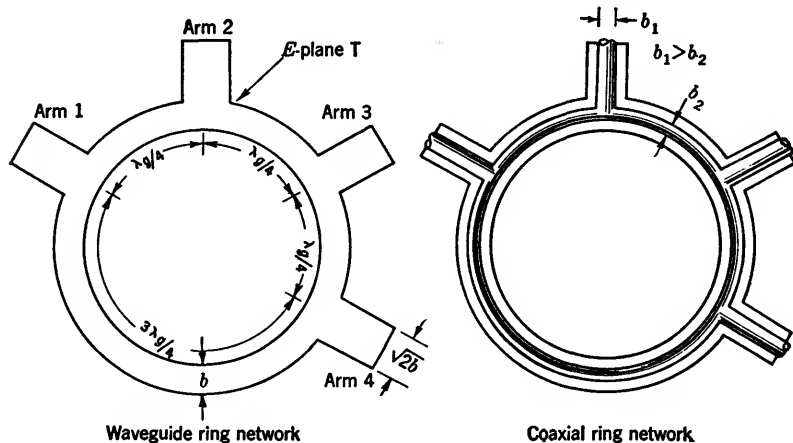


FIG. 9-13.—Waveguide and coaxial ring networks.

the ring to junction 1. If the characteristic impedance of the ring is smaller than that of the side arms by a factor  $\sqrt{2}$ , the transformations through the ring will result in matches looking into the side arms. Thus, matching is accomplished simply by choosing the proper characteristic impedance for the ring. In the case of the coaxial ring network, an analogous argument shows that the diameter of the inner conductor should be smaller for the ring than for the side arm.

Waveguide ring networks have been made so that the side arms were of  $\frac{1}{2}$ -by-1-in. waveguide<sup>1</sup> and the impedance ratio was exactly  $\sqrt{2}$ . Fortunately, over a wide frequency range the VSWR's looking into the side arms did not exceed 1.20.

While the ring network is one solution to the coaxial-T problem, Fig. 9-14 illustrates another possibility. Unfortunately, no data are available to describe its properties.

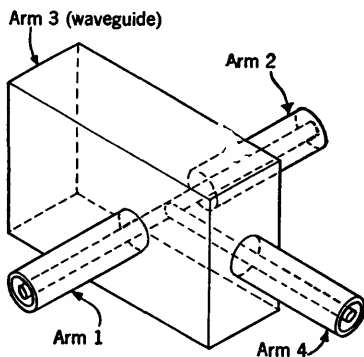


FIG. 9-14.—Coaxial T.

<sup>1</sup> This ring network resulted from duplexer developments which are described in Vol. 14, Chap. 8.

## BASIC MEASURING TECHNIQUES

Ordinary bench test equipment, such as that indicated by Fig. 9-15, is used for single-frequency operations. The components are essentially those used for slotted-section measurements. If a greater power range is desired, the r-f source may be a c-w oscillator and the detector may be a receiver or spectrum analyzer. The calibrated r-f attenuator is important for many basic measurements since the output power from a T

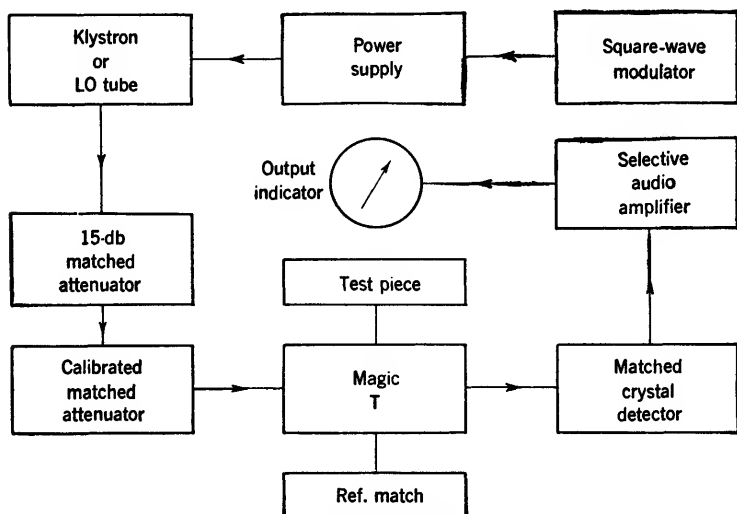


FIG. 9-15.—Typical equipment for basic measurements.

is related to the test-piece standing-wave ratio in a very definite manner. If a bolometer or crystal detector of known law is employed, the r-f attenuator may be replaced by an i-f or a-f attenuator although the range of attenuation measurement may not be large enough to permit the measurement of very small standing-wave ratios.

**9-7. The Single-frequency Bridge.**—At a single frequency it is possible to match a T so that it is truly “magic,” that is, matched looking into all arms. If unit power is incident on the bridge from a matched generator, the power to a matched detector is, from Eq. (5) Sec. 9-2,

$$P = \frac{|\Gamma_t|^2}{4}, \quad (6)$$

where  $\Gamma_t$  is the reflection coefficient of the test piece. This expression requires a symmetrical T and perfect reference match. Although neither requirement can be realized in practice, the cross-coupling that results from asymmetry can be cancelled by tuning the reference match so that

it introduces a compensating reflection. If asymmetry does not affect power division, the attenuation between the input and output powers is

$$n = 20 \log_{10} |\Gamma_t| - 6.0 \quad \text{db.} \quad (7)$$

However, asymmetry does affect the power splits and so alters the 6-db term in Eq. (7). If the T is well matched and only slightly asymmetrical, the coupling between the *E*-arm and the test arm will be proportional

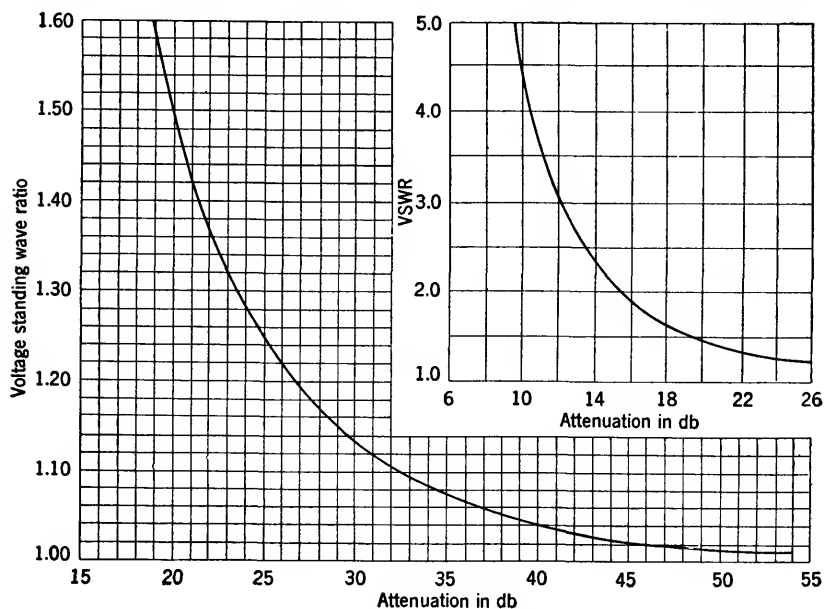


FIG. 9-16.— $r_t$  vs. equivalent line attenuation.

to  $(\frac{1}{2} + \delta)$ , and that between the *H*-arm and the test arm will be proportional to  $(\frac{1}{2} + \epsilon)$ . If the test arm appears matched looking into the T and if the cross-coupling between the side arms is negligible, conservation of energy requires a power division between the *E*- and *H*-arms so that

$$1 = (\frac{1}{2} + \delta) + (\frac{1}{2} + \epsilon)$$

when unit power is coupled into the test arm. Accordingly,  $\epsilon = -\delta$ , and the 6-db term will be in error by an amount proportioned to  $\delta^2$ , which is negligible for small amounts of asymmetry.

Since the voltage standing-wave ratio of the test piece is

$$r_t = \frac{1 + |\Gamma_t|}{1 - |\Gamma_t|},$$

a graph of  $r_t$  vs. equivalent line attenuation may be plotted as in Fig. 9-16. The measurement of  $r_t$  simply amounts to measuring attenuation through the T and reading the corresponding  $r_t$  from the graph.

The attenuation measurement may be made in several ways depending on the range of the voltage standing-wave ratio to be measured. A matched bolometer detector followed by a selective amplifier and audio attenuator or logarithmic voltmeter will provide a range of about 45 db with an accuracy of  $\pm 0.2$  db. This allows the measurement of standing-wave ratios exceeding 1.02 and means, for example, that an  $r_t$  of 1.500 will appear to be between 1.485 and 1.515. If smaller standing-wave ratios are to be measured, an r-f attenuator can be calibrated in two steps by the bolometer method. With this higher-range attenuator, a more sensitive detector such as a heterodyne receiver or spectrum analyzer should be coupled to the bridge.

The bridge-attenuation measurement necessitates disassembly of the components in the process, and this is usually an undesirable operation. The measurement can be broken effectively into two steps by using a reference mismatch. An iris is placed ahead of a well-matched termination in broached waveguide, and the standing-wave ratio of the combination is measured by attenuation through the T or by means of a slotted section. If the reference-mismatch VSWR is 1.30, the attenuation is 23.7 db; if the VSWR is 1.50, the attenuation is 20.0 db. Consequently, the attenuation measurement is not difficult.

The reference mismatch and the test piece are alternately coupled to the bridge, and the relative output powers from the bridge are compared by means of an r-f or a-f attenuator. The amplifier or spectrum analyzer is used merely as a reference indicator, and the  $r_t$  is determined from Fig. 9-16. If the reference-mismatch VSWR is 1.20, an  $r_t$  range from 1.06 to 1.90 may be covered by measuring relative attenuation of  $\pm 10$  db.

For this small range, a crystal may be assumed to be a square-law detector without excessive error for production testing of line components. An  $r_t$  of 1.06 may appear to be between 1.05 and 1.07, and an  $r_t$  of 1.70 may appear to be between 1.60 and 1.80. A good audio attenuator may be installed in the selective amplifier that follows the crystal detector, and its dial may be calibrated directly in  $r_t$ .

These techniques are accurate only when the T is well matched and asymmetric cross-coupling is eliminated. Although this can be accomplished at a single frequency, over a wide frequency range errors result from the T-mismatch, an imperfect reference match, the asymmetric cross-coupling, and the frequency sensitivity of the r-f attenuator; and these errors can combine to produce a large over-all error. Consequently, the wideband bridge is recommended for production testing and impedance-matching, and the single-frequency bridge is recommended for precision laboratory measurements, especially those involving small reflections.

**9-8. T-asymmetry.**—Cross-coupling between the *E*- and *H*-arms is caused by T-asymmetry, and the effect may be measured or eliminated

by using a termination that is tunable about the characteristic impedance of the line. For example, this termination is coupled to arm 2 and a well-matched load ( $VSWR < 1.01$ ) is coupled to arm 1; power is coupled into the  $H$ -arm, and the termination is tuned until there is no resultant wave out of the  $E$ -arm. This effect is shown in Fig. 9-17 where the wave-amplitude subscripts  $T$ ,  $A$ , and  $M$  refer to signals produced by the termination, asymmetry, and the imperfect reference match, respectively.

Now if the side arms have equal electrical lengths, interchanging the tunable termination and reference match will simply reverse the phases of  $e_T$  and  $e_M$ . In this case, the resultant wave amplitude in the  $E$ -arm

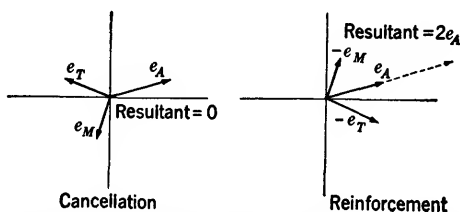


FIG. 9-17.—Cancellation and reinforcement of asymmetric cross-coupling by reflections from the side-arm terminations.

is twice that from asymmetry as shown in Fig. 9-17. This output wave is equivalent to that produced by some test piece that is coupled to a perfect bridge. The equivalent  $r_i$  can be determined from attenuation through the  $T$  or by using a reference mismatch in conjunction with a calibrated attenuator. However, since the output voltage is twice that resulting from asymmetry, 6 db must be added to the measured amount of attenuation in order to obtain the  $r_i$  equivalent to the signal caused by asymmetry.

Although asymmetry affects the power division within the  $T$ , no appreciable error is introduced in the measurement of the equivalent  $r_i$ . The side arms must have equal electrical lengths, however, or appreciable error may be introduced. The electrical length of a side arm is dependent on not only the physical length, but the average width of the waveguide as well. If the  $T$  is made of  $\frac{1}{2}$ - by 1-in. waveguide, and if the side arms differ in length by 0.005 in., the error in measuring an asymmetric  $VSWR$  of 1.01 will not exceed  $\pm 0.0001$ . If the asymmetric  $VSWR$  is 1.02, the error will not exceed  $\pm 0.0002$ . If the  $T$  is made of  $\frac{1}{4}$ - by  $\frac{1}{2}$ -in. waveguide, and if the side arms differ in length by 0.002 in., the error in measuring an asymmetric  $VSWR$  of 1.02 will not exceed  $\pm 0.0004$  and will be less if the equivalent  $r_i$  is smaller. If one side arm of a  $\frac{1}{2}$ - by 1-in. waveguide  $T$  has an average deviation of 0.001 in. from the correct width, the error in measuring an asymmetric  $VSWR$  of 1.02 will not exceed  $\pm 0.0004$  and will be less if the equivalent  $r_i$  is smaller. If one side arm of a  $\frac{1}{2}$ - by 1-in.



waveguide T has an average deviation of 0.001 in. from the correct width, the error in measuring an asymmetric VSWR of 1.02 would probably be too small to detect. If one side arm of a  $\frac{1}{4}$ - by  $\frac{1}{2}$ -in. waveguide T has an average deviation of 0.007 in. from the correct width, the error will not exceed  $\pm 0.0004$ . Thus, if close mechanical tolerances are observed, no appreciable error is caused by the unequal lengths of the side arms. The effect of unequal arms may be detected by beginning the asymmetry measurement with the tunable termination first on one side arm, and then on the other.

The major error in the measurement of asymmetry is caused by incorrect waveguide dimensions at the output-terminal planes of the side arms. Since asymmetry is defined as a function of the output wave when perfect terminations in correct-size waveguide are coupled to the side arms, the definition includes reflections from discontinuities at the output terminals of the side arms. Since these reflections do not result from asymmetry within the junction, however, their effect must be small for the measurement to be indicative of the junction asymmetry. If the T is made of  $\frac{1}{2}$ - by 1-in. waveguide, and if the narrow dimensions of the side-arm output terminals differ by 0.0004 in., the error in measuring the asymmetric VSWR will be about  $\pm 0.001$ . For  $\frac{1}{4}$ - by  $\frac{1}{2}$ -in. waveguide T's, the error will be  $\pm 0.0023$ . If the T is made of  $\frac{1}{2}$ - by 1-in. waveguide, and if the wide dimensions of the side arms differ by 0.0004 in. at the output terminals, the error will be  $\pm 0.001$ . If the wide dimensions differ by 0.0003 in. for a  $\frac{1}{2}$ - by  $\frac{1}{4}$ -in. waveguide T, the error is again  $\pm 0.001$ . If the output terminals differ from the correct dimensions by equal amounts, no error will be incurred in the measurement of asymmetry, but error may be introduced when the T is used to measure this standing-wave ratio of a test piece. In summary, if the tolerances given in the preceding paragraphs are observed, an asymmetric VSWR of 1.01 can be measured to  $\pm 0.002$  for  $\frac{1}{2}$ - by 1-in. waveguide T's, and to  $\pm 0.004$  for  $\frac{1}{4}$ - by  $\frac{1}{2}$ -in. T's. If similar tolerances are observed for  $1\frac{1}{2}$ - by 3-in. waveguide T's, the error will not be appreciable.

**9-9. Bridge Balance and the Sliding Match.**—Because of the cross-coupling that results from an asymmetrical T-junction, a bridge will appear unbalanced even if all arms are coupled to perfectly matched generators or loads. The bridge may be balanced by tuning the reference match, which is slightly imperfect anyhow, so that it produces a reflection that cancels the cross-coupling. Balancing should result in no output signal from the bridge when a perfect match is coupled to the test arm. Since a completely reflectionless termination is not realizable in practice, a "sliding match" is used instead.

The sliding match consists of a well-matched termination which may be moved lengthwise in a waveguide casing. The termination may be

a tapered piece of polyiron which is machined for a sliding fit. If the casing is made from broached or precision-drawn waveguide, and if the termination is a close fit, only the phase of the reflection varies when the termination is moved. A good termination should produce a VSWR less than 1.02, and the casing should allow a motion of at least one-half the wavelength in the line. As the termination is moved over this range, its impedance will describe a circle whose center is the characteristic impedance of the line.

If the bridge is unbalanced when the termination is moved, the reflection from the sliding match will add to, or subtract from, the unbalance signal, and the output power from the bridge will vary. If the bridge is balanced, the output signal will not vary since it results only from the sliding-match reflection, which is variable in phase but constant in amplitude.

The sliding match can be used not only to facilitate bridge balance but to measure unbalance as well. The maximum and minimum output powers are measured as the sliding match is moved, and these values are converted to equivalent  $r_i$ 's by means of Fig. 9-16. If the signal caused by bridge unbalance is less than that resulting from the sliding-match reflection, the equivalent  $r_i$  for bridge unbalance is

$$\sqrt{r_{\max}/r_{\min}},$$

and the sliding-match standing-wave ratio is

$$\sqrt{r_{\max} \cdot r_{\min}}.$$

If the bridge unbalance produces the larger output signal, the relations are reversed.

**9-10. Magic-T Alignment.**—Although the matching techniques described in Sec. 9-5 provide reasonably good operation over a wide range of frequencies, a single-frequency bridge can be matched almost perfectly by means of tuning screws. Since frequency sensitivity is unimportant, the screws may be placed sufficiently far from the T-junction so that no asymmetry is introduced. The screws should be placed in the *E*- and *H*-arms, and matching these arms automatically results in matches looking into the side arms. The easiest method of alignment is to couple the *E*- and *H*-arms alternately to another impedance bridge and to adjust them independently for minimum power reflection. Although the side arms should be coupled to well-matched terminations during this procedure, the unused *E*- or *H*-arm need not be terminated. If the radiation from the unused arm interferes with the detector by means of coupling through the intervening space, this arm may be short-circuited with a metal plate without affecting the matching procedure for the other arm.

It should be remembered that even though the T is matched according to this procedure, it will not appear matched looking into the side arms unless the *E*- and *H*-arms are coupled to a matched generator and a matched detector. For single-frequency bridges, the detectors can be matched by means of tuning screws. Although a matched generator could be achieved also by reactive tuning elements, these elements might impair the operation of those low-voltage oscillators (types 2K25 and 2K50), for example) that are purposely mismatched to the line for stability as well as power considerations. Even when tuners are used to obtain the optimum operation of high-voltage tubes, such as the 2K39, the oscillator is not necessarily matched to the line. Therefore, a matched generator is best achieved by inserting resistive attenuation between the oscillators and the T.

**9-11. The Measurement of Large Reflections.**—Both the amplitude and phase of large reflection coefficients can be measured if the reference match is replaced by a short circuit whose position is adjustable relative to the T-junction. The test piece is coupled to one side-arm of a magic T, and the position of the short circuit on the opposite arm is varied until the output wave is minimized. Accordingly, the attenuation through the T is

$$20 \log_{10} (|\Gamma_s| - |\Gamma_t|) - 6.0 \quad \text{db,}$$

where  $\Gamma_s$  and  $\Gamma_t$  are the reflection coefficients of the short circuit and the test piece. If the short circuit provides total reflection ( $\Gamma_s = 1$ ), then the attenuation is a measure of  $1 - |\Gamma_t|$ . If the side arms of the T have equal or known electrical lengths, the position of the short circuit is indicative of the phase of  $\Gamma_t$ .

Since this technique involves large reflections, the T, the generator, and the detector must all be very well matched. Also, asymmetric cross-coupling must be compensated since the output signal will be small for large values of  $\Gamma_t$ . Compensation is achieved in several steps. First, the bridge is matched and balanced as described in the preceding sections; the matching screws are placed in the *E*- and *H*-arms, and the balancing screws, in the reference arm. Second, the sliding match on the test arm is replaced by a load which is tuned until the output signal is zero, thus indicating a perfect match. Third, the termination on the reference arm is replaced by the sliding match, and the resultant output signal is caused only by asymmetry, reference-arm screw reflections, and the sliding-match reflection. If the screws are adjusted until the amplitude of the output signal is unaffected by moving the sliding match, this signal results only from the sliding-match reflection, and asymmetry is compensated. The important fact is that the T is still compensated when the reference arm is short-circuited.

If high accuracy is desired in the measurement of  $\Gamma_r$ , the loss in the sliding short circuit must be considered. A good short circuit employs chokes, rather than contact fingers, and will produce a standing-wave ratio of about 50 db. Consequently,  $|\Gamma_r|$  will be about 0.994. This can be measured with a T whose reference arm is short-circuited by a plate soldered to the waveguide.

#### DESIGN CONSIDERATIONS FOR MULTIFREQUENCY IMPEDANCE BRIDGES

The first design consideration for multifrequency impedance bridges is usually the selection of the process that provides simultaneous indications at several frequencies. The detector-indicator circuits, are therefore

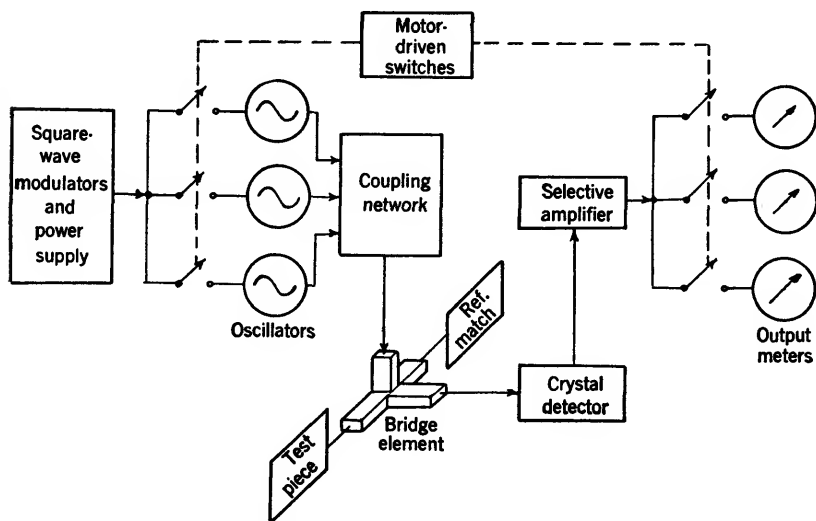


FIG. 9-18.—Simple multifrequency bridge that utilizes mechanical switching.

often predetermined, and the selection of the r-f oscillators, the coupling networks, and the other line components usually effects a compromise between accuracy and range of measurement. Although complexity, cost, and application are important, they are commonly the results of, rather than the prerequisites for, the preliminary design considerations.

**9-12. Methods Which Provide Simultaneous Indications at Several Frequencies.**—The simplest method for providing multifrequency operation is a slight elaboration of the single-frequency bridge. Figure 9-18 illustrates the method in which three oscillators are coupled to the bridge by directional couplers or magic T's. By means of a motor-driven mechanical switch, the oscillators are turned on and off in sequence, and the amplifier is coupled, in turn, to each of the three output meters.

This effect may be achieved electronically as shown in Fig. 9-19.

Three oscillators are square-wave modulated at audio rates which are not multiples of one another, and the amplifier uses three selective output channels to discriminate between the different modulation frequencies. Because of the good sensitivity afforded by a crystal detector and selective amplifier, low-voltage oscillators will deliver sufficient r-f power, and a common power supply can be used for all circuit components. If the crystal is operated as a square-law detector, an audio attenuator may be used as a calibrating device, and the number of r-f line compo-

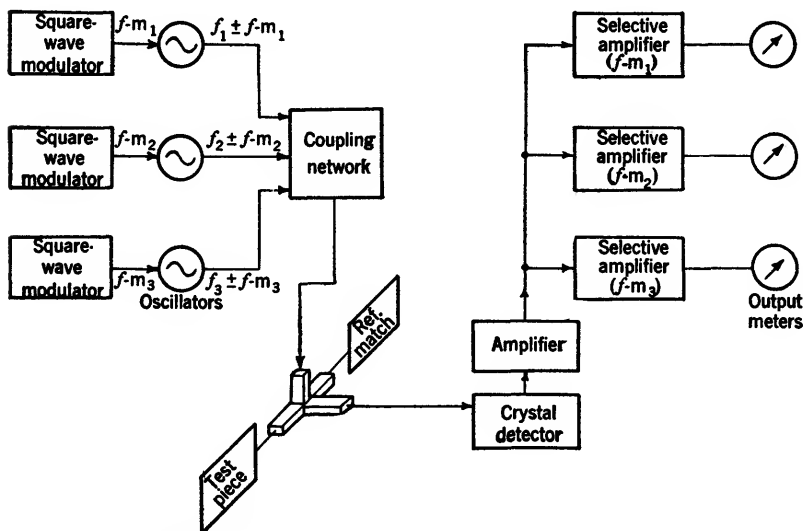


FIG. 9-19.—Multifrequency bridge that employs modulation-frequency discrimination.

nents may be held to a minimum. Both the microwave and the circuit techniques are extremely simple, and consequently, this type of bridge is recommended for applications where the investment in test equipment and its maintenance must be minimized.

A better visual presentation is obtained with a cathode-ray tube since the indications can be spaced more closely than in the case of meters. Figure 9-20 illustrates a pulse-modulated impedance bridge in which the oscillators are pulsed sequentially to provide a time separation of the corresponding pips that appear on the cathode-ray tube. Unfortunately, high-voltage oscillators are necessary to compensate for the inherent low sensitivity of the wide-band pulse amplifier, and the circuits associated with these oscillators and the cathode-ray tube make the cost and the complexity relatively high. On the other hand, these disadvantages are somewhat offset by the desirable presentation and the ease of operation; and the pulse-modulated bridge is well suited for commercial applications.

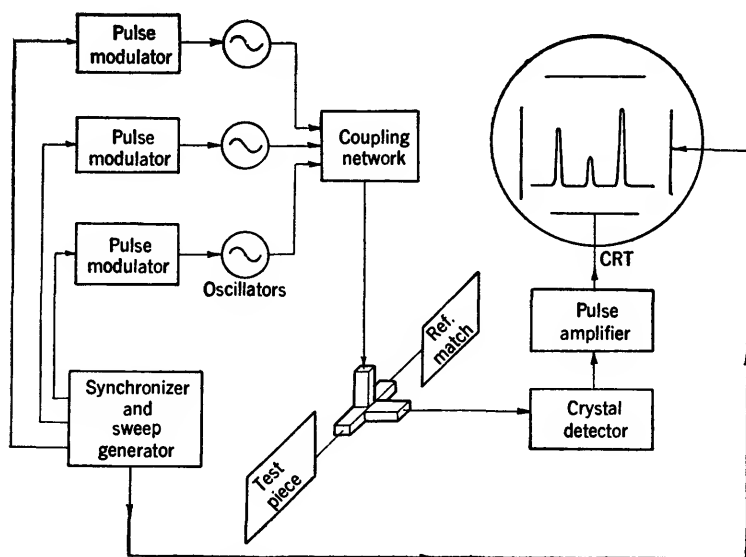


FIG. 9-20.—Multifrequency bridge that employs pulse modulation.

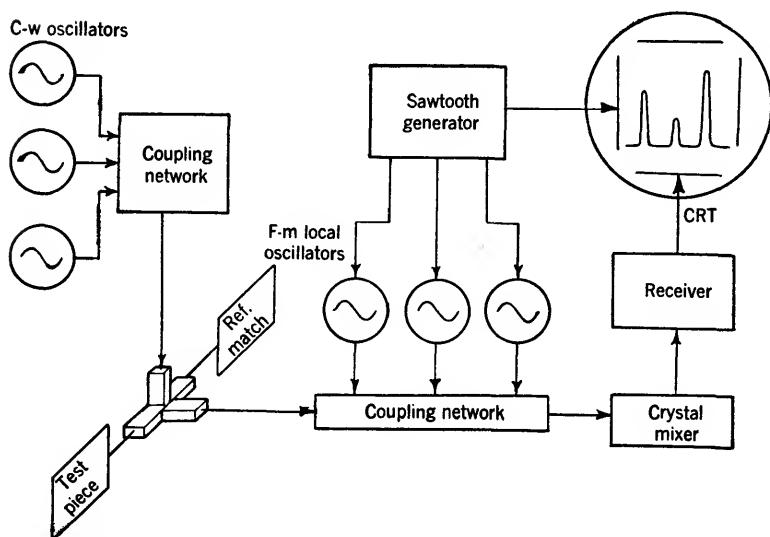


FIG. 9-21.—Multifrequency bridge that utilizes a panoramic receiver.

A similar CRT presentation is obtained with impedance bridges that employ panoramic receivers. Figure 9-21 illustrates this method in which three frequency-modulated local oscillators are coupled to a common mixer. It is also possible to use f-m sources instead of f-m local oscillators, thus minimizing spurious responses. The principle of operation is the same in both cases. Corresponding pairs of c-w and f-m oscillators are tuned so that the frequency difference between each pair is equal to the intermediate frequency at some point in the modulation cycle. Since these difference frequencies vary with time, i-f pulses are generated, and hence video output pulses result. Although the high sensitivity of the heterodyne receiver provides a large range of measurement, the use of local oscillators and their coupling networks results in a considerable increase in cost. Also, the current capacity of the power supply must be increased because of the additional oscillators. If a wide-band i-f amplifier is used for stability considerations, the current drain from the power supply will be still greater.

From an operational viewpoint, the panoramic impedance bridge is also the most complex. Commercial models provide hinged covers for the oscillator-voltage controls, and these covers are closed following alignment by an engineer. However, sometimes the oscillators drift in frequency, and their harmonics cross-modulate in the mixer and block the receiver, thus confusing the test-line operator. In general, panoramic impedance bridges are best suited for use by persons of engineering caliber who willingly tolerate the greater complexity for the increased accuracy and the greater sensitivity.

**9-13. Line Components.**—Coupling networks should introduce minimum insertion loss in order to allow the measurement of very small test-piece reflections, but should provide maximum isolation between oscillators. Both magic T's and directional couplers can be used. Directional couplers usually introduce an attenuation of at least 10 db, whereas T's introduce only 3 db. However, T's must be provided with matching elements and do not always lend themselves to mechanical arrangements in which oscillator tuning shafts must be brought out through a front panel. Directional couplers can provide 40 db of isolation between oscillators—a value that is also easily realized by T's, even those that have considerable asymmetry.

Although any number of directional couplers may be inserted in a common line, each magic T is used to couple two sources to a common line. If four oscillators are used, they may be coupled in pairs to two T's, and these T's may be coupled to a third T in order to obtain all signals in a common line. In this case, the attenuation between each oscillator and the main line is 6 db, only 4 db less than that for directional-coupler networks. If several directional couplers are inserted

in a common line, however, their individual reflections may combine so that, at some frequencies, the whole assembly, when viewed from the bridge, may appear as a very poorly matched generator. In practice, it is often possible to space the couplers so that their reflections tend to cancel rather than to reinforce. In general, matched T's provide less insertion loss than directional couplers, but a less desirable mechanical arrangement; directional couplers provide a desirable mechanical arrangement, but introduce more loss than matched T's and require judicious spacing.

Included among the line components are several attenuators, both fixed and variable. Since a crystal detector may produce a VSWR as large as 4.0 over part of a wide frequency range, it is usually padded by about 10 db of resistive attenuation in order that the VSWR, as seen from the bridge, shall not exceed 1.1. If the output powers from the oscillators are not controlled electronically, a variable attenuator can be inserted between each oscillator and the coupling network. At minimum attenuation, these attenuators should have negligible insertion loss in order to allow the measurement of small test-piece reflections. Under these conditions there is little attenuation between the oscillators and the T, and the line appears badly mismatched looking back from the T. Although the phase error tends to increase because of this mismatch, it also tends to be reduced because under these conditions a small reflection is being measured. When a larger reflection is being measured the phase error tends to increase, but sometimes the power-level attenuators can be adjusted to provide more isolation between the oscillators and the T. This increased isolation reduces the mismatch as seen looking back from the T, and consequently tends to reduce the phase error.

For example, consider a T that is matched so that the VSWR looking into all arms does not exceed 1.10 when all arms are coupled to matched generators or matched loads. The detector is isolated from the T by 10 db of attenuation so that the VSWR, as seen from the T, does not exceed 1.10. If the power-level attenuators are adjusted for the measurement of small reflections, the attenuation between each oscillator and the T may not exceed 10 db. If the coupling network alone produces a VSWR of 1.10, the VSWR, looking back from the T, can be as large as 2.20, but probably will not exceed 1.80. With *E*- and *H*-arms coupled to impedances that produce VSWR's of 1.10 and 1.80, the VSWR that is seen looking into the test arm can be increased from 1.10 to 1.65. Consequently, if an  $r_t$  of 1.02 is measured, the phase error will cause the test-piece reflection coefficient to be measured in error by a factor of 1.003, and the error in the measurement of  $r_t$  is unimportant.

Now suppose that when the bridge is used to measure an  $r_t$  of 1.6, the power-level attenuators can be adjusted to provide at least 20 db



of attenuation between each oscillator and the T. The VSWR seen looking back from the T will probably not exceed 1.15, and the VSWR looking into the test arm of the T will not exceed 1.30. Consequently, the phase error will cause the apparent  $r_t$  to fall between 1.57 and 1.62. Unfortunately, other design factors, such as the method of calibration and the over-all sensitivity, often restrict the isolating attenuation to values much less than 20 db.

If an r-f attenuator is incorporated in the bridge as a calibration device, it should be placed between the T and the detector. In this position it will be coupled to more nearly matched lines than if it were placed on the generator side of the T. Accordingly, its calibration will be much more reliable. However, if  $r_t$  is 1.60, the VSWR looking back into the T can be as large as 1.50. In bridge designs that can tolerate more line attenuation, a 5-db fixed attenuator is placed between the T and the variable attenuator so that the VSWR of 1.50 is reduced to 1.14.

All line components must furnish good protection against r-f leakage. Even if the coherent leakage is 10 db below the signal level at the detector, the signal can be changed about  $\pm 3$ db by the leakage. If this condition exists when  $r_t$  is 1.02, the measured value will be between 1.01 and 1.03. Since the total line attenuation is not less than 65 db between the oscillators and the detector for an  $r_t$  of 1.02, the leakage protection for this example is at least 75 db. If the calibration device is an audio attenuator or logarithmic voltmeter, the signal level at the detector increases 25 db when  $r_t$  is 1.60. Although the effect of the leakage is less prominent, the measurement of large test-piece reflections is more sensitive to attenuation error. Hence, the apparent  $r_t$  will be between 1.59 and 1.61, and 75 db of leakage protection may be adequate for some applications.

If an r-f attenuator is used as a calibration device, however, the detector is used merely to indicate a reference level, and hence operates at the same signal level regardless of the test-piece reflection. Consequently, the effect of leakage is always the same, and the leakage protection must be increased to about 100 db if an  $r_t$  of 1.60 is to fall between 1.59 and 1.61.

Optimum leakage protection is achieved by carefully shielding the oscillators and by providing good electrical contacts at all junctions. All electrical leads to the oscillators should enter the shield cans through coaxial fittings that have polyiron bushings between the conductors. It is usually advisable to wrap the polyiron bushings with two or three layers of varnished cambric in order to obtain greater protection against voltage breakdown. All oscillator tuning shafts and attenuator drive pins should pass through bearings that have polyiron bushings. Waveguide choke joints may be sealed by inserting a metal-textile (woven

metal strands) gasket in the choke groove. Larger gaskets can be used to seal the oscillator shield cans. Flat gaskets of metal shim-stock should be avoided since they are easily burred, scarred, and spoiled.

#### IMPEDANCE BRIDGES UTILIZING MODULATION-FREQUENCY DISCRIMINATION

The principle of operation for bridges that utilize modulation-frequency discrimination is described in Sec. 9-12 with reference to Fig. 9-19. The circuit components of this bridge can be essentially those used in bench test equipment for the measurement of standing waves by means of slotted sections. Many of the design features apply equally well to bridges that employ a mechanical switch to operate, in sequence, the oscillators and their corresponding output meters. In this bridge, however, a single amplifier channel is used since all oscillators can use the same modulation.

**9-14. Microwave Sources.**—Reflex oscillators that deliver about 25 mw of microwave power are commonly used because they are economical from the standpoint of power-supply and modulator requirements, and from the standpoint of replacement. In order to use a common power supply for all circuit components, it is desirable to operate the oscillator cathodes at ground potential and their cavities at +300 volts. The 2K25 and 2K50 tubes can be used for the 9000- and 24,500-Mc/sec regions, respectively, since the cavity (tube shell) is easily insulated from the line components. The selection of a tube for the 3000-Mc/sec region is more difficult since the 2K28 (707B) tube requires an external cavity that is usually large and difficult to insulate, especially when equipped with a micrometer-driven tuning mechanism. Although the 726 tube has its cavity as an integral part, the coaxial output fitting requires that insulating devices be provided for the coaxial line. The alternate solution is the common one: A negative-voltage power supply is used, and the oscillator cavity is operated at ground potential.

Reflex tubes are usually modulated by applying a square-wave signal to the oscillator reflector. In order to avoid frequency modulation, the square wave should have sufficient amplitude so that the oscillator drops out of oscillation for alternate half cycles. However, the amplitude also must be limited so that the tube will not be driven into the next lower mode of oscillation. When adjusting the amplitude of the modulating signal, the output signal from the detector of the bridge should be coupled to an oscilloscope in order to detect overmodulation. A diode may be connected between the reflector and the cathode of the tube in such a way that the reflector cannot be driven positive with respect to the cathode. Simple, but adequate, modulators consist of unsynchronized multivibrators which are designed so that their recurrence

frequencies are slightly adjustable in order to achieve correspondence with the selective-amplifier channels. The adjustment, however, should be limited so that the recurrence frequencies cannot be multiples of one another.

**9-15. Line Components.**—Since individual gain controls can be inserted in each channel of the selective amplifier, the r-f attenuators that are commonly used to adjust the power level may be eliminated. However, if the calibration technique is dependent on the law of the detector, error may be incurred when the different signals at the detector are not comparable in amplitude. If the power-level attenuators are omitted, and if magic T's are used for coupling networks, the bridge T may be isolated from the oscillators by only 3 or 6 db. In this case it is advisable to provide 5 to 10 db of matched attenuation in the main input line to the bridge. Correspondingly, 10 db of attenuation should be placed between the T and the detector in order that the VSWR should not exceed 1.10 looking from the T toward the detector.

Either a crystal or a bolometer may be used as a detector. Although bolometers are less sensitive than crystals and may be more difficult to procure, they have the advantage of a truly square-law behavior over a wide range of power. This fact is useful for calibration methods which utilize the law of the detector, but in many cases, the slight error that results from the uncertain law of the crystal detector will be tolerated to realize the greater sensitivity. If a calibrated r-f attenuator is used, the law of the detector need not be known, and the crystal is preferred.

Although waveguide line components are used with waveguide T's, coaxial line components will save considerable space for bridges that operate in the region of 3000 Mc/sec. Directional couplers have been designed with terminals that mate with standard 50-ohm cable plugs. If the components are connected with short cables, a good mechanical arrangement usually can be attained. Fixed attenuation may be in the form of lossy cables or coaxial metalized-glass pads. Coaxial crystal holders and double-stub tuners are also standard components for 50-ohm line.

Reaction frequency meters or wavemeters are preferable to transmission types and should be coupled to the line just ahead of the detector. In this way, any mismatch that is introduced is isolated from the T by the 10-db pad.

Leakage protection is not difficult since the sensitivity of the crystal detector and conventional amplifier produces full-scale meter deflection for an input power of about  $-80$  dbw. This level is about 35 db above the sensitivity of a heterodyne receiver, and is comparable to that used for slotted-section measurements. As in the case of slotted-section measurements, no appreciable leakage error results when only a simple

shield can (no gaskets or polyiron bushings) is placed over the oscillator. The input power leads to the oscillator run through a shield which is soldered to the tube mount, so that r-f leakage power must pass through the cable where much of it is dissipated in the insulating material. If moving a sheet of metal in close proximity to the various line components does not produce any noticeable output-meter fluctuation, the leakage protection usually meets the requirement of 100 db as specified in Sec. 9-13.

Although ordinary mixer crystals (types 1N21, 1N23, and 1N26) are often used as detectors, better results are obtained when special video crystals can be employed. Types 1N27 and 1N32 are used for the 3000-Mc/sec region; the type 1N31, for the 9000-Mc/sec region. Unfortunately, no video crystals have been produced for the 24,500-Mc/sec region.

**9-16. Selective Amplifier.**—The ordinary selective amplifier that is used for slotted-section measurements consists of a well-shielded input transformer, a pentode amplifier, a second pentode amplifier that includes a twin-T feedback network, a beam-tetrode power amplifier, a full-wave diode rectifier, and a d-c meter. This conventional design is commonly used with a 1N21, 1N23, or 1N26 crystal detector, and provides full-scale meter deflection when the average power incident on the detector is about  $-80$  dbw. Although this standard and proved design can be modified for impedance bridges, a much-improved design is feasible. In the audio range of frequencies, sensitivity is usually limited by microphonics, flicker effect, and harmonics of the power-line frequency rather than thermal noise. These effects are considerably reduced if the recurrence frequencies are increased, from the usual 500 to 1000 cps, to 15 to 20 kc/sec, and the multivibrator requirements are not increased appreciably. If the input transformer is replaced by a shielded preamplifier, less pickup and several other advantages result.

If the crystal detector is direct-coupled to the grid of the first amplifier, the open-circuit output voltage from the crystal is realized. Since conventional input transformers present a load impedance of about 400 ohms to the crystal whose video impedance is between about 2000 and 20,000 ohms, the input voltage will be increased by at least a factor 6. If a video crystal (1N27, 1N31, or 1N32) is used, the sensitivity will be increased by between 4 and 8 db. The first stage should use a tube, possibly a 6F5 triode, that has low microphonics, little hum modulation, and a low equivalent-noise resistance. The preamplifier should provide one or two stages of amplification, and a cathode-follower output stage is recommended. The effects of the power-line frequency and its harmonics are minimized if a 60-cps filter is inserted in the supply-voltage input lead, and if the heaters are operated from a selenium

rectifier. Small bridge rectifiers will deliver 12 volts and will operate both preamplifier stages if the heaters are connected in series. The effects of ground currents can be minimized by isolating the input stage from ground by means of a small resistance. Naturally the tubes should be shielded and shock-mounted, and the entire unit should be mounted close to the crystal detector.

The audio attenuator should precede the selective channels, and should be matched or calibrated for a particular load impedance. If a high-impedance network is used, the low output impedance of the preceding cathode follower need not be considered in the attenuator design. Each selective channel may consist of a buffer amplifier, a

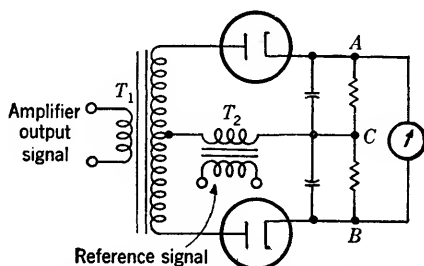


FIG. 9-22.—Coherent-signal detector.

selective amplifier, and a coherent-signal detector. If the twin-T networks are aligned carefully with the aid of standard audio test equipment,  $Q$ 's of 50 may be realized.

The greatest improvement over the conventional amplifier may be achieved through the use of a coherent-signal detector. In fact, the use of a coherent-signal detector even with conventional circuits is strongly recommended since it will reduce the pass band to about 1 cps. The twin-T selective stages should not be omitted since they remove a great deal of noise and interference prior to the detector. The principle of operation of the coherent-signal detector is illustrated by the simple diode circuit of Fig. 9-22 which is the equivalent of a hybrid coil or a low-frequency magic T. The output signal from the amplifier is coupled into  $T_1$ , and the resultant voltages between  $A$  and  $C$  and between  $B$  and  $C$  are equal and cancel unless a reference signal is coupled into  $T_2$ . If the reference signal is coherent with some component of the amplifier output signal, and if the two signals have the proper relative phase, the reference signal will reinforce the coherent component of the amplifier signal for one diode, but will reduce the component presented to the other diode. Consequently, coherent signals produce a net voltage between  $A$  and  $B$ , and if the signals have the proper relative amplitudes, the

meter deflection will be proportional to the coherent component of the amplifier output signal.

In practice, the reference signal is obtained by filtering the output signal from a multivibrator. The resultant signal is passed through a variable phase-shift network which is adjusted for maximum meter deflection. The simple circuit of Fig. 9-22 may have many variations. The transformers may be replaced by vacuum-tube circuits, and the diodes may be replaced by triodes, pentodes, or pentagrid tubes. The use of two tubes is recommended since the zero set of the meter will, in that case, be less subject to power-line variations.

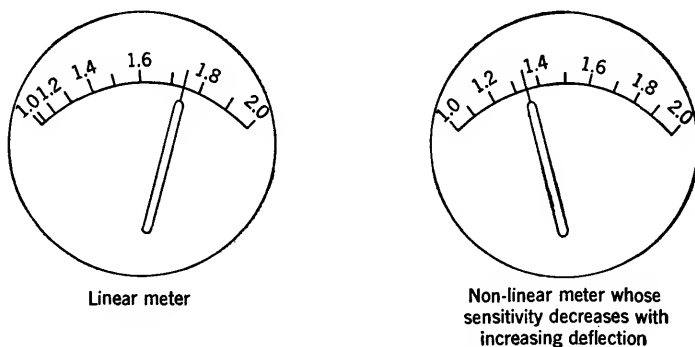


Fig. 9-23.—Meter scales for use with a square-law detector.

If the selective amplifier is constructed in accord with the previous design considerations, it should be possible to realize a stable full-scale meter deflection for r-f power levels as low as  $-90$  to  $-100$  dbw.

Since the detector is very nearly a square-law device, and since this amplifier is very linear, the output meters can be calibrated in terms of  $r_i$ . A cramped scale results, as shown in Fig. 9-23, but it may be expanded by altering the shape of the pole pieces.

**9-17. Range of Measurement.**—Since each r-f oscillator delivers square-wave-modulated power at an average power level of  $-20$  dbw, and since the crystal detector and conventional amplifier provide full-scale meter deflection when the received power level is  $-80$  dbw, a line attenuation of 60 db can be tolerated. If the attenuation between each oscillator and the T is 15 db, and if the attenuation between the T and the detector is 10 db, an attenuation through the T of 37 db corresponds to full-scale deflection. However, since  $\frac{1}{2}$ -scale deflection can be used as a reference level, the attenuation through the T can be 44 db.

If calibration is made relative to a reference mismatch whose VSWR is 1.20, the corresponding attenuation through the T is 27 db. If the reference deflection is  $\frac{1}{2}$  scale, the calibrating attenuator can have an

insertion loss that is equivalent to a line attenuation of 17 db. Since this effective attenuation is reduced in order to regain reference deflection when the test-piece reflections are small,  $r_t$ 's down to 1.025 can be measured. If the calibrating attenuator can increase the effective line attenuation 11 db (relative to that when the VSWR is 1.20), then a maximum  $r_t$  of 2.00 can be measured.

Although the calibrating attenuator is useful for accurate measurements, the meter is used to judge the success of test-piece matching procedures. If the meter is modified so that its sensitivity decreases with increasing deflection, and if the reference deflection is still  $\frac{1}{2}$  scale, then the scale can be nearly linear in  $r_t$  from 1.0 to 2.0.

Since a bridge T cannot be balanced perfectly over a wide range of frequencies, the sensitivity of the system is not always the limiting factor in the measurement of small reflections. In many cases the bridge unbalance is equivalent to an  $r_t$  of 1.02, and consequently it is hardly worth while to extend the calibration below an  $r_t$  of 1.05. If the lower limit is set at 1.05, the calibrating attenuator need introduce only 11 db of loss at the reference VSWR of 1.20, and an additional safety margin of 6 db is realized. However, in order to maintain the signal level in the range of square-law detection, it may be advisable to insert a variable level-set attenuator between each oscillator and the coupling network. If the amplifier provides a stable full-scale indication at  $-90$  dbw instead of  $-80$  dbw, the isolating attenuations between the T and the oscillators and detector can be increased, for example, 6 and 4 db, respectively, and the phase error will be reduced.

#### IMPEDANCE BRIDGES THAT EMPLOY PULSE MODULATION

The principle of operation for pulse-modulated impedance bridges is discussed in Sec. 9-12 with reference to Fig. 9-20. Several r-f oscillators are pulsed in sequence, and their output signals are coupled through the bridge T to a crystal detector. The detector is followed by a pulse amplifier which provides vertical deflection for a cathode-ray tube. The amplitudes of the resultant pips that appear on the cathode-ray tube indicate the amount of power reflected from the test piece at several corresponding frequencies.

**9-18. Microwave Sources.**—Because a pulse amplifier has a wider pass band and hence less sensitivity than a selective audio amplifier, the pulse method and the modulation-frequency method will provide comparable over-all sensitivities only if the pulsed oscillators deliver relatively higher powers. When a reflex oscillator is employed, the available pulse power is usually no greater than the available c-w power since the modes of oscillation, as well as the dissipation, determine the maximum voltages that may be applied to the tube. Whereas low-

voltage local-oscillator tubes can be used for the modulation-frequency method, the pulse method employs tubes that require voltages in the range of 1000 to 2000 volts. Since these tubes have beam currents between 50 and 100 ma, a large power supply is necessary unless the tubes are turned off, as well as driven out of oscillation, between pulses. Consequently, anode or grid modulation is preferred to reflector modulation, and the recurrence frequency should be as low as possible.

In order that a single power-supply design can serve equally well for different sets of r-f components, it is wise to choose tubes that have similar d-c characteristics. Over the frequency range from 3300 to 10,300 Mc/sec, the 2K42, 2K43, 2K44, and 2K39 tubes are a good choice since they will deliver about 250 mw. They operate with about 1250 volts applied to the anode, draw a beam current of about 45 ma, and have a focus electrode whose bias may be varied to control beam current. Since this bias may be slightly negative, pulsing may be accomplished with a high-impedance modulator; that is, no driving power is required.

The 2K33 tube, which operates in the 24,500-Mc/sec region, may be pulsed in a similar manner, but requires 1800 volts. The beam current is only about 8 ma, and the output power does not often exceed 25 mw. Although the output power is no greater than that which can be obtained from a low-voltage tube, a high-voltage power supply that employs an oscillator can be equipped with plug-in coils in order to allow the use of this tube.<sup>1</sup>

The 2K41 tube, the present design for an output power of 250 mw from 2650 to 3320 Mc/sec, has a mesh grid instead of a focusing ring. This grid is operated at a positive bias of between 0 and 50 volts. Since considerable grid current is drawn, a modulator must be capable of supplying an 80-volt pulse at about 17 ma. Since the average power consumption is very low, these drivers can be operated from the common low-voltage power supply in the bridge without increasing its capacity. The drivers can be coupled to the multivibrators which serve as modulators for the oscillators of other types, and can be mounted beside the 2K41 tubes so that they are part of the r-f package for the 3000-Mc/sec region.

If a conventional regulated supply is used, it is probably more economical to design it for 1250 volts, and use 2K50 tubes instead of 2K33's. Accordingly, the low-voltage supply is designed to withstand the current drain of the 2K50's, and modulation is applied to the reflector electrodes.

**9-19. Line Components.**—With a few exceptions, the line components for pulse-modulated bridges are the same as those discussed in Sec. 9-15 for the modulation-frequency method. The high-voltage reflex oscil-

<sup>1</sup> A power supply of this type is described in Chap. 2.



lators are not designed to operate with a matched load, and hence double-stub tuners should be inserted between each oscillator and the line. Also, these tubes have coaxial output fittings so that waveguide-to-coaxial-line adapters are necessary in many cases.

Since the oscillators are coupled to the other line components by means of cables, they may be mounted on the front panel and enclosed by a common shield. Good shielding is necessary because these tubes do not have all-metal shells and there is considerable r-f leakage from the glass portions.

Many of the high-voltage oscillators are still being improved and redesigned, and hence the available output power may vary considerably from tube to tube. Consequently, level-set attenuators should be installed between each oscillator and the coupling network. For this purpose, frequency sensitivity and gradual changes in attenuation are unimportant, and satisfactory attenuators can be made in which the absorbing elements are tapered strips of resistance-card material. For coaxial-line components, a cam-driven flap of this material may be inserted through slots in the outer and inner conductors.

**9-20. Pulse Amplifier.**—In order to provide reasonable reproduction of the pulse, arbitrary limits place the lower cutoff frequency at five times the recurrence frequency, and place the upper cutoff frequency at about 1.5 times the reciprocal of the pulse duration. The pulse will rise rather slowly, and the trailing edge will have considerable overshoot. This overshoot is not troublesome since it can be removed by a diode which also clamps the CRT baseline against the effects of varying pulse amplitudes.

If the duty ratio is limited to  $\frac{1}{10}$  by the power-supply requirements, then for a given quality of pulse reproduction the narrowest pass band is realized at the lowest possible recurrence frequency. Although this consideration produces a narrow pass band, optimum sensitivity may not be realized because considerable instability is introduced in the lower audio-frequency range by the power-line frequency and its harmonics, by microphonics, and by flicker effect. On the other hand, above 25 kc/sec, sensitivity is determined primarily by statistical noise, and increasing bandwidth results in decreasing sensitivity.

Consequently, optimum sensitivity can be realized if the lower cutoff frequency is about 10 kc/sec. This means that a recurrence frequency of 2000 cps and a pulse duration of 33  $\mu$ sec can be used, and the upper cutoff frequency for the amplifier will be 45 kc/sec. If the detector is a video crystal with a figure of merit of at least 50, a sensitivity of  $-91$  dbw can be realized. However, the minimum usable signal is about 10 db above the noise level, so that a useful sensitivity of  $-80$  dbw is achieved. Figure 9-24 shows a pulse amplifier that is slightly less sensitive because



of the linear meter, the calibration will be nonlinear. This problem may be alleviated somewhat by providing a double scale as shown in Fig. 9-25. The left-hand scale is used with a reference mismatch that produces a VSWR of 1.20, and calibration is made at maximum deflection.

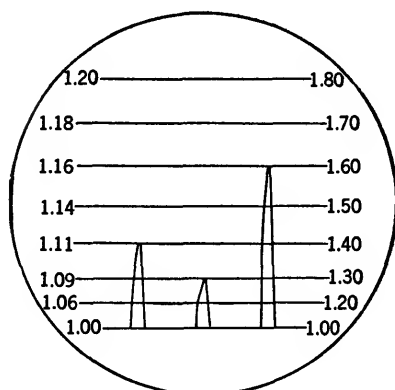


Fig. 9-25.—CRT calibration for pulse-modulated impedance bridges.

In order to use the right-hand scale, without the necessity of recalibration, a switch can be employed to reduce the amplifier gain by a factor of 10.

### IMPEDANCE BRIDGES UTILIZING PANORAMIC RECEIVERS

Chronologically, panoramic bridges were developed first because receiver components were available and because adequate sensitivity is assured even with low-power oscillators as microwave sources. The principle of operation is described in Sec. 9-12 with

reference to Fig. 9-21. Although pulse-modulated bridges have been engineered in view of production, the TBX-1BR bridge shown in Figs. 9-26 and 9-27 is the only type that has been produced commercially. It operates in the frequency range from 8500 to 9600 Mc/sec, and was produced by the Boonton Radio Corporation for the Radiation Laboratory.

**9-22. Microwave Sources and Local Oscillators.**—Low-voltage reflex oscillator tubes such as the 2K28, 726, 2K25, or 2K50 may be used as microwave sources and local oscillators for the heterodyne receiver. By operating the oscillator cathodes at ground potential, a common power supply may be used for the receiver and other low-voltage circuits. Since the tube shells will be 300 volts above ground, good insulation must be provided between the mechanical tuning shafts and the tubes. Also, because of the high sensitivity of the receiver, the oscillators should be provided with all the leakage-protection devices described in Sec. 9-13.

A total of six oscillators, three of which are frequency-modulated, is required to produce indications at three microwave frequencies, and it is not surprising that spurious signals result because of cross-modulation in the crystal mixer. Since no spurious signal can exceed the fundamental components introduced by the r-f oscillators, and since the frequency-modulated oscillators are more likely to produce spurious responses, there is a definite advantage to modulating the microwave sources because their signals are attenuated about 85 db before reaching the detector. Consequently, the main problem is the c-w local-oscillator

signals and their harmonics that can cross-modulate at a level high enough to block the receiver. This difficulty was removed from the TBX-1BR bridge by using a motor-driven switch that operated the local oscillators sequentially instead of simultaneously.



FIG. 9-26.—Front view of TBX-1BR impedance bridge.

The microwave sources are frequency-modulated by applying saw-tooth signals to the reflector electrodes. The total frequency deviation is about 10 Mc/sec in order to generate pips each of which occupies about 10 per cent of the CRT horizontal trace. The horizontal position of each pip is controlled by adjusting the d-c reflector voltage for the corresponding microwave source. Reflector-voltage variations shift the pip with respect to the sweep since they shift the operating frequency with respect to the modulation.

**9-23. Line Components.**—Since the heterodyne receiver provides more than adequate sensitivity, the line components may include sufficient attenuation so that the impedance mismatches of the oscillators and the detector do not increase the phase error excessively over that which results from the T itself. This may be achieved on the input side

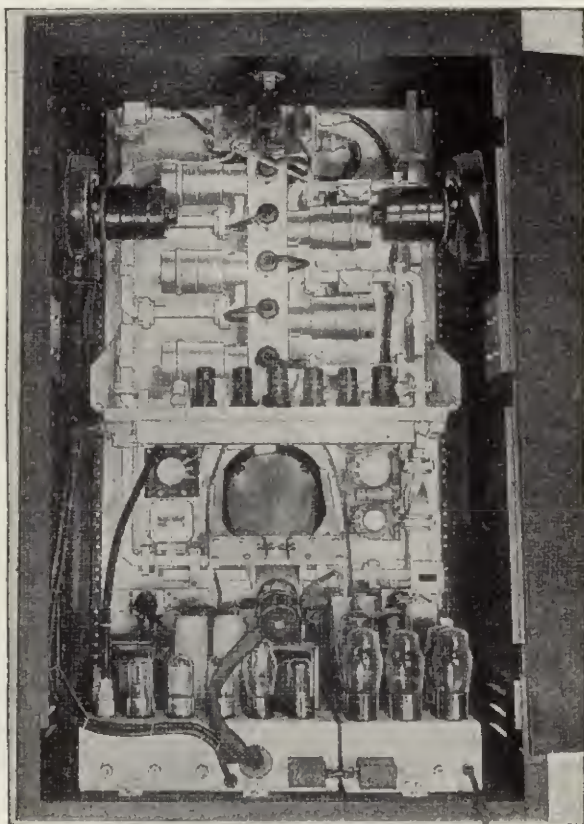


FIG. 9-27.—Rear view of TBX-1BR impedance bridge.

of the T by coupling the oscillators to the input line by 12-db directional couplers, and by inserting 10 db of matched attenuation between the couplers and the T. If the couplers are so spaced that their individual reflections do not combine adversely, the VSWR looking back from the T will not exceed 1.05. If the detector is preceded by 13 db of matched attenuation, the VSWR seen by the output arm of the T will not exceed 1.05. Although the coupling networks and the isolating attenuators have introduced 35 db of the line attenuation, the high sensitivity of the

system will still allow the use of level-set attenuators which normally are adjusted for 5 db of attenuation in order to compensate for decreases in the output powers from the oscillators.

The r-f components of the TBX-1BR impedance bridge exemplify the good mechanical arrangements that can be achieved with directional couplers. Since this bridge uses an unmatched side-outlet T, the isolating attenuation is particularly important in order to prevent an already large phase error from increasing. As shown in Fig. 9-27, the microwave sources deliver power through their level-set attenuators to the 11-db directional couplers on the right-hand side of the photograph. Power from the couplers is attenuated approximately 4 db by a metalized-glass pad, and then enters the *E*-arms of the T. Output power from the *H*-arm is attenuated about 4 db by another pad and is coupled through a 10-db directional coupler to the crystal mixer. The isolating pads are adjustable from nearly 0 to 6 db. Since they introduce small reflections themselves, and since the mismatches that they isolate vary slightly from one unit to another, the pads are adjusted for an optimum match looking into the test arm of the T. This adjustment is made with the aid of another impedance bridge. Between the isolating coupler and the mixer are the directional couplers by which the local oscillators are coupled to the mixer. These couplers and tube mounts are identical with those used for the microwave sources, and production costs are minimized by using a common design for the two similar functions. Note that the reaction frequency meter is placed between the isolating coupler and the local oscillators, and, accordingly, the reaction on a pip indicates the frequency of the signal transmitted through the T. If the meter were placed next to the mixer, it would cause confusion by producing reactions when tuned to the local-oscillator frequency.

The T is oriented so that the test arm protrudes through the front panel, and the reference match is coupled to the open junction which appears in Fig. 9-27. No r-f attenuator is included as a calibrating device, but it could be installed by removing the 4-db pad that follows the T. When used with a reference mismatch whose VSWR is 1.20 the attenuator must provide 11 db of attenuation at the reference level in order to measure an  $r_t$  as small as 1.05. In addition to serving as a calibrating device, this attenuator would provide increased isolation when the phase error tends to be large, and less isolation, but more sensitivity, when the phase error tends to be small.

**9-24. Receiver.**—Although the TBX-1BR impedance bridge employed a standard W-5 i-f amplifier and preamplifier in order to expedite production, a more suitable receiver could be designed for this application. The W-5 receiver strip and preamplifier provide 7 i-f stages, a diode detector, and two video stages. The intermediate fre-

quency is 30 Mc/sec, and the bandwidth is about 2 Mc/sec. Since a recurrence frequency of 60 cps is used in order to synchronize hum modulation, it is necessary to modify the video amplifiers designed for radar applications. This receiver provides a reliable sensitivity of about  $-120$  dbw, and very stable operation at a microwave power level of  $-100$  dbw. A more suitable receiver would provide a narrower pass band and hence could achieve greater sensitivity. The limit to which the pass band may be narrowed is determined by the duration of the i-f pulse that is generated. If the recurrence frequency is 60 cps, the pulses can have long durations, and the instability that tends to result from hum modulation is eliminated by synchronization. In addition, a more selective receiver is more economical since a high gain per stage can be realized with low current drain from the power supply.

**9-25. Range of Measurement.**—Since the microwave sources deliver power at a level of  $-16$  dbw, and since the receiver has a sensitivity of  $-120$  dbw, a line attenuation of 104 db will result in a signal equal to noise. If the line components introduce 38 db of attenuation, and if a signal level 20 db above noise is chosen from stable operation, the test-piece reflection must be large enough so that the attenuation through the T does not exceed 46 db. This corresponds to a minimum  $r_t$  of 1.02. If an r-f calibrating attenuator precedes the mixer, 6 db of isolating attenuation can be removed on the output side of the

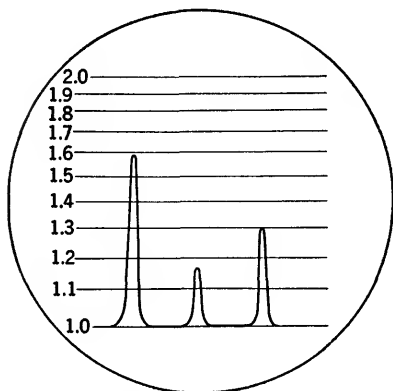


FIG. 9-28.—CRT calibration for panoramic impedance bridge.

T, and the lower limit for  $r_t$  is 1.01. Over a wide range of frequencies, bridge unbalance usually will not justify extending the calibration to this low limit.

If the receiver is linear, the CRT deflection is proportional to the magnitude of the test-piece reflection coefficient. Accordingly, a screen calibrated for  $r_t$  would appear as shown in Fig. 9-28.

#### CALIBRATING DEVICES AND SOURCES OF ERROR

There are three methods by which an impedance bridge can be calibrated in terms of  $r_t$ . An adjustable load can be calibrated and coupled to the bridge to produce an indication equal to that produced by the test piece. Although this is not a desirable method for measuring  $r_t$ , it is a convenient way of establishing an acceptance level for produc-

tion testing. A more desirable method uses a reference mismatch and a variable calibrated attenuator. The attenuator introduces or removes an amount of line attenuation equivalent to the ratio of the reference-mismatch and test-piece power reflections. However, this calibrating method necessitates coupling an accessory to the bridge. The ideal method is one in which a calibrating signal is produced by merely turning a switch while the test piece can remain coupled to the bridge. Since  $r_i$  is related to attenuation through the T, this method is achieved by using an r-f switch to direct the power around the bridge element and to the detector through an attenuation equivalent to some reference standing-wave ratio.

**9-26. Adjustable Reference Mismatches.**—The adjustable reference mismatch that was developed for use with the TBX-1BR impedance bridge consists of a micrometer-driven steel rod that protrudes from a well-matched polyiron termination. The combined reflections of the rod and the termination produce a voltage standing-wave ratio that is very nearly proportional to the micrometer adjustment from 1.20 to 1.50. The reflecting elements slide within the waveguide casing, and the effects of phase error and bridge unbalance may be averaged by "phasing" the reflection to produce maximum and minimum indications.

Since the device is frequency-sensitive, individual calibration charts were prepared. Each chart was a family of constant-VSWR contours for corresponding frequencies and micrometer settings. Although single-frequency plots of VSWR versus micrometer setting produced smooth, reproducible curves, the final charts were very erratic. The cause of these variations has not been determined completely, but their existence makes the device of dubious value. In addition, although the data were reproducible on the same day, the hygroscopic nature of the polyiron made the calibration subject to humidity conditions.

**9-27. Fixed Mismatches and Calibrated Attenuators.**—The simplest fixed mismatch can be made by placing an iris just ahead of a well-matched termination. The iris is soldered in place and then filed until the desired reflection is produced. Although the device will be frequency-sensitive, this variation can be minimized by making the reflection from the termination very small, by placing the iris very close to the termination, and by keeping the iris flat. Another type of mismatch can be made from a purposely mismatched resistive attenuator. Some of the absorbing material is removed from the leading edge of the strip, and the position of the strip in the waveguide is adjusted to produce the desired reflection. If the line is short-circuited at some point after the strip, the position of the terminating plate may be adjusted so that its reflection, reduced by the attenuating strip, is of the proper phase to minimize the over-all frequency sensitivity.



If an audio or video attenuator is used with the reference mismatch, the law of the detector must be known accurately. The attenuator can be made sufficiently accurate so that the detector law is the important factor. Measurements indicate that at low power levels, a crystal is very nearly a square-law detector. If the power level is increased 20 db from about  $-80$  dbw, a crystal detector and audio attenuator will measure the increase as about 18 db, an error of about 2 db. Although this error in attenuation may seem large, the error in measuring  $r_i$  will not be excessive for production-testing applications.<sup>1</sup>

If a calibrated r-f attenuator is employed, the law of the detector is unimportant, but the problem of frequency sensitivity arises. Actually,

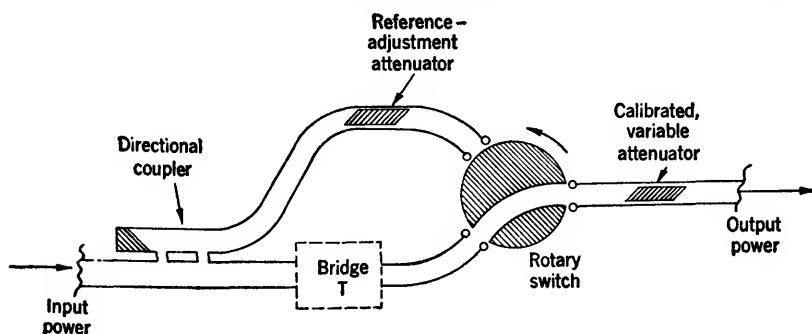


FIG. 9-29.—Built-in calibrator that employs a single directional coupler.

the frequency sensitivity of total attenuation is not important if a range of about 20 db can be obtained for which the slope of the calibration curve is frequency-insensitive. This procedure requires that some additional loss can be tolerated and that the power levels at each frequency can be adjusted to compensate for the frequency sensitivity of total attenuation. Metalized-glass attenuators are somewhat frequency-sensitive as to both total and incremental attenuation, and the calibration curves at different frequencies cross over one another. Consequently, it is desirable to plan a crossover region that corresponds to the attenuation at the reference level.

If the calibration is to cover a range of  $r_i$  from 1.05 to 1.90, a logical choice for the reference-mismatch VSWR is 1.20. In this case the calibrated attenuator must provide deviations of  $\pm 11$  db, and the drive mechanism can employ a special cam so that the scale is linear in  $r_i$ . This scale can be made sufficiently expanded so that the error in reading is negligible.

**9-28. Built-in Calibrators.**—A directional coupler and r-f switch may be used as shown in Fig. 9-29 to bypass the T and to provide a signal equivalent to that produced by, for example, an  $r_i$  of 1.20. The

<sup>1</sup> The magnitude of the error in  $r_i$  is mentioned in Sec. 9-7.

line attenuation equivalent to an  $r_t$  of 1.20 is 26.8 db, and the small trimming attenuator is adjusted accordingly. The coupler should be designed to provide an attenuation of about 25 db. There are other arrangements of the components, such as interchanging the coupler and switch, that will work almost as well. For most cases, considering the usual mismatches in the various line components, the arrangement shown will minimize the error caused by reflection losses. R-f leakage must be minimized in all cases, and a coupler design, such as the Schwinger type, should be chosen in order to avoid the necessity of a correction curve for the frequency sensitivity of coupling.

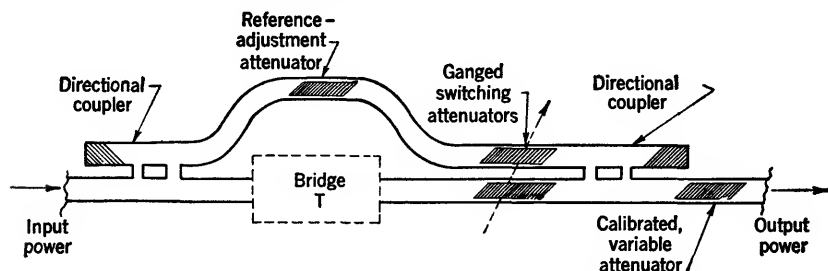


FIG. 9-30.—Built-in calibrator that employs two directional couplers.

A similar method is shown in Fig. 9-30. Two directional couplers are employed, and switching is accomplished by two attenuators which are operated by a single cam drive so that attenuation is introduced in one line as it is removed from the other line. The attenuators should be variable from about 0 to 40 db. This method may prove more expensive from the standpoint of components, but different designs can be chosen for the two couplers so that their frequency sensitivities tend to cancel.

Since the errors resulting from the calibrated attenuator are the same for this as for other methods of calibration, the error of interest is that incurred in the reference-level determination. If it is assumed that a VSWR of 1.20 can be measured to  $\pm 0.01$  by, for example, slotted-section techniques, then the built-in calibrator must have its insertion loss of 27 db known to  $\pm 0.40$  db for comparable accuracy. This accuracy applies to matched line components, and since reflection losses can be between 0 and 0.15 db in practice, the attenuation should be measured to  $\pm 0.25$  db. It was shown in Sec. 9-7 that a slightly asymmetrical T does not introduce appreciable power-split error, and hence this error is not considered here.

**9-29. Sources of Error.**—Although the sources of error can be enumerated, it is difficult to estimate the over-all error unless a specific bridge design is considered. In general, the output signal from bridge unbalance

will be equivalent to an  $r_t$  of between 1.01 and 1.02. If a rotating post within the T, or an adjustable reference match, is employed, a sliding match can be used on the test arm to facilitate optimum bridge balance at several frequencies simultaneously. By following this procedure and by checking it over the entire operating range of frequencies, bridge unbalance should not exceed 1.01.

Phase error is given by Fig. 9-2 and amounts to  $\pm 0.01$  when  $r_t$  is 1.60 and the VSWR looking into the test arm is 1.10. This is a very well-matched T, and does not include the reflections from a mismatched generator and mismatched detector. In practice the VSWR looking into the side arm may be 1.50 and the corresponding phase error is  $\pm 0.036$  for an  $r_t$  of 1.60. For small test-piece reflections, the phase error is usually unimportant.

The other main source of error is the method of calibration. For accurate measurements, the detector is used as a reference indicator whose level can be reproduced to approximately 1 per cent. A reference mismatch, or built-in calibrator, is used with a calibrated attenuator to measure  $r_t$ . If the reference level corresponds to a VSWR of 1.20, it can be determined to  $\pm 0.01$ . If the attenuation relative to this level is known to  $\pm 0.1$  db, an  $r_t$  of 1.60 will be in error by  $\pm 0.008$ . For small  $r_t$ 's the attenuation error is unimportant. If a reference mismatch is used which is not of the sliding type, the phase error can enter into the calibration procedure. In estimating over-all error, however, this factor will not be included since a sliding mismatch or built-in calibrator could be employed.

Over-all error for a multifrequency impedance bridge is shown by Table 9-1. Errors that might arise from r-f leakage, incorrect side-arm dimensions, instability, and an illegible attenuator dial are not considered. Also, it must be remembered that the errors in the table apply only to the hypothetical bridge considered in this section.

TABLE 9-1.—PROBABLE ERROR FOR TYPICAL IMPEDANCE BRIDGE

Source of error	Error in $r_t$	
	$r_t = 1.05$	$r_t = 1.60$
Bridge unbalance equivalent to an $r_t$ of 1.01	$\pm 0.011$	$\pm 0.017$
Phase error for test-arm VSWR = 1.50	0.000	0.036
Reference-level reproducibility of 1 per cent	0.000	0.004
Reference VSWR = $1.20 \pm 0.01$ , or equivalent attenuation	0.002	0.035
Calibrated attenuator error of $\pm 0.1$ db	0.000	0.008
Maximum error	$\pm 0.013$	$\pm 0.100$
Probable error	$\pm 0.011$	$\pm 0.054$

## CHAPTER 10

### THE MEASUREMENT OF DIELECTRIC CONSTANTS

By R. M. REDHEFFER

#### INTRODUCTION

In an ordinary material, which is the only type to be considered here, the electromagnetic field equations are linear, and the properties of the material that are relevant to a study of these equations may be completely specified by two complex constants. These constants, called the *complex dielectric constant* and the *complex permeability*, are designated respectively by  $\epsilon_0$  and  $\mu_0$  (real) for free space and by  $\epsilon$  and  $\mu$  (complex) for the material;  $\epsilon$  and  $\mu$  are usually separated into real and imaginary parts, with the notation

$$\begin{aligned}\epsilon &= \epsilon' - j\epsilon'' = \epsilon'(1 - j \tan \delta) = \epsilon_0 k_\epsilon (1 - j \tan \delta), \\ \mu &= \mu' - j\mu'' = \mu_0.\end{aligned}\tag{1}$$

The equation for  $\mu$  is true for most nonmetallic materials, including all those with which the present discussion will be concerned. The dimensionless quantity  $\tan \delta$  in Eq. (1) is called the *loss tangent*; it is equal to the power dissipated divided by the power stored per cycle (Refs. 2b to 5b)<sup>1</sup> and is thus a measure of the energy lost in the form of heat when a wave is propagated through the material. The quantity  $k_\epsilon$ , likewise dimensionless, is properly called the *specific inductive capacity*; in the present text, however,  $k$  will be written in place of  $k_\epsilon$  and referred to simply as the *dielectric constant*. Since the parameters  $\epsilon_0$  and  $\mu_0$  for free space are known, being in fact determined by the choice of measuring units, it is clear that the two constants  $k$  and  $\tan \delta$ , rather than  $\epsilon'$  and  $\epsilon''$ , may be used to specify any given material, and these quantities will be taken as fundamental throughout the ensuing discussion.

For reasons which are too well known to require enumeration here the values of  $k$  and  $\tan \delta$  are frequently required in both industrial and laboratory work. With especial regard to experimental procedures as well as theoretical principles, and with emphasis on results rather than on derivations, it is the purpose of the present chapter to describe the chief means by which these parameters are evaluated at microwave frequencies. Certain of the methods of measurement in the microwave

<sup>1</sup> All references in text are to the Bibliography at the end of chapter.

region are similar, as far as principles are concerned, to the standard techniques used in other frequency ranges. For various reasons, however, there is little in common besides this similarity of principle, the details of equipment and procedure being different from those of either the ordinary electrical or the optical frequencies. The necessity of preventing radiation requires rather extensive modification of the low-frequency techniques. The optical methods, on the other hand, are not directly applicable because of the reduced sample dimensions, as measured in terms of wavelengths, and, until recently, because of the difficulty of obtaining a constant frequency from a microwave generator. The method of detection is unlike those customarily used in either the low- or high-frequency ranges, moreover, as are the procedures for determining impedance or wavelength; and for microwaves, resonant-cavity techniques may be used which would be impractical in other cases. Because of these differences, microwave measurement of  $k$  and  $\tan \delta$  should be approached as a field of study in its own right, even though the same problem has been extensively investigated for neighboring ranges of the spectrum.

#### 10-1. Derivation of Relations for Proceeding from Data to Results.—

Since the electromagnetic behavior of the material is completely specified by the parameters in question, it is possible to find their values by many different methods; in principle, practically any measurable effect the material may have on an electromagnetic field can be used for such a determination. If a wave of known wavelength  $\lambda$  is incident upon a plane sheet of known thickness  $d$ , for example, there will be a certain transmission coefficient  $te^{-it'}$  and a certain reflection coefficient  $re^{-ir'}$ , all quantities permitting direct measurement. In principle, any two of the four values  $t$ ,  $r$ ,  $t'$ , and  $r'$  usually suffice to determine both  $k$  and  $\tan \delta$ , whereas if  $\tan \delta$  is known to be negligible, only one measurement is needed for  $k$ . There is, to be sure, an ambiguity in that an infinite set of values of  $k$  and  $\tan \delta$  will reproduce the observed data; but this difficulty, which is often encountered when the minimum possible number of measurements are used, may be avoided in practice by making a suitable estimate of the true value, or by repeating the measurement with slightly different initial conditions as will be described. It is clear that the experiment can be performed at a known angle of incidence  $\theta_0$  or in a waveguide of known properties; and, instead of a direct measurement of  $t$ ,  $t'$ ,  $r$ , and  $r'$ , a determination of related quantities, such as the angle of incidence for minimum reflection, the thickness for minimum reflection, or the cutoff wavelength of the filled guide, can be made. Further variation may be obtained by changing the so-called "termination" of the sheet which, instead of being backed by free space or by a matched load, may be backed by any suitable source of reflection; for

example, it may be backed by a second sheet similar to the first, by a metal plate, or by a termination that eliminates the reflection at the second air-sample interface. In all such cases two electrical measurements usually suffice to determine both  $k$  and  $\tan \delta$ , whereas with negligible loss only one measurement is required for  $k$ .

Because of this great variety of methods which, in principle, make possible the evaluation of  $k$  and  $\tan \delta$ , it is inexpedient to derive the necessary theoretical expressions afresh for each case. Such an approach not only leads to an exposition of excessive length, but also obscures

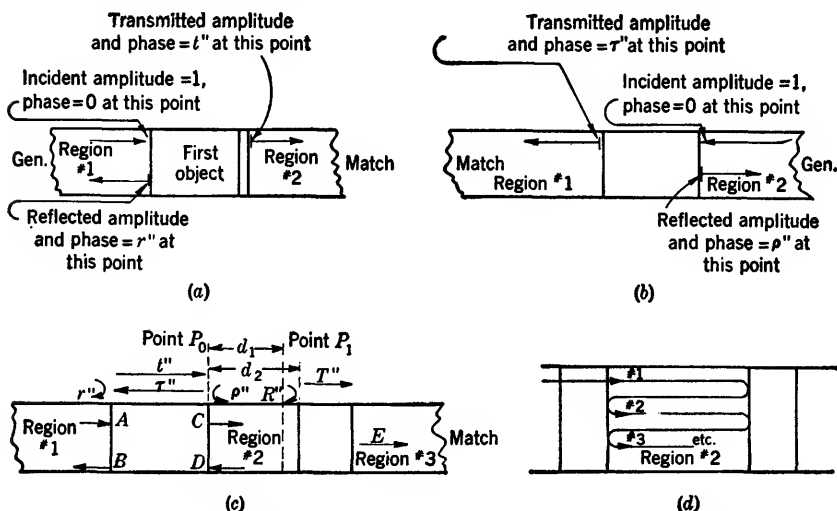


FIG. 10-1.—Reflection and transmission coefficients for one or two objects.

the underlying unity of the methods, giving an impression of complete independence that does not correspond to the facts. Instead of this procedure of obtaining each equation from first principles as it is required, the following four results are presented, which are found to include every relation for the transition from measured to desired quantities which will be needed in twenty-eight of the thirty methods here considered.

**A Basic Configuration.**—If the complex transmitted and reflected amplitudes in Fig. 10-1 are proportional to the incident amplitudes, and if the fields in the indicated regions of Fig. 10-1c can be resolved into one or two waves as there shown, then the complex amplitude of the resultant wave moving from left to right at point  $P_0$  of that figure will be given by

$$C = \frac{At''}{1 - \rho''R''e^{-2j\beta d_2}} \quad (2)$$

where

$$j\beta = \frac{2\pi}{\lambda_2} \quad (3)$$

and  $\lambda_2$  is the wavelength in region No. 2, which is assumed to be lossless. The complex coefficients  $t''$ ,  $\tau''$ ,  $r''$ ,  $\rho''$  are defined in Figs. 10-1a and b, and  $R''$  and  $T''$  are to be similarly interpreted; the propagation constant for general media is defined in the next section.

Because of the importance of this result in the sequel, two derivations of it are given. Thus, the wave in question is equal to the sum of waves (1), (2), (3), . . . in Fig. 10-1d provided the sum is evaluated with due regard to phase; thus (cf. Ref. 7b),

$$C = At'' + At''(R''\rho''e^{-2j\beta d_2}) + At''(R''\rho''e^{-2j\beta d_2})^2 + \dots + ,$$

which is equivalent to Eq. (2), since the series is obviously convergent. For the second derivation, it should be noted that the amplitudes  $A$ ,  $B$ , . . . satisfy the relations (Ref. 6c)

$$\begin{aligned} D &= R''e^{-2j\beta d_2}C, \\ C &= At'' + D\rho'', \\ B &= Ar'' + D\tau'', \\ E &= T''e^{-j\beta d_2}C, \end{aligned} \quad (4)$$

by virtue of the superposition principle and the definition of  $t''$ ,  $\tau''$ , . . . . The solution of this system for  $C/A$  again gives Eq. (2).

If the wave in region 2 is allowed to travel to the second source of reflection, and through it,

$$\frac{E}{A} = \frac{t''T''e^{-j\beta d_2}}{1 - \rho''R''e^{-2j\beta d_2}} \quad (5)$$

is obtained for the transmission coefficient of the whole arrangement; and similarly,

$$\frac{B}{A} = r'' + \frac{R''t''\tau''e^{-2j\beta d_2}}{1 - \rho''R''e^{-2j\beta d_2}} \quad (6)$$

for the over-all reflection. Analogous procedure gives  $D$ , the amplitude of the wave moving from right to left at point  $P_0$  of the figure. If this is added to the amplitude  $C$ , with due regard to phase, the field at the arbitrary point  $P_1$  between the two objects, Fig. 10-1c is

$$\frac{At''e^{-j\beta d_1}[1 + R''e^{-2j\beta(d_2-d_1)}]}{1 - \rho''R''e^{-2j\beta d_2}}. \quad (7)$$

These equations, which are immediate corollaries of the fundamental Eq. (2), may also be derived from the system of Eq. (4); their relevance to the theory of dielectric measurement will become apparent in the ensuing discussion.

*Interface Reflection.*—Like Eq. (2), the following result also will be used repeatedly for relating  $k$  and  $\tan \delta$  to measured quantities: If a plane wave is incident normally on the interface between two lossless dielectrics  $k_1, k_2$ , then the complex reflection coefficient will be given by

$$r_i e^{-ir'_i} = \frac{\sqrt{k_1} - \sqrt{k_2}}{\sqrt{k_1} + \sqrt{k_2}}, \quad (8)$$

and the complex transmission coefficient by

$$t_i e^{-ir'_i} = 1 + r_i e^{-ir'_i} = \frac{2\sqrt{k_1}}{\sqrt{k_1} + \sqrt{k_2}}. \quad (9)$$

The wave is assumed to be traveling from the medium with constant  $k_1$  to that with constant  $k_2$ . The variation of  $r_i$ , or  $t_i - 1$ , with  $k_1/k_2$  is shown in Fig. 10-2a. A special case of the Fresnel equations, this result may be found in any text on optics; it is rigorously derived in Ref. 1b.

*Arbitrary Incidence or Waveguide.*—There will frequently be occasion to analyze measurements made in waveguide or at arbitrary incidence, as well as those for free space at normal incidence. On the other hand, a separate derivation of the results appropriate to these modified situations is undesirable for reasons already stated. It is easily shown, however, that any relation of the type under consideration here may be used in these more general circumstances, if  $\beta$  of Eq. (2) and its corollaries, and  $k$  of Eqs. (8) and (9), be replaced by appropriate quantities as indicated in Table 10-1 (cf. also Fig. 10-2b).

TABLE 10-1.—EQUIVALENCE RELATIONS FOR OBTAINING EQUATIONS AT ARBITRARY INCIDENCE OR IN GUIDE FROM THOSE FOR FREE SPACE AT NORMAL INCIDENCE

Situation	To obtain the correct expression for the given situation, $k$ in the free-space normal-incidence equation must be replaced by	The propagation constant $\beta$ must be taken as the following, if $k$ is the dielectric constant of region No. 2 in Fig. 1c
Free space, normal incidence; or coaxial line, fundamental mode	$k$	$\frac{2\pi\sqrt{k}}{\lambda}$
Waveguide propagating a $TE$ -wave with cutoff wavelength $\lambda_c$ for the mode in question; or free space, incidence $\theta$ , $E$ -vector polarized perpendicular to plane of incidence	$\frac{k - p}{1 - p}$	$\frac{2\pi\sqrt{k - p}}{\lambda}$
Same, propagating a $TM$ -wave; or parallel polarization in free space	$k^2 \frac{1 - p}{k - p}$	$\frac{2\pi\sqrt{k - p}}{\lambda}$



The symbol  $p$  of the table stands for the squared ratio of free-space to cutoff wavelength,

$$p = \left( \frac{\lambda}{\lambda_c} \right)^2, \quad (10)$$

whenever the equations are concerned with waveguide (Ref. 27b). When the result is for free space, on the other hand,  $p$  is defined as

$$p = \sin^2 \theta, \quad (11)$$

where  $\theta$  is the angle of incidence. This abbreviated representation, which will be used throughout the present chapter, is possible because the condition  $\sin \theta = \lambda/\lambda_c$  leads to an exact equivalence between the results for free space and waveguide without further complication; perpendicular polarization corresponds to a  $TE$ -wave, parallel polarization to a  $TM$ -wave. Like the equivalence relations of Table 10-1, this one is actually of considerable generality, applying to any series of parallel plates with arbitrary thicknesses and dielectric constants (cf. Refs. 6b, 7b, and 8b). Since  $TE$ -waves have apparently been most often used in practice, all waveguide results in the present text are presented for  $TE$ -waves alone, unless the contrary is expressly stated; the extension to  $TM$ -waves is readily made by means of Table 10-1 if it should become necessary. The waveguides customarily used in dielectric measurement are coaxial, circular, or rectangular; and the cutoff wavelengths for the lowest (or most commonly used) mode in these three cases are respectively infinity, 1.706 times the inside diameter, and 2.000 times the larger of the two inside widths. The quantity  $p$  for waveguide is thus determined whenever  $\lambda$  is known, since these dimensions of the guide are readily measured. An alternative procedure which is sometimes more accurate is to determine the guide wavelength  $\lambda_g$ , for example as twice the difference between successive minima, and then to evaluate  $p$  by the relation

$$p = 1 - \left( \frac{\lambda}{\lambda_g} \right)^2.$$

Equipment and methods for finding the free-space wavelength are described in Chap. 5.

*Loss.*—Although the general expression Eq. (2) assumes nothing about loss, those of the foregoing relations which involve  $k$  explicitly are valid only when  $\tan \delta = 0$ . To the three fundamental results, Eq. (2), Eq. (8), and Table 10-1, must therefore be added a fourth which will allow the case  $\tan \delta > 0$  to be taken into account. The equivalence relation here is even simpler than those for arbitrary incidence or waveguide, namely,

$$k(1 - j \tan \delta) \equiv (k \sec \delta) e^{-\delta} \quad (12)$$

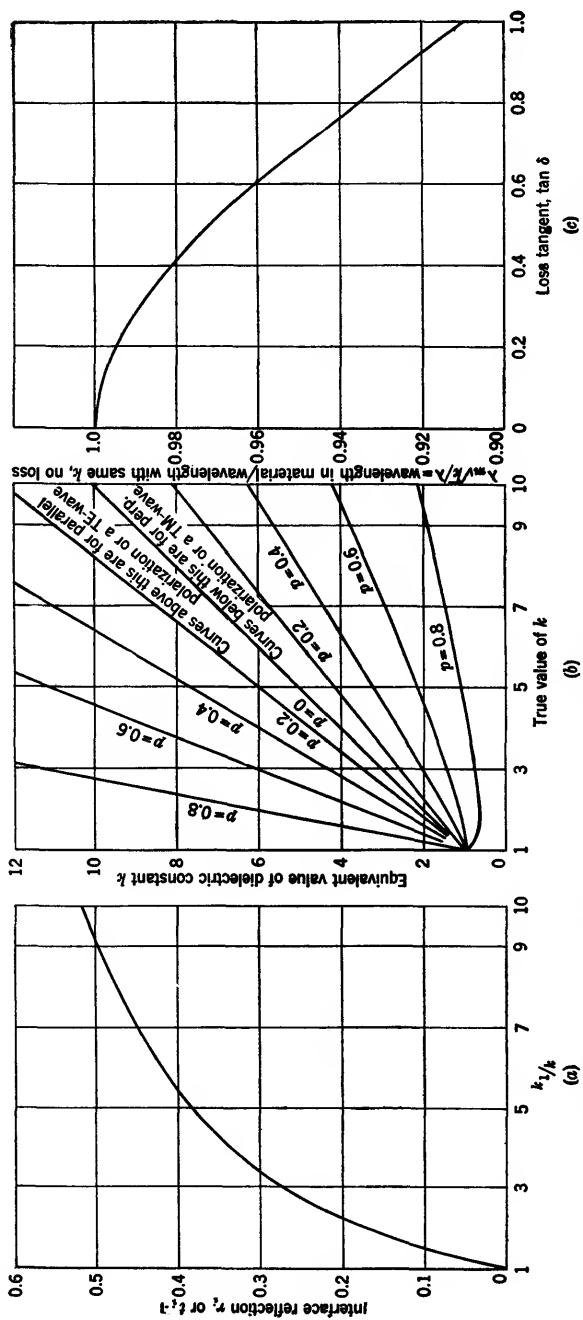


FIG. 10-2.—A few general relations for dielectric materials. (a) Interface reflection for a lossless sheet in free space at normal incidence. (b) The equivalent dielectric constant (Table 10-1) for arbitrary incidence or for waveguide. (c) The effect of conductivity on wavelength: incidence is normal, sheet is in free space.

replaces  $k$  wherever it appears. This procedure, which follows easily from relations derived in Ref. 1b, applies without error to any result based on Maxwell's equations, provided only that the original equation for zero loss be written in complex form; specifically, no separation of real and imaginary parts or taking of absolute values can have occurred at any point in the derivation. When Eq. (12) is used in conjunction with Table 10-1, the operations must be carried out in the proper order. Thus, starting with the equation in complex form the relations of Table 10-1 should be used to obtain the complete result for zero loss, and then  $k$  is replaced in this expression by its complex analogue. The reverse order of substitution will not in general give the correct result.

**10-2. General Considerations Influencing Choice of Method.**—In the foregoing discussion a number and variety of methods were noted by which  $k$  and  $\tan \delta$  may be determined. Five or ten different possibilities were specifically mentioned, each of which may in turn be carried out by a number of experimental techniques. These methods themselves are only representative of the many which may be used. Besides affecting the general treatment of derivation, this diversity of method also shows that some criterion for selection is much to be desired.

*Practical Considerations.*—In a consideration of requirements, it should be noted that the choice of method will depend to a large extent upon the type of work contemplated; a method which is satisfactory in research is sometimes undesirable for routine measurement, and conversely. Further subdivision is found when the preparation of the sample is considered, an operation which often takes more time than the actual process of measurement. Thus, a method requiring rod-shaped samples is almost impossible to use with certain types of laminates, which are ordinarily supplied in sheet form; but on the other hand, free-space methods, which require fairly large sheets, are inconvenient when the temperature and humidity are to be controlled or when the material is not available in quantity. The choice of method is likewise influenced by the properties of the material itself, apart from its form or availability; for example, those with high losses are not always conveniently treated by the methods used for low-loss materials, and similarly, materials of low dielectric constant ( $k < 2$ ), which are often inhomogeneous, are most accurately measured by methods utilizing a large sample, with the consequence that an average result is obtained. Still another item influencing the utility of a given method is the type of equipment available; for example, it may or may not be easy to change the oscillator wavelength, the use of a traveling probe may be recommended or prohibited for various reasons, or the transmitter output power may be sufficient for some methods but not for others. The evaluation of the methods described in the ensuing discussion is based on considerations

of this type, which have been found of considerable practical importance in certain cases.

*Theoretical Requirements.*—Before these methods are discussed in detail it is perhaps worth while to consider the respective roles played by the two parameters being measured, as this question too has considerable influence on the choice of procedure. First, it is found, in general, that the effect of  $k$  cannot be separated rigorously from that of  $\tan \delta$ , since any electrical phenomenon that depends upon the one will likewise depend to some extent upon the other. Quantitative consideration of the relations given in Ref. 1b or Eq. (12) easily leads to

$$\kappa = \left( \frac{2\pi}{\lambda} \right) \sqrt{6k \sec \delta} e^{-\frac{j\delta}{2}}, \quad (13)$$

$$\kappa = \left( \frac{2\pi}{\lambda_m} \right) \left[ 1 - j \tan \left( \frac{\delta}{2} \right) \right], \quad (14)$$

where  $\lambda$  is the wavelength in free space,  $\lambda_m$  in the material, and  $\kappa$  is the propagation constant as usually defined. In other words, multiplication by  $e^{-j\kappa d}$  gives the change in amplitude and phase experienced by a plane electromagnetic wave when propagated a distance  $d$  through the material. The wavelength  $\lambda_m$  is inversely proportional to the real part of  $\kappa$ ,

$$\lambda_m = \left( \frac{\lambda}{\sqrt{k}} \right) \left[ \frac{\sqrt{\cos \delta}}{\cos \left( \frac{\delta}{2} \right)} \right], \quad (15)$$

whereas the imaginary part gives a measure of the attenuation. Briefly, if the wave is propagated a distance  $\lambda_m$ ,

$$\text{the phase increases by } 2\pi \text{ radians;} \quad (16)$$

$$\text{the amplitude is multiplied by } e^{-2\pi \tan(\delta/2)}. \quad (17)$$

These two effects, phase and attenuation, depend upon  $\lambda_m$ , which involves both  $k$  and  $\tan \delta$ ; and hence  $k$  cannot be determined from a single measurement of phase alone nor  $\tan \delta$  from a measurement of amplitude alone; a simultaneous solution is necessary for the general case.

Although separation of  $k$  and  $\tan \delta$  in this sense is impracticable with the exact equations, it is feasible if certain approximations are allowed. In most cases of practical interest  $\tan \delta$  is small compared with unity, and the expansion of  $\lambda_m$  (Ref. 1b) may be written

$$\lambda_m = \frac{\lambda}{\sqrt{k}} \left[ 1 - \frac{\tan^2 \delta}{8} + O(\tan^4 \delta) \right] \quad (18)$$

for the wavelength in the material, where, as elsewhere in this chapter, the symbol  $O(x)$  means "terms of the order of  $x$ ." To the extent that

$\tan^2 \delta$  may be neglected,  $\lambda_m$  depends on  $k$  alone, and many equations giving  $k$  from measured quantities will in fact be the same as they are when  $\tan \delta = 0$  (cf. Fig. 10-2c). This approximation is the basis of a procedure often used in optics, where the effect of loss is considered for questions involving attenuation but is ignored for both measurement and computation of the index of refraction. In microwave work the approximation  $\tan^2 \delta \approx 0$  is equally useful; not only does it facilitate computation, but it allows the proper choice of the general type of measurement to be made for determining each of the two parameters. It should be noted from Eqs. (17) and (18) that any effect depending primarily on wavelength may lead to an accurate method of finding  $k$ ; and once  $k$  has been determined, any effect depending primarily on power absorption may be expected to give  $\tan \delta$ . Although derived here only for plane waves in an infinite medium, considerations of this sort are shown by Table 10-1 to be qualitatively valid for the majority of configurations encountered in the actual process of microwave measurement, and they will be frequently used in the following sections.

#### METHODS DEPENDING ON TRANSMISSION IN GUIDE

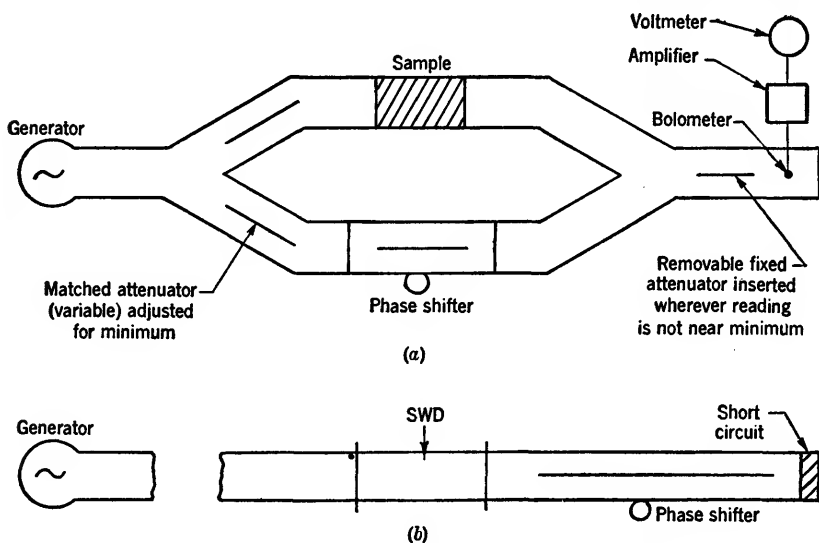
When  $\tan \delta = 0$  it is readily shown that  $k$  can be determined by measurement of either the amplitude transmission  $t$  or the phase shift  $t'$ . Upon more detailed examination, however, it is found that determination from  $t$  is, in general, considerably less accurate than determination from  $t'$ , even in the assumed situation  $\tan \delta = 0$ ; and when this condition is only approximately satisfied, which is always the case in practice, the errors are found to be much increased, being of the order of  $\tan \delta$  in the first case,  $\tan^2 \delta$  in the second. For the determination of loss, on the other hand, the situation is reversed, measurement of  $t$  giving an accurate, measurement of  $t'$  an inaccurate, result. Because of these considerations, which, incidentally, agree with the discussion of the relative effect of the two parameters, it will be assumed throughout the present section that  $k$  is to be determined from  $t'$ , whereas  $\tan \delta$  is to be found from  $t$ .

**10-3. Techniques for Phase Measurement.**—Measurement of  $t$  may be made with the equipment of Fig. 10-3a. The procedure as described in Ref. 6a is to adjust the phase shifter for minimum voltmeter reading (1) when the sample is not present, and (2) when it is present; the setting of the phase shifter should be noted in each case. With the arrangement of Fig. 10-3b, the phase difference corresponding to these two settings is then determined or, when many measurements are to be made, the equipment may be completely calibrated. If  $\Delta$  denotes the difference in probe position for the two settings in the equipment of Fig. 10-3b, then Eq. (16) combined with Table 10-1 gives the relation plotted in

Fig. 10-4,

$$k = 1 + \left(\frac{\Delta}{d}\right) \left(2 + \frac{\Delta}{d}\right) (1 - p), \quad (19)$$

for waveguide propagating a *TE*-wave (Ref. 6a). There is a certain ambiguity in the value of  $\Delta$ , as anticipated in the introduction, for the addition of  $n\lambda_g$  has no apparent effect on the relative phases of the two waves, so that  $\Delta$  may be increased or decreased by this quantity at discretion. The ambiguity may be resolved by estimating the dielectric

FIG. 10-3.—Measurement of  $k$  by phase shift in guide.

constant, or by repeating the measurement with a different sample thickness.

**R-f Errors.**—The foregoing discussion is intended to illustrate principles only, and it includes a number of tacit assumptions that are not necessarily satisfied in practice. In deriving Eq. (19) it is assumed, for example, that the phase shift on transmission through a sheet of thickness  $d$  is exactly equal to  $2\pi d/\lambda_m$ , that is, to the phase shift obtained for propagation a distance  $d$  through an infinitely long medium. This relation, which is physically equivalent to neglecting the reflection  $r_i$  at the two air-sample interfaces, may be shown to be true without error if and only if the thickness is an integral number of quarter wavelengths,

$$d = \frac{n\lambda}{4\sqrt{k-p}} \quad (n = 0, 1, 2, \dots), \quad (20)$$

or the dielectric constant is unity,  $k = 1$ . In other cases, the error may be exactly compensated by a procedure similar to that to be described for the same error in free-space measurement; or it may be reduced to negligible proportions by the use of a sufficiently long sample. If the use of a long sample is impracticable,  $\Delta$  may be taken as the average of the two values found for two values of  $d$  differing by approximately  $\lambda_m/4$ . With this procedure (Ref. 6a), it is not difficult to show that the

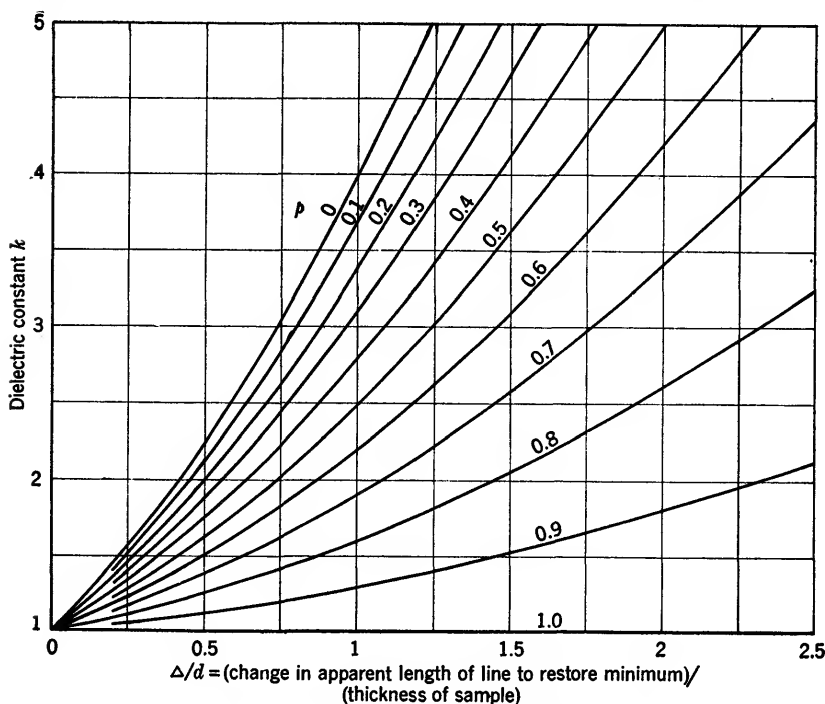


FIG. 10-4.—Dielectric constant vs. phase shift in guide.

deviation in the final value of  $\Delta$  will be of the order of  $r_i^4$ , if  $r_i$  is the reflection at the interface between material and air. The deviation as found from a single measurement is of the order of  $r_i^2$ .

Closely analogous to the above error is the error due to reflection from the Y-joints of the equipment, which is shown by Eq. (5) to be of the second degree in the three variables: reflection of sample, combined reflection of first Y-joint and attenuator, and reflection of second Y-joint. The error is therefore small when these joints are moderately well matched, and all terms that involve the sample reflection  $r$  become of the fourth degree (Ref. 4a) when two measurements are taken with a quarter-wave displacement of the sample and the results are averaged. The use

of a magic T for these Y-joints will also decrease the error in certain cases. If still further accuracy is desired, at least for the shorter wavelengths, it is a simple matter to design attenuators giving a standing-wave ratio not much over 1.01 in power, although the design of well-matched joints and indeed of most other r-f components is difficult. In such cases it is sometimes helpful to precede each source of unwanted reflection by an attenuator, as suggested by Fig. 10-5. Except for terms of the order of  $T^2AJ$ , it follows from Eq. (6) that

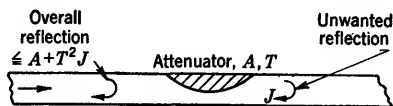


FIG. 10-5.—Use of an attenuator to reduce reflection.

$$\text{Over-all reflection} \leq A + T^2J, \quad (21)$$

for such an arrangement, if  $T$  is the transmission coefficient of the attenuator and  $A$  and  $J$  are respectively the reflection coefficients of the attenuator and termination. To apply this principle to the case at hand two attenuators are added to the right-hand Y-joint of Fig. 10-3a, located more or less symmetrically with respect to those already present, which are necessary in any case to prevent interaction between the two branches of the circuit.<sup>1</sup>

Additional r-f error is contained in the assumption of a constant generator frequency. Clearly, if this frequency is not the same when the readings are taken with and without the sample, or when the phase shifter is calibrated, than  $\Delta$  will be in error by a corresponding amount. The error of calibration due to this difficulty is usually negligible in practice, and if necessary, it may be compensated by using appropriate values of the wavelength. Error due to frequency drift occurring in the actual process of measurement, on the other hand, may become serious if no precautions are taken in the design of the equipment. With  $A$  and  $B$  as the lengths of the two branches of the circuit (Fig. 10-3a), it is not difficult to show that the error in  $\Delta$  is given by

$$\frac{(B - A)(\Delta\lambda)}{\lambda(1 - p)} + O[(\Delta\lambda)^2], \quad (22)$$

where  $\Delta\lambda$  represents the difference in transmitter wavelength with and without sample. The effect of the sample has been neglected, a procedure that is usually justified in calculations of this sort; it is discussed briefly in connection with Eq. (43). Since the error is proportional to  $(B - A)$ , it may become large when the equipment is used for measuring

<sup>1</sup> In Ref. 6a a set of values of  $k$  versus  $d$  was obtained without isolation of this type and the measured values varied from 2.4 to 3.1. When a single attenuator was added to the equipment, however, all values fell between 2.59 and 2.65. Except for this one change, the addition of an attenuator, identical equipment was used in both cases.



gases, and on the other hand the error is practically zero, independently of the total lengths  $A$  and  $B$  of either guide, when these lengths are equal. It is evident, then, that equipment of this type should be designed to be symmetrical; the two branches should not only use guides with the same internal dimensions (as here assumed) but also have substantially the same length. Of course such considerations are relevant only when the transmitter is moderately unstable, permitting a frequency drift of perhaps one part in five or ten thousand; instability of this or higher order was often encountered when the work here presented was first carried out. Recently, however, methods have been found by which the frequency of a klystron transmitter can be stabilized to within one part in  $10^8$ , and if such equipment is used for dielectric measurement the expedients here described are unnecessary. In the present chapter this remark applies whenever questions of frequency stability are discussed.

*Other Errors.*—If the error due to loss, which is of the order of  $\tan^2 \delta$  and negligible for our present purposes, is omitted, the above discussion summarizes the significant r-f errors in the derivation of Eq. (19) from measured quantities. Besides these errors, some inaccuracy due to the equipment and the experimental procedure is inevitable; much of this may be avoided by the use of precision instruments and sufficient care in taking the readings. The standing-wave detector used to calibrate the phase shifter, for example, must have the same internal width as the guide containing the sample; or, if not, the measured value of  $\Delta$ , as determined from Fig. 10-3b, should be corrected by the relation

$$\Delta_{\text{true}} = (\Delta_{\text{measured}}) \left( \frac{\lambda_g}{\lambda_s} \right), \quad (23)$$

where  $\lambda_s$  is the wavelength in the standing-wave detector, and  $\lambda_g$  that in the portion of guide which is to contain the sample. The remaining details of the proposed method of calibration are similar to those of the short-circuited-line method for measuring dielectric constants, which will be discussed subsequently. Other procedures are possible; for example, the meter reading may be taken as a function of the position of the phase shifter with the guide empty, and the resulting sine curve may be used to determine the relative phases of the two waves. Partly because the attenuation depends to some extent on phase-shifter setting, however, this method is usually less accurate than that of Fig. 10-3b. A third procedure, of course, is to use a phase shifter that is known to be linear and hence to require no calibration. Such a device is described in connection with free-space measurement.

Throughout the foregoing analysis it was assumed that the physical lengths of all waveguides remained unchanged while the experiment

was being carried out. In normal circumstances such an assumption is justified whenever the r-f paths are sufficiently short, since the actual (as well as the percentage) expansion due to temperature variation will then be very small. As in the case of frequency instability, however, to which the present effect has a certain formal resemblance, it is found that variation due to temperature changes may become serious whenever the path differences are large. Such large differences are likely to occur in the measurement of gases. Thus, the error results from the magnitude of the change in length and may be considerable for moderate temperature variation when the original length is large. It must be noted too that the cutoff wavelength  $\lambda_c$  depends on the temperature. The result of this variation, which happens to enhance the effect of the change in length, is to alter the guide wavelength in accordance with Table 10-1. It has already been shown that the error resulting from a change of wavelength is proportional to path difference [Eq. (22)]. A precise expression for the particular effect in question, may be obtained by replacing  $\Delta\lambda/\lambda$  in Eq. (22) by  $d\Delta T$ , with the result

$$\text{Error in } \Delta = \alpha(B - A) \frac{(\Delta T)}{(1 - p)} + O(\alpha^2),$$

where  $\alpha$  is the coefficient of expansion for the metal of which the guide is made,  $\Delta T$  is the temperature change in units appropriate to the value of  $\alpha$  chosen, and  $(B - A)$  represents the difference in geometrical path lengths as shown in Fig. 10-3a. This result, which does not assume a rectangular guide, takes account of the change in  $\lambda_c$  as well as of that in  $(B - A)$ ; the effect of the sample itself is neglected as in the derivation of Eq. (22), however, and  $\alpha$  is assumed independent of temperature over the range  $\Delta T$ .

Since the error is proportional to  $(B - A)$ , the equality of paths should be retained regardless of the over-all length required, and since the error is proportional to  $\Delta T$ , compensation may be necessary, even with small path differences, when the dependence of  $k$  and  $\tan \delta$  on temperature is being investigated (cf. Ref. 16a). Since the value of  $\Delta T$  is usually known, in order to compensate the error the measured value of  $\Delta$  may be corrected, and either the computed or the measured values of  $d$  and  $\lambda_c$  appropriate to the new temperature may be used in all calculations. For such a procedure only approximate values for  $\alpha$  of the sample and the guide are required; in fact the value for the guide may be evaluated in terms of the shift in  $\Delta$  with temperature. Any error from clearance, produced by the difference of expansion of the guide and the sample, may be compensated as described subsequently, if necessary, although the effect due to temperature alone is completely negligible in ordinary practice. If a complete curve of  $k$  vs. temperature is taken,

such a condition requires merely that the setting be repeated without the sample and that  $d$  and  $\lambda_c$  be evaluated from time to time as the experiment progresses. When practicable, this procedure is usually preferred. The same or substantially equivalent methods are valid for estimating or compensating the effect of temperature in all methods to be considered.

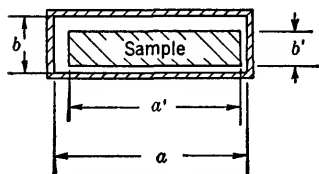


FIG. 10-6.—Clearance in a rectangular waveguide.

A third source of error is the clearance between the sample and the guide, which is necessarily present to some extent in all methods not carried out with the sample in free space. Although the exact theoretical results are available for the situation illustrated in Fig. 10-6,

it suffices here to give the empirical equation

$$k_{\text{true}} = (k_{\text{measured}} - 1) \frac{b}{b'} + 1, \quad (24)$$

which has been experimentally verified in a number of cases (Ref. 4a). The stated dependence on  $b'$  is suggested by the uniformity of the  $E$ -field in the vertical direction; that the result is substantially independent of  $a'$  for small clearance, follows from the fact that the field is zero at the sides of the guide. Corrections for clearance may be given in other cases, for example, for round or coaxial waveguides, although it is usually necessary to assume that the sample is centered for an exact theoretical derivation. It must be mentioned that errors from clearance can be greatly reduced by use of a mode in which the  $E$ -field is tangential to the inner surface of the guide at all points. The field must then be nearly zero at the edges of the sample, and hence, for all dimensions, a reduction of error is obtained which is similar to that noted in connected with dimension  $a'$  of Fig. 10-6. An example of such a mode is the  $TE_{01}$ -mode in circular waveguide, which was suggested and actually used in Ref. 13a as a means of eliminating this source of error.

A final error is found in the actual process of determining  $\Delta$ , as the phase shifter evidently cannot be adjusted exactly to give minimum power. This error is reduced to a small value, however, if the waves in the two branches of the equipment have amplitudes so nearly equal that the minimum meter reading is practically zero. The result may be magnified by an increase of over-all gain or, what is essentially the same thing, by the use of a logarithmic meter, and hence a small change in setting of the phase shifter suffices to produce a large change in meter reading. Because the minimum can be made very small by appropriate adjustment of the variable attenuator in Fig. 10-3a, the only obvious limitation to the accuracy that may be obtained (with constant generator

frequency) is set by the transmitter power and the signal-to-noise ratio of the receiver. In practice, however, it is not usually possible to obtain zero both with and without the sample, as the transmission coefficient  $t$  is less than unity. Since the phase shift of an attenuator depends upon its setting, moreover, this difficulty cannot be completely overcome by any simple procedure. It may be partially obviated by adjusting the attenuator initially to give somewhat too little power in one branch when the sample is not present, and somewhat too much when it is. This adjustment, which is made by observing meter reading vs. attenuator position, depends for its efficacy upon the fact that  $t$  is usually close, even though not exactly equal, to unity. The error in  $\Delta$  is thus made negligible compared with the other errors, for most applications, especially if the sample is reasonably long. The increase in accuracy here described is, of course, obtained only when the phase shifter is set for minimum or near-minimum meter reading; in particular, the whole method of measurement is inaccurate if the attempt is made to set on a maximum. It is perhaps worth noting that transmission errors have much in common with errors encountered in the other procedures to be investigated; these other errors may often be treated by the same methods or even by the same equations that are presented in detail here.

**10.4. Techniques for Amplitude Measurement.**—The general procedure used and the chief difficulties encountered when  $k$  is found by measurement of transmission in guide have been indicated. With regard to the question of loss, from Eqs. (12), (13) and Table 10-1,

$$\tan \delta = -\frac{\lambda \sqrt{k-p} \ln t}{\pi k d} + O(\tan^2 \delta) \quad (25)$$

may be obtained for  $\tan \delta$  in terms of the amplitude transmission coefficient  $t$ , if it is assumed for the moment that no power is reflected at the interface between air and medium.

*Direct Measurement of Transmission.*—To measure  $t$  directly the procedure suggested in Fig. 10-7a, may be used, which leads to

$$t^2 = \left[ \frac{\text{receiver reading with sample}}{\text{receiver reading without sample}} \right] \times \left[ \frac{\text{monitor reading without sample}}{\text{monitor reading with sample}} \right] \quad (26)$$

whenever second-order terms in the generator reflection, the sample reflection, and the reflection of the termination may be neglected. As previously, all terms except the product of the generator reflection and the reflection of the termination are reduced to the fourth degree if the experiment is repeated with a quarter-wavelength displacement of the sample. When the isolating attenuator is properly designed and placed

in the position shown, rather than in the fixed part of the line as might perhaps seem more natural, then it is seen from Eq. (21) that this product term will be negligible irrespectively of slight inaccuracies in the joints. Quantitative evaluation of the maximum error in this and similar methods of transmission measurement may be made by means of Table 10-2 if  $A$  is taken to mean the reflection from the sample. The effect of detector nonlinearity is the same for measurement of transmission

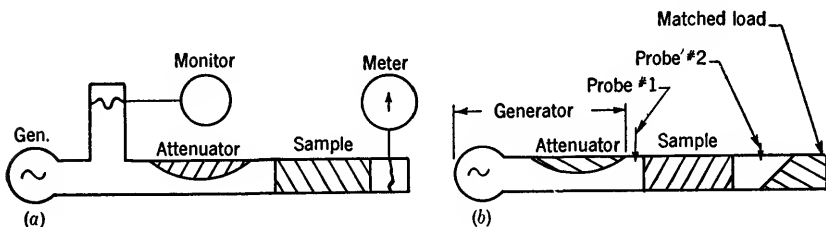


FIG. 10-7.—Direct measurement of transmission.

by this method as for measurement of a power standing-wave ratio by the maximum-to-minimum technique. The ratio of transmissions for different sample lengths is often required rather than the actual value of the transmission, and a modified procedure that eliminates error from the terminating reflection may then be employed. Thus, instead of reducing this reflection to a zero or near-zero value, the phase may be adjusted in such a way as to maximize the receiver reading; or, what is nearly the same thing, the bolometer may be matched to generator plus sample rather than to the line. For the validity of either procedure, it is necessary and sufficient that the reflection of generator plus sample be constant, a condition that will usually be realized only when the sample transmission is so low that the over-all reflection  $r$  nearly equals the interface reflection  $r_i$ . Thus, the method should not be used for short low-loss samples. Another property of this method which makes it unsuitable for such samples is that the transmission of the phase shifter itself will depend to some extent upon the setting; the change in transmission so introduced must be compensated by previous calibration unless it is negligible in comparison with the change in transmission being measured. The error from generator reflection persists in general even with this modified procedure, but if the sample has low transmission—which is a desirable property with this method in any case—then the error is eliminated whenever the distance from the generator to the nearest sample interface is held constant. It must be mentioned again, however, that the ratio of two transmissions only is considered here. The procedures outlined in this paragraph are incorrect when the value is desired in an absolute sense. An illustration of the correct application of the

method is given in Ref. 8a, where the loss tangent of water is evaluated.

Still a third method of finding  $t$  directly is suggested in Fig. 10-7b, for which a relation is given in Ref. 17a,

$$t = \left[ \frac{\sqrt{\text{max}} + \sqrt{\text{min}} \text{ for probe \#2}}{\sqrt{\text{max}} + \sqrt{\text{min}} \text{ for probe \#1}} \right] \div [\text{same, without sample}], \quad (27)$$

with an apparent error of the order of the sample reflection times the reflection of the termination independently of generator mismatch. Unlike the procedures hitherto described, however, this one involves the use of a traveling probe, which is shown in Ref. 5a to lead to large inaccuracy in certain cases. The fractional error is of the second degree in the five quantities: reflection of generator, reflection of first probe, reflection of sample, reflection of second probe, reflection of load; several of the terms involving probe reflection remain of the second degree, in general, even if an average with quarter-wavelength displacement is taken. The need for reducing this source of reflection is thus apparent.

*Measurement of the Difference between Transmission and Unity.*—Although the foregoing methods of finding  $t$  are simple and direct, they are not entirely satisfactory when the loss is low. Thus, it is seen from Eq. (25) that it is essentially  $1 - t$  rather than  $t$  which is desired, with the result that the fractional error in  $\tan \delta$  greatly exceeds that in  $t$  when  $t \approx 1$ . To overcome this difficulty the bridge method previously described may be used, which gives  $1 - t$ , essentially, rather than  $t$ . Thus,

$$1 - t = \frac{2m}{M + m}, \quad (28)$$

where  $M^2$  is the maximum,  $m^2$  the minimum meter reading observed as the setting of the line stretcher is changed with the sample in place, if the variable attenuator has been adjusted to give a minimum of zero with the sample removed. To avoid overloading the detector, the maximum  $M^2$  is taken with the fixed attenuator present, the minimum  $m^2$  with it absent; the true maximum for substitution in Eq. (28) is then equal to the measured maximum divided by the transmission coefficient of the attenuator.

Such a procedure reduces errors due to nonlinearity, as may be easily shown, but its indiscriminate use is likely to lead to errors of another kind. Thus if the insertion of an attenuator reduces the power by a given amount in Fig. 10-8a, it causes, in general, a different reduction in Fig. 10-8b; the ratio of power with and without the attenuator is, however, independent of probe position in both cases. For quantitative treatment  $T^2$  is defined as the ratio of powers with and without attenuator in Fig. 10-8a,  $\tau^2$  as the ratio in Fig. 10-8b,  $R$  as the amplitude reflection coefficient

for the load,  $G$  for the generator, and  $A$  for the attenuator. If the attenuator is not symmetrical,  $A$  is the reflection coefficient from the right for the first situation, from the left for the others in Table 10-2. With the aid of this table, in which only the last two entries are approximate, the

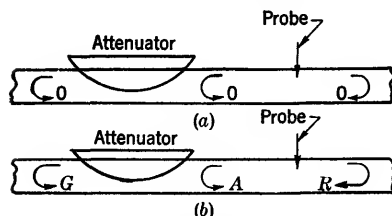


FIG. 10-8.—Typical application of an attenuator.

attenuation is found to be independent of the position of the attenuator, of the position of the load, and of the magnitude of the reflection from the load if, and only if, two of the three quantities  $A$ ,  $R$ , and  $G$  are equal to zero (Ref. 2a). In particular, the generator must be matched to the line rather than to the load if the errors for high stand-

ing-wave ratios are not to be prohibitively large; the corresponding reduction in available power leads to complications in certain cases.

TABLE 10-2.—THEORETICAL ERRORS INTRODUCED BY IMPROPER USE OF AN ATTENUATOR

Situation	Least possible value of $T/\tau$	Greatest possible value of $T/\tau$	Extremes possible in ordinary cases
$G = 0$ , $R$ and $A$ finite	$(1 - RA)^2$	$(1 + RA)^2$	Yes
$R = 0$ , $G$ and $A$ finite	$(1 - GA)^2$	$(1 + GA)^2$	Yes
$A = 0$ , $G$ and $R$ finite	$\left(\frac{1 - RGT}{1 + RG}\right)^2$	$\left(\frac{1 + RGT}{1 - RG}\right)^2$	No
$A = 0$ , $G$ and $R$ finite, phase shift through attenuator same as for empty line	$\left(\frac{1 + RGT}{1 + RG}\right)^2$	$\left(\frac{1 - RGT}{1 - RG}\right)^2$	Yes
$G$ , $R$ , $A$ , finite $T \ll 1$	$\left(\frac{1 - RA}{1 + RG}\right)^2 (1 - GA)^2$	$\left(\frac{1 + RA}{1 - RG}\right)^2 (1 + GA)^2$	Yes, for certain attenuator lengths.
$T \ll 1$ , generator initially matched to load	$\frac{(1 - RA)^4}{(1 - R^2)^2}$	$\frac{(1 + RA)^4}{(1 - R^2)^2}$	Yes

If the calibration of the variable attenuator is known, an alternative procedure is to adjust the attenuator for zero minimum with and without the sample, whereupon the ratio of the attenuator transmissions for the two cases is easily seen to be equal to the transmission desired; that is,

$$t = \frac{T_1}{T_2} \quad (29)$$

if  $t$  is the transmission coefficient of the sample, as usual, and  $T_1$ ,  $T_2$  are those of the attenuator when adjusted to give a minimum meter reading of zero with and without the sample, respectively. The chief advantage of this procedure over those discussed hitherto is that the result is now independent of the linearity of the receiver. This independence of linearity is characteristic of all procedures that merely require two readings to be equalized, and, although not explicitly mentioned in all cases, it is of frequent application in the present discussion. Error from reflection is again given in Table 10-2.

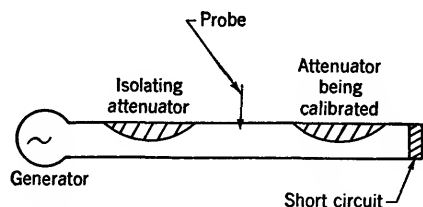


FIG. 10-9.—Calibration of a low-loss nonreflecting attenuator.

Because the range of attenuation is small for most applications, the calibration may be carried out by the method suggested in Fig. 10-9; from Eq. (6) with  $r'' = \rho'' = 0$

$$T^2 = \frac{[(\text{SWR}) - 1]}{[(\text{SWR}) + 1]} \quad (30)$$

is obtained for the attenuator transmission  $T$  in terms of the measured standing-wave ratio. The error in the method of Fig. 10-9 due to attenuator reflection, which must be small anyway for the application suggested, is shown by Eq. (6) to be of the first degree when a single measurement is made, of the second if two measurements are averaged with a quarter-wavelength displacement. When the attenuation exceeds 1 db, the measurement of the standing-wave ratio must be carried out by taking maximum and minimum meter readings, as usual, whereas for lower attenuation, the procedure is preferably that described in connection with the short-circuited-line method. In the first case probe errors are of the order of the product of the reflection being measured and the probe reflection; in the second they are negligible (Ref. 5a). From this and other considerations it is concluded, finally, that the attenuator should be calibrated by one of the methods of Fig. 10-7 for moderate or large attenuation, and by the method of Fig. 10-9 for small attenuation.

Thus far it has been assumed that the transmission coefficient of the phase shifter is independent of setting, which is actually not the case in normal practice. The error due to this variation may be shown to be



negligible when  $t'$  is being considered, but when  $t$  is to be found by the method just described the error must be considered in somewhat greater detail. By application of Eq. (28) to the situation illustrated in Fig. 10-3b it is a simple matter to calibrate the phase shifter, and the transmission, although not constant, is then known as a function of the setting. With this information available the error due to the effect in question is readily corrected by the relation

$$t = \frac{(Mt_1 - mt_3)}{(Mt_2 + mt_2)}, \quad (31)$$

which replaces Eq. (28), and by

$$t = \frac{T_1 t_1}{T_2 t_2} \quad (32)$$

instead of Eq. (29). In these equations, which are valid without appreciable error if the reflection from the phase shifter may be neglected,

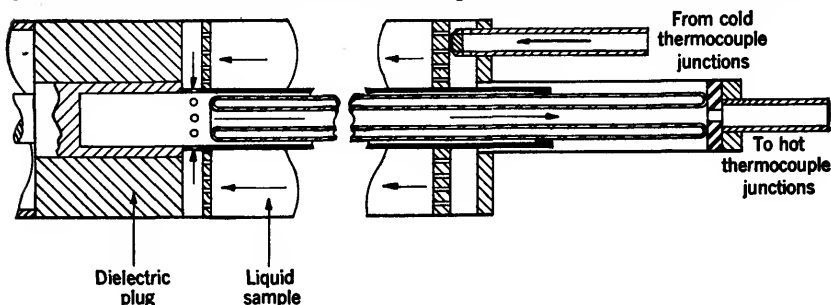


FIG. 10-10.—A calorimeter for measuring loss.

$t_2$  is the transmission of the phase shifter when it is set for minimum reading with no sample, and  $t_3$  and  $t_1$  are the transmissions when it is adjusted for maximum and minimum readings, respectively, with the sample in place.

*A Calorimeter Method.*—Attention hitherto has been confined to the standard methods of r-f power measurement. Partly because of its novelty one other procedure is considered which requires none of the r-f components that have played an essential role in the foregoing discussion. With the procedure in question, developed in Ref. 15a, the temperature change caused by the r-f power absorbed is measured, and from this temperature change the loss tangent of the material is obtained (see Fig. 10-10). If  $(\Delta T)_t$  denotes the difference between input and output temperatures at time  $t$  after the r-f power is turned on, a plot of  $(\Delta T)_\infty - (\Delta T)_t$  vs.  $t$  is a straight line on semilogarithmic paper with slope  $s$  given by

$$s = -2\alpha \frac{q}{A},$$

where  $A$  is the cross-sectional area of the coaxial line,  $q$  the rate of flow of liquid, and  $\alpha$  the attenuation constant, defined by the relation

$$E(x) = E(0)e^{-\alpha x},$$

which gives the amplitude  $E(x)$  at point  $x$  inside the liquid. The foregoing result was obtained for the period of temperature rise. After the steady state has been reached the transmitter may be turned off. The temperature difference will now decrease exponentially, in such a way that  $(\Delta T)_t$  vs.  $t$  will be a straight line with the same slope as that formerly obtained for  $(\Delta T)_t - (\Delta T)_\infty$ . As a check for experimental accuracy, the slope  $s$  is evaluated in practice by both methods. The method appears to be most feasible in coaxial line, since the center conductor supplies a convenient return path; in this case Eq. (17) of the introduction, together with the above equation, gives the simple result

$$\sec \delta = 1 + \frac{1}{8} \frac{1}{k} \left( \frac{\lambda s A}{\pi q} \right)^2$$

for  $\sec \delta$  in terms of the measured quantities  $s$ ,  $A$ ,  $q$ , and  $k$ , provided the first three are expressed in a consistent system of units.

The experimental procedure is to measure the temperature difference at regular intervals from the time at which the transmitter was turned on, with due care to keep the input power and rate of flow constant. From a logarithmic plot of temperature difference vs. time, the slope  $s$  is obtained. The quantities  $A$  and  $q$ , and with them the ratio  $A/q$ , giving the velocity of the liquid, are determined by standard methods, whereas  $k$  is found by a separate r-f measurement of the type considered elsewhere in this chapter.

The foregoing discussion gives only the essentials of the method, and it remains to consider the conditions for its validity. In the first place, the power was assumed to be traveling in a direction opposite to that of the liquid flow, as illustrated in Fig. 10-10. It was shown in Ref. 15a that this condition is the most satisfactory experimentally; it leads to a time constant that is smaller than that obtained in other circumstances, and that is, moreover, independent of the length of the liquid column. The limitation on this last statement is that the length must be sufficient to absorb practically all the r-f power, that is, a traveling wave must exist in the sample rather than a standing wave, and only negligible power must reach the termination. This condition, which requires either very long or very lossy samples, seriously restricts the utility of the method, apart from the fact that it is applicable to liquids only. The use of a short circuit for the termination, if accompanied by a suitable modification of the theory, could be expected to allow lengths half as great as those otherwise permitted; but the restriction on length would still be incon-

venient for most materials. Another assumption was that the flow is laminar, a condition which need be only approximately satisfied in practice and which is sufficiently assured by the proper design of the end plates. Local velocity variations with time must be avoided, however, and precautions must be taken to prevent heat interchange between the input and output pipes. In conclusion, the method has the disadvantages of giving loss alone, and of applying only to a very special type of sample. Its accuracy is apparently not sufficient, moreover, to permit measurement of small losses. On the other hand it is advantageous in that it requires no r-f equipment besides the generators, and it has a certain theoretical interest in that it can be used for absolute power measurement. Henceforth, however, only the more familiar r-f techniques will be described. The following discussion is not intended to apply to the calorimeter method.

**10.5. Details of Computation.**—It is possible to determine transmission with considerable accuracy. Most causes of error noted above in connection with  $t'$ , such as clearance or generator instability, are relatively less serious for  $t$ , and may be corrected when necessary in the same way as before. For the computation of  $\tan \delta$  from the accurate value so obtained, however, it may be observed that the simple equation given for this purpose is actually incorrect in many cases. By analogy to the procedure used in deriving Eq. (19), the interface reflection  $r$ ; was neglected and the attenuation was computed as though the wave were simply traveling a distance  $d$  through a continuous medium. In the equation for  $k$ , Eq. (19), the error due to this neglect of  $r$ ; was found to be of the second order and to be, moreover, rigorously equal to zero for many values of the thickness. In the present case, on the contrary, not only does the error persist for all values of  $d$ , but the change in  $t$  due to interface reflection—far from being negligible—is often fifty or a hundred times greater than the change due to a nonzero  $\tan \delta$ . In other words the terms neglected in the derivation of Eq. (25) are usually more significant than the terms retained, and the need for further investigation is clear.

*Exact Solution.*—In the first place, the problem may be solved exactly by the relations given in the Introduction. Thus, if  $r_i e^{-j\tau'}$  and  $t_i e^{-j\tau'}$ , as given by Eqs. (8) and (9), are substituted for the quantities  $t'$ ,  $T''$  and  $\rho''$ ,  $\tau''$  of Eq. (5),

$$te^{-i\tau'} = \frac{4 \sqrt{k} e^{-i\beta d}}{(\sqrt{k} + 1)^2 - (\sqrt{k} - 1)^2 e^{-2i\beta d}} \quad (33)$$

is found to be the complex transmission coefficient of a single lossless sheet of thickness  $d$ , when a plane wave is incident normally upon it in free space (Ref. 1b). The corresponding equation for guide is obtained

from Table 10-1, and finally application of Eq. (12) to the resulting expression gives the general relation for arbitrary loss. The two non-complex equations eventually obtained in this way are unfortunately transcendental as well as simultaneous; they may, however, be solved graphically or by successive substitution. In this latter case use is made of the fact that the computation of  $k$  is practically independent of  $\tan \delta$ , and an accurate value may be found directly by Eq. (19). This preliminary value for  $k$  is then substituted in the final form of Eq. (33), which thereupon becomes quadratic and may be solved by elementary methods. With  $\tan \delta$  equal to the value thus obtained instead of zero, Eq. (33) is used to find a more accurate  $k$ , and so on. The process converges rapidly in most cases; in fact, as was observed in connection with Eq. (19), the first value of  $k$ , computed for  $\tan \delta = 0$ , will ordinarily be correct within the experimental error.

Although numerical solution of Eq. (33) is not convenient, the values of both  $k$  and  $\tan \delta$  are obtained in principle from the measured quantities  $t$ ,  $t'$ ,  $d$ ,  $\lambda$ . If conductor losses be dealt with as suggested, no theoretical error is introduced in the transition from data to results. Of course the experimental errors remain, however, and upon more detailed investigation it is found that those in  $\tan \delta$  will be excessive for all but certain limited ranges of the parameters. Thus, the percentage change in  $t$  or  $1 - t$  caused by a positive rather than a zero value of  $\tan \delta$  is usually small; conversely, a small change in the measured transmission will often lead to a large, or even infinite, percentage error in  $\tan \delta$ . In this situation, which is the usual case for arbitrary values of  $d$  and moderate loss, the present method of loss measurement is relatively useless whether or not the exact equation be employed.

*Low Transmission.*—To obtain a large percentage change in a measured quantity, as  $\tan \delta$  increases from zero to a finite value, two procedures may be used, namely, a large value of  $d$ , or a lossy sample may be taken so that the change will actually be great in magnitude; or a sample that will have almost complete transmission for zero loss may be used, so that the percentage change in  $1 - t$  caused by  $\tan \delta$  will be large whether or not the actual magnitude is large. The first situation is expressed by the inequality

$$\exp \left[ \left( \frac{-2\pi d}{\lambda_m} \right) \left( \tan \frac{\delta}{2} \right) \right] \ll 1 \quad (34)$$

for which Eq. (5) leads to

$$te^{-jt'} \approx (1 - r_i^2 e^{-2j\pi d}) e^{\left( \frac{-2\pi jd}{\lambda} \right) \sqrt{k(1-j \tan \delta) + p}}, \quad (35)$$

instead of the exact equation corresponding to Eq. (33). Equation (35), which is valid whether the wave be *TE* or *TM*, suggests that the measure-

ments be repeated with two different values of  $d$ , as such a procedure will eliminate  $r_i$  or  $r'_i$  and lead to a nontranscendental solution for both  $k$  and  $\tan \delta$  without further approximation of any kind. Thus,

$$k = 1 + \left(\frac{\Delta}{d}\right) \left(2 + \frac{\Delta}{d}\right) (1 - p) - \left[\frac{(\lambda \ln t)}{(2\pi d)}\right]^2, \quad (36)$$

$$\tan \delta = \left(\frac{2}{k}\right) \left(1 + \frac{\Delta}{d}\right) \sqrt{1 - p} \frac{(\lambda \ln t)}{(2\pi d)}, \quad (37)$$

where  $d$  now stands for the difference between the two values of  $d$ ,  $\Delta$  for the difference in the two values of  $\Delta$ , and  $t$  for the ratio of the two values of  $t$ . For its validity this equation requires only that interaction between the two faces of the sample be negligible; in particular, it is not even assumed that  $\tan \delta$  is less than unity. To compute  $k$  and  $\tan \delta$  the result for zero loss is obtained, Eq. (19), to which Eq. (34) evidently reduces whenever  $\tan^2 \delta = 0$ ; and from this the term indicated in Eq. (36) is subtracted. Having thus found  $k$ ,  $\tan \delta$  may be computed from Eq. (37), which is equal to the square root of the correction term already found, multiplied by an easily computed factor. As may be seen from Eq. (5), the theoretical error in Eqs. (36) and (37) is of the order of

$$r_i^2 \exp \left( -\frac{4\pi d}{\lambda_m} \tan \frac{\delta}{2} \right),$$

or somewhat less if the two values of  $d$  differ by  $n\lambda_m/2$ . The experimental errors will be relatively small for the assumed situation, as the effect being measured is large in both percentage and magnitude.

The method just described was used in Ref. 8a to evaluate the loss tangent of water, for which the transmission is low enough to satisfy all the requirements noted above. It was verified that  $p$  can be neglected when  $k$  is sufficiently large, a result which is evident from Eq. (35) or from Table 10-1 of the present text. The equations appropriate to free space were used accordingly in Ref. 8a even though the measurement was carried out in guide. Such a procedure, it is perhaps worth mentioning, is usually valid for the propagation constant alone; the effective  $k$  used for interface reflection involves  $(1 - p)$  as a factor, and hence the dependence must be retained regardless of its magnitude (Table 10-1).

With the propriety of the simplified equations for  $p = 0$  verified, the presence of negligible interaction between the sample faces, which follows theoretically from Eq. (34), was checked experimentally. To this end a complete curve of transmission vs. thickness, rather than only two points as hitherto described, was obtained (see Fig. 10-11a), and  $\log t$  was plotted as shown in Fig. 10-11b. The thickness itself, which was

too small to measure directly, was obtained as the quotient of the volume of the water and its surface area. If Eq. (35) of the present text is valid, then a curve of the type given in Fig. 10-11b should be a straight line.

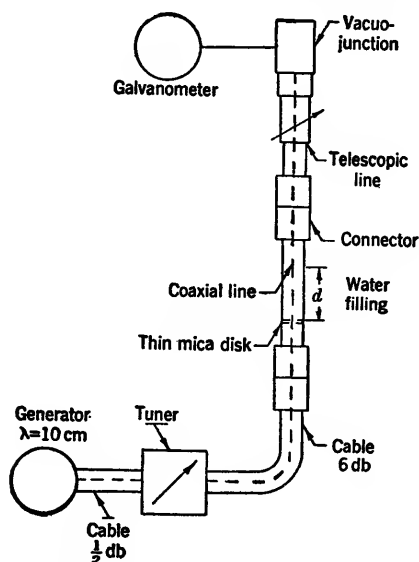


FIG. 10-11a.—Use of transmission in coaxial line to determine the loss tangent of water (from Ref. 8a).

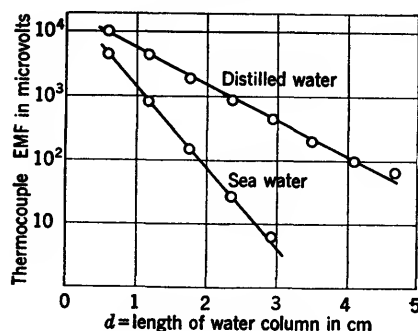


FIG. 10-11b.—Data obtained with the apparatus shown in Fig. 10-11a.

It may be shown, conversely, that if this curve is a straight line, then Eq. (35) is valid. With axes chosen to give such a linear relation, the best-fitting curve is particularly easy to find by least-square methods. The slope of this best-fitting curve (that is, straight line) gives the proper values for substitution in Eq. (35). No error is introduced by the mica partition, for Eq. (5), which leads immediately to Eq. (35), assumes

nothing about the origin of  $t''$ ,  $r''$ ,  $T''$ ,  $R''$ . Thus, Eq. (35) and the cancellation attendant upon taking the ratio of  $t$ 's, remain valid for the present situation if  $t_i e^{-j\alpha}$  be interpreted as the transmission coefficient of the three-medium transition from air to mica to water. Similarly, the error term  $r_i^2 \exp [-(4\pi d/\lambda_m) \tan \delta/2]$  remains valid if  $r_i$  be taken as the over-all reflection of the same three-medium transition.

This investigation described in Ref. 8a, which has been here discussed in some detail, was carried out with regard to water alone, but many of the principles employed have a general validity that is relevant to less specialized problems and may well be given a place in the present discussion. Such a principle is embodied in the use of a complete curve of  $k$  or  $\tan \delta$  vs. some easily varied parameter (Fig. 10-11b); not only does it give a check for certain inaccuracies but it often leads to an increase in accuracy by virtue of the well-known behavior of probable error in such circumstances. Similarly, cancellation of the effect of the mica separator, which is shown by Eq. (5) to be obtained regardless of the transmission or loss, is often found for extraneous effects of this sort if a ratio is taken as here described. A third principle, which is likewise of general utility, is the modification of procedure and theory to suit the special problem at hand. Thus, the fact that  $k$  was large in this particular case permitted use of the somewhat simpler free-space equations; similarly, the fact that the interface reflection is large with  $k$  large suggested that the maximizing procedure described, rather than some other method, be used for finding the transmission. And finally, the fact that the sample was a liquid permitted use of a novel and accurate method of measuring the thickness. Although they are not specifically

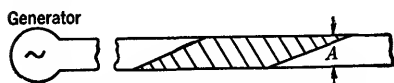


FIG. 10-12.—Use of tapered ends to eliminate interface reflection.

mentioned here with every method treated, it is clear that such procedures, and similar ones which will suggest themselves to the reader, are sometimes of considerable utility in dielectric measurement.

*Moderate or High Transmission.*—It frequently happens that the loss is too low for Eq. (34) to be satisfied with conveniently small values of  $d$ . In this case a large magnitude for the measured effect of  $\tan \delta$  cannot be obtained, but it is still possible to obtain a large percentage effect by the procedure outlined above. Specifically, a sample is used that would have high transmission for zero loss, whereupon the value of  $1 - t$ , which can be measured directly, will depend critically on  $\tan \delta$ . Thus, instead of measuring a large quantity with high accuracy a small quantity is measured with moderate accuracy, an operation which is considerably more practicable. To achieve the desired characteristics of the sample the technique suggested in Fig. 10-12 may be used, where

reflection at the air-sample interfaces is practically eliminated by the taper.<sup>1</sup> Higher modes are obviated when the inner dimension  $A$  of the guide satisfies the condition

$$A < \frac{\lambda}{2\sqrt{k}}, \quad (38)$$

and in other particulars the equipment remains as described above. There is an error in  $t$  caused by the less-than-unity transmission of the taper, which is eliminated by the following procedure: two measurements with different values of  $d$  are taken and the difference between these values, the difference between corresponding  $\Delta$ 's, and the ratio of the  $t$ 's are used rather than the quantities themselves in Eqs. (36) and (37). The conditions for validity and errors are the same as before but where the accuracy was formerly attained by making  $d \tan \delta$  large, it is now attained by making  $r_i$  small. It should be observed that Eq. (37) reduces to Eq. (25) whenever  $\tan^2 \delta \approx 0$ , although the symbols must be given their present significance of differences or ratios. Despite the fact that complete neglect of  $r_i$  is inadmissible, it is thus apparent that appropriate experimental conditions allow the treatment of the theory as if it were indeed a valid approximation. It is in this sense that Eq. (25) may be considered correct.

*Half-wavelength Sample.*—Although the foregoing techniques arose from experimental necessity rather than from theoretical convenience, they actually led to much more manageable relations than those obtained for the general case. The need for having  $1 - t$  depend critically on  $\tan \delta$  suggests one other specialization of this type, which likewise gives simple theoretical relations, namely, a sample with  $d = n\lambda_m/2$  may be used. The necessary preliminary estimate of  $\lambda_m$  causes no difficulty, as it depends primarily on  $k$ , which may be determined with an arbitrary value of  $d$ . Thus a simplified form of the exact expression for Eq. (33) is obtained, which reduces to

$$t = \frac{4ae^{-b}}{(a+1)^2 - (a-1)^2e^{-2b}}, \quad (39)$$

$$a = \sqrt{\frac{k-p}{1-p}}, \quad b = \frac{k\pi n}{2(k-p)} \tan \delta,$$

when  $\tan^2 \delta = 0$ , as may be seen from Refs. 6b and 8b. The two results are compared in Fig. 10-13, where the elementary quadratic Eq. (39) is shown to be valid in all cases not covered by Eq. (34). Although

<sup>1</sup> This method of measurement, with an  $E$ -plane taper to eliminate interface reflection, was suggested and used by E. L. Younker (Ref. 6a). Waveguide transmission was apparently used to determine  $\tan \delta$  for solid low-loss materials in Refs. 17c, 18c, though no description of procedure is given.



the thickness for maximum transmission is an exact half-wavelength only when  $\tan \delta = 0$ , the deviation is negligible for the present application; hence the value of  $t$  for substitution in Eq. (39) may be most accurately determined by measuring transmission vs. thickness near  $d = n\lambda_m/2$ .

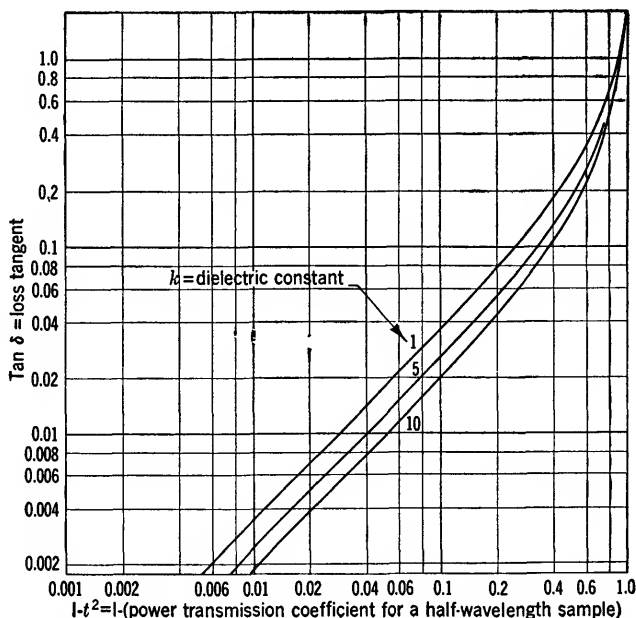


FIG. 10-13.—Exact and approximate curves for  $\tan \delta$  from the transmission of a half-wavelength sample. If the approximate equation is valid, these curves may be used for a sample of thickness  $n\lambda_m/2$  provided  $\tan \delta$  is replaced by  $n \tan \delta$ .

**Wall Losses.**—The loss introduced by the waveguide itself has hitherto been neglected, although it is frequently comparable with that of the sample. This loss is not the same with the filled as with the empty guide, for not only are the energy relations changed by the presence of a dielectric, but the field in the sample is often a standing-wave field rather than the traveling-wave field formerly obtained. The error is accordingly not canceled by the bridge procedure as would perhaps be expected, and special compensation is necessary.

If the *empty* guide were completely lossless,

$$(\tan \delta_{\text{measured}}) = (\tan \delta_{\text{sample}}) + (\tan \delta_{\text{wall}}) \quad (40)$$

would be obtained<sup>1</sup> when measuring the transmission of the sample con-

<sup>1</sup> This method of treating wall losses, which will be repeatedly used in the present text, is due to A. R. von Hippel (Ref. 1a).

tained in a piece of the actual lossy guide. The condition of zero loss for the empty guide may be simulated if the substitution is made

$$t = t_{\text{measured}} \cdot \exp \left[ \left( -\frac{\pi d}{\lambda} \right) (\tan \delta_{\text{wall}}) \sqrt{1 - p} \right], \quad (41)$$

and hence wall losses may be readily corrected whenever  $\tan \delta_{\text{wall}}$  is known. To determine this parameter,  $t$  is measured for two widely differing lengths of empty guide, whereupon the appropriate form of Eq. (25), with  $k = 1$  and  $t =$  ratio of transmissions, gives the desired result. Since the loss is of concern here rather than  $k$ , the large path difference used for finding  $\tan \delta_{\text{wall}}$ , with consequent magnification of the effect of frequency drift, causes no undue error in normal practice.

**10-6. Uses.**—The utility of the present method lies chiefly in two characteristics, namely, it does not require a probe of any sort and sharpness of resolution may be attained even with great path lengths. The first characteristic is relevant because of the demonstrated superiority of the short-circuited-line method presently to be described which, however, requires a traveling probe. Although standard at the longer wavelengths, equipment of this type is not easily designed for wavelengths much below one centimeter. On the other hand, it is precisely in this range of very short wavelengths, for which  $d$  may be much greater than  $\lambda_1$  that the present method appears to best advantage.

The second property, independence of path length, is particularly useful for the study of gases, in which the necessarily long guides, with their attendant high losses, give such a broad minimum with the short-circuited-line method as to render it practically useless. Transmission techniques are open to no such objection, the sharpness of the minimum depending on waveguide attenuation only to the extent that this attenuation reduces the available power. For measurement of gases, incidentally, not only is the advantage just described obtained, but also most of the sources of error, including all those involving  $r_i$ , are negligible since  $k \approx 1$ .

#### MEASUREMENT BY TRANSMISSION IN FREE SPACE

In all methods requiring the use of a guide, the preparation of the sample usually takes much more time than the actual process of measurement. If the methods are modified as suggested in Fig. 10-14 this preliminary step is eliminated for most production materials that are normally supplied in sheet form, and the resulting saving of time is considerable. Besides this increase in speed and simplicity, the experimental procedure, which is evident from the preceding discussion and from Fig. 10-14, has the additional advantages that there are no errors from clearance and that systematic error from other causes may be

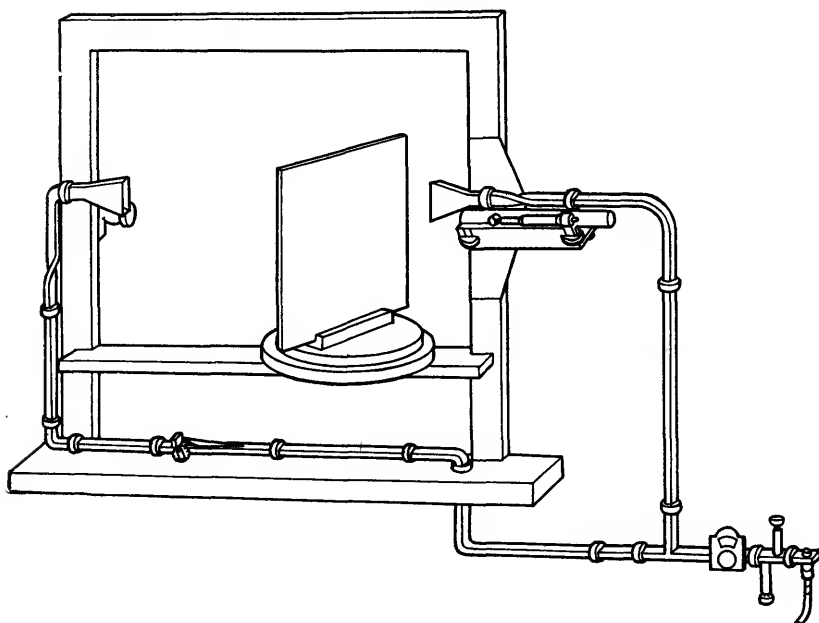


FIG. 10-14a.—Equipment for measurement of phase in free space.

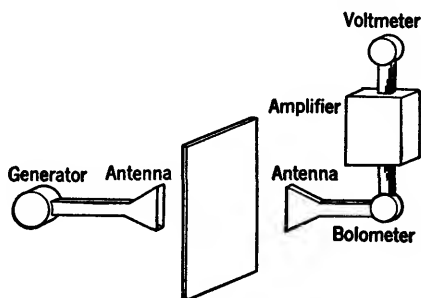


FIG. 10-14b.—Equipment for measurement of transmission in free space.

conveniently investigated by the use of several angles of incidence. If  $p$  is set equal to zero in Eq. (19), or by direct calculation from Eq. (15) with  $\delta = 0$ , the relation

$$k = \left(1 + \frac{\Delta}{d}\right)^2, \quad \theta_0 = 0, \quad (42)$$

results as an approximate equation for the dielectric constant  $k$  in terms of the sample thickness  $d$  and the phase difference  $\Delta$  obtained for the air gap with and without sample (Ref. 6a). The details for more rigorous

calculation will be given; it suffices here to observe simply that  $k$  can be determined once  $\Delta$  is known.

**10-7. Experimental Procedure for Normal Incidence.**—Although much of the discussion given in Secs. 10-3 to 10-5, including almost all results on amplitude measurement, applies without change to the present situation, there are a few differences for phase measurement which are of sufficient importance to be mentioned explicitly. With regard to the equipment itself (cf. Ref. 6a), a sufficiently long guide must be used in Fig. 10-14a to avoid undue strain as the micrometer setting is altered; the horn must be constrained to move in a straight line without nodding; and the micrometer itself must be aligned parallel to the direction of this motion. With these precautions, the first important difference between this and the previous techniques is that the present equipment need not be calibrated and  $\Delta$  may be read directly from the micrometer. Unlike those customarily used in waveguide work, moreover, a phase shifter of this type gives an accurately symmetrical minimum; hence the position may be computed as the average of two values for equal meter readings, (see Fig. 10-15). This process leads to a significant increase in accuracy by virtue of the nonzero derivative (cf. Sec. 10-13). With drift eliminated as described later, absolute accuracies of the order of 0.0005 $\lambda$  are found to be attainable with relatively crude equipment, and the sensitivity is such that a single sheet of paper inserted in the air gap may increase the meter reading by a factor of ten.

*Inconstant Frequency.*—With such precision the effect of drift becomes increasingly important; on the other hand, the expedient of using equal paths no longer avails for the equipment of Fig. 10-14. Upon calculation of the derivative, the equation

$$a = 2b + c\sqrt{1-p} \quad (43)$$

should be satisfied for minimum sensitivity to drift (Ref. 6a), in which case

$$c' = c \left[ \frac{\lambda\lambda'}{\lambda_0^2} + \sqrt{(1-p)(1-p')} \right], \quad (44)$$

for the change  $c$  to  $c'$  in micrometer setting produced by a change of  $\lambda$  to  $\lambda'$  in transmitter frequency when the sample is not present. An exact criterion of this kind of course depends to some slight extent on the material between the horns, and is moreover impossible to satisfy exactly

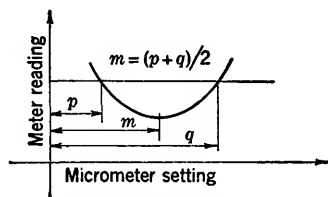


FIG. 10-15.—The location of the minimum of a symmetrical curve by using points of nonzero slope;  $m = (p + q)/2$ .

for two different materials, for example, for air alone and at the same time for air plus dielectric. As a compromise adjustment for this effect, which is of secondary importance, a value may be given to  $a$  slightly higher than that indicated by Eq. (43). A similar method is applicable to the waveguide equipment already treated, although for all ordinary work it is unnecessary in either case.

If the equipment is designed with paths of equal geometrical or electrical lengths, rather than with paths satisfying Eq. (43), the equations corresponding to Eq. (44) indicate considerably greater sensitivity to drift, as would be anticipated from the nonzero derivative. By Table 10-3, which gives a comparison of such equations with that just obtained, it is seen that the optimum condition Eq. (43) is satisfactory even with rather unstable oscillators, and that these other conditions may on the contrary lead to large errors in practical work (cf. Ref. 6a). Unlike the result for waveguide measurement, the present relations sug-

TABLE 10-3.—THEORETICAL EFFECT OF FREQUENCY DRIFT IN FREE-SPACE EQUIPMENT

Transmitter wavelength, in.	Change in micrometer setting for minimum, $c = 22$ in., $\lambda_c = 0.84$ in.		
	Equal geometrical lengths, $a = 2b + c$ , in.	Equal electrical lengths, in.	Correct adjustment, in.
0.5000	0.000000	0.000000	0.000000
0.5001	0.001100	0.002442	0.000000
0.5005	0.005412	0.012100	0.000002
0.5010	0.010736	0.024112	0.000013
0.5100	0.110638	0.245256	0.002442

gest that complete insensitivity to drift is unattainable even when the effect of the sample is neglected. From more detailed analysis it is indeed found that such insensitivity may be achieved if, and only if, every guide with a given dielectric and  $\lambda_c$  in one branch of the circuit be balanced by a similar guide of the same length in the other. For the present case, a second air gap would be required, which would be inconvenient in normal practice.

*Errors Similar to Those in Guide.*—Except for inaccuracy specifically caused by the use of a guide, which is not found in the free-space measurement, the errors are essentially the same as those described in Secs. 10-3 to 10-5. Analogous to the clearance error, for example, is the error produced by diffraction around the edge of the sample, which is discussed quantitatively in what follows. For our present purposes, the error analogous to clearance may be eliminated altogether if the sample is

sufficiently large. Besides this error, which is corrected without the use of accurately prepared samples, additional inaccuracy occurs as before from interaction between various parts of the equipment. In Ref. 6a it is shown theoretically and experimentally that the effect of interaction between the two antennas is practically negligible. By the methods of Refs. 6a and 7a it is also possible to eliminate error from the interaction between antenna and sample. Thus, a graph of measured  $\Delta$  vs. the distance from sample to antenna should theoretically<sup>1</sup> be a sine curve, nearly, with period  $\lambda/2$ , as is seen from Ref. 7a. Hence the procedure previously advocated for compensating Y-joint reflection likewise applies in the present instance, that is,  $\Delta$  may be taken as the average of the two values found for a quarter-wavelength motion of the sample (Ref. 6a). Other details of this sort need not be reiterated here; in particular the comments of Sec. 10-5 relative to the measurement of  $\tan \delta$  remain valid for free space.

*Spherical Wavefront.*—A source of error which is unlike interaction in that it has no analogue for waveguide work is the fact that the wavefront incident on the sample is essentially spherical rather than plane. As is seen from Fig. 10-16, the effect is qualitatively similar to that obtained by taking a number of readings for various angles of incidence near normal and averaging the results in some suitable way. To the extent that this simple mechanism represents the true effect it can be said, by virtue of Eqs. (47) and (52) and the accompanying remarks, that the error in practice will usually be very small. It may be investigated experimentally by taking measured  $k$  or  $\tan \delta$  vs. the distance from transmitter to sample, a procedure which was suggested and used in Ref. 14a.

Besides thus changing the "effective angle of incidence" (if one may be permitted such a term for waves which are not plane), the spherical phase-front has the added effect of producing inverse-distance attenuation; hence the amplitude distribution through the sample will not have the uniformity hitherto assumed, even along the axis. Points off the axis are illuminated nonuniformly in accordance with the antenna pattern, an effect commented on in Ref. 7a. Whether significant error from this attenuation would be encountered in practice is a matter not easy to determine with assurance, although the similarity of propagation constants for plane and spherical waves would indicate that no appreciable error should be observed when interface effects are negligible. For moderately thin samples the effect in question would likewise be expected to be small, a conclusion which has been verified experimentally in that the results are independent of both thickness and angle of incidence (cf. Refs. 6a, 7a, and Sec. 10-18). It is worth noting, incidentally, that

<sup>1</sup> That such behavior is found in practice is verified by the curves of Fig. 19c.

this inverse-distance attenuation gives a simple and accurate method of investigating the receiver characteristics. Thus, if the antennas are sufficiently far apart for the application of Fraunhofer theory, if they are kept oriented for maximum pickup, and if care is taken to avoid interference between the antennas themselves (Ref. 7*a*) or from surrounding objects, then a log-log plot of receiver reading vs. the distance between antennas should be a straight line with slope equal to the law of the detector. Such a curve was actually obtained in Ref. 14*a*, and used as a check on the linearity of the receiving system.

In connection with error from the spherical wavefront it is natural to inquire whether more accurate results will be obtained, for given antenna separation, with the sample near the receiver than with the

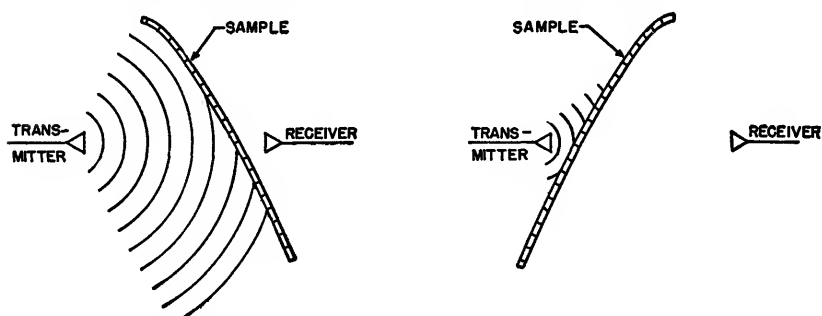


FIG. 10-16.—Spherical wavefront obtained in free-space measurement. The sample is shown as curved to indicate the generality of the result in the text, which is valid for such samples or for arbitrary incidence, and to illustrate the nature of the symmetry required.

sample near the transmitter. Intuitively an affirmative answer would perhaps be expected to this question, since the incident wave certainly becomes more nearly plane, both in phase and in amplitude, as the distance from sample to transmitter increases (Fig. 10-16). Despite this intuitive reasoning, however, the two positions are found to be essentially equivalent whenever the antennas are alike: for the situation of Fig. 10-16*b* can then be obtained from that of Fig. 10-16*a* by merely reversing the direction of power flow. If the general reciprocity theorem is applied to the system when the sample is not present, and then when it is, the ratio of complex transmission with sample to that without, which is the measured transmission coefficient, will be the same in Fig. 10-16*a* as in Fig. 10-16*b*. It follows that  $\Delta$  and  $t$  are both unchanged, and hence the error due to the curved wavefront is presumably the same in both cases. Some slight error in this argument is to be anticipated in that one of the antennas is moved during the measurement, though the qualitative conclusion is not thereby invalidated. In practice, nevertheless, the sample should be placed nearer to the receiver, though for an

entirely different reason (Ref. 6a), namely, to prevent the so-called "pulling" of the microwave generator.

**10-8. Computations for Normal Incidence.**—The calculation of  $k$  from  $\Delta$  may be made, in principle, by setting  $p = 0$  in the waveguide equations, which then become equally valid for free space. Because of the restrictions introduced by having the sample in sheet form, however, these relations are for the most part rather inappropriate and therefore may be supplemented with equations specifically derived for the case at hand. The restrictions in question chiefly involve the sample thickness  $d$ , which can be given fairly large values and changed at will in guide, but which is usually small and difficult to change for free space. With the choice of  $d$  thus circumscribed, the analogue of Eq. (19), Eq. (42), is quite inaccurate theoretically, a situation that is the more serious in view of the high precision possible experimentally. For quantitative consideration Eq. (42) actually represents the exact limiting value (always neglecting  $\tan^2 \delta$ ) which would be approached as  $d$  approaches infinity; and when  $d$  approaches zero, on the other hand, this exact limiting value is given by

$$k = 1 + \frac{2\Delta}{d},$$

as can be seen by Ref. 6a or by Eq. (45). In intermediate cases Eq. (33) gives the transcendental but real equation

$$\left(\sqrt{k} + \frac{1}{\sqrt{k}}\right) \tan\left(\frac{2\pi d \sqrt{k}}{\lambda}\right) = 2 \tan t', \quad (45)$$

which is likewise exact for  $\tan^2 \delta = 0$  and which may be solved by graphical means (Fig. 10-17). With a direct solution of this kind, however, the plot required for accurate work is of almost prohibitive size, and therefore another procedure is sought.

*Method Permitting Accurate Graphical Computation.*—If Eq. (42) and Eq. (45) are combined (Ref. 6a),

$$\Delta_{\text{meas}} - \Delta_{\text{desired}} = \frac{\lambda}{4} - d \sqrt{k} - \left(\frac{\lambda}{2\pi}\right) \tan^{-1} \left[ \frac{2 \sqrt{k}}{1 + k} \cot \left( \frac{2\pi d \sqrt{k}}{\lambda} \right) \right] \quad (46)$$

is obtained for the difference between the  $\Delta$ 's which would lead to Eq. (42) and the true value of  $\Delta$  as actually measured. From this equation, which is plotted in Fig. 10-18, the value of the error in question cannot only be estimated but can also be corrected. Thus, the value of  $k$  is found from Eq. (42), which usually gives a value accurate enough for negligible error in Eq. (46). From Eq. (46) or from Fig. 10-18 the desired value of  $\Delta$  may be obtained and substituted in Eq. (42) to find the true value of  $k$ . Although essentially a process of successive sub-



stitution which may be indefinitely continued, the values converge so rapidly that a single operation suffices for practically all cases. By virtue

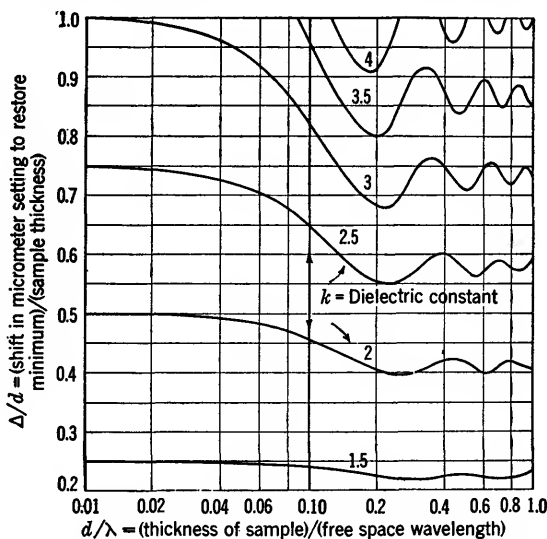


FIG. 10-17.—Exact relation between  $k$  and  $\Delta$  for free space, normal incidence, and negligible  $\tan^2 \delta$ .

of the equivalence relations of Table 10-1, this method of compensation may also be applied to measurements in guide, although the use of samples

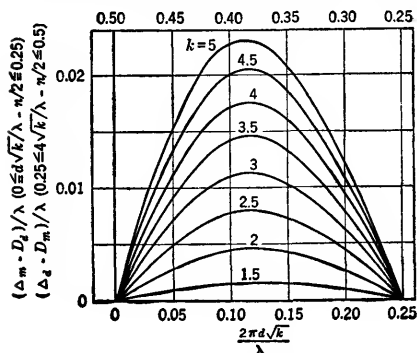


FIG. 10-18.—Error in approximate equation as a function of thickness and dielectric constant. The quantity  $\Delta_m$  is equal to the measured value of  $\Delta$  and  $\Delta_d$  represents the desired value, that is, the value of  $\Delta$  for which  $k = (1 + \Delta/d)^2$ .

implicitly, Eq. (39) explicitly, and in other cases the free-space method should not be used at normal incidence for finding loss. If  $\tan \delta$  is already

thin enough to make such a procedure necessary is not particularly to be recommended.

*Loss.*—It has so far been assumed that  $\tan^2 \delta \approx 0$ . In the few cases for which this assumption is not valid certain of the waveguide equations may be used, although the expedients suggested for eliminating the effect of  $r_i$  in guide are usually no longer practicable here. Similarly, it is not usually possible to obtain a large effect from  $\tan \delta$  in free space, unless the sample happens to be such that  $d = n\lambda_m/2$ . For this case Eq. (33) gives the required result

known, however, its effect on the measured value of  $k$  may be compensated, the procedure being to use  $(1 + r_i)^2/(1 - r_i)^2$  in place of  $k$  in Fig. 10-18,  $d/\lambda_m$  in place of  $d\sqrt{k}/\lambda$ , and from the value of  $k$  thus obtained to subtract the correction term of Eq. (36) with  $p = 0$ . Such complications seldom arise, however, in ordinary practice.

It must be mentioned that there is one notable exception to these inconveniences that are usually attendant upon free-space measurement of  $\tan \delta$ . The exception in question concerns the sample itself, which may be readily and accurately measured provided it is sufficiently lossy for the validity of Eq. (34) with manageable values of  $d$ , and of such a form (almost necessarily liquid) that  $d$  may be easily changed, and available in sufficient quantity to permit use of a sample large enough to obviate diffraction. With such samples the procedure suggested for comparable circumstances in guide is valid for free space as well; in particular the calculations may be made by Eqs. (36) and (37) with the symbols as there defined and with  $p = 0$ . Of course the number of materials fulfilling the above requirements is somewhat limited, although the requirements are admirably met by water, which was successfully investigated (Ref. 14a) by the free-space method as described here. For reasons already mentioned, however, free-space measurement of  $\tan \delta$  is not to be recommended as a procedure of general utility.

**10-9. Arbitrary Incidence.**—Although error due to interaction may be canceled with the foregoing procedures, the labor of experiment and computation is considerably increased. The possibilities of the free-space method are not exhausted by the foregoing discussion, however, since the process of measurement is often more convenient and accurate at arbitrary than at normal incidence. In this case the errors due to interaction are automatically eliminated. Thus, instead of returning to the antenna, as in Fig. 10-19a, the wave reflected from the sample is directed away from the equipment as shown in Fig. 10-19b, and thus the measured value of  $\Delta$  should be substantially independent of sample position. That such is the case in practice is shown in Fig. 10-19c; it is therefore unnecessary to duplicate the measurement with a quarter-wavelength

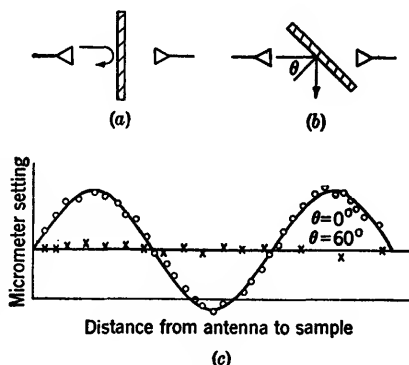


FIG. 10-19.—Interaction between sample and antenna at arbitrary incidence. (a) Normal incidence. (b) Not normal incidence. (c) Micrometer setting vs. sample position at  $\lambda = 1.25$  cm. Points are experimental, curve is best-fitting sine curve with period  $\lambda/2$ .

displacement when the incidence is far from normal. The appropriate form of Eq. (42) with either polarization may be written

$$k = 1 + 2 \left( \frac{\Delta}{d} \right) \cos \theta + \left( \frac{\Delta}{d} \right)^2, \quad (47)$$

for incidence  $\theta$  and negligible interaction between the sample faces (see Fig. 10-20). The equation may be obtained by setting  $p = \sin^2 \theta$  in Eq. (19), or directly by Eq. (42) and the  $\beta$ -equivalence of Table 10-1, since the phase is measured perpendicular to the wavefront in free space

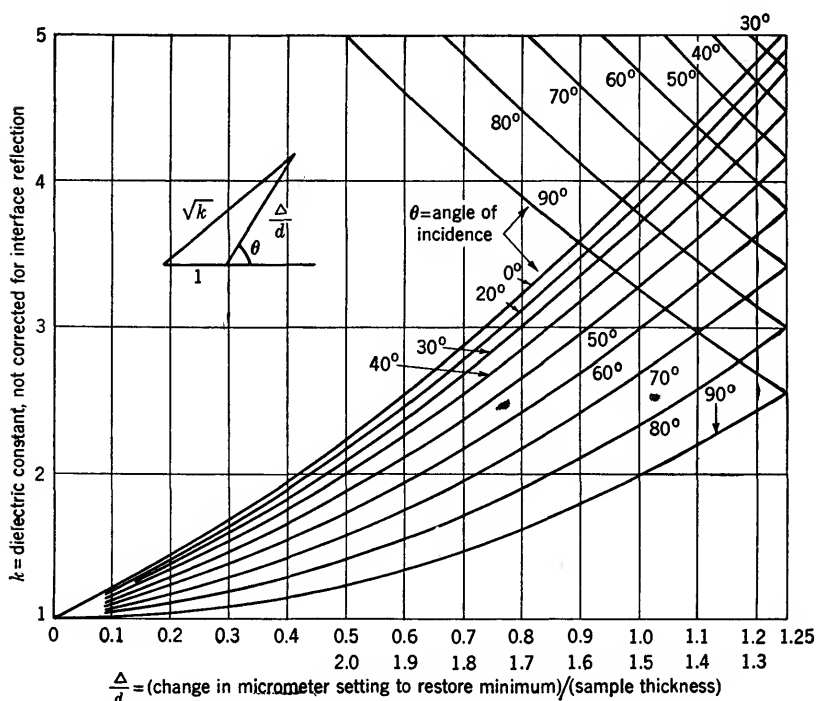


FIG. 10-20.—Approximate curves giving dielectric constant in terms of the phase shift at arbitrary incidence in free space.

and perpendicular to the sample in guide. Thus, the value of  $\Delta$  in the earlier result or in the table corresponds to  $\Delta \cos \theta$  in the present case, a substitution which is frequently necessary in progressing from normal incidence or guide equations to those of the type in question here.

*Interface Reflection.*—Like interaction between sample and antenna, the interaction between the two faces of the sample, which necessitated the correction associated with Fig. 10-18, may be eliminated automatically by the use of arbitrary incidence in many cases. For quantitative

investigation (cf. Refs. 7b, 6a),

$$\frac{\lambda}{2\pi} \sin^{-1} r_i^2 \approx \frac{\lambda}{2\pi} [r_i^2 + O(r_i^6)] \quad (48)$$

is found to be the maximum error in  $\Delta$  due to  $r_i$  as the thickness is changed. This expression follows directly from Eq. (5) and is correct without approximation in guide as well as for arbitrary incidence at either polarization in free space, if the appropriate value of  $r_i$  be used in each case. From the curves of Fig. 10-21 it is seen that the error is much larger for

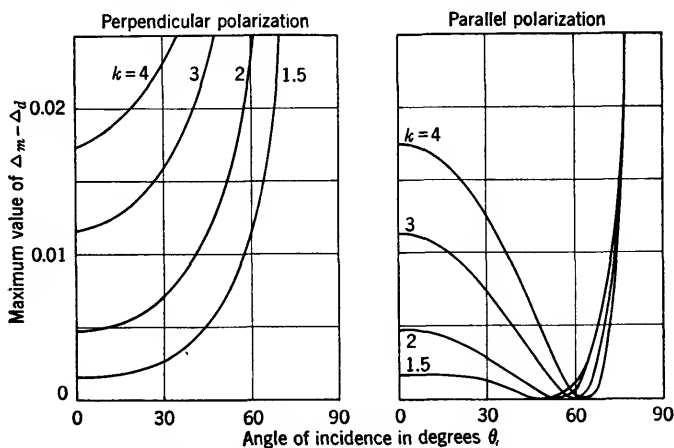


FIG. 10-21.—Maximum error in  $\Delta$  due to interface reflection for polarization perpendicular or parallel to the plane of incidence.

perpendicular than for parallel polarization, in agreement with the well-known behavior of interface reflection; with parallel polarization the error is zero, as it should be, when  $\theta$  equals the polarizing or Brewster angle,

$$\theta_b = \tan^{-1} \sqrt{k}. \quad (49)$$

In practice it is inconvenient to set  $\theta$  to this value exactly, particularly when  $k$  is unknown; however, the error is so small that the exact determination of the proper  $\theta$  is unnecessary in any case. For example, if  $\theta = 60^\circ$  is taken independently of  $\Delta$ , the maximum possible error is shown by Fig. 10-21b to be less than  $0.001\lambda$  whenever  $1 \leq n \leq 4.5$ , an error which is negligible for all but the most exacting work. If for any reason  $\theta$  must be very far from  $\theta_b$ , however, the correction of Fig. 10-18 may also be used at arbitrary incidence by means of the substitutions of Table 10-1. Such a situation arises when the sample is unusually thick, as the beam shift, due to refraction, will then lead to erroneous results whenever  $\theta$  deviates appreciably from zero (cf. Ref. 6a). It is worth

remarking that a similar reduction of interface reflection is obtained when a *TM*-wave is used in a guide giving an appropriate value of  $p$ , though such a procedure has apparently not yet been used in practice.

*Loss.*—The reduction of  $r_i$  obtained with incidence other than normal may also be applied to measurement of loss, which satisfies

$$\begin{aligned}\tan \delta &= -\frac{\lambda \ln t}{\pi k d} \frac{\sqrt{k-p}}{k} + O(\tan^2 \delta), (\theta \approx \theta_b), \\ &= -\frac{\lambda \ln t}{\pi d \sqrt{k+1}} + O(\tan^2 \delta), (\theta = \theta_b),\end{aligned}\quad (50)$$

whenever  $\theta$  is sufficiently near to  $\theta_b$ .

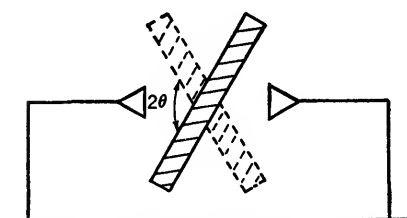


FIG. 10-22.—Determination of the true angle of incidence.

In the few cases for which neglect of  $\tan^2 \delta$  is inadmissible the appropriate relation may be obtained by Eqs. (12) and (33) and Table 10-1, with due regard to the mode of measuring  $\Delta$  [cf. Eq. (47) and accompanying remarks]. In both Eqs. (47) and (50) it is worth noting that change of polarization affects only the error term  $r_i$ , not the value of the main expression;

hence the presence of slight cross-polarization may be justifiably neglected.

*Measurement of Angle of Incidence.*—With the above procedure it is necessary to know the true value of  $\theta$ , which cannot be found by geometrical measurements alone. For this reason it is advisable to modify the normal-incidence technique, taking  $\theta$  rather than the micrometer setting as the variable used to minimize the received power. Thus,  $\theta$  is set at about  $60^\circ$ , or at any other desired value, and the micrometer is adjusted for minimum. With this fixed micrometer setting,  $\theta$  is adjusted for minimum reading on the original and on the other side of  $\theta = 0$ , as suggested in Fig. 10-22, the fixed attenuator being inserted during the transition. The average of the two values so obtained is the true angle of incidence (Ref. 6a), and  $\Delta$  is found, as usual, from the fixed micrometer setting as compared with that obtained without the sample. Because  $\cos \theta$  varies so slowly when  $\theta$  is near zero, this difficulty does not arise with the normal-incidence method, that is, Eq. (42) remains valid over a range of perhaps  $\pm 10^\circ$  in most cases, and hence the adjustment may be made by inspection (cf. Eq. (52)).

*Sample Size.*—Besides this extra difficulty in determining  $\theta_0$ , the use of arbitrary incidence has the disadvantage of leading to large errors from diffraction in certain cases. Although the error can still be eliminated when the sample is sufficiently large, the size required is often prohibitive for materials not in industrial production. At the shorter

wavelengths this diffraction effect should theoretically depend chiefly upon the projected width of the sample, the minimum permissible size being accordingly given by an equation of the form

$$\text{Minimum permissible width} = A \sec \theta, \quad (51)$$

with the constant  $A$  depending only on the sample position and type of equipment. That such intuitive results are valid in practice is verified

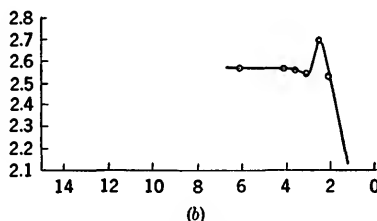
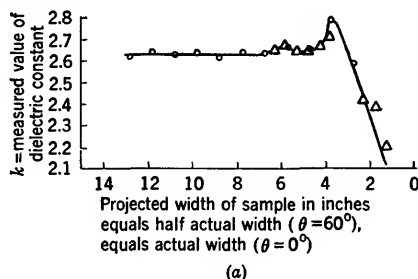


FIG. 10-23.—Effect of diffraction on apparent value of  $k$ , as measured by the phase shift for transmission in free space. In *a* the distance from the center of the sample to the receiver is 4.5 in.; the circles are for  $\theta = 0^\circ$ , the triangles are for  $\theta = 60^\circ$ . In *b* the center of the sample is 0.5 in. from the receiver, and  $\theta = 0^\circ$ .

by Fig. 10-23*a*, where a curve of measured  $k$  vs. projected width is seen to be nearly the same at  $\theta = 0$  as at  $\theta = 60^\circ$ . For this particular case the constant  $A$  of Eq. (51) happens to be about 7 in. when the axis of rotation is 4.5 in. from the antenna, and about 4 in. when the distance is 0.5 in. (Fig. 10-23*b*). This decrease of  $A$  with the distance to the nearest antenna is likewise to be expected intuitively; obviously the axis and antenna should in practice be as close as the construction of the system will permit. Although no reliable method of compensation has been found, curves of the type shown in Fig. 10-23 permit estimation of the error in question or, alternatively, of the sample size required to reduce this error to negligible proportions, and only one or two curves are required for any given equipment. If it is desired merely to verify that the particular sample used is sufficiently large, without determining

the minimum size, a nontransmitting sample of the same size may be substituted. If the receiver reading is zero, independently of the micrometer setting, the size is ample. Such a procedure is described for checking the amplitude measurement in Ref. 14a.

**10-10. Comparison with Optical Methods.**—Before the subject of transmission as a means of determining  $k$  is left, a brief comparison of the microwave techniques described here with the closely analogous interferometer procedures of optics will be given. In optics the phase is usually measured by counting interference fringes, whereas in microwave techniques the micrometer setting is adjusted for minimum received power. The results obtained in the optical region are evidently considerably less accurate; phase errors of many degrees are possible. With microwave techniques, accuracies of the order of  $0.1^\circ$  are regularly obtained. In optical work, moreover, the effects of interaction are neglected, all results being computed from Eq. (42) or similar equations without correction of any kind; but this source of error has been considered in detail and compensated for in the microwave procedures just outlined.

From this superficial examination it might perhaps be concluded that optical methods usually lead to less precise values for  $k$  than those obtained with microwaves. Actually, however, such is far from the case. In fact, optical methods usually give two or three more significant figures than are at present attainable in the microwave region, quite irrespective of the inaccuracies noted. The approximate relations for  $k'$ , the numerical error in  $k$ , may be written

$$k' \approx \left(\frac{2}{d}\right) \left[ \left( \cos \theta + \frac{\Delta}{d} \right) \left( \Delta' - \frac{d'\Delta}{d} \right) - \theta' \Delta \sin \theta \right],$$

and

$$k' \approx \left( \frac{2\sqrt{k}}{d} \right) [\Delta' - d'(\sqrt{k} - 1)], \quad \theta = 0,$$

in terms of  $\Delta'$ ,  $d'$ ,  $\theta'$ , the numerical errors in  $\Delta$ ,  $d$ ,  $\theta$  respectively. From this equation it is seen, among other things, that the error depends on the ratios  $\Delta'/d$ ,  $d'/d$ ; it does not depend on the angular errors  $\Delta'/\lambda$ ,  $d'/\lambda$ . Thus, although  $\Delta'$  can be measured with only moderate angular accuracy at optical frequencies, it can be measured with high accuracy in length; it is in this sense that accuracy is required by Eq. (52). Looking at the question from a different point of view it may be said that the actual phase change  $\Delta$ , in degrees, is extremely large for optical work, and hence an error  $\Delta'$  of ten or twenty degrees is a negligible fraction of the total. From still a third point of view it may be found that  $\Delta$  is really its measured value, which is less than a wavelength, plus a term  $n\lambda$ ; although  $n$  is usually zero or a small integer in microwave work, it may

be as high as 10,000 in optics. By far the greater contribution to the  $\Delta$  substituted in Eq. (47) accordingly comes from  $n\lambda$ , which is accurately known because  $\lambda$  is; and a given percentage error in the measured quantity  $\Delta$  will therefore lead to a smaller percentage error in  $\Delta + n\lambda$ . Such considerations all depend on the fact that  $d \gg \lambda$ , and it is this condition that gives to optical methods their superior accuracy. Such a condition is unattainable to anything like the same extent with microwaves. The advantage of greater accuracy in phase measurement and in computation, then, is more than offset by the decreased sample thickness as measured in terms of wavelengths; whereas the refinements here mentioned would perhaps affect the eighth significant figure in optics, and could be ignored, they will usually affect the second or third figure in microwave work, and must be retained.

**10-11. Uses.**—The experimental and theoretical procedures for determining  $k$  by measurement of transmission in free space having been indicated, the applications will be discussed briefly. There are two characteristics of especial interest, namely, the method entails no preparation of the sample, and the phase shifter can be designed in such a way as to require no calibration. Because of this first property the method is particularly suitable for routine testing, in which a large number of determinations are to be made in a short time. Although many applications are of this type, it is often desirable to achieve great accuracy in a few determinations. The free-space method offers certain advantages here also, as the errors all decrease with increasing sample thickness and there are no serious systematic errors. In particular, there are no errors from clearance if the sample is sufficiently large. Accuracies of the order of a few tenths of one per cent are readily achieved for thick low-loss samples, and variation of  $\theta$ , which is quite convenient in practice, leads to independent values of  $k$  as a check for consistent error. These advantages of having the sample in free space and unprepared are especially noteworthy for the measurement of certain materials. For those such as glass, which cannot be machined, the method is often convenient, and similarly for materials which are not strictly uniform, where the use of a large area automatically gives an average determination, which is often desirable. Examples of such materials are low-density materials, certain laminates, plain or conducting cloth, and wood. In particular for oriented materials, such as wood, it is possible to take a complete curve of  $k$  vs. the direction of polarization, although this presents considerable difficulty with any waveguide or cavity method.

The foregoing advantages follow from the fact that the sample need not be accurately machined to fit a cavity or guide. When combined with the fact that no calibration is required, this property shows the



method to be particularly applicable at the shorter wavelengths; with negligible error in  $d$ ,  $\theta$ ,  $\lambda$  and with a given angular error in  $\Delta$ , the error in  $k$  is directly proportional to  $\lambda$ . Moreover, difficulties from diffraction decrease rapidly as the frequency increases. Apart from this increase in accuracy, the equipment is suitable for use at the shorter wavelengths because of the simplicity of the r-f components required. Given a suitable generator, it is sufficient to have unmatched T-joints, simple horns, variable attenuators, and some means of measuring power, all of which are relatively easy to make in small sizes. In particular, no slotted section, probes, or phase shifters are required either for calibration or for measurement.

To these advantages must be added the corresponding disadvantages. For example, the use of large samples in sheet form is not only possible, but necessary; hence small samples or materials available only in the form of rods cannot be tested. Similarly, the increase in accuracy found with thick samples, which is easily attained in guide, is usually impracticable in free space. Even though the higher precision of  $\Delta$  compensates this difficulty to some extent, it is nevertheless found that accurate results cannot be achieved with very thin sheets. Such considerations are particularly true of  $\tan \delta$ , in which the only compensating feature analogous to this higher accuracy of  $\Delta$  is the slight advantage of having zero wall losses. And finally, instead of saying that the method improves with decreasing wavelength it may be said that it deteriorates with increasing wavelength; not only is the precise measurement of  $\Delta$  more difficult, but errors from diffraction and stray radiation may become prohibitively large. At the same time the alternative waveguide and cavity methods become more accurate. It may be concluded that the present method is suitable for measurement at short wavelengths only.

#### GENERAL METHODS DEPENDING ON REFLECTION

**10.12. Interface Reflection.**—The discussion has hitherto been concerned solely with transmission. As noted, however, both  $k$  and  $\tan \delta$ , in principle at least, can be likewise determined from reflection. This procedure may well be considered in greater detail.

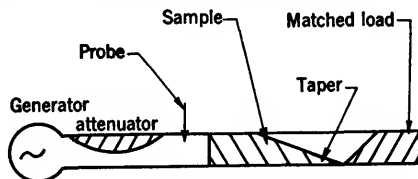


FIG. 10-24.—Experimental procedure for measuring interface reflection.

**Waveguide.**—With the arrangement of Fig. 10-24 it is clear that the complex interface reflection  $r_i \exp(-j\tau_i)$  is obtained, which gives  $k$

and  $\tan \delta$  by the exact Eqs. (54) and (55) for coaxial line. The corresponding result for waveguide in general is somewhat complicated, and therefore terms of the order of  $\tan^2 \delta$  are neglected to obtain the approximate forms (cf. Fig. 10-27)

$$k \approx \frac{(1 + r_i)^2 - 4r_i p}{(1 - r_i)^2} \quad (53)$$

$$\tan \delta \approx \frac{k - 1}{k} \sqrt{\frac{k - p}{1 - p}} \tan r'_i,$$

which follow easily from Eqs. (8), (12) and Table 10-2. Like Eqs. (54) and (55), these relations lead to simple numerical calculations. They

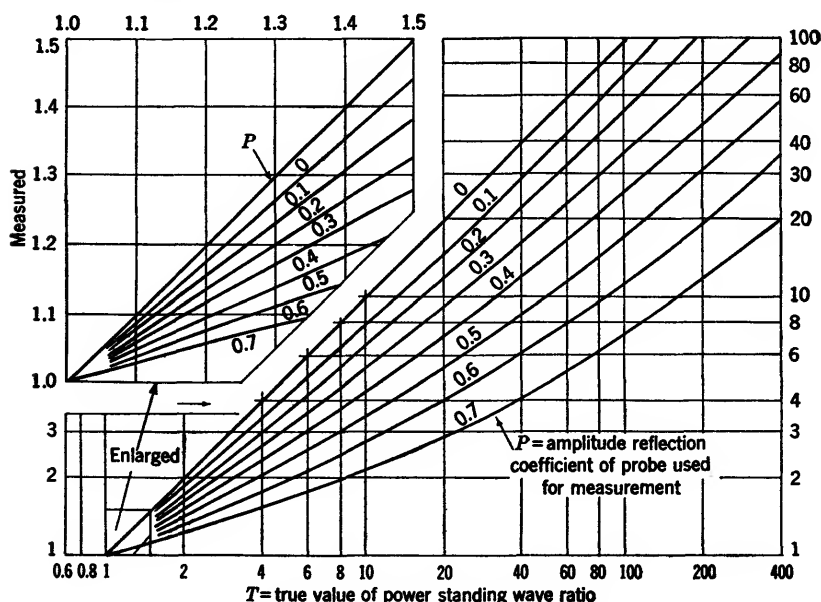


FIG. 10-25a.—Effect of probe reflection on apparent power standing-wave ratio; theoretical true vs. measured power standing-wave ratio with generator matched to line.

show that loss is determined from the phase shift  $r'_i$ , essentially, whereas  $k$  is found from the absolute magnitude of  $r_i$ . To cancel the small reflection from the taper, the measurement is repeated with  $d$  replaced by  $d - \lambda_m/4$ , and to cancel the error due to load reflection the measurement is repeated with a quarter-wavelength motion of the sample as a whole. As an alternative procedure, which is especially useful when the measured reflection is small, the probe may be kept stationary, with the generator matched to the line, and the ratio of the maximum to the minimum probe reading may be taken as the sample is moved. A rather

detailed account of this and other methods of measuring small reflections or the associated phase shifts is given in Ref. 4a. Similarly, errors due to the measuring probe are discussed at length in Ref. 5a; if  $Pe^{-iP'}$  is the probe reflection, it is sufficient here to observe that the fractional error in  $r_i$  is of the order of  $r_i P \cos P'$ , when the generator is matched to the line, whereas that in  $r'_i$  is negligible in comparison with the other errors. If the generator is matched to the load and if the probe is tuned

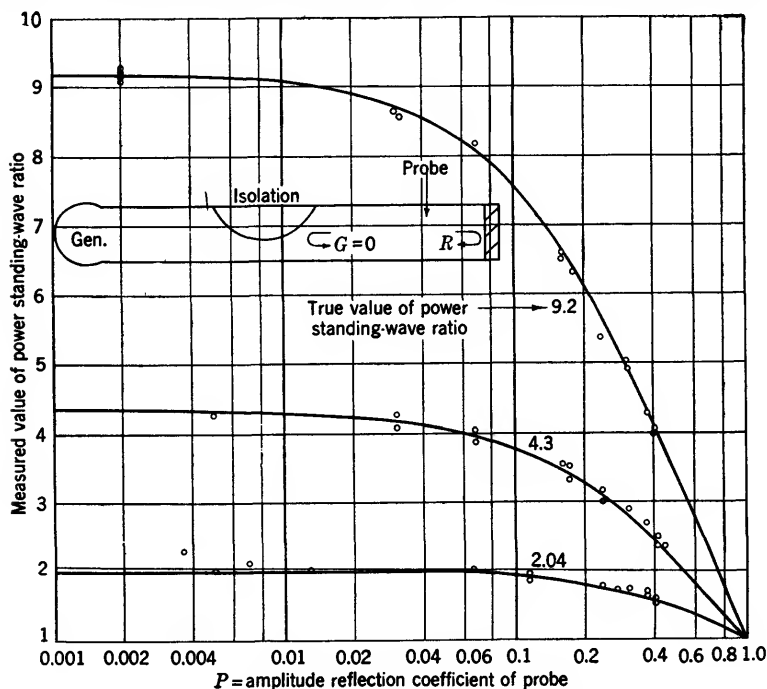


FIG. 10-25b.—Effect of probe reflection on apparent power standing-wave ratio; comparison of theory and experiment, generator matched to line.

for maximum pickup, which conditions should both be satisfied in good practice, then the error in reflection may be corrected by the curves of Fig. 10-25a. Experimental illustrations showing the general behavior are given in Figs. 10-25b, c. Wall losses are compensated by extrapolating the measured reflection to the sample interface, as described in Sec. 10-18, and subtracting  $(\tan \delta_{\text{wall}})$  from  $(\tan \delta_{\text{measured}})$ .

Interface reflection in guide was used in Ref. 11a to evaluate the dielectric constant and loss tangent of water, which is one of the few materials giving a sufficiently high reflection for accurate results. Precautions were taken to avoid error from probe reflection, and other r-f errors were investigated by the use of several depths for the water column. Because

of the high attenuation it was unnecessary to use a tapered sample. Loss was determined by the phase shift, as here described, and  $k$  was found from  $r_i$ . The size of waveguide used, combined with the large value of  $k$ , permitted substitution of the free-space equations, Eqs. (54) and (55), for the guide equation, Eq. (53). The method seemed to be satisfactory in this case. It was similarly used in Ref. 16a to determine  $k$  for water, although  $\tan \delta$  was found by a procedure presently to be described rather than by the phase shift  $r_i'$ . The general utility of this

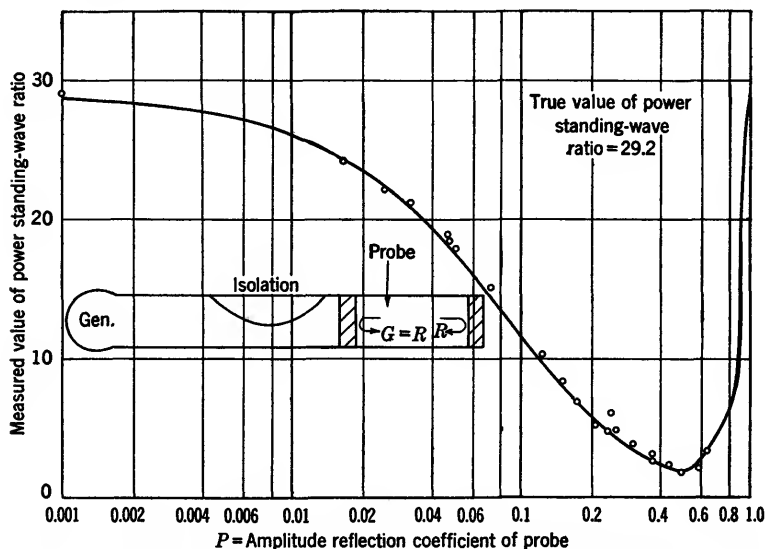


FIG. 10-25c.—Effect of probe reflection on apparent power standing-wave ratio; comparison of theory and experiment, generator matched to load.

interface method will be commented upon; the examples here cited show, for certain circumstances at least, that it can be successfully used in practical work.

*Free Space.*—In the course of the foregoing discussion it was noted that the methods depending on transmission in guide could be readily extended to free space—the process being regarded as an extension, despite the slight simplification of theory, because of the nonstandard experimental techniques required. A similar extension may be made for the methods just described; as before, it is found to lead to certain advantages, as well as disadvantages, not offered by the waveguide procedure. If Eq. (12) is substituted in Eq. (8), the following equations are obtained (cf. Fig. 10-26):

$$k \sec \delta = \frac{1 - 2r_i \cos r_i' + r_i'^2}{1 + 2r_i \cos r_i' + r_i'^2} \quad (54)$$

$$\sin\left(\frac{\delta}{2}\right) = \frac{1}{2} \left( \sqrt{k \sec \delta} - \frac{1}{\sqrt{k \sec \delta}} \right) \tan r'_i \quad (55)$$

for  $\tan \delta$  in terms of  $r_i e^{-jr'_i}$ , the interface reflection when the incidence is normal in free space. Since the right-hand side of Eq. (54) involves measured quantities only, the need for simultaneous solution is obviated when the results are presented in the form here given. Thus,  $k \sec \delta$  is obtained from Eq. (54), and is substituted in Eq. (55) to find  $\sin(\delta/2)$  which in turn gives  $\delta$ , the loss tangent  $\tan \delta$ , and the term  $\sec \delta$  required to complete the computation of  $k$ .

With arbitrary incidence the corresponding equations are somewhat involved, and, as in the derivation of Eq. (53), terms of the order of  $\tan^2 \delta$  are neglected to obtain

$$k = \frac{A(1 + \sqrt{1 - 4p(1-p)/A})}{2(1-p)}, \quad (56a)$$

where

$$A = \frac{(1 + r_i)^2}{(1 - r_i)^2}$$

and

$$|k - pk - p| \gg \tan \delta.$$

Similarly, when

$$\begin{aligned} |(k-1)(k-2p)(k-pk-p)| &\gg \tan \delta, \\ \tan \delta &= \frac{\sqrt{k-p}(k-1)(k-pk-p)}{\sqrt{1-p}(k)(k-2p)} \tan r'_i \end{aligned} \quad (56b)$$

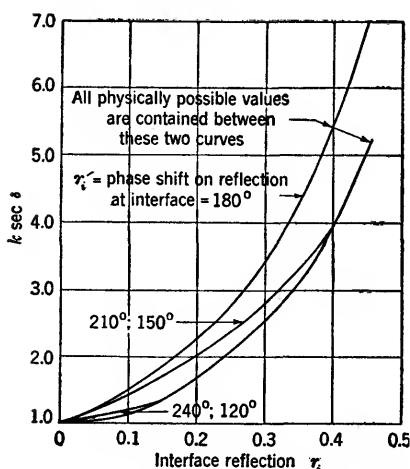


FIG. 10-26.—Dielectric constant vs. interface reflection for arbitrary loss in free space at normal incidence.

is found for polarization parallel to the plane of incidence. The result for perpendicular polarization is given, to the same approximation, by Eq. (53). Both equations, plotted in Fig. 10-27, follow from Eqs. (8) and (12) and Table 10-1. Parallel polarization admits a possibility not presented by any of the other conditions in that the effective dielectric constant for zero loss would be unity at the polarizing angle  $\theta_b$ , which is found when  $p$  satisfies

$$p = \frac{k}{k+1}, \quad (57)$$

as is seen by setting the effective

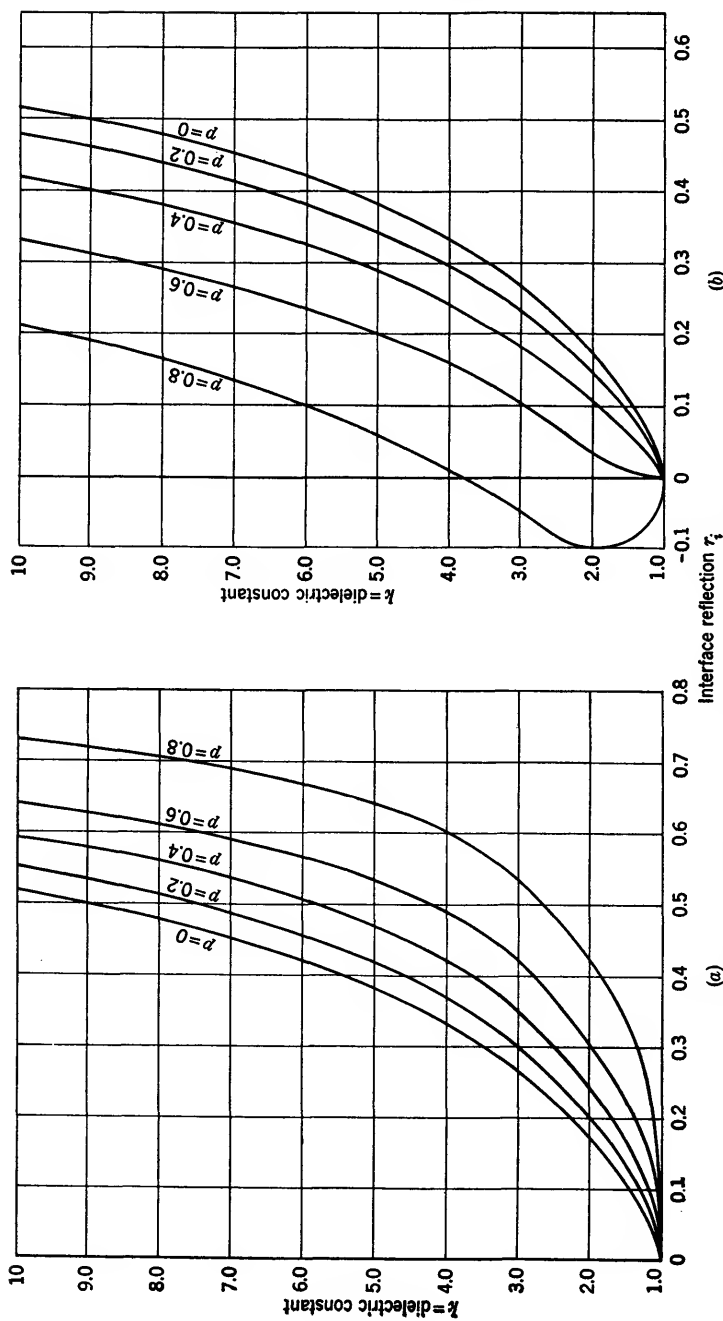


Fig. 10-27.—Dielectric constant vs. interface reflection for low-loss materials at arbitrary incidence or in waveguide. (a) Perpendicular polarization or  $TE$ -wave. (b) Parallel polarization or  $TM$ -wave.

value equal to unity in Table 10-1, or by Eq. (49). With this angle of incidence (which may be found with sufficient accuracy by taking reflection vs. angle over a small range and noting the minimum value) the approximations used in the derivation are incorrect; instead of Eq. (56), the equations obtained are

$$\tan \delta = \frac{4kr_i}{k-1}, \quad p = \frac{k}{k+1}, \quad (58)$$

if again terms of the order of  $\tan^2 \delta$  are neglected. Thus, the amplitude of the interface reflection cannot be used to determine loss, in general, as it involves only the small quantity  $\tan^2 \delta$ ; but if parallel polarization is used and the angle of incidence is adjusted in accord with Eq. (49), then on the contrary, the amplitude reflection not only depends on the first power, but is directly proportional to it. The situation is unique in that it represents perhaps the only case in which small loss may be accurately determined from measurement of amplitude reflection without the use of a short circuit or its equivalent. Of course these results concerning parallel polarization are equally valid for waveguide propagating a *TM*-wave, although *TM*-waves have apparently not been used in experimental work.

**10-13. Reflection Measurement in Free Space.**—Turning now to the question of free-space measurement, three different methods are available from current practice.

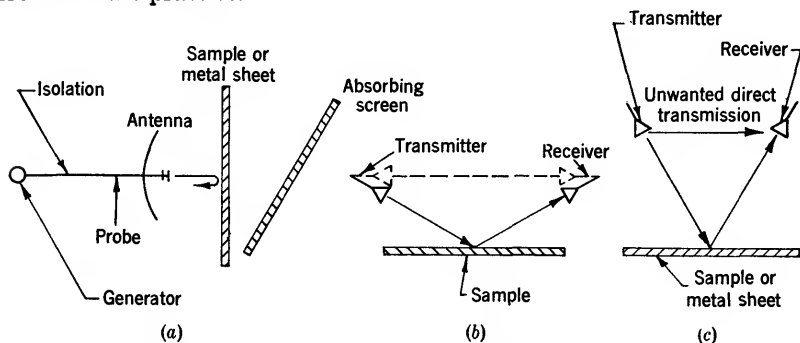


FIG. 10-28.—Equipment for reflection measurement in free space: (a) normal incidence, (b) incidence far from normal, and (c) general case.

**Normal Incidence.**—The first of these methods is to measure the reflection in the line from the sample, then from a metal sheet, as shown in Fig. 10-28a. If the antenna is matched to free space, the ratio of the two measured reflections gives the reflection coefficient desired (Refs. 7a, 20a). The dependence on sample size is investigated in some detail elsewhere (Ref. 7a). The sample may be considerably smaller than is permissible with transmission; a safe criterion is to have it cover the

antenna aperture if in the Fresnel region, and a larger area if in the Fraunhofer region. The effect of sample curvature is likewise investigated theoretically and experimentally in Ref. 7a, where the error is found to be theoretically negligible whenever the product of the radius of curvature of the surface and the wavelength is greater than one hundred times the square of the radius of the antenna for a paraboloidal antenna. Error from interaction between antenna and sample is canceled in the usual way by repeating the measurement with a quarter-wavelength displacement and using the average of the two values so obtained, rather than either value alone, as the measured reflection. Additional error is noted when the angle of incidence is not the same for the metal sheet as for the sample; thus, (Refs. 7a; 20a)

$$(\text{Measured reflection in amplitude}) = (\text{constant})(\text{reflection coefficient of sample}) P(\theta), \quad (59)$$

where  $P(\theta)$  is the one-way secondary power pattern of the antenna and  $\theta$  is the (small) angle between the electrical axis and the normal to the sheet. Essentially the same result is obtained for the methods considered below, if  $\theta$  is suitably interpreted. Because erratic values with a metal sheet are obtained at the shorter wavelengths, this method is suitable only when the microwave frequency is relatively low; even then a certain amount of care must be exercised since the measured power standing-wave ratio is usually small.

*Incidence Far from Normal.*—The foregoing procedure is operable only when the incidence is normal. With the arrangement of Fig. 10-28b, however, reflections in more general circumstances may be determined; the procedure as described in Ref. 14a is to compare the reflected power (solid path in the figure) with that received directly (dotted path). To check for cross-polarization, which is of moment whenever the incidence is far from normal, the ratio of maximum to minimum received power is noted as one of the antennas is rotated about its axis (Refs. 14a, 22a); with suitable antennas the ratio so obtained should be of the order of  $10^3$  or higher. The experiments of Ref. 14a were all carried out with perpendicular polarization; if the polarization is parallel, as required, for example, by Eq. (58), it is clear that error from cross-polarization becomes considerably more serious. Thus, the interface reflection is now higher for the unwanted component, whereas previously the reverse was the case.

A second source of error is the simultaneous presence of both direct and reflected waves, an effect which is unavoidable in that any real antenna has but limited directivity. This difficulty was considered in Ref. 14a, the procedure being to take reflection vs. angle and to draw a



smooth curve through the mean of the points so obtained. It was expected that the error in question would be sometimes positive, sometimes negative, and would thus be averaged out by the procedure described. An alternative—or rather a supplementary—method of cancelation is to change the distance from the receiver to the transmitter or the metal sheet, as the case may be, and to use the average of the maximum and minimum received amplitudes so obtained in all equations. Such a procedure, which is closely analagous to that to be treated in detail, will lead to slightly different values for the average path length with the direct and reflected waves—a difference which is present to some extent in any case. The attendant error may be corrected by the relation

(Receiver reading with path length  $D$ )

$$= (\text{receiver reading with length } D') \left( \frac{D'}{D} \right)^2, \quad (60)$$

which is valid whenever the antennas are sufficiently far apart for inverse-distance attenuation (Refs. 7a, 14a). A square-law detector is assumed, and the receiver reading is taken as proportional to the received r-f power. As was the case for direct measurement of transmission, here too the error is the same as that in the power standing-wave ratio, and hence the discussion may again be deferred. Strictly speaking, the path length  $D$  must be measured from the effective center of the antenna (Ref. 7a), though for our present purposes it suffices to measure  $D$  from the antenna aperture.

*Incidence Not Normal but Otherwise Unrestricted.*—When the incidence is near normal, it is impracticable to send the power directly from the transmitter to the receiver along the dotted path in Fig. 10-28b. Thus, although error from interference between the two antennas may be canceled out by the usual quarter-wavelength motion (cf. Ref. 7a), error caused by the now great difference in path lengths cannot be compensated for by Eq. (60), which is valid only in the Fraunhofer region. To obviate this difficulty a metal plate may be used as before, the reflection coefficient being again obtained as a ratio of two measured values (Refs. 7a, 14a, 20a). The sources of error are for the most part similar to those already described, and, with one exception, they need not be reconsidered here. The exception concerns the problem of direct pickup between antennas, which is made more serious than before by their increased proximity in spite of the large angle in the secondary pattern at which it must occur (Ref. 14a). If  $A$  or  $A'$  denotes the amplitude of this directly transmitted wave, after it has entered the r-f line of the receiver, and if  $B$  or  $B'$  is proportional to the amplitude of the reflected wave, the unprimed quantities referring to the metal sheet, the primed ones to the dielectric, then the received power will be given approximately by (Ref. 14a)

$$\begin{aligned}\text{receiver reading} &= \left| A + \frac{B}{D} e^{-\frac{2\pi j D}{\lambda}} \right|^2 \\ &= \left| A' + \frac{B'}{D} e^{-\frac{2\pi j (D-C)}{\lambda}} \right|^2,\end{aligned}\quad (61)$$

where  $D$  again stands for the total length, between suitably chosen end points, of the r-f path. The constant  $C$  is necessary because the phase shift on reflection from the sample need not be the same as that for the metal. The ratio  $B'/B$  may be determined from Eq. (61), since this is easily seen to be equal to the reflection coefficient of the material. Such a determination was made in Ref. 14a by adjusting  $D$  for maximum receiver reading  $M^2$ ,  $M'^2$  in each case, whereupon second-order terms may be neglected (Ref. 14a), and

$$\frac{B'}{B} \approx \frac{M'}{M} \left( 1 + \frac{C}{D} \right) \left( 1 + \frac{AD}{B} \right) \left( 1 - \frac{A'(D+C)}{B'} \right) \quad (62)$$

is the desired ratio  $B'/B$  in terms of the variables of Eq. (61), if  $D$  now stands for the particular value of  $D$  which gave a maximum with the metal sheet. With regard to inverse-distance attenuation, the unknown quantities  $AD/B$ ,  $A'(D+C)/B'$  are then determined from the ratio of maximum to minimum received power with the metal sheet or sample, as the case may be, and substituted in Eq. (62).

Although this method has been used with success it is somewhat complicated in practice. The following procedure, which is simpler and more consistent with the experimental techniques developed in this chapter, is presented. For compensating error from extraneous r-f power, it is required that an average of two readings be obtained, with the error positive for one reading and negative for the other. It is instructive to investigate the same operation as applied to Eq. (61). Since it may be assumed that  $A < B/D$  and  $A' < B'/D$ , Eq. (61) gives

$$\begin{aligned}M + m &= B \left( \frac{1}{D + \lambda/8} + \frac{1}{D - \lambda/8} \right) \\ M' + m' &= B' \left( \frac{1}{D + C + \lambda/8} + \frac{1}{D + C - \lambda/8} \right),\end{aligned}\quad (63)$$

if  $D$  stands for the average of the two lengths noted for  $M$  and  $m$  and if  $M$  and  $M'$  are the maximum,  $m$  and  $m'$  the minimum receiver readings obtained by changing the distance to the metal sheet and to the sample, respectively. Thus both of the unknown amplitudes  $A$  and  $A'$  have been eliminated. From Eq. (63)

$$\frac{B'}{B} = \frac{M' + m'}{M + m} \left( 1 + \frac{C}{D} \right) + e \quad (64)$$

is obtained for the desired ratio  $B'/B$ , with the error-term  $e$  easily shown to be  $\leq (\frac{1}{32})(\lambda/D)^3$  since  $|C|$  may be assumed  $\leq \lambda/8$ . Besides having the small coefficient  $\frac{1}{32}$ , this error term is of the third degree in a quantity whose square was neglected throughout the previous calculation; hence it may be justifiably ignored. Equations (62) and (64) are, of course, valid whether the antennas or the sample be moved to change  $D$ ; they may also be used when only one antenna is moved, provided the amplitudes  $A, A'$  remain substantially constant.

*Phase.*—Phase may be determined in principle by comparing the minimum positions for metal and dielectric in Fig. 10-28*a*, as described in Ref. 7*a*, or by the free-space bridge method applied to the systems of Figs. 10-28*b* and *c*. Because of the low standing-wave ratio, the first method is very inaccurate, however, and both methods present certain difficulties in that the metal surface, if employed, must be placed precisely at the position formerly occupied by the sample. In using free-space reflection, therefore, the amplitude alone is usually measured, and the transmission or some other easily measured property is relied upon for the information that would normally be obtained from  $r'_i$ . This is the procedure followed in Ref. 14*a*, where the free-space methods here outlined were used to evaluate the dielectric constant and loss tangent of water. Because of the high loss the equations were too complicated for convenient simultaneous solution, and instead a graphical method was adopted, which is of sufficiently general application to be given a place here. The slope of the transmission curve was determined experimentally, whereupon Eq. (35) of the present text became an implicit relation between  $k$  and  $\tan \delta$ , and the locus of values could be plotted as a single curve. Next, the interface reflection  $r_i$  was obtained experimentally, and a similar locus derived therefrom. The computations are relatively convenient in each case; the intersection of the two loci gives the true values of both  $k$  and  $\tan \delta$ .

**10-14. Change of Termination.**—In transmission measurement nothing is usually gained by use of an unmatched termination for the sample; indeed, whether it be part of the sample itself or of the r-f measuring equipment, such a termination was found in the foregoing pages to be a serious source of error, and much of the experimental procedure was accordingly designed to simulate the condition of zero reflection for both sample and load. With reflection, on the other hand, quite the opposite behavior is found to prevail. Not only is it permissible to use an unmatched termination (with suitable changes in the theory, of course) but it is often necessary for the attainment of high accuracy. Such questions perhaps merit further consideration.

*Terminations Not Containing a Short Circuit.*—One of the simplest unmatched terminations is the second interface of the sample itself,

which need not be tapered as shown in Fig. 10-24. Instead of interface reflection, it is the over-all reflection  $re^{-ir'}$  for an entire sheet of material that is obtained here. This reflection in turn may be evaluated

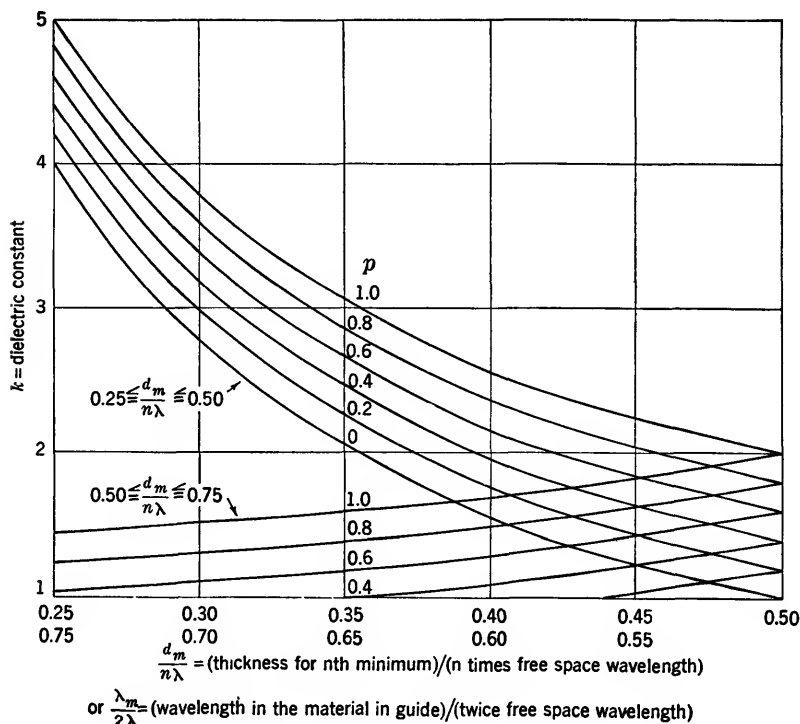


FIG. 10-29.—Dielectric constant vs. thickness for minimum reflection or vs. wavelength in the material.

by substituting  $t_i e^{-jt'}$ ,  $r_i e^{-ir'}$  as obtained from Eqs. (8) and (9) for  $t''$ ,  $T''$ ,  $\tau''$  and  $r''$ ,  $R''$ ,  $\rho''$  in Eq. (6). Thus (Ref. 1b)

$$re^{-ir'} = - \frac{(k-1)(1-e^{-2i\beta d})}{(\sqrt{k}+1)^2 - (\sqrt{k}-1)^2 e^{-2i\beta d}} \quad (65)$$

is found for zero loss and normal incidence, with the result in more general circumstances to be derived as usual from Eq. (12) and Table 10-1. Equation (65) easily leads to

$$\left(\sqrt{k} - \frac{1}{\sqrt{k}}\right) \sin\left(\frac{2\pi d \sqrt{k}}{\lambda}\right) = \pm \frac{2r}{\sqrt{1-r^2}},$$

$$k \approx 1 + \frac{r\lambda}{\pi d}, \quad d \ll \lambda, \quad (66)$$

for the amplitude, and the corresponding result for phase is given by Eq. (45) with  $t' = r' + \pi/2$  (cf. Refs. 20a, 8b). In particular, the thickness  $d_m$  for minimum reflection gives a relation plotted in Fig. 10-29,

$$k = \frac{(n\lambda)^2}{(2d_m)^2} + p, \quad (67)$$

and the maximum reflection  $r_M$  gives the relation

$$k = \frac{1 + r_M(1 - p)}{1 - r_M}. \quad (68)$$

In Fig. 10-30 are plotted curves showing this function, for the general case of waveguide. Besides being nontranscendental, Eq. (67) is superior

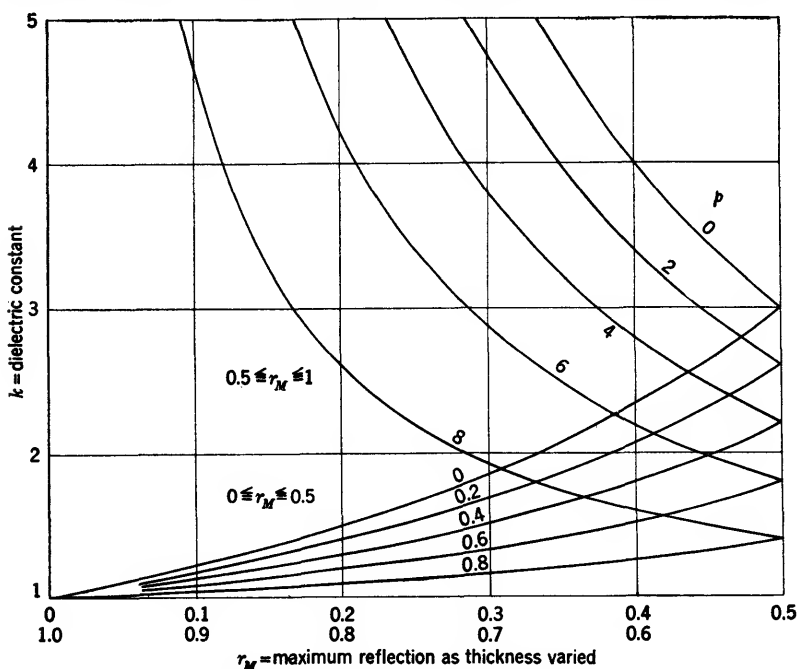


FIG. 10-30.—Dielectric constant vs. maximum reflection in waveguide.

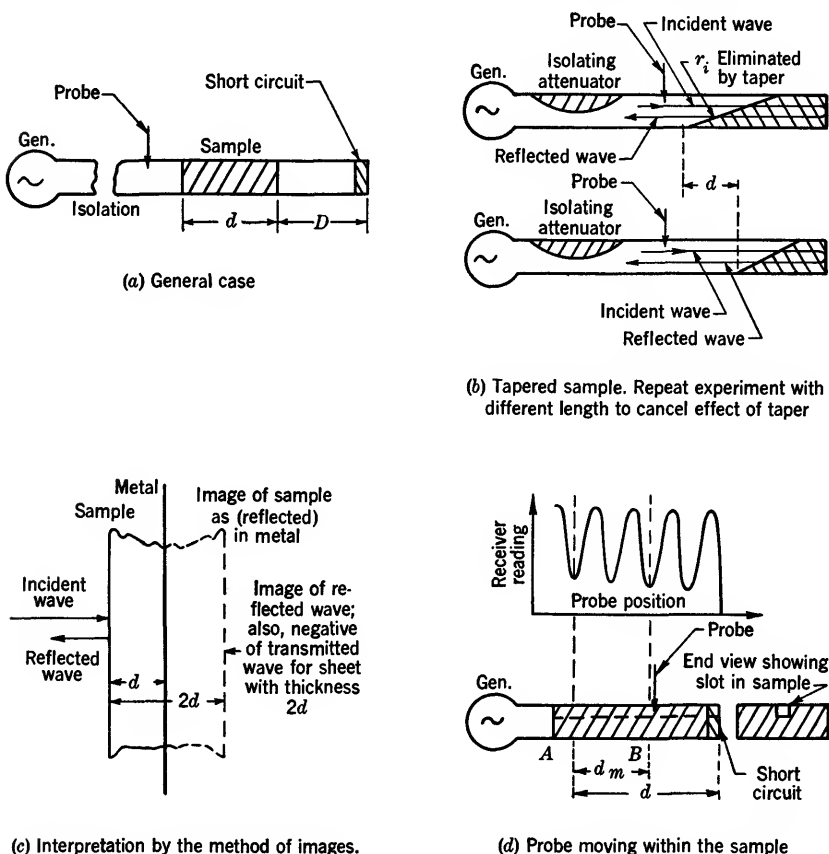
to Eq. (60) because a large reflection can be measured with greater percentage accuracy than a smaller one, as may be easily shown (Ref. 2a), and because the derivative of the final result with respect to  $d$  is zero, the error due to inaccuracy in measuring the thickness is minimized. This process of maximizing the reflection while minimizing the derivative may be extended to several samples. Thus, if each of  $n$  sheets has its thickness adjusted for maximum reflection, then the reflection for the

whole series in free space will be maximum when the sheets are uniformly spaced exactly a quarter-wavelength apart. The over-all reflection so obtained equals the maximum reflection attainable with a single sheet of dielectric constant  $k^n$  (Ref. 8b).

*A Digression Concerning Merit.*—The use of various terminations in reflection procedure has been briefly considered; first a termination which matched out the reflection of the second interface was assumed, then one which consisted of this second interface itself, and finally a special case of a termination consisting of extra samples similar to the original one. Each of these terminations, as it happens, has actually been used in practice. Thus, the first occurred in sources already quoted; the second [Eqs. (66) to (68)] was studied in Refs. 6a, 21b, the approximate form of Eq. (60) being given in Refs. 6b, 21b; and the third has been used in unpublished laboratory work. There is apparently but one other termination, namely, a short circuit at some point behind the sample, which has been used in the measurement of dielectrics by reflection methods, and this termination is discussed in detail in Sec. 10-15.

Before proceeding to this final method, however, the merit of those just described will be considered. In the first place, the use of interface reflection has led to accuracy of the order of  $\pm \frac{1}{2}$  per cent in practical work (Ref. 14a), and measurement of the over-all reflection of an entire sheet can likewise give precision of this order (cf. Refs. 4a, 7a). Such accuracy compares favorably with that obtained by the best methods at present available. Hence, inquiry should be made to determine whether it is a general property of these reflection techniques, or whether it is caused by an unusually favorable set of special circumstances. That the accuracy is caused by special circumstances is easily seen for the interface method; the material used was water, for which the interface reflection and loss are both high. Large reflection is desirable, although perhaps not absolutely necessary (Ref. 4a) for accurate measurement in guide. With ordinary precautions in evaluating the reflections usually encountered,  $k$  could hardly be determined to more than two figures, and because of the difficulty of measuring the minimum position associated with a moderate power standing-wave ratio, the loss  $\tan \delta$  will usually fare even worse. Similarly, the use of interface reflection in free space is not only inaccurate, in general, but impossible to use, for the effect of the second interface cannot be eliminated when the sample is of ordinary thickness and moderate loss. Free-space measurement, in particular, permits no matching device analogous to the taper shown in Fig. 10-24. Hence for the high values of  $k$  or  $\tan \delta$  obtained in the special investigations cited above, the interface method presents many advantages, but when regarded as an over-all procedure of general utility, it is nevertheless inferior to the methods presently to

be described. Similar considerations apply to the other methods, for example, to measurement of reflection for the complete sample and use of the approximate Eqs. (66) to (68), or their precise analogues for finite loss.



(c) Interpretation by the method of images. Zero reflection at the interface is assumed here.

(d) Probe moving within the sample

FIG. 10-31.—The general short-circuited-line method; and two special forms of it which illustrate principles and lead to simple calculations. (a) General case. (b) Tapered sample. (c) Interpretation by the method of images. (d) Probe moving within the sample.

Since the emphasis here is upon techniques that are applicable in general, the discussion may proceed forthwith to methods using a short circuit.

**10-15. Short Circuit, Zero Reflection at Interface.**—By the equipment of Fig. 10-31a the reflection coefficient and minimum position may be obtained for the short-circuited line with and without the dielectric sample, whereupon from Eq. (18) and the accompanying remarks it is

seen that the change in minimum position gives  $k$ , essentially, whereas the change in reflection coefficient gives  $\tan \delta$ . The general arrangement of Fig. 10-31a, for which the interface reflection  $r_i$  has not been eliminated, is discussed at length in the following sections. For our present purposes a qualitative description of the type just given is sufficient.

From this so-called "short-circuited-line method," which was developed by A. R. von Hippel and his associates (Refs. 1a, 2b, 3b, 5b), many advantages are obtained over the mere measurement of  $r_i$  or  $r$ . Not only do given errors in measurement usually lead to smaller errors in the result, but these measurements themselves may be carried out with far greater accuracy. Instead of being perhaps 3 or 4, the power standing-wave ratios are now anywhere from  $10^3$  to  $10^7$ , with a corresponding increase in the accuracy with which minimum position, and hence  $k$ , may be determined. For  $\tan \delta$  the situation is analogous to that noted in connection with Fig. 10-12, where it was found desirable to have  $t = 1$  when  $\tan \delta = 0$ . Here  $R = 1$  for zero loss, if  $R$  is the amplitude reflection of sample and short circuit; hence the error in  $\tan \delta$  is comparable with that in  $1 - R$ , which may be measured directly. Thus, instead of measuring a minute variation in a large quantity, as is necessary for finding  $\tan \delta$  from  $r$  or  $r_i$ , the actual value of a small quantity is measured, a procedure which here too, as with  $t$  above, is more accurate.

*Methods Using a Probe.*—There is indeed more than a superficial similarity between this procedure and the transmission procedures hitherto described, although the wave now traverses the sample twice instead of once. This equivalence, intuitively evident in any case, becomes formally exact when  $r_i$  is negligible, for the solution is then given, without further approximation, by Eqs. (36) and (37), with  $2d$  written in place of  $d$  and with  $R$ , the over-all reflection of sample and short circuit, in place of  $t$ . The quantity  $\Delta$  represents twice the difference in minimum positions with and without the sample (cf. Fig. 10-31c). These results, which follow by setting  $r'' = \rho'' = 0$ ,  $t'' = 1/r''$ ,  $R'' = -1$  in Eq. (6), may be used for actual measurement if the effect of  $r_i$  be properly eliminated. Thus, when  $k \approx 1$ , the usual quarter-wavelength change is made in  $d$ . For general values of  $k$  the same effect is achieved by the use of two measurements with a tapered sample (Fig. 10-31b). When the quarter-wavelength change is made, the average of the two computed values is used; when the tapered sample is used, the difference of the two  $d$ 's and the ratio of the two  $R$ 's are substituted, rather than the quantities themselves, into the equation. Wall losses are compensated, *mutatis mutandis*, by the procedure of Secs. 10-5 or 10-18. This is true of all the methods of this section.

A second method of achieving much the same result is given in Fig.



10-31*d*, where the measuring probe is so located that the measured reflection must be completely independent of  $r_i$ . This property, which is easily proved by Eq. (7) of the introduction, also follows from the well-known fact that the impedance of a termination depends only on the termination, not on the items that may have preceded it in the line. In terms of the measured reflection at the point *A*, which is a distance *d* from the short circuit (Fig. 10-31*d*), the transmission equations of the foregoing pages, with the substitutions described in the above paragraph, will again give *k* and  $\tan \delta$ . The result involves no theoretical approximation.

As far as the present theory is concerned, the choice of point *A* is arbitrary; in particular, it need not be at a voltage node as shown in Fig. 10-31*d*. But when measurement instead of theory is considered, the advantage of this choice becomes at once apparent, for the reflection, as well as the phase, cannot be readily determined at any other points of the line. In connection with measurement procedure it is worth noting also that, for measurement of reflection at a point within the sample as here required, it will not do to take the ratio of maximum to minimum power in the conventional manner, since the attenuation produced by the sample may become appreciable over the region thus traversed by the probe. Instead the procedure to be discussed is used noting that Eq. (79) for reflection in terms of the width at twice minimum is valid here if  $\lambda_r$  be replaced by  $\lambda_m$ , the wavelength in the material in guide. The dielectric constant *k* may usually be determined first from the minimum position alone. After *k* has been thus determined,  $\lambda_m$  is computed without difficulty, and with  $\lambda_m$  known the reflection is obtained from Eq. (79), which in turn gives  $\tan \delta$  by the procedure outlined. If the loss is so high that it appreciably affects the value of  $\lambda_m$ —which is almost never the case in practice—then the equations are transcendental; they may, however, be solved by successive substitution in the manner suggested for Eq. (33).

The foregoing method neglects loss in the short circuit itself, which is not compensated even when  $\tan \delta_{\text{wall}}$  is subtracted from  $\tan \delta_{\text{measured}}$  as prescribed. To obviate this difficulty the reflection may be measured at two points, for example, *A* and *B* of Fig. 10-31*d*; *d* is taken now as the distance  $d_m$  between the points, and the reflection as the ratio of the two measured values. Because of the need for a slot in the sample, the method of Fig. 10-31*d* is not well suited for measurement at very short wavelengths, although the same or a similar procedure appears to have been employed successfully (Ref. 17*c*) for measurement of *k* in the 3-cm range. Since the slot is in a region of maximum field, the error is probably somewhat larger than that for an equivalent area spread over the top of the sample. In other words, the present failure of the sample

to fill the guide completely is more serious than the ordinary clearance problem. It must be mentioned, however, that this method has an outstanding advantage over all the others involving a short circuit in that the character of the load does not change while the measurements are being made. The results for different sample lengths or for sample and guide need not be compared. The necessity for generator isolation is thus materially reduced, since the free-space wavelength can be measured while the sample is in place.

The use of a probe and a short circuit for dielectric measurement as described permits a physical interpretation somewhat different from the one here given. Thus, the problem has been regarded as analogous to transmission, a procedure which was made plausible by Figs. 10-31*b,c,d* and which was proved by Eq. (6). If the dielectric constant is considered, however, the method of Fig. 10-31*d* may be interpreted as a means of measuring the wavelength in the material, without regard either to transmission or to reflection as such. For negligible  $\tan^2 \delta$  the distance between the  $i$ th and  $(i + n)$ th node is equal to  $n\lambda_m/2$ , and hence  $k$  is given by the relation plotted in Fig. 10-29 and Eq. (67), with  $d_m = d$ . This point of view, which is the one adopted for such methods in Ref. 6*a*, may be used here and in the following paragraphs to supplement the transmission analogy noted. The wavelength presentation is in some respects the simpler when loss is not in question, whereas the transmission analogy is to be preferred for the general case.

*Methods Not Using a Probe.*—At short wavelengths the design of traveling probes becomes difficult, and methods have accordingly been devised for obtaining the necessary information by other means. Several of these methods have already been described in the foregoing sections of the present text, with regard to measurement of both transmission and reflection. For the present situation, in which the sample is followed by a short circuit, the procedure suggested in Fig. 10-32*a* may be used. As the plunger and with it the sample are moved along the line, the receiver reading will take on maximum or minimum values; the difference between plunger positions for corresponding values will be equal to  $\lambda_m/2$ , and  $k$  is thus to be found from Eq. (67). In other respects too the method is equivalent, as far as principles are concerned, to that of Fig. 10-31*d*. Thus, it is possible to imagine the sample and plunger positions held constant while the generator and receiving system are moved; all theoretical relations or procedures for the previous case are therefore applicable here. With regard to actual operation in practice, however, there are several differences in addition to the valuable property of not requiring a traveling probe. The line leading to the load is of variable length, for example, with the result that the usual measures must be taken to prevent interaction between the two components of the system—in the present

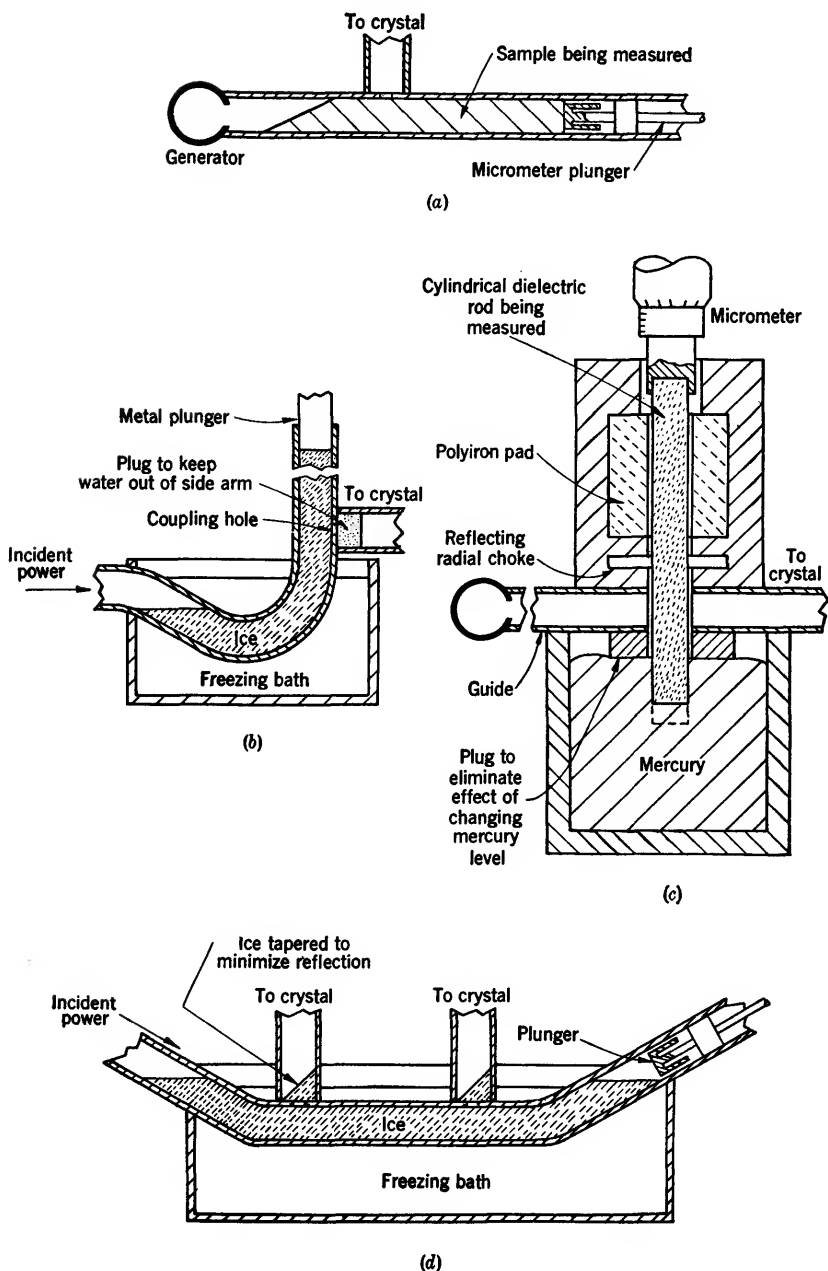


FIG. 10-32.—Methods of making measurements on a sample, backed by a short circuit, without the use of a probe.

case, between generator and load. Added to this requirement, which is essentially that the generator reflection must be small, is a second requirement that the sample be tapered, for the sidearm, corresponding to the probe in Fig. 10-31*d*, has a relatively high reflection of its own. Partly because of this reflection the method is found not to be satisfactory for evaluation of loss; its originator, E. L. Younker, has used it successfully, however, for measurement of  $k$  (cf. Ref. 6*a*).

In Ref. 16*a* the foregoing procedure was modified as illustrated in Fig. 10-31*d* and used for measurement of the dielectric constant of ice. The plunger is now moved by melting the sample, which thus changes in length while the interface position remains constant; but in all respects relevant to the present discussion the method is equivalent to that of Fig. 10-32*a*. A second modification, developed by E. L. Younker and E. M. Purcell (cf. Ref. 6*a*) is represented in Fig. 10-32*c*, where the use of a mercury well eliminates error due to clearance. The samples, which must be in the form of rods, should be of a diameter  $D$  satisfying

$$0.765\lambda \geq D \sqrt{k} \geq 0.585\lambda$$

to permit propagation at one and only one mode; but in other respects the theory and equations remain the same as for Fig. 10-31*a*. A final modification (Ref. 16*a*), which gives information on  $\tan \delta$  rather than on  $k$ , is that shown in Fig. 10-32*d*. The ratio of maximum to minimum power is taken, first in one side arm and then in the other, as the plunger is moved. From this the ratio of the reflection coefficients at the two points is computed and the procedure thenceforward is the same as that described in connection with Fig. 10-31*d*.

### THE SHORT-CIRCUITED-LINE METHOD

**10-16. Theory.**—Although sufficiently exact for numerical computation when  $r_i = 0$ , the precise analogy to transmission is no longer obtained when  $r_i > 0$ . The following relation, however, which is suggested by Fig. 10-31*c*, may be proved by direct substitution from Eqs. (33), (65), and (69):

$$\left. \begin{array}{l} \text{Complex reflection for a sheet of} \\ \text{thickness } d \text{ backed by a metal} \\ \text{plate } (D = 0) \end{array} \right\} = \left\{ \begin{array}{l} \text{Complex reflection minus com-} \\ \text{plex transmission for a similar} \\ \text{sheet of thickness } 2d \text{ backed} \\ \text{by a matched load.} \end{array} \right.$$

A special case of a similar result which has been proved from the relations of the Introduction, this equation is easily shown, by the methods here adapted for such extension, to be valid without error for lossy materials in waveguide or at arbitrary incidence. This affords another proof

of the unity so often observed in the present text, in that the relations for the short-circuited-line method are contained in those for a single sheet. Of course the details of actual computation require further study, which will be given in the present section; as far as principles are concerned, however, the equivalence has been completely established.

*General Considerations.*—From the result just stated, it may be shown that one of the most significant practical differences between the short-circuited-line method and transmission methods is the behavior of errors. Thus, when dealing with transmission, it was found necessary to have  $1 - t$  small, so that the measured effect would be due to  $\tan \delta$  alone. This condition, which arose through experimental requirements, immediately led to the theoretically simple situations  $r_i \approx 0$  (tapered sample) or  $r \approx 0$  (half-wavelength thickness). It was therefore unnecessary to give a detailed consideration of rectangular samples for general values of  $d$ . When dealing with reflection, on the contrary, no such artifices are required to achieve experimental accuracy; the quantity  $1 - R$  will automatically approach zero with  $\tan \delta$ , irrespective of the value of  $d$  or  $r_i$ . Physically, this behavior follows from the fact that all power not measured must now be absorbed, since none is transmitted through the termination; but in the transmission measurement the power not measured could be either reflected or absorbed. The use of tapered samples, samples an integral number of half wavelengths long, or the other modifications heretofore described, is therefore unnecessary with the short-circuited-line method, and an investigation of the theory for the general case (Fig. 10-31) is well worth while.

If a lossless sheet is backed immediately by a metal plate in free space, the normal-incidence reflection  $Re^{-iR'}$  for the whole is given by

$$Re^{-iR'} = - \frac{(\sqrt{k} - 1) + (\sqrt{k} + 1)e^{-2i\beta d}}{(\sqrt{k} + 1) + (\sqrt{k} - 1)e^{-2i\beta d}}, \quad (69)$$

as is seen if values from Eqs. (8) and (9) are substituted for  $t''$ ,  $\tau''$ ,  $r''$  and  $\rho''$ ; and  $R''$  is set equal to  $-1$  in Eq. (6). By reference to Eq. (12) and Table 10-1, the exact solution is obtained for the general case represented with  $D = 0$  in Fig. 10-31a. The equation so obtained can be put into strikingly simple form without approximation of any kind; whether in free space or guide, the entire problem reduces to the transcendental equation (Refs. 2b, 5b)

$$\frac{\tanh(ae^{ib})}{ae^{ib}} = ce^{rd}, \quad (70)$$

where  $c$  and  $d$  are known and  $a$  and  $b$  are required. Since it involves but two variables, the left-hand side of Eq. (70) may be plotted or tabu-

lated without difficulty (Ref. 5b) and thus, in principle at least, a general solution of the problem with arbitrary thickness, interface reflection, and loss is obtained. It is worth noting that the short-circuited-line method, or modifications of it, are apparently the only ones for which the general equation simplifies in this way. Although simple results can be found for the other methods, they depend upon neglect of  $\tan^2 \delta$ , elimination of  $r_i$ , or some similar artifice.

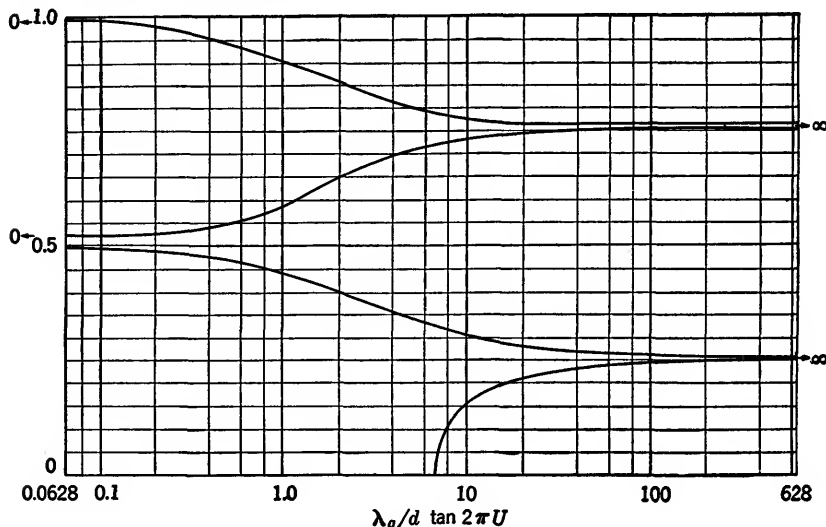


FIG. 10-33.—A plot of  $2\pi \tan x/x$  giving the general solution of Eq. (71);  $x = 2\pi V$ .

In spite of this increased simplicity (as compared with the corresponding result for other methods) actual computation from Eq. (70) leads to a certain amount of difficulty in practice. The mathematical methods whereby such difficulty is circumvented are not relevant in a discussion of measurement procedure, and are moreover described at length elsewhere (Refs. 1a, 2b, 5b). It therefore suffices here to point out the existence and theoretical advantages of Eq. (70). Attention is henceforward confined to the case  $\tan^2 \delta = 0$ , which leads to simple relations, and actually includes most situations of practical interest. The results, to this approximation, are given in Refs. 26b, 9b, and, together with correction terms for more accurate approximation, in Ref. 22b:

$$\frac{\tan 2\pi V}{V} = \frac{\lambda_0}{d} \tan 2\pi U, \quad (71)$$

$$\tan \delta = W \left( \frac{k-p}{k} \right) \frac{4\pi \csc 4\pi U}{4\pi V \csc 4\pi V - 1} \quad (72)$$

The quantities  $U$ ,  $V$ ,  $W$  are given by

$$\begin{aligned}
 U &= \frac{(\Delta + d)}{\lambda_g}, \\
 V &= \frac{d \sqrt{k - p}}{\lambda}, \\
 W &= \frac{1}{\pi} \frac{1 - R}{1 + R},
 \end{aligned}
 \tag{73}$$

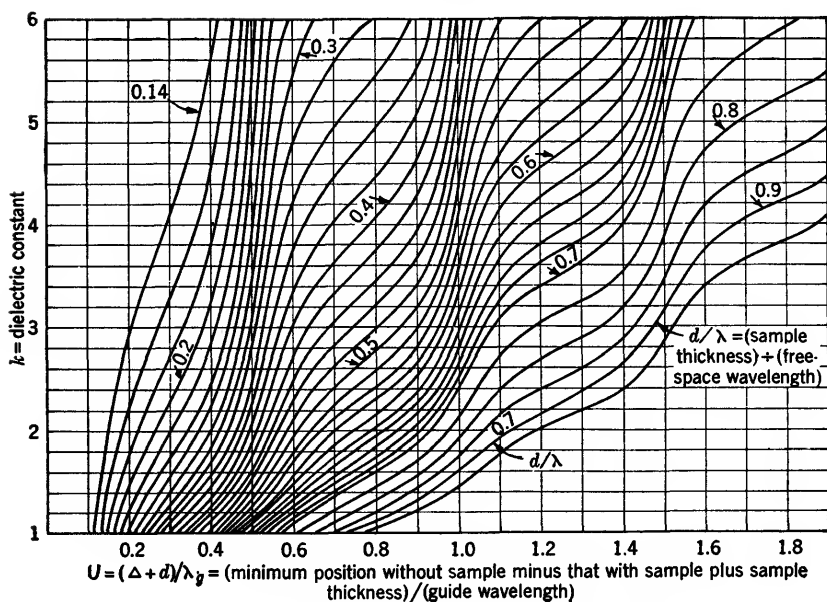


FIG. 10-34.—Explicit curves of  $k$  vs. measured quantities, valid for  $p = 0.345$ .

in terms of the amplitude reflection coefficient  $R$  and the shift in minimum position  $\Delta$  produced by insertion of the sample. Although transcendental, Eq. (71) is readily solved by graphical means; indeed, a plot of  $(\tan x)/x$  is all that is required (Fig. 10-33). When much work is to be done for a given value of  $p$ , however, it is expedient to give a less general presentation such as that shown in Fig. 10-34. The equation for  $\tan \delta$  is likewise solved conveniently by means of graphs; because of periodicity, a single set of curves covering a limited range suffices for all cases (Fig. 10-35). When the thickness is an integral number of quarter wavelengths, this graph cannot be accurately read; but its equation then takes the simpler forms

$$\begin{aligned}
 \tan \delta &\approx \frac{W\lambda^2}{kd\lambda_g} \\
 \tan \delta &\approx W \frac{\lambda_g}{d} \left( \frac{(k - p)}{k} \right),
 \end{aligned}
 \tag{74}$$

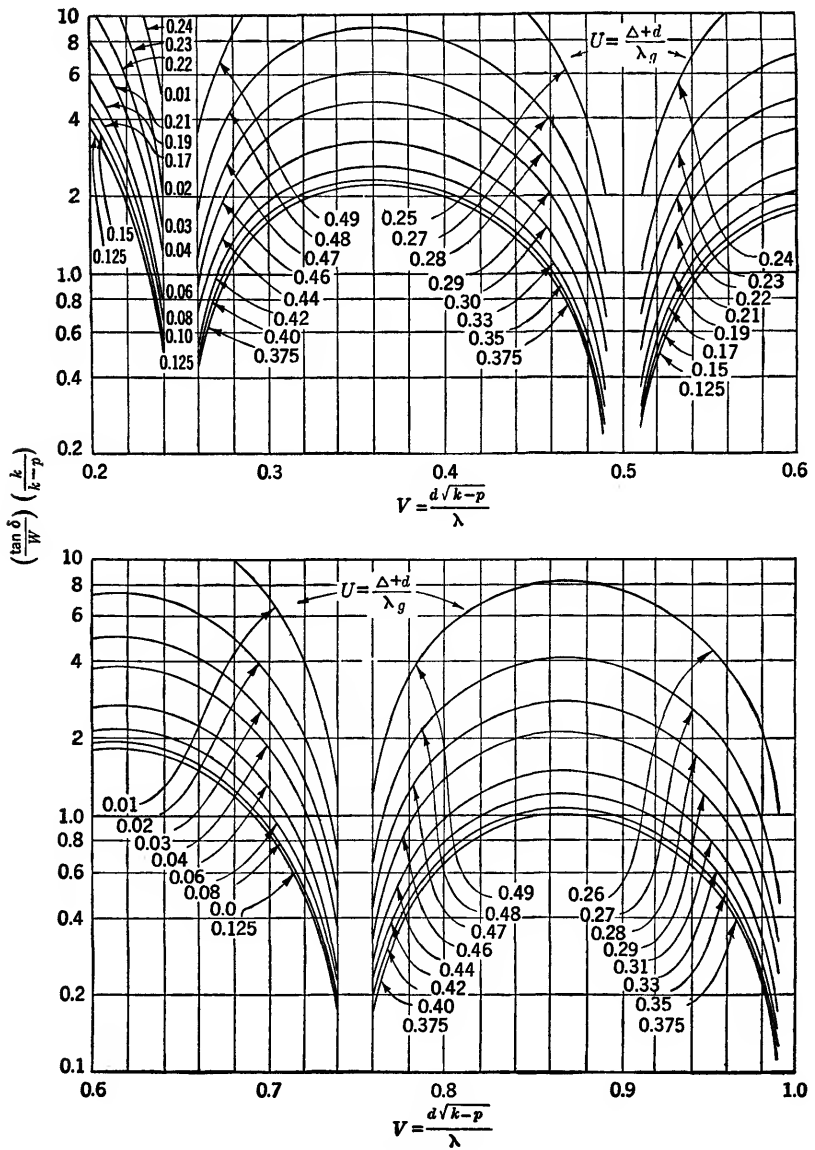


FIG. 10-35.—Curves for computation of  $\tan \delta$ , valid for all values of  $p$ .



and graphical computation is less convenient than direct computation for this case. The error is less than 5 per cent in the first equation when  $0.73 < V < 0.77$ , in the second when  $0.48 < V < 0.52$ . Wall losses are compensated as described in Sec. 10-18.

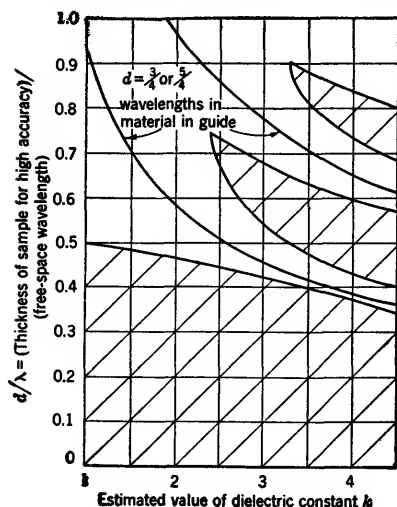


FIG. 10-36a.—Value of sample thickness for maximum accuracy with short-circuited-line method. Condition for minimum slope in Fig. 10-34. The slope is greater than  $60^\circ$  in the shaded region, less than  $60^\circ$  elsewhere.

thickness is an odd number of quarter wavelengths (Ref. 5b). Thus, Eq.

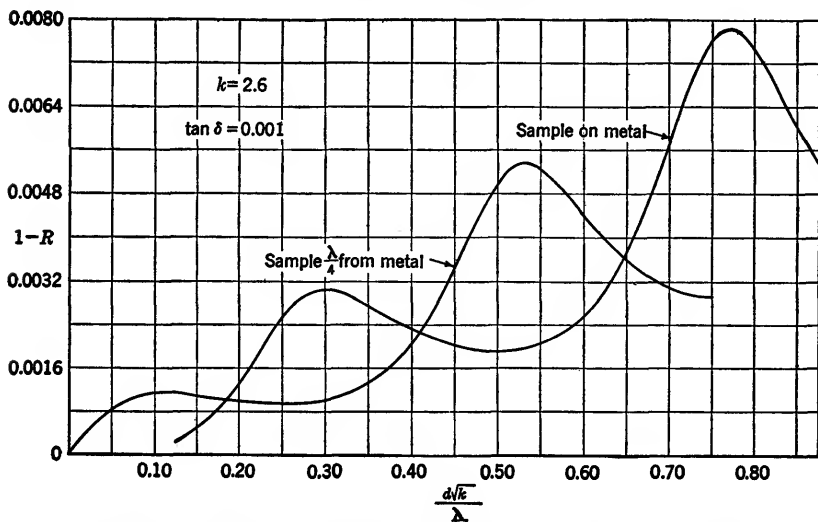


FIG. 10-36b.—Relation of the measured quantity  $(1 - R)$  to sample thickness.

(20) with  $n$  odd is the condition for minimizing the slope of the curves in Fig. 10-34. To estimate the permissible deviation, a point on the curve may be found where the slope has some preassigned constant value; although highly arbitrary, such a procedure does give an indication of the general behavior (Fig. 10-36a). The same condition maximizes the value of  $1 - R$  and thus minimizes the error in  $\tan \delta$  (cf. Ref. 5b and Fig. 10-36b). On account of these considerations, which are shown by Fig. 10-36c to be important in practice as well as in theory, the original data should fall in a restricted region of the curves. For purposes of computation this restricted region may be plotted on an expanded scale, as shown in Fig. 10-37, the remainder of the curves being omitted. Alternatively, a preliminary value of  $k$  may be obtained with any thickness, this preliminary value may be used to satisfy Eq. (20), and the final values of  $k$  and  $\tan \delta$  may be computed from the resulting simplified form of Eq. (70). The merit of this procedure (cf. Refs. 5b, 24b) is most evident when  $\tan^2 \delta \neq 0$ , as the computations are then greatly facilitated. For low-loss materials of the type here considered, however, the equations are sufficiently simple in the first place without this experimental complication; and in most cases  $k$  can be estimated well enough beforehand to come within the range required by Figs. 10-36a and 10-37.

Before this question of the optimum value for  $d$  is left, it should be noted that another consideration will lead to the opposite conclusion from the one just obtained. Thus, an error is produced by irregularity in the air-sample interface or by a failure to have it perpendicular to the waveguide axis; this error will presumably be minimum when the interface is in a region of minimum field (Ref. 13a). The "optimum" thickness on this basis is an integral number of half wavelengths,  $d = n\lambda_m/2$ , a value that is also obtained for  $k$  by maximizing the slope in Fig. 10-38 rather than in Fig. 10-34 (cf. Ref. 18b). Thus, the previous argument is to be regarded with a certain diffidence in some cases.

*Gap between Sample and Short Circuit.*—The foregoing results assume that the sample is immediately followed by the short circuit, which is perhaps the most convenient situation in practice. There may, however, be a gap between sample and termination, as shown in Fig. 10-31a, and it is of interest briefly to consider this new arrangement. It is clear that the necessary theoretical relations are contained in the introduction for that case also; it suffices in fact to substitute  $r'' = \rho'' = r$  as determined by Eq. (65),  $t'' = r'' = t$  as found from Eq. (33), and

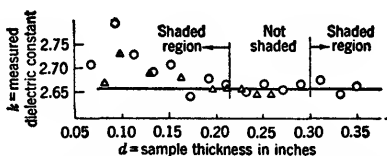


FIG. 10-36c.—Measured dielectric constant vs. sample thickness at  $\lambda = 1.25$  cm.

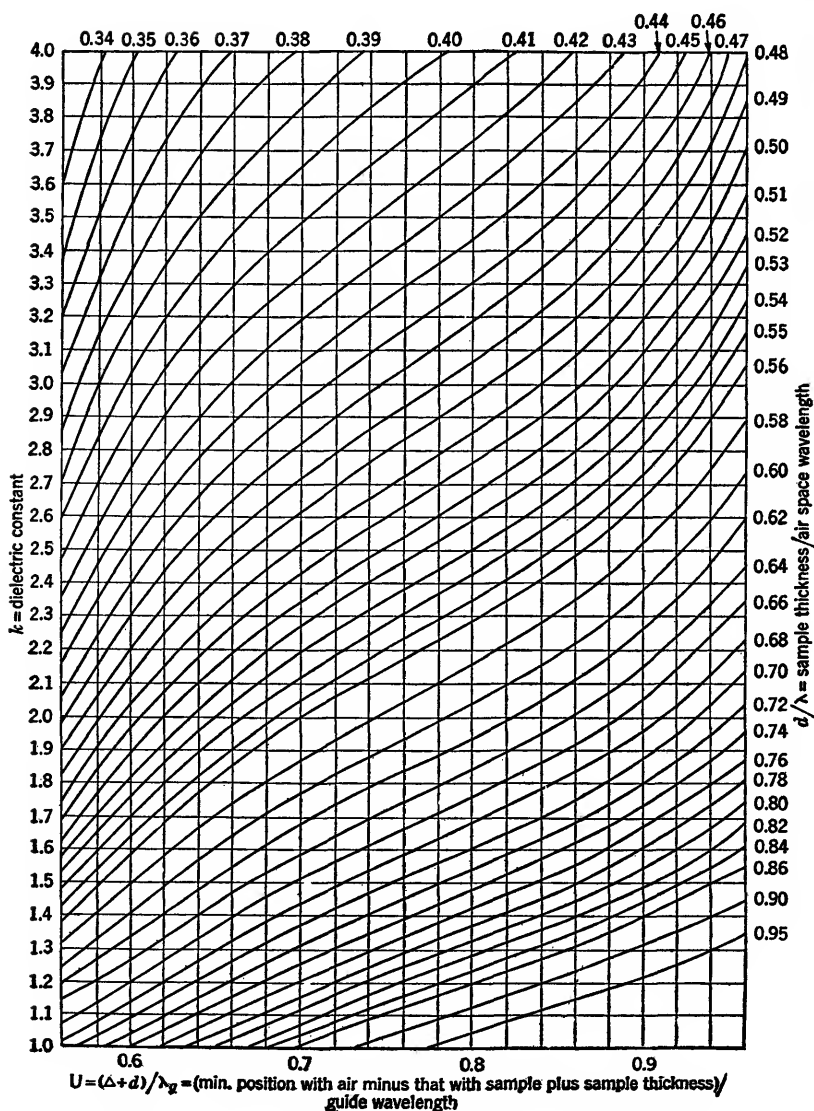


FIG. 10-37.—Expanded chart for computation of  $k$  when  $p = 0.345$ , giving region of high accuracy only.

$R'' = e^{-\frac{4\pi j D}{\lambda}}$ , for the variables of Eq. (6), which then gives  $B/A$ , the over-all reflection of sample and short circuit in the free-space analogue of Fig. 10-31a. The extension to guide is made in the usual way; specifically  $t$  and  $r$  are taken appropriate to that case and  $\lambda$  is replaced by  $\lambda_g$ ,

in the relation for  $R''$ . Since it illustrates no new principles, and is moreover rarely used in practice, the somewhat complicated relation so obtained is omitted (see Ref. 5b). The exact solution, however, leads to an equation of the form of Eq. (70). Perhaps the most significant change, from a practical point of view, is in the behavior of errors. Thus, the optimum thickness is found to be an odd number of quarter wavelengths when  $D = 0$ ; but if on the other hand  $D = (2n + 1)\lambda_g/4$ , then the optimum thickness for both  $k$  and  $\tan \delta$  is an even number of quarter wavelengths (Ref. 5b) (cf. Ref. 5b and Fig. 10-36b). For a thin sample, near-optimum accuracy is obtained if the location of the sample is symmetrically disposed about an antinode (cf. Ref. 12b), but for practical

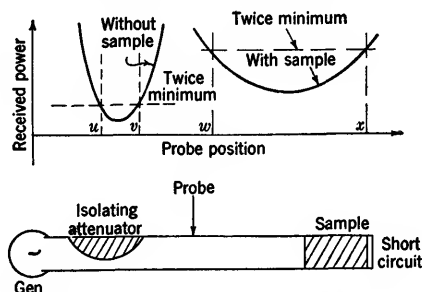


FIG. 10-38.—Measurement of reflection by taking probe positions at which the power equals twice its minimum value.

work the two values  $D = 0$  or  $D = \lambda_g/4$  are usually sufficient. It must be noted, in this connection, that the reflection for several values of  $D$  may be taken (Refs. 19a, 23b) and that  $k$  and  $\tan \delta$  may be computed by relations somewhat different from those given here. It is not apparent, however, that any appreciable advantage is obtained thereby, and the duplication of effort, the need for moving the sample, and the difficulty of compensating for wall losses between sample and short circuit are undesirable in practical work.

**10-17. Measurement Procedure.**—Hitherto theoretical methods of finding  $k$  and  $\tan \delta$  from the measured quantities  $R$  and  $\Delta$  have been considered. The experimental techniques merely concern the problem of impedance measurement, for which a number of different methods are available from current practice. Free-space methods have been considered in detail, and no new problems are presented by the short-circuited-line procedure. In fact the experimental operations are somewhat easier to perform than in other methods, since the metal plate can remain stationary at all times, while the sample is placed on it or removed as required. The problem of locating sample and metal at precisely the same distance from the antennas, which is one of the chief difficulties of measuring phase in free space, accordingly does not arise in

the short-circuited-line method. A similar advantage is that the reflection of the combination of sample and metal is usually about the same as that from metal alone, and thus a sharp minimum for phase measurement can be obtained in both cases.

*Direct Measurement of Standing-wave Ratio.*—Perhaps the most widely known of the waveguide methods is that in which the maximum and minimum received powers,  $M^2$  and  $m^2$ , are measured as the probe is moved along the line, whereupon the reflection is computed from

$$R = \frac{(M - m)}{(M + m)}, \quad (75)$$

and  $\Delta$  is determined by setting the probe on a minimum. Despite its general acceptance, this method has certain shortcomings for the case at hand. In the first place, r-f detectors obey the square law only approximately, and often the voltage  $V$  from the detector is

$$V \propto E^\alpha, \quad (76)$$

where  $E$  is the electric field in the r-f line. If  $\alpha \neq 2$ , such a relation never gives true proportionality of r-f power and receiver reading, and it is apparent that both the magnitude and the percentage error approach infinity with power standing-wave ratio, no matter how small the deviation of  $\alpha$  from the ideal value 2 may be. Nor is it easy to correct the error by evaluation of  $\alpha$  and by use of Fig. 10-39, for  $\alpha$  is likely to depend on field strength over the wide ranges encountered in the present application, since a detector sufficiently sensitive to respond to the minimum is usually overloaded at the maximum. For the measurement of high-power standing-wave ratios by the proposed method a calibrated attenuator must be used in somewhat the same manner as that previously described for transmission; specifically, the maximum when the attenuator is present and the minimum when it is absent are measured—a procedure which introduces new errors, however, in accordance with Table 10-2.

From the foregoing it appears, first, that errors due to nonlinearity become excessive when high standing-wave ratios are measured by the maximum-to-minimum technique; and second, that these errors can be reduced by the use of an attenuator, although a certain amount of care must be exercised in this operation. Direct measurement of high standing-wave ratios in the manner described is open, however, to still another objection, namely, in the derivation of Eq. (75) not only is the voltmeter reading assumed to be proportional to the r-f power at the probe but also it is assumed that this r-f power itself remains unchanged when the probe enters the line. For quantitative investigation, the generator may be regarded as matched to the line,  $G = 0$ , which condition has just been shown to be desirable in any case. The true value

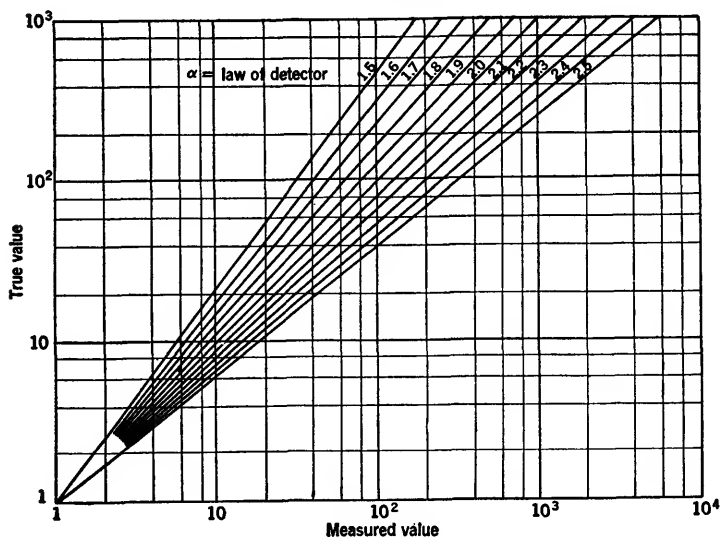
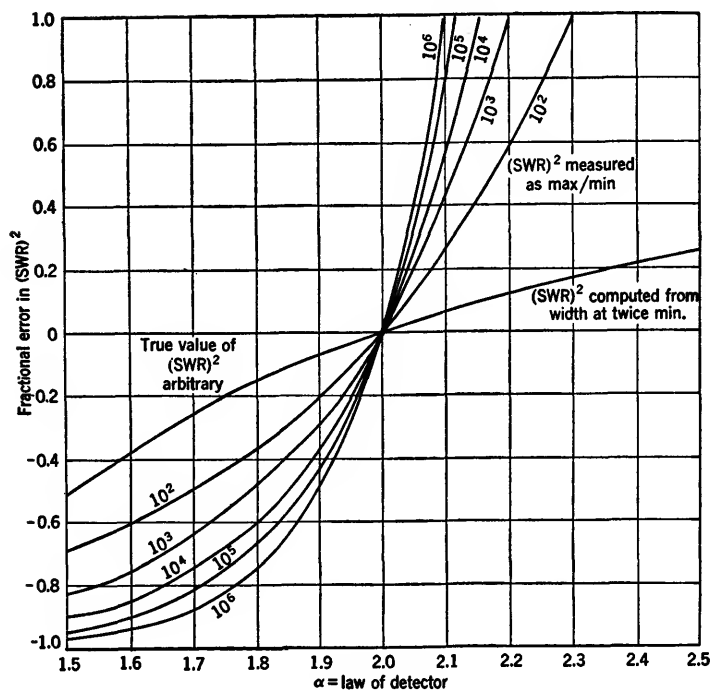


FIG. 10-39.—Theoretical effect of detector nonlinearity on certain r-f measurements. Lower curves: Effect on power transmission as measured directly; or on power reflection as measured at incidence far from normal; or on  $(SWR)^2$  as measured by the maximum-minimum technique. Upper curves: Comparison of the effects of nonlinearity in the maximum-minimum method of reflection measurement and measurement from the width at twice the minimum.

of the reflection  $R$  may be assumed to differ but slightly from unity. By the methods of Ref. 5a, or directly from Eq. (7) of the present text, the relation plotted in Fig. 10-40 is obtained,

$$\text{fractional error in } (1 - R) = -2 \frac{P + \cos P'}{1 + 2P \cos P' + P^2}, \quad (77)$$

or, for  $P' = \pi$ ,

$$\text{fractional error} = \frac{2P}{1 - P}, \quad (78)$$

for the fractional error in  $1 - R$  produced by a thin probe with reflection coefficient  $Pe^{-iP'}$ . Equation (78) is usually valid if the probe is tuned

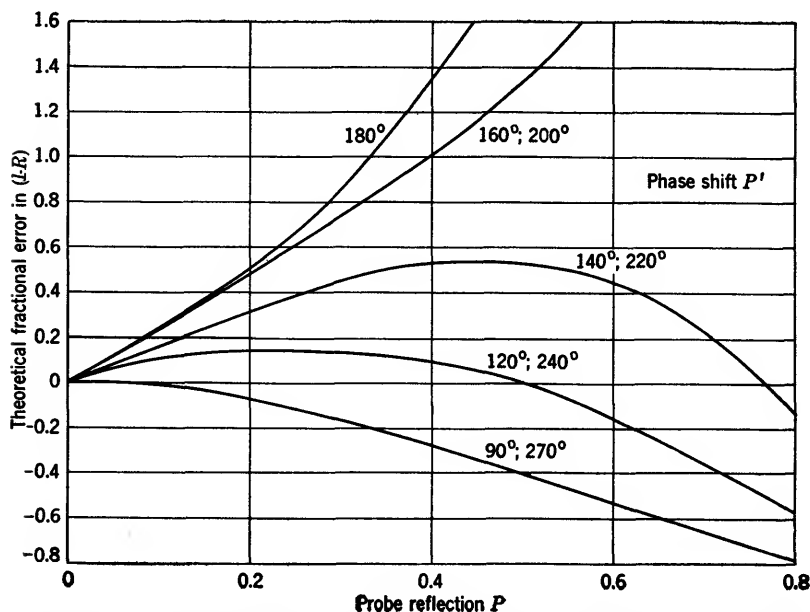


FIG. 10-40.—Fractional error in  $(1 - R)$  produced by a probe reflection  $P \exp (iP')$  when a high reflection  $R$  is measured by the maximum-minimum technique and the generator is matched to the line.

for maximum pickup, as was shown in Ref. 5a, where it was also found that the dependence of  $P$  on the probe depth  $\delta$  is essentially exponential:

$$P = Ae^{B\delta}. \quad (79)$$

The error in minimum position is also given in Ref. 5a; it is of the order of  $P \sin P' (1 - R)^2$  and is entirely negligible here.

When added to those just obtained, this result on probe reflection permits numerical estimates of the over-all error to be anticipated in ordinary practice. Suppose, for example, that a power standing-wave ratio of  $10^5$  is to be measured directly as the quotient of maximum and

minimum. If no attenuator is used it is seen that a detector law of 2.02 (instead of 2.00) leads to an error of 26 per cent in the final result, exclusive of inaccuracy caused by the probe. To avoid this error, an attenuator known to have exactly 40 db attenuation and a reflection coefficient, from either side, of 0.01 per cent in power is used. Error due to non-linearity is now reduced to about 5 per cent. Since an attempt to match generator to load, if successful, might lead to an error of over  $10^5$  per cent upon insertion of the attenuator, the generator is isolated by an attenuator whose reflection is likewise 0.01 per cent in power. The maximum error due to reflection is then about  $\pm 8$  per cent, as seen by Table 10-2; thus the over-all error is now 12 per cent instead of 26 per cent. To either figure must be added the inaccuracy due to the probe, however, which is shown by Eq. (78) to be about 30 per cent in power standing-wave ratio if the probe reflects as much as 0.5 per cent in power. With these rather conservative estimates for detector law and reflection coefficients, errors as high as 40 to 50 per cent may be expected in the final power standing-wave ratio if it is measured by the procedures here described.

*Computation from Width at Twice Minimum.*—The foregoing method has been considered in some detail, partly because it is standard practice for most types of reflection measurement, and partly because the excellent alternative method developed by A. R. von Hippel (Refs. 2b to 5b) can be properly appreciated only after a discussion of the sort just given. In this alternative method the probe positions  $u$  and  $v$  at which the power has twice its minimum value are measured as illustrated in Fig. 10-38. If a lossless line, exact linearity of all receiver components, and zero probe reflection may be assumed, then the expression

$$(SWR)^2 = 1 + \csc^2 \left[ \frac{\pi(v-u)}{\lambda_g} \right] \\ \approx \frac{1}{[\pi(v-u)/\lambda_g]^2} \quad (80)$$

is obtained for the standing-wave ratio produced by the termination. The approximate Eq. (80) is valid with an error less than 1 per cent whenever the standing-wave ratio is greater than 133, and it will henceforward be treated as a strict equality. In terms of the measured positions  $u$  and  $v$  without the sample,  $w$  and  $x$  with the sample (Fig. 10-38) the quantities  $U$  and  $W$  of Eq. (73) take the form

$$U = [(u+v) - (w+x) + 2d] \frac{1}{2\lambda_g}, \quad (81)$$

$$W = \frac{(x-w)}{\lambda_g}, \quad (82)$$



and preliminary computation of the reflection coefficient  $R$  is unnecessary in practice. It must be mentioned, incidentally, that the three quantities  $1/(SWR)$ ,  $(1 - R)$ , and  $(x - w)$  all vary in approximately the same way. As is seen from Eqs. (75) and (80) they are in fact almost proportional whenever  $R \approx 1$ . Hence the fractional error of any one is nearly equal to that of any other; and the three quantities shall therefore be regarded as interchangeable. Whichever one happens to give

the simplest result for the problem at hand should be used.

In a consideration of experimental errors, it is found that those discussed in the preceding paragraphs are practically eliminated by the method in question. The effect of nonlinearity is represented by

$$\text{fractional error in } (SWR)^2 = 2 - 2^{2/\alpha}, \quad (83)$$

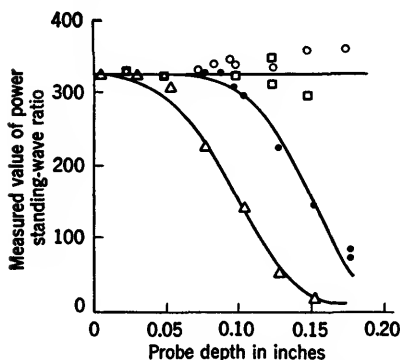


FIG. 10-41.—Experimental comparison of the effects of probe penetration on  $(SWR)^2$  as measured by the maximum-minimum and twice-minimum techniques in guide at  $\lambda = 3.2$  cms. The points  $\circ$ ,  $\square$  represent values taken by the twice-minimum method with the generator matched to the line and load, respectively, while the points  $\bullet$ ,  $\Delta$  represent corresponding results as measured by the maximum technique. The curves are theoretical with the constants  $A$ ,  $B$  of Eq. (79) adjusted for optimum fit, the same values being used for each curve; data from Ref. 6a.

is eliminated. From the fact that the probe is in a region of low field it may be concluded (Ref. 5b) that these errors too, although not obviated entirely, are greatly reduced. Intuitive reasoning of this sort is indeed verified by quantitative calculation. Probe errors with a matched generator are completely negligible in the sense that the approximations made in the derivation of Eq. (80) are equally valid whether  $P$  be zero or positive (Ref. 5a). In other words, irrespective of the value of  $P'$ , the only terms in  $1 - R$  which are affected by probe reflection are terms of the order of  $1/(SWR)^2$  or higher, and are of no significance here. That this relative insensitivity to probe reflection is found in practice is verified by Fig. 10-41.

**Power Level for Optimum Accuracy.**—This superiority of the alternative method is not confined to measurement of standing-wave ratios, but is

found for the minimum position as well. Thus, instead of a setting on a point of zero slope being attempted, two points for which the slope is positive are averaged, a procedure that is feasible by virtue of the symmetrical curve shape (cf. Fig. 10-15 and accompanying remarks). If the determination of minimum position is considered in more detail, the error in position is found to be about equal to that in the two measurements of distance  $v$  and  $u$ . These errors will be least if the power level at which they are made is such that the slope of the curve of meter-needle displacement vs. distance is a maximum. If the meter is linear, the maxi-

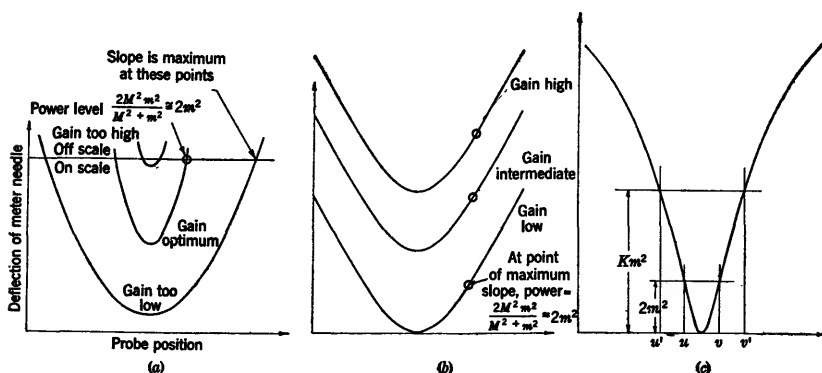


FIG. 10-42.—Conditions on receiver gain and portion of curve selected, to obtain optimum accuracy. (a) Effect of gain on slope with a linear meter. (b) Same, logarithmic meter. (c) Measurement of width at twice minimum from that at  $K$  times minimum.

imum of the curve will be far off scale in normal practice, and the points of greatest slope occur at full-scale deflection. As the gain is increased, this maximum slope will likewise increase up to a certain point, then decrease to zero when the minimum itself causes a full-scale deflection. Quantitative investigation shows this point of maximum slope to occur at the harmonic mean of maximum and minimum as illustrated in Fig. 10-42a. To determine phase with optimum accuracy when a linear meter is used for large standing-wave ratios the gain should be adjusted until the minimum leads to half-scale deflection, and the two probe positions that are then found to lead to full-scale deflection should be averaged. If the meter is logarithmic rather than linear, all properties relevant to the present discussion are independent of receiver gain (Fig. 10-42b), in contrast to the results noted. When the derivative is maximized, however, the harmonic mean of maximum and minimum represents the condition for maximum slope and hence, as before, the optimum points for high standing-wave ratios are the ones actually used. The methods and results of this paragraph are valid for any curve which approximates a parabola near the minimum.

The question of slope is somewhat more complicated when the width of the curve rather than minimum position is considered. Thus, if the length of a segment is measured at a power level  $K$  times the minimum, as shown in Fig. 10-42c, then the desired twice-minimum segment is given by (Ref. 2a)

$$v - u = \frac{\lambda_g}{\pi \sqrt{K-1}} \sin \frac{\pi(v' - u')}{\lambda_g} \approx \frac{(v' - u')}{\sqrt{K-1}} \quad (v' - u') \ll \lambda, \quad (84)$$

and the error in  $v - u$  is thus less than that in  $v' - u'$  by a factor  $\sqrt{K-1}$ , approximately. For this reason greater accuracy is sometimes achieved by taking one-third the width at ten times the minimum, for example, rather than by direct measurement of the width at twice the minimum. Despite the fact that the end points of such a segment are determined with less accuracy than is the case for  $v - u$ , the additional error is often more than compensated by Eq. (84). No such desirable behavior is found for errors from nonlinearity, however; instead of Eq. (83),

$$\text{fractional error in } (SWR)^2 = \frac{K - K^{2/\alpha}}{K - 1}. \quad (85)$$

The expedient of Fig. 10-42c is to be recommended, then, only for unusually low-loss samples that give a minimum too narrow to be measured with precision, and only when the detector is accurately linear. In other cases the increase in accuracy, if obtained at all, would scarcely warrant the added complications.

**10-18. A Few Sources of Error.** *Impurity of Generator Output Power.* It has been assumed throughout the foregoing discussion that only a single frequency is generated by the source of r-f power. The output power of a modulated klystron does not always satisfy this condition, however, but sometimes has components at frequencies different from the fundamental. This behavior is the result of improper modulation of the generator (Ref. 1a); it is quite different from the normal presence of harmonics in the frequency spectrum of a pulse. Since they deal chiefly with generator adjustment or design rather than with measuring techniques, methods of correction are not included here (cf. Ref. 1a). It is of interest, however, to investigate the effect as to order of magnitude, an investigation that is readily made by Eq. (7) of the Introduction. As described in Ref. 1a, the r-f power is not present simultaneously at two different frequencies, but rather one frequency exists for alternate pulses of the modulator, or one frequency at one point of each pulse, a different frequency at a later point of the same pulse. For approximate quantitative computation, therefore, powers are added instead of amplitudes, and the meter reading is assumed to be the sum of the values for the two individual frequencies. With such an approach neither equal

resonance of the cavity nor equal sensitivity of the receiving system need be assumed, and in addition, the power need not be equally divided between the two frequencies. If the load reflection is independent of frequency over the small variation in question, then

$$\frac{1}{(SWR)_{\text{measured}}^2} = \frac{1}{(SWR)_{\text{true}}^2} + \frac{1}{1-p} \left( \frac{\pi X}{\lambda} \right)^2 \left( \frac{2\rho}{1+\rho^2} \right)^2 \left( \frac{\Delta f}{f} \right)^2 \quad (86)$$

gives the measured standing-wave ratio at a distance  $X$  from the interface in terms of its true value, and the ratio  $\rho^2$  of received powers at frequencies  $f, f + \Delta f$ . The error in minimum position is of the order of  $\Delta f$ ; but when the results for sample and short circuit are compared, the error is found to be nearly the same in both cases and thus to cancel out.

The result of Eq. (86) was obtained for direct measurement of the power standing-wave ratio as the ratio of maximum to minimum. If the power is set equal to twice its minimum value, however, and the above assumptions are retained, an identical expression is found for the error, except that the power standing-wave ratios are replaced by the squares of the twice-minimum widths as given by Eq. (80). Thus, direct measurement of the standing-wave ratio and computation from the width of the curve are equivalent as far as sensitivity to impurity of the frequency is concerned (Ref. 2a). The error in width, which has been seen to be essentially equivalent to that in  $1/(SWR)$ , is proportional to the right-hand term of Eq. (86) if the error is small compared with the actual width; but if the reverse is the case then the error is proportional to the square root of this term. In particular, for a perfect short circuit, which gives a true width of zero,

$$\text{measured width} = \left( \frac{X}{1-p} \right) \left( \frac{2\rho}{1+\rho^2} \right) \left( \frac{\Delta f}{f} \right) \quad (87)$$

The first factor shows that the error increases as the average frequency approaches the cutoff wavelength of the guide, and that it is proportional to the distance from the minimum to the sample; the second indicates that the error is proportional to the geometric mean of powers at  $f$  and  $f + \Delta f$  divided by the arithmetic mean; from the last factor it is seen that the error is proportional to the percentage change in frequency,  $\Delta f/f$ . These remarks apply to the general case of nonzero width, if the error in width and each factor mentioned are squared. For example, if the frequency is 3000 Mc/sec and  $p = \frac{1}{2}$ , the measured width at the second minimum for a perfect short circuit [Eq. (87)] is found to be about 0.0019 in. when the power ratio  $\rho^2$  is unity and the frequency difference is  $\frac{1}{2}$  Mc/sec, whereas it is 0.001 in. when this difference is  $\frac{1}{4}$  Mc/sec. If the true width is 0.002 in., however, then the error becomes 0.0007 or 0.0002 in., respectively. These computed values are consistent with the experimental

results of Ref. 1a, where a transmitter bandwidth of  $\frac{1}{2}$  Mc/sec was found to be satisfactory and a bandwidth of  $\frac{1}{2}$  Mc/sec caused a noticeable increase in the measured width of the curve.

**Wall Losses.**—The foregoing errors occur in the actual process of finding  $U$  and  $V$ . When the quantities  $k$  and  $\tan \delta$ , are computed from these measured quantities, an additional error is found to be introduced by the neglect of wall losses. To correct this error much the same procedure is used as for transmission. The data are manipulated to obtain the values for lossy guide surrounding the sample, lossless guide elsewhere, and the computed result is interpreted by Eq. (40). With the short-

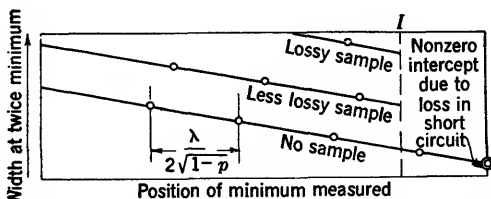


FIG. 10-43.—Detailed behavior of width at twice minimum.

circuited-line method the calculation (Ref. 1a) is particularly simple. As illustrated in Fig. 10-43, the width at twice minimum increases almost linearly with distance from the short circuit (Ref. 5b), and the curves for different terminations are all parallel to one another. Both results have been verified by experiment; theoretically they follow from the fact that  $\tan \delta_{\text{wall}}$  is small enough to give  $\exp(\tan \delta_{\text{wall}}) \approx 1 - (\tan \delta_{\text{wall}})$ . With such linear dependence it is a simple matter to extrapolate the minimum width from the point at which it actually occurred to the air-dielectric interface  $I$  of the figure. Although appropriate only to point  $I$  for lossy guide, this same extrapolated width would be appropriate to any point when the guide leading to the sample is lossless. With this procedure, which neglects the small loss in the short circuit, it is found (Ref. 1a) that  $\tan \delta$  equals the value of  $\tan \delta$  as obtained from Eq. (72) with extrapolated width, minus  $\tan \delta_{\text{wall}}$ . The quantity  $\tan \delta_{\text{wall}}$  is obtained from

$$\tan \delta_{\text{wall}} = D(1 - p) \quad (88)$$

if  $D$  represents the difference in the  $W$ 's obtained, either with or without the sample, for the  $k$ th and  $(k + n)$ th minima. Losses in the  $(v - u)$  length of guide over which the probe moves are neglected, as well as all wall losses, in computing phase. These approximations were also used in the transmission methods already described; that they are justified is easily proved theoretically. Additional verification is given in Fig. 10-44, where neglect of loss is actually permissible over a portion of line much larger than the length  $(v - u)$  in question here.

*Insufficient Power.*—A third source of error sometimes encountered is the frequency shift produced by the changing character of the load, or, with adequate isolation, the increase in apparent signal due to receiver noise. Thus, the short-circuited-line method differs from the others mentioned in that it leads to high mismatches that are of variable phase. Hence, whereas isolation of the generator was formerly of only secondary importance, it is now necessary to provide the requisite stability, for

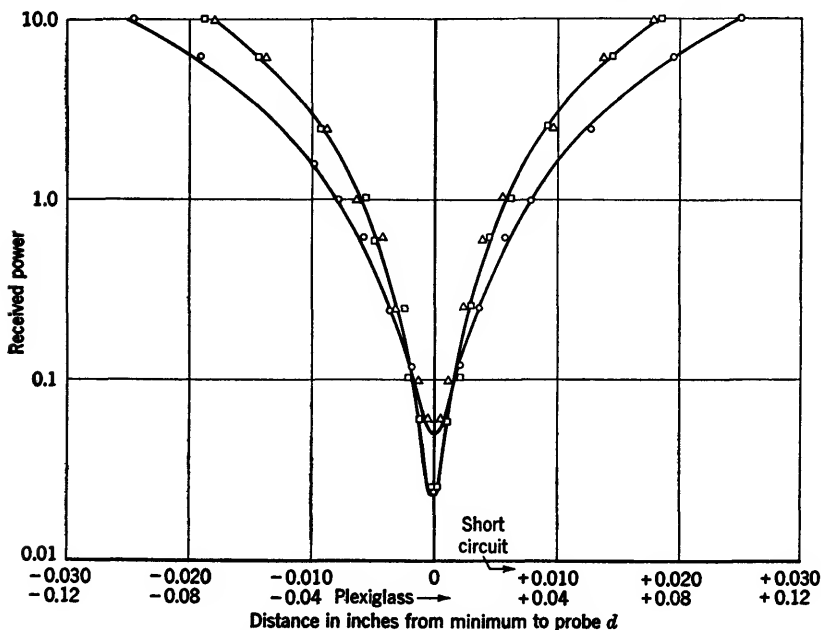


FIG. 10-44.—Experimental verification that neglect of loss is permissible in the region traversed by the probe. The points are experimental at  $\lambda = 3.2$  cm; the curve is theoretical, matched at two points. The triangles are for the probe near the short circuit, the squares are for the probe a half wavelength farther from the short circuit, and the circles are for plexiglas plus short circuit.

despite the high and variable mismatch, the generator frequency must be the same when the two measurements are taken with and without sample. Even if the receiving systems were of equal sensitivity in both cases, the short-circuited-line method would require more power, for a given signal-to-noise ratio, than methods depending on transmission. In actual practice, however, this difference in available transmitter power caused by the need for isolation is enhanced by a similar difference in the receiving equipment. Thus, for transmission, a bolometer or similar device is used, placed in the line at the antinode of a short circuit, with the result that most of the r-f power actually contributes to receiver

reading. In the short-circuited-line method, on the other hand, the role taken by the bolometer is now taken by a traveling probe, which responds to only a small fraction of the total power available. Indeed it has been shown (Ref. 5a) that a thin probe cannot remove more than one-fourth of the power from the line, irrespective of its depth, and that the figure in ordinary practice is considerably less than this. Because of this combined loss of transmitter power and receiver efficiency it is found, at the higher frequencies, that klystron oscillators usually provide insufficient power<sup>1</sup> for the short-circuited-line method to be successfully used. A magnetron transmitter leads to no improvement, as the use of a bolometer instead of a crystal, necessitated by the short pulse, offsets the gain in transmitter power by a corresponding decrease in detector sensitivity (Ref. 6b). In principle the power standing-wave ratio may be increased by artificial means, and thus the need for readings at low power is avoided; for example, a poor short circuit may be used or a quarter-wave sheet of lossy material may be placed between the sample and the termination (Refs. 23b, 24b). Such expedients, however, are easily seen to destroy the inherent accuracy of the method. Thus, the value of  $\tan \delta$  depends essentially on the difference of the two widths when the sample is present or removed (Ref. 23b). Not only will this difference be small when the sample has loss low enough to require an artificial increase, but the original measurement of the width loses accuracy because of the decreased slope. These considerations are not to be confused with those of the foregoing discussion, where it was found preferable to adjust  $d$  for a large value of  $(1 - R)$ . The increase in  $(1 - R)$  there obtained was entirely due to the desired quantity  $\tan \delta$ , whereas it is now the result of the introduction of an extraneous loss that must be later subtracted. In view of these problems, then, there is need for a modified procedure that will give essentially the same information as that obtained from the points  $u, v, w, x$ , of Fig. 10-38, but which will nevertheless presuppose no knowledge of the minimum.

**10-19. Modified Procedure for Low Power.**—Determination of the minimum position  $(u + v)/2$  presents no difficulties. If the attenuation is neglected in the part of the line in which the measurement is made (not in the load, nor in the line leading to it) it may be shown that the average of any two suitable probe settings for which the voltmeter readings are equal will give the minimum position. This is true independently of the law of the detector. Although the condition of maxi-

<sup>1</sup> This problem has been recently attacked by electronic methods that are quite different from the r-f methods to be considered here. Besides being at present incomplete, however, such procedures are concerned chiefly with the means of power detection or with receiver design. As far as r-f dielectric measurement itself is concerned they suggest no new principles, and are therefore omitted from the present discussion.

imum slope is no longer obtained, the curve is steep enough to give accuracy adequate for most purposes, and there is some compensation too in that fluctuations from noise are reduced. That such considerations are valid in practice was verified in Ref. 2a, where accuracies of the order of  $\pm 0.0002\lambda$  for a short circuit and  $\pm 0.0004\lambda$  for a sample were consistently obtained at power levels 20 to 25 db above the minimum.

*Derivation.*—From the ease with which the minimum position  $(u + v)/2$  may be found at low power it might be expected that equally

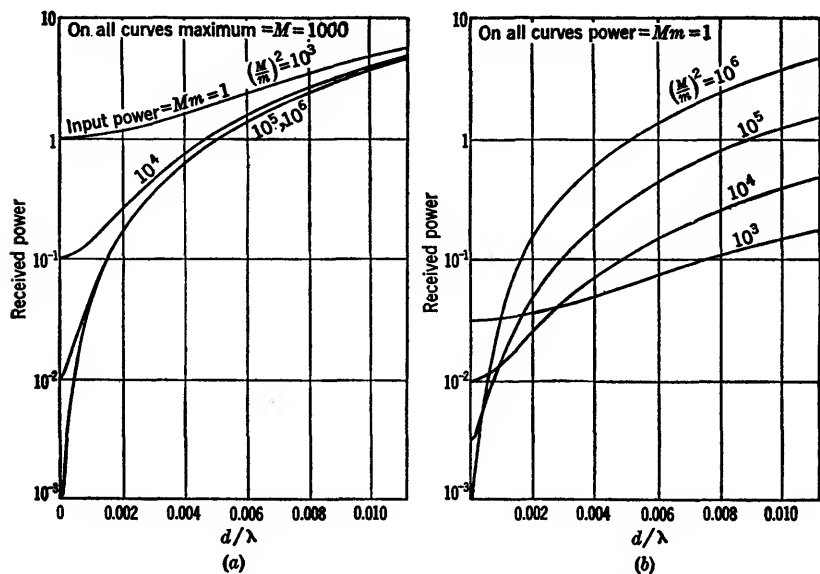


FIG. 10-45.—Comparison of probe power vs. position when maximum is constant (a) and when input power is constant (b).

simple methods would give the width of the curve  $(v - u)$ . Thus, since the general equation for probe power vs. position is known, the entire curve may be determined—and with it the twice-minimum points—by making any two independent measurements; for example, the width at a known fraction of the maximum power may be measured, or the two widths for any known power ratio. Despite the simplicity and similarity to the procedure for minimum position, however, such expedients are unsuccessful in practice; as was shown in Ref. 2a, the experimental errors are multiplied by 100 or 1000 in typical cases. Upon closer investigation it is found that there is nothing surprising in this behavior of errors, since the shape of the power-vs.-distance curve near the maximum is practically the same for all large values of the standing-wave



ratio (Fig. 10-45a). It is therefore impossible to measure high reflections at low power by any method depending on shape alone.

If the net input power were kept constant, however, the height of the curve (not its shape) would show a marked dependence upon standing-wave ratio even near the maximum, as is seen by Fig. 10-45b, and the use of some sort of matching device is at once suggested. It is found, in principle, that only approximate matching suffices for measurement of

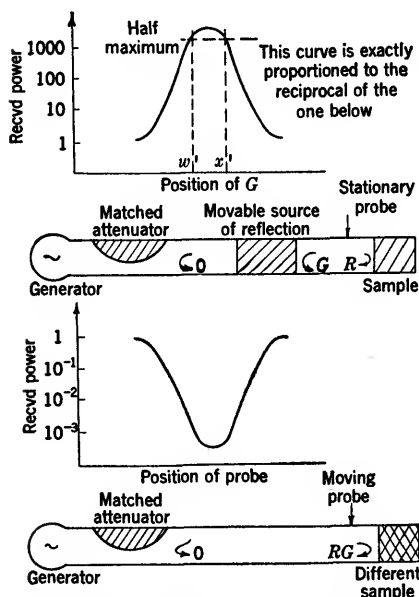


FIG. 10-46.—Modified short-circuited-line method. Diagram illustrating principles.

the net input power, and hence for accurate determination of  $1 - R$  (Ref. 2a); but in practice there are large errors from tuner loss, and the necessary adjustments are somewhat inconvenient (Ref. 3a). Without changing the essential features of the method, however, these difficulties may be obviated by the procedure suggested in Fig. 10-46a, in which a curve of power vs. phase of generator mismatch with constant probe position is measured. By inspection of Eq. (7) a relation for the r-f power at the probe is obtained, and from this is found the theoretical equation of the curve just described, if the receiver reading is assumed to be proportional to r-f power. The curve of power vs. phase of the generator mismatch is thus shown to be inversely proportional to a curve of power vs. probe position with a load reflection  $RG$ , if  $G$  is the coefficient for the moving mismatch (Ref. 2a). From this property, which is illustrated in Fig. 10-46a, it follows that the behavior of the one curve near the maximum is essentially the same as the behavior of the other near the minimum. Thus,

$$(x - w) = (x' - w') - (x_g - w_g), \quad (89)$$

after making the same approximation as that used for Eq. (80). In Eq. (89) the quantities  $(x - w)$ ,  $(x_g - w_g)$  are the widths at twice minimum which would be found in a curve of power vs. probe position with load reflections of  $R$  and  $G$ , respectively, and  $(x' - w')$  is the measured width at half maximum found in a curve of probe power vs. the position of  $G$  (Fig. 10-46a). The equations for the unmodified short-

circuited-line method, Eqs. (71), (72) and all others, are valid here. If  $u'$  and  $v'$  denote the two positions at half maximum without the sample, and  $w'$ ,  $x'$  the positions with the sample, then

$$U = \frac{[(u' + v') - (w' + x') + 2d]}{(2\lambda_g)}, \quad (90)$$

$$W = \frac{[(x' - w') - (v' - u')]}{\lambda_g}, \quad (91)$$

instead of Eq. (81). Equation (91) follows directly from Eq. (89), and Eq. (90), which is evident by inspection of Fig. 10-46a, may be proved by Eq. (7).

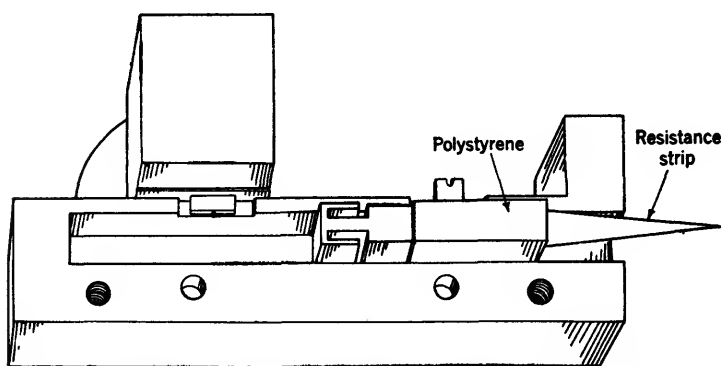
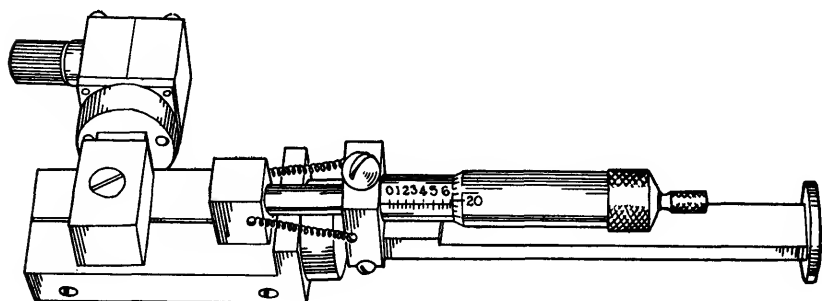


FIG. 10-46b.—Modified short-circuited-line method. Diagram showing details of equipment.

**Power Gain.**—Up to this point it has been shown that the alternative procedure of Fig. 10-46a gives all data needed for computation of  $k$  and  $\tan \delta$  by the unmodified short-circuited-line method. The errors are not excessive, being essentially the same as those in the unmodified

method with  $R$  replaced by  $RG$ . It remains to investigate the power requirement, which is determined by the equation

$$\text{Power at minimum} = (1 - R)^2, \quad (92)$$

with the generator matched to the line, and

$$\text{Power at minimum} = \frac{(1 - R)}{(1 + R)}, \quad (93)$$

with the generator matched to the load. The latter condition may be approximated in practice by use of a plunger similar to that of Fig. 10-46b (cf. Refs. 2b, 25b). With a lossless source of reflection  $G$ , on the other

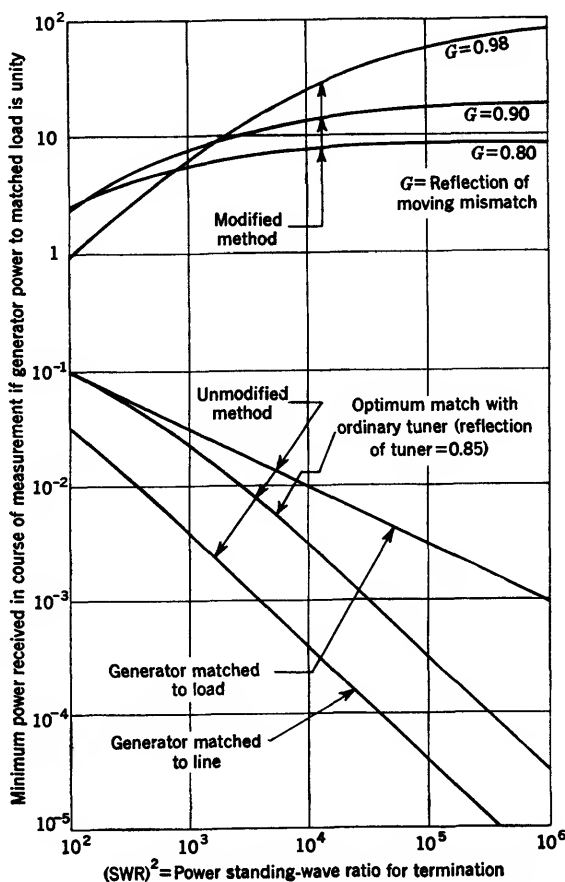


FIG. 10-47.—Comparison of power requirements in modified and unmodified methods.

hand, the modified method gives

$$\text{Power at half maximum} = \frac{(1 - G^2)(1 + R)^2}{2(1 - RG)^2} \quad (94)$$

for the power at half maximum which, like Eq. (93), represents the smallest power level required for measurement. In Eqs. (92), (93) and

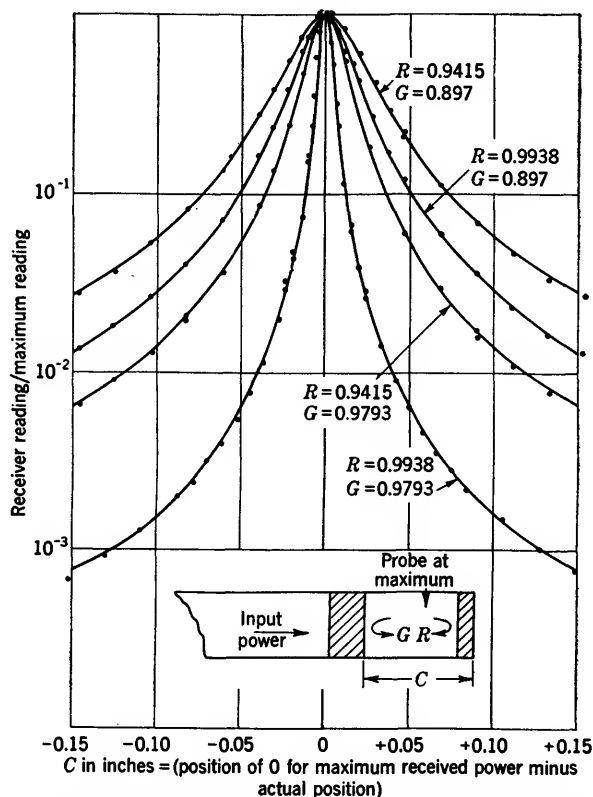


FIG. 10-48.—Detailed comparison of experiment and theory for modified short-circuited-line methods. The points are experimental, the curves are theoretical from independent measurements of  $R$  and  $G$ .

(94) the received power for the isolated generator connected directly to a matched load has been taken as unity. These results are compared in Fig. 10-47, where the modified method is seen to be operable at relatively low power; there is in fact a power gain, so that if the power be sufficient to give a reading with a matched load it will usually be more than sufficient to permit measurement of high power standing-wave ratios. In contrast to the behavior of most other methods for reflection measurement, moreover, the available power is found to increase rather

than to decrease as the load reflection approaches unity. With very large  $G$ , Eq. (94) can be used for measurement of  $R$ , if the value of  $G$  is known and the generator is supplied with a suitable monitor (cf. Ref. 2a and Table 10-4).

*Accuracy in Practice.*—In regard to the question of error it may be observed that the foregoing results are correct without theoretical approximation, irrespective of probe position and of the loss associated with  $G$ , if line losses may be neglected and if power is propagated in only one mode. Thus, in practice, a low-loss source of reflection  $G$  is used with the probe set on or near the maximum to increase the available power; no theoretical error is incurred by a failure to satisfy these conditions. Experimental verification is given in Fig. 10-48, where the values of  $G$

TABLE 10-4.—COMPARISON OF FOUR METHODS FOR MEASURING HIGH REFLECTIONS

Termination	Value of $G$ used					
	0.897		0.9490		0.9793	
	Without sample	With sample	Without sample	With sample	Without sample	With sample
$(u - v)$ as computed from maximum/minimum.	0.0020 in.	0.0180 in. 0.0171	0.0023 in.	0.0166 in.	0.0020 in.	0.0175 in.
$(u - v)$ as computed from over-all maximum, Eq. (83).	0.0020	0.0198 0.0151	0.0011	0.0154	0.0014 0.0014	0.0174
$(u - v)$ as obtained by modified method, Eq. (78).	0.0016	0.0168	0.0017	0.0169	0.0017	0.0168
$(u - v)$ as measured directly by unmodified method.	0.0013	0.0168 0.0178	0.0016	0.0171	0.0015	0.0170

and  $R$  used for the theoretical curve were independently measured by the twice-minimum procedure. An additional check on the theory is given in Table 10-4, which compares the twice-minimum widths as obtained by direct measurement, by the standard maximum or minimum technique, by Eq. (94) and by the modified method, Eq. (84).

The theoretical and experimental accuracy of the method naturally presupposes that the conditions for its use are satisfied in practice. The

probe reflection must be negligible, the value of  $G$  must remain constant, and the slopes must be such that the true points at half maximum can be accurately determined. The true points can be determined whenever  $RG$  is sufficiently large, the slope on a logarithmic meter being in fact equal to that obtained in the twice-minimum method for a reflection of this magnitude. The discussion of Fig. 10-42 is therefore essentially valid for this case also; in particular, the points of optimum accuracy for determining minimum positions are the half-maximum points actually used. The value of the maximum slope so obtained increases steadily with  $G$ , and for this reason it is desirable to give  $G$  as large a value as is convenient. Such a condition not only gives greater accuracy but also leads to a higher output power, as the attendant loss in the transmission of  $G$  is usually more than compensated by the increased resonance effect of the cavity (Fig. 10-47). It is worth noting too that Eq. (84) involves the same approximation applied to  $RG$  as was applied to  $R$  in the derivation of Eq. (81). Hence  $RG$  must be greater than 0.84 if the error is not to exceed 1 per cent. With sufficiently large  $G$  (0.95 to 0.98), but not otherwise, the inequality is usually satisfied. When  $R$  is so small that this is not the case, the exact equation analogous to Eq. (79) may be used or the comparatively small standing-wave ratio may be measured directly.

*Probe Errors.*—Since the measurement is carried out in a region of high field, the impurity of the frequency might be expected to be less important and probe errors more important than in other cases. This latter conclusion was quantitatively verified in Refs. 2a, 5a, 6a. Thus, when the probe is at the maximum, the equation

$$(R_{\text{measured}}) = R \sqrt{\frac{1 + 6P \cos P' + 9P^2}{1 - 2P \cos P' + P^2}}, \quad P(1 - R) \approx 0 \quad (95)$$

$$(R_{\text{measured}}) = R \frac{(1 - P)^2}{1 + RP} - P, \quad P' = \pi$$

give the measured reflection coefficient in terms of its true value  $R$  and the probe reflection  $P e^{-iP'}$ . This result may be derived from the relations of the Introduction; the measured reflection is in fact equal to that for the probe and termination together, which is given by Eq. (6) with  $t'' = \tau'' = 1 - P e^{-iP'}$ ,  $r'' = \rho'' = P e^{-iP'}$ ,  $R'' = R$ ,  $d = 0$ —the last two substitutions being valid because the probe position is that for maximum power. In the course of dielectric measurement, the difference of the two determinations with and without sample is measured, a procedure that is found to cancel out the first-order terms in probe reflection (Ref. 5a). The probe insertion must still be less than that permitted by the unmodified method; but so great is the power gain that an improvement of 20 to 30 db is obtained even with the probe sufficiently retracted to

lead to negligible error. Experimental examples are given in Fig. 10-49; the curves are computed from an equation analogous to Eq. (84).

*Errors from Moving Plunger.*—As was observed, the reflection  $G$  must be both high and constant, because a low value leads to small slopes and invalidates the approximation made in Eq. (89), and a value that varies with position will introduce errors in accordance with the same equation. To obtain a large value a choke-plunger short circuit may be used as shown in Fig. 10-46b. For constancy, accurately machined

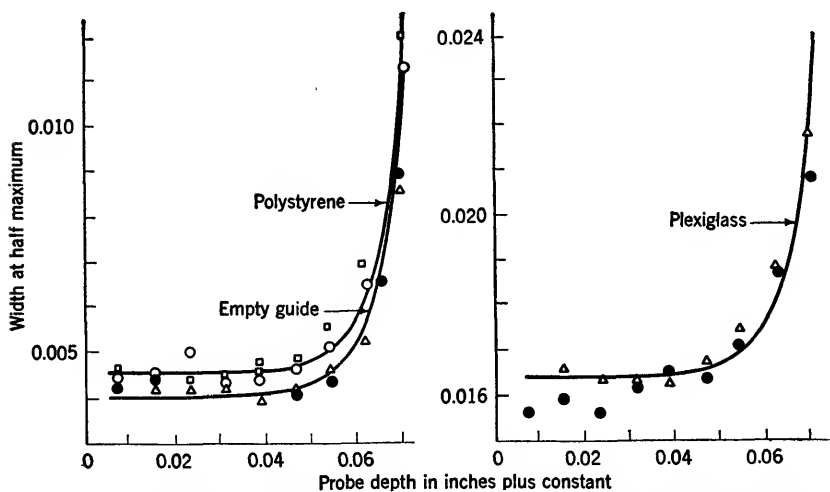


FIG. 10-49.—Effect of probe depth on measured width of curve at half maximum power (modified method). The points  $\circ$ ,  $\bullet$  are measured directly and the points  $\square$ ,  $\Delta$  are determined from the width at one-tenth maximum. The curves are theoretical, computed as in Fig. 10-41.

parts and a generator matched to the line are used. With regard to constancy, the error in  $G$  is found to be approximately

$$\text{Error} = \pm G_1 T_G^2, \quad (96)$$

if  $T_G^2$  is the power transmission coefficient of  $G$ , and  $G_1$  is the reflection looking into the generator as shown in Fig. 10-50. The use of a large

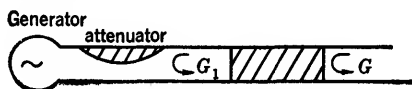


FIG. 10-50.—Generator reflection  $G_1$ .

$G$  is thus recommended to reduce  $T_G^2$ , as well as for the reasons just mentioned. For further reduction a small attenuator may be added as shown in Fig. 10-46b. If this small attenuator has a one-way power transmission of 0.2, for example, then the error from  $G_1$  is reduced by a

factor of five; a power standing-wave ratio of 1.05 for  $G_1$  is now no more serious than one of 1.01 was before. The power requirement is not increased, since the need for generator insulation is obviated in proportion as the attenuation associated with  $G$  becomes large.

*Radiation.*—Even with these two requirements of accurate machining and low  $G_1 T_0^2$  both satisfied, however, there may still be a slight error from radiation. Thus, the current lines are strictly parallel to the slot only when it is infinitely narrow; in actual practice there is always a certain amount of leakage. To avoid the consequent interference of  $G$  with the performance, the dimensions are adjusted in such a way as to have the choke plunger entirely enclosed at all times; that is, it is never allowed to extend to either of the two slots as  $G$  is moved (Ref. 2a). Error from radiation is further decreased by the use of a narrow slot and by arranging the probe carriage in such a way as to cover it completely for all probe positions. This expedient is of value only when error from variable contact is less serious than that from radiation, which appears to be the case at least for the shorter wavelengths (Ref. 2a). Radiation from slots causes difficulty in maintaining  $G$  constant and in measuring high standing-wave ratios. Radiation is present whenever slotted equipment is used, for example, the phase shifters illustrated in connection with the transmission method.

It may be eliminated by similar procedures in these other cases, of course, although the effect is usually negligible for all work not involving high reflection.

*Errors Analogous to Those Previously Discussed.*—Most of the errors discussed heretofore are peculiar to reflection measurement. Because of the above-mentioned analogy between reflection and transmission procedure, other errors are similar to those previously discussed and need not be considered in detail. From clearance, for example, the behavior shown in Fig. 10-51 is obtained. Although presented only for the modified method, the same result would evidently have been obtained with the maximum/minimum or twice-minimum techniques, as is seen by Table 10-4 and the accompanying remarks. Similarly, the treatment of wall losses, although slightly complicated by the term  $(x_g - w_g)$  of Eq. (89), is still analogous to the procedures heretofore described. If linear variation like that of Fig. 10-43 is assumed, the half-maximum width is extrapolated without sample to the position at which the maximum occurred with sample, whereupon the term in question

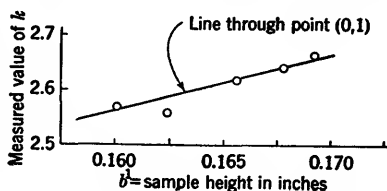


FIG. 10-51.—Experimental effect of clearance on measured value of  $k$  in rectangular guide at  $\lambda = 1.25$  cm. Points are experimental, curve empirical as given by Eq. (24).



is canceled by subtracting the two widths. To this difference must be added the change in width due to loss in the portion of line containing the sample, which is given by

$$\text{Change in width} = \frac{2Dd}{n\lambda_g}, \quad (97)$$

if  $D$  represents the difference in the two widths found, either with or without sample, for any two positions of  $G$  differing by  $n\lambda_g/2$ . The modified width so obtained is then substituted in Eq. (72) and finally the computed value of  $\tan \delta$  is corrected by Eq. (40), where  $\tan \delta_{\text{wall}}$  is found from Eq. (88) with  $D$  defined as in Eq. (97). As before, the loss in computing phase and in the portion of line over which  $G$  moves in a single measurement has been neglected, and the error is entirely negligible (cf Fig. 10-48). Strictly speaking, the present procedure is also incorrect in that it assumes the loss in the short circuit to be the same with and without sample, but the error so introduced usually does not exceed that in the unmodified method, where loss due to the short circuit was neglected altogether. In fact, the former assumption is sometimes the more accurate, especially when  $\sqrt{k} \approx 1$ . In such circumstances the method of compensation suggested for the modified method may be profitably applied to the unmodified method as well, the procedure being in all respects the same as that just described.

**10-20. Uses.**—One of the more important characteristics of the short-circuited-line method is that it requires only a relatively small sample for precise measurement—a length of  $\lambda_m/4$  or, at the higher frequencies, of  $3\lambda_m/4$ , being sufficient for high accuracy. This property of the method is due partly to the fact that the wave traverses the sample twice and partly to the increase of the standing-wave ratio usually found with decreasing sample length. Thus, although the measured effects, width and shift of minimum position, are smaller with a short sample, these measurements themselves may be made with correspondingly higher accuracy. Since the method requires only small samples, it is thus especially satisfactory for research and other work involving materials not available in quantity.

A related advantage is found in the location of the sample, which is placed at the end of the line rather than at some intermediate point as in the other methods discussed hitherto. The method is accordingly adapted to experiments in which the temperature is to be controlled, and is to be recommended especially for measurement of liquids. For such measurement the transmission methods can usually be used, if at all, only with clumsy expedients that are inconvenient and in general introduce considerable error. With the short-circuited-line method it suffices merely to have the equipment vertical (Refs. 1a, 5b). Because

of surface tension there is difficulty in deciding on a precise value for  $d$ , but this is a magnitude rather than a percentage error and may therefore be reduced by the use of a long sample, since the error in both  $k$  and  $\tan \delta$ , due to a given magnitude error in  $d$ , approaches zero as  $d$  increases indefinitely. A second expedient, by which the error is eliminated altogether, is the use of a window of mica or some other suitable material, a procedure that also prevents condensation of the liquid in the upper part of the guide. A detailed account of equipment for such measurements and of means for compensating the electrical effect of the window is given in Ref. 1a.

The short-circuited-line method, besides using a small and easily accessible sample, gives high accuracy both theoretically and practically, particularly at wavelengths not much below 10 cm. Thus, the sources of error are few and well defined. Instead of a host of extraneous reflections, as in the transmission methods, only the probe reflection exists, and this has been shown, for the unmodified method at least, to be completely negligible in practice. Similarly, no calibration is required for the r-f components, and the detector itself may deviate widely from linearity with but slight effect on the measured results. Because of the relatively short sample permissible, errors from clearance are readily minimized, and because of the high standing-wave ratios, the necessary measurements of field can be carried out with considerable accuracy. If care is taken in the machining of the equipment and the sample, this method is found to be about as accurate as any other for the measurement of  $k$ , and perhaps more accurate than any other for  $\tan \delta$ . With regard to this last, in particular, not only is the general behavior of the errors favorable, but the theoretical compensation of the effects of  $r_i$  and wall losses is found to be both possible and relatively convenient without approximation of any kind, provided that the short circuit itself produces negligible loss. In other words, the exact equation, with all parameters arbitrary, assumes the simple and manageable form of Eq. (70).

Only the unmodified method is clearly superior in regard to loss measurement; errors in the modified method are no longer eliminated with the same simplicity, and those remaining after compensation are usually somewhat higher because of the inconstancy of  $G$  and the decreased slope of the curve. The modified method, nevertheless, offers an advantage not possessed by any of the other methods discussed so far in that it is operable even when the power is insufficient to give a receiver reading when the line is matched. Although found only in the modified method, this characteristic of low power requirement is perhaps of sufficient importance to be set down as a fourth advantage peculiar to the short-circuited-line procedure.

In a consideration of the unfavorable properties of the method, it is observed that it has a failing common to all procedures not carried out in free space inasmuch as it presupposes an accurately prepared sample. At best a tedious process, this preparation becomes exacting for short wavelengths, and it is at these short wavelengths that the alternative free-space methods appear to best advantage. A second disadvantage, which again is especially noteworthy at the short wavelengths, is that a considerable supply of accurately machined equipment is required; in particular, a traveling probe of some sort is required for either method, and an accurately constructed reflector  $G$  is required as well for the modified procedure. A third disadvantage is the high power requirement of the unmodified method, which is surmounted by the suggested modification only with an attendant loss in accuracy for  $\tan \delta$ . And finally, the method is unsuitable for measurement of gases: the use of a short sample is not only permissible but imperative if the standing-wave ratio is not to become too small, and the path lengths of  $500$  to  $2000\lambda_m$  required for even moderate accuracy in measurement of gases would lead to prohibitively low values from the effect of line losses alone.

### CONCLUSION

*Retrospect.*—In the course of the foregoing pages the great variety of experimental techniques by which dielectric measurement can be made in the microwave region was noted; and at the same time an equally great uniformity in the theoretical principles required was observed. The equations for every method were, in fact, deduced from Eq. (2) of the Introduction with its corollary Eqs. (5), (6), and (7), and from Eq. (8) with the supplementary results, Eqs. (9), (12), and Table 10-1. Not only did these few relations suffice for the transition from data to results in ideal circumstances, but they also allowed an investigation of many of the sources of r-f error. An illustration of this repeated application of a few simple equations is found in the modified short-circuited-line method just considered; and the deviations for this method, which is of importance in the sequel, may be summarized in the following manner. The first step was the computation of  $r_i$  from Eq. (8); with  $r_i$  known, the corollaries of Eq. (2) gave both reflection and transmission for a lossless sheet of arbitrary thickness in free space. In the situation in which the sheet is followed at a distance  $D$  by a metal plate, it was found that this more difficult configuration also depended for its solution upon Eq. (2), the extension to lossy materials in guide being made by Eq. (12) and Table 10-1. The fact that the measuring probe has, in general, a non-zero reflection led to the investigation of the consequent error—a computation which required only that the over-all reflection of probe and

termination be computed, which could accordingly be done by the same methods. The next step was to relate receiver reading to plunger position, a problem that was likewise solved by a corollary of Eq. (2); and finally the error due to generator reflection was investigated by the same means. This uniformity of theory has been noted for each of the other methods, the derivations from Eqs. (2) and (8) being, in fact, more immediate than in the case described.

To the mathematical equivalence just observed must be added a similar correspondence in the physical principles required. Thus, the last procedure was proved essentially equivalent to the short-circuited-line method; the only change was in the actual manner of obtaining the data since all relations between measured quantities,  $k$  and  $\tan \delta$ , were the same in the two cases. The short-circuited-line method, in turn, was seen to be closely related to the transmission procedures with which the present discussion was begun; as far as principles are concerned, the equivalence was established on both intuitive and mathematical grounds, the chief difference again consisting in the method of obtaining the data. Moreover, the two transmission methods, free space and waveguide, are evidently equivalent to each other in all essentials; and, with the exception as before of measurement technique, they are likewise equivalent to the standard interferometer methods of physical optics. If the relatively unimportant procedures discussed in Secs. 10-12 to 10-14 are omitted the methods hitherto considered may be regarded as forming a sort of sequence: from the familiar technique of optics to its microwave analogue, transmission in waveguide or free space; from this to the short-circuited-line method, where the "transmitted" and incident waves are compared on the generator side, rather than on the load side, of the sample; and from the short-circuited-line method to the modified procedure last described.

**10-21. Resonant-cavity Methods.**—This modified procedure, which requires a high mismatch on both sides of the sample, permits continuation of the sequence mentioned, making a simple and natural transition from the elementary methods first discussed to the apparently more difficult ones forming the topic of this section.

*Methods Included in Preceding.*—In the resonant-cavity method of Fig. 10-52a the plunger position is adjusted for resonance with and without the sample; the change in position gives  $k$ , essentially, and  $\tan \delta$  is found from the change in resonant current (cf. Eq. (94)) or from the width of the resonance curve (cf. Eq. (92)). This procedure, discussed at length in Ref. 18b, is evidently equivalent to that of Fig. 10-46a; the only change is to introduce the generator power by a second probe or coupling loop rather than by the transmission of the plunger. The entire discussion of Sec. 10-19 is therefore valid almost word for word

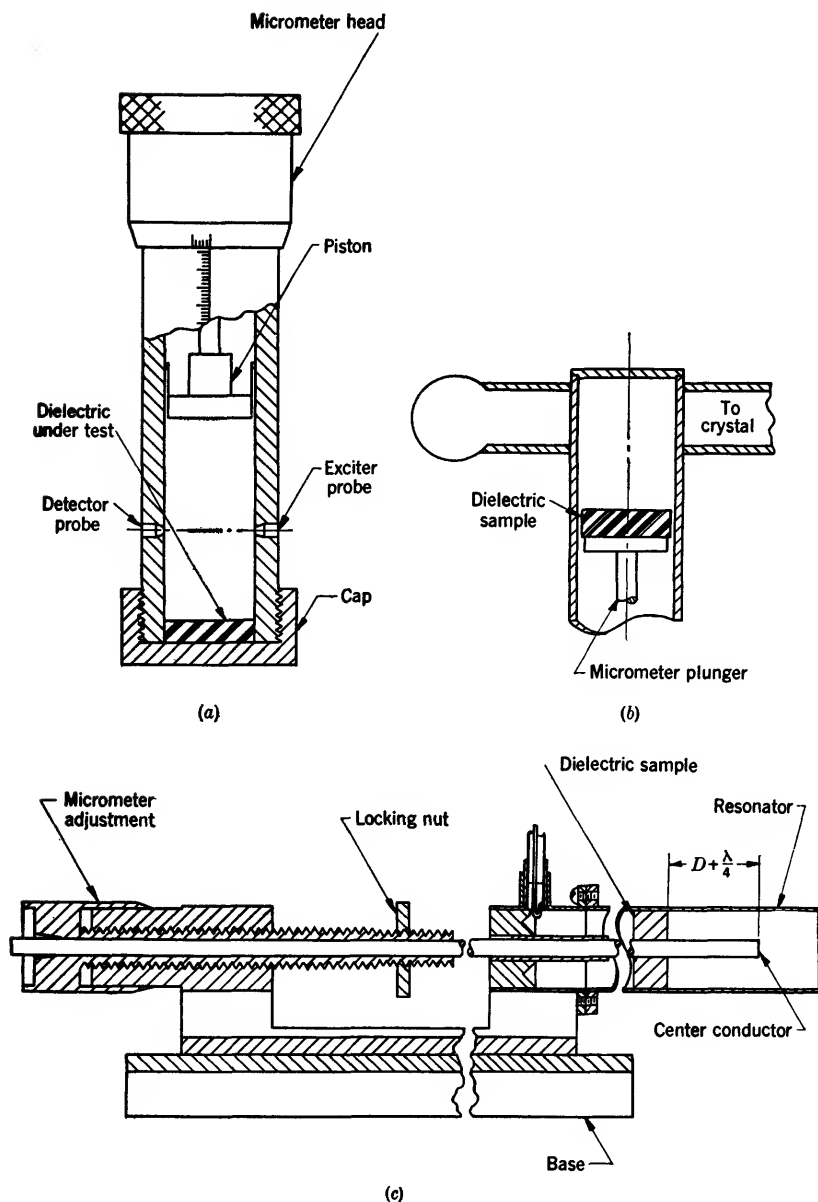


FIG. 10-52.—Resonant-cavity methods. In (c) a second coupling loop, not shown, is placed  $90^\circ$  from the first. The resonator may have an open end, as shown, or may be closed.

in the present case, and Eqs. (71) and (72) again give  $k$  and  $\tan \delta$  (Ref. 18b), whenever terms of the order of  $\tan^2 \delta$  may be neglected. The same remarks apply to the method of Fig. 10-52b developed in Ref. 13a; and because of the complete equivalence to what has gone before it is unnecessary to present more than the most cursory discussion of either method. It is observed, however, that these methods are superior to the former insofar as the equipment is considerably easier to construct. Instead of a traveling probe, for example, there is a simple coupling loop; and the sliding plunger, which need not be adjusted to have a constant nonzero transmission, may have a reflection coefficient of unity. For this reason the plunger is more easily designed and its reflection more easily maintained constant. There is, on the other hand, some slight disadvantage in that the received power is not usually the maximum possible. Thus, neither the penetration of the coupling loops nor their position is adjustable, and, since the position of the minimum will depend on the sample, it is clear that the two loops will not generally be on an antinode. Moreover, when the loops are near a node, an increase in coupling, which is then permissible, cannot be obtained. In other words, the coupling coefficient must be sufficiently small to permit operation at an antinode even when the loops are actually located near the minimum. In the previous method no such difficulty was found, and there was also a possible advantage in that only one source of extraneous reflection (the probe) was required, rather than two.

Difficulty due to variation of the minimum position may be obviated, in principle, by using two traveling probes in place of the coupling loops of Fig. 10-52a. A better method, however, is that suggested in Fig. 10-52c (Refs. 11b, 12b, 15b, 16b, 17b, 12c, 18c) where the two loops are located at the short circuit and hence are always at a node. The length of the line is changed, but the distance from the sample to one end remains constant. Whether this constant distance happens to be measured to the generator end or the load end is unimportant in this discussion, for in either case the opposite end of the line may be replaced by a short circuit shifted a distance zero or  $\lambda_g/4$  according to whether this opposite end was itself a short or open circuit. The method is thus seen again to be equivalent to that of Sec. 11-19; if the fixed distance from the sample to the end of the line is represented by 0 or  $\lambda/4$  plus the distance  $D$  of Fig. 10-31a, as shown in Fig. 10-52c, then the whole of the foregoing theory applies without approximation to the present case. It is observed in passing that the methods of Fig. 10-52 may be used with variable frequency rather than variable length—a remark which applies to almost all the methods here considered. In principle, the free-space wavelength  $\lambda$  is adjusted for resonance with and without the sample. At the same time the resonant current or the width at half

maximum is noted. For the empty guide of resonant length  $n\lambda_g/2$  the width  $\Delta l$ , when the length  $l$  is variable, is related to that found when  $\lambda$  is variable by the approximate equation (Ref. 12a)

$$\Delta l \text{ for half power} = \left(\frac{n}{2}\right) \left(\frac{\lambda_g}{\lambda}\right)^3 \times \Delta \lambda_{\text{half power}}. \quad (98)$$

This is seen by differentiating the relation of Table 10-1 for waveguide in terms of free-space wavelength. In a similar manner the change  $\Delta \lambda_g$  in guide wavelength needed to restore resonance after insertion of the sample is related to the change in length  $\Delta l$  by

$$(\Delta l) = -\frac{n(\Delta \lambda_g)}{2}, \quad (99)$$

where  $\Delta l$  is measured at the wavelength that gave resonance when the sample was in place, and  $n$ , as before, represents the number of antinodes in the resonating empty guide. This last equation is valid

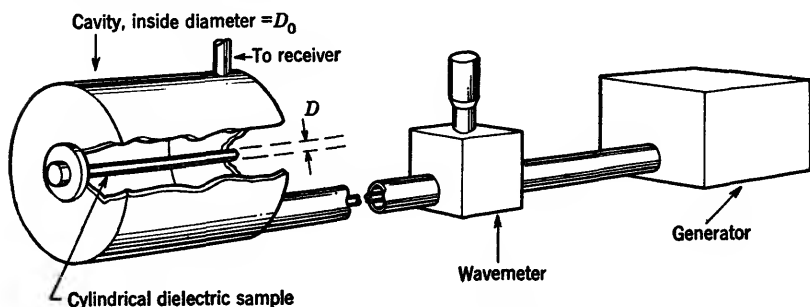


FIG. 10-53a.—A resonant-cavity method using cylindrical samples and variable frequency, Ref. 9a.

without approximation, whereas Eq. (98) is to be used only when terms containing the square of the width may be neglected—a situation which is, as will be shown, the only one that should be allowed to occur. Equation (98) may be regarded as correct, to a first approximation, when the sample is in place, although a rigorous treatment is made difficult by the fact that the total electrical length, which is involved in the constant  $n$  of the equation, then depends in a complicated way on the frequency. The maximum power, however, is the same for variable frequency as for variable length (cf. Ref. 12a); hence Eq. (94) may be used without change in either case. The merit of using a variable frequency will be commented upon; it is sufficient to note that the foregoing results may be used in this case also, provided that the resonant width is suitably determined, the equivalent change in length is computed from Eq. (99), and the parameter  $\lambda$  in all equations is taken as equal to its value for resonance when the sample is in place.

*A Method Not Included.*—The summary dismissal of the resonant-cavity methods shown in Fig. 10-52 was possible because of their close similarity to procedures already discussed. In the method of Fig. 10-53 it is found that the general form cannot readily be subsumed in this way; there is, however, a special case that has considerable practical importance and is at the same time amenable to treatment by the elementary methods hitherto employed. This special case, which forms a convenient introduction to the general method, is found when the resonator is entirely filled with the material being tested so that, with the notation of Fig. 10-53,  $D = D_0$ . Although its attainment with solid samples is somewhat inconvenient, such a condition is easily obtained in practice whenever the sample happens to be in liquid or gaseous form. With all air-dielectric boundaries perpendicular to the axis of the system, this special configuration is now included among those

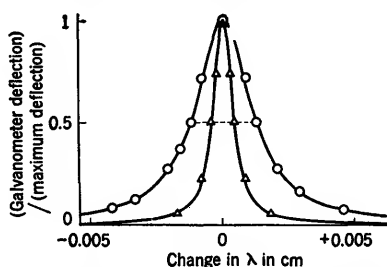


FIG. 10-53b.—Example of resonance curves, received power vs.  $\lambda$ , for the empty cavity (triangles) and for the cavity containing a dielectric sample (circles). The points are experimental, the curves theoretical fitted at the half-maximum points.

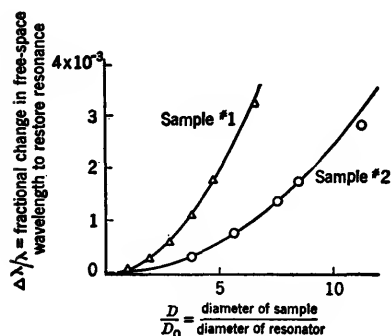


FIG. 10-53c.—Experimental verification of Eq. (105a) for two dielectric materials. The points are experimental and the curves are calculated from Eq. (105a).

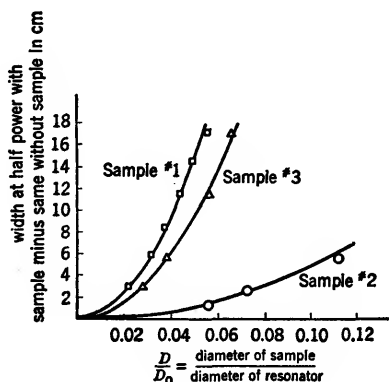


FIG. 10-53d.—Experimental verification of Eq. (105b) for three materials. The theoretical curves are determined from the best experimental value of  $\tan \delta$ .

hitherto treated; and the condition for resonance is thus seen to be (cf. Ref. 12a)

$$(\text{length of resonator}) = \left(\frac{n}{2}\right) (\text{wavelength in material in guide}), \quad (100)$$



whence is obtained

$$k = \left(\frac{m}{n}\right)^2 \left(\frac{\lambda}{\lambda_0}\right)^2 + \left[1 - \left(\frac{m}{n}\right)^2\right] \left(\frac{\lambda}{\lambda_c}\right)^2, \quad (101)$$

$$k = \left(\frac{\lambda}{\lambda_0}\right)^2, \quad m = n, \quad (102)$$

for the dielectric constant  $k$  in terms of the resonant (free-space) wavelengths  $\lambda$ ,  $\lambda_0$ , with or without the sample, and the ratio  $m/n$  of the number of antinodes in the filled or empty guide. The normal situation is represented by the case  $m = n$ , for which the equation takes the simple form Eq. (102) given in Refs. 10a, 10b, 17b. Equations (101), (102) are valid only for negligible  $\tan^2 \delta$ ; the general result is obtained by substituting an appropriate value for guide wavelength in Eq. (100), as computed from Eq. (12) and Table 10-1. It must be noted, however, that Eq. (100) itself ceases to be valid for very lossy samples; the condition of resonance, as determined by maximum power, gives a length somewhat smaller than the length there indicated.

For the loss tangent (Refs. 10b, 13b, 14b, 17b),

$$\tan \delta = \frac{\Delta\lambda}{\lambda} - \left(\frac{\Delta\lambda}{\lambda}\right)_0, \quad (103)$$

where the first term stands for the width of the resonance curve at half power divided by the resonance wavelength for the actual sample (Fig. 10-39b), while the second is the corresponding quantity for a hypothetical sample with the same dielectric constant but zero loss. With negligible  $\tan^2 \delta$  this second quantity is equal to the corresponding result for the empty resonator multiplied by  $\sqrt{k}$  (Ref. 17b). Instead of taking the width of the resonance curve, the following relation (Ref. 10a) may sometimes be used,

$$\frac{\text{Width for first sample}}{\text{Width for second}} = \frac{\text{power at resonance for second}}{\text{power at resonance for first}}. \quad (104)$$

This equation gives the ratio of widths in terms of the received power at resonance. Besides requiring use of a monitor, the procedure has the disadvantage of being relative only, with the result that one of the widths must be directly measured in any case. After such a determination is made, however, the evaluation of the other is sometimes facilitated.

The foregoing discussion has been devoted to the special case for which the sample entirely fills the resonating chamber, and the relations obtained were both convenient and elementary. In the general situation of Fig. 10-53a, on the other hand, the corresponding results become considerably more complex than any hitherto encountered. Not only are the equations for both  $k$  and  $\tan \delta$  transcendental even when

$\tan^2 \delta = 0$  (see Refs. 14b, 19b, 20b), but they involve too many parameters to be readily solved by graphical methods. Moreover, the functions themselves are not elementary; instead of the exponential or circular functions that have hitherto sufficed in all cases, Bessel functions must be used. These difficulties, noted when  $\tan^2 \delta$  is set equal to zero, are naturally enhanced when a truly general computation is attempted; for not only will the equations be transcendental involving functions which are not elementary, but the arguments of these functions will be complex as well. It is clear, then, that any theoretical investigation aiming at completeness will necessarily be somewhat involved. Before embarking on such an enterprise, it is perhaps worth while to consider the experimental conditions imposed on the method in question. Thus, with some of the transmission procedures considered above it was found that the quantity  $r_0 e^{-d \tan \delta}$  should be small for experimental convenience. Hence the theory could justifiably be confined to the simple relations obtained when this condition is satisfied. A similar approach is found valid for the present method too, in that the general situation is somewhat impracticable from an experimental standpoint irrespective of its theoretical difficulty. Before extending the theory, therefore, the question of experimental procedures is to be considered.

In the first place it is noted that variation of frequency presents considerable difficulty when the range of variation is large. With the microwave generators available at present a change of much over twenty per cent is hardly feasible, and for convenience the figure should be considerably less than this. Even the small variation required to measure the width presents certain problems, in that due care must be taken to ensure constant output of the generator and constant sensitivity of the receiving equipment, or of the monitor if one is used, over this range. There is, moreover, a theoretical objection in that both  $k$  and  $\tan \delta$  depend on frequency, although this objection is somewhat academic in ordinary practice (cf. Ref. 9a). A more serious problem occurs, however, when the empty resonator rather than the filled is considered, for the frequency shift so required will, in general, be far beyond the capacity of most microwave generators to achieve, apart from incidental difficulty due to frequency sensitivity of the r-f components. To obviate this difficulty the resonant wavelength for the empty guide may be computed, instead of measured, easily and accurately from Eq. (100) whenever the resonator length is known. This length is so chosen that resonance is obtained, with the sample in place, at a frequency that is within the range of the generator and that is also sufficiently close to the frequency at which the values of  $k$  and  $\tan \delta$  are desired. In this way the measurement of  $k$  is carried out with but slight change of frequency, even when the difference as given by Eq. (102) is large. Such a procedure, which

was used with success in Refs. 10*b* and 14*b*, requires knowledge of the approximate value of  $k$  and demands that the resonator length be adjusted accordingly, since different lengths are necessary for different samples.

The foregoing limitations were concerned chiefly with the dielectric constant, as it is this parameter rather than loss that is primarily determined from the frequency shift [cf. Secs. 10-3 to 10-6 and Eq. (102)]. For measurement of  $\tan \delta$ , however, another difficulty is encountered in that Eq. (103) presupposes knowledge of the width for a hypothetical sample with the same dielectric constant as that of the original sample, but of zero loss. Of course, no such sample can be actually produced and measured, and the question must be considered in more detail. Theoretically this hypothetical loss may be computed from the dimensions of the resonator and the conductivity (or more particularly, the so-called "skin depth") of the walls (Refs. 10*b*, 13*b*, and 14*b*), but such a computation neglects all extraneous losses, including those from the junctions and coupling loops. For this reason it is found that the values computed differ perhaps by a factor of two from the ones actually measured (Refs. 10*b* and 14*b*). In Ref. 14*b* it was assumed, therefore, that the ratio of computed to measured width would be the same for the empty cavity as for the cavity filled with the hypothetical lossless dielectric; but, as was there observed, no proof has been obtained, nor is it to be supposed that such a procedure is of general validity. Even if it be permissible, however, there is still difficulty because the determination of width for the empty cavity itself must be made at a frequency that is too far from that with the sample to be readily attained in practice. To obviate this added difficulty a new and larger cavity that will resonate at a convenient wavelength when empty, may be constructed and from measurement on this new cavity the width that would have been obtained for the original one can be estimated. Although such a procedure has been actually used (Refs. 10*b* and 14*b*), the inconvenience as a matter of general practice is evident.

From this discussion, much of which applies to all methods using a variable wavelength, it is seen that considerable experimental difficulty is often to be anticipated in the method of Fig. 10-53; and although such difficulty can be circumvented by various devices, these devices are sufficiently inconvenient to be of but limited utility. Instead of seeking a general theory, therefore, the problem is to find the particular circumstances in which the method appears to best practical advantage. Once this has been decided, the special theory appropriate to that case may be exhibited in simple form. The complications noted consisted chiefly in the large frequency change for proceeding from the filled to the empty guide, and in the difficulty of computing a sort of "comparison loss"

corresponding to the empty-guide loss. Both difficulties would be obviated if, and apparently only if, the character of the resonator were not appreciably changed by insertion of the sample. In other words, the resonant wavelength should remain nearly the same, and the loss when empty should be nearly the same as the loss when filled by a lossless sample of the same dielectric constant. These conditions are met whenever  $k \approx 1$ ; in particular for a gas the method is most convenient and was used for such measurement in Refs. 10a and 12a. The length rather than the frequency, however, is varied in Ref. 12a. After it was verified that no undue absorption was to be anticipated from dry air at the frequency used, the width for the empty resonator was taken as equal to the value for the air-filled resonator, and this value was substituted for the second term of Eq. (103). Because of the low dielectric constant, such a procedure was entirely justified in that case. The remainder of the measurement too could be carried out with ease, since all frequency shifts were very small; and  $k$  was readily computed from Eq. (102). In Ref. 12a the accuracy was increased by use of a large cavity, and due precautions were taken to prevent oscillation at unwanted modes (cf. Ref. 13b). The method is in many respects the best for measurement of gases; not only is the cavity airtight whenever the coupling loops are suitably sealed off, but also the method allows accuracies that are scarcely attainable by other procedures. The power requirement is not excessive, and the equipment itself, which requires no moving plunger, is perhaps as simple as any hitherto discussed.

It is not necessary to use materials of low dielectric constant; a sample of such small diameter may be used that the resonant frequency is only slightly affected. There is, to be sure, a limit to the reduction that is permissible in good practice, since both the frequency shift and the rod diameter must be known within a small percentage error, rather than a small absolute error, if accurate results are to be obtained; for diameters  $D \approx 0.05D_0$  this effect is still of secondary importance when the sample is accurately machined. For a  $TM$ -wave the general equation takes the simple form (Refs. 9a and 14b)

$$k \approx 1 + 0.538 \left( \frac{D_0}{D} \right)^2 \left( \frac{\lambda}{\lambda_0} - 1 \right), \quad D \ll D_0, \quad (105a)$$

$$\tan \delta \approx 0.269 \left( \frac{D_0}{D} \right)^2 \left( \frac{\Delta \lambda}{\lambda} - \frac{\Delta \lambda_0}{\lambda_0} \right). \quad (105b)$$

Equations (105) indicate that the effect of the sample is proportional to its volume (see Fig. 10-53c). Because of the similarity to the equations previously discussed, the sources of experimental error need not be further investigated.

**10-22. Summary. Methods Tabulated.**—The great variety of experimental methods, which has been so often observed in the discussion, suggests that a brief summary will be of use, and such a summary is accordingly presented in Table 10-5. The descriptions given, which are suggestive only, are intended to aid recollection and are in no sense an adequate presentation of the method described. Because the emphasis has been on measurement procedure, a fine subdivision in Table 10-5 is used, despite the theoretical homogeneity. Thus, two methods are classified separately when they differ appreciably in experimental technique, even though they may be, in principle, entirely equivalent.

**Consistency of Results.**—Before the subject of dielectric measurement can be dropped, the order of accuracy that may be expected in typical

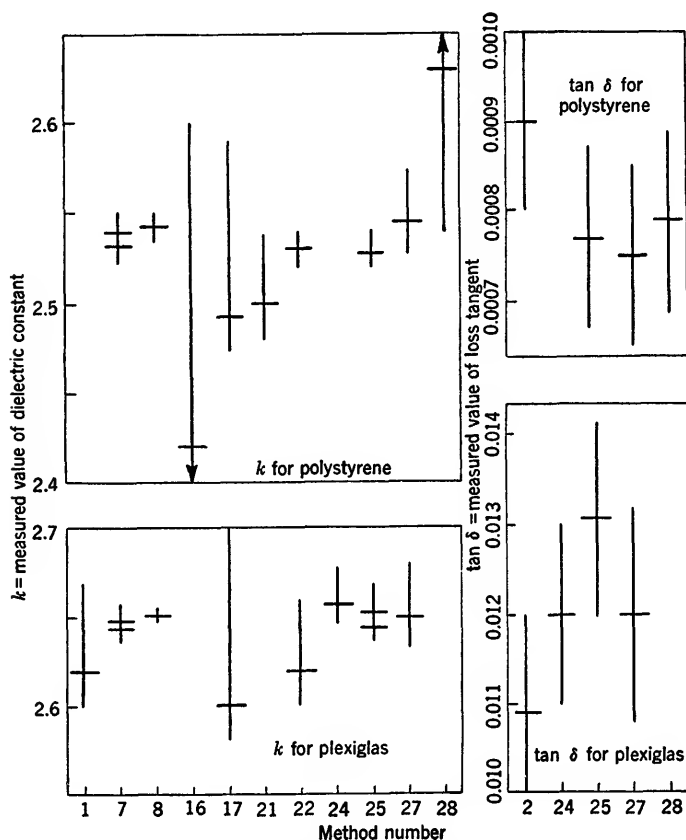


FIG. 10-54.—Comparison of values as measured by various methods. Horizontal line shows average value of  $k$  or  $\tan \delta$  for a given sample, vertical line shows estimated error.

TABLE 10-5.—SUMMARY OF METHODS

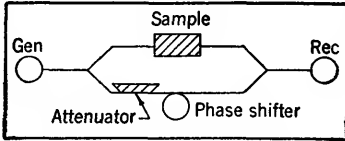
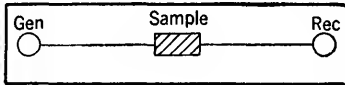
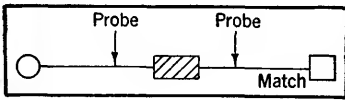
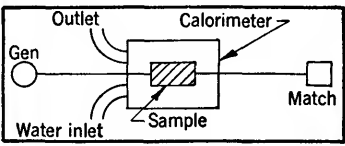
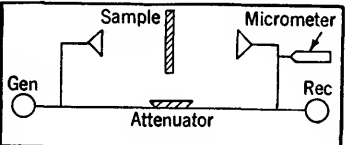
Method number	Quantity determined when loss is low	Procedure	Equipment	Discussed in section	References		
					a	b	c
Measurement from transmission in guide							
1	$k$	Set phase shifter for minimum with and without sample.		10-3, 10-5, 10-6	6		
2	$\tan \delta$	Take receiver reading with and without sample using tapered, $n\lambda_g/2$ or high-loss sample.		10-4, 10-5, 10-6	6		
3	$\tan \delta$	Take max. and min. with each probe, sample as in No. 2.		10-4, 10-5, 10-6.	17 7		
4	$\tan \delta$	Take max. and min. power as phase shifter is varied, sample as in No. 2.	Same as No. 1	10-4, 10-5, 10-6			
5	$\tan \delta$	Set calibrated attenuator to minimize the minimum with and without sample, sample as in No. 2.	Same as No. 1	10-4, 10-5, 10-6			
6	$\tan \delta$	Measure rate of temperature rise with power on, fall with power off.		10-21	15		
Measurement from transmission in free space							
7	$k$	Adjust micrometer for minimum with and without sample.		10-7, 10-8	6 7	6	

TABLE 10-5.—SUMMARY OF METHODS.—(Continued)


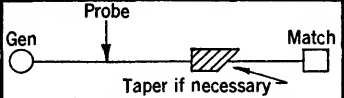
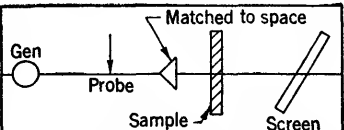
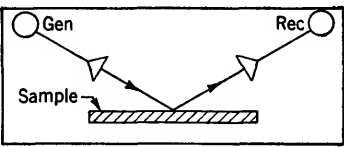
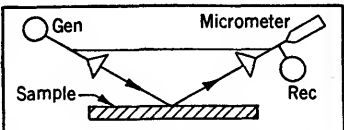
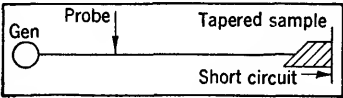
Method number	Quantity determined when loss is low	Procedure	Equipment	Discussed in section	References		
					a	b	c
8	$k$	Adjust angle of incidence for minimum on each side of $\theta = 0$ .	Same as No. 7	10-9	6		6
9	$\tan \delta$	Take receiver reading with and without half-wavelength or lossy sample.		10-7 10-8	14		
10	$\tan \delta$	Same, ordinary sample at Brewster's angle.	Same as No. 9	10-9			
General methods depending on reflection							
11	$k, \tan \delta$	Measure interface reflection and phase shift with a traveling probe.		10-12	8 11		
12	$k$	Compare (SWR) <sup>2</sup> for sample and metal sheet. Sample should be an interface, or a quarter wavelength thick.		10-13	7 20		
13	$k$	Compare reflected with directly received power. Sample as in No. 12		10-13	14 21		
14	$k$	Compare received power from sample and metal sheet in same position. Sample as in No. 12	Same as No. 13	10-13	14 20 7		
15	$\tan \delta$	Adjust antenna position for minimum with sample and metal sheet in same position.		10-13	14		

TABLE 10-5.—SUMMARY OF METHODS.—(Continued)

Method number	Quantity determined when loss is low	Procedure	Equipment	Discussed in section	References		
					a	b	c
16	$k$	Measure reflection of a sheet, preferably a quarter wavelength thick.	Same as No. 11	10-14	6	21	
17	$k$	Take thickness for minimum reflection.	Same as No. 11	10-14	6		
18	$k$	Take maximum reflection of two or more samples.	Same as No. 11	10-14	8		
19	$k, \tan \delta$	Measure reflection and minimum position for two sample lengths.		10-15			

## General methods depending on reflection

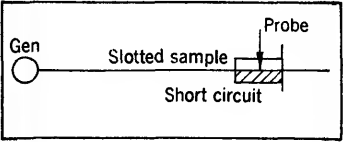
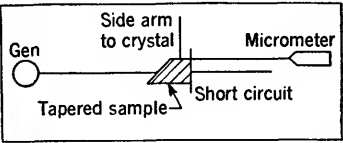
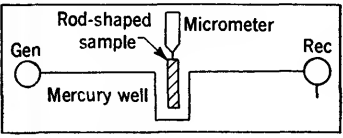
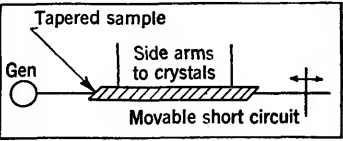
20	$k, \tan \delta$	Measure distance between minima, and take width at twice minimum, probe being in sample.		10-15			17
21	$k$	Take distance between minima, as sample moves past side arm.		10-15	16	6	
22	$k$	Take difference of sample positions for resonance		10-15	6		
23	$\tan \delta$	Take ratio of max. to min. power in each side arm as plunger is moved.		10-15	16		



TABLE 10-5.—SUMMARY OF METHODS.—(Continued)

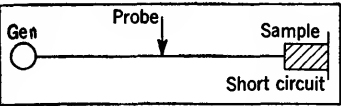
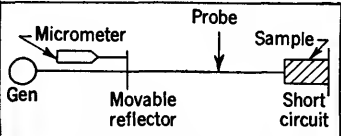
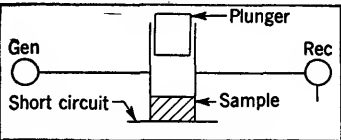
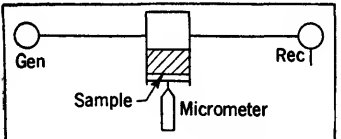
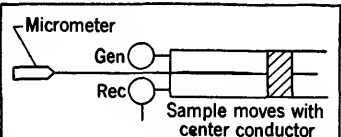
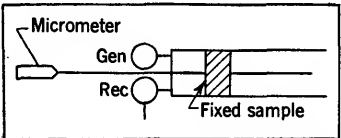
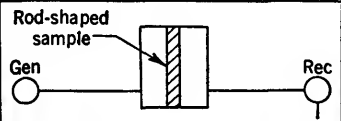
Method number	Quantity determined when loss is low	Procedure	Equipment	Discussed in section	References			
					a	b	c	
The short-circuited-line method								
24	$k, \tan \delta$	Measure minimum position and width at twice minimum with and without sample.		10-17 10-18	19 1	26 22	2 1	1 2
25	$k, \tan \delta$	Take plunger position for maximum and width of curve at half-maximum, or maximum power, with and without sample.		10-19	6			6
Resonant-cavity methods								
26	$k, \tan \delta$	Same as No. 25		10-21	12			19
27	$k, \tan \delta$	Same as No. 25		10-21	13			
28	$k, \tan \delta$	Adjust line length for resonance with and without sample. Take width or max. power.		10-21			16 17 15 11 12	
29	$k, \tan \delta$	Same as No. 28		10-21			16 17 18	12
30	$k, \tan \delta$	Same, frequency varied instead of length.		10-21	9 10	14 10	13 9	

TABLE 10-6.—COMPARISON OF METHODS WITH REGARD TO INTERNAL CONSISTENCY FOR MEASUREMENT OF  $k$ 

Method number	$\lambda$ cm	Parameter varied	Number of measurements	Greatest value obtained	Least value obtained	Average deviation for all values	Material used	From Ref.
1	1.25	Sample thickness	10	2.65	2.59	0.02	Plexiglas	6a
7	1.25	Sample thickness	4	2.65	2.64	0.00	Plexiglas	6a
7	1.25	Sample thickness	2	2.54	2.53	0.00	Polystyrene	6a
7	1.25	Sample thickness	3	3.47	3.41	0.02	Dielectene	6a
8	1.25	Angle of incidence	8	2.659	2.648	0.002	Plexiglas	6a
8	1.25	Angle of incidence	9	2.550	2.542	0.002	Polystyrene	6a
8	1.25	Angle of incidence	3	3.41	3.40	0.00	Dielectene	6a
8	1.25	Angle of incidence	13	3.456	3.441	0.003	Dielectene	6a
12	9.1	Antenna size	5	2.72	2.63	0.03	Plexiglas	7a
21	1.25	.....	4	2.65	2.59	0.02	Plexiglas	6a
21	1.25	.....	2	2.50	2.50	0.00	Polystyrene	6a
22	1.25	.....	4	2.66	2.64	0.01	Plexiglas	6a
22	1.25	.....	2	2.53	2.53	0.00	Polystyrene	6a
24	1.25	Sample thickness	14	2.68	2.64	0.02	Plexiglas	6a
25	1.25	Sample thickness	2	2.65	2.64	0.01	Plexiglas	6a
25	1.25	Sample thickness	5	2.66	2.65	0.01	Plexiglas	6a
25	1.25	Sample thickness	6	2.67	2.65	0.01	Plexiglas	6a
25	1.25	Sample thickness	5	2.53	2.52	0.00	Polystyrene	6a
25	1.25	Sample thickness	6	3.45	3.42	0.01	Dielectene	6a

circumstances is to be considered. A precise investigation of this question presents considerable difficulty in that the accuracy of a given method depends on the nature of the sample. Thus, a method that is suitable for thick samples may be inaccurate for thin ones, and a method satisfactory for high loss may be almost useless when the loss is low. Added to the theoretical complication is the fact that experimental precision depends on the care with which the measurement is conducted. It is therefore clear at the outset that results only of the most qualitative kind will be presented. Because of the novelty of microwave procedures, however, it is believed that even such results have a certain value, in that they prevent serious misconceptions. With these preliminaries, it is noted that error appears in two forms: the results obtained with a given method disagree among themselves, to some extent, as the conditions are varied; on the other hand, the average results obtained for different methods are not exactly equal to each other. The error of the first type, which is concerned with reproducibility of the results in a given method, is illustrated in Table 10-6, where the variation of values is noted as various parameters are changed. The second error is considered in Fig. 10-54 where values as measured by the different techniques summarized in Table 10-5 are compared. The results for methods 21 and 22 were obtained with different samples from that used in the others and hence the agreement, or lack of it, has only doubtful significance. The materials used, plexiglas and more especially polystyrene, are known to be fairly uniform; but the evidence of this uniformity depends in no small measure on data of the type shown in Fig. 10-54, and it cannot validly be urged in the present case. With this reservation, however, the agreement is within the experimental error as estimated from Table 10-6 and from *a priori* considerations. Because of the lack of extensive data on  $\tan \delta$  with uniform samples, no result such as that of Table 10-6 or Fig. 10-54 is presented for loss. It is observed, however, that typical values for error would be perhaps  $\pm 5$  per cent or  $\pm 0.0001$ , whichever is the larger. In exceptional cases, accuracies as great as  $\pm 0.00001$  may be achieved, although the techniques then become somewhat exacting. The accuracy with which  $k$  can be measured is of the order of  $\pm 2$  per cent to  $\pm 0.2$  per cent in typical cases, where only a high grade of engineering precision in the design and operation of the equipment is assumed. With the refinements that are to be expected in research work, this accuracy can no doubt be greatly exceeded.

#### BIBLIOGRAPHY

Because of the number of references dealing with the subject matter of this chapter, it has been thought best to present a classified bibliography, where the references are divided into classes dealing with

experimental techniques (*a* references), theory (*b* references), or tabulated values of  $k$ ,  $\tan \delta$  (*c* references). If a report appeared to fit equally well into the *a* or *b* category, it was arbitrarily placed under *a*.

The following references are concerned chiefly with experimental procedures for finding the original data.

- 1a. VON HIPPEL, A., D. JELATIS, W. WESTPHAL, and M. HAUGEN, "Auxiliary Equipment for the MIT Coax Instrument and its Use," Laboratory for Insulation Research, MIT, NDRC 14-210, November, 1943.
- 2a. REDHEFFER, R. M., "Radome Bulletin Number 7: The Measurement of High Reflections at Low Power," RL Report 483-7, Nov. 20, 1944.
- 3a. REDHEFFER, R. M., "Radome Bulletin Number 9: The Matching of High Standing Wave Ratios," RL Report 483-9, Dec. 22, 1944.
- 4a. DOWKER, Y., and R. M. REDHEFFER, "Radome Bulletin Number 10: The Measurement of Small Reflections," RL Report 483-10, Feb. 6, 1945.
- 5a. DOWKER, Y., and R. M. REDHEFFER, "Radome Bulletin Number 14: An Investigation of R-F Probes," RL Report 483-14, Feb. 6, 1946.
- 6a. REDHEFFER, R. M., and E. D. WINKLER, "Radome Bulletin Number 15: The Measurement of Dielectric Constants in the One-Centimeter Band," RL Report 483-15, May 11, 1945.
- 7a. REDHEFFER, R. M., "Radome Bulletin Number 18: The Interaction of Microwave Antennas with Dielectric Sheets," RL Report 483-18, Mar. 1, 1946.
- 8a. TURNER, L. B., "Conductivities of Sea, Tap and Distilled Water at  $\lambda = 10$  cm," Admiralty Signal Establishment, Lythe Hill House, Haslemere, Surrey, Report M496, April 1943.
- 9a. BORGNIS, F., "Measurement of the Dielectric Constants and Loss Factor of Dielectric Substances with a Wavelength of 17 cm. with the Help of Cavity-Resonators," *Phys. Z.*, **43**, 284-291 (Aug. 1942).
- 10a. SAXTON, J. A., "The Dielectric Constant and Absorption Coefficient of Water Vapour for Wavelengths of 9 cm. and 3.2 cm. (Frequencies 3,300 and 9,350 Mc/s.)," The National Physical Laboratory, Paper No. R.R.B./S.11., Apr. 12, 1943.
- 11a. COLLIE, C. H., "Preliminary Report on the Dielectric Properties of Water in the K-Band," The National Physical Laboratory, C.V.D. Report CL, Misc. 25.
- 12a. SAXTON, J. A., "The Dielectric Constant and Absorption Coefficient of Water Vapour for Radiation of Wavelength 1.6 cm. (Frequency 18,800 Mc/s.)," The National Physical Laboratory, Paper No. R.R.B./S.17., Apr. 22, 1944.
- 13a. PENROSE, R. P., Clarendon Laboratory, Oxford University. "A Method for the Determination of Permittivity for Power Factors of Low Loss Dielectrics in the K-Band," C.V.D. Report CL Misc. 32, Dec. 1944.
- 14a. SAXTON, J. A., and J. A. LANE, "The Dielectric Properties of Water in the Temperature Range 0°C. to 40°C. for Wavelengths of 1.24 cm. and 1.58 cm.," The National Physical Laboratory, Paper No. R. R. B./C.116, Mar. 7, 1945.
- 15a. CALBICK, C. J., "Ultra-High Frequency Attenuation in Liquids with Experimental Data for Water and Ethyl Alcohol," BTL MM-42-140-53, Sept. 16, 1942.
- 16a. YOUNKER, E. L., "Dielectric Properties of Water and Ice at K-band," RL Report 644, Dec. 4, 1944.
- 17a. LEITER, H. A., "Dielectric Transmission Measurements," RL Report 244, Jan. 15, 1943.

- 18a. ENGLUND, C. R., "Series of Ultra Short Wave Dielectric Measurements," *Proc. Inst. Radio Engrs*, **23**, 114 (Jan. 1944).
- 19a. ALTAR, W., "Measurement of Dielectric Properties of Lossy Materials," Westinghouse Research Report R-94318-E, Sept. 13, 1944.
- 20a. REDHEFFER, R. M., "Radome Bulletin Number 2: An Outline of the Electrical Properties of Radomes," RL Report 483-2, Dec. 20, 1943.
- 21a. PFISTER and ROTH, *Hochfrequenztechn. u. Elektroakust.*, **51**, 156 (1938).
- 22a. REDHEFFER, R. M., "Radome Bulletin Number 13: Elliptical Polarization Produced by Streamlined Radomes," RL Report 483-13, Feb. 12, 1945.

The following references deal chiefly with the theoretical relations between the original data and the desired results,  $k$ ,  $\tan \delta$ .

- 1b. STRATTON, J. A., *Electromagnetic Theory*, McGraw-Hill, New York, 1941.
- 2b. ROBERTS, S., and A. VON HIPPEL, "A New Method of Measuring Dielectric Constant and Loss in the Range of Centimeter Waves," Department of Electrical Engineering, MIT, Mar. 1941, pp. 1-19.
- 3b. VON HIPPEL, A., "Progress Report on Ultra-High Frequency Dielectrics," Laboratory for Insulation Research, MIT, NDRC Report 14-121, Jan. 1943.
- 4b. VON HIPPEL, A., and R. BRECKENRIDGE, "The Interaction Between Electromagnetic Fields and Dielectric Materials," Laboratory for Insulation Research, MIT, NDRC Report 14-122, Jan. 1943.
- 5b. VON HIPPEL, A., D. G. JELATIS, and W. B. WESTPHAL, "Measurement of Dielectric Constant and Loss with Standing Waves in Coaxial Wave Guides," Laboratory for Insulation Research, MIT, NDRC Report 14-142, April 1, 1943.
- 6b. REDHEFFER, R. M., "Radome Bulletin Number 4: Transmission and Reflection of Single Plane Sheets," RL Report 483-4, July 12, 1944.
- 7b. REDHEFFER, R. M., "Radome Bulletin Number 11: Electrical Properties of Double-Wall and Sandwich Radomes," RL Report 483-11, Feb. 1, 1945.
- 8b. REDHEFFER, R. M., "Radome Bulletin Number 12: Transmission and Reflection of Parallel Plane Sheets," RL Report 483-12, Jan. 26, 1945.
- 9b. DOWKER, Y., "Radome Bulletin Number 19: Dielectric Constant and Loss Tangent Computation," RL Report 483-19, Aug. 7, 1945.
- 10b. TAYLOR, T. A., and W. JACKSON, "The Use of the Closed Cylindrical Resonator for Dielectric Loss Measurements," Ministry of Supply, Advisory Council on Scientific Research and Technical Development, R.D.F., Application Committee, Communications Committee, A.C. 1425, RDF. 100, Com. 70, Nov. 25, 1941.
- 11b. GENT, A. W., "Theory of Permittivity and Loss Factor Measurements Using Resonant Transmission Lines," Standard Telephones and Cables Limited, London, England, Valve Laboratory Report No. G.48, June 1942.
- 12b. GRANT, A. S., "The Measurement of Dielectric Constant and Power Factor of Insulating Materials at 10-cm. Wavelength," Standard Telephones and Cables Limited, London, England, Valve Laboratory Report No. G. 49, June, 1942.
- 13b. HANSEN, W. W., "A Type of Electrical Resonator," *J. Appl. Phys.*, **9**, 654-663 (1938).
- 14b. HORNER, F., and T. A. TAYLOR, "The Use of Cylindrical Resonators for Dielectric Measurements at Centimeter Wavelengths," Electrotechnics Department, Manchester University, Report No. 38, June 12, 1942.
- 15b. HORNER, F., "Measurement of Loss Factor of Low Loss Dielectrics at U.H.F." Extra-mural Research, Ministry of Supply, 287/Gen/35 D.S.R., Electrotechnics Dept., Manchester Univ., June 12, 1941.

- 16b. HORNER, F., and W. JACKSON, "Interim Report on Dielectric Loss Measurements at 3200 mc/sec.," Ministry of Research, D.S.R. Report No. 14, Feb. 15, 1941.
- 17b. DUNSMUIR, R., "The Resonant Frequency and Q Value of a Half Wave Coaxial Line Resonator Containing Dielectric Media with Transverse Discontinuities," Electrotechnics Department, Manchester University, June 20, 1944.
- 18b. SEAMAN, E. C. H., J. C. SIMMONDS and C. F. DAVIDSON, "A Resonant Cavity Method of Measuring Relative Permittivity and Loss Tangent," Radio Branch Laboratories, Wembley, England, Post Office Engineering Department, Radio Report No. 1240, Oct. 22, 1944.
- 19b. APKER, L., and L. TONKS, "Measurement of Dielectric Loss in the Microwave Region," GE, Schenectady, Nov. 18, 1942.
- 20b. FEENBERG, E., "Use of Cylindrical Resonator to Measure Dielectric Properties at Ultra-High Frequencies," Sperry Report GC 16907, July 21, 1942.
- 21b. BURROWS, C. R., "Transverse Dielectric Slab in a Wave Guide," BTL MM-43-160-46, Apr. 13, 1943.
- 22b. FEENBERG, E., "The Measurement of Dielectric Properties on an Impedance Meter," Sperry Report 5220-114, April 10, 1943.
- 23b. FEENBERG, E., "The Measurement of Dielectric Properties on an Impedance Meter," Supplement to Report No. 5220-114, Sperry Report 5220-124, Aug. 2, 1943.
- 24b. FEENBERG, E., R. LOUGHLIN, and R. MERCHANT, "The Measurement of Dielectric Properties on an Impedance Meter," Supplement to Report No. 5220-124, Sperry Report 5220-125, Sept. 15, 1943.
- 25b. DAKIN, T. W., "The Hollow Pipe Method of Measuring Dielectric Constant and Loss Factor," Westinghouse Research Report SR-134, Aug. 25, 1942.
- 26b. DAKIN, T. W., "Dielectric Constant and Dissipation Factor Calculation Methods from Wave Guide and Co-ax Standing Wave Measurements," Westinghouse Research Report R-94308-V, Oct. 5, 1944.
- 27b. SPERRY GYROSCOPE COMPANY, INC., *Microwave Transmission Design Data*, Publication No. 23-80, Sperry Gyroscope Company, Inc., Brooklyn 1, New York, 1944.

The following references give measured values of dielectric constant loss tangent, or both.

- 1c. VON HIPPEL, A., "Tables of Dielectric Materials," Laboratory for Insulation Research, MIT, NDRC Report 14-237, Feb. 1945.
- 2c. VON HIPPEL, A., "Tables of Dielectric Materials," Vol. II, Laboratory for Insulation Research, MIT, NDRC Report 14-425, June 1945.
- 3c. VON HIPPEL, A., L. G. WESSON, and S. L. WHITCHER, "The Polystyrene Plastics as High-Frequency Dielectrics," Laboratory for Insulation Research, MIT, NDRC Report 14-276, May 1944.
- 4c. CHECKENRIDGE, R. G., A. P. DE BRETTEVILLE, JR., J. M. BROWNLOW, F. G. CHESLEY, G. OSTER, L. TISZA, W. B. WESTPHAL, and A. VON HIPPEL, "High Dielectric Constant Ceramics," Laboratory for Insulation Research, MIT, NDRC Report 14-300, August 1944.
- 5c. EVERHART, E. M., "Radome Bulletin Number 5: Recent Dielectric Constant and Loss Tangent Measurements," RL Report 483-5, July 14, 1944.
- 6c. HEGARTY, M., Y. DOWKER, R. M. REDHEFFER, and E. D. WINKLER, "Radome Bulletin Number 17: Current Progress on R-f Research," RL Report 483-17, May 10, 1945.

- 7c. SUEN, T. J., and E. M. EVERHART, "Dielectric Constants and Loss Tangents of Radome Materials," RL Report 483-25, Jan. 11, 1946.
- 8c. BIRKS, J. B., "Expanded Dielectrics," TRE Report T.1812, Feb. 27, 1945.
- 9c. TAYLOR, T. A., and W. JACKSON, "The Electrical Properties of Ice," Ministry of Supply, Advisory Council on Scientific Research and Technical Development, R.D.F., Application Committee, Communications Committee, A.C. 1516, RDF. 110, Com. 78, Dec. 22, 1941.
- 10c. REDDISH, W., "The Use of a Cylindrical Cavity Resonator for Measurement of Permittivity and Power Factor of Low-Loss Dielectric Materials at 10,000 Mc/sec. (3 cms.)," Ministry of Supply, Advisory Council on Scientific Research and Technical Development, R.D.F., Application Committee, Communications Committee, A.C. 3056, Com. 140, RDF. 162, Nov. 21, 1942.
- 11c. JACKSON, W., "The Permittivity and Power Factor Values of a Range of Dielectric Materials Measured at Room Temperatures and 3000 Mc/sec. (approx.)," Ministry of Supply, Advisory Council on Scientific Research and Technical Development, Communications Committee, A.C. 3784, Com. 167, Mar. 31, 1943.
- 12c. HORNER, F., and T. A. TAYLOR, "Measurement at 3200 Mc/sec on a Series of Glasses Supplied by the B.T.H. Co.," Ministry of Supply, Extra-mural Research F 72/74, 287/gen/35 PSR, Electro-Technics Dept., Manchester Univ., Sept. 2, 1943.
- 13c. JACKSON, W., "The Permittivity and Power Factor Values of a Range of Dielectric Materials Measured at Room Temperature and 3000 Mc/sec (approx.)," Ministry of Supply, Advisory Council on Scientific Research and Technical Development, Communications Committee, Extra-mural Research F 72/74, Apr. 7, 1943.
- 14c. STRACHEY, C., "Dielectric Constant of Paraffin Wax-Rutile Mixtures," Standard Telephones and Cables Limited, London, England, Valve Laboratory Report No. G. 85, Aug. 1943.
- 15c. PENROSE, R. P., "Further Measurements on the Permittivity and Power Factor of Low Loss Dielectrics in the K-Band," Admiralty Department of Scientific Research and Experiment, Committee on Valve Development Report CL. Misc. 53; Clarendon Laboratory, Oxford University, July 1945.
- 16c. SAXTON, J. A., "The Dielectric Properties of Water at Wavelengths from 2 mm. to 10 cm., and over the Temperature Range 0°C. to 40°C.," The National Physical Laboratory, Radio Research Board Report C.115, Mar. 20, 1945.
- 17c. HUNT, L. E., "Dielectric Constant and Attenuation of Micalex at 3 cm.," BTL MM-42-160-125, Oct. 20, 1942.
- 18c. ROBERTSON, S. D., "Properties of Dielectric Materials at K-Band Frequencies," BTL MM-43-160-131, Aug. 13, 1943.
- 19c. MEAHL, H. R., and R. F. WOOD, "Power Factors and Dielectric Constant Data at 10 cm and 3 cm Wavelengths," General Engineering Laboratory, GE, Schenectady, Data Folder No. 72335, Oct. 16, 1942.

**PART IV**

**ATTENUATORS AND RADIATION  
MEASUREMENTS**



## CHAPTER 11

### MICROWAVE ATTENUATORS. CUTOFF ATTENUATORS

BY RUDOLPH N. GRIESHEIMER

Microwave attenuators fall naturally into two groups which differ in the means by which the power is attenuated. The first group utilizes a waveguide operated at a frequency which is below the cutoff frequency characteristic of the size and shape of the waveguide. Electromagnetic fields excited at one end of the waveguide couple weakly to a receiving element at the other end of the waveguide, the amount of coupling depending on the length and size of the waveguide. This technique is particularly suitable for application in the microwave region, although it has been employed at frequencies as low as a few megacycles per second. In the second group of attenuators, power is absorbed in poorly conducting materials and transformed into heat as in a resistor used at low frequencies. In this chapter, cutoff attenuators are discussed. In the following chapter, resistive attenuators that are suitable for microwaves are described. In Chap. 13 the techniques by which attenuation may be measured are presented.

#### INTRODUCTION

**11.1. Definitions of Attenuation.**—The concept of attenuation is that of a reduction in the amplitude and a change in the phase of the voltage or current at the load impedance caused by the introduction of some circuit element, the attenuator, between the generator and the load. In most microwave transmission-line problems one is interested only in the amplitude reduction effected by the attenuator and can disregard the accompanying phase shift. On the other hand, when the attenuator causes no amplitude change but only a phase shift, it serves as a dissipationless "line stretcher."

Although the concept of attenuation is direct and elementary, there exists considerable confusion with regard to what constitutes a proper, quantitative definition of attenuation. Various authors have defined such quantities as insertion loss, transmission loss, attenuation, attenuation factor, attenuation constant, complex attenuation constant, transfer constant—all of which are rooted in the fundamental concept of an amplitude reduction and a phase shift of the wave. It is, therefore, necessary to establish the definitions and concepts on which subsequent discussion

within this chapter will be based. Despite the fact that microwave transmission is commonly discussed in terms of distributed-parameter transmission lines, it is sometimes advantageous to revert to concepts familiar in the lower frequency ranges, and to treat a relatively short, high-loss length of microwave transmission line as a dissipative, two-terminal-pair network. The term "attenuator" as used below may be considered to apply equally well to a distributed-parameter line or to a lumped-constant, dissipative, two-terminal-pair network.

The first quantity to be defined is insertion loss. If a generator of arbitrary impedance delivers an amount of power  $P_1$  to a load of arbitrary impedance, and if the power to this same load is reduced from  $P_1$  to  $P_2$  when the attenuator is inserted in the line, the *insertion loss*  $L$  in decibels is given by

$$L = 10 \log_{10} \frac{P_1}{P_2}. \quad (1)$$

As so defined, insertion loss is not a quantity exclusively characteristic of the attenuator and will depend on the generator and load impedances. If the generator and load impedances are not equal, the insertion loss of the attenuator will, in general, be different, depending on which terminal-pair of the attenuator is considered as the input pair. If we further specify that the attenuator is to be installed in a transmission line of known, real characteristic impedance, which is terminated at both the generator and load ends in matched impedances, then we have a specific quantity which is characteristic of the attenuator. Insertion loss with these additional specifications will be defined as the *attenuation*  $A$ .

An equivalent way to define attenuation is

$$A = 10 \log_{10} \frac{P_1}{P_2}, \quad (2)$$

where  $P_1$  is the maximum *available* power from the generator, and  $P_2$  is the power delivered to a matched terminal load, with the attenuator inserted. Such a definition does not preclude the possibility of having the matched generator in a line of one characteristic impedance and the matched load in a line of different characteristic impedance. The equation can then specify, for example, the attenuation of a dissipative adaptor from waveguide to coaxial line.

There are several facts implicit in this definition of attenuation which deserve careful comment. It is important to note that a transmission-line element may produce attenuation, yet have no internal dissipation of power. For example, a dissipationless metal obstruction placed in a transmission line will cause a change in the power delivered

from generator to load. If the generator or load is not matched, this change can be such as to either increase or decrease the power to the load so that insertion loss  $L$  may be either a positive or negative quantity. However, the attenuation  $A$  of the metal obstruction can only be positive since a matched generator delivers maximum power to a matched load. In terms of waves traveling along the transmission line, it can be said that the metal obstruction introduces a reflected wave in the line, thereby reducing the amplitude of the wave which continues in the direction of the load. We shall speak of such attenuation as *reflective attenuation* in contrast to *dissipative attenuation*. Often the attenuator is mismatched

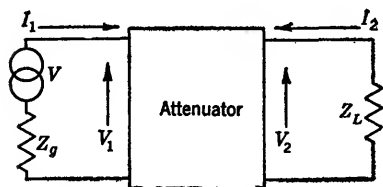


FIG. 11-1.—Four-terminal network.

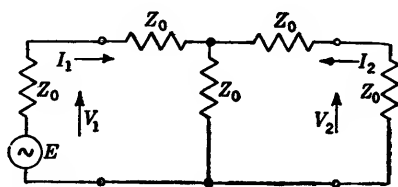


FIG. 11-2.—Example of attenuator network.

to the line, and may have different input impedances at the two pairs of terminals, that is, it is unsymmetrical. In such a case the attenuation it introduces is in part dissipative and in part reflective.

A rather common definition of attenuation is given by the expression

$$A' = 10 \log_{10} \frac{\text{Re}(V_1 I_1^*)}{\text{Re}(V_2 I_2^*)}, \quad (3)$$

where  $V_1$ ,  $V_2$ ,  $I_1$ , and  $I_2$  are indicated on Fig. 11-1. Attenuation defined in this way is wholly dissipative as contrasted to our chosen definition of  $A$  which has both dissipative and reflective components. A simple example will serve to demonstrate this important difference. Consider the network shown in Fig. 11-2. The input impedance at terminal (1) is  $2Z_0$ , and the input power is  $\frac{2}{3} E^2/Z_0$ . The output power is  $E^2/36Z_0$ , and the attenuation given by Eq. (3) is

$$A' = 10 \log_{10} 8 = 9.03 \text{ db.}$$

Using our chosen definition of  $A$ , Eq. (2), we have

$$A = 10 \log_{10} 9 = 9.54 \text{ db.}$$

The reflective component of attenuation is therefore  $9.54 - 9.03 = 0.51$  db. The reflective component can be calculated alternatively from the voltage standing-wave ratio  $r$  in the line connecting the matched generator and the attenuator. Here  $r = 2$ . The power drawn from the generator will be

$$1 - \left( \frac{r-1}{r+1} \right)^2 = \frac{8}{9}$$

of that which would be delivered to a matched load. The reflective component of attenuation is therefore equal to

$$10 \log_{10} \frac{2}{3} = 0.51 \text{ db.}$$

In a distributed-parameter transmission line there is defined a quantity  $\gamma$  which is called the *propagation constant* or complex attenuation constant of the line. The amplitude of the voltage wave is proportional to  $e^{-\gamma z}$ , where  $z$  is measured along the line and

$$\gamma = \alpha + j\beta, \quad \beta = \frac{2\pi}{\lambda_g}.$$

The real part  $\alpha$  is called the *attenuation constant* of the line and is measured in nepers per unit length of line. The imaginary part  $\beta$  is called the *wavelength constant* and is a measure of the phase shift along the line. It is expressed in radians per unit length of line. The attenuation constant is a measure of the *dissipative* attenuation per unit length of line, and is a quantity which is a function solely of the dissipative line.

The *attenuation constant* is not to be confused with the quantity we have chosen to define as attenuation. Both quantities are commonly used in the province of microwaves, and each has its place of importance. A dissipative line is often used as an attenuator. If  $\alpha$  is small, the characteristic impedance of the dissipative line has only a small reactive component. If the resistive component of the characteristic impedance is nearly equal to the characteristic impedance of the line in which it is to be used as an attenuator, the reflective component of attenuation is then small. The attenuation is closely equivalent to the product of the attenuation constant and electrical line length of the attenuator. Cables and other relatively long lines with a low attenuation constant are commonly characterized by a value of the attenuation constant. This is often expressed in decibels per meter.

**11-2. General Design Considerations.**—One of the important requisites of a good attenuator is that the input impedance at both terminals shall be matched to the characteristic impedance of the transmission line in which it is to be used. It is not possible to match an attenuator perfectly over a band of frequencies, although it is relatively simple to accomplish this at any specific frequency through the use of reactive tuning elements. However, it is not uncommon to require that an attenuator be well matched over a band of frequencies, for example, that it have a voltage standing-wave ratio of less than 1.20. For the purposes of this chapter we shall speak either of a perfectly matched attenuator, that is, VSWR equal to unity within the limits of experimental error, or of an attenuator which is matched to a VSWR of 1.10, or less, over the band in question.

Our definitions of insertion loss and attenuation have shown that regardless of which quantity we consider, the measured magnitude of the quantity will be influenced by the extent to which the attenuator has been matched to the transmission line. If, in calibrating an attenuator, one is very careful to match the generator and load to the transmission line, the attenuation can be measured with good accuracy. However, when the carefully calibrated attenuator is placed in the transmission line in which it is to be used, it is often difficult to provide an equally well-matched generator and load, particularly over a broad band. It therefore follows that calibration of the attenuator is no longer meaningful since the reduction in power received by the load is directly related to the insertion loss of the attenuator, and not to the quantity we have defined and measured as its attenuation. One calibrates the attenuator in terms of attenuation, and attempts when using it to meet the conditions of matched generator and matched load as closely as possible. Recognizing that one cannot meet these conditions exactly, the next best procedure is to minimize the mismatch contributed by the attenuator itself. The better matched the attenuator, the less error can result from failure to match the generator and load perfectly. Also, this error will be less sensitive to small variations (with frequency, for example) of the generator and load impedances. Therein lies the importance of impedance matching of the attenuator.

In a majority of cases the attenuator is used over a band of frequencies, and one must inquire into the frequency sensitivity of both its impedance match and its attenuation. When the utmost in accuracy is required, it is necessary to prepare a calibration curve showing the variation of attenuation with frequency. However, one is usually asked to design an attenuator which has an attenuation of  $X$  db, constant to  $\pm Y$  db over the band. In general, the quantity  $Y$  has three components: (1) the inherent calibration error, (2) the frequency sensitivity of attenuation, and (3) the error that can arise from having a mismatched generator and mismatched load in the line in which the attenuator is to be used. In evaluating this third error, one usually calculates the greatest possible error from the known characteristics of the attenuator and an assumed set of maximum values for the voltage standing-wave ratios of generator and load. It is obvious that for a given allowable value of  $Y$ , the attenuator with greater frequency sensitivity of attenuation must be better matched. The problem of designing an attenuator with very small frequency sensitivity of attenuation is considerably more difficult (particularly for variable, resistive attenuators) than that of designing an attenuator matched over a broad band. The latter problem becomes serious only when dimensional limitations of the sort that preclude the use of long matching tapers are imposed.

Another factor of importance in the design of many attenuators is the maximum power capacity. Excessively high power levels can burn out an attenuator, or can change its calibration temporarily, or permanently. It is important to note that burnout may result either from arcing, when operating under pulsed-power conditions, or from the high temperatures associated with large average power. Consequently, it is essential in many cases to determine maximum values for both pulse and average power. Partial or complete burnout may lead to either increased or decreased attenuation. For example, a coaxial-line attenuator with a resistive center conductor will show increased attenuation for partial burnout, and nearly infinite attenuation for complete burnout. In contrast, a waveguide attenuator which uses a resistive film lying parallel to the narrow side of the guide will show decreased attenuation with partial burnout, and almost no attenuation with complete burnout. Some types of attenuators, particularly the resistive-film types, will change calibration with power level or temperature. Films with low temperature coefficients of resistance are chosen to circumvent this difficulty.

A practical consideration of occasional importance is the matter of deciding whether to use a single attenuator, or two in cascade. If the total attenuation required is as large as 70 or 80 db, it may be desirable to use a pair of attenuators. The sum of the calibration errors for two 40-db attenuators may easily be less than the calibration error associated with a single 80-db attenuator. Further, it is sometimes possible to use two cascaded attenuators of opposite frequency sensitivity so that the resultant combination is more accurate over a wide band than is a single attenuator.

Unfortunately, if there is a stringent restriction on the length of the attenuating element, the design problem, particularly for resistive-film attenuators, may become very difficult. Short lengths of film will necessarily have a high resistivity, and consequently a low power capacity. Further, so long as the r-f skin depth exceeds the film thickness, it is usually true that greater frequency sensitivity of attenuation and poorer matching result from decreasing the length of the attenuating element. The reasons for this will be made apparent in the subsequent discussion of specific attenuator designs.

In the design of a variable attenuator there are additional considerations of importance. For example, the shape of the calibration curve (db vs. displacement) is very often of interest. In a majority of problems one is asked to provide an attenuator with an approximately linear calibration curve. In some instances it has been possible to meet this requirement by a proper choice of the shape and resistivity gradients of the attenuating element; more frequently, it is accomplished by mechani-

cal means such as proper shaping of the cam which drives the movable element. If one is interested in greater accuracy at small attenuation levels, the calibration curve should have a slope which increases with the attenuation level. On the other hand, the calibration curve for attenuators used in microwave impedance bridges (see Chap. 9) should have a slope which decreases with increasing attenuation. The design of the drive mechanism for a variable attenuator is an important factor, and it is usually necessary to take great precautions against backlash, mechanical play, wear on moving parts, and r-f leakage.

### CUTOFF ATTENUATORS

**11.3. Principles of Cutoff Attenuators.**—One of the most common types of microwave attenuator is that which utilizes a waveguide beyond cutoff. It is well known that, for a given frequency of oscillation, one can reduce the dimensions of either circular or rectangular waveguide to a point where energy of this frequency can no longer be propagated in the waveguide. Below the cutoff frequency, the fields decay exponentially along the waveguide, and the phase is changed a negligible amount by losses in the walls. It is possible to excite fields in a waveguide beyond cutoff in several ways, and to couple selectively to a mode of transmission whose attenuating characteristics can be calculated. For example, a simple means of constructing a cutoff attenuator is to terminate the inner conductor of a coaxial line by folding it back in a loop to the outer conductor. The outer conductor is continued as a length of waveguide beyond cutoff, and the receiving element consists of a similar loop-terminated coaxial line which slides in the cutoff tube. This construction is shown in Fig. 11-3. Circular waveguide is commonly used because simple mechanical arrangements can be provided to adjust the separation of the coupling elements.

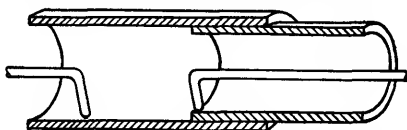


FIG. 11-3.—Simplest cutoff attenuator; *TE*-mode.

A cutoff attenuator may be designed for either a *TM*- or a *TE*-mode of transmission. In the *TM*-mode designs the coaxial lines are usually terminated in circular metal disks, the coupling between the two disks being capacitive. In *TE*-mode designs the coaxial lines are usually terminated by metal loops, and the coupling is inductive.

In circular waveguide the cutoff wavelength (the free-space wavelength corresponding to the cutoff frequency) is given by

$$\lambda_c = \frac{2\pi r \sqrt{k_e}}{s_{mn}}, \quad (4)$$

where  $r$  is the inside radius of the circular waveguide,  $s_{mn}$  is a dimensionless quantity characteristic of the specific mode (see Table 11.1), and  $k_e$  is the relative dielectric constant of the medium filling the waveguide. ( $k_e = 1$  for free space.)

TABLE 11.1.—VALUES OF THE CUTOFF PARAMETER,  $s_{mn}$ , IN EQ. (4)

$TM_{mn}$ -modes			
$s_{01} = 2.405$	$s_{02} = 5.520$	$s_{03} = 8.654$	$s_{04} = 11.79$
$s_{11} = 3.832$	$s_{12} = 7.016$	$s_{13} = 10.17$	$s_{14} = 13.32$
$s_{21} = 5.136$	$s_{22} = 8.42$	$s_{23} = 11.62$	$s_{24} = 14.80$
$s_{31} = 6.38$	$s_{32} = 9.76$	$s_{33} = 13.02$	$s_{34} = 16.22$
$TE_{mn}$ -modes			
$s_{01} = 3.832$	$s_{02} = 7.016$	$s_{03} = 10.17$	
$s_{11} = 1.841$	$s_{12} = 5.33$	$s_{13} = 8.54$	
$s_{21} = 3.05$	$s_{22} = 6.71$	$s_{23} = 9.97$	
$s_{31} = 4.20$	$s_{32} = 8.02$	$s_{33} = 11.35$	

In rectangular waveguide the cutoff wavelength for either the  $TE_{mn}$ - or  $TM_{mn}$ -modes is given by

$$\lambda_c = \frac{2\sqrt{k_e}}{\sqrt{\left(\frac{m}{a}\right)^2 + \left(\frac{n}{b}\right)^2}}, \quad (5)$$

where  $a$  and  $b$  are, respectively, the wide and narrow inside dimensions of the waveguide. In the  $TE$ -mode series,  $m$  and  $n$  have integral values and either  $m$  or  $n$  may be zero. In the  $TM$ -mode series  $m$  and  $n$  have integral values equal to or greater than unity.<sup>1</sup>

When the frequency is varied from a value greater than the cutoff frequency to one less than the cutoff frequency, there is a continuous transition through the cutoff point from a slightly attenuated sinusoidal field to a highly attenuated exponential field. Expressions for the attenuation of either the traveling wave or the highly attenuated field are simple. The expression for the attenuation in the case in which  $\lambda$  is very slightly greater than  $\lambda_c$  is rather complicated, and is seldom used. For  $\lambda/\lambda_c \geq 1.05$ , however, it is sufficiently accurate to write the following expression for the attenuation constant  $\alpha$

$$\alpha = \frac{2\pi}{\lambda_c} \sqrt{1 - \left(\frac{\lambda_c}{\lambda}\right)^2} \quad \text{nepers per unit length.} \quad (6)$$

This equation is valid for  $TE$ - or  $TM$ -modes, and for circular or rec-

<sup>1</sup> In this numbering system the  $TE_{10}$ -mode is the dominant mode in rectangular waveguide.



tangular waveguide, if the proper value of  $\lambda_c$  is used. Moreover, the value of  $\alpha$  is independent of the material from which the waveguide is made if the material has a high conductivity.

It is interesting to note from Eq. (6) that  $\alpha$  increases rapidly with  $\lambda$  for small values of  $\lambda/\lambda_c$ , but increases slowly with  $\lambda$  as  $\lambda/\lambda_c$  becomes large. In order to reduce the frequency dependence of  $\alpha$ , it is customary to select a tube diameter such that  $\lambda/\lambda_c$  is large over the range of wavelengths in which the attenuator is to be used. For example, if the attenuator is to be used over a range of wavelengths from  $\lambda_1$  to  $1.5\lambda_1$ , and if it is desired that  $\alpha$  be constant to within one per cent over this wavelength range, then the tube diameter must be chosen so that

$$\lambda_c \leq 0.19\lambda_1.$$

It is important to recognize that the dimensions of the waveguide must be known precisely if  $\alpha$  is to be known with the accuracy customarily required. For example, for circular waveguide,

$$\frac{d\alpha}{\alpha} = - \left[ \frac{1}{1 - \left(\frac{\lambda_c}{\lambda}\right)^2} \right] \frac{dr}{r}.$$

Or, for  $\lambda_c \ll \lambda$

$$\frac{d\alpha}{\alpha} = - \frac{dr}{r}.$$

Consequently, electroformed or carefully broached tubing is commonly used for these attenuators in order to avoid variations in  $\alpha$  that may be caused by dimensional variations along the length of the tube.

**11.4. Purity of Useful Mode.**—The two major problems in the design of a cutoff attenuator are r-f impedance-matching of the antenna elements and mode purity. The importance of impedance-matching in any type of attenuator has been discussed in Sec. 11.2. The problem of mode purity, however, is peculiar to the cutoff attenuator.

One of the most attractive features of the cutoff attenuator is the fact that its attenuation constant can be predicted exactly by theory, and with certain limitations the attenuator may, therefore, be considered a primary standard. If only one mode exists in the cutoff tube, the attenuation constant is given exactly by Eq. (6), and is independent of the total attenuation. However, if more than one mode is excited in the cutoff tube, Eq. (6) is no longer sufficient to specify the attenuation constant. In this case  $\alpha$  will vary with  $x$ , the separation of the antenna elements, and will approach a constant value only at large values of  $x$ . The variation of  $\alpha$  with  $x$  is determined by the relative amplitudes and phases of the specific modes excited in the cutoff tube. Since the various modes have different values for  $\alpha$ , their relative intensities vary with  $x$ .

As  $x$  increases, one mode after another decays into insignificance, until  $\alpha$  becomes essentially independent of  $x$  when only the single mode with the smallest value of  $s_{mn}$  remains.

In most applications of cutoff attenuators it is desired to effect a known change in attenuation. Seldom is it necessary to know accurately the total attenuation introduced by the device. Consequently, greatest accuracy results from using the attenuator in the linear region—at large values of  $x$  where  $\alpha$  is independent of  $x$ . Although it may not be necessary to know accurately the total attenuation under such circumstances,

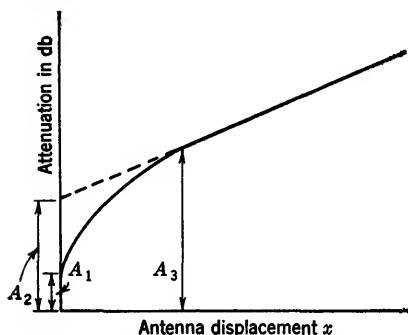


FIG. 11-4.—Representative calibration curve for a cutoff attenuator.

it is often desirable to keep it reasonably small. In order to obtain linearity in the calibration without having to accept objectionably large values of total attenuation, it is necessary to design at least one of the antennas so that it excites a single mode, the mode with the smallest value of  $s_{mn}$ .

In Fig. 11-4 three quantities are indicated which are commonly used to characterize a cutoff attenuator.

The quantity  $A_1$  represents the minimum attenuation that is available from the cutoff attenuator. The attenuation is minimized by bringing the antenna elements into contact, but, in general, cannot be made zero. Discontinuities in the transmission line at the antennas account for some reflective attenuation, and the impedance-matching devices commonly incorporated in a cutoff attenuator add a dissipative component to  $A_1$ .

$A_2$  is the attenuation value determined by extrapolating the linear part of the calibration curve to the  $x$  axis. The total attenuation at large values of  $x$  may be calculated from the simple linear equation

$$A = A_2 + \alpha x,$$

where  $\alpha$  is the slope of the linear region of the curve.

$A_3$  is the smallest value of attenuation where the calibration curve is linear. Unfortunately, this definition is not specific, and there is lack of agreement with regard to how it should be further qualified. One may say either that the slope of the curve at this point is within a given percentage (for example, 1 per cent) of that of the linear portion of the curve, or that the attenuation at this point is within a given fraction of a decibel (for example, 0.5 db) of that associated with the extrapolated linear region of the curve. Any reference to  $A_3$  in the following material

will be specifically qualified to avoid confusion. For most applications of cutoff attenuators it is important to have  $A_3$  as small as possible. To meet this condition it is necessary to strive for high mode purity, and to design the impedance-matching networks in such a manner that satisfactorily low reflection can be obtained with networks having relatively small attenuation.

**11-5. Separation of Undesirable Modes.**—As previously mentioned, the nonlinearity of the calibration curve of a cutoff attenuator in the region of relatively close coupling between the antennas is largely a result of multimode coupling between the two antennas. Both antennas must be capable of exciting (or coupling to) more than a single mode in order for this nonlinearity to occur. Much of interest can be learned about cutoff attenuators by examining the mechanism of this multimode coupling.

Consider, for example, the case of a loop-coupled  $TE_{11}$ -mode attenuator. This mode is commonly used in cutoff-attenuator design because it has the smallest attenuation constant of all modes. The modes with larger  $\alpha$  or  $s_{mn}$  values decay more rapidly, and the calibration curve for the attenuator must necessarily approach linearity at large values of loop displacement. By reference to Table 11-1 we note that the  $TM_{01}$ -mode is likely to be the most troublesome mode from a point of view of linearity since its  $s_{mn}$  value is closest to that of the  $TE_{11}$ -mode. Experience substantiates this prediction, particularly if the metal coupling-loop wires have diameters that are large enough for ruggedness. Referring now to Fig. 11-4, let us arbitrarily divide the curve into three regions: (1) the linear region where only the  $TE_{11}$ -mode exists, (2) an intermediate region where the curvature results from a combination of  $TE_{11}$ - and  $TM_{01}$ -modes, and (3) the region near  $x = 0$  where the curvature is influenced by many modes and by other factors not yet mentioned. Let us concentrate on the intermediate region where only two modes need be considered. The  $TM_{01}$ -mode has a field intensity which is independent of the angle of rotation  $\theta$  between the two loops; the intensity of the  $TE_{11}$ -mode (see Fig. 11-5) varies with  $\cos \theta$ , however, if both loops are grounded on the same generator of the cylinder where  $\theta = 0$ .

Let  $V_1$  and  $V_2$  represent, respectively, the voltages induced in the receiving loop by the  $TE_{11}$ - and  $TM_{01}$ -modes; then

$$V_1 = B_1 e^{-\alpha_1 x} \cos \theta, \quad (7)$$

$$V_2 = B_2 e^{-\alpha_2 x}, \quad (8)$$

where  $\alpha_1$  and  $\alpha_2$  are the corresponding attenuation constants.

In combining the vectors  $V_1$  and  $V_2$  it is necessary to take into consideration the fact that, in general, the two modes are separated in time phase by an angle  $\psi$ . Therefore, the resultant vector voltage  $V$  induced

in the receiving loop is given by

$$V^2 = V_1^2 + V_2^2 + 2V_1V_2 \cos \psi,$$

or

$$V^2 = (B_1 e^{-\alpha_1 x})^2 (1 + r^2 e^{-2\rho x} + 2r e^{-\rho x} \cos \theta \cos \psi - \sin^2 \theta), \quad (9)$$

where

$$\rho = \alpha_2 - \alpha_1,$$

and

$$r = B_2/B_1.$$

If  $V_0^2$  is defined as the value of  $V^2$  for  $x = 0$  and  $\cos \theta = 1$ , and if the attenuation in decibels is arbitrarily taken as zero for this case, then it

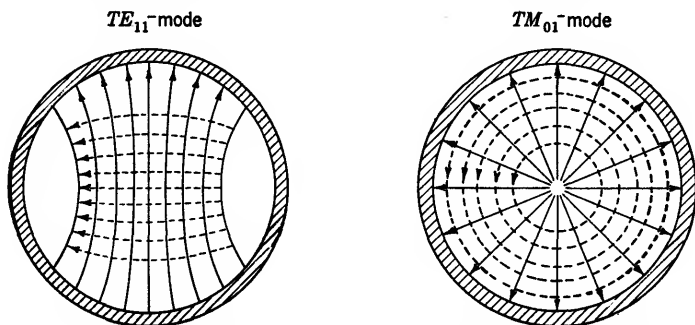


FIG. 11-5.—Field configurations of the  $TE_{11}$ - and  $TM_{01}$ -modes in circular waveguide.

follows from Eq. (9) that

$$A = 8.686\alpha_1 x + 10 \log_{10} \left( \frac{1 + r^2 + 2r \cos \psi}{1 + r^2 e^{-2\rho x} + 2r e^{-\rho x} \cos \theta \cos \psi - \sin^2 \theta} \right). \quad (10)$$

Equation (10) is the general equation for the attenuation of the cutoff attenuator, except for an additive constant, resulting from a combination of the two modes. The equation includes the effects of both linear and angular displacement of the loops. The first term of Eq. (10) is the attenuation resulting from the desired  $TE_{11}$ -mode, and the second term is of the nature of a correction term which arises because of the existence of the  $TM_{01}$ -mode. Implicit in Eq. (10) are the assumptions that (1) the cutoff tube has a circular cross section with no elliptical eccentricity, (2) the plane of each of the two loops includes the center line of the cutoff tube, and (3) the transfer impedance effects, to be discussed later, are negligible.

For further considerations it is convenient to rewrite Eq. (10) for the special case,  $x = 0$ . The angular dependency of attenuation is thus

$$A = 10 \log_{10} \frac{1 + r^2 + 2r \cos \psi}{1 + r^2 + 2r \cos \theta \cos \psi - \sin^2 \theta}. \quad (11)$$

Values for  $r$  and  $\cos \psi$  may be calculated from measurements of  $A$  as a function of  $\theta$ , taken at the arbitrarily chosen,  $x = 0$  plane. As one loop is rotated with respect to the other, the power coupled from one loop to the other varies. It will have a maximum value at  $\theta = 0$ , by previous definition. As  $\theta$  is increased, the power transferred will decrease, pass through a minimum, and will then increase again to a second maximum at  $\theta = 180^\circ$ . This second maximum will be smaller than the first since in this case the electric-field vectors of the two modes oppose each other, whereas they reinforce each other in the case of larger maximum at  $\theta = 0$ . By differentiating the right-hand side of Eq. (11) with respect to  $\theta$  and equating to zero, one obtains the condition that

$$\sin \theta (\cos \theta + r \cos \psi) = 0. \quad (12)$$

The maxima in power transfer occur for  $\sin \theta = 0$ , or  $\theta = 0$  and  $180^\circ$ , respectively. The minimum power transfer exists when

$$\cos \theta_m = -r \cos \psi. \quad (13)$$

Therefore, if we define  $A_{sm}$  as the attenuation when  $\theta = 180^\circ$ ,  $A_{mi}$  as the attenuation when  $\theta = \theta_m$ , we may rewrite Eq. (11) in the forms

$$A_{sm} = 10 \log_{10} \frac{1 + r^2 + 2r \cos \psi}{1 + r^2 - 2r \cos \psi}, \quad (14)$$

$$A_{mi} = 10 \log_{10} \frac{1 + r^2 + 2r \cos \psi}{1 + r^2 + 2r \cos \psi \cos \theta_m - \sin^2 \theta_m}. \quad (15)$$

Equations (13), (14), and (15) may be solved simultaneously to determine  $r$ ,  $\psi$  and  $\theta_m$  in terms of  $A_{sm}$  and  $A_{mi}$ . Thus

$$r = \left( \frac{1 - J}{1 + J} \right) \sqrt{1 + \frac{4g^2}{1 - t^2} \left( \frac{1 + J}{1 - J} \right)}, \quad (16)$$

$$\tan \psi = \pm \sqrt{\frac{4g^2}{1 - t^2} \left( \frac{1 + J}{1 - J} \right)}, \quad (17)$$

$$\cos \theta_m = \mp \left( \frac{1 - J}{1 + J} \right), \quad (18)$$

where

$$J = \sqrt{\frac{t^2 - g^2}{1 - g^2}},$$

$$A_{mi} = 20 \log_{10} \left( \frac{1}{g} \right), \quad (19)$$

$$A_{sm} = 20 \log_{10} \left( \frac{1}{t} \right).$$

The calculation of  $\theta_m$  from Eq. (18) may be checked by an experimental measurement of  $\theta_m$ , provided that the assumed conditions are satisfied. An indication of the presence of other modes is asymmetry

of the angle calibration curve. For example, if the two minima (one between 0 and  $\pi$  and the other between  $\pi$  and  $2\pi$ ) are not symmetrically located or differ in the value of  $A_{mi}$ , at least one other mode is present. The choice of sign in Eq. (18) is dictated by whether the experimentally determined  $\theta_m$  is in the first or second quadrant. The choice of sign in Eq. (17) is dictated by the fact that  $\psi$  is a second-quadrant angle if  $\theta_m$  is in the first quadrant, and vice versa. This is apparent from Eq. (13).

If  $r$  and  $\psi$  have been found, Eq. (10) can be used to predict the attenuation as a function of  $\theta$  and  $x$ . In particular, the value of  $x$  and the attenuation corresponding to the point  $A_3$  of Fig. 11-4 may be determined. If we let  $Y$  equal the logarithmic correction term of Eq. (10), then the slope of the calibration curve is

$$\frac{\partial A}{\partial x} = 8.686\alpha_1 + \frac{\partial Y}{\partial x}. \quad (20)$$

By setting the ratio of  $\partial A/\partial x$  to  $8.686\alpha_1$  equal to 1.01, for example, one can determine the value of  $x$  at which the slope is within 1 per cent of the pure  $TE_{11}$ -mode slope; or one may calculate the value of  $x$  at which the attenuation is 0.5 db lower than that of the extrapolated linear portion of the curve. It will be remembered that these are the two alternatives for specifying the quantity  $A_3$ .

Several other bits of useful information may be extracted from the above equations. For example, referring to Eq. (20), the slope correction term  $\partial Y/\partial x$  should be made as small as possible for best linearity. By differentiation,

$$\frac{\partial Y}{\partial x} = 8.686\rho r e^{-\rho x} \left( \frac{r e^{-\rho x} + \cos \theta \cos \psi}{r^2 e^{-2\rho x} + 2r e^{-\rho x} \cos \theta \cos \psi + \cos^2 \theta} \right). \quad (21)$$

For  $\cos \psi = 0$  or unity, the value of  $\partial Y/\partial x$  is minimized with respect to variations in  $\theta$  by setting  $\cos \theta = \text{unity}$ . Moreover, this condition on  $\cos \theta$  holds, regardless of the value of  $x$ . To obtain the smallest possible  $A_3$  value, the attenuator should be operated with the loops adjusted to meet the  $\theta = 0$  condition.

If the cross section of the cutoff tube is not accurately circular, it is possible to get into peculiar difficulties. For example, in a slightly elliptical tube it is possible for the  $TE_{11}$ -mode to be excited as two modes, polarized at right angles with respect to each other. Since they have the same attenuation constant, the variation with  $x$  is not affected, but the variation with  $\theta$  suffers a marked change. It is essential to guard against any twist along the length of a slightly elliptical tube. Such a twist rotates the plane of polarization of all modes that do not have circular symmetry, and this affects the coupling to these modes. Thus

it is possible to have a cutoff tube in which only the  $TE_{11}$ -mode exists, but which nevertheless has a nonlinear calibration curve because of the fact that the coupling to the mode varies with the twist angle of the tube. It is apparent that twist can be even more harmful in distorting the calibration curve if more than one mode is being coupled.

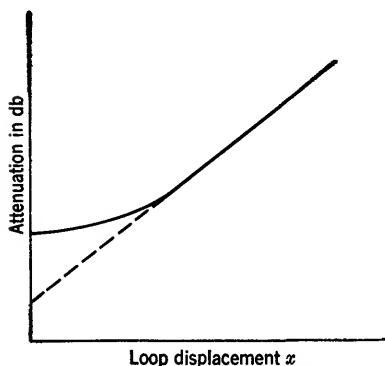


FIG. 11-6.—Calibration curve of a cutoff attenuator with  $TE_{11}$ - and  $TM_{01}$ -modes in opposite time phase.

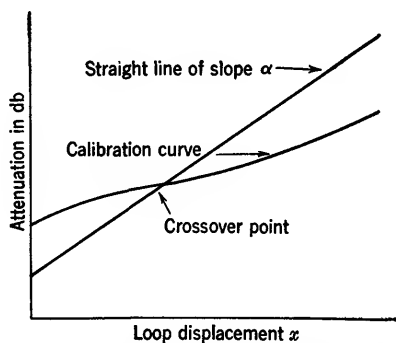


FIG. 11-7.—Calibration curve illustrating the crossover phenomenon.

The correction term  $Y$  may be either positive or negative; if it is positive, the general shape of the calibration curve is that shown in Fig. 11-4; if it is negative, the calibration curve approaches linearity by a decreasing slope, rather than by an increasing slope as in Fig. 11-6. The sign of the correction term  $Y$  changes from plus to minus for a value of  $\psi$  somewhat greater than  $90^\circ$ . If  $\theta = 0$ , then the sign of  $Y$  depends on whether the argument of the logarithm is greater or less than unity. Therefore, if  $Y = 0$ ,

$$1 + r^2 + 2r \cos \psi = 1 + r^2 e^{-2\rho x} + 2r e^{-\rho x} \cos \psi,$$

and

$$\cos \psi = -\frac{1}{2}r(1 + e^{-\rho x}). \quad (22)$$

This equation states that it is possible to have  $Y = 0$  at  $x = 0$ , an important observation. In other words, it permits the calibration curve to have a "crossover point" of the kind shown in Fig. 11-7.

The parenthetical quantity in Eq. (22) varies from 2 to 1 as  $x$  varies from 0 to  $\infty$ . Therefore, the crossover point occurs when  $\cos \psi$  lies within the range between  $-r/2$  and  $-r$ . As the value of  $\cos \psi$  varies from  $-r/2$  to  $-r$ , the crossover point moves out along the straight line toward infinity. Crossover from the opposite direction (that is, the mirror image of the calibration curve shown) is not possible if  $r$  is less than unity.

**11-6. Principle of Mode Filtering.**—A potentially powerful tool in the design of cutoff attenuators, and one which unfortunately has not been

utilized as often as it might have been, is the principle of mode filtering. One may select a waveguide such that, at the frequency of interest, propagation is possible only in the lowest, or dominant, mode. Modes of higher order will be beyond cutoff and will therefore be attenuated. A sufficient length of such a line can be used as an effective mode filter, maintaining unattenuated propagation of the fundamental mode while the higher modes decay into insignificance. After passing through the filter, the fundamental mode is used to excite a length of waveguide which is beyond cutoff for this mode. It is essential, of course, to design the junction between the filter and cutoff sections so that higher modes are not excited again. The principle is quite simple, but there are practical problems involved which are not always simple.

If the cutoff region for the dominant mode is to be in circular waveguide, the filter section is customarily designed for circular waveguide; similarly, rectangular filter sections are used with rectangular waveguides beyond cutoff. Consider, for example, the design of a circular-waveguide filter section for operation at a wavelength of 9.5 cm. From Eq. (4), it can be calculated that an air-filled tube of 2.93 cm radius will propagate the fundamental  $TE_{11}$ -mode at wavelengths of 10.0 cm or less and will propagate the next higher mode, the  $TM_{01}$ , at wavelengths of 7.6 cm or less. This tube radius would therefore be an acceptable one for use at 9.5 cm. There is no danger of cutoff attenuation in the fundamental mode, and the mode of the next higher order is sufficiently far beyond cutoff so that its attenuation constant is not too frequency-sensitive at this wavelength. The length of filter section used would depend on the time phases and intensities of the higher modes relative to those of the fundamental mode at the input end of the filter section. A waveguide diameter of 5.86 cm is apt to be objectionably large for some applications, so that it is desirable to fill the waveguide with a dissipationless material of relatively high permittivity. The reduction in tube radius, according to Eq. (4), is governed by the relation

$$a\sqrt{k_e} = \text{constant.}$$

Since it is possible to obtain a usable, easily machined  $TiO_2$ -impregnated polystyrene for which  $k_e = 10$ , the use of this dielectric permits reduction in radius of the tube by a factor of three or more.

The use of a dielectric-filled waveguide for the filtering section affords another advantage over an air-filled filter section. In using a filter with no dielectric, it is necessary to constrict the waveguide section following the filter in order to bring the fundamental mode beyond cutoff. This constriction might, for example, take the form of an abrupt decrease in the diameter of a circular waveguide, or an abrupt decrease in both the  $a$  and  $b$  dimensions of a rectangular waveguide.



Such a discontinuity in the waveguide will excite higher modes in the cutoff section, and much if not all of the usefulness of the mode filter will be lost. However, if a dielectric of high permittivity is used in the mode filter, there need be no discontinuity between the filter and cutoff sections aside from the simple dielectric-air interface which lies normal to the axis of the waveguide. The field boundary conditions at such an interface guarantee that if only the fundamental mode exists in the dielectric, adjacent to the interface, then only the fundamental mode can exist in the air region beyond. It is advantageous to use a material with a large dielectric constant in the filter section. In this case the fundamental mode will be far beyond cutoff in the air-filled cutoff section, and the attenuation constant for the mode will be relatively insensitive to frequency.

The use of a mode filter restricts the wavelength range in which the cutoff attenuator may be used. This range can at the most be the difference between the cutoff wavelengths for the fundamental and next higher mode. In practice it is necessary to sacrifice part of this range. For example, since there are small variations in the permittivity of the dielectric from one attenuator to the next, it is unwise to operate at wavelengths close to the cutoff wavelength of the fundamental mode. In working very close to the short-wavelength limit of the allowable range, variations in permittivity may allow the next higher mode to be propagated together with the fundamental. Also, the attenuation of this second mode will be slight in this wavelength region, and the filter section to be effective must be made objectionably long. It should be noted that the use of a dielectric-filled line in place of an air-filled line does not change the wavelength spread between the fundamental and next higher mode, provided that both arrangements have the same cutoff wavelength for the dominant mode.

Rectangular waveguide has an advantage over circular waveguide for mode filtering because the cutoff wavelengths (and cutoff attenuation constants) for the various modes are more widely separated when rectangular waveguide is used. Consequently, the rectangular mode-filtered cutoff attenuator is operable over a much broader wavelength range than is the circular mode-filtered attenuator. Reference to Table 11-2 should clarify this point. The data apply strictly for  $\lambda \ll \lambda_c$ , but are indicative of the situation when  $\lambda$  approaches  $\lambda_c$  closely.

In studying Table 11-2 note particularly the additional advantage gained from using a very flat waveguide. In such waveguide only the series of  $TE_{m0}$ -modes is of importance; all other modes have relatively large attenuation constants. However, regardless of the value of  $a/b$ , a considerably greater usable wavelength range is obtained with rectangular waveguide than with circular.

Because of the larger mode separation in rectangular waveguide, the input impedance for the filter section is less frequency-dependent and hence more susceptible to matching over a broad band. The higher modes that are attenuated in the filter section store power that is reflected back into the transmission line toward the generator. By no means all of the power associated with the main mode is coupled through the attenuator, and much of the total power reflection is from this mode. In the rectangular waveguide the phase shift in the dominant mode and the attenuation constants of the higher modes are less frequency-sensitive than in circular waveguide, and consequently the input impedance is less frequency-sensitive.

TABLE 11-2.—SPREAD IN CUTOFF WAVELENGTHS AND RATIO OF ATTENUATION CONSTANTS FOR VARIOUS WAVEGUIDE MODES

Circular Waveguide					
Parameter (see notes)	$TE_{11}$	$TE_{01}$	$TE_{21}$	$TM_{11}, TE_{01}$	$TE_{31}$
X	....	0.23	0.40	0.52	0.56
Y	1.00	1.31	1.66	2.08	2.28

Rectangular Waveguide								
Param- eter (see notes)	$TE_{10}$	$TE_{20}$	$TE_{18,0}$	$TE_{01}$	$TE_{11}, TM_{11}$	$TE_{21}, TM_{21}$	$TE_{02}$	$TE_{12}, TM_{12}$
$\frac{a}{b} = \frac{9}{4}$								
X	....	0.50	0.94	0.56	0.59	0.67	0.78	0.78
Y	1.00	2.00	18.0	2.25	2.46	3.01	4.50	4.61
$\frac{a}{b} = \frac{9}{1}$								
X	....	0.50	0.94	0.89	0.89	0.89	0.94	0.94
Y	1.00	2.00	18.0	9.00	9.05	9.22	18.0	18.0

X represents the expression  $\left[ \frac{(\lambda_c)_f - (\lambda_c)_q}{(\lambda_c)_f} \right]$ .

Y represents the expression  $\left( \frac{\alpha_q}{\alpha_f} \right)$ .

$(\lambda_c)_f$  is the cutoff wavelength for the fundamental mode.

$(\lambda_c)_q$  is the cutoff wavelength for the specific, tabulated mode.

$\alpha_f$  is the attenuation constant for the fundamental mode.

$\alpha_q$  is the attenuation constant for the specific, tabulated mode.

**11-7. Variation of Input Impedance with Close Coupling.**—Multimode cutoff is not the only cause of nonlinearity in the calibration curve of a cutoff attenuator. A second source of nonlinearity is the variation in the input impedance of the attenuator, for a given load impedance, with a displacement of the coupling elements. For large separations of the

coupling elements the input impedance is wholly reactive, whereas for tight coupling the input impedance approaches the load impedance. The change in input impedance with antenna displacement is rapid for small separations, and very slight at large separations. This change in input impedance affects the power drawn from the generator, and consequently has an influence on the shape of the calibration curve. In many cutoff-attenuator designs the multimode coupling extends over such a large range of attenuation that the coupled-impedance effect is almost completely masked and can be ignored. However, in one or two of the specific designs to be discussed the mode purity is so good that impedance coupling becomes the limiting factor on linearity at the lower end of the calibration curve. Impedance coupling is also an

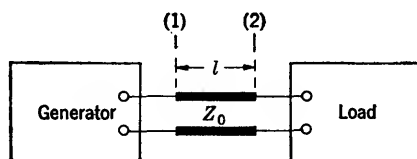


FIG. 11-8.—Diagrammatic representation of a transmission line.

important consideration in calculating the impedance-matching networks that are frequently built into cutoff attenuators.

The input impedance can easily be calculated as a function of the load impedance and the cutoff attenuation, either by formula or by reference to impedance-circle diagrams. In fact, the procedures are analogous to those used for a propagating waveguide. In the case of a propagating waveguide the magnitude of the voltage reflection coefficient  $\Gamma$  is not changed as the plane of reference is moved along the waveguide, but the phase angle of  $\Gamma$  varies twice as fast as the angle  $2\pi l/\lambda_0$  through which the reference plane is moved. In contrast, the phase angle of  $\Gamma$  does not change with  $l$  in cutoff waveguides, but the magnitude of  $\Gamma$  does change with  $l$ .

In any transmission line, represented diagrammatically in Fig. 11-8, we can apply two fundamental formulas

$$\begin{aligned}\Gamma_1 &= \Gamma_2 e^{-2\gamma l}, \\ \Gamma &= \frac{Z - Z_0}{Z + Z_0}.\end{aligned}$$

For propagating waveguides, where the magnitude of  $\Gamma$  does not change with  $l$ ,

$$\begin{aligned}\gamma &= j\beta = j\frac{2\pi}{\lambda_0}, \\ \Gamma_1 &= \Gamma_2 e^{-2j\beta l}.\end{aligned}$$

The characteristic impedance of the line is real, and we may write

$$Z_0 = R_0.$$

The transformation along the line may be represented graphically by the impedance-circle diagrams of Fig. 11-9. Here lines of constant  $|\Gamma|$  are shown as solid lines, while lines of constant phase are dotted. To transform an impedance along the transmission line, moving  $\theta$  degrees toward the generator, one moves  $2\theta$  degrees in a clockwise direction across the dashed constant-angle lines. Limiting the impedance to the right half of the  $Z$ -plane restricts the reflection coefficient to within the unit circle on the  $\Gamma$ -plane.

In the case of cutoff waveguides  $\gamma = \alpha$  and  $Z_0$  is pure imaginary. Let us write

$$\begin{aligned} Z_0 &= jX_0, \\ \Gamma_1 &= \Gamma_2 e^{-2\alpha l}. \end{aligned}$$

The impedance diagrams for this case are shown in Fig. 11-9. Here also lines of constant  $\Gamma$  are solid, and the phase lines dotted. The characteristic impedances of the lines, whether or not they are operated at frequencies below cutoff, may be taken as proportional to the wave impedances in the line. For  $TE$ -modes the wave impedance is

$$Z_0 = \frac{j\omega\mu}{\gamma}.$$

If  $\gamma$  is imaginary, and we have propagation,

$$Z_0 = R_0 = \frac{\lambda_g}{\lambda} \sqrt{\frac{\mu}{\epsilon}}.$$

If  $\gamma$  is real,

$$Z_0 = jX_0 = j \frac{\omega\mu}{\alpha}.$$

For  $TM$ -modes, the wave impedance is  $\gamma/j\omega\epsilon$ , and

$$\begin{aligned} R_0 &= \frac{\lambda}{\lambda_g} \sqrt{\frac{\mu}{\epsilon}}, \\ X_0 &= -\frac{\alpha}{\omega\epsilon}. \end{aligned}$$

For cutoff waveguides having  $TM$ -modes,  $X_0$  is negative, and the equation of transformation from the  $Z$ - to the  $\Gamma$ -plane becomes

$$\Gamma = \frac{Z + j|X_0|}{Z - j|X_0|}.$$

This corresponds to a geometrical reflection on the resistance axis of the

diagram in the impedance plane so that going toward the generator now corresponds to a clockwise rotation on the diagram. The diagrams can also be used for admittances. In this case there is a geometrical

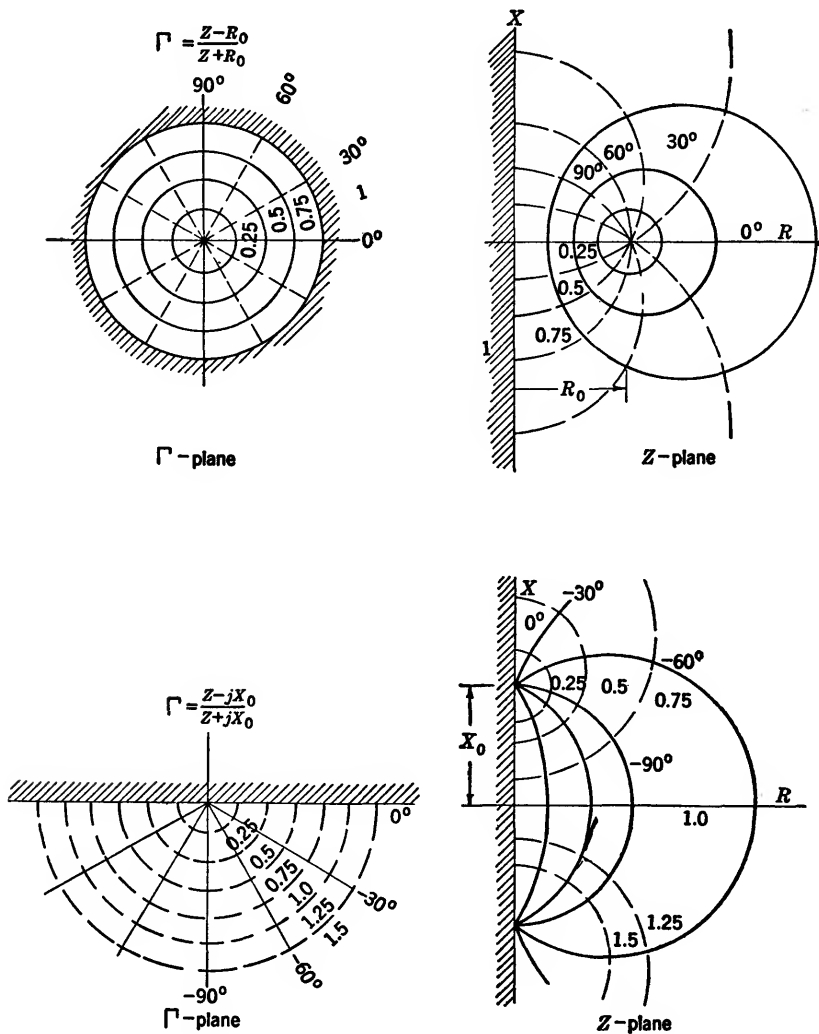


FIG. 11-9.— $\Gamma$ - and  $Z$ -planes for a  $TE$ -mode beyond cutoff.

reflection on the resistance axis, and the angles are changed to their negative complements.

These calculations are applicable only for single-mode excitation

in the cutoff waveguide. In the event of multimode coupling, the situation is much more complicated, and we shall not discuss it here.

The junction between a propagating waveguide and one beyond cutoff may be represented as a four-terminal network whose parameters depend on the geometrical configuration of the junction as well as the characteristic impedances of the lines connected to the junction. Thus a complete cutoff attenuator has the equivalent circuit shown in Fig. 11-10. If the characteristics of the input and output junctions are known, the complete behavior of the attenuator can be calculated as outlined above. In Sec. 11-11 an attenuator is described for which this calculation has been carried out.

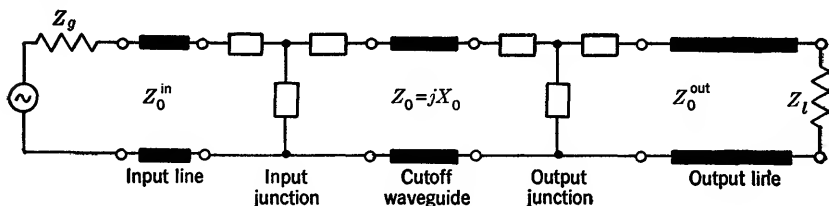


FIG. 11-10.—Equivalent circuit of a cutoff attenuator.

**11-8. Impedance-matching Techniques.**—In Sec. 11-2 an attempt was made to justify the importance of matching an attenuator. The cutoff attenuator particularly demands impedance-matching since its input impedance is wholly reactive for large separations of the coupling elements. The voltage standing-wave ratios are very high, around 40 or 50, and a small change in frequency can markedly affect the power drawn from the generator and delivered to the load which terminates the transmission line. There are several factors to be considered in the design of a matching network, and the choice of matching section depends on how one wishes to weight the various design factors. In general, the important factors are (1) maximum allowable input voltage standing-wave ratio, and the wavelength band over which the attenuator is to meet this maximum VSWR specification; (2) maximum reflections from the generator and load in the transmission line in which the attenuator is to be used; (3) magnitude of the dissipative attenuation introduced by the matching section; (4) relative importance of good matching at tight coupling and at loose coupling; (5) power-handling capacity of the matching section; (6) physical size of the matching section; (7) availability and ease of construction of the matching section; and, (8) reproducibility of the matching section.

The maximum allowable VSWR is, as previously explained, important from the viewpoint of ascertaining reflection errors when the generator and load are not perfectly matched. In attenuators which use matching

sections consisting of a lumped resistive element, the mismatched generator and load take on added significance. There is a power split between the matching element and the terminal load, this split being determined by the impedances of the two, and the effective dissipative attenuation of the matching element is therefore dependent on the load impedance. Consequently, a small change in load impedance can, under certain circumstances, exert a big influence on the over-all attenuation of the cutoff attenuator. More will be said about this in following paragraphs. Often one wishes to have good impedance-matching at the least possible cost in attenuation from losses in the matching section. The need for reducing this attenuation to a bare minimum will greatly influence the choice of the matching section. If the need for good impedance-matching is greatest under the condition of tight coupling, the design of a matching section is a much more severe problem than if the matching is to be made optimum at loose-coupling conditions. This follows from the fact that, at tight coupling, the impedance which is to be matched is varying much faster with antenna separation. The fact that the power level will be very low when the attenuator is in use does not allow one to neglect the power capacity of the matching section; relatively high-power levels must be used in calibrating the attenuator at large values of attenuation. The last three items in the above list are of relatively minor importance within the laboratory but can be quite troublesome if large-scale production of attenuators for field use is contemplated.

Most of the information available on resistive matching sections pertains to attenuators employing circular waveguide. In these designs the coupling elements terminate coaxial lines so that the matching sections are also in coaxial line. Matching sections of three types have been used in such attenuators: distributed-parameter resistive attenuators, i.e., microwave T-pads; resistive coupling loops; and a single, lumped-constant, series or shunt resistive element which is properly located with respect to the coupling element.

TABLE 11-3.—DATA ON CABLE ATTENUATION AND CHARACTERISTIC IMPEDANCE

Cable	$\lambda$ , cm	$Z_0$ , ohms	$A$ , db/ft
RG-21/U	10.0	52	0.83
RG-21/U	3.3	52	1.6
RG-9/U	3.3	52	0.33

Undoubtedly the most commonly used matching device with distributed parameters is a long length of lossy cable. Typical data on cable attenuation and characteristic impedance are given in Table 11-3. In determining how much attenuation should be used, it is convenient to

refer to Fig. 11-11. This is a graph of the voltage standing-wave ratio of a short-circuited line which is "padded" with  $n$  db of matched attenuation. Thus, if the voltage standing-wave ratio looking into the attenuator is not to exceed 1.05, it is necessary to use at least 16 db of matched-cable attenuation. Actually, however, it is almost impossible to reduce the input VSWR to a value as small as 1.05 because of the reflections introduced by the cable fittings. If the cable attenuation reduces the VSWR of the short-circuited line to a value  $r_1$ , and if the

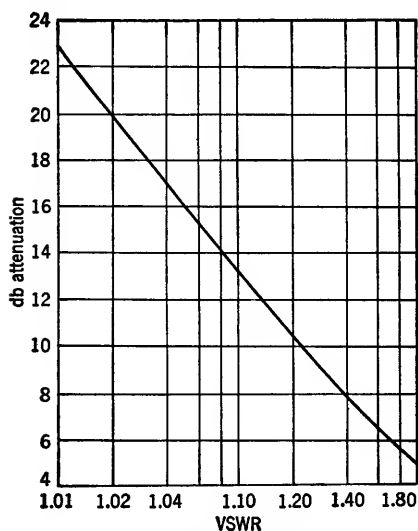


FIG. 11-11.—Change in VSWR with line attenuation.

cable fitting has a  $VSWR = r_2$  when followed by a  $Z_0$  load, then the actual or effective VSWR  $r'$  may lie anywhere within the range bounded by the product and quotient of  $r_1$  and  $r_2$ . Thus the reflections from the connectors impose a limit on the goodness of matching.

It should be noted that  $r'$  need not be particularly small if the cutoff attenuator is used only to effect a known change in attenuation, and if it is operated in the range of relatively loose coupling where the previously discussed coupled-impedance effect is negligible. It is, nevertheless, safe practice to minimize  $r'$  since the attenuation error associated with

a small and often unavoidable frequency drift will be less if  $r'$  is small.

Lossy cable has the advantage of being readily obtainable, but it is very bulky. Its attenuation constant is somewhat sensitive to changes of temperature and frequency, although if enough cable is used these variations are not disturbing. Flexion of the cable adjacent to the connectors can be very bothersome because it moves the center conductor pin of the plug (male) connector and changes the reflection. It is helpful to install a six-inch length of metal tube at the back end of the connector to prevent the cable from bending in this critical region. Lossy cable is capable of greater power dissipation than are most other types of matching sections.

There are many kinds of coaxial attenuators using metalized glass, polyiron, Bakelite, and other dissipative materials, that can be considered for use as cutoff-attenuator matching sections. In principle they do not differ from lossy cable but are often preferable because of their



compactness. Such designs will be discussed in detail in Chap. 12. In general, they are not well matched over as broad a wavelength band as is lossy cable.

The idea of using a resistive coupling loop which itself provides a satisfactorily matched termination for the coaxial line is an interesting one. This has been accomplished, in 0.5-in. 10-cm cutoff tubes, in two ways. The Carborundum Co. manufactures a midget carborundum resistor of 50-ohm nominal value in a 0.1-watt size. It is only  $\frac{1}{8}$  in. in diameter and  $\frac{1}{4}$  in. in length and has metalized ends for soldering. Figure 11-12 shows how such a resistor might be installed.

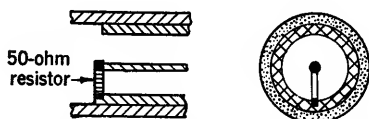


FIG. 11-12.—Coupling loop for a  $TE_{11}$ -mode cutoff attenuator with midget 50-ohm resistor.

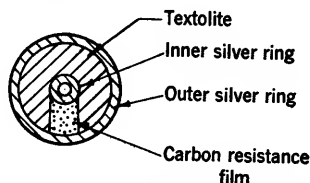


FIG. 11-13.—Resistive-stripe coupling loop for a  $TE_{11}$ -mode circular cutoff attenuator.

While rated for only 0.1 watt, the resistor will apparently carry several times this amount without harm. The standing-wave ratios obtained in the 10-cm band were considerably larger than those obtained using a "carbon stripe," so that the use of these resistors was abandoned except for a few instances where power capacity was of greater importance than low reflection. However, this method of matching would probably be very successful for application at longer wavelengths and would seem to deserve further investigation.

The carbon stripe is a coating of carbon on a thin  $\frac{1}{32}$ -in. textolite disk. The carbon material used is the same as that used in making the common carbon-strip potentiometers. The disk has a hole in its center through which the inner conductor of the coaxial line may protrude and silver-paste rings baked onto the disk to facilitate soldering or good pressure contact to the inner and outer conductors of the line. The hole diameter and disk diameter are chosen to be compatible with the coaxial-line size used. The construction is shown in Fig. 11-13.

The VSWR data in Table 11-4 indicate what can be expected in the impedance-matching of a resistive-stripe coupling loop. The cutoff tube is a 0.5-in. diameter tube; the sliding insert is a 50-ohm coaxial line terminated in the resistive stripe. The VSWR data were taken with the sliding insert installed in the cutoff tube but with no second loop to couple power from it. The resistivity of the carbon film was varied so that the d-c resistance of the stripe was 50 ohms in all cases.

TABLE 11-4.—IMPEDANCE-MATCHING DATA FOR A CARBON-STRIPE COUPLING LOOP

Stripe width, in.	VSWR less than	Over the band, cm
$\frac{5}{16}$	1.08	8.5 to 12.2
$\frac{3}{16}$	1.10	8.6 to 12.2
$\frac{2}{16}$	1.4	8.6 to 12.3
$\frac{3}{32}$	1.6	8.6 to 11.8

It will be noted from the data tabulated above that the wide stripes are preferable to the narrow ones from the viewpoint of broadband matching. The simplest explanation is that the wider stripes have less inductance, and thus contribute a smaller reactive component to the load impedance. An alternative, but perhaps less likely, explanation is that the inductance associated with the wide stripe, together with the inductive reactance which is reflected into the loop from the cutoff tube, is enough to resonate the capacitance of the high-permittivity textolite disk. Such a resonant circuit, heavily loaded by the resistance of the stripe, may be expected to have a very low  $Q$  and hence an impedance which is relatively insensitive to changes of frequency.

The carbon stripe unfortunately has a low power-handling capacity. Because of variations in the thickness of the resistive film, it is unwise to use such a stripe at power levels in excess of 0.1 watt. There seems to be no reason why the metalized-glass techniques used in making resistive attenuators could not be utilized in applying a metal-film stripe to a glass or a nonflaking synthetic-mica disk. Such techniques should produce a uniform, reproducible resistive coupling loop. The resistive stripe has two fundamental disadvantages: the appreciable width of the stripe enables it to couple well to the undesired  $TM$ -modes, and extremely tight coupling in the desired mode is impossible because of the difficulty of bringing two such stripes into intimate contact.

The third general procedure for matching the coaxial-line coupling element involves the use of a small, lumped-constant resistor in series or in shunt with the line. To idealize the situation, assume that the metal coupling loop in a design for the  $TE_{11}$ -mode is exactly equivalent to a short circuit at the loop, and that the metal disk used in the designs for the  $TE_{01}$ -mode is exactly equivalent to an open circuit at the metal disk. In the case of the short circuit at the loop, a tiny resistor of  $Z_0$  ohms in series with the center conductor, at a distance of a half wavelength from the loop, would effect a matched termination. In other words, the load impedance is zero at this half-wavelength point, and a  $Z_0$  series resistor installed at this point should provide a match. Similarly, if a shunt resistance is to be used, it would be installed at the quarter-wavelength point where its resistance would be in parallel with an open circuit

and would therefore present a match. Similar reasoning, applied to the design for the  $TM_{01}$ -mode, suggests that the series resistor should be inserted at the quarter-wavelength point and the shunt resistor at the half-wavelength point. Normally one would prefer the element placed at the quarter-wavelength point, as this obviously leads to a less frequency-sensitive load than would a half-wavelength spacing of the resistor. In any case, this third type of matching cannot be expected to be good over as broad a band as either of the first two mentioned.

Actually, conditions are not quite as we have assumed them to be. The reactive impedance of the cutoff tube must be considered and this may be inductive or reactive depending on whether the coupling is to  $TE$ - or  $TM$ -modes. In  $TE$ -mode designs the coupling loop has an appreciable inductance. In  $TM$ -mode designs there is a heavy capacitive loading from the fringing of the  $E$ -lines in the neighborhood of the periphery of the metal disk. Because of these factors, it is usually found that the resistors must be properly placed through trial and error to obtain the best results. The line distances are for this reason often far different from the simple quarter- and half-wavelength values. However, good impedance-matching is possible over limited wavelength bands.

In the above discussion of matching sections it is tacitly assumed that the optimum standing-wave ratio is required under loose-coupling conditions. As previously indicated, multimode coupling, in cutoff attenuators of most designs, discourages the use of these attenuators at small values of total attenuation. Since the attenuators are usually used in a loosely coupled condition, it is customary to match the impedances for this condition.

Series-matching resistors have been made from Erie<sup>1</sup>  $\frac{1}{2}$ -watt and 1-watt carbon resistors by cracking away the protective covering from the resistor material beneath it. The kernel of the  $\frac{1}{2}$ -watt resistor is approximately 0.11 in. by 0.5 in.; that of the 1-watt resistor is approximately 0.19 in. by 0.7 in. By use of a 0.500-in. OD, 0.217-in. ID coaxial line and a properly placed 50-ohm, 1-watt series resistor of this type, it was found possible to match a loosely coupled oscillator cavity to a VSWR of 2, or less, over the 8.9- to 11.1-cm band. Tolerances of  $\pm 5$  ohms on d-c resistance were found to affect the maximum standing-wave ratio very little. It is occasionally desirable to do most of the impedance-matching with such a lumped-resistor element and to reduce the VSWR further by using lossy cable.

The shunt resistor commonly used is a thin resistive disk since a disk presents a less serious discontinuity in the coaxial line than would a

<sup>1</sup> Erie Resistor Corp., Erie, Pa.

midget resistor installed across the line. The plane of the disk is normal to the axis of the coaxial line. Figure 11-14 shows the construction of a 50-ohm disk.<sup>1</sup> The disk is the correct size for installation in the coaxial sliding insert used with most 0.5-in. 10-cm cutoff attenuators. The

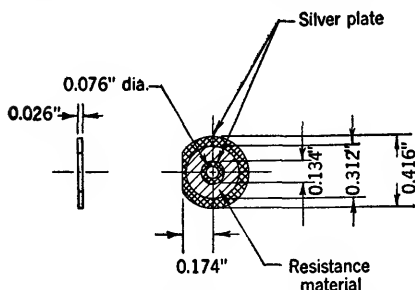


FIG. 11-14.—Resistive disk for matching attenuators.

construction is similar to that of the carbon stripe shown in Fig. 11-13, but, instead of a stripe, the entire annular region between the two silver rings is coated with carbon material. The resistance measured between the inner and outer rings is  $50 \pm 2.5$  ohms with the dimensions as shown. The power capacity of such a disk is somewhat greater than 0.5 watt.

Some idea of the effectiveness of the resistive disk as an impedance-matching device may be attained from the following data which apply to the use of the disk in a  $TM_{01}$ -mode circular cutoff design. Figure 11-15 shows the installation of the resistive disk behind the metal disk

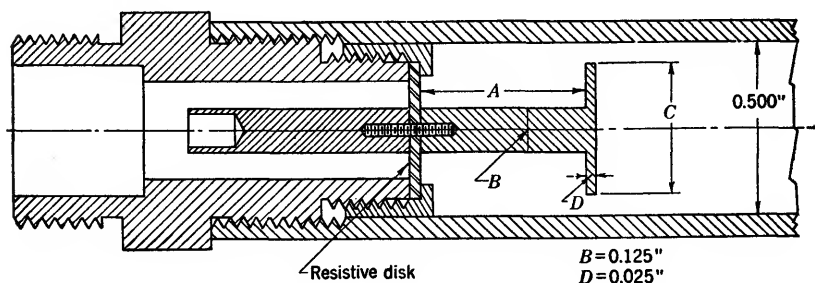


FIG. 11-15.—Installation of a resistive matching disk in a  $TM_{01}$ -mode cutoff attenuator.

which acts as the coupling element. The two most pertinent dimensions are the diameter  $C$  of the metal disk and the length  $A$  of the coaxial line between the metal disk and the resistive matching disk. The carbon side of the resistive disk is the side toward the right in the figure.

Impedance measurements were made by directing power from left to right. The VSWR-vs.- $\lambda$  curves were found to be consistently parabolic. Holding the value of  $C$  constant at 0.400 in., a graph of  $A$  vs. the wavelength for minimum VSWR ( $\lambda_b$ ) was plotted. The curve was found to be accurately a straight line for the entire range of  $A$  (0.85 in. to

<sup>1</sup> Manufactured by the International Resistance Company of Philadelphia (Catalogue number VC 14204).

1.60 in.) investigated. The value of  $dA/d\lambda_b$  was found to be 0.178 in. per cm with  $\lambda_b$  being 10.0 cm for  $A = 1.20$  in. Holding the value of  $A$  constant at 1.33 in., a graph of  $C$  vs. the wavelength for minimum VSWR ( $\lambda_b$ ) was plotted. This curve was also found to be linear for the entire range of  $C$  (0.250 in. to 0.400 in.) investigated. The value of  $dC/d\lambda_b$  was found to be 0.096 in. per cm. with  $\lambda_b$  being 10.0 cm for  $C = 0.330$  in. The optimum VSWR (at  $\lambda_b$ ) was, in almost all instances, between 1.05 and 1.10. The VSWR rose from its lowest value to a value of 1.20 at approximately  $\lambda = (1 \pm 0.08)\lambda_b$ . Ten different matching disks with d-c resistances in the range of  $50 \pm 8$  ohms were used in taking these data. Disk variations appeared to be relatively unimportant.

Since a reasonably good impedance match can be obtained at a given wavelength by any one of a number of combinations of the  $A$  and  $C$  dimensions, an additional criterion is needed to specify the best combination. This criterion is concerned with mode purity of excitation in the cutoff region and will be discussed subsequently in Sec. 11-12. Assuming that the carbon disk is a pure 50-ohm shunt resistance, and having experimental data on  $\lambda_b$  for a given line length  $A$ , it is possible to calculate the value of capacitance which, representing the metal coupling disk in an equivalent circuit, produces an infinite impedance in shunt with the 50-ohm disk. The input VSWR of the over-all combination may then be calculated as a function of  $\lambda$ , and the calculated curve compares very well with the experimentally determined one. This is another way of saying that the disks have a small reactance, and that it is insensitive to frequency. Separate experiments involving impedance measurements on disks installed in short-circuited coaxial lines verify this conclusion.

**11-9. Examples of Waveguide Attenuators for 3000 Mc/sec.**—Having discussed most of the basic principles of cutoff-attenuator design, we may now consider the details of some specific designs that have been developed. First to be considered is a series of 10-cm circular  $TE_{11}$ -mode cutoff attenuators. These will be discussed in approximately the chronological order of their development so that the improvements effected can more easily be followed and understood. All attenuators in this series use a  $\frac{1}{2}$ -in. diameter cutoff tube.

*The TPS-15 Attenuator.*—The first 10-cm attenuator produced in quantity for use within the Radiation Laboratory was the TPS-15. An assembly sketch of the TPS-15 is shown in Fig. 11-16, and a photograph of the attenuator is shown in Fig. 11-17. The two coupling loops in this design are shown in contact in the figure. The rigidly mounted loop at the left terminates a short length of 50-ohm coaxial line. The loop at the right terminates the 50-ohm coaxial line in the sliding insert. Eight to ten fingers are cut into the left end of the sliding insert in the vicinity of its coupling loop, and the loop is grounded to one of these fingers. The

fingers are given sufficient spring to provide good electrical contact between the end of the slider and the wall of the cutoff tube. The slider is driven by a rack and pinion, and a dial is mounted on the shaft of the pinion gear. The spacing of teeth on the rack, the diameter of the

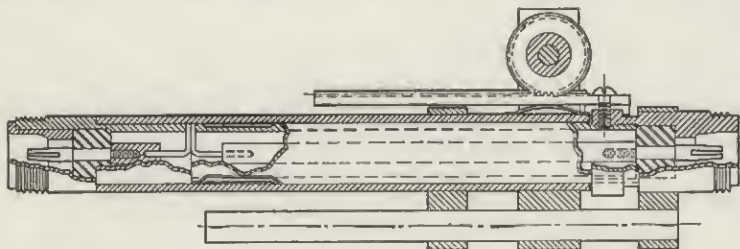


FIG. 11-16.—Assembly sketch of the TPS-15 cutoff attenuator.

pinion gear, and the dial engraving are so chosen that one dial division corresponds to one decibel of attenuation. Wobble of the insert is avoided by the use of a steel guide rod of large diameter which slides through oiled bearing holes in two brass blocks rigidly fastened to the cutoff tube. Note that no impedance-matching devices are designed

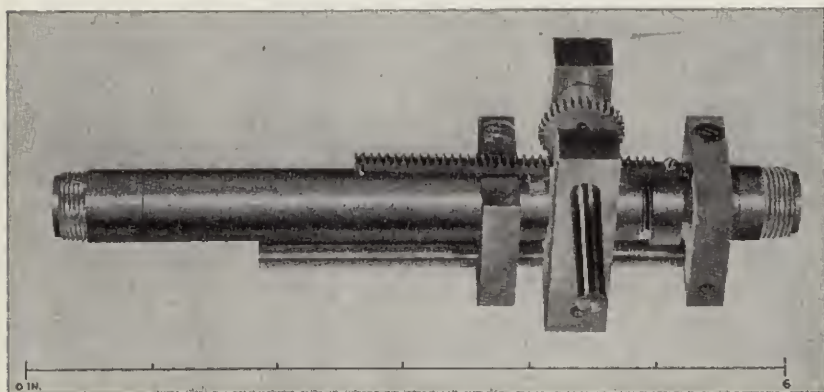


FIG. 11-17.—Photograph of the TPS-15 cutoff attenuator.

into this model; consequently, long lengths of lossy cable are required on each side of the attenuator.

Whereas the attenuator is simple to construct, it leaves much to be desired electrically. The coupling is by no means pure  $TE_{11}$ -mode coupling and the attenuation (exclusive of that in the cable) at a point within 0.5 db of linearity is approximately 30 db. When properly padded with lossy cable, the minimum attenuation that permits operation on the linear part of the calibration curve is, therefore, objectionably high for many purposes. The cutoff tube gradually becomes scored through wear

from the fingers and the finger contacts are not perfect enough to prevent r-f leakage between the sliding insert and the wall of the cutoff tube. R-f leakage either into or out of the attenuator can under certain circumstances (see Sec. 13-5) cause appreciable errors in measurements made with the attenuator.

A number of attempts to improve the purity of mode in this attenuator by radical changes in loop shape or by the use of solid silver contact fingertips on the slider were fruitless. Changes in the variation of attenuation with both distance and angle of loop orientation were effected in this manner, but none seemed to offer a sufficiently great improvement to suggest that the problem of nonlinearity could be solved in this way. Subsequently, there was conceived the idea of exciting the  $TE_{11}$ -mode by means of an iris instead of a loop, and later developments proved the merits of this suggestion.

*The Model O Attenuator.*—The first attenuator design making use of such an iris was called the Model O. The novel features of the design are shown in Fig. 11-18. The cutoff tube is joined at right angles to a coaxial line of comparable diameter, using a  $180^\circ$  circumferential slot in the outer coaxial conductor to couple the two lines electrically. The slot acts as a nonplanar iris which can excite or couple to a  $TE_{11}$ -mode in the cutoff tube, but discriminates against  $TM$ -modes. The coupling loop of the slider (not shown in the figure) lies in the plane which includes the axis of the coaxial line. The coaxial line is short-circuited a distance  $\lambda/2$  from the coupling slot so that a current maximum exists at the slot. This facilitates tightest coupling. Because of the frequency sensitivity of the half wavelength of coaxial line, the attenuator has an obvious bandwidth limitation in so far as tight coupling is concerned. Also, higher-mode coupling still exists, although to a lesser degree than in the TPS-15 design. The calibration curve for the Model O reaches linearity to within 0.5 db at an attenuation (exclusive of lossy cable) of approximately 25 db.

*The Model T Attenuator.*—A further improvement in linearity was made in the Model T design shown in Fig. 11-19. A coaxial line of much larger diameter is used so that the cutoff tube can easily be projected

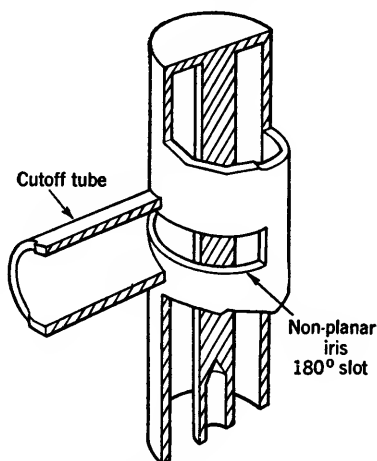


FIG. 11-18.—Iris-coupling mechanism used in the Model O attenuator.

through its outer conductor. This permits the use of a planar iris at the end of the cutoff tube and also permits tighter coupling, since the iris is brought nearer the center conductor of the coaxial line where the field is more concentrated. The calibration curve reaches linearity within 0.5 db at an attenuation of approximately 20 db.

*The Model S Attenuator.*—The minimum attenuation of an iris attenuator can be reduced several decibels by coupling to the iris through a highly resonant cavity. The cavity has the function of building up the electric potential across the edges of the gap to a high value, and thereby tightens the coupling. The Model S attenuator makes use of this principle. It has proved to be a quite satisfactory design, and has served faithfully as a primary standard attenuator.

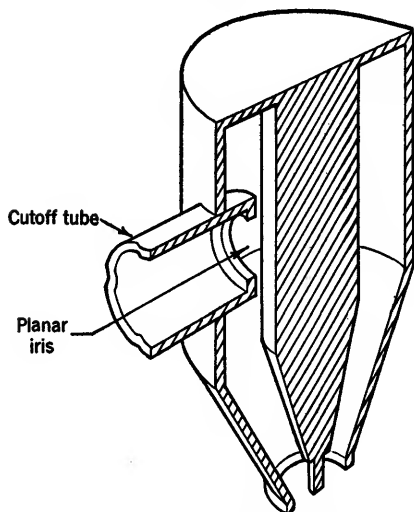


FIG. 11-19.—Iris-coupling mechanism used in the Model T attenuator.

Figure 11-20 shows a sketch of the pertinent features of the Model S attenuator. The cavity used is a round pillbox type with metal walls and an axial tuning rod. It normally resonates in a  $TM_{010}$ -mode although, possibly, the heavy capacitive loading associated with a small gap between the end of the tuning rod and the cavity bottom plate can make the cavity resonate in a coaxial mode at the long-wavelength end of its tuning range. It is good practice to keep the height of the cavity a little less than a

half wavelength and the diameter somewhat greater than a half wavelength. The tuning rod may be either metal or a relatively high-permittivity (for example, glass) dielectric; the effect of either material is to concentrate the fields in the vicinity of the tuning rod. The dielectric tuning rod is preferable from the viewpoint of coherent-leakage protection since its diameter may be chosen so that the metal tube through which it slides is beyond cutoff. In contrast, one must depend on good electrical contact in the screw threads of the tuning mechanism to prevent leakage when a metal tuning rod is used. The cavity commonly used in this design will tune over a minimum wavelength band of 9 to 11 cm. Irregularities in the walls of the cavity show no appreciable effect on the shape of the calibration curve. Likewise, because of the relatively low loaded  $Q$  of the cavity, highly polished plating is unessential.



The input coupling loop is rigidly fixed with respect to the cavity and has dimensions which make it nearly resonant so that it couples tightly to the cavity. In contrast, the coupling through the planar iris to the loop of the slider in the cut-off tube is relatively weak. The large input coupling loop is approximately square, and oriented in a plane parallel to the tuning rod. It is grounded next to the flat bottom end of the cavity. The loaded  $Q$  of the cavity used in this design is of the order of 100 to 150, and decreases with the resonant frequency of the cavity. It was found preferable to locate the capacitive tuning gap at the bottom of the cavity, instead of at the center.

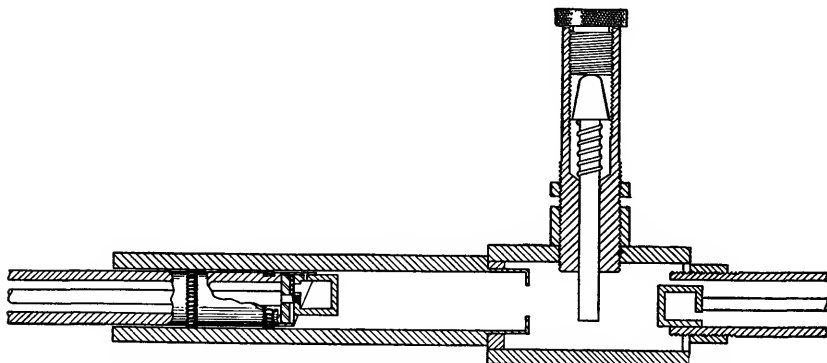


FIG. 11-20.—Sketch of the pertinent features of the Model S attenuator.

It is occasionally advantageous to install in the cavity another coupling loop which couples to a short length of coaxial line terminated by a crystal. The current induced in the loop is rectified by the crystal and measured by a d-c microammeter. For a given cavity, the crystal monitor provides a measure of the electric potential across the iris. Thus frequency-drift or output-power variations in the oscillator, either of which will affect the field intensity in the cavity, can easily be followed. The coaxial line should be extended a short distance beyond the crystal and filled with a tube of high-loss polyiron material. By bringing the d-c leads to the microammeter through such an attenuating line, one can avoid r-f leakage into or out of the cavity at this point.

The design of the planar iris terminating the cutoff tube is based on the necessity of a compromise between the purity of mode excitation and small cavity insertion loss. For a 0.5-in. cutoff tube, an iris width of  $\frac{1}{8}$  in. to  $\frac{1}{4}$  in. was found to provide good linearity. If the planar iris is approximately flush with the cylindrical wall of the cavity, the insertion loss is rather high, but the calibration curve reaches linearity almost immediately. On the other hand, if the cutoff tube and terminating iris are projected into the cavity a short distance, it is found that the insertion loss drops while the nonlinear part of the calibration curve is

extended. Consequently, the over-all attenuation level at which the calibration curve of the attenuator becomes linear to within a specified fraction of a decibel is not appreciably affected by the extent of projection of the iris. The best compromise is a projection into the cavity of approximately  $\frac{3}{16}$  in. The iris is made  $\frac{1}{32}$  in. thick, and the slot is carried all the way across the cutoff tube. Although, as indicated above, there is some latitude in choice of slot width, a  $\frac{1}{4}$ -in. width is commonly used.

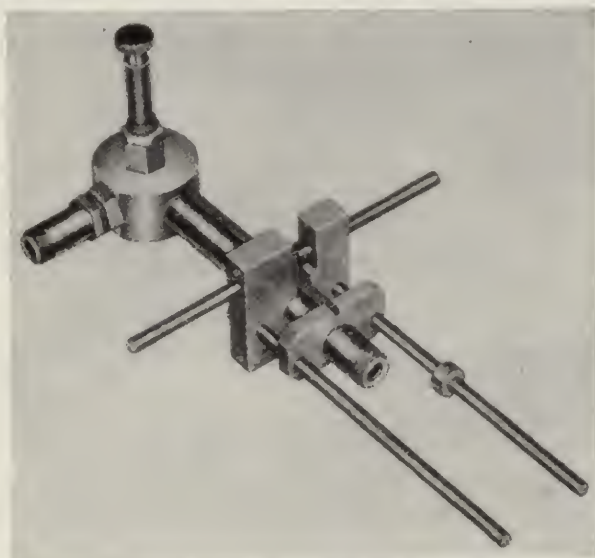


FIG. 11-21.—Photograph of the Model S attenuator.

The length of the slot lies in a direction normal to the plane of the coupling loop of the sliding insert.

The design of the sliding insert has likewise been given careful attention. The coupling loop (see Fig. 11-20) is a rather large one, and is formed from a thin metal strap of rectangular cross section. The 50-ohm IRC resistive disk used for impedance-matching is located at the base of the loop where it is easily installed. It is convenient for optimum impedance match that the sizable inductance associated with this large loop demands that the disk be placed at this point. Over the 9- to 11-cm band, the VSWR of the matched loop does not exceed 1.15. The cutoff tube in which the slider operates need not be built diametrically opposite the input coupling loop to the cavity, as shown in Fig. 11-20. Figure 11-21, a photograph of the Model S attenuator, shows the cutoff tube 90° from the input coupling loop.

It is not so easy to match the cavity loop because the position of the voltage maximum in the standing-wave pattern looking into the cavity

loop is critically dependent on tuning. To compensate for this two disks may be inserted. The first is in the normal position of the voltage minimum, and is inoperative when the cavity is tuned. The second disk is placed a quarter wavelength down the coaxial line from the first. When the cavity is detuned, the decreased effectiveness of the second disk is partially compensated for by the action of the first disk which is no longer located at the voltage minimum. With this arrangement the VSWR was reduced to 1.35 for a tuned cavity, and to 1.80 for a badly detuned cavity. The pair of disks introduced an additional attenuation of 4 to 6 db depending on the tuning. This represents a distinct improvement over the use of lossy cable, but the mechanical complication of installing the pair of disks may be too costly.

Sliding contacts which are electrically good are always difficult to obtain in the microwave region. The slider in the Model S offers no exception. The split-tubing finger construction, mentioned in connection with the TPS-15 attenuator, has many disadvantages. The finger to which the center conductor is grounded by the loop appears to be the important one, but unfortunately it is the least dependable because of the restraint put on it by the mechanical tie to the center conductor. The difficulty may be alleviated by stiffening the loop finger and bending it back so that it must be compressed slightly when inserted into the cutoff tube. Unless the insert is very tightly fitted in the cutoff tube (which is bad from other points of view), forces exerted on the slider can cause troublesome contact variations. Helical-spring contacts were designed for use in the Model S attenuator. Figure 11-22 shows in detail the method of constructing the helical springs and the method of installing them on the slider.

The wearing qualities of uncoiled sliders are very poor, in general. No combination of brass, steel, solid silver, silver plate, or nickel plate evidenced good wearing qualities when operated dry. However, a good grade of low-viscosity motor oil used for slider lubrication effected a marked improvement. An attenuator design in which the slider must depend on pressure contact with the inside of the cutoff tube for mechanical support is particularly bad; rather severe gouging develops in time. It is desirable to use external guide rods to support the slider, although this procedure usually demands a larger tolerance between the slider and the cutoff tube. In turn, this larger tolerance invites greater r-f-leakage difficulties. However, the helical springs are not handicapped by this larger tolerance, as are the conventional split-finger contacts, and can serve simultaneously as effective leakage inhibitors and good electrical contactors. Optimum leakage protection is gained by using a pair of the springs, spaced  $\lambda/4$  apart along the length of the slider. The springs have been shown to provide from 80 to 100 db of leakage pro-

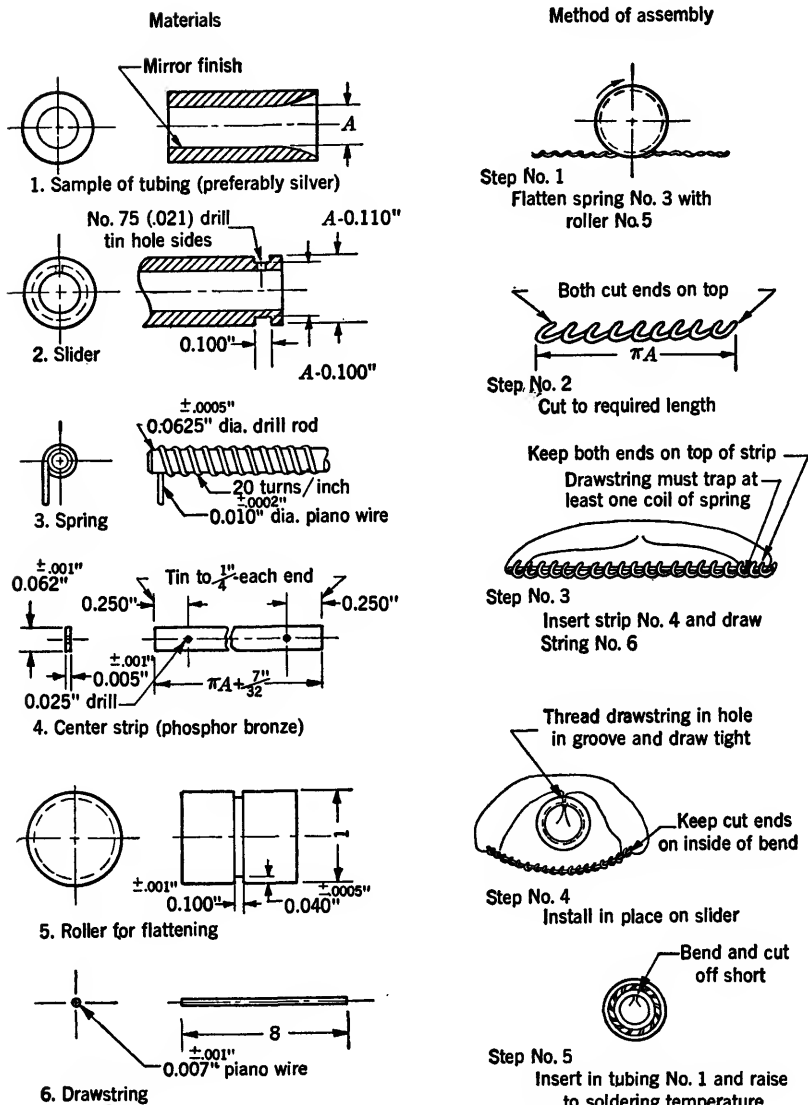


FIG. 11-22.—Method of constructing helical-spring r-f contacts.

tection when used in pairs. If desired, further leakage protection can be obtained by using a thin-walled tube of polyiron around the slider, locating it between the second helical spring and the r-f connector at the end of the slider. The polyiron should not touch the wall of the cutoff tube.

A spring-loaded rack with pinion gear is a commonly used drive mechanism for the slider. The dial attached to the pinion gearshaft may have an accurate vernier scale associated with it, or a dial indicator (Ames Gauge) may be used to indicate the position of the slider. The latter method escapes backlash troubles with the drive mechanism, and provides a least count of 0.001, or even 0.0001 in., of slider movement.

The Model S attenuator has a calibration curve which is within 0.5 db of linearity when the over-all attenuation (including loss in the slider matching disk) is 6 db, and is within 0.1 db of linearity at 14 db. The attenuators have been quite reproducible. The calibration curve includ-

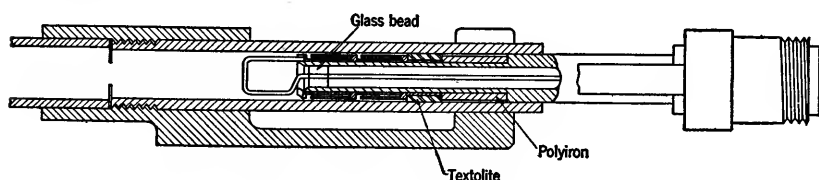


FIG. 11-23.—Sketch of a 3-cm-band  $TE_{11}$ -mode cutoff attenuator.

ing the nonlinear region is almost wholly independent of wavelength from 9 to 11 cm except for the slope change specified by Eq. (6). This is small: the slope is 0.975 db per dial division at 9 cm, and 0.985 db per dial division at 11 cm. Calibration curves taken with the cavity detuned by as much as 75 Mc/sec have shown that detuning to this degree has no appreciable effect on the extent of the nonlinear region. Of course, the insertion loss of the cavity is increased by such detuning.

**11-10. A Waveguide Attenuator for 9000 Mc/sec.**—The sketch of a design for frequencies near 9000 Mc/sec is shown in Fig. 11-23. It is somewhat dimensionally distorted to make possible the inclusion of all pertinent features in the single sketch. Figure 11-24 shows a photograph of the assembled attenuator.

The circular cutoff tube is approximately  $\frac{1}{4}$  in. in diameter, and is coupled to the 0.400- by 0.900-inch rectangular waveguide by a planar iris similar to that used in the Model S designed for the 10-cm band. The circular and rectangular waveguides have a common axis. Experiments were conducted with a variety of iris shapes and the one finally selected as optimum for use over the band from 3.13 to 3.53 cm has a width approximately equal to the radius of the cutoff tube. The iris extends entirely across the cutoff tube, with its length parallel to the wide side of the rectangular waveguide.

The slider has a large rectangular loop of approximately resonant dimensions, and the loop is given rigidity at its base by a glass bead which mechanically supports the inner conductor of the coaxial line. No

impedance-matching network is built into the slider. A pair of stagger-tuned half-wavelength choke cups are installed on the slider immediately behind the coupling loop. Then follows a hard, smooth-surfaced textolite bushing which makes sliding contact with the cutoff tube. Behind the bushing is a polyiron sleeve of slightly smaller diameter to assist the tuned choke cups in providing adequate leakage protection. The minimum attenuation (with loop touching the iris) is 7 to 10 db over the above-mentioned wavelength band. The calibration curves require an additional 8 to 10 db to reach linearity within 0.5 db.

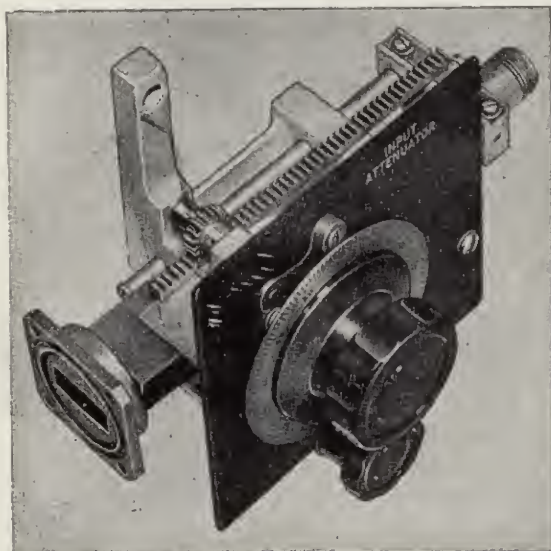


FIG. 11-24.—Photograph of the 3-cm-band cutoff attenuator.

**11-11. An Attenuator for 24,000 Mc/sec.**—Figure 11-25 shows the design of an attenuator for frequencies near 24,000 Mc/sec which utilizes a dielectric rod as the sliding member.

The  $\frac{1}{2}$ -in. by  $\frac{1}{4}$ -in. rectangular guide carries power from a generator to a power-monitoring termination (for example, a thermistor) or a matched load. A round waveguide beyond cutoff extends to the right, normal to the broad side of the rectangular waveguide. A polystyrene rod of approximately  $\lambda_c/2$  in length is seated in the end of the cutoff tube. Its exact length is chosen such that, for loose coupling in the attenuator, the reactive impedance of the cutoff tube referred to the junction of the rectangular and cutoff waveguides is zero and no reflection is produced in the rectangular waveguide. A polystyrene rod is driven along the cutoff tube by a micrometer, thus varying the length of the air region which is beyond cutoff for the  $TE_{11}$ -mode. The  $TE_{11}$ -wave which is propagated

then couples into the rectangular waveguide and passes out of the attenuator. A tuned 1-cm-band choke facilitates coupling into the rectangular waveguide by preventing propagation further in the dielectric rod. A resistive matching disk is installed in the polystyrene rod, so that the wave moving through the dielectric rod proceeds from a matched generator. The extension of the rectangular waveguide and the location of its short-circuited end are carefully chosen so that the circular-to-rectangular-waveguide transition is reflectionless.

Resistive matching disks of several types have been tried, but none has been entirely satisfactory. Cloth soaked in Aquadag (a carbon suspension) has been used, for example. For the proper disk resistivity, a match can be obtained with a thin, uniform disk. Correction for an unfavorable resistivity can be made by cutting a hole of the proper size in the center of the disk. Since the disk is spliced between two dielectric rods, the adhesive presents a problem which has not been solved with entire satisfaction.

The position of the matching disk with reference to the dielectric-air interface is important. The disk should be placed at a current node in the polystyrene rod. Since the reflected inductive reactance of the cutoff tube is approximately  $j$ , the polystyrene cap placed over the resistive disk should be approximately  $\lambda_g/8$  in length.

A desirable feature of this variable attenuator is that it employs no sliding metal contacts. The diameter of the cutoff tube is so chosen that when it is filled with the dielectric it propagates the  $TE_{11}$ -mode but it is still below cutoff for the  $TM_{01}$ -mode. The short length of polystyrene, therefore, acts as a mode filter for energy coupled out of the main waveguide by the electric field. If the ends of the dielectric rods are accurately perpendicular to the cutoff tube, no higher modes are excited.

One of the big advantages inherent in the dielectric cutoff attenuator is that its calibration curve can be accurately predicted, including the nonlinear part that arises from interaction or reflection effects at the dielectric-air interfaces. The effect has been discussed in Sec. 11-7. The expression derived<sup>1</sup> for the attenuation (that is, ratio of power trans-

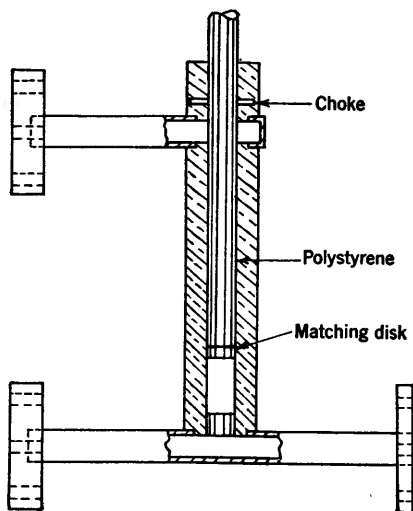


FIG. 11-25.—Attenuator with polystyrene rod for 1-cm band.

<sup>1</sup> N. H. Frank, private communication.

mitted through the air cutoff region to the power incident on the input dielectric-air interface) is

$$A = 10 \log_{10} \left\{ 1 + \frac{(k_e - 1)^2}{4 \left[ k_e - \left( \frac{\lambda}{\lambda_c} \right)^2 \right] \left[ \left( \frac{\lambda}{\lambda_c} \right)^2 - 1 \right]} \sinh^2 \frac{2\pi l}{\lambda} \sqrt{\left( \frac{\lambda}{\lambda_c} \right)^2 - 1} \right\}, \quad (23)$$

where  $\lambda_c$  is the cutoff wavelength in the  $TE_{11}$ -mode for the tube when no dielectric is present. This equation can be simplified considerably if we choose the diameter of the waveguide beyond cutoff so that

$$W = \frac{(k_e - 1)^2}{4 \left[ k_e - \left( \frac{\lambda}{\lambda_c} \right)^2 \right] \left[ \left( \frac{\lambda}{\lambda_c} \right)^2 - 1 \right]} = 1. \quad (24)$$

This condition is met when

$$\lambda_c = \lambda \sqrt{\frac{2}{1 + k_e}}. \quad (25)$$

In this case the simplified equation becomes

$$A = 10 \log_{10} \cosh^2 \left[ \frac{2\pi l}{\lambda} \sqrt{\left( \frac{\lambda}{\lambda_c} \right)^2 - 1} \right]. \quad (26)$$

Since, for large  $x$ ,

$$\sinh^2 x = \frac{e^{2x}}{4},$$

we can write Eq. (23), for  $l \gg \lambda$ , as

$$A = \frac{10}{\ln 10} \frac{4\pi l}{\lambda} \sqrt{\left( \frac{\lambda}{\lambda_c} \right)^2 - 1} + 10 \log_{10} \frac{W}{4}. \quad (27)$$

Thus the attenuation becomes a linear function of  $l$  with the slope

$$\alpha = \frac{40\pi}{\ln 10} \sqrt{\left( \frac{1}{\lambda_c} \right)^2 - \left( \frac{1}{\lambda} \right)^2}.$$

The term independent of  $l$  in Eq. (27) can be made independent of wavelength, if we impose the condition that

$$\frac{\partial W}{\partial \lambda} = 0. \quad (28)$$

This leads again to Eqs. (25) and (26), while Eq. (27) becomes

$$A = \frac{40\pi}{\ln 10} \sqrt{\left( \frac{1}{\lambda_c} \right)^2 - \left( \frac{1}{\lambda} \right)^2} l - 20 \log_{10} 2. \quad (29)$$

These relations have been verified to within the experimental error.



### 11-12. The Design of Cutoff Attenuators Using the $TM_{01}$ -mode.—

Until recently little attention has been given to the design of cutoff attenuators using the  $TM_{01}$ -mode. It was felt that the slightest amount of plate ellipticity or eccentricity in the centering of the plate in the cutoff tube would lead to excitation of modes in the  $TE$ -mode series. Even if the  $TE_{11}$ -mode is excited very weakly, it will cause trouble at large attenuations because it decays in intensity less rapidly than does the  $TM_{01}$ -mode. For example, if the  $TE_{11}$ -mode is excited with an intensity 40 db down from that of the  $TM_{01}$ , it will be only 20 db down after the  $TM_{01}$ -mode has been attenuated 80 db. It is, therefore, necessary to check calibration of such an attenuator over the entire range of attenuation for which it is to be used. If this range is 70 db or greater, such a procedure imposes severe experimental difficulties.

It has been pointed out that one should be able to circumvent the effects of  $TE_{11}$ -modes by properly orienting the two antenna plates. Two antenna plates which are slightly elliptical may be oriented in such a way that their major axes are at right angles to each other so that, if the first plate excites the  $TE_{11}$ -mode, the second one will not couple to it. This alignment cannot be based on mechanical measurements since the eccentricity is extremely small. However, an experimental determination of the proper alignment can be made. It is not unreasonable to suppose that proper orientation will reduce by 30 to 50 db the coupling to the  $TE_{11}$ -mode. Consequently, if the plates are turned down on a lathe after installation on their respective coaxial lines, and carefully oriented by means of an angle calibration, satisfactory freedom from  $TE$ -mode coupling can probably be achieved.

A brief investigation was made of a 10-cm-band  $TM_{01}$ -mode cutoff attenuator using 0.400-in.-diameter metal plates in a 0.5-in. cutoff tube. The inner conductors of the coaxial lines were supported by polystyrene beads located a short distance behind the plates. The minimum attenuation, plates touching, was less than 1 db in the wavelength range from 10 to 12 cm, and the calibration curve reached linearity within 0.5 db after 10 db of decoupling. The linearity was checked up to an attenuation of 50 db, and was found to be exact within the limits of experimental error.

In order to improve further the linearity of a  $TM_{01}$ -mode cutoff attenuator in the low-attenuation range, it would be necessary to suppress the excitation of the higher  $TM$ -modes. A means of accomplishing this has been suggested, but unfortunately has not been verified experimentally. The principle is to select different diameters for the two metal-disk antennas such that one disk cannot excite the  $TM_{02}$ -mode, and the other disk cannot excite or couple to the  $TM_{03}$ -mode.

## CHAPTER 12

### MICROWAVE ATTENUATORS. RESISTIVE ATTENUATORS

BY E. WEBER AND R. N. GRIESHEIMER

For general laboratory use, many devices are available which give fixed or variable attenuation of the main power flow, or which permit power sampling for power-monitoring purposes without reacting perceptibly upon the main power flow. For low power ranges it is usually permissible to insert in the main power path elements of dielectric base materials which have thin coatings of power-absorbing materials such as carbon or Aquadag. For larger powers, in order to provide for efficient heat transfer to the ambient air, power-absorbing materials in greater bulk and with proper metal casings are inserted. Finally, in order to separate the directly transmitted power from that absorbed in a properly designed terminal load, the principle of power division can be used.

The design of dissipative attenuators involves two problems of paramount importance: the choice of the material in which the power is to be lost, and the impedance-matching of the attenuator to the transmission line. These problems must also be solved in the design of a termination for a transmission line which will absorb without reflection all the power incident upon it. The design of a termination or load is often simpler than that of an attenuator because the impedance-matching need be done at one end only. The first part of this chapter is, therefore, devoted to a discussion of terminations.

Most of the general-purpose laboratory attenuators admit of calibration in a limited sense only, over narrow frequency ranges, either because of the frequency dependence of the loss characteristics of the materials, or because of the influences of temperature and humidity. For this reason, a separation is made between the general-purpose attenuators and the attenuators which by the use of precision metalized glass, justify higher accuracy in calibration and are therefore even useful as standards.

### MATCHED TRANSMISSION-LINE TERMINATIONS

BY R. N. GRIESHEIMER

There are innumerable applications in microwave work for matched-impedance transmission-line terminations, or "loads" as they are more commonly called, and the number of materials and designs employed in

their construction has been as great as the number of applications. Terminations are commonly classed as either high-power or low-power terminations. High-power terminations are designed to take the full output power of a transmitter tube; that is, power ranging from a few watts to several hundred watts. They are used to replace the transmitting antenna under conditions where radiated power would violate secrecy or would interfere with neighboring receivers. In addition, the high-power load sidesteps the objection that within the confines of a laboratory an antenna offers a varying load impedance as objects move in its immediate vicinity. High-power loads are usually required to have a VSWR not greater than 1.05 to 1.10.

Low-power loads may be grouped into two classes. Some applications demand that the loads be almost perfectly matched; that is, their VSWR should be no greater than 1.01 or 1.02. The reference match in a magic T that is used for impedance measurement is such an application. Impedance measurements on lossless or low-loss line components are often conducted with a matched line termination placed after the component under test, and such a termination should also have a VSWR which is as small as 1.01. In contrast, the terminations used in the secondary lines of directional couplers, for example, can often be allowed a maximum VSWR as great as 1.1 or 1.2. In these applications a compromise is usually necessary between the allowable voltage standing-wave ratio and the allowable physical dimensions of the termination, with the directivity of the directional device being the determining factor in setting the maximum allowable voltage standing-wave ratio. Low-power loads are seldom designed to dissipate more than 0.5 watt.

In the design of a line termination there are a number of factors which must be taken into consideration. The most important electrical specifications are the maximum allowable voltage standing-wave ratio and the bandwidth over which the voltage-standing-wave ratio specification is to be met. The maximum safe power capacity of the load is also of considerable importance. For high-power loads it is necessary to consider both average power dissipation and pulse-power breakdown, or "arc-over." The impedance match should be independent of temperature within the stated safe average-power limit, and should not be affected by humidity variations or by aging. Many applications, for example the reference match for the magic T, demand that the loads be very carefully protected against r-f leakage. The impedance match of the load should be quite insensitive to shock and vibration, and, in the event that large-scale production is anticipated, it should also be reproducible from unit to unit. As previously suggested in the comments on directional couplers, the size, primarily the length, of the termination is important in some applications. In constructing very-

well-matched loads with VSWR less than 1.02, it is of particular importance to obtain precision waveguide or coaxial line for their construction. The reflection from a small discontinuity at the junction of the load and the line which it terminates can easily account for a VSWR of 1.01 or 1.02.

The metal housing for the load is customarily terminated by an r-f short circuit in order to avoid r-f leakage from the load. This imposes a lower limit on the attenuation of the termination if a broadband impedance match is to be obtained. Figure 11-11 shows that the VSWR of a short circuit, measured through 23 db of matched attenuation, is 1.01. Since the termination is not likely to be exactly matched, it is essential to have a minimum of 30 db of attenuation in the load if there is to be any hope of obtaining a load VSWR less than 1.01 over a sizable wavelength band.

The most difficult problem in load design is, of course, the impedance-matching problem. A number of techniques have been employed for impedance-matching; most of these techniques are also applicable to the matching of resistive attenuators. The most commonly used matching devices are long tapers, or one or more quarter-wavelength transformers. However, examples of other techniques will also be cited.

**12-1. Low-power Coaxial-line Terminations.**—Two coaxial-line terminations have been developed which meet a maximum VSWR specification of 1.02 to 1.04 over an 8 to 10 per cent band. One design utilizes a thermosetting plastic, Durez 7421, which is cast in a section of the line to be terminated. Then, because the temperature coefficient of expansion of Durez is greater than that of brass, it can be removed from the center conductor by heating and from the outer conductor by cooling. It is a relatively easy material to machine, and a conical matching taper of the correct length can be cut on a lathe. The taper is carried all the way to a knife edge at the center conductor, with the experimentally determined optimum taper length being approximately two wavelengths. The solid plastic provides a good support for the center conductor and consequently the load is a rugged one. A second well-matched load has been made from a resistive cloth, Uskon.<sup>1</sup> The cloth used has a resistivity of approximately 440 ohms per square. A long trapezoidal piece of the cloth is tightly wrapped around the inner conductor of the coaxial line in such a way that a conical matching taper, followed by a completely filled length of line, is formed. This is a less durable load than the one made from Durez, particularly since the cloth has a tendency to fray at the tip of the taper, and thereby produces a reflection. These loads may be made for a variety of sizes of coaxial lines but may become objectionably long at wavelengths longer than microwaves.

<sup>1</sup> Manufactured by the U. S. Rubber Co., Rockefeller Center, New York.

Various polyiron materials have been used effectively in making 10-cm-band and 3-cm-band step terminations in coaxial lines. Figure 12-1a shows a cross section of a polyiron cylinder commonly used for a  $\frac{1}{8}$ -in. coaxial line; Fig. 12-1b shows a preferable shape for a  $\frac{5}{16}$ - or  $\frac{1}{2}$ -in. line. In the smaller size the step shown in Fig. 12-1a is so thin that it is too easily broken. Polyiron has the advantage of having a very large attenuation constant for microwaves; consequently, polyiron terminations can be made relatively short. Moreover, polyiron terminations can be made for use at wavelengths considerably longer than microwaves. This material has the disadvantage, up to the present, that its microwave properties vary considerably from batch to batch, and the dimensions often need to be corrected when units are made from a new batch. Typical data on two coaxial polyiron terminations are given in Table 12-1.

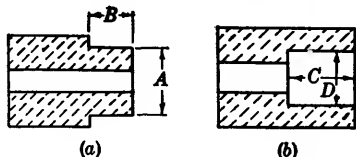


FIG. 12-1.—Cross section of polyiron cylinder for (a) large and (b) small coaxial lines.

TABLE 12-1.—DATA ON TWO COAXIAL POLYIRON TERMINATIONS  
Crowley\* material MP-1826

50-ohm,  $\frac{1}{8}$ -in. coaxial line

$A = 0.511$  in.

$B = 0.295$  in.

VSWR  $< 1.10$  from 9 to 11 cm

50-ohm,  $\frac{5}{16}$ -in. coaxial line

$C = 0.188$  in.

$D = 0.228$  in.

VSWR  $< 1.10$  from 3.1 to 3.5 cm

\* Henry L. Crowley Co., West Orange, N. J.

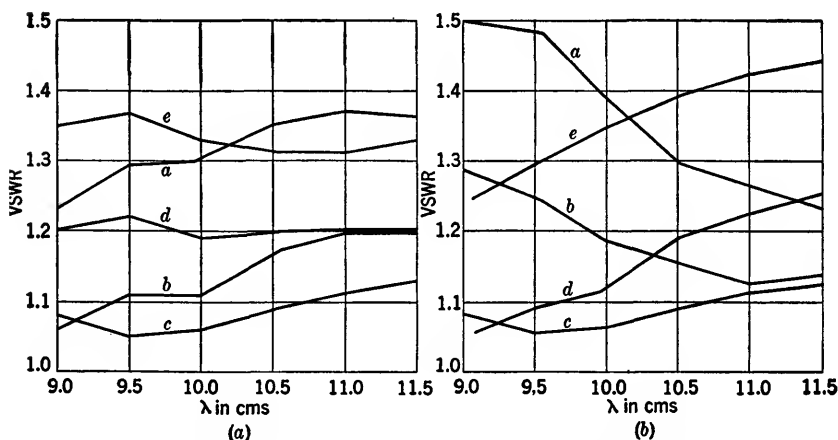


FIG. 12-2.—Tolerance study on a  $\frac{1}{8}$ -in. coaxial-line polyiron load of Fig. 12-1a. For curves  $a$ , dimension  $A = 0.511$  in., dimension  $B$  for the various curves as follows (a) 0.220 in., (b) 0.260 in., (c) 0.295 in., (d) 0.350 in., (e) 0.400 in. For curves  $b$ ,  $B = 0.295$  in.,  $A$  equals the following: (a) 0.570 in., (b) 0.530 in., (c) 0.511 in., (d) 0.500 in., (e) 0.480 in.

The tolerances on the step dimensions must be very small, even for loads made from a given batch of material. The graphs shown in Fig. 12-2 offer an indication of the criticalness of the dimensions. Such families of tolerance curves have proved to be very helpful in establishing dimensional corrections for a new batch of the material. Unfortunately polyiron is not an easy material to machine. Diamond-dust grinders and Carboloy-tipped drill bits and lathe tools are needed to cut it. An effective ventilating system is required to protect the machinist from the iron dust. Attempts have been made to match coaxial-line polyiron loads by machining conical tapers at the front ends of the pieces, but low standing-wave ratios with acceptably short taper lengths have not been obtainable.

Impedance data for cylinders of polyiron in 50-ohm,  $\frac{7}{8}$ -in. coaxial line (see Table 12-2) show that the impedance of the various materials is

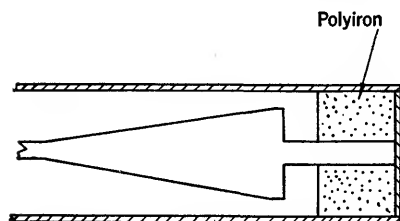


FIG. 12-3.—Proposed broadband polyiron coaxial termination.

remarkably independent of wavelength. Although a termination of this design has not been built and tested, the tabulated data suggest that a broadband device could be made according to the construction shown in Fig. 12-3. The conical taper should be at least one-half wavelength long. There is a very good correlation between the degree

of mismatch of the materials and the loss per unit length of the materials. For example, the attenuation constants for MP-1548, MP-1826, and MP-1822 are 20, 60, and 110 db/in. respectively.

TABLE 12-2.—IMPEDANCE DATA FOR CYLINDER OF POLYIRON IN 50-OHM,  $\frac{7}{8}$ -IN. COAXIAL LINE

Crowley material	$Z/Z_0$ at 11.5 cm	$Z/Z_0$ at 10.1 cm	$Z/Z_0$ at 8.9 cm
MP-1826	0.39 — $j0.16$	0.38 — $j0.15$	0.39 — $j0.21$
MP-1822	0.14 — $j0.09$	0.13 — $j0.09$	0.13 — $j0.16$
MP-2884D	0.42 — $j0.18$	0.39 — $j0.20$	0.39 — $j0.25$
MP-1529B	0.42 — $j0.08$	0.41 — $j0.10$	0.43 — $j0.10$
MP-1548	0.53 — $j0.16$	0.52 — $j0.19$	0.49 — $j0.16$
MP-2875D	0.47 — $j0.04$	0.45 — $j0.09$	0.46 — $j0.09$

A design for  $\frac{7}{8}$ -in. coaxial-line termination which shows promise of extreme bandwidth employs a short length of metalized-glass center conductor in a line with appropriately stepped or tapered outer conductor. Thus far it has been found possible to cover a bandwidth of 7.5 to 30 cm with a maximum VSWR well below 1.20. Such a design is

based on the following considerations. The impedance  $Z$  of a coaxial line with shunt conductance and series resistance losses is given as a function of distance along the line  $x$  by

$$\frac{dZ}{dx} = (GZ^2 - R) + j\omega(CZ^2 - L), \quad (1)$$

where  $R$ ,  $G$ ,  $L$ , and  $C$  are respectively the resistance, the conductance, the inductance, and the capacitance per unit length of line, and  $\omega$  is the angular frequency. If it is desired to select a line taper such that  $Z$  will have no reactive component, Eq. (1) demands that

$$\frac{dZ}{dx} = GZ^2 - R, \quad Z = \sqrt{\frac{L}{C}}. \quad (2)$$

Equation (2) dictates the spacing of the conductors as a function of  $x$ . If an inner conductor which is a dielectric rod coated with an extremely thin resistive film is considered, it may be said that  $G = 0$ , and  $R$ , because of the thinness of the film, is essentially frequency-independent. If the line is tapered by changing the diameter of the outer conductor  $b$ , while keeping the diameter of the inner conductor  $a$  constant, then

$$Z(x) = -Rx = 60 \ln \frac{b(x)}{z},$$

where  $x = 0$  when  $b = a$  and  $z = 0$ ,  
or

$$b(x) = ae^{-\frac{Rx}{60}}.$$

Therefore, if the outer conductor is tapered to make contact with the inner conductor at the end of the termination, and if the taper length  $l$  is chosen to be

$$l = \frac{Z_0}{R}, \quad (3)$$

the termination should absorb all incident power without reflection at all frequencies. Also, the power dissipation will be constant along the length of taper. It should be noted that, according to Eq. (3), the total resistance of the film should be equal to the characteristic impedance of the lossless coaxial line.

If, for constructional reasons, it is impossible to continue the taper until the outer and inner conductors meet, other means to terminate the tapered line may be used. For example, if the line is terminated in a short circuit, the impedance of the termination is given by<sup>1</sup>

<sup>1</sup> E. Feenberg, "Resistance Attenuators and Terminations," Sperry Report 117, Apr. 10, 1943.

$$\frac{4\pi}{\lambda R} Z(\eta) = \eta - \frac{\eta_0 e^{-j(\eta - \eta_0)}}{1 - \frac{j\eta_0}{2} e^{+j\eta_0} \int_0^\eta \frac{e^{-j\eta'}}{\eta'} d\eta'} \quad (4)$$

where

$$\eta_0 = -\frac{4\pi x_0}{\lambda}, \quad \eta = -\frac{4\pi x}{\lambda},$$

and the short circuit is placed at  $x = x_0$ . The real and imaginary parts of Eq. (4) for various values of  $\eta_0$  may be plotted, and that point at which the short circuit should be placed in order to make  $Z$  real and equal to  $Z_0$  may be observed. This construction is not as inherently broadband as the first construction mentioned, nor is the power dissipation constant along the length of taper.

**12.2. Low-power Waveguide Terminations with Polyiron.**—The variety of low-power waveguide terminations exceeds that of coaxial loads. Those to be discussed are grouped according to the materials used in their fabrication.

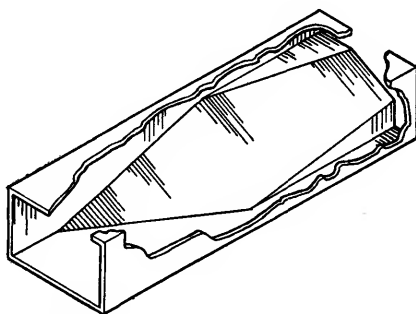


FIG. 12.4.—A well-matched polyiron termination for  $\frac{1}{2}$ -by 1-in. waveguide.

An excellent polyiron termination has been made for  $\frac{1}{2}$ -by 1 in. waveguide, using Crowley material MP-2884D, or Chromet 4. It has been found that the double-slant taper used in this construction (see Fig. 12.4) is better than a single taper to either the narrow or the wide side of the waveguide. It has a VSWR less than 1.01 over the 3.13- to 3.53-cm band. A similar termination, made from the same material, has an equally good impedance match in 1.25-cm-band waveguide. Polyiron waveguide terminations are capable of greater power dissipation than most of the terminations of other types that are to be considered, but the size and weight of a polyiron termination make it impractical for waveguides as large as those used at 10-cm band.

The step-matched polyiron piece shown in Fig. 12.5 may be used either as a load or as a bilaterally matched 40-db attenuator in  $\frac{1}{2}$ -by 1-in. waveguide. It is made from Crowley material MP-2312 (D-1). Its



VSWR specifications are 1.02 or less at 3.3 cm, and 1.06 or less at the edges of a  $\pm 6$  per cent wavelength band centered at 3.3 cm. As was shown to be true in the case of coaxial-line polyiron matching steps, the waveguide matching steps are also dimensionally critical. Furthermore, small dimensional corrections are usually necessary when loads are machined from a new batch of polyiron material. This must be taken into account when designing dies to be used in pressing the polyiron pieces into approximately the correct shape. A matching step which is centered in the waveguide has been found to be considerably more broadband than an unsymmetrically located step which rests on the broad side of the waveguide.

A compact polyiron termination for use in a 3-cm-band directional coupler has been made from a rectangular block of MP-1826 polyiron, 0.458 in. in width, 0.183 in. in height, and 0.895 in. in length. The block is laid across the waveguide, and rests on a broad side of the waveguide. The waveguide is short-circuited by a metal plate soldered across its end, and touches the polyiron block which has been cemented in place. In this design, reflections from the front face of the block are canceled by those from the short circuit, and therefore, broadband matching cannot be expected. The VSWR of the termination is less than 1.15 over the 3.16- to 3.33-cm band. Such a load is to be recommended only when the space limitation is as severe as the impedance-matching requirement.

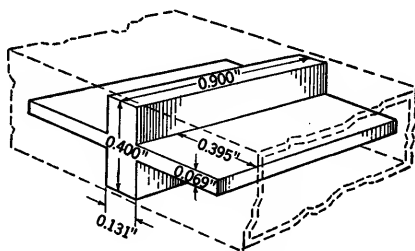


FIG. 12-5.—A step-matched polyiron termination for  $\frac{1}{2}$ -by 1-in. waveguide.

TABLE 12-3.—IMPEDANCE AND ATTENUATION DATA FOR BLOCKS OF POLYIRON IN  $\frac{1}{2}$ -BY 1-IN. WAVEGUIDE

Crowley* material	$\lambda = 3.13$ cm		$\lambda = 3.33$ cm		$\lambda = 3.53$ cm	
	Z	db/in.	Z	db/in.	Z	db/in.
MP-2875D	$0.32 - j0.03$	30	$0.29 - j0.03$	30	$0.28 - j0.04$	30
MP-2325	$0.31 - j0.03$	40	$0.28 - j0.06$	30	$0.26 - j0.04$	30
MP-1529B	$0.27 - j0.02$	60	$0.23 - j0.02$	60	$0.22 - j0.04$	50
MP-1548	$0.29 - j0.07$	80	$0.27 - j0.08$	80	$0.26 - j0.08$	70
MP-2312	$0.23 - j0.12$	180	$0.22 + j0.02$	160	$0.20 + j0$	140
MP-2884D	$0.20 - j0.12$	180	$0.19 - j0.01$	170	$0.19 - j0.02$	150
MP-1826	$0.21 - j0.12$	210	$0.20 + j0$	190	$0.19 - j0.02$	180
MP-1842	$0.08 - j0.11$	220	$0.07 + j0.06$	220	$0.07 + j0.03$	220

\* Henry L. Crowley Co., West Orange, N. J.

Table 12-3 has been included to show the microwave differences among various polyiron materials that can be considered for attenuator or load design in  $\frac{1}{2}$ - by 1-in. waveguide. The impedance data were more carefully taken than the attenuation data. It is to be noted that, in general, the materials with larger conductance values have larger attenuation constants. The impedances have small reactive components, and while the reactances apparently vary somewhat more with wavelength than in the case of coaxial lines (see Table 12-2), the polyiron impedances are nevertheless surprisingly independent of wavelength.

Only scattered and incomplete data are available, but there is evidence for believing that the voltage standing-wave ratio of a well-matched polyiron load is subject to variation with humidity. The higher the frequency, the more likely this is to be true. Therefore, it is good practice to dry carefully the polyiron pieces in an oven after machining, and to impregnate them immediately with a moisture-resisting lacquer.

**12-3. Low-power Waveguide Terminations Which Use Other Lossy Materials.**—A well-matched termination for a circular  $E_0$ - or  $H_1$ -mode waveguide can easily be made by machining a long, sharp-pointed conical taper on a Durez or soft-pine rod of appropriate diameter. The taper length and the rod length for optimum broad-band matching are determined experimentally. For example, a Durez 7421 load for an  $H_1$ -mode waveguide of 0.350 in. ID, using a 2.5-in. taper length and a 4-in. over-all length, has a VSWR less than 1.01 over the 1.20- to 1.30-cm band. A soft-pine  $E_0$ -load for a tube of 1.150 in. ID, using a taper length of 14 in. and an over-all length of 28 in., has a VSWR less than 1.02 over the 3.13- to 3.53-cm band. An appreciable saving in length can be made by using a 400-ohms-per-square IRC resistance strip for the load element. If this strip is used, a symmetrical V is cut into the end of a rectangular strip of the material, so that the taper is toward the wall of the tube instead of toward its axis. If a taper length of 6 in. and an over-all length of 15 in. are used, the load VSWR can be held under 1.01 over the entire 3.13- to 3.53-cm band. The taper tips must touch the wall of the tube.

Well-matched terminations for rectangular waveguide may also be made from tapered IRC resistance strip. The strip is placed in the center of the waveguide, aligned in the direction of the electric field, and except for the tapered section, touches the two broad walls of the waveguide. The taper may be a single taper which touches one wall at the tip of the taper, or a double taper which tapers from both broad walls to the axis of the waveguide. A single taper is usually used except in flexible waveguide, but terminations of either type can be made which are well matched over a broad band. In order to combat the flexibility of the strips and to shorten the length required to provide the attenuation

necessary for low voltage standing-wave ratios, it is advisable to use a combination of two strips side by side, glued together, one shifted with respect to the other. Figure 12-6 illustrates these designs. The strips are supported mechanically by the short-circuiting block at the end of the waveguide.

If loads are made from IRC strip, care must be taken to obtain smooth edges, and to avoid chipping off the resistive coating. This can be done by using a shearing cutter similar to those used for cutting paper and sheet metals. It may be necessary to remove rough edges and chips by hand-smoothing the taper on emery cloth or sandpaper. The taper

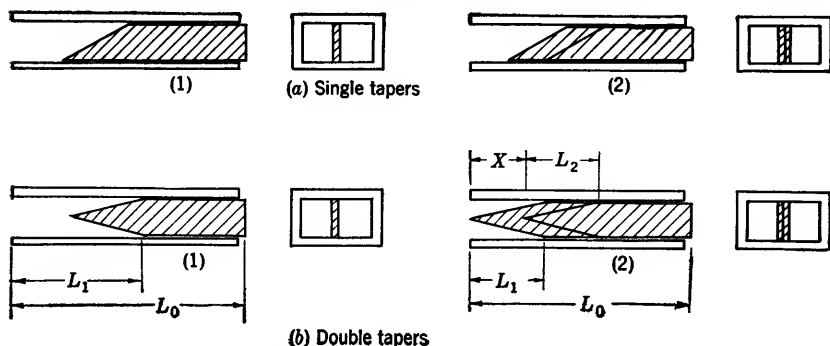


FIG. 12-6.—Various designs of IRC resistance loads for rectangular waveguide.

length is not critical except at wavelengths which are near the cutoff wavelength of the waveguide. Typical tolerances call for  $\pm \frac{1}{2}^\circ$  in the taper angle, and  $\pm \frac{1}{4}$  in. in taper length, at 3-cm band. In general, the tolerances become larger as the taper length is increased. In all single-taper designs the end of the taper must rest flat against the waveguide wall. A small clearance, a few thousandths of an inch, is allowable between the other edge of the strip and the wall. The vertical position of the tip in the double-taper designs is not critical.

A taper length of one-half guide wavelength or slightly longer is satisfactory for single-taper designs. The attenuation per unit length  $A$  of an IRC strip in rectangular waveguide decreases linearly with increasing resistivity  $\Omega$  measured in ohms per square. The following formulas have been determined empirically, and have been checked experimentally for the range of 100 to 800 ohms per square. For  $\lambda_0 = 3.3$  cm, 1- by  $\frac{1}{2}$ -in. waveguide, 0.050-in. wall,

$$A = 15.7 - 1.5 \frac{\Omega}{100} \quad \text{db/in.}$$

For  $\lambda_0 = 10.0$  cm, 3- by  $1\frac{1}{2}$ -in. waveguide, 0.080-in. wall,

$$A = 5.0 - 0.38 \frac{\Omega}{100} \quad \text{db/in.}$$

The over-all lengths of single-taper loads can be estimated by using these formulas and assuming that the attenuation contributed by the taper is one-half that of an equivalent length of strip which completely fills the waveguide. This assumption has been verified experimentally. It is advisable to allow a small additional length to compensate for the change of attenuation with wavelength. Table 12-4 summarizes the designs involving these strips. Reference should be made to Fig. 12-6 for the significance of the various dimensions.

A very compact termination from IRC strip material can be made by completely blocking off the waveguide with a strip placed normal to the axis of the waveguide. The waveguide is short-circuited at an experimentally determined position which is effectively one-quarter guide wavelength behind the resistive strip. If a 600 ohms per square strip in 1- by  $\frac{1}{2}$ -in. waveguide is used, it is possible to obtain a load VSWR less than 1.2 over a  $\pm 6$  per cent band. At the design wavelength, the VSWR can be brought below 1.05. The strip is introduced through a slot in the narrow side of the waveguide, and cemented in position.

TABLE 12-4.—SUMMARY OF IRC STRIP LOADS IN RECTANGULAR WAVEGUIDE

Line size	Strip material	Band, cm	VSWR over band	Dimensions*			
				$L_1$	$L_2$	$L_0$	$X$
1½-in. by 3-in. OD	400 ohms	8 to 10.5	<1.01	4½ in.		10 in.	
0.080-in. wall							
Same	400 ohms	8 to 11.1	<1.02	4½ in.		10 in.	
Same	400 ohms	8 to 11.1	<1.01	4½ in.		10 in.	
Same	400 ohms	8 to 12	<1.02	4½ in.		10 in.	
Same	600-ohms long strip	9 to 11.1	<1.01	4½ in.	4½ in.	8 in.	2½ in.
	400-ohms short strip						
Same	600-ohms long strip	8 to 12	<1.03	4½ in.	4½ in.	8 in.	2½ in.
	400-ohms short strip						
½-in. by 1-in. OD	100 ohms	3.13 to 3.53	<1.01	3½ in.		5 in.	
0.050-in. wall							
⅝-in. by 1½-in. OD	100 ohms	3.13 to 3.53	<1.01	2½ in.		5 in.	
0.062-in. wall							

\* Refer to Fig. 12-6.

The IRC strip material can be easily damaged by the high temperatures associated with excessive average-power dissipation or soldering operations on the metal casing. It is usually easy to recognize an overheated strip by the small welts that rise on the resistive film. Because of this limitation it has been necessary in certain load designs for directional couplers to use other materials such as Uskon cloth, and Synthane. Uskon cloth of 6-ply lamination can be cut into a single-taper load

resembling the IRC strip loads shown in Fig. 12-6. In this application the material has an attenuation constant of approximately 30 db/in. at 3-cm band and 10 db/in. at 10-cm. band. Reasonably short taper lengths provide VSWR's less than 1.10 over a  $\pm 5$  per cent band. In addition to its ability to withstand higher temperatures than the IRC strip material, Uskon is more durable with respect to shock and vibration. However, the electrical properties of the material appear to vary con-

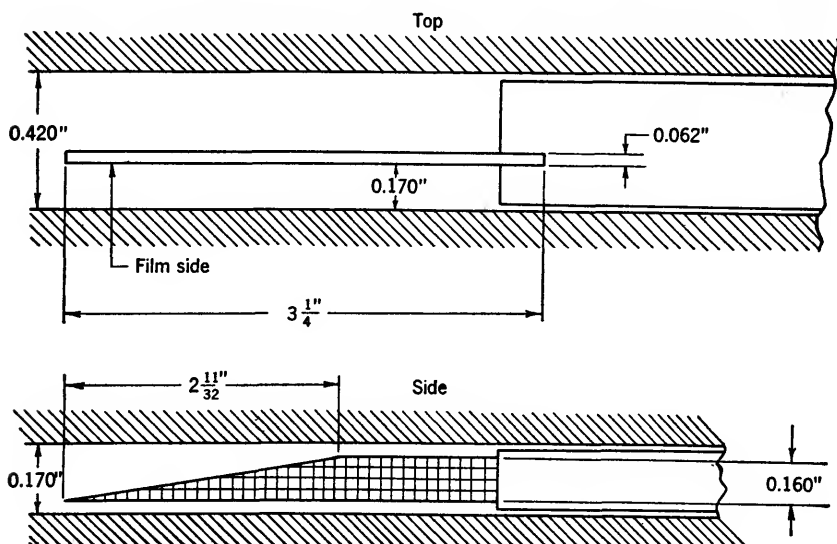


FIG. 12-7.—A metalized-glass load for 1.25-cm waveguide.

siderably from batch to batch. At high relative humidities the 6-ply cloth tends to split apart. The application of a silicone lacquer coating to the cloth would probably prevent this, but it has not yet been tried. Synthane is a material similar to Uskon, but it is mechanically stiffer than Uskon cloth of the same thickness and resistivity.

**12-4. Low-power Terminations Using Metalized Glass.**—A thin, evaporated Nichrome film sandwiched between a glass-plate support and a thin protective magnesium fluoride film can be used in place of the IRC strip material. It is more expensive than the IRC material although a preferable substitute since it has good mechanical rigidity and is unaffected by moisture, and aging. Figure 12-7 shows a 1.25-cm-band load of this type which has a VSWR less than 1.01 over the 1.215- to 1.285-cm band.

In developing this termination, tests were made first with a No. 774 Pyrex glass plate of 0.038 in. thickness. A film resistivity of approximately 300 ohms per square was found to be optimum according to

impedance-matching data taken with an untapered film. However, the taper length and over-all length required to meet a VSWR  $< 1.01$  specification were found to be excessive, and not at all compatible with the mechanical strength of such a thin glass plate. In order to increase the mechanical strength, a thicker, soft-glass plate was tried. The thicker plate has a second advantage in that the guide wavelength is reduced because of the larger permittivity of soft glass as compared with Pyrex. If no detrimental field distortion is incurred, a reduction in the necessary taper length can be expected. Similar reasoning may be applied to the film resistivity. Although a film resistivity close to the characteristic impedance of the waveguide will, in general, match better than a smaller resistivity, its rate of attenuation will be much smaller. It may therefore have to be made objectionably long in order to provide sufficient attenuation to eliminate effectively reflections from the short circuit of the mechanical holder. The final soft-plate design is that shown in Fig. 12-7. The film resistivity is 110 ohms per square. Note that the strip is not centered with respect to the waveguide, but is displaced to the side where it has been found experimentally that lower voltage standing-wave ratios can be obtained.

**12-5. High-power Coaxial-line Loads.**—The first high-power 10-cm load made in  $\frac{7}{8}$ -in., 50-ohm coaxial line used Aquadag-coated sand as a dissipative medium. Two quarts of 20 to 30 testing sand<sup>1</sup> are stirred thoroughly in a fluid suspension consisting of  $\frac{1}{2}$  pt. of Aquadag in  $\frac{1}{2}$  gal. of water. The heavily-coated sand is then drained and allowed to dry in shallow trays at an elevated temperature. A 50-50 mixture of coated and uncoated sand is used as a filling material for the load. It is necessary to prepare a reflectionless, temperature-resisting bead to hold the sand within the line. Of the several bead designs investigated, the best appeared to be a  $\frac{1}{16}$ -in.-thick steatite washer which is held in place by Insalute Cement applied around its edges. After installation of the steatite bead, the sand is poured in from the rear end of the line and compacted by gentle tamping. A metal end plug is then soldered in place to terminate the line. In order to preserve the characteristic impedance of the line in the region of the sand which has a relatively high permittivity, the inner conductor of the line is undercut throughout the entire 9-in. length occupied by the bead and sand mixture. If a dozen 3-in.-diameter radiating fins equally spaced along the sand-filled section of line are used, it is possible to dissipate 60 watts average power and 50 kw pulse power. Unfortunately, the load was difficult to reproduce and the reject percentage was high even for a lenient maximum VSWR specification of 1.10 or less over the 8.5- to 11.5-cm band.

The sand load just described suffers in two respects because it does

<sup>1</sup> Ottawa Silica Co., Ottawa, Ill.

not make use of steps or of a continuous taper at its input end. Steps or a smooth taper facilitate impedance-matching and tend to allow a more uniform power dissipation along its length. In contrast, the sand load gets very hot at its input end where half of the power is dissipated in the first 3 db of attenuation. It may easily be shown that if the power dissipation is to be uniform along the length of the load, the attenuation constant must vary with position along the line according to the following formula

$$\alpha = 10 \log_{10} \frac{y + 1}{y}, \quad (5)$$

where  $y = 0$  at the short-circuited end of the load, and where the total length of the load is large compared with the unit length. The formula may be applied either to steps or to a smooth taper. For example, if matching steps are used, the attenuation for successive steps of equal length, counting backwards from the short-circuited end of the load, should be  $\infty$ , 3 db, 1.8 db, 1.25 db, 1.0 db, and so forth, for as many steps as are to be used. The inclusion of additional steps does not alter the attenuation per step of the rear steps. Equation (9) offers an alternative expression for the attenuation constant of a line continuously tapered for uniform power dissipation along its length. This equation, unlike Eq. (5), had no restriction on the magnitude of a "unit length" as compared with the total length of the load. This equation is useful principally in step-matched constructions. It is customary to step or taper toward the outer rather than toward the inner conductor, since the outer conductor can more effectively carry away the heat developed in the load. Furthermore, a rough lip on the taper edge has less effect on the voltage standing-wave ratio of the load if the taper is carried to the outer conductor where the fields are weak rather than to the center conductor.

Figure 12-8 shows a  $\frac{1}{8}$ -in. coaxial-line load which makes use of a straight, conical taper to the outer conductor. The load material first used with this design was polyiron made resistant to high temperatures by a ceramic binder. However, it was impossible to mold the taper lip properly, and the machining of such a taper into polyiron was objectionably difficult in production. Consequently, it became necessary to choose another load material, and the final choice was a mixture of powdered flake graphite (Dixon's No. 2 grade) and X-Pandotite cement.<sup>1</sup> A mixture of 40 per cent graphite and 60 per cent cement by weight is ball-milled for two hours, care being taken to keep the cement dry to ensure satisfactory milling. Water is then added to the mixture—two parts

<sup>1</sup> X-Pando Corporation, Long Island City, N.Y.

of water to five parts of powder, by weight—and the whole is mixed thoroughly. The mixture is poured into a coaxial mold and allowed to set, partially before the tapered center mold is withdrawn to permit hard setting over a 24-hr period. The outer cylinder of this mold is the outer conductor of the load line. Then follows a 6-hr oven-drying treatment at 200°C. After the center conductor of the line is installed, the load material is impregnated with a fluid Dow-Corning resin No. 2102, allowed to air-dry for a few hours, and then oven-baked at 200° to 250°C for a period of 8 hr. At the end of this baking treat-

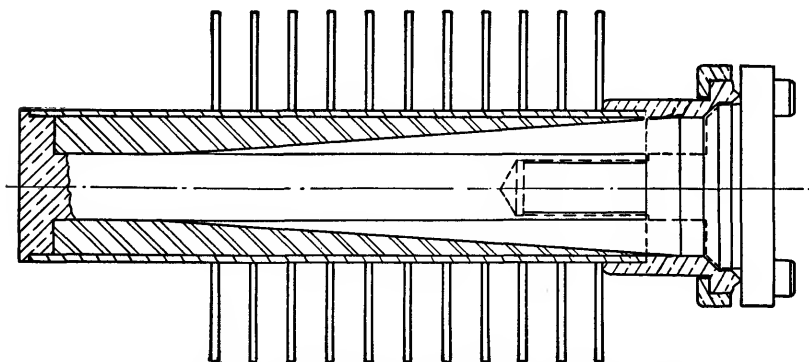


FIG. 12-8.—Sketch of a graphite-cement high-power coaxial-line load.

ment, all toluene from the resin should have evaporated. Benzene may be used to clean any resin from the coaxial-line coupling. The brass casing is painted with a dull black finish which is capable of withstanding a temperature of 200°C. The cement adheres well to the brass casing, and does not crack at temperatures of approximately 200°C. The load is rated at 100 watts average and 200 kw pulse power. The production VSWR specification is less than 1.10 over the 8-to-12-cm wavelength band. Laboratory-built models were all well within this specification. The high-temperature drying and the resin impregnation of the cement are essential, since absorbed water in the load has been found to affect appreciably the attenuation constant and to alter the impedance match.

Some helpful hints can be offered to facilitate the design of matching tapers for lines (coaxial or waveguide) which are filled with an attenuating dielectric. If the experimentally determined wavelength for smallest voltage standing-wave ratio for a given taper is *longer* than the wavelength at which optimum match is desired, a shorter taper and a material of higher conductivity (therefore larger attenuation constant) should be used in the line. Conversely, if the taper matches best at a wavelength



*shorter* than the design wavelength, a longer taper and a material of smaller attenuation constant should be used.

**12-6. High-power Waveguide Loads.**—In the microwave region more work has been done on high-power waveguide loads than on coaxial loads. There are several reasons for this. Waveguide has a greater pulse-power capacity than coaxial line, the skin loss in the metal walls of the line is smaller in waveguide than in a coaxial line, and the shortest wavelengths in the microwave region demand an unmanageably small coaxial line which is much more difficult to build than an appropriate rectangular waveguide. For these reasons there has been a growing trend, particularly for high powers and short wavelengths, to use waveguide loads.

A sand load for the 10-cm band in waveguide  $1\frac{1}{2}$  by 3 in. by 0.080-in. wall has been made from the same sand mixture used in the previously described coaxial-line high-power load. Impedance-matching is obtained by tapering the input end of the sand load, holding the sand in the tapered position by a  $\frac{1}{8}$ -in. Transite plate which is made fast by Insalute cement. The taper is from narrow wall to narrow wall of the waveguide; the taper length, measured in the direction of the waveguide, is 12 cm. The load has a VSWR less than 1.1 over the 8.5- to 11.5-cm band, and is rated for 300 watts average and 300 kw pulse power. The power limitation of the load is the inability of the Transite material to withstand high temperature. The waveguide tapered sand loads have more reproducible impedance characteristics than do the coaxial sand loads, but all of them suffer from varying impedance as the moisture absorption of the sand changes. Moreover, their construction permits shock and vibration to break the sand seal, or even to change the match of the load because of a change in the compactness of the sand. A similarly constructed load for 3 cm with a thick sheet of mica replacing the Transite plate, has a VSWR less than 1.1 over a  $\pm 5$  per cent band. It is rated for 70 watts average and 150 kilowatts pulse power.

The Bell Telephone Laboratories have produced a satisfactory porcelain-silicon load<sup>1</sup> for use in  $\frac{5}{8}$ -in.-by- $1\frac{1}{4}$ -in. waveguide. A combination of 30 per cent silicon in porcelain provides an attenuation of 50 db for a 6-in. length of load,  $4\frac{1}{2}$  in. of which is a continuous linear taper from one broad side of the waveguide to the other. Silicon is not readily obtainable, but 220-mesh silicon carbide has been found to be a good substitute. This material withstands high temperatures without oxidation, and has good thermal shock and thermal conductivity characteristics. Because of the relatively large (10 per cent) shrinkage when the mixture is fired at 1250°C, the fired ceramic

<sup>1</sup> S. O. Morgan, "Ceramic Attenuators for Dummy Loads," BTL MM 44-120-36, Mar. 1, 1944, p. 2.

pieces must be ground to exact dimensions. The grinding operation is a rather tedious one, particularly in the vicinity of the taper tip. If the taper is sufficiently long, the standing-wave ratio depends primarily on the thickness of the tapered edge. Although it is desirable to make this edge as thin as possible, it is not feasible to grind it to a feather edge because of excessive breakage in manufacture and use. As a compromise, an edge thickness of  $\frac{1}{8}$  in. was chosen. The VSWR of such a load can be less than 1.05 over an appreciable bandwidth. It is capable of dissipating 200 watts average and 200 kw pulse power. The ground ceramic pieces may be cemented into the waveguide with Insalute cement or Pliobond.

The most novel, and probably the most satisfactory, method of constructing a waveguide high-power load is to use waveguide walls which are poor conductors instead of using attenuating material which fills the waveguide. Such a construction facilitates a more effective removal of the heat generated in the load, and is not as subject to pulse-power breakdown (arcing) as are the designs which use filling materials in the waveguide. It has been shown experimentally that satisfactory impedance-matching can be obtained with this construction. Also, the waveguide walls may be tapered in order to effect a reasonably uniform power dissipation along the length of the load. The conditions under which a good impedance match in waveguide may be expected can be determined by comparison of the waveguide with a low-frequency transmission line.

The characteristic impedance of a dissipative transmission line is in general a complex quantity given by

$$Z_0 = \sqrt{\frac{R + j\omega L}{G + j\omega C}}.$$

However,  $Z_0$  is real and equal to  $\sqrt{L/C}$ , the characteristic impedance of a nondissipative line of the same size, if

$$\frac{R}{L} = \frac{G}{C}. \quad (6)$$

The series resistance losses are proportional to the square of the current, and hence are proportional to the square of the magnetic field strength. The shunt conductance losses are proportional to the square of the voltage in the line and hence proportional to the square of the electric field strength. From these facts it can easily be shown that the condition expressed by Eq. (6) is equivalent to the statement that the series resistance losses are exactly equal to the shunt conductance losses in the dissipative medium.

The  $L$  and  $C$  of a line depend to a certain extent on  $R$  because of the skin effect which changes the dimensions of the line. Equation (6) is easily applied to the matching of a dissipative to a nondissipative line at low frequencies, since the dimensional adjustments necessary to make the ratio  $\sqrt{L/C}$  of the dissipative line equal to that of the nondissipative line do not produce appreciable reflections. When the line dimensions are comparable with the wavelength, however, geometric discontinuities have an appreciable effect. Although it has not been possible to derive the condition for impedance match from theoretical considerations, it is likely that this relation is given by

$$\frac{\lambda_c}{\lambda} = \frac{2a}{\lambda} = \sqrt{1 + \frac{2b}{a}}. \quad (7)$$

Table 12-5 shows values of the parameters calculated from this equation.

TABLE 12-5.—APPLICATION OF EQ. 12-7 TO SEVERAL STANDARD WAVEGUIDES

Waveguide, in.	$b$ , in.	$a$ , in.	$\lambda_c$ , cm	$\lambda_c/\lambda$	Calculated $\lambda$ , cm
$1\frac{1}{2} \times 3$	1.340	2.840	14.4	1.40	10.3
$\frac{1}{2} \times 1$	0.400	0.900	4.57	1.38	3.32
$\frac{1}{4} \times \frac{1}{4}$	0.170	0.420	2.13	1.35	1.58

Data taken on loads of this type have verified the usefulness of Eq. (7) as a design formula. A typical 10-cm laboratory-made load gave VSWR's of 1.015 at 10 cm, 1.04 at 8 cm, and 1.06 at 12 cm. A typical 3-cm laboratory-made load gave VSWR's of 1.01 at 3.3 cm, and 1.025 at 3.1 and 3.5 cm. A load in  $\frac{1}{4}$ -by- $\frac{1}{2}$  in. waveguide gave a VSWR of approximately 1.07 at 1.25 cm, and progressively lower values as the wavelength was increased toward 1.58 cm. No oscillator was available that would operate in the wavelength range for which the voltage standing-wave ratio was a minimum. It has been observed that the input impedance of the lossy waveguide at the calculated wavelength is very nearly resistive, but slightly greater than unity. This can be accounted for by the effective increase of the  $b/a$  ratio caused by an appreciable skin depth in the dissipative walls of the load.

Figure 12-9 shows the broad-side and narrow-side views of the 3-cm-band load with dissipative walls. The 10-cm-band load has a similar construction. The dissipative material used in this design is a mixture of 35 per cent Portland cement and 65 per cent Dixon's No. 2 powdered flake graphite. It should be noted, however, that Eq. (7) assumed no specific dissipative material. The choice of Portland cement and graphite is dictated not so much by an impedance-matching consideration as by

considerations of thermal shock, durability of the load, the adhesive bond of the material to the metal walls of the waveguide, and ease of casting the mixture. Excessive graphite results in a crumbly material; too little graphite makes the attenuation constant too high.

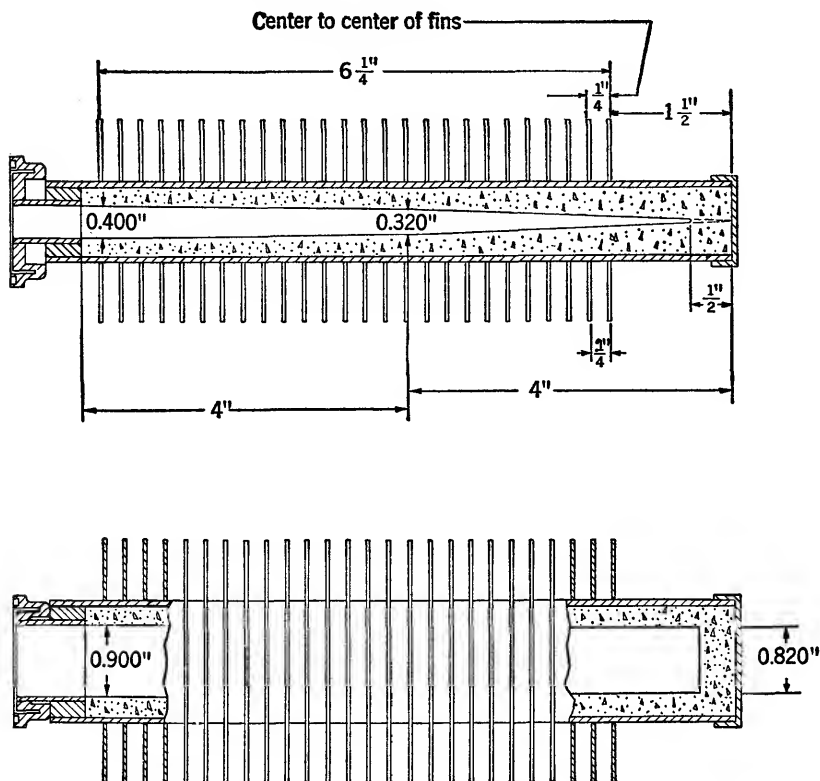


FIG. 12-9.—Construction of a 3-cm-band waveguide high-power load that uses attenuating walls.

The graphite-cement mixture is ball-milled for at least two hours and is then thoroughly mixed with water in the proportions of three parts water to four parts of dry mixture, by weight. A properly shaped center mold is inserted into the load casing, and the graphite-cement-water mixture is poured into the back end of the casing so as to fill the space between the waveguide walls and the center mold. The load should be shaken during the casting process to facilitate the removal of air bubbles. After the cement has set for approximately 4 hr, the center mold may be removed. After an additional 48-hr setting period, the load is allowed to dry for 6 hr in an oven at 200°C. This is followed

by impregnation with Dow-Corning Resin No. 2102. The baking of the impregnated load to remove the toluene, and the associated steps in this process are conducted according to the procedure outlined for the coaxial high-power load. It is extremely important that the transition between metal wall and graphite-cement wall inside the load should be smooth. No gap can be tolerated and small steps at the junction should be filed off.

If the transition has been made smoothly, as has been emphasized, the load accomodates, without breakdown, pulse-power levels almost as

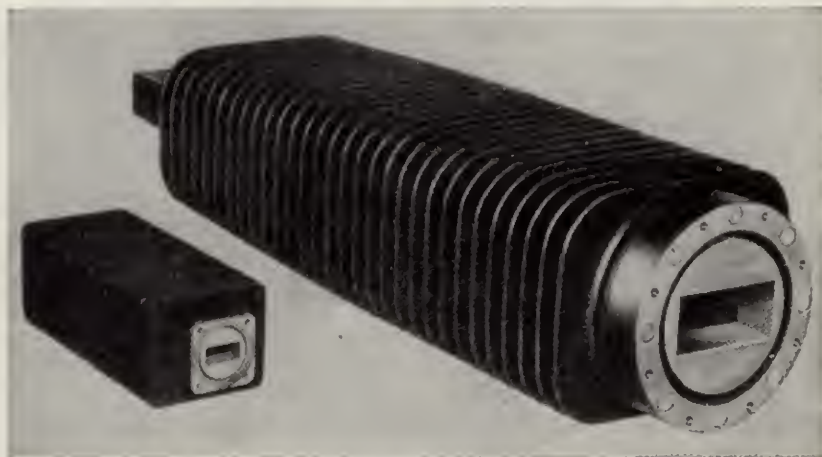


FIG. 12-10.—Photograph of the 10-cm-band and 3-cm-band dissipative-wall high-power loads.

great as those which the nondissipative waveguide accepts. Production specifications, however, have been made more lenient. The 10-cm-band load is rated for 2 Mw pulse power and 1 kw average. The 3-cm-band load is rated for 0.5 Mw pulse power and 0.2 kw average. As may be seen from Fig. 12-10, ample radiating fins are used to dissipate the heat generated in the load. Production voltage-standing-wave-ratio specifications have also been made rather lenient. The 10-cm-band load must have a VSWR less than 1.1 from 8 to 12 cms. The 3-cm-band load has a similar specification of 1.1 or less for the 3.13- to 3.53-cm band. The laboratory-made models were considerably better matched than these specifications require. The attenuation constant of the material is approximately 2 db/in. at 3-cm band, and 1 db/in. at 10-cm band. Experiments indicate that it is unaffected by the input-power level.

The dimensions of the load should be adjusted, in so far as it is possible, to obtain a uniform power dissipation on all four walls of the waveguide and throughout the length of the dissipative section. It may be shown

that the density of power dissipation is constant over the four walls of the waveguide when

$$\frac{\lambda_c}{\lambda} = \sqrt{2}. \quad (8)$$

When this condition is satisfied, the proper  $b/a$  ratio becomes equal to one-half, which is a very convenient value. It should be noted from Table 12-5 that  $\lambda_c/\lambda$  for standard waveguide sizes does not differ greatly from the preferred value given by Eq. (8).

In order to effect uniform power dissipation along the line, it is necessary to vary, in a prescribed manner, the attenuation constant with  $x$ , the distance along the waveguide. This can be done more easily by tapering the walls of the waveguide than by varying the composition of the material as a function of  $x$ . It is possible to derive an expression for the attenuation constant  $\alpha$  as a function of  $x$  by starting with the well-known equation

$$\frac{dP_z}{dx} = -2\alpha P_z,$$

where  $P_z$  represents the power in the dissipative line at the point  $x$ . The equation is integrated from  $x = 0$  to  $x = x$ , and the constant of integration is determined by setting  $P_z = P_0$  when  $x = 0$ . Thus

$$P_d = 2\alpha P_z = 2\alpha P_0 \exp\left(-2 \int_0^x \alpha dx\right),$$

where  $P_d$  represents the power dissipated per unit length of line. But

$$\frac{P_d}{2P_0} = \alpha_0,$$

where  $\alpha_0$  must be a constant if  $P_d$  is to be a constant, and is equal to the value of  $\alpha$  at  $x = 0$ . This leads to the simplified form

$$\ln\left(\frac{\alpha}{\alpha_0}\right) = 2 \int_0^x \alpha dx.$$

The solution to this equation is

$$\alpha = \frac{\alpha_0}{1 - 2\alpha_0 x}. \quad (9)$$

Equation (9) specifies how  $\alpha$  should vary with  $x$ , but it is also necessary to have an expression for  $\alpha$  as a function of  $a$  and  $b$ , the waveguide dimensions, if Eq. (9) is to be used effectively. This form is

$$\alpha = \frac{k}{a} \cdot \frac{\frac{a}{2b} + \left(\frac{\lambda}{2a}\right)^2}{\sqrt{1 - \left(\frac{\lambda}{2a}\right)^2}}, \quad (10)$$

where  $k$  is a constant that need not be evaluated.

At this point, it is wise to summarize the conditions which dictate the design of the load. Equation (7) specifies the impedance-matching condition. Equation (9) specifies  $\alpha$  as a function of  $x$  for uniform power dissipation along the length of the load, and Eq. (10) dictates the tapering of the dimensions  $a$  and  $b$  in order to meet the condition stated by Eq. (9). Equation (8) specifies the condition necessary for all four walls of the dissipative waveguide to have the same density of power dissipation. There is also the additional consideration that the internal shape of the load must be such that the center mold used in the casting process can easily be withdrawn from the waveguide.

Since there are essentially only three variables with which to work,  $a$ ,  $b$ , and  $x$ , all of the desired conditions cannot be met simultaneously. The compromises made in the design of the 3-cm- and 10-cm-band loads are the following. Since a low voltage standing-wave ratio is usually more essential than uniformity of power dissipation, the linear tapering of the dimensions  $a$  and  $b$  for the first 5 to 8 db of attenuation is made to conform with the condition expressed by Eq. (7). The tapering must be slight in order to avoid bringing the waveguide too near cutoff by making the  $a$  dimension too small. By taking differentials in Eq. (7) it may be shown that, to a first-order approximation, a linear tapering of the dimension  $a$  demands a linear tapering of the dimension  $b$ . If Eq. (7) is obeyed throughout the first few decibels of attenuation, no serious effect on the input voltage standing-wave ratio will be noticed if, for the remainder of the load, emphasis is given to distributing the losses more evenly along the length of the waveguide. In other words, Eq. (7) is discarded in favor of Eq. (9) for the remainder of the length. It should be noted from Eq. (10) that either  $a$  or  $b$  or both may be varied to get the value of  $\alpha$  demanded by Eq. (9). Most of the variation is taken in the  $b$  dimension. In the final load design the  $a$  dimension is given a slight linear taper throughout the entire length of the load, whereas the taper on the  $b$  dimension changes abruptly after several decibels, when making the transition from an impedance-matching to a uniform-power-dissipation condition.

The same material used in constructing the dissipative-wall waveguide load can also be used for making a filled waveguide load. If the waveguide is properly tilted when the cement-graphite mixture is allowed to dry, the desired taper can be automatically cast. As previously mentioned, the filled waveguide load has less desirable electrical characteristics than the dissipative-wall load; however, it is more easily made.

A variation on the above theme was introduced in the design of a 1.25-cm-band waveguide load. It was felt that additional mechanical strength and a more gradual power dissipation could be achieved by introducing loss only in the narrow sides of the waveguide. Furthermore, lower voltage standing-wave ratios are possible in this design

because, as has been shown, the dimensions of standard 1.25-cm-band waveguide are not correct for impedance-matching at 1.25 cm if all walls of the waveguide are made to attenuate. To increase the mechanical strength of the load, the use of a continuous lossy wall was abandoned for a lattice structure in which sections of dissipative material  $\frac{5}{8}$  in. long are separated by sections of conductor  $\frac{1}{8}$  in. long. The attenuation

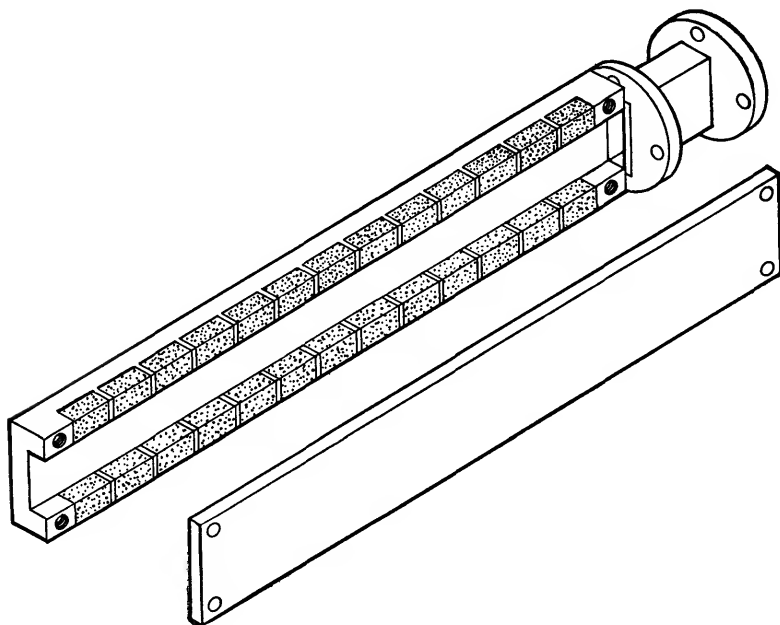


FIG. 12-11.—1.25-cm-band waveguide high-power load.

of a load 5 in. long was approximately 20 db. Figure 12-11, with a broad side of the waveguide removed, explains this construction.

The dissipative material consists of a mixture of a metal powder and a cement. Iron powder gave lower voltage standing-wave ratios than either nickel or nickel-copper mixtures. Consequently, a mixture of iron powder and X-pandotite was chosen as the attenuating material for the load. The iron powder is very fine, and presumably has grain dimensions which are less than the skin depth in iron at 1.25 cm. To a 4-to-1 mixture by weight of X-pandotite and iron powder (Cenco hydrogen-reduced iron) is added enough water to make a workable paste. After the load lattice is filled by the cement, the cement is allowed to harden for a few hours at 200°C. To protect the load material against moisture absorption it is coated with a 2 per cent solution of silicone (Dow-Corning Fluid No. 200) in carbon tetrachloride.



Production models of the load have a VSWR less than 1.1 over a band of  $\pm 2$  per cent centered at 1.25 cm. The load absorbed, without breakdown or other ill effects, the highest pulse power, 115 kw, and the highest average power, 35 watts, available at the time of test. At these power levels no radiating fins need to be used.

### GENERAL LABORATORY ATTENUATORS

By E. WEBER

At microwave frequencies, practically all dielectric materials that are mechanically satisfactory absorb a considerable amount of electromagnetic power, and therefore, can be used as attenuating materials in either coaxial or waveguide transmission systems.

**12-7. Cables as Coaxial Attenuators.**—One of the most common, and also one of the most practical, dissipative attenuators is a piece of high-frequency coaxial flexible cable, usually constructed with a high-resistance inner conductor of nichrome wire. A description of cables of various types and their general characteristics as transmission lines is given in Vol. 9, Chap. 5. The old cables, with solid rubber dielectrics, had rather high power factors and the losses varied appreciably with changes in temperature. The recent cables have solid polyethylene insulation, a low-loss dielectric developed in England, which is much more stable and varies less with temperature.

Theoretically, attenuation should vary with wavelength in accordance with the form

$$\alpha = \frac{p}{\sqrt{\lambda}} + \frac{q}{\lambda}, \quad (11)$$

where  $p$  and  $q$  are constants;  $p$  indicates essentially the conductor losses which are proportional to the square root of frequency, whereas  $q$  indicates essentially the dielectric losses, which are directly proportional to frequency. Thus, for the low-loss cable RG-9/U, the coefficients are numerically  $p = 0.392$ ,  $q = 0.360$ , for the wavelength  $\lambda$  in cm, which lead to values of  $\alpha$  in db per foot.<sup>1</sup> For the high-loss cable RG-21/U, the coefficients are  $p = 2.4$ ,  $q = 0.81$ , and indicate the larger contribution of the high-resistance inner conductor. The attenuation values were obtained at the Radiation Laboratory from measurements made at room temperature at two wavelengths, as shown in Table 12-6. The values of the coefficients can be used for approximate determination of  $\alpha$  at other wavelengths down to wavelengths corresponding to several hundred megacycles per second.

<sup>1</sup> F. E. Ehlers, "Attenuation of RG-9/U Cable as a Function of Temperature and Frequency in the X-Band," RL Report 754, June 18, 1945.

TABLE 12-6.—CABLE ATTENUATION AS FUNCTION OF WAVELENGTH

Kind of cable	Type	Measured attenuation in db/ft		Coefficients of Eq. (11)	
		at $\lambda = 10$ cm	at $\lambda = 3.30$ cm	$p$	$q$
Low-loss cable	RG-9/U	0.16	0.326	0.392	0.360
High-loss cable	RG-21/U	0.83	1.60	2.40	0.81

TABLE 12-7.—MEASURED ATTENUATION VALUES OF MICROWAVE CABLES

Cable type	Manufacturer	Characteristic impedance $Z_0$ (ohms)	Attenuation in db/ft as function of	
			wavelength	temperature
D163296 (obsolete)	BTL	50 (nominal)	$9.55/\lambda$ $8.5 \text{ cm} < \lambda < 11.5 \text{ cm}$ at $T = 26^\circ\text{C}$	$0.74 + 0.0082T$ $25^\circ\text{C} < T < 85^\circ\text{C}$ at $\lambda = 10 \text{ cm}$
RG-21/U	BTL	52 (approx.)	$2.64/\sqrt{\lambda}$ $8.7 \text{ cm} < \lambda < 12.6 \text{ cm}$ at $T = 26^\circ\text{C}$	$0.834 = 0.054 \times$ $(T - \frac{80}{100})^2$ $-40^\circ\text{C} < T < +60^\circ\text{C}$ at $\lambda = 10 \text{ cm}$
RC-21/U	BTL	52 (approx.)	$5.3/\lambda$ $3.12 \text{ cm} < \lambda < 3.53 \text{ cm}$ at $T = 26^\circ\text{C}$	$1.677 - 0.09 \times$ $(T + \frac{50}{100})^2$ $-46^\circ\text{C} < T < 89^\circ\text{C}$ at $\lambda = 3.23 \text{ cm}$
RG-9/U	Federal Tel. and Radio Co.	52 (approx.)	$1.08/\lambda$ $3.14 \text{ cm} < \lambda < 3.56 \text{ cm}$ at $T = 26^\circ\text{C}$	See text

However, as the empirical formulas in Table 12-7 indicate, the variation over narrower wavelength ranges can be simplified with closer approximation to measured values. This is particularly true for the shorter wavelengths where the braid of the outer conductor apparently influences the attenuation values rather markedly. For this reason, the cables must be securely anchored during measurements to avoid flexing. It was found that the attenuation could easily be varied from 5 to 10 per cent by moving the cable; it was also observed that if the cable were disturbed at all, a period of several minutes was required to allow the attenuation to stabilize. Flexure near the fittings can be particularly troublesome and can cause much larger errors in measurement.

The variation of attenuation with temperature is also indicated in Table 12-7 insofar as reliable results could be obtained. At the shorter wavelengths, temperature cycling produces hysteresis effects with permanent increases in the attenuation values. Thus, RG-9/U cable

showed, after about nine temperature cycles from room temperature to 65°C, a permanent increase of the losses of about 0.06 db per foot to a final value of about 0.40 db per foot. Similarly, a hysteresis effect occurs at low temperatures. Moving and shaking the cable after or during temperature cycling usually causes a sudden increase in the attenuation of about 0.01 db per foot. Such erratic values in the attenuation have been attributed to variation in the contact resistance between the braid wires, and have been observed only at the highest range of frequencies at which these cables can be used, namely at or near 9000 Mc/sec.

The input impedance of cables was originally chosen to be close to the standard characteristic-impedance values of coaxial transmission lines. However, the actual value of cable impedance varies from 52 to 48 ohms for cables with a nominal characteristic impedance of 50 ohms. If a cable of 52-ohm impedance is connected to a  $\frac{5}{16}$ -in. coaxial line of 49.6 ohms it leads to an unavoidable VSWR of 1.047. Careful measurements have also shown, particularly in low-loss cables, a periodicity

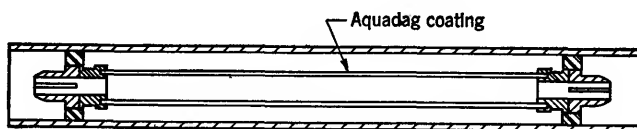


FIG. 12-12.—Carbon-coated coaxial attenuator.

effect introduced by the production method which causes large and rather sharp VSWR maxima of 1.4 or higher at some wavelengths between 8.4 cm and 10.6 cm. Lesser maxima occur at the harmonic multiples of the corresponding frequency. Finally, the input impedance can vary appreciably as a function of frequency since the connectors have to be considered an integral part of the cable assembly for testing and use. The characteristics of cable connectors are described in Vol. 9, Chap. 5.

Thus, while cable has the unquestioned advantage of simplicity for providing attenuation, care has to be exercised in any assumption of its attenuation or input-impedance value. It has the added advantage of large power capacity, but becomes bulky if large values of total attenuation are required.

**12-8. Fixed Coaxial Pads.**—One of the earliest attenuating materials used in the microwave region was Aquadag, a colloidal suspension of fine carbon powder. For use in coaxial lines, it is painted on a glass or ceramic rod of the same diameter as the inner conductor of a coaxial system and then dried in a baking oven at about 100°C. If the rod is furnished with standard end bullets and the outer casing with standard couplings for the particular line size, a fixed-value coaxial attenuator is obtained as shown in Fig. 12-12. The values of attenuation obtainable vary with the

thickness of the coating, but it is difficult to control the uniformity of the coating as well as its thickness. For attenuations up to about 8 db, the voltage standing-wave ratio is generally tolerable, and increases with attenuation for a fixed film length. The higher the value of attenuation the more dependent it is on frequency; it also depends on humidity and, to a slighter extent, on temperature. Although these attenuators, as laboratory instruments, are simple and convenient, they are restricted to low values of attenuation because of the difficulty of proper impedance-

matching, and they are not suitable as standards because of possible changes with moisture.

Attenuators with higher values of attenuation in coaxial systems have been designed with good matching characteristics by combining carbonized shunt disks with series rods in  $\Pi$ - or T-network fashion. The very close tolerances required in order to achieve desirable wideband performance have

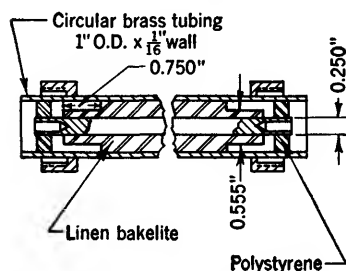


FIG. 12-13.—Coaxial attenuator.

militated against more widespread use of these attenuators. Designs up to 500 and possibly 1000 Mc/sec are available at Bell Telephone Laboratories, and a few models have been built.

Fixed coaxial attenuators have also been produced by filling the space between inner and outer conductor with a lossy dielectric material or with a dispersion of conductive particles in a neutral binder. Practically all of these materials are described in greater detail in Secs. 1 to 6, inclusive, as illustrations of well-matched transmission-line terminal loads. For values of attenuation of 20 db or more, the matching shapes which have been described can be directly copied, since the reflection from the far end of the attenuator will be insignificant and without effect at the input end. For values of attenuation below 20 db, the matching sections must be modified in order to minimize or eliminate this reflection. As in the original design, only procedure by trial and error will lead to a satisfactory solution.

One illustration, Fig. 12-13 shows the construction of a fixed attenuator pad for a 75-ohm transmission system with linen Bakelite as the lossy dielectric.<sup>1</sup> The matching section is designed for a wavelength of 10 cm and a relative dielectric constant of approximately  $k_s = 4$ . Instead of Bakelite, either mahogany wood or Transite could be used. Both the wood and the Transite have about the same loss factor as Bakelite, but are even more subject to the influence of humidity than is Bakelite.

<sup>1</sup> Used by Sperry Gyroscope Co., Garden City, Long Island, N. Y.

Of course, a coating of a sealing, moisture-proof varnish can be used to reduce the effect of humidity, although usually its effect cannot be eliminated entirely.

Other materials that have been used are Durez 7421, which is a thermosetting plastic, and various polyiron materials.

**12-9. Fixed Waveguide Attenuators.**—A material of a somewhat different type is the IRC resistance card, a phenol fiber, approximately  $\frac{3}{8}$  in. thick, on which is sprayed a mixture consisting of graphite and a binder; the latter volatilizes when heated to about 100°C and leaves a carbon coating of reasonable uniformity and adequate resistance values depending upon the length of baking. It is easy to cut this card material into different shapes and to use it, particularly in waveguides, as a power-

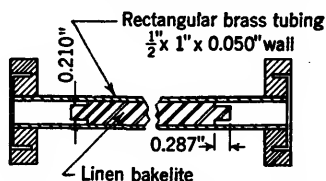


FIG. 12-14.—Waveguide attenuator.

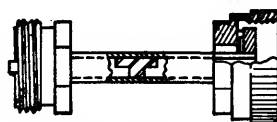


FIG. 12-15.—Polyiron waveguide pad for 1.25 cm.

absorbing element. In the form of a tapered vane, it can be placed in the center plane of the waveguide parallel to the small dimension and used for small power levels as a fixed attenuator. Data on the measured attenuation rates, voltage-standing-wave-ratio values for different waveguide sizes, and resistance values of the strips have been collected in Table 12-4; therefore, the design of simple waveguide pads is relatively easy. As has been indicated, the IRC strip might be replaced by a strip of Uskon cloth that has better mechanical strength.

For large power levels it is necessary to use material of greater bulk in order to provide proper heat exchange with the ambient air. A fixed waveguide pad of approximately 10 db attenuation at a wavelength of 3.2 cm, in which linen Bakelite is used as the lossy dielectric,<sup>1</sup> is shown in Fig. 12-14.

Polyiron materials have also been used very effectively in waveguides with stepped cross sections to provide proper matching. The characteristics of polyiron of several types have been determined (see Table 12-3) and therefore, the design of attenuator pads for the wavelength range from 3.13 cm to 3.53 cm in a waveguide of inner dimensions 0.400 by 0.900 in. is relatively simple. For other frequency ranges and other waveguide sizes, new designs would have to be made, although the values given can serve as a guide.

<sup>1</sup> Used by Sperry Gyroscope Co., Garden City, Long Island, N. Y.

The design of a waveguide pad for the wavelength range of 1.25 cm  $\pm 1$  per cent, with a nominal attenuation of 22 db, is shown in Fig. 12-15. The waveguide has inner dimensions of 0.169 by 0.419 in. and the polyiron used is material No. 1725. As a bilaterally matched pad, the VSWR was held to less than 1.2, but the dimensions had to be met very closely in order to stay within these specifications.

Of course, any lossy material can be used for the design of fixed pads as long as provision can be made for matching sections and machining, or if other suitable forming processes are applicable.

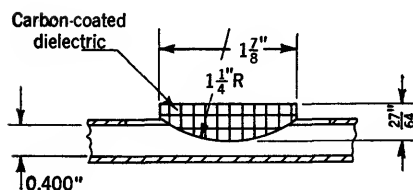
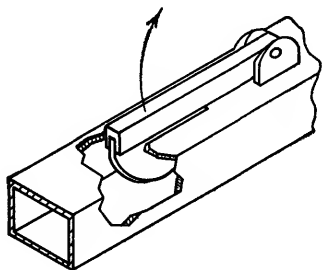


FIG. 12-16.—Variable waveguide attenuator of the flap type.

**12-10. Variable Waveguide Attenuators.**—The simplest type of variable attenuator for waveguides is the so-called flap attenuator, shown schematically in Fig. 12-16. The dissipative element is again an IRC resistance card, cut along a circle in order to achieve good voltage standing-wave ratio. A single strip, of resistivity 200 ohms per square, with the dimensions shown will give about 10 to 15 db attenuation in a waveguide whose inner dimensions are 0.400 by 0.900 in. In order to provide mechanical rigidity, two resistance cards of 200 ohms per square can be glued together back to

back. This results in a combined film resistivity of 100 ohms per square and in a somewhat higher value of attenuation. Insertion into the guide is made through the broad top side of the guide and the vane swings about a hingelike holder. Because of the simplicity of its construction, an attenuator of this type is probably the most frequently used attenuator in test setups where the obvious leakage from the slot in the guide is of no particular concern. It is used near the oscillator as a buffer attenuator to avoid reaction of the load changes upon the oscillator; it is used as a variable buffer in the detector section of attenuation-measuring arrangements, but only if it cannot influence the input power to the detector through leakage coupling; it is also used to adjust power to predetermined levels where the amount of attenuation needed is of no interest. Building a casing over the central part of the waveguide and driving the resistive-strip holder suitably by means of a shaft extending through the casing, has produced calibrated

flap attenuators for about 24,000 Mc/sec and with maximum attenuation values of 90 db. These flap attenuators, however, were found to be very sensitive with respect to exact centering in the guide, parallelism to the guide walls, and exact shape of the resistive vane.

A variation of a flap attenuator of this type is shown in Fig. 12-17 where the resistance card is cut in spiral shape and is attached to a circular metal disk. This disk is centered on a shaft which penetrates a leakage-proof casing. The rotation of the shaft might also move a pointer or a dial calibrated directly in decibels of attenuation as measured against a comparison standard. By properly shaping the resistance card, a scale of attenuation which is almost linear can be attained with

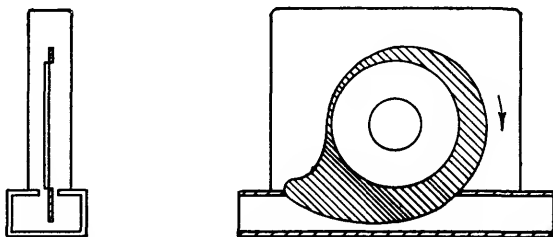


FIG. 12-17.—Attenuating strip moving vertically in guide.

rather good voltage standing-wave ratio. Although the construction is again simple, lack of mechanical rigidity and the possibility of a slight deformation under the influence of temperature and humidity would militate against the use of this card as a precision attenuator. Values of attenuation up to about 40 db are obtained easily, whereas higher values present considerable difficulties. These difficulties result from the coupling of the guide with the casing above, which permits much of the electromagnetic power to flow through the less attenuating path through the casing.

Instead of insertion through a slot in the guide, a vane can be fitted into the guide parallel to the small waveguide dimension as shown in Fig. 12-18. For mechanical reasons, two resistance cards can be used, cut either with tapered matching sections as shown in Fig. 12-18*a* or with notches as in Fig. 12-18*b* and glued back to back. Depending on the type of drive chosen, considerable accuracy of setting can be achieved.<sup>1</sup> However, temperature and humidity occasionally cause deformations of the strip which make reproducibility and reliability somewhat questionable particularly at the high values of attenuation where variation with position is very rapid. An illustration of this performance, Fig. 12-19, shows the attenuation versus position of a vane, as in Fig. 12-18*a*, at

<sup>1</sup> E. I. Green, H. J. Fisher, and J. F. Ferguson, "Techniques and Facilities for Microwave Radar Testing," AIEE Technical Paper No. 46-40, January, 1946, p. 22

the three wavelengths 3.1, 3.32 and 3.5 cm and in a waveguide of inner dimensions 0.400 by 0.900 in. It can be observed from this figure, that the variation of attenuation with wavelength is large and not very systematic and therefore interpolation is very difficult. Another

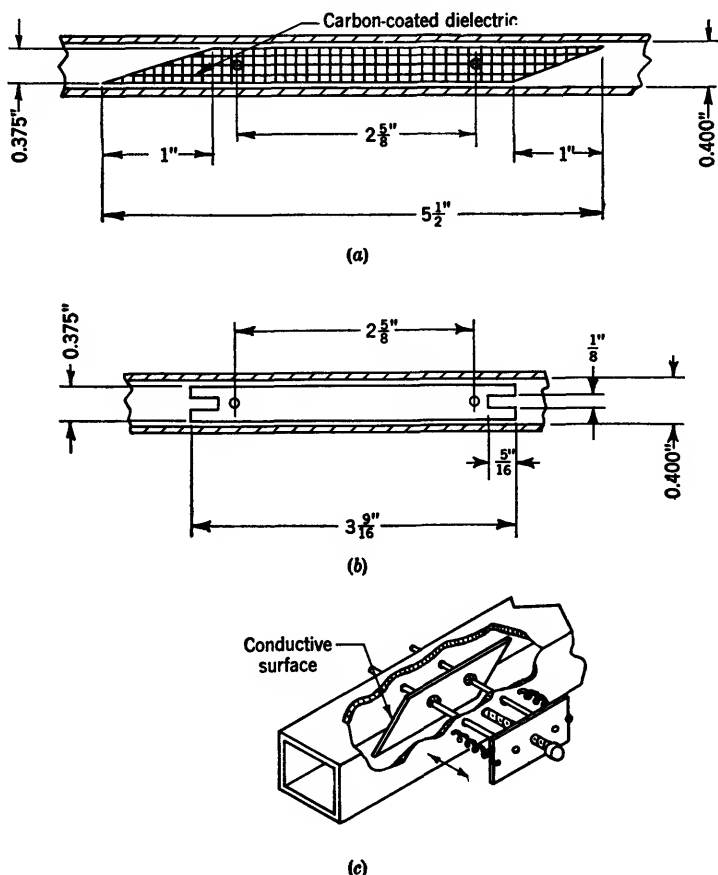


FIG. 12-18.—Variable waveguide attenuator of the vane type. (a) tapered vane, (b) notched vane, (c) perspective of assembly.

illustration of performance, Fig. 12-20, shows the calibration curves for the notched-end plate of Fig. 12-18 for different widths of the vane and for a fixed wavelength of 3.20 cm in a waveguide whose inner dimensions are 0.400 by 0.900 in. It is important to observe the critical influence of the width of the vane upon the attenuation curve which leads to a resonance peak for a width of 0.355 in. at a distance of  $\frac{5}{8}$  in. from the



side wall. The design of the resistive strips is still an art, and from new applications unexpected results can be anticipated.

It is possible to obtain improved performance with respect to variation of attenuation with frequency if two vanes moving simultaneously from

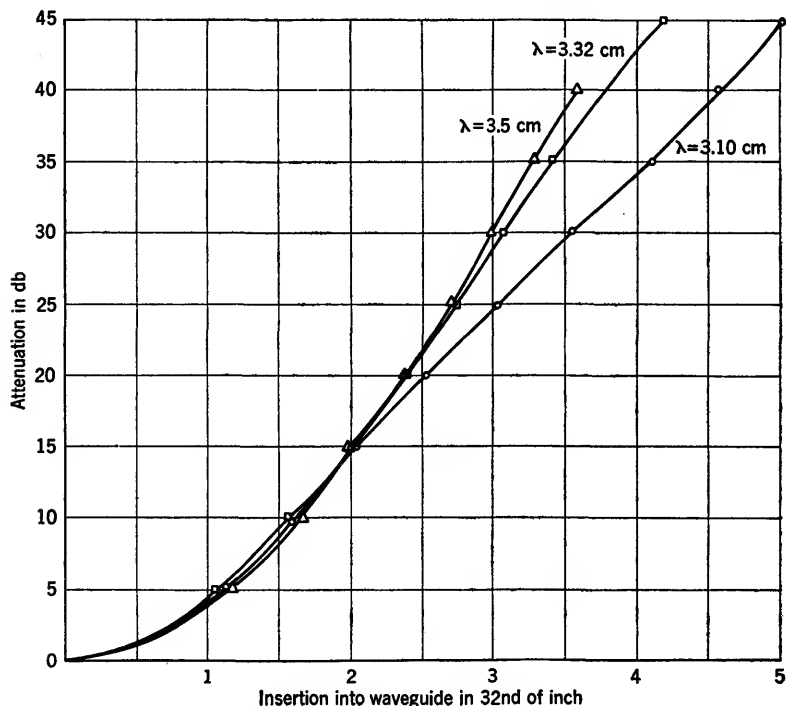


FIG. 12-19.—Calibration of tapered-end IRC resistive-vane attenuator.

the opposite small sides of the waveguide toward the center are used. The complication in construction is, however, considerable, and the increase in total attenuation is not uniform.

### PRECISION METALIZED-GLASS ATTENUATORS

BY E. WEBER

The depth of the penetration of electromagnetic fields into metals can be derived by means of Maxwell's field equations as<sup>1</sup>

$$\delta = \sqrt{\frac{2}{\omega\mu\sigma}},$$

where  $\omega = 2\pi f$  and  $f$  is the frequency of the oscillation in cycles per

<sup>1</sup> J. A. Stratton, *Electromagnetic Theory*, McGraw-Hill, New York, 1941, p. 504.

second,  $\mu$  is the absolute permeability of the metal, and  $\sigma$  is its conductivity. For copper, at microwave frequencies of about 10,000 Mc/sec, a depth of penetration of  $7 \times 10^{-5}$  cm is obtained. Very thin metal films, appropriately applied to dielectric carriers, can be made of thicknesses of  $10^{-6}$  to  $10^{-5}$  cm; they will then exhibit essentially uniform current distribution even at the highest practical microwave frequencies.

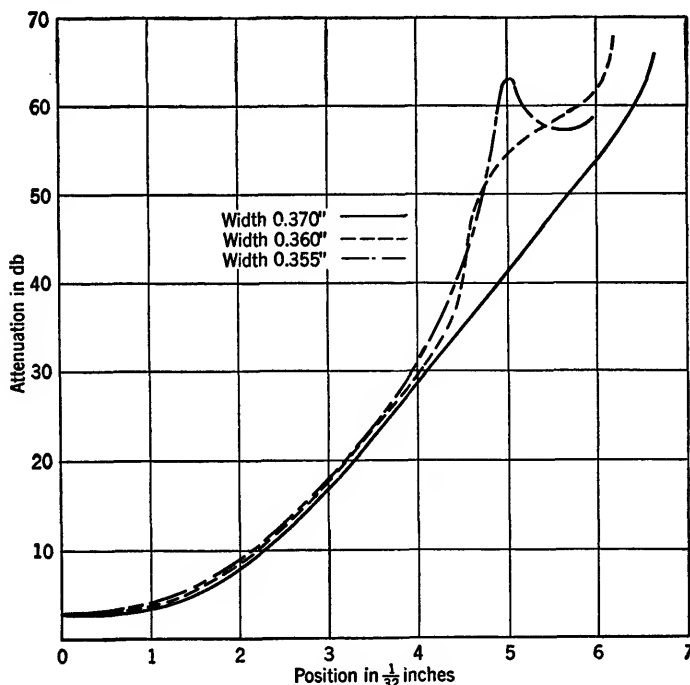


FIG. 12.20.—Calibration of notched-end IRC resistive-vane attenuator for varying widths of the vane.

Moreover, these metallic films, with glass as a foundation, can be made stable, unaffected by humidity, controllable as to resistance, and reproducible.

If these metal films on glass tubing are used as the inner conductor of a coaxial system, precision attenuators of fixed values can be obtained if suitable casings are provided which permit insertion in a standard coaxial line. With a variable metallic shunt path to the film, variable attenuators can be obtained which are of particular use as laboratory instruments.

**12.11. Electrical Design of Coaxial-pad Inserts.**—In the electrical design of the coaxial attenuator insert, dimensions and resistances of

film sections on insulators must be specified so that the over-all unit matches and has the required attenuation. In order to design units of various types, it is necessary to refer to the basic principles of transmission lines with series loss.

A section of uniform transmission line, in which the center conductor is a thin metallic film on a dielectric carrier, has a complex characteristic impedance with a real part greater than the characteristic resistance corresponding to the dimensions of the lossless line, and a capacitive reactive component; thus,

$$\begin{aligned} Z_c &= \sqrt{\frac{R + j\omega L}{j\omega C}} \\ &= \sqrt{\frac{L}{C}} \sqrt{1 + \frac{R}{j\omega L}} = Z_0(u - jv), \end{aligned} \quad (12)$$

where  $R$ ,  $L$ , and  $C$  are the resistance, the inductance, and the capacitance, all per unit length (neglecting radiation resistance). The quantities  $u$  and  $v$  then are, respectively, the resistive component and the reactive component of the impedance normalized with respect to the geometric characteristic resistance,  $Z_0 = \sqrt{L/C}$ .

If the quantities  $u$  and  $v$  are considered as functions of the resistance per unit length, they are related and define a curve on the impedance chart. For convenience, let

$$x = \frac{R}{\omega L} = \frac{R\lambda_0}{2\pi Z_0}, \quad (13)$$

where  $\lambda_0$  is the wavelength for the lossless line in which  $R = 0$ . If the substitution

$$x = \sinh 2\theta \quad (14)$$

is used, there is obtained from Eq. (12)

$$u = \cosh \theta \quad \text{and} \quad v = \sinh \theta. \quad (15)$$

From this, it is seen that the real part of the characteristic impedance is always greater than the lossless ( $R = 0$ ) characteristic resistance. The

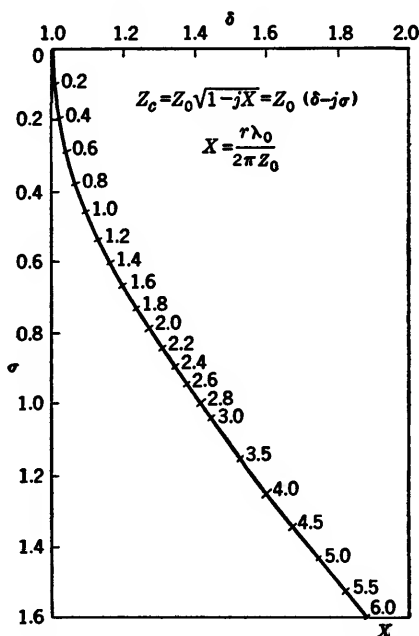


FIG. 12-21.—Normalized impedance chart for a line with series resistance.

locus of the normalized complex characteristic impedance, for a portion of the impedance chart, is shown in Fig. 12-21, with values of the parameter  $x$  indicated along the curve. For greater accuracy, special tables<sup>1</sup> of the functions in Eqs. (14) and (15), or conventional tables of the hyperbolic functions, may be used.

Similarly, the general expression for the propagation constant of a uniform transmission line can be reduced to functions of  $u$  and  $v$ ,

$$\gamma = \sqrt{j\omega C(R + j\omega L)} = j\omega \sqrt{LC} \sqrt{1 - j\frac{R}{\omega L}} = \frac{2\pi}{\lambda_0} (v + ju). \quad (16)$$

With the general form  $\gamma = \alpha + j\beta$ , the attenuation constant becomes

$$\alpha = \frac{2\pi}{\lambda_0} v \quad \text{nepers/meter}, \quad (17)$$

and the phase constant becomes

$$\beta = \frac{2\pi}{\lambda_0} u = \frac{2\pi}{\lambda_a}, \quad (18)$$

where  $\lambda_a = \lambda_0/u$  is the actual wavelength in the resistive line, which is thus always shorter than the free-space wavelength.

Therefore, if any one of the three quantities,  $x$ ,  $u$ , or  $v$ , and the

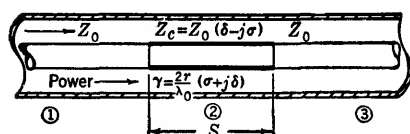


FIG. 12-22.—Schematic diagram of single metal-film section.

lossless wavelength  $\lambda_0$  are known, the calculation of the normalized line characteristics—characteristic impedance  $Z_c$ , attenuation constant  $\alpha$ , and phase constant  $\beta$ —necessary for the design of the attenuator, can proceed. In fact,

from Eq. (17) an expression for the attenuation per wavelength (measured in the lossless line) can be obtained

$$a = \lambda_0 \alpha = 2\pi v. \quad (19)$$

This expression can be considered as a measure of all the design parameters, and it determines the performance that may be expected of an attenuator.

Let us assume first a single coaxial-line section of length  $s$  with metal film as shown schematically in Fig. 12-22, and with the same diameter ratio of conductor surfaces as the lossless line, so that the same geometric impedance holds for all three sections. From transmission-line theory, the expression for the input impedance to the film section is found to be

$$Z = \frac{1 - R_{23}e^{-2\gamma s}}{1 + R_{23}e^{-2\gamma s}} Z_c, \quad (20)$$

<sup>1</sup> R. W. P. King, *Electromagnetic Engineering*, Vol. I, Appendix II, McGraw-Hill, New York, 1945

where the reflection coefficient at the junction of lines (2) and (3) is defined by

$$R_{23} = \frac{Z_c - Z_0}{Z_c + Z_0}. \quad (21)$$

The over-all reflection coefficient at the beginning of the film section becomes

$$R_L = \frac{Z_0 - Z_L}{Z_0 + Z_L} = \frac{R_{12} + R_{23}e^{-2\gamma s}}{1 + R_{12}R_{23}e^{-2\gamma s}}, \quad (22)$$

where  $R_{12}$  is the (fictitious) reflection coefficient at the junction of lines (1) and (2), if line (2) is assumed of infinite length (or properly terminated); namely,

$$R_{12} = \frac{Z_0 - Z_c}{Z_0 + Z_c}. \quad (23)$$

By symmetry,  $R_{12} = R_{23}$ . Very frequently, especially in the design of attenuators,

$$|R_{12}R_{23} \cdot e^{-2\gamma s}| < 0.01,$$

and therefore, the approximate and very much simpler form

$$R_L \approx R_{12} + R_{23} \cdot e^{-2\gamma s} \quad (24)$$

can be used without appreciable loss in accuracy.

The design of the single metal-film section, which has a given attenuation  $A = \alpha s$  and an ideal match  $R_L = 0$ , can now be attempted. From Eq. (24) together with Eqs. (21) and (23), there results, for  $R_L = 0$ ,

$$e^{2\gamma s} = 1, \quad 2\gamma s = j2\pi;$$

and with Eqs. (17) and (18)

$$4\pi \frac{s}{\lambda_0} \cdot v + j4\pi \frac{s}{\lambda_0} \cdot u = j2\pi,$$

which leads to  $v = 0$ ,  $u = \frac{1}{2}\lambda_0/s$ . The exact solution is trivial, namely,  $A = \alpha s = 0$ . However, if the condition on the match is relaxed to permit an input VSWR of 1.02,  $|R_L| = 0.01$ , and therefore

$$\left| \frac{Z_0 - Z_c}{Z_0 + Z_c} 1 - e^{-2\gamma s} \right| = 0.01. \quad (25)$$

If the value of  $Z_c$  from Eq. (12) and of  $\gamma$  from Eq. (16) are introduced, there is obtained, for the condition for match,

$$\frac{(1-u)^2 + v^2}{(1+u)^2 + v^2} \cdot \left[ 1 - 2e^{-4\pi \frac{s}{\lambda_0} v} \cos \left( 4\pi \frac{s}{\lambda_0} u \right) + e^{-8\pi \frac{s}{\lambda_0} v} \right] = 0.01, \quad (26)$$

while for the total attenuation Eq. (17) gives

$$A = \alpha s = 2\pi \frac{\lambda_0}{s} \cdot v. \quad (27)$$

By trial and error a combination of  $s/\lambda_0$  and a proper pair  $(u, v)$  from Fig. 12-21 can be found, which satisfies simultaneously Eqs. (26) and (27). With this solution, it is possible to evaluate  $x$  according to Eq. (14).

$$x = \sinh (2 \cosh^{-1} u). \quad (28)$$

Since  $s/\lambda_0$  is now known, Eq. (13) is best rewritten as

$$x = \frac{1}{2\pi} \frac{\lambda_0}{s} \cdot \frac{R_s}{Z_0},$$

from which the value of the resistance  $R_s/Z_0$  can be determined. For

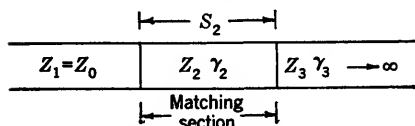


FIG. 12-23.—Schematic diagram of single matching section.

small values of attenuation  $A$ , satisfactory film sections can be designed.

With proper modifications, the same relations can be used for the design of a metal-film transformer section interposed between the

lossless line  $Z_1 = Z_0$  and a main attenuating film of total attenuation large enough to make it appear of infinite electrical length, as shown in Fig. 12-23. The condition for match is again given, with slight modifications, by Eq. (24), namely,

$$R_L = R_{12} + R_{23}e^{-2\gamma_2 s_2} = 0, \quad (29)$$

$$R_{23} = \frac{Z_2 - Z_3}{Z_2 + Z_3}, \quad R_{12} = \frac{Z_0 - Z_2}{Z_0 + Z_2}, \quad (30)$$

whereas the total attenuation of line section (2) is, in accordance with Eq. (27),

$$A_2 = \alpha_2 s_2 = 2\pi \frac{\lambda_0}{s_2} \cdot v_2. \quad (31)$$

By trial and error the complex equation (29) may be readily solved for the possible combinations of the pairs  $(v_2, u_2)$ ,  $(v_3, u_3)$ , and  $s_2/\lambda_0$ . The solutions are unique if the restriction of shortest possible length,  $s_2/\lambda_0$ , is imposed. For this condition the results are plotted in Fig. 12-24 and the over-all attenuation  $A_2$  follows from Eq. (31). It is observed that the length of the compensator approaches a quarter wavelength, and that  $v_2$  approaches  $\frac{1}{2}v_3$  as the resistances of both sections approach zero; these conditions are identical with those for the quarter-wave geometric-mean impedance transformer, and are to be expected. For

films of higher resistances, the length of the matching section increases beyond a quarter wavelength, and the ratio  $v_3/v_2$  increases rapidly, and becomes 6.5 in the range covered by the curve. The ratio of the resistance value per unit length in line section (3) to the value in section (2) increases at a rate even more rapid than  $(v_3/v_2)$ . This holds approximately for all attenuators with single matching sections.

An appropriate extension to  $n$  sections of metal film of different individual characteristics makes possible the design of more complex attenuator inserts for good matching conditions over broader frequency bands. In all cases, the trial-and-error method, if applied from the background of experience, yields the quickest results.

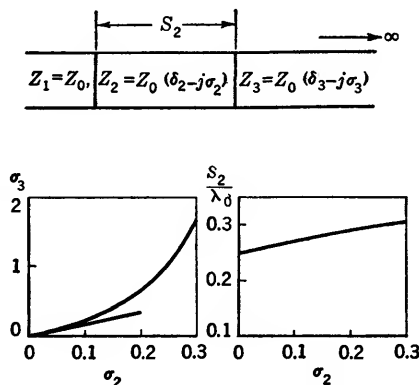


FIG. 12-24.—Attenuator design with single matching section.

**12-12. Construction of Coaxial Fixed Pads.**—A complete, fixed-value attenuator pad consists of the metalized-glass insert with metal bullets soldered to its ends for insertion into the metallic center conductor of the coaxial-line system; a support structure of the inner conductor; and a coaxial outer conductor or casing with suitable coupling elements with which to connect the pad rigidly to the adjoining line sections.

*Metalized-glass Inserts.*—Although several different methods have been developed for deposition of thin metallic films<sup>1</sup> on glass or similar nonmetallic carriers—for example, the Brashear and the Rochelle Salt methods of chemical deposition, cathode sputtering, spraying, and other methods—there are only two methods which by effective control provide the requisite precision for electrical applications: the burning-on method, and the evaporation method. Because of the broad range of its application, the burning-on method will be described in some detail here; the evaporation method will be discussed in Sec. 12-15.

The burning-on method of metal deposition has been known to china

<sup>1</sup> Strong, *Procedures in Experimental Physics*, Prentice-Hall, New York, 1943.

decorators and other artisans for a very long time; it is applicable only to noble metals, those metals that are reduced by heating. To form a resistive film on the glass, an oily solution of one of the metallic salts is painted, sprayed, brushed, or wiped on the glass. When heat is applied, the oil burns off and reduction of the salt occurs, leaving a metallic deposit on the glass. The glass is then heated to the softening point. This causes the deposit to form a compact adherent film on the glass. These films are mechanically sound; if they are formed on a clean glass surface they withstand considerable abrasion, are little affected by humidity changes, and retain good electrical characteristics. The ease with which such films are formed expedites production methods. The control of the resistance, however, is dependent on the metals used and upon their concentration in the original liquid coating, while the uniformity of the films is dependent on the method of application.

The most useful types of metallic solutions are those which contain mixtures of platinum and palladium with some rhodium. These are particularly useful for fairly high resistance values. For medium resistance values, platinum-gold solutions have been used, and for low resistances, pure platinum, gold, silver, or palladium solutions are available. Where it is necessary to make provisions for solderable connections, a paste of platinum-gold has been found most satisfactory. It is, however, not a thin film, and its resistance is negligible.

There are several ways in which the metallic solutions may be applied to the glass. In the case of tubing, four procedures have been tried: painting with a soft camel's-hair brush; spraying with an atomizer; drawing of the tubing through a cup filled with solution; and finally, applying by means of a saturated felt washer. Only the last-named method proved suitable for close and not too critical control of uniform film thickness. In this method, a felt washer is clamped between two metal washers. The diameter of the hole cut in the felt is about  $\frac{1}{8}$  in. less than the diameter of the glass tubing to be coated. The metal washers used are approximately 2 in. in diameter, with  $\frac{5}{8}$ -in. holes, and are clamped together with four machine screws which pass through one washer and are threaded into the other. The washers and screws are made of brass. The felt is saturated with the solution used, and the glass tube to be coated, after thorough cleaning of the glass surface, is forced through the hole in the felt. The tube is run up and down through the hole two or three times and is rotated slightly while the washer is held in a horizontal position and the tube is held in a vertical position. On the final passage, as the tube is being withdrawn from the washer, the speed of withdrawal is held as constant as possible. The rotation of the tube and the constant speed of withdrawal tend to cause a uniform coating on the tube. This method of coating is affected by many variables; for



example, the concentration of the solution, the degree of saturation of the felt, the number of times the tube is passed through the felt, the speed of passage, and, particularly, the speed of the final withdrawal. However, this method for experimental work has proved to be the most successful of the methods tried.

After the glass tube has been coated with the metallic solution, it is placed immediately on a rotating spindle in a drying oven maintained at a temperature of approximately 100°C. During this drying period, which lasts about 5 min., the volatile oils in the solution evaporate and leave the surface film dry to the touch. The tube is then placed on a rotating spindle and inserted into a firing oven where it is kept from 5 to 7 min. at a temperature of 650°–680°C; the length of time and the temperature depend upon whether a metallic solution or a paste has been used. The rotating spindles in this step ensure uniform heating and maintain the alignment of the tube. The rods which form the spindles must be of some material that can withstand these temperatures for the time required without appreciable softening and consequent bending. During this period in the oven, the metallic salts are reduced, and the metal is deposited and then bonded onto the semiplastic surface of the glass.

After proper cooling, the resistance of the film is measured. If it is too high, another coating may be applied to form a second metallic layer on the first, and bonded with it. If the resistance is too low, it is advisable to vary the concentration of the solution by the addition of thinning agents. If it is necessary to produce resistive films on glass tubing in sections with different resistance values, then the higher resistance film is formed first over the entire tube. The section which now has the final desired resistance is covered with masking tape, and the sections that are to have a lower resistance are coated with additional solution. The unit is dried again, the tape removed, and the film cleaned with carbon tetrachloride.

After a film or complex films of correct resistance have been attained, collars of platinum-gold paste are burned on at the ends of the glass tube, which has previously been ground to the correct over-all length. The collars formed by this paste can be soldered readily; thus, they serve as a means by which the resistive film can be soldered to metal connectors, and thereby form a complete unit which may be inserted in, or removed from, a section of a coaxial line.

It is apparent that the attainment of exact resistance values by this "hand method" is almost an art. For better economy, an adaptation of the evaporation method has been developed. This consists of placing a special mechanical drive into the bell jar which revolves the individual spindles carrying the glass tubes. Since the process of

evaporation and the vacuum system with the bell jar will be described in Sec. 12-15, the discussion here will be restricted to the mechanical setup for evaporation on glass tubing. The machine consists of a cage which supports twenty spindles, and which turns in a horizontal plane about a center line drawn vertically through the center of the base plate and, therefore, through the center of the filaments. The spindles have small gears at their inner ends which are meshed with a fixed bevel

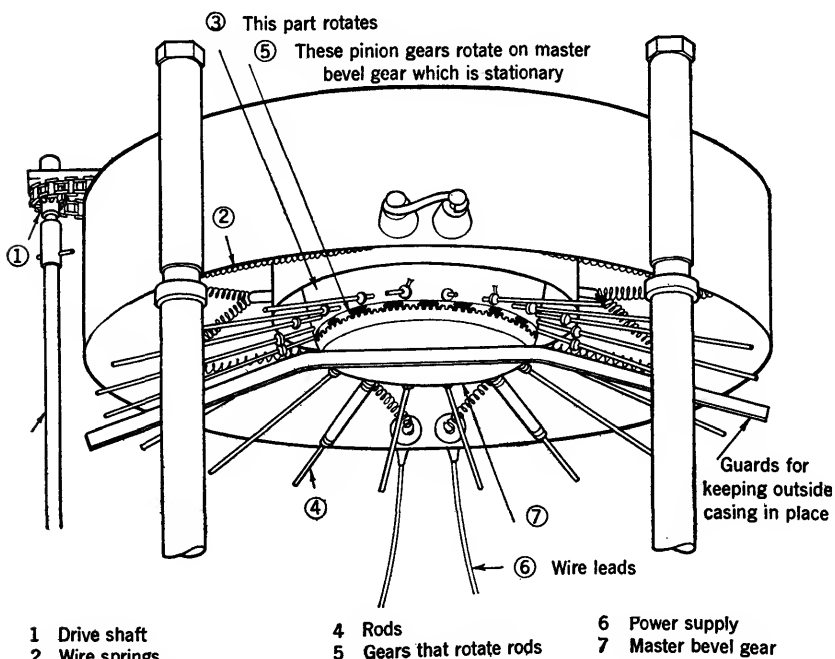


FIG. 12-25.—Mount for attenuator inserts in evaporation chamber.

gear. The supporting shaft of this bevel gear serves as the axis for the cage and spindles. The cage is turned by means of a chain drive which runs over a large sprocket wheel mounted over the cage and fastened rigidly to it, and also over a small sprocket wheel mounted vertically on a shaft offset to one side of the machine. To this small sprocket wheel is pinned a drive shaft that extends down, through a Wilson seal in the base plate, to a geared electric motor which drives it through a flexible coupling. When the cage is turned by the chain and sprocket drive, the spindles rotate on their axes and also revolve about their common center. The glass tubes, mounted on the spindles, are rotated on their axes and revolved, in a horizontal plane, about the central

vertical axis, and thus expose all of their outer surfaces to the molecular rays of the evaporating metal.

The assembly of this machine is shown in Fig. 12-25. In order to produce, in a single cycle of evaporation, a resistive film consisting of three sections—the end sections having a specified low resistance, and the center section a specified, relatively high resistance—a fixed mask made of curved sheet metal is mounted just beneath the spindles. The radial dimension of the mask is equal to that of the center section of the desired element, and its angular extent is about the same fraction of  $2\pi$  as the ratio of the resistances per unit length of the center and end sections.

*Assembly with End Connectors.*—As an example of the brass end connectors directly soldered to the metalized-glass insert, Fig. 12-26 shows the bullet for  $\frac{3}{8}$ -in.-diameter tubing and a midband frequency of 3000 Mc/sec. The cylindrical cup at the left end is the receptacle into which the collars at the ends of the metalized-glass tube are soldered. The outside wall of this cup is made very thin in order to minimize electrical reflections and to prevent an excessive strain on the glass as a result of the soldering process. To reduce still further the electrical effect of this increase in diameter, an adjacent corresponding decrease in diameter is provided. By this procedure, the voltage standing-wave ratio is reduced to less than 1.02 over a  $\pm 10$  per cent frequency band. The remainder of the bullet is so constructed as to connect into a standard-line inner conductor. A hole is provided in the bullet to permit the escape of gas which is formed during the soldering of the glass tubing.

In order that the metalized-glass inserts may be mechanically strong and may fit interchangeably into various coaxial-line systems, the soldering technique must meet three requirements; the bullets must form a strong bond with the glass insert to which they are soldered, the bullets must be axially aligned, and the length between the bullet shoulders at the ends of the inserts must be maintained to the correct tolerance. The last two requirements are best met by the use of special jigs.

*Protective Coating of Metalized-glass Inserts.*—Although the metallic films, as produced by the burning-on method, are quite rugged, they can

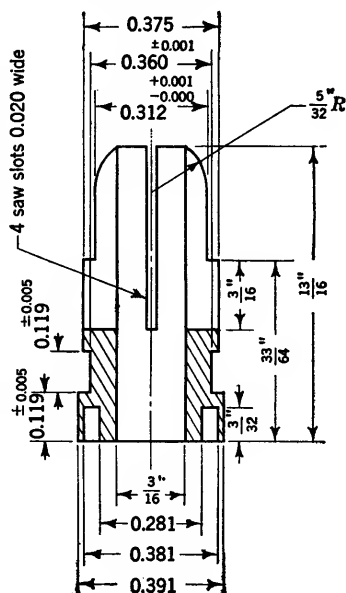


FIG. 12-26.—End bullet for metalized-glass insert of  $\frac{3}{8}$ -in. diameter.

be damaged by abrasion. To protect them during assembly in the casing that forms the outer conductor of the coaxial line, and to protect them from rough or thoughtless handling, a coat of wire varnish is usually painted on the completed element. This includes the glass tube with its metallic film and the soldered end connectors. This varnish is baked at 150°C for one hour, which causes it to set as a hard film that withstands all abrasion except that caused by sharp-pointed tools. It also serves as a protection against the effects of prolonged exposure to high humidity which might cause oxidation or corrosion of the metallic film. To prevent fungus growth which might occur in wire varnish if the units are to be used in tropical climates, a plastic, fungus-resistant varnish has been used. This also requires baking at 150°C.

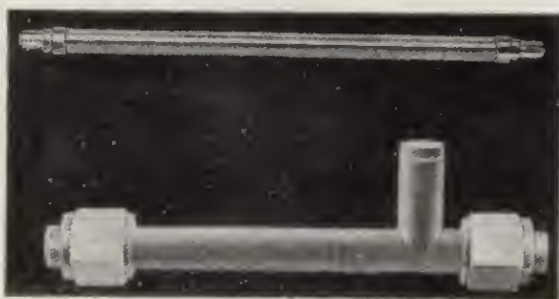


FIG. 12-27.—A  $\frac{1}{2}$ -in. coaxial-line attenuator and insert.

If the metal films have been formed with proper attention to the cleanliness of the glass surface and if care has been taken in all operations of coating, baking, and firing, these films are mechanically strong and can withstand considerable abrasion; they cannot be rubbed off the glass. Dirt, or contamination of the glass surface or of the solution, is always evidenced in poorly bonded films that are easily removed from the glass. A well-formed, well-bonded metal film resists removal by any means except forcible removal by a sharp-edged instrument. The metallic films are not permanently affected, either mechanically or electrically, by thermal changes between  $-50^{\circ}$  and  $150^{\circ}\text{C}$ , the baking temperature of the varnish. The temperature coefficient of resistance of the films has an average value of 0.0007 per degree C; slight variations probably result from differences in the composition of the solutions used.

*Complete Assembly of Coaxial Pads.*—The over-all length of the casing is short enough to be convenient and still ensure broadband operation. In the case of the  $\frac{5}{8}$ -in.-line and the  $\frac{7}{8}$ -in.-line units, casings of two types have been designed. One type has only one broadband (Pound) T-support as shown in Fig. 12-27; this casing is particularly convenient when frequent interchange of the attenuator elements is

desired. The other type of casing uses two broadband T-supports as shown in Fig. 12-28; this casing is recommended for standard attenuators which have been carefully calibrated and are to be used as reference attenuators. The small  $\frac{5}{8}$ -in.-line casing is made only as a complete unit, with the insert already bead-supported inside the casing. The construction is mechanically very rugged, and is shown in Fig. 12-29.

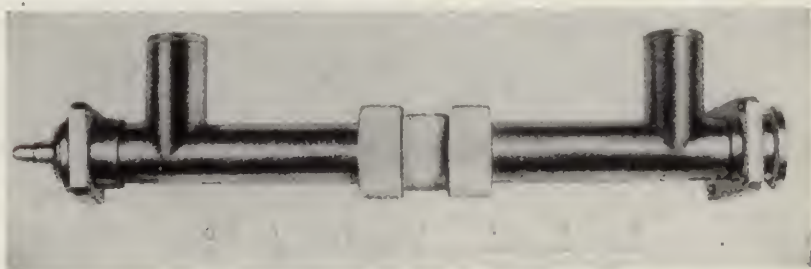


FIG. 12-28.—Standard coaxial attenuator.

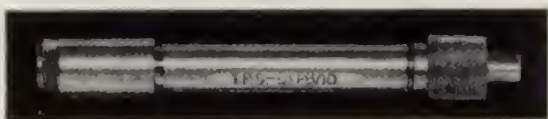


FIG. 12-29.—A  $\frac{5}{8}$ -in. coaxial-line attenuator.

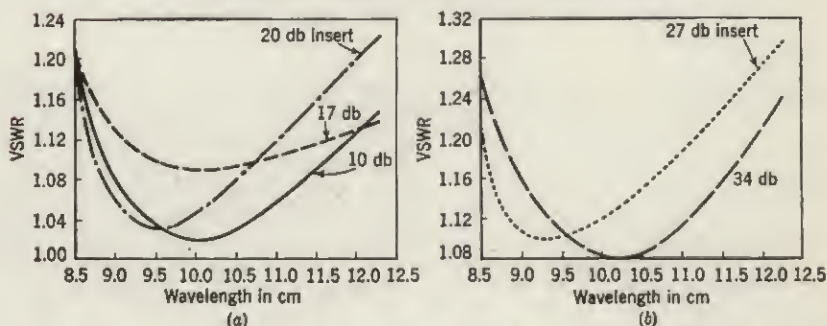


FIG. 12-30.—Voltage standing-wave ratio vs. wavelength of attenuator inserts for  $\frac{1}{4}$ -in. coaxial line.

All casings are provided with the proper coupling elements and they can be inserted easily in transmission systems of standard size.

**12-13. Performance Characteristics of Fixed Coaxial Pads.**—The most important characteristics of attenuators for broadband use are the variations of the voltage standing-wave ratio and of the attenuation with frequency. Their power capacity is also of considerable interest. The attenuator pads for  $\frac{7}{8}$ -in. coaxial line, which are used principally as laboratory units for precise measurements, have been studied in con-

siderable detail. As illustration of the results, Fig. 12-30, shows the variation, with wavelength, of the voltage standing-wave ratio for pad inserts designed for different values of attenuation. Each insert has a total film length of one wavelength at a center frequency of 3000 Mc/sec. Each curve represents an average of four measurements of voltage standing-wave ratio taken on a pair of attenuators; the voltage standing-wave ratio is measured at each end of the attenuator with a matched terminal at the output. Single-stub casings with especially low standing-wave ratios were used with each insert. The inaccuracy of the measurements is probably less than  $\pm 0.03$  in VSWR. The shape of the curves approximates that which is predicted theoretically. Since these attenuator inserts originally were designed for a  $\pm 10$  per cent frequency band, the performance is quite satisfactory. The inserts for higher values of attenuation have a center film of rather high specific resistance, and therefore nonuniformities in production tend to have a greater effect upon the resultant standing-wave ratio than at lower values of attenuation.

For these laboratory attenuators the variation of attenuation with frequency is very nearly linear. For the pads mentioned above, attenuation was very accurately measured at nine different wavelengths, ranging from 8.5 to 12.3 cm (3530 to 2440 Mc/sec). Straight lines could be drawn through the experimental points with less than  $\pm 0.1$  db deviation for any one point. The data at 8.5 cm and 12.3 cm are given in Table 12-8 with the measured slope and the theoretical slope calculated from the design theory.

TABLE 12-8.—ATTENUATION VS. WAVELENGTH FOR  $\frac{3}{8}$ -IN. COAXIAL-LINE ATTENUATORS

Nominal attenuation value, db	Measured attenuation in db		Measured slope, db per cm change of wavelength	Calculated slope, db per cm change of wavelength
	At 8.5 cm (3530 Mc/sec)	At 12.3 cm (2440 Mc/sec)		
10	9.9	9.7	0.05	0.05
10	11.0	10.6	0.10	0.05
17	16.6	15.7	0.20	0.20
17	17.1	16.1	0.20	0.20
20	20.0	18.6	0.30	0.33
20	21.5	20.3	0.40	0.33
27	28.0	25.8	0.60	0.65
27	29.5	27.2	0.60	0.65
34	35.4	32.4	0.80	0.95
34	36.0	33.0	0.80	0.95

The measured values are in good agreement with the calculated values. It can be observed that the frequency sensitivity increases with the attenuation value. This effect can be noted by comparing two 17-db units, connected in tandem so as to give 34 db, with a 34-db unit. The frequency sensitivity of the two 17-db units is 0.40 db/cm, whereas for the 34-db unit it becomes 0.80 db/cm, or twice that for the tandem connection.

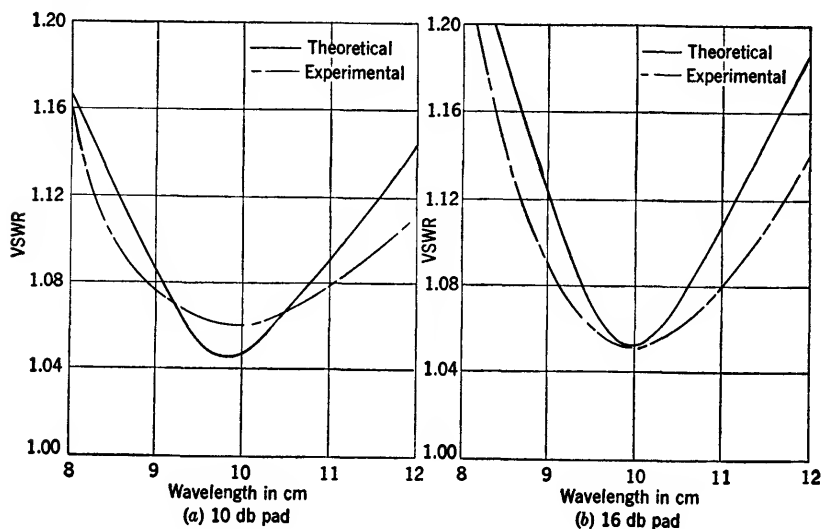


FIG. 12-31.—Wavelength vs. voltage standing-wave ratio for a  $\frac{5}{16}$ -in. coaxial line pad.

The attenuator pads for  $\frac{5}{16}$ -in. coaxial line, which are used principally in field instruments, have end-connectors in the form of cable fittings of essentially narrow-band design. To study the frequency sensitivity of these attenuators, the effects produced by the inserts must be distinguished from those produced by the casing. Fig. 12-31 shows the voltage standing-wave ratio vs. wavelength for the metalized-glass inserts of attenuation values of 10 and 16 db. These inserts were tested in special casings which permitted the evaluation of the performance of the inserts alone, and excluded the reflections of the cable fittings and the associated bead structures. Here, also, two inserts of each type were tested, which permitted four voltage standing-wave-ratio measurements per type to be averaged. The inaccuracy of measurement is considered to be less than  $\pm 0.03$  in VSWR. In addition to the experimental data, calculated curves are drawn according to the design theory of Sec. 12-11. Since the design is based on film length of one wavelength at a center wavelength of 10 cm, the agreement between theory and measurement

can be considered satisfactory. However, the cable fittings add reflections, particularly at the ends of the wavelength band, and consequently the over-all voltage standing-wave ratio of the completed pad may show

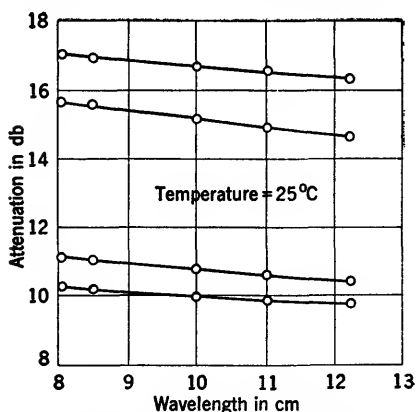


FIG. 12-32.—Attenuation vs. wavelength of inserts for  $\frac{1}{8}$ -in. coaxial line.

values up to 1.34 either at the short or at the long wavelength end, depending on the type of cable fitting used. This demonstrates the frequency limitation of the existing cable fittings, which with proper redesign will eventually be removed.

For the same attenuator pads, Fig. 12-32 shows the attenuation as a function of frequency, obtained by very careful measurements. Within experimental error, these curves can also be approximated by straight lines.

The data on the rate of variation of attenuation with wavelength are given in Table 12-9. For use over rather broad frequency bands, a smaller frequency sensitivity would be required, and a better voltage standing-wave ratio would be needed. This indicates a need for a design which is basically new and on such a design work has already been begun.

TABLE 12-9.—ATTENUATION VS. WAVELENGTH FOR  $\frac{1}{8}$ -IN. COAXIAL-LINE ATTENUATORS

Nominal attenuation value, db	Measured slope, db per cm change of wavelength	Calculated slope, db per cm change of wavelength
10	0.15	0.1
10	0.10	0.1
16	0.25	0.3
16	0.20	0.3

With a film length of about two and one-quarter wavelengths, attenuation inserts for use at a center frequency of 9091 Mc/sec have been designed and built. An insert of this type has a considerably lower attenuation value per wavelength, which, according to Sec. 12-11, is a basic quantity for the electrical design. As a result, a lower voltage standing-wave ratio can be expected for the insert. However, for this insert also, the end connectors are of the cable-fitting type and, therefore, are inherently frequency-sensitive. Special improved end-fittings have been designed to reduce this frequency sensitivity, but the principal



requirement that they should mate with the existing cable connectors so restricted the freedom of design that only limited gain could be achieved. Thus, for ten samples of the 20-db unit, and six samples of the 10-db unit, the average voltage standing-wave ratio for the complete units with the improved casing was measured with the results given in Table 12-10.

TABLE 12-10.—VSWR vs. WAVELENGTH FOR ATTENUATORS FOR  $\frac{1}{16}$ -IN. COAXIAL LINE

Nominal attenuation value, db	VSWR values at		
	wavelength 3.5 cm (8570 Mc/sec)	wavelength 3.3 cm (9091 Mc/sec)	wavelength 3.1 cm (9680 Mc/sec)
10	1.21	1.17	1.20
20	1.10	1.10	1.14

The insert for the 10-db unit has no impedance-matching sections (compensators), and consequently has a VSWR of approximately 1.08 at the longest wavelength. For this reason, the 10-db units exhibit, on the average, a somewhat higher voltage standing-wave ratio than the 20-db units which do have compensators. From the design theory it is also predicted that only a slight variation in the voltage standing-wave ratio should occur over the frequency band and this contention is supported by the results of measurements.

For these same attenuators, the variation of attenuation over the frequency band of  $\pm 6$  per cent is theoretically predictable as about  $\pm 0.02$  db for the 20-db unit; measurements indicate practically unobservable variation of attenuation. This excellent result stems from the choice of the length of the attenuator inserts and suggests the possibility of further improvements.

*Effect of Ambient Temperature.*—If coaxial attenuators are used as standards in the laboratory, or if they are used over widely varying temperatures in the field, consideration must be given to the attenuation of the unit as a function of temperature. Although the temperature coefficient of resistance of the metal film is small, it is appreciable. The temperature coefficient of the film material of the main section is measured as 0.0006 per  $^{\circ}\text{C}$ , while that of the compensator is 0.0008 per  $^{\circ}\text{C}$ , for the majority of attenuators. With these values, the performance may be calculated as summarized in Table 12-11. The performance is substantially independent of line size and of the frequency at which the attenuators are used.

Attenuator inserts produced by means of the evaporation process (see Sec. 12-12) should be insensitive indeed to large variations in tem-

perature, since the nichrome film obtained by this process has a very low temperature coefficient, about  $\frac{1}{10}$  of that of the burned-on films for which the above data are valid.

The effect of ambient-temperature changes upon the match characteristics of all coaxial attenuators is negligible.

TABLE 12-11.—EFFECT OF AMBIENT TEMPERATURE

Nominal attenuation value of units, db	Change in attenuation, db per 10°C rise in ambient temperature
10	+0.080
17	+0.124
20	+0.136
27	+0.167
30	+0.180
34	+0.196

*Power Capacity.*—In order to check the power capacity of the matalized-glass attenuators, tests of two types were made. In the first test, the power was increased slowly to the point of failure; this is a slow, tedious, and costly test, and invariably ends in the destruction of the unit. From the results of tests of this type it can be concluded that inserts of proper uniformity for  $\frac{5}{16}$ -in. coaxial lines at a center frequency of 3000 Mc/sec will withstand one watt of average power under any condition of pulsed operation; and attenuators for large line sizes will withstand larger amounts of average power, at least in the ratio of the insert diameters. In the second test, units were subjected to specified values of power and the number of failures were recorded. The results of tests on units for  $\frac{5}{16}$ -in. coaxial line and center frequency 3000 Mc/sec are summarized in Table 12-12:

TABLE 12-12.—POWER TEST OF ATTENUATORS

Attenuation value, db	Number of units tested	Number of failures with 1.5 watts con- tinuous r-f power	Number of failures with pulse power
20	4	0	1
16	5	0	0
10	5	0	1

In the 14 units tested by applying 1.5 watts of c-w power, no failures occurred. These 14 units were then tested at 1.0 watt average power with a pulse length of 1.0  $\mu$ sec, and a repetition rate of 1000 cps. Two failures occurred. The fact that two units failed on 1 watt average power at a thousand-cycle repetition rate, after withstanding 1.5 watts of average continuous power, indicates that the pulse-power application is the more critical test.

Because of the reflections at the intersection of the first impedance-matching section (compensator) and the main film section, the current is not exponentially distributed along the metallic film. In the case of the 20-db insert one wavelength long, the theoretical distribution of the current was determined. The calculations show that in the first centimeter of the compensator the current remains virtually constant. This corresponds to the experimental fact that a large majority of the failures occur in the first centimeter of the leading end of the attenuator.

The actual failure of an insert is initiated by an arc which forms along its surface, travels at a rapid rate completely around the insert, and burns off an insulating ring. A d-c continuity test quickly indicates the failure which is always complete. The failure also causes bad mismatch and consequently the attenuation becomes appreciably higher.

All power tests so far described were restricted to attenuators which were not artificially cooled. With water cooling, sufficient to keep the temperature of the film to within several degrees of room temperature, 1 kw of continuous power has been dissipated in a film of 50-ohm resistance and of 3-in. length. This might indicate that the temperature rise of the film has an effect on the breakdown power.

*Power Attenuators.*—Under proper conditions the metallic films used in these attenuators can withstand considerable power. Special attenuators have been designed for powers ranging up to 30 watts average. This has been done by extending the length as far as convenient, and by arranging a low-attenuation section in front of a high-attenuation section. As a result, a large fraction of the power, about one-half, is absorbed in the first section. Such a design is necessary since the exponential decrease in voltage in a section of film causes most of the power to be dissipated in the leading parts of the film. For a special application at 7000 Mc/sec, an attenuator was designed in which the first section of 6-in. length had an attenuation of 6.67 db, whereas the second section, also of 6-in. length, had an attenuation of 13.33 db.

If air cooling can be arranged, the conventional 20-db unit in  $\frac{1}{8}$ -in. coaxial line, one wavelength long, at 3000 Mc/sec, can withstand continuous power up to 20 watts. For this high-power application, rather thick, low-resistance films are used. If an accurate knowledge of the attenuation is desired the attenuator must be calibrated against power.

**12-14. Variable Metalized-glass Coaxial Attenuators.**—The principle of very thin metal films on glass tubing as inner conductor of a coaxial system is also applicable to variable attenuators if a mechanism is arranged for effectively short-circuiting a part of the metal film. Two possible solutions have been suggested. In the first solution, a metal rod is inserted into the metalized-glass tubing from the far end of the attenuator, and coupling takes place through the glass wall to the metal

film; the attenuation is varied by varying the position of the metal rod. In the second solution, the short-circuiting member is a close-fitting metal tube which slides over the metalized-glass element and which is insulated from the metal film by a layer of varnish in order to avoid uncertain metallic contact.

The chief advantage of a metalized-glass variable attenuator lies in the possibility of a very low minimum attenuation of from 2 to 5 db, attained by permitting the movable element to short-circuit the entire attenuating metal film. In order to achieve this low loss and yet maintain a low input voltage standing-wave ratio to the attenuator at all positions of the movable metallic element over a reasonably broad frequency band, special types of matching were developed.

The input impedance to a long section of the main attenuating metal film was given by Eq. (12) and was seen to be complex. Broad-band matching of the main film to a lossless line can, therefore, be obtained only by lossy matching elements, and again, two solutions have been found. In one case, there is interposed a short section of line which has a center conductor, the resistance of which varies gradually from zero to the resistance of the attenuating film. Such a transition film, or resistance-tapered transformer, provides a very good match in both directions over a wavelength band of  $\pm 5$  per cent, the VSWR being generally less than 1.05. In the other case, a film of uniform thickness is used, but applied in longitudinal stripes varying in width and number according to the required resistance. A resistance-tapered transformer of this type gives as good results as the first one, and is considerably simpler to apply. It is evident that these transformers absorb considerable power, but this is desirable in an attenuator.

*A  $\frac{5}{8}$ -in.-line Variable Attenuator.*—For application in a range near 3000 Mc/sec, a laboratory attenuator has been developed for rather coarse measurement work in  $\frac{5}{8}$ -in. coaxial line as shown in Fig. 12-33. Designed for use with type N connectors, its casing is made of standard  $\frac{5}{8}$ -in. line. The tubular element is made of glass coated with metal resistive film and is terminated at both ends by brass bullets whereby it is supported between a solid T-joint and a hollow joint. Through the center of the hollow joint and into the interior of the element is inserted the short-circuiting rod the motion of which is controlled by a rack and pinion. A central coupling unit is provided to facilitate installation of the element. The end shown on the left side of Fig. 12-33 is called the input end of the instrument. The tapered adaptor and the T-support are of proved design, therefore the first source of possible reflection is met at the input end of the element. A proper metal-film transformer is therefore inserted at that end. Reflections from the back end of the attenuator are generated both at the end of

the element and at the end of the sliding rod. The shape of the tip of the rod that gives the best results is that of an inverted cone as shown. A tip of this shape causes reflections which partially neutralize the

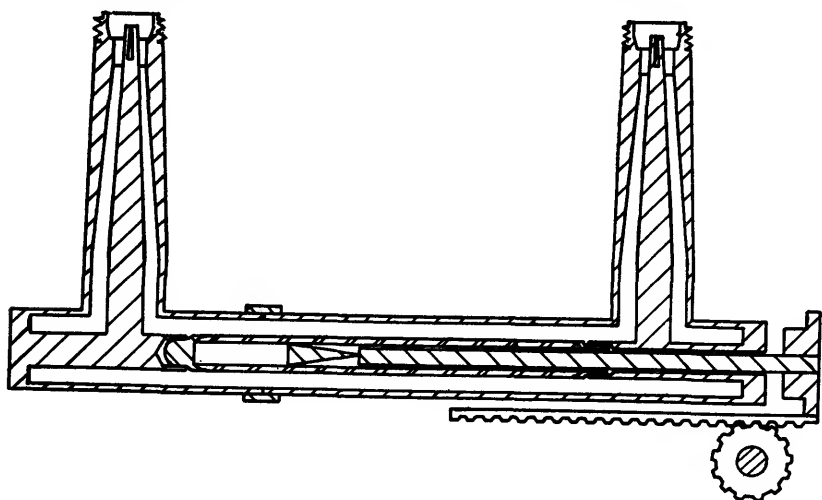


FIG. 12-33.—Schematic section of  $\frac{1}{8}$ -in. coaxial variable attenuator.

reflections at the end of the element. The compensation, however, is more or less imperfect according to the position of the slider, leading to variations in VSWR between 1.0 and 1.45. The total attenuation can be made to vary between 5 and 50 db, in a nearly linear manner over a considerable range.

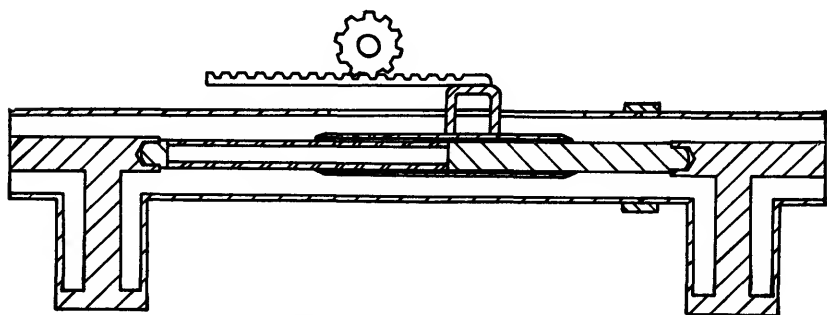


FIG. 12-34.—Schematic section of  $\frac{1}{8}$ -in. variable attenuator.

*A  $\frac{1}{8}$ -in.-line Variable Attenuator.*—For precise laboratory measurements, an attenuator in a  $\frac{1}{8}$ -in. coaxial line has been developed and has served both as a standard attenuator and as a general laboratory instrument. A schematic section is shown in Fig. 12-34. The element

consists of a metalized-glass tube equipped with brass-bullet terminals by which it is supported between two T-joints at the ends of a length of standard size  $\frac{7}{8}$ -in. line. Fitting over the element is a thin-walled metal tube or slider which serves to short-circuit the required length of the film on the element. This slider is controlled from the outside by a rack-and-pinion mechanism attached to it by an insulating handle which passes through a longitudinal slot in the outer conductor. The mechanism is concealed and protected by suitable metal covers and the only exposed moving parts are the control knob and the pointer by which the setting is indicated on an engraved scale.

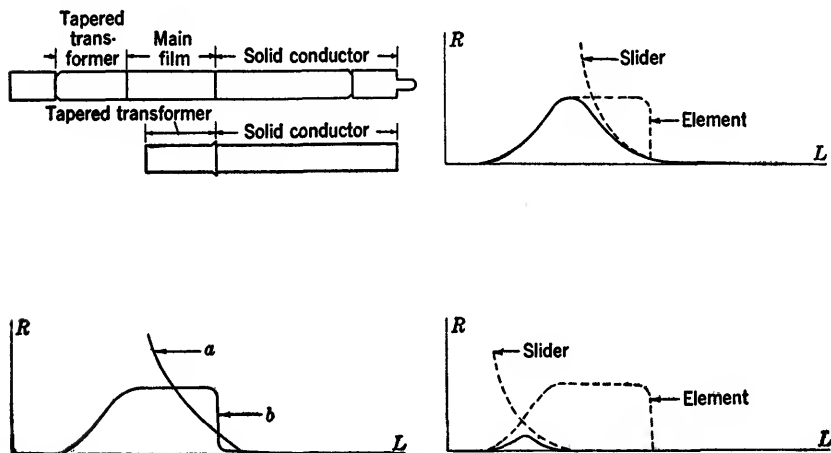


FIG. 12-35.—Diagrams to illustrate the matching of a variable coaxial-line attenuator. The curve at the upper right shows the combined resistance of element and slider at the position of maximum attenuation. On the lower left are the resistance characteristics of the slider (curve  $a$ ) and the element (curve  $b$ ). The curve at the lower right is the combined resistance at the position of minimum attenuation.

In this attenuator, the element is coated with metal film so as to produce the resistance distribution shown in Fig. 12-35. To the slider Fig. 12-34, is attached a short glass tube with stripes of film to form a tapered transformer as shown in the photograph, Fig. 12-36, and therefore the resistance distribution of the sliding system becomes as shown in Fig. 12-35. The slider transformer lies directly over the film of the element and the two films are separated only by a layer of baked enamel; consequently, at the frequencies employed the capacitance between them is very great. Therefore, the resistances of the two films may be added in parallel combination. If this be done, it is found that the effective resistance characteristic of the element and the slider combined is as shown in Fig. 12-35. But the characteristic there shown is simply that of a section of attenuating line joined at both ends by

tapered resistance transformers to normal lossless lines. The combination is therefore well matched in both directions even though the slider be moved, for this motion only varies the length of the central flat portion of the curve. When the slider system is moved all the way forward and the whole length of the uniform portion of the element film is covered by the metal slider, then the two tapered transformers are together, but



FIG. 12-36.—Slider assembly for  $\frac{3}{4}$ -in. variable attenuator.

face in opposite directions. Their added characteristic is as shown in Fig. 12-35 and is equivalent to two tapered transformers back-to-back with no intermediate attenuating line. A distinct advantage of the design is here evident, for the added characteristic, in this setting of minimum attenuation, shows that a very low insertion loss may be expected.

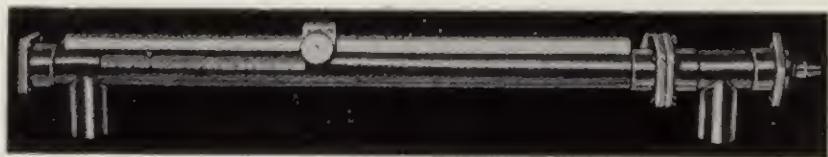


FIG. 12-37.—Side-outlet  $\frac{3}{4}$ -in. variable attenuator.

In Fig. 12-37 is shown a photographic view of the assembled attenuator with end sections that permit power flow into, and out of, the attenuating element at right angles to the element. The performance of an average standard unit is summarized by the following data: maximum attenuation, 40 db; minimum attenuation, about 3 db; VSWR less than 1.25 in both directions, at all settings and throughout a wavelength range of  $\pm 10$  per cent; power capacity, 10 watts continuous. A typical calibration curve shown in Fig. 12-38 indicates a parabolic variation of

attenuation with position of the slider, which is convenient if uniform relative accuracy of attenuation measurement is desired.

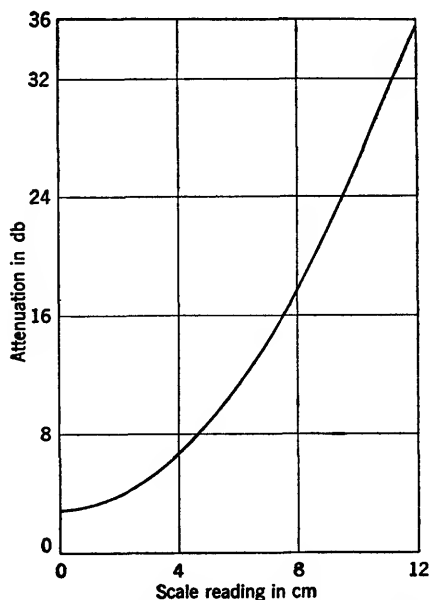


FIG. 12-38.—Calibration of typical  $\frac{7}{8}$ -in. coaxial variable attenuator.

**12-15. Design of Elements for Waveguide Attenuators.**—The use of metalized glass as a dissipative element in waveguide transmission systems is most convenient in the form of thin glass plates; usually, these plates carry metal film only on one side, and are suspended in the waveguide with the film parallel to the electric field lines. In the simplest construction, the glass plate has one or two holes drilled along its long center line and is cemented to one or two metal struts. These struts penetrate the guide wall, preferably at right angles to the electric field lines. These struts can, in turn, be made to move and carry the glass plate across the waveguide, as in the variable waveguide attenuators.

The most reliable cement to use in this construction is Sauereisen<sup>1</sup> Insalute Cement No. 1. It shows strong cohesion and permanence, easy applicability, and cold-drying qualities. Although this cement is not waterproof, a thick coating of Glyptol cement will minimize any detrimental effects from moisture. Humidity tests on cement-held plates of this type without the Glyptol coating have shown a "breathing" effect as large as  $\pm 0.002$  in. within several hours, during which time

<sup>1</sup> Made by Sauereisen Cements Co., Pittsburgh, Pennsylvania.



the relative humidity varied from 20 to 80 per cent. Although this effect apparently cannot be completely eliminated, the Glyptol-coated cement showed not only less but greatly retarded action. Figure 12-39 shows, schematically, the glass as it is cemented directly to continuous struts going completely across the waveguide.

A much more satisfactory method of fastening the glass plate to the waveguide struts was developed by the Corning Glass Works. First, instead of drilling holes, which always causes slight chipping and thus weakens the glass section, Corning used a very fine gas flame to burn out or melt out the holes; the sides of these holes are perfectly smooth and fire-polished, and have a small crater of glass which actually strengthens the glass locally. Second, Corning designed German-silver eyelets as shown in Fig. 12-40 which are crimped onto the glass by special jigs; these eyelets permit soldering to the struts, which now have to be of solderable material. Shock and vibration tests on plates mounted

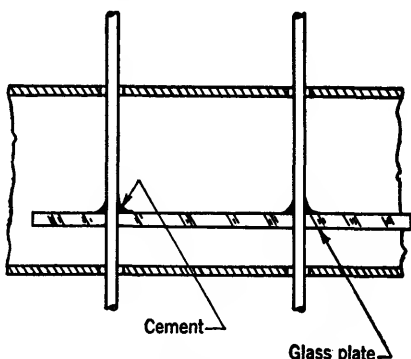


FIG. 12-39.—Cement mounting of glass plate in waveguide.

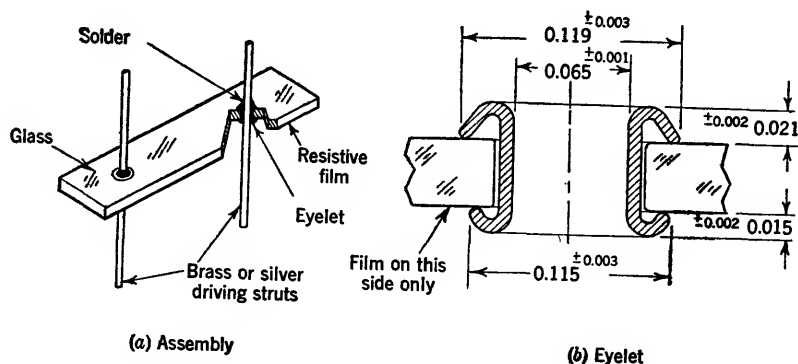


FIG. 12-40.—Eyelet mounting of glass plate on waveguide struts.

by this method have given completely satisfactory results; the effects of temperature and humidity are also eliminated.

*Metalization of Glass Plates.*—The metalization of the glass plates can be done by different chemical or mechanical processes of metal deposition. Utmost uniformity, together with the close control of thickness for the

proper rate of attenuation, can, however, be attained only with the evaporation process.<sup>1</sup>

In the evaporation process, the pieces to be coated with film are placed in an airtight chamber. In this chamber, and at a considerable distance from the pieces, is a heating element to which is attached a sufficient quantity of the material desired for the film. The chamber is evacuated to a low pressure during which time the filament is heated, which in turn melts and volatilizes the material to be evaporated. Molecular particles of the material deposit on relatively cool surfaces, and form a thin film. The amount of material required to produce a film of known resistance, and the rapidity at which it is formed, can be easily controlled by varying the temperature of the filament. The resistance of the film formed can be measured continually throughout the process by means of clips fastened to a glass plate placed in the chamber. Leads from the clips, brought out from the chamber through insulated and vacuum-tight seals, can be connected to an ohmmeter or other resistance-measuring device. By this means, the resistance of the film formed can be continually followed throughout the process, and the process can be stopped when the exact value of resistance is attained. The films formed on glass by this process are very adherent, are of considerable uniformity, and have excellent electrical properties for microwave work.

The equipment needed for evaporation of metals or nonmetals has already been described in detail in available literature.<sup>2</sup> The first, and most obvious, unit of equipment is a large, high bell jar with an accompanying oil diffusion pump and forepump. The pumps must have sufficient capacity to exhaust the bell jar fairly rapidly to an ultimate pressure of  $10^{-4}$  to  $10^{-5}$  mm Hg and they must have an ionization gauge for measurement of low pressures. To heat the filaments, a controllable power source, either d-c or a-c, of low voltage and high current is needed. This source is most conveniently provided by a low-voltage power transformer controlled by means of a Variac in the primary circuit. The glass plates should be supported from 10 to 15 inches above the filaments. As the distance between the filaments and the plates increases the degree of uniformity of deposition of the metal evaporated increases. The base plate of the vacuum system should be equipped with as many insulated and vacuum-sealed binding posts as are required to satisfy the demands for electrical connections within the bell jar.

It appears reasonable, at first, to use the noble metals, gold, platinum,

<sup>1</sup> A. A. S. Moore, "Production of Semi-reflecting Films of Chromium on Plane Mirrors," *J. Sci. Instrum.*, Vol. 22, June 1945.

<sup>2</sup> J. Strong, *Procedures in Experimental Physics*, Prentice-Hall, New York, 1943.

and silver, for evaporation because of their immunity to oxidation and corrosion. However, in order to obtain a reasonable amount of electrical resistance of the film, the thickness of the film needs to be only a few times greater than the molecular diameter. For example, consider a film of platinum having a resistivity of 100 ohms per square and evaporated onto a glass plate 5 cm long and 1 cm wide. The resistance from end to end is then 500 ohms. Since

$$R = \frac{\rho l}{A} = \frac{\rho l}{wt}, \quad (32)$$

in which  $R$  is the resistance in ohms,  $\rho$  the resistivity in ohm cm,  $l$  the length of film,  $w$  the width of film, and  $t$  the thickness of film, then, under the assumed conditions

$$t = \frac{\rho l}{wR} = \frac{9.83 \times 10^{-6} \times 5}{1 \times 500} = 9.83 \times 10^{-8} \text{ cm} = 9.83 \text{ \AA}.$$

This is an extremely thin film, approximately 5 molecules in thickness. Films of this thickness are difficult to obtain and are usually unstable. Of various metals and alloys which were tested, the most useful was found to be the resistive alloy nichrome. Films prepared by evaporation of nichrome exhibit the high resistivity and also the low temperature coefficient of resistivity which are characteristic of nichrome in bulk. The thickness of a nichrome film of the same type and value as that chosen in the above example is, however,

$$t = \frac{\rho l}{wR} = \frac{100 \times 10^{-6} \times 5}{500} = 100 \times 10^{-8} \text{ cm} = 100 \text{ \AA}.$$

This film is approximately 50 molecules in thickness and is very stable. The only difficulty in producing uniform films of such resistance alloys arises from the large amounts of nickel that they contain. Nickel, when melted, dissolves most other metals, particularly the high-melting-point metals, such as tungsten, molybdenum, and others, which are suitable for use as heater elements in the evaporation process. This might cause a disintegration of the heater before a film of sufficient thickness is deposited, and furthermore, the dissolved heater material is also evaporated and has an adverse effect on the electrical properties of the film. It is, therefore, necessary to use tungsten wire of excessive thickness as a heater and a larger quantity of nichrome than is actually required for the film, so that, when it melts, the tungsten is coated with a nichrome layer so thick that a satisfactory film can be formed before tungsten has time to diffuse through the nichrome layer to the surface.

Because of the extreme thinness of the film, even the slightest deterioration of the surface seriously alters the resistance of the film. It is

therefore necessary to apply by evaporation a protective coating to the metal film before removing it from the vacuum. Magnesium fluoride was found to be the most convenient material for this purpose because of its low temperature of volatilization. A very thin coating of magnesium fluoride not only protects the metal film completely from chemical deterioration but, because of the great hardness and strength, it also prevents accidental mechanical injury of the film.

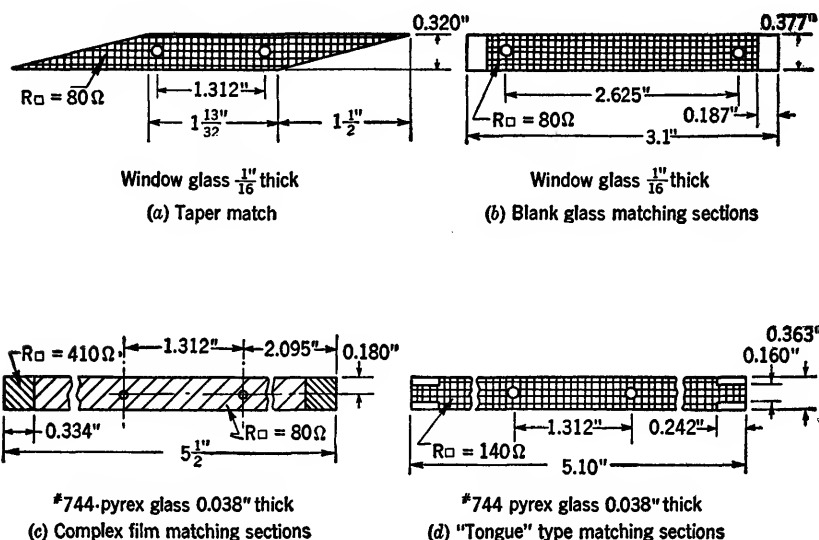


FIG. 12-41.—Types of matching of metalized-glass plates.

If all precautions have been taken in cleaning the surface of the plates, or tubes, the film deposit has considerable adherent strength. The combination of the film and the protective coating of magnesium fluoride which covers it has such great strength that ordinary abrasion from rubbing does not scratch the film; indeed, only a very sharp instrument pressed hard against the film, can penetrate the coating and damage the film. Further, since the fluoride coating completely covers the metallic film, the films are unaffected by change of humidity. The films also after having been subjected to temperature changes between  $-50^\circ\text{C}$  and  $150^\circ\text{C}$  show no permanent change in their resistance. Within this temperature range the temperature coefficient of resistance has been repeatedly checked and has an average value of  $6 \times 10^{-5}$  per degree C.

**Matching Characteristics of Glass Plates.**—Most attenuators require, in addition to stability, that the input impedance to the unit be almost equal to the characteristic impedance of the line or waveguide used. Unless the metallic-film resistance is very high and the supporting glass

dielectric is very thin, resistive plates will not match well without a transition or matching section preceding the active attenuating element. Four separate types of transitions, or matching sections, have been developed for use on the glass plates which are shown in Fig. 12-41. Two kinds of glass, either window glass  $\frac{1}{8}$  in. thick or 0.038-in. No. 774 Pyrex glass, are used for all plates. Some of the matching arrangements prove more satisfactory with one of the glass types.

The possibilities of the taper match are perhaps most apparent. The taper section in Fig. 12-41 is actually a transition section and depends

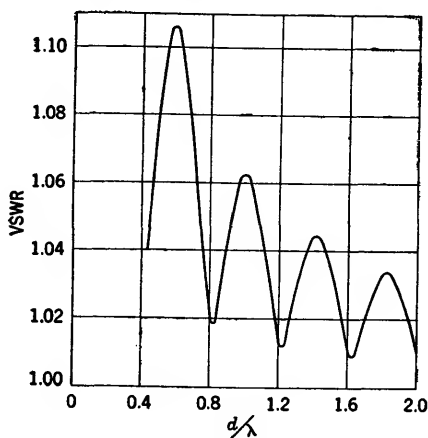


FIG. 12-42.—Variation of voltage standing-wave ratio with length of taper.

for match upon a small rate of transition, or change in characteristic impedance, per wavelength. The response curve shown in Fig. 12-42 is common for most taper transition sections and shows the variation of match as the taper is increased to several wavelengths in length. Film resistance, the dielectric constant of glass, and the thickness of the glass determine for a given wavelength the length of taper required for best match. Window-glass plates, with the relatively high dielectric constant  $k_e = 7$ , usually require a shorter taper than the Pyrex-glass plates. As an example of the results that can be expected with soft glass, plates 0.375 in. wide with a film resistance of 80 ohms per square and a taper length of  $1\frac{1}{4}$  in. can be made to have VSWR's of less than 1.1 in a waveguide of 0.400 by 0.900 in. ID and over a frequency band of  $\pm 6$  per cent centered near 9000 Mc/sec. In fact, the VSWR can be below 1.1 for all positions of the plate in the guide, a very desirable characteristic for application in variable attenuators.

In order to reduce the length of the matching sections, the transformer shown in Fig. 12-41b has been developed for window-glass plates.

The theoretical details for this type of match have not been fully explored; it is known, however, that the blank glass present in the guide changes locally the characteristic impedance, which, together with the effective reactance provided by the shunt field distortion at the front edge of the glass, is apparently capable of matching window-glass plates with metal films which have a resistance of 100 ohms per square. This matching arrangement is most useful in narrow-band, variable attenuators. The dimensions have to be specifically determined for each frequency.

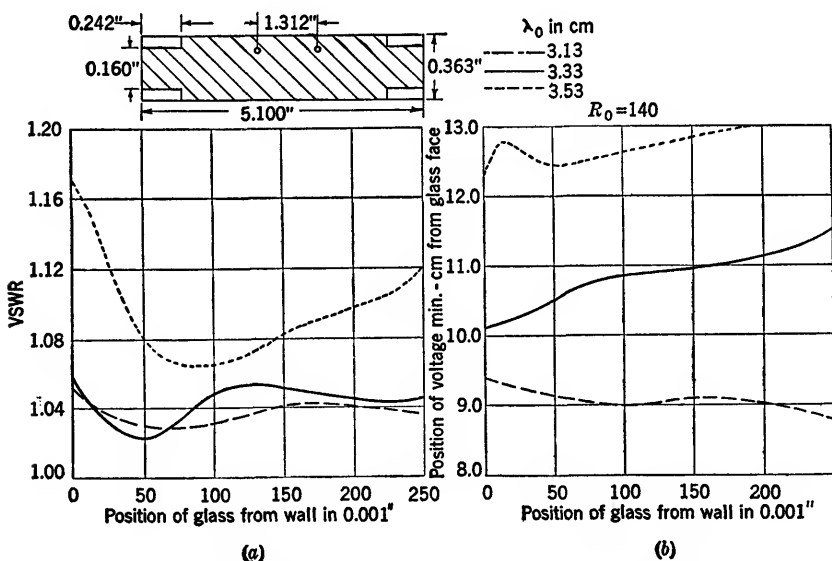


FIG. 12-43.—Impedance data for tongue-matched Pyrex plate.

The "complex film" transforming section shown in Fig. 12-41c is most useful for very thin Pyrex plates. The length and the resistance of the film transformer sections are determined experimentally. As an example, a main-film resistance of approximately 140 ohms per square could be matched by a transformer length of 0.330 in. with a matching-film resistance of approximately 400 ohms per square over a frequency range of about  $\pm 6$  per cent centered at 9000 Mc/sec if used in a waveguide of 0.400 by 0.900 in. ID. The need of different film resistances on the same plate makes the use of the evaporation technique imperative. In order to metalize the element, the transforming sections are shielded, and the main section is evaporated first. When metalization has been completed, the shields are removed and the transformer section coated to the proper resistance. Since, for the second evaporation, the main

section is not shielded, two parallel coatings of resistive film exist in the main section, separated by a film of magnesium fluoride.

For broadband match on thin Pyrex plates a matching section of the type shown in Fig. 12-41*d* has proved to be the most satisfactory. The tongue section is made by suitable masking during evaporation. It provides a transforming section with a complex characteristic impedance similar to the complex film match. Film resistance is uniform, however, and the tongue width determines the difference in characteristic impedance between the matching and the main sections. The critical transformer dimensions have to be determined experimentally and

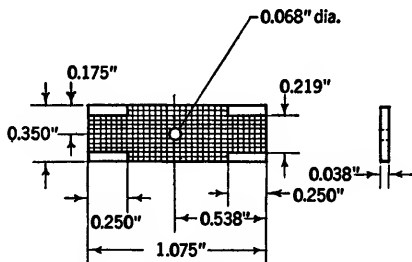


FIG. 12-44.—TMX-18PB film specifications.

differ for different film resistances of the main section. The broadband input impedance data for a typical plate using a match of this type are shown in Fig. 12-43 for a rectangular waveguide of 0.400 by 0.900 in. ID and used over a band of  $\pm 6$  per cent with a center frequency of 9000 Mc/sec.

**12-16. Waveguide Pads of Fixed Values.**—In the study of the dependence of attenuation at various frequencies on the position of a metalized-glass plate within the waveguide, it has been found by careful measurements

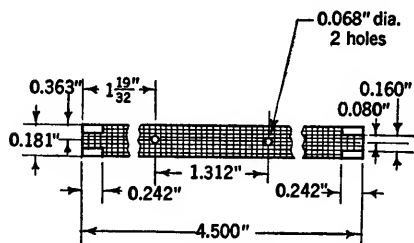


FIG. 12-45.—TMX-16PB film details.

that there exists a region of minimum frequency dependence of attenuation over a broad frequency band at a distance of about  $a/8$  from the side wall of the guide. Usually, the glass plate carries the metal film facing the nearer side wall and the distance is measured from the film surface to the wall. If a properly designed glass plate is

located in this region of minimum variation of attenuation with frequency, particularly desirable fixed waveguide pads are obtained, which can be used as calibrated attenuation "gauge blocks" to extend the range of power meters without appreciable loss of accuracy.

Figure 12-44 shows the dimensions of a metalized-glass plate which gives an attenuation of 3 db in a waveguide of 0.400 by 0.900 in. ID when spaced 0.1 in. from the side wall and supported by a strut which, for mechanical reasons, extends completely across the waveguide. The design of the matching sections of this plate must take into account not only the match to the main attenuating film itself, but also the fact

that the main-film section is very short, has low attenuation, and therefore has an input impedance which depends on the termination of the pad. In addition, the supporting strut presents a local capacitive susceptance of appreciable value (see Sec. 12-18). Under these conditions, the accurate measurement of attenuation becomes an important problem

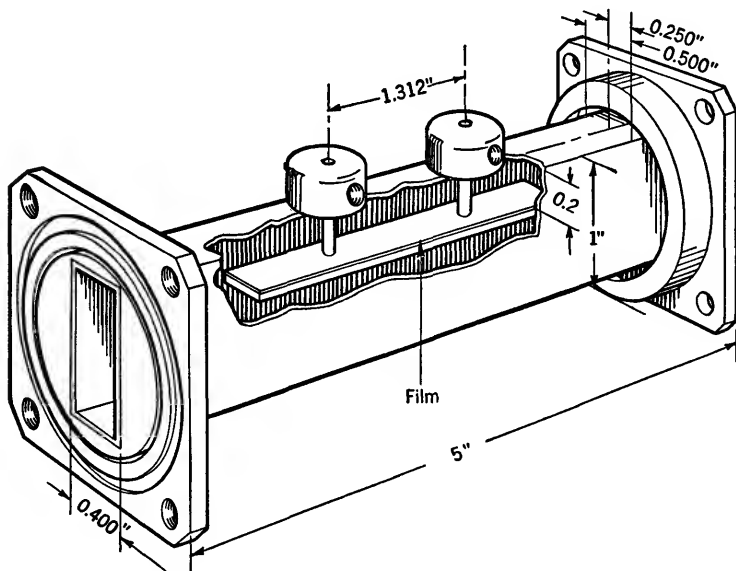


FIG. 12-46.—TMX-81PB fixed attenuator in casing.

and is discussed further in Chap. 13. Variation of attenuation with frequency over a 6 per cent band, centered at 9000 Mc/sec, is less than 0.2 db, and thus this pad makes a very accurate gauge block to establish the half-power point for measurements of  $Q$ . To demonstrate the influence of the positioning of the plate upon the variation of attenuation with frequency, a special casing was constructed with a fine micrometer drive and the same plate moved successively to positions giving 3, 4, 5

TABLE 12-13.—VARIATION OF ATTENUATION WITH FREQUENCY FOR DIFFERENT POSITIONS OF THE SAME PLATE

Position of plate	$\lambda = 3.13$ cm	$\lambda = 3.33$ cm	$\lambda = 3.40$ cm	$\lambda = 3.53$ cm	Spread of attenuation
3 db	3.03 db	2.97 db		2.86 db	0.17 db
4 db	4.0	4.0		3.7	0.30
5 db	4.90	5.01		4.50	0.51
6 db	6.1	6.0	5.67 db	5.55	0.55



and 6 db of attenuation at 9000 Mc/sec. The variation of attenuation with frequency is shown in Table 12-13, and the variation of the voltage standing-wave ratio is given in Table 12-14. For accurate measurements of voltage standing-wave ratio, it is also important to observe the effect of the coupling flanges, which cause additional frequency sensitivity beyond that of the metalized-glass plate itself. This effect is evident from the results given in Table 12-14.

Another example of the advantageous use of the frequency-insensitive region is the design of the metalized-glass plate shown in Fig. 12-45. This design is for a fixed waveguide pad of attenuation values between 25 and 30 db. In this case, the matching section can be designed to match the main film. To improve the voltage standing-wave ratio, the two struts used to support the plate do not continue beyond the glass plate, as shown in Fig. 12-46. The performance of this attenuator over the frequency band from 9000 to 9470 Mc/sec is given in Fig. 12-47 and shows particularly low voltage-standing-wave-ratio values for attenuations above 20 db.

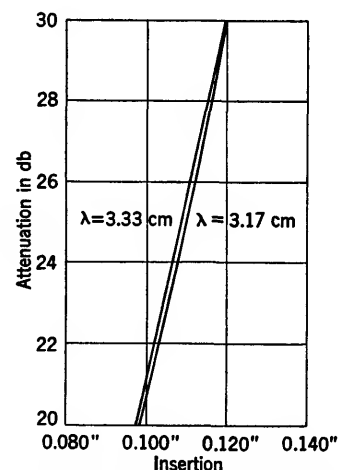
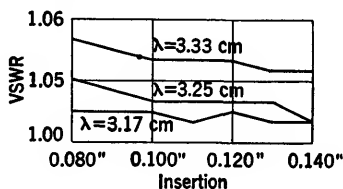


FIG. 12-47.—TMX-16 attenuator characteristics vs. insertion.

TABLE 12-14.—VARIATION OF VOLTAGE STANDING-WAVE RATIO WITH FREQUENCY FOR DIFFERENT POSITIONS OF THE SAME PLATE

Position of Plate	Direction of measurement*	$\lambda = 3.13$ cm	$\lambda = 3.33$ cm	$\lambda = 3.53$ cm
3 db	Choke end	1.065	1.041	1.055
	Flange end	1.03	1.062	1.079
4 db	Choke end	1.082	1.064	1.042
	Flange end	1.065	1.065	1.082
5 db	Choke end	1.09	1.10	1.045
	Flange end	1.07	1.105	1.09
6 db	Choke end	1.11	1.10	1.08
	Flange end	1.10	1.145	1.12

\* Casing was furnished with one choke and one flange coupling. For "choke" reading, attenuator is coupled in through flange-choke combination. For "flange" reading, the coupling is through a flange-flange joint.

**12-17. Construction of Variable Waveguide Attenuators.**—In principle, the construction is of the same type for variable waveguide attenuators with metalized-glass inserts as for laboratory attenuators which use carbon paints or deposits on dielectric carrier plates (see Sec. 12-10). However, the driving mechanism for variable attenuators incorporating metalized-glass plates must be of considerable precision in order to avoid the imposition of undue mechanical stresses upon the glass. The result-

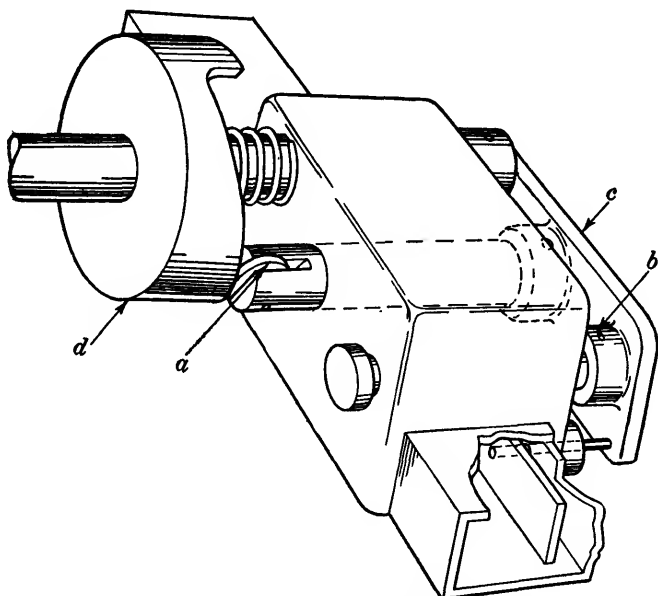


FIG. 12-48.—Cam drive for variable attenuator.

ing accuracy of positioning the dissipative metal film, together with the stability of the film itself, make these variable attenuators almost necessarily of the precision type suitable for permanent calibration.

The distinguishing features of the variation of attenuation have resulted in the development of three principal methods for the constructing of attenuators. These methods are incorporated in the single-vane type shown in Fig. 12-48, the double-vane type shown in Fig. 12-49, and the guillotine type, with either one plate in the center as shown in Fig. 12-50, or two plates symmetrically located, as shown in Fig. 12-51.

*Single-vane Attenuators.*—In attenuators of the single-vane type, two struts, accurately aligned, carry the single metalized-glass plate across a part of the guide. Special bosses on the side walls of the waveguide casing provide bearings as seen at *b* in Fig. 12-48. The actual driving

pin *a* is carefully aligned with the two struts and is attached to a heavy plate *c* which carries these struts. The driving pin in this model<sup>1</sup> is driven by a cam *d* against a restoring spring located within the superstructure. For accurate setting, the camshaft carries an engraved dial,

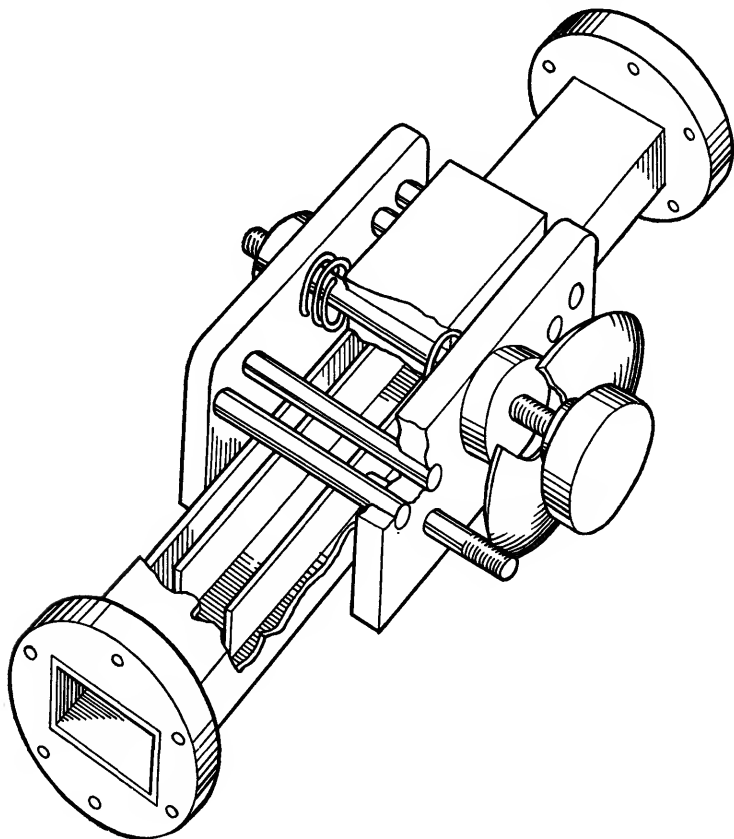


FIG. 12-49.—Double-vane attenuator.

while a gear-set vernier is usually attached directly to the casing. The cam drive has the advantages that the driving pin can be located in the center plane between the struts and that the cam can be designed to linearize the attenuation curve. It has the disadvantage, however, that any noticeable play of the camshaft makes resetting difficult. As an example, a metalized-glass insert designed for a maximum attenuation of 75 db in a waveguide of 0.400 by 0.900 in. ID has a change of attenua-

<sup>1</sup> This cam drive was designed by Philharmonic Radio Corporation, New York, N. Y.

tion of 0.8 db for each mil of displacement which occurs near a position corresponding to 66 db total attenuation. Obviously, the construction must be sufficiently sound to permit the resetting of the plate to small

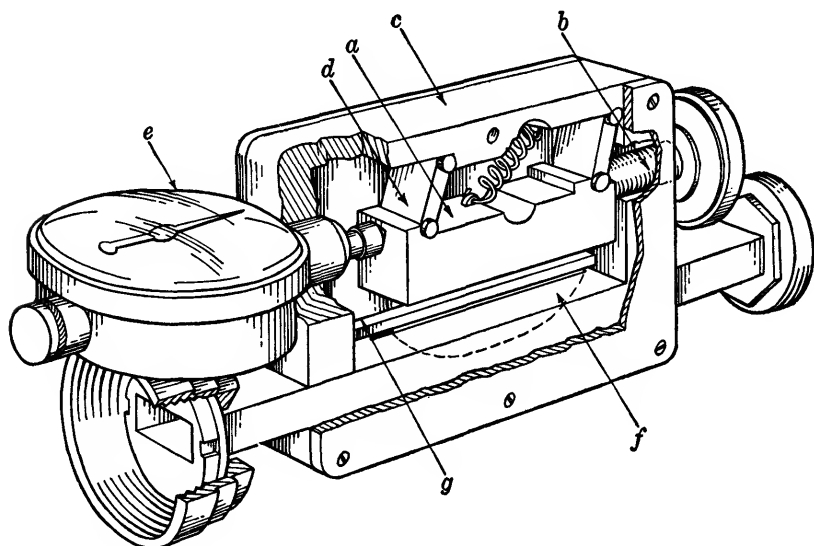


FIG. 12-50.—Precision 1-cm-band variable attenuator, TPK 35/PB/40.

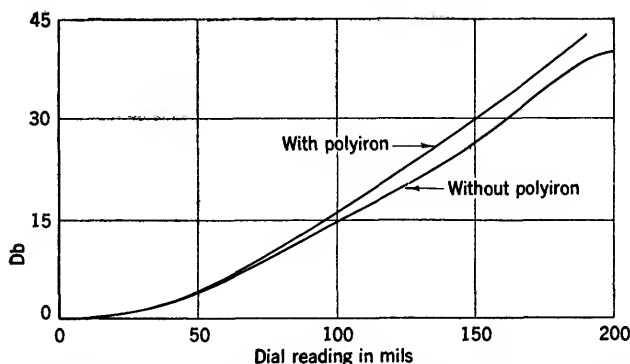


FIG. 12-51.—Effect of polyiron on attenuator loss. The ordinate scale is in decibels above the minimum insertion loss.

fractions of one mil. Frequently, a cam follower is built into the main pin *a* to avoid friction and wear; however, this follower must be accurately round in order to avoid errors in case of slippage. Furthermore, the restoring spring action must be strong enough to prevent the main pin from sticking when the cam is turned from higher to lower attenuation.

The cam drive can be replaced by a multithread screw drive.<sup>1</sup> The driving pin carries a very heavy plate, and the plate carries the struts supporting the glass plate. A guide pin keeps the plate from rotating or becoming misaligned. This casing is simple to construct, has directness of drive, and is easily reset. Hence, it has been widely used for attenuators where careful calibration is needed.

Instead of a dial and vernier, a micrometer drive can be installed and the position of the plate can be read on the micrometer head. Or, a counter device can be connected to the driving pin which has a fine screw thread so that each revolution corresponds to one mil advancement of the plate into the guide.

Another important consideration in the design of casings of the vane type is the exact spacing of the supporting struts. The strut-spacing tolerance and glass-hole-spacing tolerance must be kept small to permit ease of plate mounting. The struts should at no time exert undue pressure on the glass plate because pressure may cause breakage. This entails equal and exact strut spacing for all plate positions in the guide. It is important that no r-f power leak from the drive openings in the waveguide walls. Tests have shown little power leakage from the small  $\frac{1}{16}$ -in. driving holes in attenuators of the vane type. Although it is possible to provide small polyiron bushings to absorb the small leakage power, in most cases this is not necessary.

*Double-vane Attenuator.*—From theoretical considerations of the field distribution in the waveguide it can be shown that a symmetrical arrangement of two glass plates in the waveguide leads to a smaller voltage standing-wave ratio than is possible with a single glass plate, and it also results in a decreased frequency sensitivity of attenuation. Figure 12-49 gives a schematic view of the construction needed if two metalized-glass plates are driven simultaneously from opposite sides of the waveguide towards the center. The supporting struts cannot in this case extend across the waveguide. Although this construction affords an electrical advantage the mechanical construction is considerably weaker than the construction when one plate is used. For large plates, advanced far into the guide, the danger of mechanical resonance with impressed vibrations exists. This construction, therefore, has not been used for field-test attenuators.

*Guillotine Attenuators.*—An entirely different principle of variation of attenuation is the insertion of a metalized-glass plate through a slot in the broad side of the waveguide. Figure 12-50 shows the construction of a single-plate attenuator, for a center frequency of 24,000 Mc/sec, with a shape resembling that of a guillotine blade. On the broad side of the waveguide a frame *c* is built. From this frame the carrier *a* is

<sup>1</sup> Designed by F and R Machine Works, Long Island City, New York.

suspended by links  $d$  which are held in the bearing surfaces of the frame by a pair of strong springs. As a special feature of this construction, the glass plate  $f$  mounted on the carriage block  $a$  moves in the arc of a circle as the drive screw  $b$  is turned. During a constant turning of the drive screw, the vertical insertion of the glass in the guide is at first rapid, but its speed gradually tapers off as the glass swings to the lower extremity of the arc. If the dial indicator  $e$  is used, horizontal rather than vertical movement is measured. The form of variation of attenuation with plate insertion, combined with the nonlinear characteristic of the precision drive, results in an attenuation calibration which is nearly linear and which affords accurate setting.

Since the slot through which the glass plate is inserted is located in a region of strong electric field, the inserted glass acts as an antenna, and causes power to leak into the cavity formed by the attenuator casing. Thus energy is shunted from the main waveguide path, and the maximum attenuation obtainable is limited to the attenuation of this shunt path. In order to prevent this leakage, a frame of polyiron  $g$  is mounted on a metallic reinforcement of the top wall of the waveguide. Figure 12-51 demonstrates the effectiveness of the polyiron choking. Without polyiron, the maximum attenuation is about 40 db. The variation of the attenuation of the leakage path with glass insertion alters the shape of the calibration curve.

This single-plate guillotine attenuator can be contrasted with a double-plate guillotine attenuator of the symmetrical or balanced type.<sup>1</sup> Two plates are mounted on a common carrier as shown in Fig. 12-52. The carrier is driven by a cam which is mounted on a fixed frame of the casing, while the cam follower is affixed to a vertical structure of the carrier. Guidance is provided by a pin to avoid rotation about the vertical axis. Precise construction of this attenuator casing is necessary in order to avoid rocking of the carrier and to maintain strong contact between cam and cam follower. In order to avoid the shunt leakage provided by the metalized-glass plates, a polyiron frame closely surrounds the slots. Without this polyiron frame, the maximum attenuation obtainable is about 50 db, while with this frame, attenuation values up to 80 db can be obtained with very small variation of attenuation over a frequency band of  $\pm 6$  per cent centered at 9000 Mc/sec.

*Mechanical Tests on Attenuators.*—In many practical applications of attenuators, it is necessary that the complete attenuators withstand not only mechanical shock and vibration tests, but also corrosion tests under salt sprays. The cement mounting of the glass plates is satisfactory under dry conditions, but will not withstand salt spray. The

<sup>1</sup> Designed by Sperry Gyroscope Company, Garden City, N. Y.

eyelet mounting as described in Sec. 12-15 is completely satisfactory under all test conditions.

The mechanical strength of the glass plates might be a matter of concern under severe test conditions, particularly for long plates such as shown in Fig. 12-41*d*. For calculations on the strength of the cross section about the  $\frac{1}{8}$ -in. mounting hole, it was assumed that the plate was rigidly clamped at the point of strut support with a 4.8-cm length of

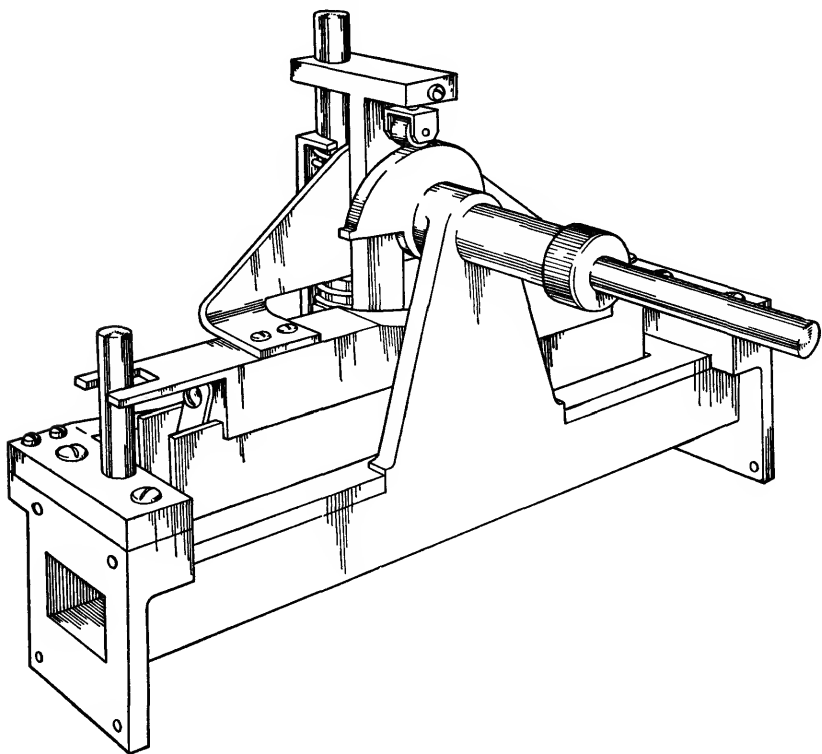


FIG. 12-52.—Double-plate guillotine attenuator.

glass extending out from the support. These calculations show that glass is strong enough to withstand the stress imparted by a sinusoidal vibration of the glass and the mounting with a maximum acceleration of  $430g$ . The impressed vibration must have a frequency well below the natural frequency of 281 cps of the 4.8-cm length of extending glass. Static tests made on eleven plates with holes showed them to break when the stress applied corresponded to an acceleration of  $200g$ . This reduction from the theoretical strength is probably caused by small fractures and strains in the glass.

Dynamic shake tests have been made on plates supported outside of casings, as well as on plates mounted in commercial casings of the type shown in Fig. 12-48 which use both cement and eyelet mounting. The shake tests were made by securely fastening the samples to the table of a vibration fatigue-testing machine.<sup>1</sup> In operation, the table had a sinusoidal vibration with a periodic change of frequency of from 10 to 50 cps over one-minute periods. Each sample was tested for vibration, in the plane of the glass and perpendicular to the plane of the glass, for

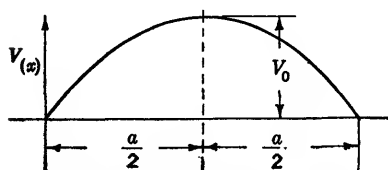
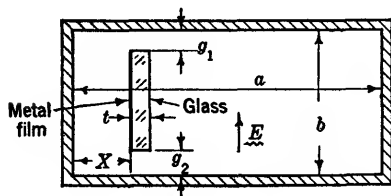


FIG. 12-53.—Coordinate system for circuit representation of attenuator.

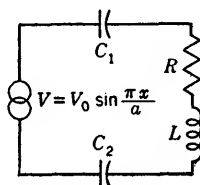


FIG. 12-54.—Simplified lumped-circuit representation of metal film in waveguide.

wall and with the plate out in the center of the guide. There was no glass breakage nor did the joint between the glass and strut become loose. Several of the casings, however, were shaken so violently that the set screws on the drive mechanism were loosened, and indicated the necessity for cementing the set screws securely. Shock tests were conducted by directing severe hammer blows against a table on which the complete test set was mounted. No harm was done to the glass plates. Thus, with proper methods of mounting, the metalized-glass attenuators can be used as field instruments as well as for laboratory instruments.

**12-18. Performance Characteristics of Variable Waveguide Attenuators.**—It is possible to devise a simple equivalent circuit for the dissipative action of an attenuator vane in a waveguide, and to explain, in a nearly quantitative manner, the variations of attenuation with the resistance of the metallic film, the position of the film in the guide, and the relative width of the glass plate carrying the film. Thus, if a transverse electric field is assumed, the designations in Fig. 12-53 used, and the current per unit length in the metallic film in the direction of the electric field

<sup>1</sup> Model 10-HA, manufactured by All-American Tool and Mfg. Company, Chicago, Ill.



defined as  $I$ , a shunt impedance to the local effective voltage  $V$  can be supposed as in Fig. 12.54. The resistance  $R$  and the inductance  $L$  are parameters per unit length of the resistive film, and the value of  $L$  varies with the plate position in the magnetic field of the guide. The condensers  $C_1$  and  $C_2$  represent the effective gap capacitances between the metalized-glass plate and the metal guide and depend inversely upon the gap values  $g_1$  and  $g_2$  and the resistance  $R$  of the film, since they represent the fringing effect of the electric field. This lumped-circuit representation is far from complete, but does allow for the possibility of the occurrence of resonance, which explains, at least partially, some of the attenuation characteristics experimentally observed.

Defining the effective voltage as

$$V = V_0 \sin \frac{\pi x}{a}, \quad (33)$$

and assuming, as a rough approximation,

$$\begin{aligned} L &= L_0 \sin \frac{\pi x}{a}, \\ C &= C_0 \frac{R_0 g_0}{R} \sin \frac{\pi x}{a}, \end{aligned} \quad (34)$$

where  $L_0$ ,  $R_0$ ,  $g_0$  and  $C_0$  are quantities either empirically determined from tests or semiempirically determined from qualitative considerations, the current through the metallic film is

$$|I| = \frac{|V|}{|Z|} = \frac{V_0 \sin \frac{\pi x}{a}}{\left[ R^2 + \left( \omega L - \frac{1}{\omega C} \right)^2 \right]^{1/2}}$$

and the dissipated power per unit length is

$$|I|^2 R = \frac{V_0^2}{R_0} \cdot \frac{\left( \sin \frac{\pi x}{a} \right)^2}{\left( \frac{R}{R_0} \right) + \left( \frac{L_0}{R_0^2 C_0} \cdot \frac{g}{g_0} \right) \left( S - \frac{1}{S} \right)^2}, \quad (35)$$

where

$$S = \omega \sqrt{L_0 C_0} \sqrt{\frac{R_0 g_0}{R}} \sin \frac{\pi x}{a}. \quad (36)$$

It is readily recognized that resonance occurs at the position  $x_0$  for which

$$\sin \frac{\pi x_0}{a} = \frac{1}{\omega \sqrt{L_0 C_0}} \cdot \sqrt{\frac{R}{R_0 g_0}}, \quad (37)$$

and that this resonance point is dependent on the width of the plate, on the resistance  $R$ , and on the frequency  $\omega/2\pi$ . No resonance exists if the right-hand term in Eq. (37) is larger than unity.

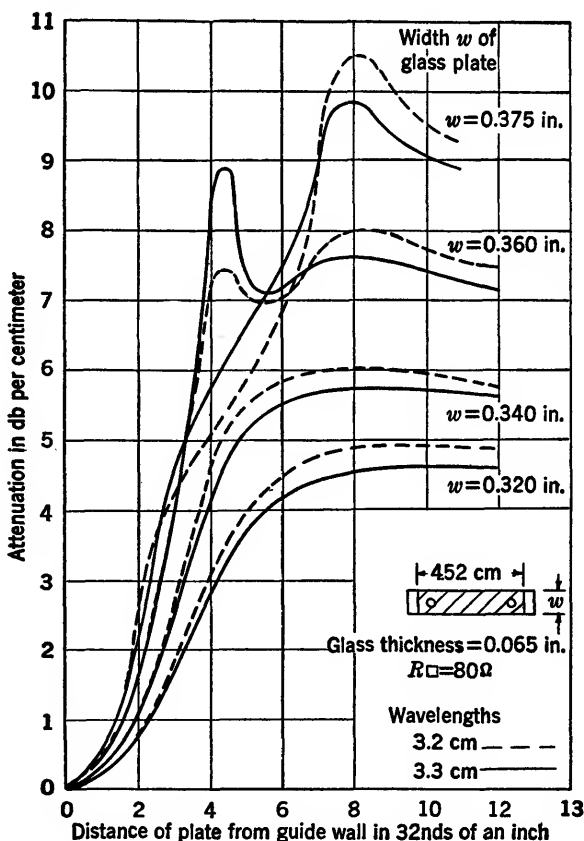


FIG. 12-55.—Attenuation characteristics of soft-glass vane coated with metallic film.

Figure 12-55 shows the measured values of specific attenuation of a metalized plate of soft glass in a waveguide the inner dimensions of which are 0.4 by 0.9 in. The match characteristics, over all tested values of width and for both frequencies, were good, with a VSWR of less than 1.15 even at the point of resonance, and therefore no possibility of a reflective resonance effect need be considered. The curves illustrate shift of resonance with increasing gap values  $g$ ; they show the proper variation with frequency, and indicate that, in choosing a glass width for a certain film resistance, combinations close to resonance must be avoided. The change of attenuation with frequency usually becomes

large for plate widths near resonance. However, for some applications with the plate fixed in position, the attenuation-frequency crossover points caused by resonance can be used to reduce the variation of attenuation with frequency.

The curves in Fig. 12-56 illustrate the effect on attenuation, for various positions in the guide, as the film resistance is varied. The resistance

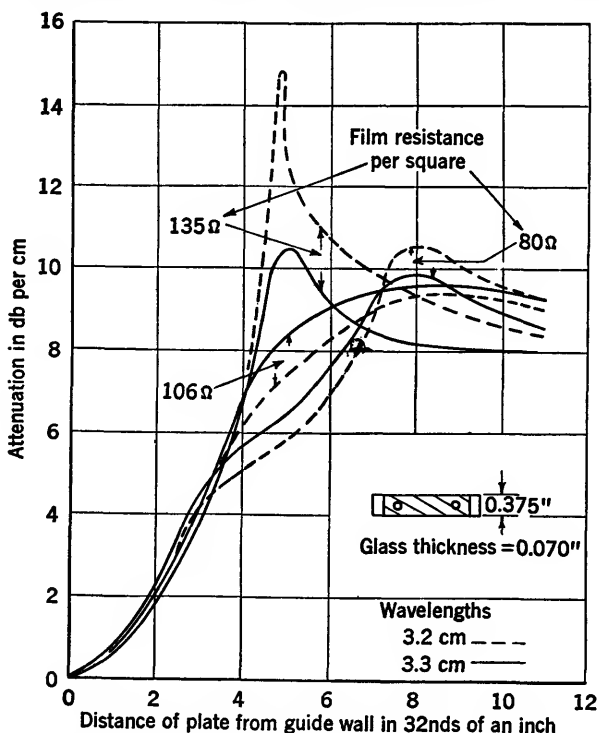


FIG. 12-56.—Attenuation characteristics of soft-glass vane coated with metallic film.

values shown are only approximate, since the metal films were not completely uniform. The shape and frequency characteristics of the curves justify the tentative acceptance of the equivalent series-resonant circuit. Thus, for a resistance of 135 ohms per square at a wavelength of 3.2 cm, the attenuation of the plate approaches the value for cutoff waveguide at the position corresponding to the cutoff width of the guide formed by the metal film and the larger section of the guide. As the plate moves out into the guide, the value of the attenuation decreases. However, a more complete equivalent circuit would be necessary to explain the shape of the attenuation curves of wide plates with a resistance of 80 ohms per square, particularly the hump in the curve at lower attenuation.

As an example of the over-all performance of a particular metalized-glass-plate design, Fig. 12-57 gives the voltage standing-wave ratio and the attenuation characteristics of the plate shown in Fig. 12-58. The design is for a frequency of 9000 Mc/sec, or a wavelength of 3.33 cm, and the inner dimensions of the waveguide are 0.4 by 0.9 in. The

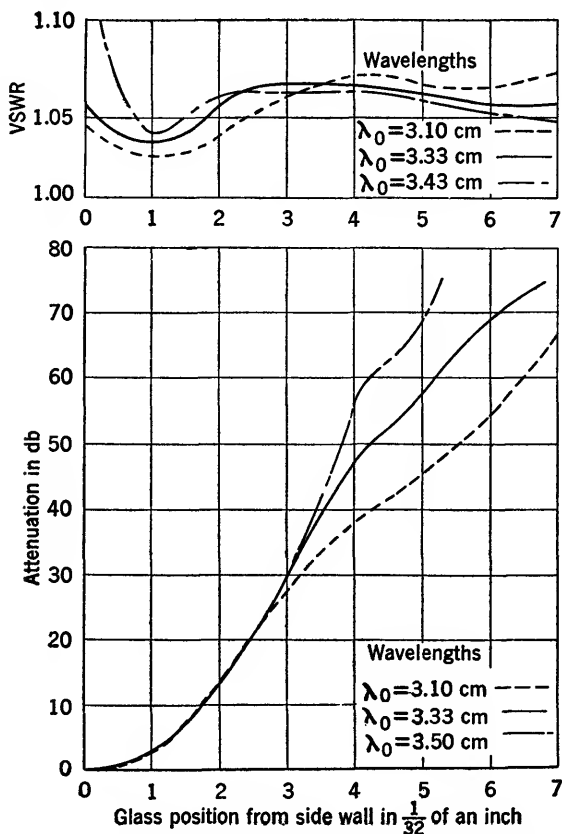


FIG. 12-57.—Attenuation characteristics of typical window-glass plate.

VSWR for this wavelength is less than 1.075 for all positions in the waveguide; and the attenuation curve, although not linear, is nearly so for high values of attenuation. The minimum value of attenuation, with the metal film very close to the side wall, is normally about 0.1 to 0.2 db. Although the match characteristics of the long taper are good over a rather broad band, the frequency dependence of attenuation is undesirably large. This is characteristic of vanes made of window glass.

The voltage standing-wave ratio of Fig. 12-57 shows the rise of the

voltage standing-wave ratio for small insertions of the metalized-glass plate into the guide, when only small effects from the plate itself might be expected. However, the glass plates in an attenuator of this type are usually supported by  $\frac{1}{8}$ -in. brass rods that extend across the guide in the plane normal to the electric lines of force (see Sec. 12-17). Since the supporting struts also reflect a small amount of power, the transforming section is designed to compensate for these reflections. If there is

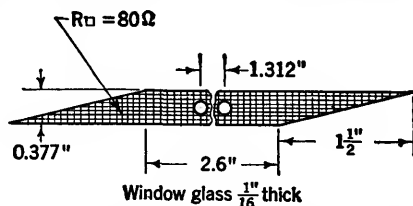


FIG. 12-58.—Metalized-glass plate dimensions for characteristics shown in Fig. 12-57.

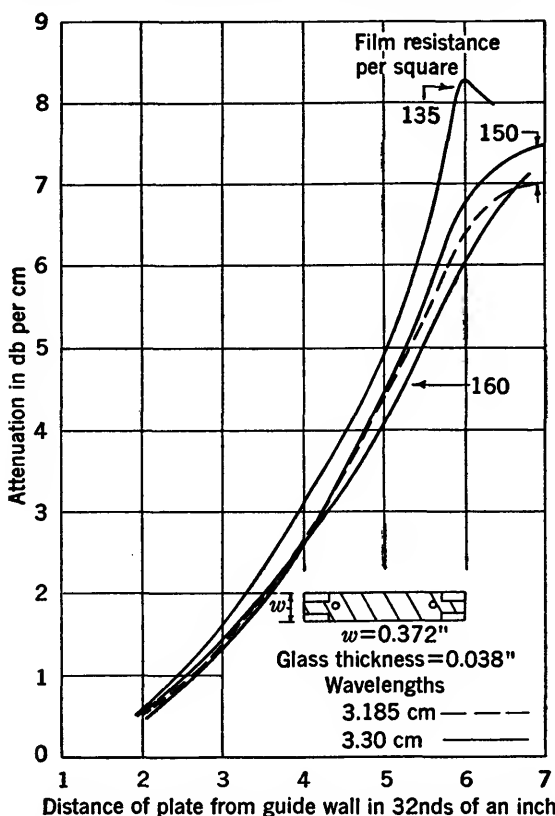


FIG. 12-59.—Attenuation characteristics of Pyrex glass with metallic film.

sufficient attenuation between the struts and the matching section to absorb this reflected power, then the strut problem is of no concern.

However, as the glass plate is also used in zero position or in positions of small attenuation, it is necessary to space the two struts an approximate distance apart of  $n\lambda/4$ , where  $n$  is an odd integer, in order to cancel the two strut reflections. Such cancellation can be perfect at only one wavelength, and in applications over a broad band of frequencies the strut effect becomes noticeable at the edges of the band, as seen in Fig. 12-57.

For the same waveguide size (0.4 by 0.9 in. ID), the thin pyrex plates with metal films should have a width of about 0.372 in. and a thickness

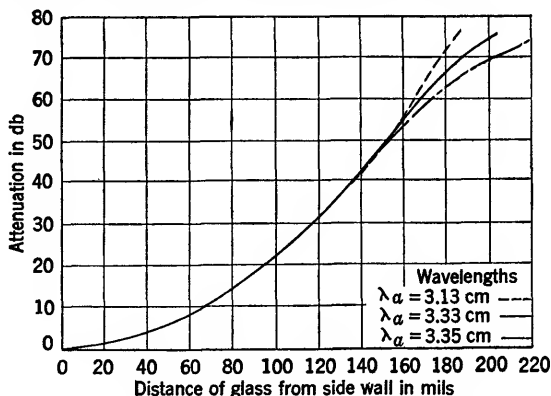


FIG. 12-60.—Attenuation characteristics for typical Pyrex plate with metallic film.

of about 0.038 in. in order to obtain a large range of attenuations, and at the same time to avoid the resonance characteristics shown in Figs. 12-55 and 12-56. The effect of the resistance is shown in Fig. 12-59, which indicates a resonance peak for a film of about 135 ohms per square at a position  $\frac{3}{8}$  in. from the wall. It has been found that a film resistance of about 140 ohms per square gives best results with the above plate dimensions.

Figure 12-60 shows the over-all performance of the plate of Fig. 12-41d. The match characteristics are given in Fig. 12-43. This plate demonstrates very slight variations of attenuation with frequency up to values of 45 db and is therefore exceptionally well suited for broadband attenuators in low ranges of attenuation. In fact, if space permits, two of these can easily be placed in tandem in order to provide values of attenuation up to 90 db with a maximum variation of attenuation of about 2 db over the  $\pm 6$  per cent frequency band centered at 9000 Mc/sec. The minimum attenuation obtained with the metalized-glass plate close to the side wall of the guide and the metal film facing the wall, is practically negligible, in most instances less than 0.1 db.

For very small sizes of waveguide used for frequencies of about 24,000

Mc/sec, the use of metalized-glass vanes moving across the waveguide imposes extremely rigorous tolerances on the mechanical construction, and therefore, the desirable characteristics of the tongue-matched pyrex plate cannot be utilized. The most suitable attenuator construction is that of the guillotine, described in Sec. 12-17, with a metalized-glass plate, as shown in Fig. 12-61, whose matching characteristics depend on the gradual transition provided by its circular shape.

An attenuator with a maximum attenuation of 40 db was designed for use over a band of  $\pm 2$  per cent, centered at 24,000 Mc/sec, or for wavelengths from 1.225 to 1.275 cm, with a guide of inner dimensions

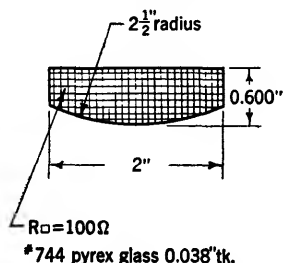


FIG. 12-61.—Metalized-glass plate dimensions for characteristics shown in Fig. 12-62.

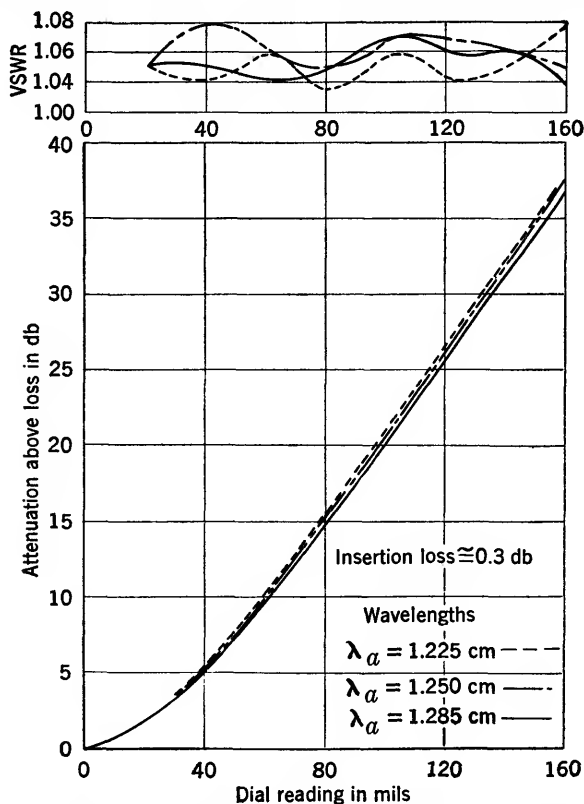


FIG. 12-62.—Performance characteristics of single-plate guillotine attenuator.

0.17 by 0.42 in. The minimum insertion loss of the complete unit was not more than 0.3 db and Fig. 12-62 shows the typical variation of attenua-

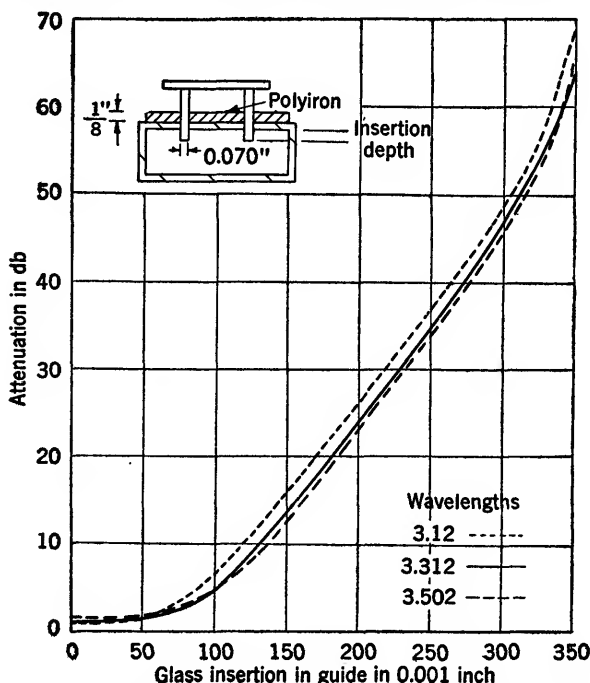


FIG. 12-63.—Attenuation characteristics of experimental model of 75-db balanced guillotine attenuator.

tion and voltage standing-wave ratio at three different frequencies. The maximum variation of attenuation between the edge frequencies is below  $\pm 0.75$  db.

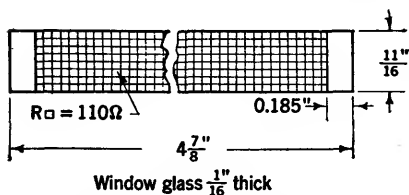


FIG. 12-64.—Metalized-glass plate dimensions for characteristics shown in Fig. 12-63.

Figure 12-63 shows the attenuation characteristics of this attenuator, and also indicates the schematic arrangement. Figure 12-64 shows the glass-plate dimensions with the clear glass matching sections used in this attenuator. The match characteristics are considerably poorer than those of the tongue-matched pyrex plate. They give VSWR values up to 1.24, but

An attempt to reduce the frequency sensitivity of attenuation for high values of attenuation in the range of 9000 Mc/sec resulted in the construction of the guillotine attenuator with two metalized-glass plates inserted into the guide as described in Sec. 12-17.



the variation of attenuation with frequency over the band of  $\pm 6$  per cent centered at 9000 Mc/sec is less than 3.5 db for all depths of insertion into the guide. This is the result of the interaction between the metalized-glass plates within the guide and the cavitylike casing which encloses the driving mechanism and superstructure as shown in Fig. 12-52. The attenuation curves in Fig. 12-63 show a second crossover region near 60-db attenuation values, which obviously tends to reduce the divergence found in the other regions. Such interaction is necessarily critical, however, in mechanical precision, metal film resistance, polyiron framing, and possibly other factors, and consequently, reproducibility under normal production processes is difficult to achieve.

### POWER DIVIDERS AS ATTENUATORS

By E. WEBER

In power measurements it is often convenient to use a sensitive power indicator because of its greater individual accuracy and also because of its quicker response. If a power indicator is used it is necessary to interpose between the input terminal of the power indicator and the main power flow an accurately known amount of attenuation. This attenuation is usually provided by radiation coupling either through appropriate holes or through pickup antennas. Power dividers of several types are used successfully; among those used are calibrated pickup probes, directional couplers, bifurcated lines, and branched lines.

**12-19. Calibrated Pickup Probe.**—A power-monitoring device of the very simplest type is a common slotted section with an adjustable bolometer-probe pickup, provided that this probe can be calibrated by

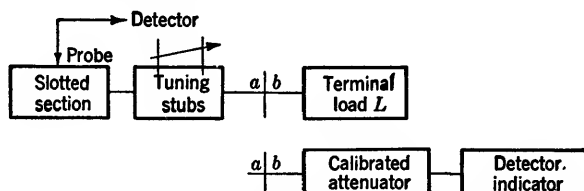


FIG. 12-65.—Use of calibrated bolometer probe with terminal load as attenuator.

an independent power measurement. Figure 12-65 shows an arrangement whereby the power into the terminal load  $L$  is to be measured by a sensitive power detector coupled through the probe to the main power flow. The calibration of the bolometer probe can be accomplished by substituting for the terminal load a well-matched calibrated attenuator and detector. For a certain fixed probe depth and for a fixed setting of the calibrated attenuator, the absolute probe indications over a selected frequency range can then be defined as the equivalent attenuation values.

By variation of the probe depth, different values of attenuation can be attained; but the probe depth must be so chosen that no appreciable reflection of power occurs since this reflection detracts from the accuracy of the power indication. Furthermore, in order to assure general validity of the calibration, the terminal load must be well matched; this can be achieved with the tuning stubs, and the bolometer probe in the slotted section can also be used to indicate proper match. If no matching stubs are available, then the forward power delivered into the terminal load can be computed from maximum and minimum values of power by

$$P = [\frac{1}{2} (\sqrt{P_{\max}} + \sqrt{P_{\min}})]^2. \quad (38)$$

If the bolometer-probe indications have been calibrated in terms of a well-matched calibrated attenuator, the assembly of the slotted section with the probe, the tuning stubs, and the terminal load represents an attenuator of adjustable values. These values of attenuation are usually large, above 30 db. This method is particularly useful for large

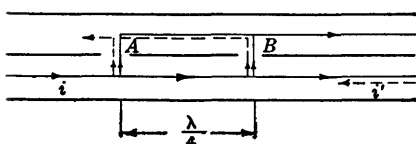


FIG. 12-66.—Principle of directional coupler.

powers, since the dissipation of the terminal load can be increased to absorb practically all the main power. If the terminal load is very well matched over the entire useful frequency band, then the probe can be kept in a fixed location and can be made an integral part of the load; for calibration purposes, however, it still has to be detachable. This method is, of course, equally applicable to waveguide and to coaxial transmission systems.

**12-20. Directional Couplers.**—In Chap. 14, it is observed that directional couplers can be designed for broadband applications to measure voltage standing-wave ratio or to act as power monitors. In principle, two coupling holes between parallel transmission systems are spaced one-quarter wavelength apart as in Fig. 12-66, which shows a sketch for a waveguide system. The incident wave radiates through the holes *A* and *B* into the neighboring system; both forward waves are in time phase at *B* (having traveled the same distance) and support each other to form the outgoing wave *O*. The backward waves which issue from *A* and *B* travel to the left, but the phase difference between the waves from *A* and those from *B* at the point *A* is exactly 180°, and therefore cancellation results and no resultant wave issues to the left. For an incident wave *i'*, the results are opposite, and therefore, the forward and the reflected wave intensities can be measured separately.

On the other hand, this simple directional coupler can be used as a fixed attenuator pad if the remaining incident wave *i'* is absorbed in the main system and the remaining reflected wave *r'* is absorbed in the other

system as shown in Fig. 12-67. In this way, it is easy to obtain attenuator pads for large power and for high attenuation values. Coaxial systems at approximately 3000 Mc/sec have been built for 30-db attenuation or more with small variations with frequency over a frequency band of 30 per cent.<sup>1</sup> For waveguide systems, such attenuator pads have

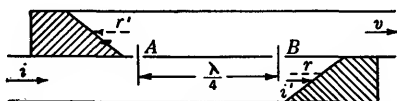


FIG. 12-67.—Use of directional coupler as attenuator.

been built for about 3000 Mc/sec down to values of 15 db, and at 9000 Mc/sec for values of 10- and 20-db attenuation. The variation in coupling was less than 0.3 db for a frequency band of 12 per cent. With well-matched terminations, the problem of the directivity of the coupler, that is, the fact that incomplete cancellation of the backward-traveling waves occurs, is of less importance. Of course, it is necessary to determine the attenuation values by accurate calibration, and it does not seem possible to control mechanical and material factors in such a way as to obviate this necessity.

**12-21. Bifurcated Lines.**—A very convenient power divider of fixed ratio is obtained by the introduction of a very thin partition into a transmission-line system, as shown in Fig. 12-68 for a waveguide. The

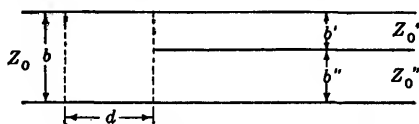


FIG. 12-68.—Bifurcation of a waveguide.

guide of small dimension  $b$  is divided into two guides of small dimensions  $b'$  and  $b''$ . If the characteristic impedances are chosen as

$$\frac{Z_0'}{Z_0} = \frac{b'}{b}, \quad \frac{Z_0''}{Z_0} = \frac{b''}{b}, \quad (39)$$

and

$$Z_0 = Z_0' + Z_0'', \quad (40)$$

the three guides can then be considered in series combination and no power reflection takes place if the two smaller guides are individually terminated in their characteristic impedances. For use of this arrangement as an attenuator, one of the smaller guides would be terminated in a well-matched power-absorbing section and the other used as the

<sup>1</sup> R. S. Julian, "Directional Transmission Line Taps," BTL MM-44-170-6, Jan. 26, 1944.

output guide, connected to the transmission system with the reduced power. By the use of a proper taper transition section this output guide can, of course, be brought back to the characteristic impedance  $Z_0$  of the input system. The actual value of attenuation can be determined from the power split. If the guide with impedance  $Z'_0$  is the output guide, then the output power  $P''$  is, in terms of the input power  $P_0$ ,

$$P'' = \frac{Z'_0}{Z_0} P_0, \quad (41)$$

and therefore, the attenuation becomes

$$A = 10 \log_{10} \frac{P_0}{P''} = 10 \log_{10} \frac{Z_0}{Z'_0} = 10 \log_{10} \left( 1 + \frac{Z''_0}{Z'_0} \right) \text{ db.} \quad (42)$$

This attenuation is defined directly in terms of the impedance ratio. If the termination in the guide  $Z'_0$  can be made frequency-insensitive and if the characteristic impedances are reasonably constant, the attenuation can be made substantially constant over a considerable range of frequencies. The termination must, of course, be able to absorb the power  $P'$  and this determines the material that can be used.

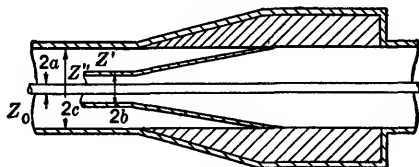


FIG. 12-69.—Attenuator using the bifurcation of a coaxial transmission line.

Figure 12-69 indicates a power split in a coaxial transmission system whereby the impedance must now be related according to

$$\frac{Z'_0}{Z_0} = \frac{\ln \frac{c}{b}}{\ln \frac{c}{a}}, \quad \frac{Z''_0}{Z_0} = \frac{\ln \frac{b}{a}}{\ln \frac{c}{a}}, \quad (43)$$

and where

$$Z_0 = Z'_0 + Z''_0 \quad (44)$$

in order to lead to the three lines in electrical series combination. To bring the output system to the same impedance as the input system a taper transition section is shown. This section, if made somewhat longer than the longest wavelength in the selected wavelength range, usually results in a satisfactorily low voltage standing-wave ratio over a considerable range.

The simple concept of direct series connection holds strictly for

infinitesimally thin partitions<sup>1</sup> and also for any chosen reference plane in the main guide, but practically, little disturbance is observed with thin but finitely thick partitions.

**12-22. Branched Lines.**—As an alternative to the series combination of transmission lines, two transmission lines in parallel to a main system can be connected as illustrated in Fig. 12-70 for a coaxial line. Since

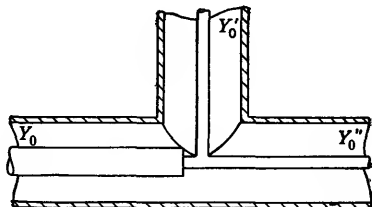


FIG. 12-70.—Attenuator using parallel power split.

the two branch lines are in parallel, they are best represented in terms of their characteristic admittances  $Y'_0$  and  $Y''_0$ , and again satisfy the condition that

$$Y'_0 + Y''_0 = Y_0. \quad (45)$$

If one of the branches,  $Y'_0$ , is terminated in a well-matched power absorber of proper characteristic impedance, and if the other branch  $Y''_0$  is used as the power output system, the over-all attenuation is given as in Eq. (42) by

$$A = 10 \log_{10} \frac{P_0}{P''} = 10 \log_{10} \frac{Y_0}{Y''} = 10 \log_{10} \left( 1 + \frac{Y'_0}{Y''} \right) \quad \text{db.} \quad (46)$$

In order to bring the output admittances again to standard coaxial-line values, impedance transformers can be added in the output section. The transformers may be either the quarter-wavelength type or the tapered type. From the point of view of frequency sensitivity, the bifurcated line has numerous advantages, while mechanically, both the bifurcated line and the branched line present moderate design difficulties.

<sup>1</sup> See Waveguide Handbook, Vol. 10.

## CHAPTER 13

### THE MEASUREMENT OF ATTENUATION

BY ERNST WEBER

To be meaningful the term "attenuation" must be associated with a measurable physical quantity, such as voltage, current, or power, which can be uniquely established at two terminal pairs of an otherwise unrestricted network (see Sec. 11·1). At microwave frequencies, the most readily measured quantity is power, whereas terms like voltage and current would in many cases require explanatory definitions. Attenuation has become associated principally with power and, furthermore, is, as demonstrated in Sec. 11·1, defined in terms of a measurement under ideally normalized conditions; namely, by inserting the pertinent micro-

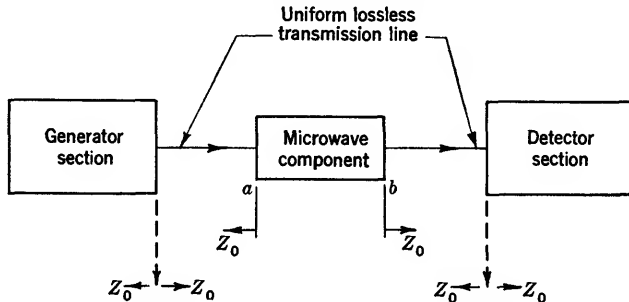


FIG. 13-1.—Schematic arrangement for measurement of attenuation at a microwave frequency.

wave component into a lossless transmission line of defined characteristic impedance  $Z_0$  (see Fig. 13-1) terminated at one end by an ideally matched generator section, and at the other end by an ideally matched detector section. Maintaining these conditions, two principal methods of measurement can be devised; one in which the unknown microwave component is actually removed and the power ratio measured as "insertion loss," another, in which the unknown microwave component, together with a standard of comparison, establishes a fixed over-all power ratio by mutual substitution; both these methods will be described in detail. Other methods of attenuation measurement have been proposed and used; these, however, deviate from the above concept of attenuation and need qualifying elucidation.

**13.1. Direct Measurement of Power Ratio.**—The simplest arrangement for the direct measurement of the power ratio as insertion loss under normalized conditions involves the use of two slotted sections with probe detectors of identical characteristics. Figure 13-2 indicates schematically the arrangement of the equipment, and clearly indicates to the left of  $a$  the generator section, and to the right of  $b$  the detector section. In order to establish proper matching conditions in both directions, two complete modulated-oscillator assemblies with power supply and square-wave modulator are needed. With the oscillator unit  $A$

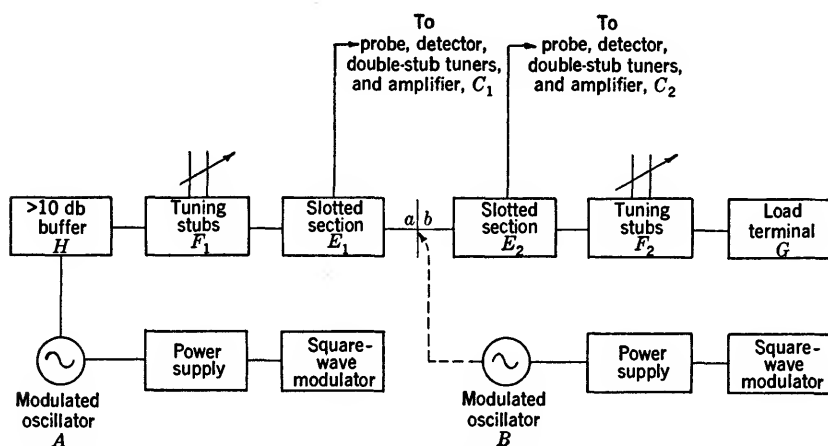


FIG. 13-2.—Schematic arrangement for measurement of attenuation with two slotted sections.

connected to the closed assembly joined at  $ab$ , the tuning stubs  $F_2$  are adjusted to a VSWR  $< 1.02$  as read in either slotted section  $E_1$  or  $E_2$ . With the oscillator unit  $B$  connected to the left section of the assembly at  $b$  and with oscillator unit  $A$  inactive, the tuning stubs  $F_1$  are adjusted to a VSWR  $< 1.05$  as read in slotted section  $E_1$ . To assure no noticeable subsequent disturbance of the match looking back into the active oscillator unit  $A$ , the buffer attenuator  $H$  must have a minimum value of 10 db for most oscillators.

The measurement of attenuation proceeds by first normalizing the probes in slotted sections  $E_1$  and  $E_2$  to the same power level with  $a$  and  $b$  directly joined. Inserting then the unknown microwave component between  $a$  and  $b$ , and maintaining the same power level in the probe of slotted section  $E_1$ , the needed gain in the amplifier  $C_2$  will be a direct measure of the power loss or attenuation caused by the unknown component. Obviously, the gain in the amplifier  $C_2$  can be directly marked in decibel values and thus permit direct reading of attenuation as long as

the detector characteristic follows the square law, that is, is linearly related to the absorbed power. This is usually assured with Wollaston-wire bolometers which are therefore preferred to crystal detectors for attenuation measurements. If crystal detectors are used, it is best to determine their detection characteristics by calibration with a standard signal generator. In order to assure greater accuracy, the arrangement in Fig. 13-2 can be made perfectly symmetrical by placing the second modulated oscillator *B* behind the terminal load *G*, which can then take the form of a buffer attenuator similar to *H*, and which performs the

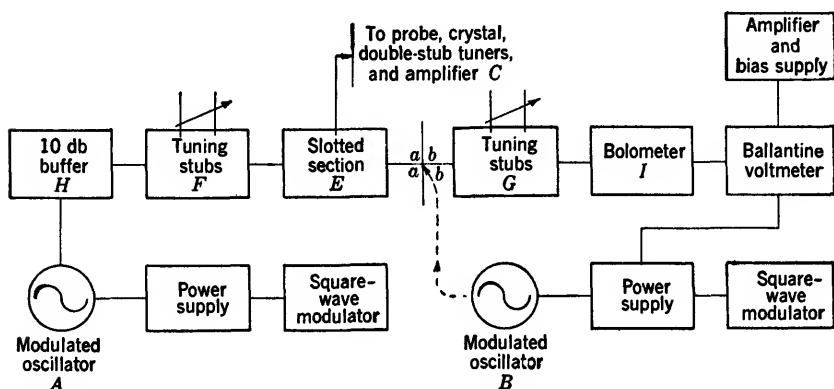


FIG. 13-3.—Schematic arrangement for measurement of attenuation with Ballantine voltmeter.

attenuation measurement alternately with source *A* active and *B* inactive, and vice versa. This requires complete identity of the probe-detector characteristics. This method can be used conveniently for attenuations up to 15 db and for frequency ranges for which the microwave accessories have been designed, since the ultimate indicator, namely, the amplifier, responds only to the modulating frequency of the oscillator which is usually chosen in the audio range.

This method will, however, not measure the value of attenuation as insertion loss according to the definition in Sec. 11-1 if the unknown component is badly mismatched. In this case, the reflective attenuation is disregarded by trying to keep the input power level constant; but even this becomes difficult to assure because the power level is actually determined from the VSWR of slotted section *E*.

**Ballantine-voltmeter Method.**—Another very convenient method of attenuation measurement replaces the detector section in Fig. 13-2 by a bolometer terminal in conjunction with a Ballantine voltmeter as shown schematically in Fig. 13-3. Here, detection of the modulated r-f power by the bolometer develops a voltage across the input terminals



of the special, tuned audio peaked amplifier which is amplified and indicated on the voltmeter. The basic assumption<sup>1</sup> is made that with the proper amount of d-c bias power in the bolometer, the a-c voltage developed across the amplifier input terminals is proportional to the r-f input power to the bolometer which therefore acts as a square-law detector. If the amplifier is strictly linear, a change on the voltmeter of  $n$  db indicates a change in attenuation in the transmission line of  $n/2$  db. Since the calibrated voltmeter is actuated by the audio component of the bolometer output voltage, this method is not limited to a specific range of microwave frequencies unless difficulties are encountered in matching the bolometer at some frequencies.

The range on the voltmeter that may be used in practice is limited on the low-power end by noise and on the high-power end by nonlinearity of the bolometer. By checking the various scales of the voltmeter as well as the linearity of the amplifier, it has been found that the maximum safe range usually extends from 0.01 to 10 volts, permitting, together with the tuned amplifier, the measurement of power ratios up to 30 db. Larger ranges of attenuation may be measured in two steps by subdivision into two ranges, each of which is smaller than 30 db and by establishing the terminal point of the lower range as a new fixed reference point for the upper range. Of course, the error of measurement in such a procedure is doubled and the limit is probably set by the power capacity of the source as well as all the microwave components in the assembly. For greater accuracy, the voltmeter should be calibrated. The calibration may be made with an audio attenuator of negligible reactance which has in turn been calibrated with a potentiometer (see Sec. 13-7).

In order to establish proper matching conditions in both directions the same procedure should be followed as above. With source *A* inactive, source *B* connected at *b*, adjust the tuning stubs *F* for good match as read in the slotted section *E*; then, with source *A* active, the system closed at *ab*, adjust tuning stubs *G* for good match as again read in slotted section *E*. If the bolometer mount is tunable, it should be matched independently by using a slotted section with the proper d-c bias current circulating through the bolometer.

The actual measurement of attenuation then proceeds in the following manner: With the components assembled as in Fig. 13-3 and matched, the r-f power level is adjusted by means of the buffer *H* so that no more than the maximum permissible power enters the bolometer. The amount of buffering may be increased when necessary in order to fulfill this condition; however, a buffer of at least 10 db must be used, as

<sup>1</sup> The validity of this assumption is discussed in R. L. Report No. 55.1—10/16/45, "Notes on the Use of Bolometers for Pulsed R-f Power Measurements," by George Guthrie.

explained above. After the frequency of the oscillator is checked, the modulation frequency is set at 1000 cps to correspond with the frequency at which the preamplifier is peaked. This setting gives maximum deflection on the Ballantine voltmeter. The gain control on the preamplifier is adjusted so that the Ballantine voltmeter reads 20 on any range other than the 100-volt range. Switched to the next higher range, the meter should then read exactly 0. If it fails to do this, mechanical adjustment of the voltmeter must be made until this condition is met. By setting the gain control on the preamplifier, a reference level on the voltmeter is established, the system disconnected at points *a* and *b* and the unknown microwave component inserted and the new reading taken. One half of the difference between the reference and final readings gives the power attenuation of the unknown component. For better accuracy, repeated checks should be made on all initial adjustments, such as oscillator frequency, modulator frequency, reference power level, and matching conditions.

For various frequency ranges, different types of bolometers are available, which are described in Chap. 3. For frequencies in the range of 3000 Mc/sec or above, Littelfuse elements for  $\frac{1}{2}$  amp can be used as bolometers; they require a d-c bias current of about 5.5 ma. Most Wollaston-wire bolometers can carry a permissible maximum power between 1 and 30 mw. Bolometers have been made with metalized-glass fibers which can carry up to 0.1 and 0.2 watt of maximum power. Further extension of the power range is possible by insertion of carefully calibrated precision attenuators between the bolometer and the tuning stubs *G* in Fig. 13-3. The accuracy of the attenuation measurement will then be influenced by the accuracy of the additional attenuator.

**Water Calorimeter.**—For still higher power capacities the bolometer-detector section in Fig. 13-3 is replaced by a water calorimeter, described in Secs. 3-32 to 3-36. The power-detecting medium is the circulating water absorbing the heat generated. With proper calibration and well-controlled water-pump speeds, the accuracy can be made satisfactory for most practical purposes.

**13-2. Substitution Methods.**—A different method of attenuation measurement particularly suitable for high values of attenuation is the *substitution method*, in which, at some point in the detector system, the power level is maintained constant upon insertion of the unknown microwave component by adjusting the attenuation of an appropriate standard attenuator, which can be a part of either the generator section or the detector section. Several schemes are possible based on the same principle and differing only with respect to the choice of the section in the detector system in which the power level is maintained constant. Thus, in the microwave substitution method, the microwave power at the

detector is maintained at a constant level with the aid of a microwave standard attenuator, located in series with the unknown attenuator, either in the generator section or in the detector section. In the intermediate-frequency substitution method, the power level is maintained constant at the i-f detector by adjusting an i-f standard attenuator to compensate for the insertion of the unknown microwave component. Finally, in the d-c substitution method, the power level in one arm of a d-c bridge circuit is maintained constant, as with the use of a bolometer bridge detector.

*Microwave Substitution Methods.*—The specific arrangement of equipment will in most cases depend on the power range of the microwave

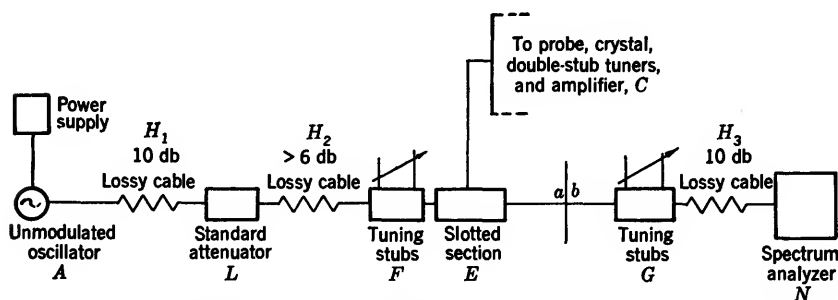


FIG. 13-4.—Schematic arrangement for measurement of attenuation at 3000 Mc/sec with microwave standard attenuator in generator section.

source, on the sensitivity of the detector, on the availability of a suitable standard, and on the over-all characteristics of the equipment. As will be pointed out in Sec. 13-6, the waveguide-beyond-cutoff standards can be considered primary standards, but they usually have a rather large minimum attenuation value necessitating very sensitive detectors to permit the measurement of large ranges of attenuation. Although the resistive precision attenuators have nearly zero minimum attenuation, they must be calibrated absolutely. Of the three principal types of power detectors that are commonly used; namely, the crystal, the bolometer, and the spectrum analyzer, only the spectrum analyzer has a sensitivity sufficiently high to permit attenuation measurements up to 70 or 80 db. The maximum sensitivity of the crystal or of the bolometer limits the range to about 30 db. In view of the fact that the substitution methods are particularly suitable for wide ranges of attenuation measurements, the spectrum analyzer primarily will be considered here.

As an illustration of an arrangement with the standard attenuator in the generator section, Fig. 13-4 shows the system used for frequencies of about 3000 Mc/sec, for which a special primary-standard attenuator has been developed with a tunable transmission cavity on one end that

must be tuned for maximum power transfer (see Sec. 11-9). It is advisable to use the cavity at the input end of the standard attenuator. The standard attenuator should be located near the oscillator since the effective load impedance at this point is constant and the frequency of the cavity will not be pulled. Power is coupled into the cavity with a loop and out of the cavity through an iris to the cutoff tube. If the attenuator is held in a position so that the rotating drive shaft is horizontal, the planes of both loops will be vertical and a line passing through the long dimension of the iris will be horizontal. The standard attenuator is isolated from the rest of the system by means of pieces of lossy cable so that the maintenance of a good match, looking towards the generator from point *a* after it has once been matched by means of the tuning stub *F*, is assured.

Similarly, the spectrum analyzer is isolated from the output end *b* of the unknown microwave component by a lossy cable of at least 10-db attenuation in order to maintain a match once a match has been established by the tuning stub *G*. The spectrum analyzer consists of a well-shielded superheterodyne receiver employing a crystal mixer and having a local oscillator that is frequency modulated in sawtooth fashion. A frequency spread of  $\pm 20$  Mc/sec about the frequency setting of the local oscillator is available. The sawtooth voltage that produces the frequency modulation of the local oscillator is also applied as the horizontal deflection voltage to a cathode-ray oscilloscope. The video output voltage of the receiver is connected to the vertical plates of the oscilloscope. Thus, when a signal is applied to the input terminals of the receiver, a pip appears on the screen. The receiver bandwidth is about 50 kc/sec. The magnitude of the pip is a measure of the input power to the receiver. To measure attenuation, the standard attenuator is set for a value that is a few decibels higher than the attenuation to be measured. By means of the gain control, the pip of the spectrum analyzer is set at a convenient level on the screen of the oscilloscope. The unknown microwave component is inserted at *ab* and the attenuation of the reference standard is reduced until the pip returns to the level previously set. As a check, removing the unknown component and returning the dial setting of the reference standard to the value initially selected should bring the pip to the same level again. If the level has changed, the measurement is to be discarded as erroneous. The error may be caused by instability either in the source or in the spectrum analyzer. The maximum usable range of this system for measuring attenuation is limited to about 54 db. The range of the power ratios that the spectrum analyzer can detect is of the order of 95 db. The various buffer-cable sections consume at least 26 db and the nonlinear region in the standard cutoff attenuator extends to 15 db resulting in an actual minimum attenuation in the system, exclusive of the unknown component, of 41 db.

Figure 13-5 shows the schematic arrangement of a system for the measurement of attenuation in the range of 9000 Mc/sec with the standard attenuator in the detector section. For better accuracy, rectangular

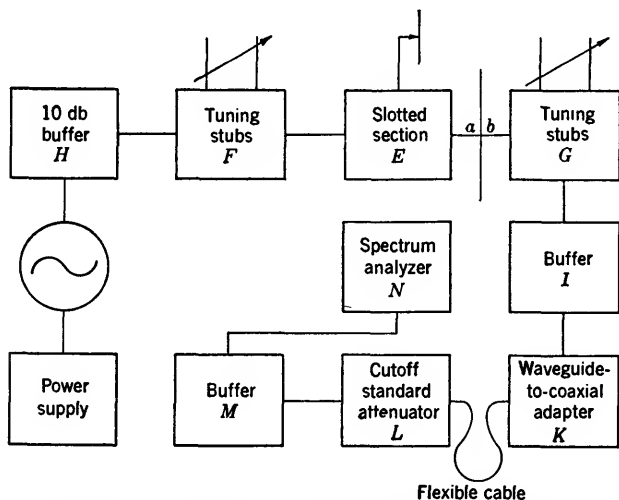


FIG. 13-5.—Schematic arrangement for measurement of attenuation at 9000 Mc/sec with microwave cutoff standard attenuator in detector section.

waveguide is used for the power-transmission system, necessitating an appropriate adaptor to permit insertion of the reference standard. The movable end of the cutoff attenuator is joined to the line by means of a flexible cable employing cable connectors. Since no cutoff standard has been designed for this frequency range which incorporates a frequency-sensitive cavity, it can be placed close to the receiver-type detector. As above, the over-all attenuation needed in the system, exclusive of the unknown component, is about 41 db so that the same range of attenuation measurements can be covered.

A considerable extension of the range of attenuation measurements can be achieved by the use of a resistive variable attenuator standard such as is described in Secs. 12-18 and 13-6. The arrangement of the components is shown in Fig. 13-6. Essentially, the cutoff standard attenuator with the adaptor is replaced by the resistive precision

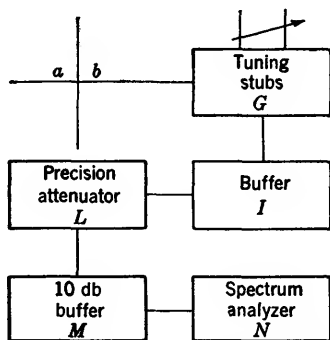


FIG. 13-6.—Schematic arrangement of detector section for measurement of attenuation at 9000 Mc/sec with microwave resistive attenuator in detector section (generator section same as Fig. 13-5).

attenuator. The minimum attenuation of the resistive attenuator is almost zero, in any case less than 0.5 db. Since resistive attenuators are usually well matched, the buffer attenuator  $I$  can have very low attenuation. Therefore the minimum attenuation in the system, exclusive of the unknown component, can, in this case, be made about 20 db and the range of attenuation measurements can be extended to 75 db. With a proper r-f source or with reduced buffering and acceptance of loss of accuracy, this extension can possibly be carried even further.

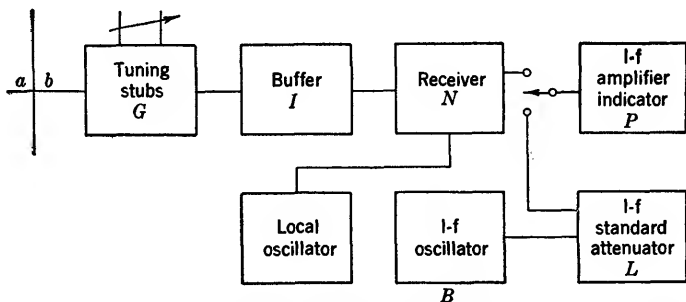


Fig. 13-7.—Schematic arrangement of detector section for measurement of attenuation with i-f standard attenuator.

*I-f Substitution Method.*—Instead of compensating for the attenuation of the unknown component in the microwave system itself, a receiver can be used as a detector and compensation can be made in the i-f part of the detector section. Figure 13-7 indicates one possible arrangement<sup>1</sup> whereby the i-f amplifier-indicator is designed for 20 Mc/sec and is used principally as a power-level indicator. The measurement of attenuation proceeds by first adjusting the gain control on the i-f amplifier to a convenient level for reception from the microwave line. The i-f amplifier-indicator is then connected to the i-f standard attenuator, which in turn is adjusted to give the *same* indication on the amplifier. The receiver is switched back to the microwave line, and the unknown microwave component inserted, the gain control on the i-f amplifier is adjusted to give a convenient reading; then the i-f amplifier is again switched over to the i-f standard attenuator and this is adjusted to bring the i-f amplifier to the new reading set by the microwave signal. The change in setting in decibels of the i-f standard attenuator is thus identical with the attenuation of the inserted microwave component at the microwave frequencies. In using the i-f standard attenuator, the frequency and power level of the i-f source should be carefully checked. It is advisable to use a special i-f amplifier with humped frequency

<sup>1</sup> See F. G. Gainsborough, "Notes on the Calibration of High-frequency Attenuators at the National Physical Laboratory," B.C.S.O. Report No. 343, Jan. 24, 1945.

response to make the tuning unambiguous. Likewise, the i-f standard attenuator should be very carefully constructed, preferably so that it can be calibrated with direct current to avoid additional sources of error.

The accuracy of the method depends on the linear relationship existing between the i-f beat-frequency amplitude and the power level of the microwave signal, which in turn depends on the mixer characteristics. If the local-oscillator input signal into the mixer can be kept at least 10 times stronger than the microwave signal, this linearity will be maintained with sufficient accuracy in diode mixers and even in crystals, as has been

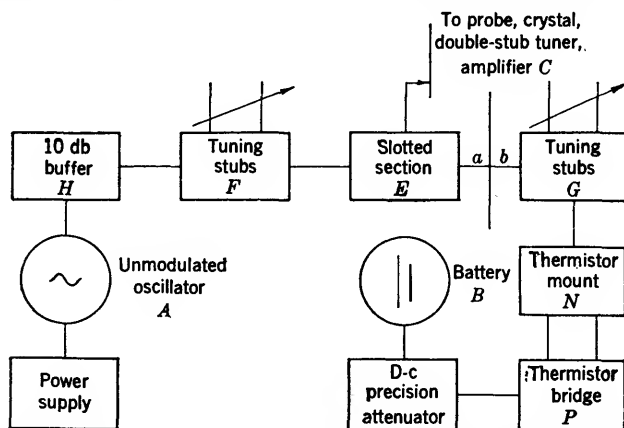


FIG. 13-8.—Schematic arrangement for measurement of attenuation with the thermistor bridge.

shown experimentally at the National Physical Laboratory.<sup>1</sup> The advantage of the method is, however, that the i-f attenuator standard can be the same for practically any microwave frequency if proper changes are made in the local oscillator of the receiver.

**Thermistor-bridge Methods.**—The use of thermistors as high-frequency power-measuring elements has been discussed in Chap 3. In almost all applications the basic assumption is made that equal amounts of d-c and microwave power have the same effect on the temperature rise of the element and therefore cause the same resistance change. This principle can be used to extend the substitution method to include d-c substitution by employing the thermistor as a power detector and a properly designed bridge circuit as a power-level indicator as shown schematically in Fig. 13-8.

The thermistor bridge itself consists of three 600-ohm resistors connected to a thermistor element to form a Wheatstone-bridge circuit

<sup>1</sup> See also L. C. Peterson and F. B. Llewellyn, "The Performance and Measurement of Mixers in Terms of Linear Network Theory," *Proc. I.R.E.*, 1, **33**, 458 (1945).

as shown in Fig. 13-9. The d-c voltage source supplies the bridge through several attenuators  $R_1$ ,  $R_2$ ,  $R_3$ , and  $R_4$ . Three of these attenuators are T-pads having a characteristic impedance equal to the input impedance of the bridge and calibrated in decibels. The resistor  $R_1$  is an uncalibrated voltage divider that permits the effective input voltage of the bridge to be varied. The thermistor should preferably be mounted in a constant-temperature oven to minimize the effect of ambient-temperature changes. In order to measure microwave attenuation, first, with only direct current supplied to the bridge and the microwave source inactive, adjust the voltage divider  $R_1$  until the bridge is balanced. The calibrated attenu-

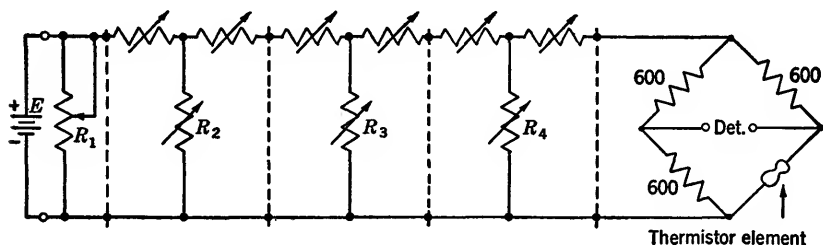


FIG. 13-9.—Thermistor-bridge circuit.

ators  $R_2$ ,  $R_3$ , and  $R_4$  should read zero during this adjustment of  $R_1$ . The d-c calibrated attenuators should then be set at least 4 db higher than the attenuation to be measured, for example, to  $A_1$  db, thus reducing the d-c current through the thermistor to  $i_1$ . Turning on the microwave power and adjusting it by means of buffer  $H$  to such a value that the bridge will again be balanced establishes the reference microwave power  $P_1$ . The unknown microwave component is inserted into the line between points  $a$  and  $b$ , maintaining the established input power  $P_1$  at the transmission line. The unknown component decreases the microwave power in the thermistor bead to  $P_2$ , so that the bridge must be rebalanced by adjusting the d-c calibrated attenuators  $R_2$ ,  $R_3$ , and  $R_4$ . The new setting of these attenuators should be  $A_2 < A_1$ , whereas the d-c current should be increased to  $i_2 > i_1$ . Since direct substitution of d-c power for microwave power necessitates constant resistance values in all four arms of the bridge (precluding any heating effects in the three fixed arms), the attenuation of the unknown component can be defined as

$$A = 10 \log_{10} \frac{P_1}{P_2} = 10 \log_{10} \frac{1 - a_1}{1 - a_2}, \quad (1)$$

where

$$\frac{1}{a_1} = \text{antilog}_{10} \frac{A_1}{10}, \quad \frac{1}{a_2} = \text{antilog}_{10} \frac{A_2}{10} \quad (2)$$

Since the minimum power measurable to any degree of accuracy is about 50  $\mu$ w, and the maximum power of the thermistor is in the neighbor-



hood of 4 mw, the largest attenuation range that can be measured is just under 20 db. To extend this range, standard attenuators can be used as gauge blocks. The power  $P_1$  can be established with the standard attenuator in the microwave line and  $A$  can be set on the d-c attenuators. The unknown component can be substituted for the standard attenuator, and  $P_2$  can be measured with the  $A_2$  setting. The total attenuation of the unknown component is then the sum of the differential attenuation computed by Eq. (1) and the value of the standard attenuator. Although this method seems simple, it requires a powerful microwave source. The practical limit of measurements using this method and thermistor elements with no refinements is about 40 db with good accuracy, and 50 db with reasonable accuracy.

Instead of using accurately calibrated d-c attenuators, the d-c current measurements as indicated can be used and the measured attenuation can be defined

$$A = 20 \log_{10} \frac{i_2}{i_1}. \quad (3)$$

In order to preserve accuracy, however, the meter has to be of very high accuracy itself, although the d-c attenuating network can now be uncalibrated. Finally, if the low-resistance d-c attenuators are accurately calibrated, lower values of attenuated power  $P_2$  can be measured and the range of measurement can be further increased. The practical limit in the measurement of very small powers lies in the necessity of using a sensitive galvanometer in the bridge circuit. If the thermistor element can be considered to be a linear detector of microwave power over a reasonably small resistance change, then the deflection of the galvanometer will be proportional to the input microwave power and an unbalanced bridge reading can be taken. The proportionality constant for this deflection can be obtained by calibration with a directly measurable small power. With a sensitive galvanometer of  $1\mu\text{a}$  full-scale deflection and 50 ohms internal resistance, sizable deflections can be obtained with an input power of a microwatt or less. However, bridge-balance drifts make such measurements difficult and time consuming, and this method will usually be used only if microwave substitution methods cannot be applied.

*Wire-bolometer-bridge Methods.*—Instead of using the thermistor bead as a power detector, a hot-wire bolometer that employs a very thin Wollaston wire of a length that is small compared with a wavelength can be used. With a properly designed bridge circuit, attenuation measurements can be made in exactly the same manner as with the thermistor bridges, balanced or unbalanced. These bridges are described in detail in Chap. 3.

Similarly, thin metalized-glass fibers have been used as power-detector elements. Again with properly designed bridge circuits, these elements have been used for attenuation measurements.<sup>1</sup> Metalized-glass fibers have a higher power capacity than thermistor elements, their larger diameters permit better broadband matching than the hot-wire elements. They are, however, somewhat more difficult to produce.<sup>2</sup>

**13-3. Measurement of Attenuation by Standing-wave Effects.**—For measurement of small values of attenuation, neither substitution methods nor direct measurement of the power ratio with or without the unknown component are adequate if accuracies of 0.1 db or less are required. From basic transmission-line theory, however, it can be shown that the attenuation of any lossy four-terminal network may be determined from the knowledge of either of the following quantities: (1) the effect of the insertion of such a network on the voltage distribution and the phase shift in a short-circuited section of a lossless line following the unknown component, (2) the magnitude of the voltage standing-wave ratio of the unknown component terminated in a short circuit. Either effect can be made the basis for measurement of attenuation.<sup>3</sup>

*Measurement of Power Ratios Referred to Line-voltage Distribution.*—The methods of measuring attenuation discussed so far use either a defined standard attenuator, or square-law response of a detector, or correspondence between a-c and d-c voltage as a basis. Most of these assumptions are reasonably justified, but they have nevertheless been questioned from time to time. It seems desirable, therefore, to have still another method available which involves none of the previous assumptions, but rather measures attenuation in terms of a theoretically defined voltage distribution. Figure 13-10 shows the schematic arrangement for such a system in which the slotted section  $G_2$ , next to the short circuit, is the attenuation-measuring instrument. This apparatus must be particularly well constructed. Relative movement of its probe must be measurable to fractions of a mil; a 1-in. precision dial indicator with scale divisions of 1 mil, which is directly attached to the drive mechanism of the probe, is usually satisfactory.

In order to measure attenuation of an unknown component, both the detector and generator sections are first matched as well as possible by means of the slotted section  $G_1$ . The unknown component is then inserted between  $a$  and  $b$ . Maximum indication in the slotted section  $G_2$  is determined and noted as a reference level. After removal of the

<sup>1</sup> J. Ebert, "Notes on the Use of Bolo-meters for Ultrahigh Frequency Attenuation Measurements," NDRC 14-219; PIB-7, June 2, 1943.

<sup>2</sup> S. A. Johnson, "Metalized-glass Bolometers," NDRC 14-524, Oct. 31, 1945.

<sup>3</sup> J. Ebert, "Notes on the Accurate Measurement of Small Attenuations," NDRC 14-439; PIB-43, Apr. 5, 1945.

unknown component, the distance is measured between two successive points about a voltage minimum in  $G_2$  which give the same indication

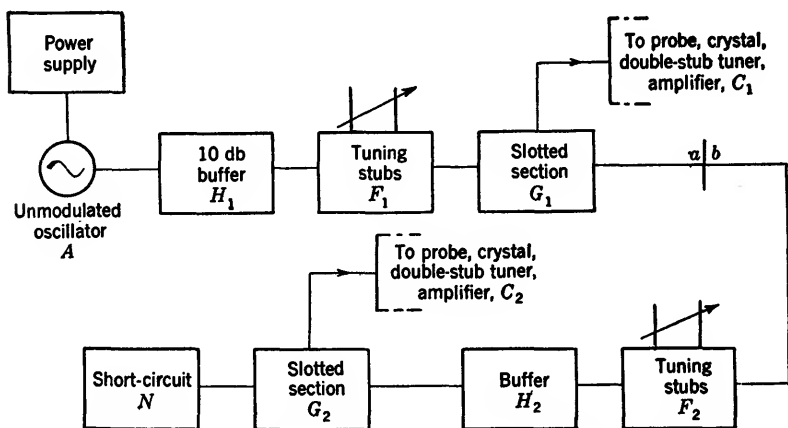


FIG. 13-10.—Schematic arrangement for measurement of attenuation by reference to line voltage distribution.

as the reference level previously noted. Knowing this distance, the frequency of the generator, and the voltage distribution, the power ratio or attenuation can be calculated in a simple manner. Assuming the entire detector section to be nearly lossless, the voltage distribution in the slotted section  $G_2$  will be sinusoidal. Let  $E_1$  represent the maximum voltage and reference level when the unknown component is inserted between  $a$  and  $b$ , and let  $E_2$  be the maximum voltage when the unknown component is removed, as indicated in Fig. 13-11. Then the attenuation of the unknown component is by definition

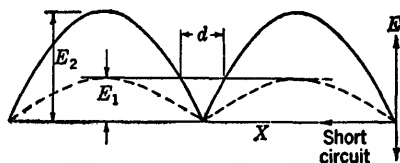


FIG. 13-11.—Voltage distribution in the slotted section  $G_2$  of Fig. 13-10. The dotted line is the absolute value of the voltage with the unknown component present, the solid line is the voltage without the unknown.

$$A = 20 \log_{10} \frac{E_2}{E_1} \quad \text{db.} \quad (4)$$

Since the voltage distribution is sinusoidal, however,

$$E_2 \sin \frac{\pi d}{\lambda} = E_1,$$

where  $\lambda$  is the wavelength in the slotted section  $G_2$ . Thus, Eq. (4)

becomes

$$A = 20 \log_{10} \left( \frac{1}{\sin \pi d / \lambda} \right) \quad \text{db.} \quad (5)$$

Figure 13-12 gives the graphical representation of Eq. (5) for small values of attenuation.

The expression in Eq. (5) is an approximation since the short circuit and the transmission line are not lossless; the actual voltage distribution

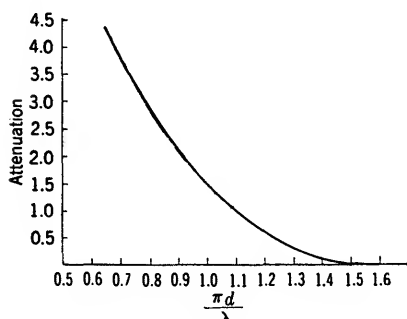


FIG. 13-12.—Attenuation values as measured by voltage distribution.

will therefore deviate appreciably from the assumed sinusoidal distribution. In the simple form given the method does not apply for attenuations much above 4 or 5 db. It is necessary, even at lower values of attenuation, to keep to a minimum the extension of the exploring probe into the active field in order to minimize its field-distorting effects and to maintain the voltage distribution close to sinusoidal. The main

advantage of the method, however, is that the crystal or detector law of the exploring probe need not be known, because the same power level is used throughout.

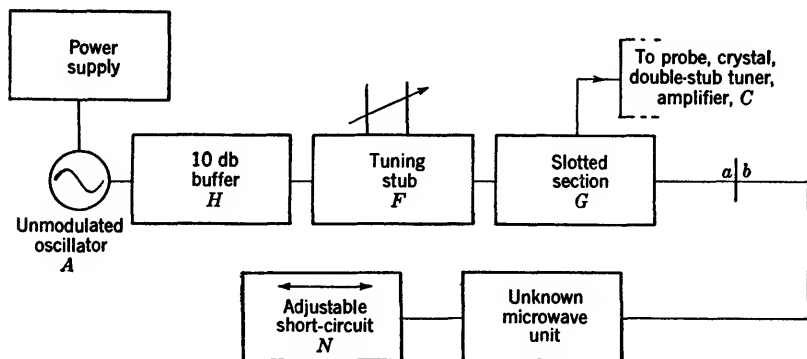


FIG. 13-13.—Schematic arrangement for measurement of power reflection ratio.

**Measurement of Power-reflection Ratio.**—If the unknown unit is terminated by a short circuit and if the ratio of incident to reflected power is known, the attenuation of the unknown unit can be computed. This power ratio may also be measured by determining the input standing-wave ratio in the arrangement shown in Fig. 13-13. The unknown

unit remains connected in the line system, making this method independent of the generator impedance.

Assuming a perfectly matched device to be measured, the relationship between voltage standing-wave ratio and attenuation can be found in the following way. Referring to Fig. 13-14, let  $P_1$  represent the power incident on the unknown unit. Let the power transmitted by the unit be denoted by  $P_2$ . The power  $P_2$ , after being totally reflected from the short

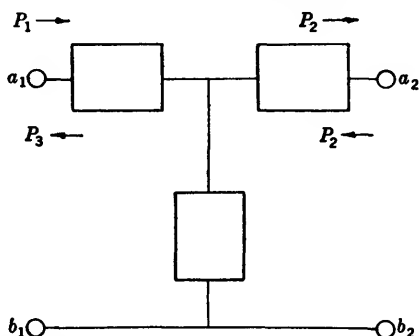


FIG. 13-14.—Power reflection from the terminals of short-circuited four-terminal network. circuit, is again attenuated in passing through the unknown unit. If the power then emerging from the unit is represented by  $P_3$ , the attenuation of the unit can be written as

$$A = 10 \log_{10} \frac{P_1}{P_2} = 10 \log_{10} \frac{P_2}{P_3} = 5 \log_{10} \frac{P_1}{P_3} \quad \text{db.}$$

The quantity  $P_3/P_1$  is, however, the ratio of incident to reflected power and is independent of generator impedance. If  $r$  is the input voltage standing-wave ratio, then

$$\frac{P_3}{P_1} = \frac{(r - 1)^2}{(r + 1)^2}.$$

Introducing this into the expression for  $A$  above,

$$A = 10 \log_{10} \frac{r + 1}{r - 1} \quad \text{db.} \quad (6)$$

This relationship is represented graphically in Fig. 13-15.

Most of the devices to be measured will not be perfectly matched, but will have reflections of their own, which will make the input standing wave dependent upon the phase of the reflection from the short circuit, and will make it vary from a maximum  $r_M$  to a minimum  $r_m$ . In this more general case, the relation

$$A = 10 \log_{10} \left[ \left( \frac{r_M + 1}{r_M - 1} \right) \left( \frac{r_m + 1}{r_m - 1} \right) \right]^{1/2} \quad \text{db} \quad (7)$$

can be derived, or

$$A = \frac{1}{2} \left( 10 \log_{10} \frac{r_M + 1}{r_M - 1} + 10 \log_{10} \frac{r_m + 1}{r_m - 1} \right) \quad \text{db.} \quad (8)$$

If  $r_M$  as well as  $r_m$  is measured with an adjustable short circuit, Fig. 13-15 can be used to determine the attenuation. Equation (8) is an expression for dissipative attenuation alone (see Sec. 11-1), and does

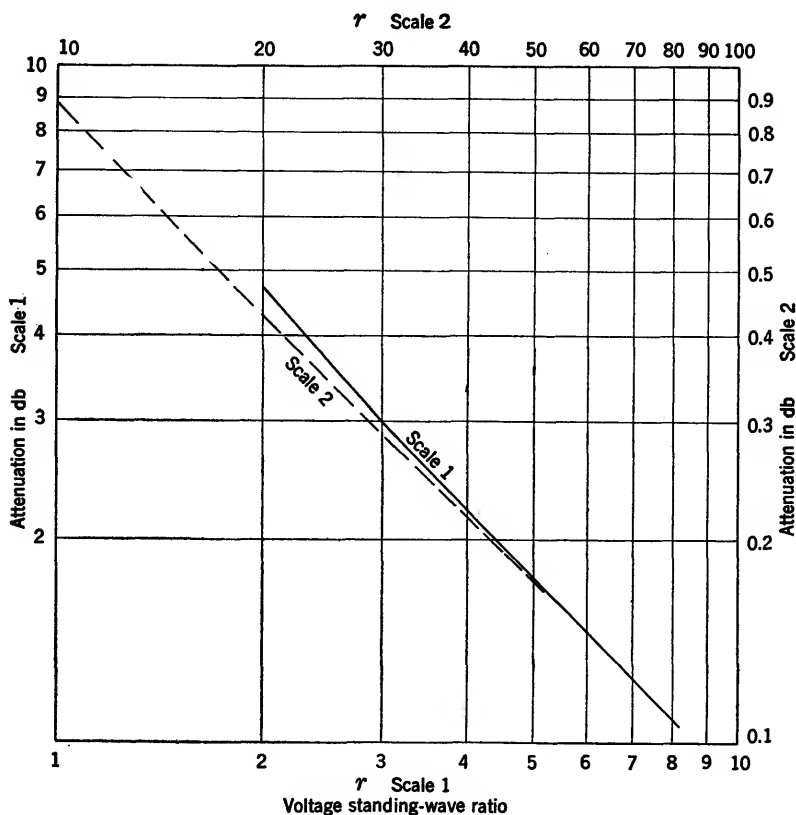


Fig. 13-15.—Plot of relation between attenuation and voltage standing-wave ratio.

not include the apparent increase of attenuation caused by power reflection from mismatches. Such reflection effects are included in all other measuring systems discussed above.

If the short circuit is imperfect, it can be regarded as a series combination of a perfect short circuit terminating a small fixed attenuating pad. The attenuation measured is the sum of the unknown unit and the attenuation of the imperfect short circuit. The attenuation value of

the hypothetical short-circuit pad can itself be measured by the method as outlined above.

In using this short-circuit method, it is necessary to measure input standing-wave ratios accurately. This can be done either with a hot-wire bolometer serving as a detector and as a standard in the slotted-section probe circuit, or by using some other sensitive microwave detector with a calibrated variable attenuator preceding it. When using the bolometer method, the powers at maximum- and minimum-voltage positions are measured and the ratio of the powers is the power standing-wave ratio  $r^2$ . When using the calibrated variable attenuator and detector in the probe circuit much larger standing-wave ratios can be measured. The change in attenuation necessary to equalize maximum and minimum indications is a measure of the reflection. Frequently a spectrum analyzer is used as the detector and a cutoff waveguide attenuator as the standard.

The advantage of using bolometers or standard attenuators in this method is the increase in sensitivity and accuracy of the measurements. Thus, measuring an unknown unit of 3-db attenuation, a change of approximately 0.3 db in power standing-wave ratio will correspond to a change of 0.1 db in the value of the unit. Measuring 1 db, the attenuation-sensitivity factor is roughly 8.4 and increases as the attenuation of the unknown unit decreases. However, since very large standing-wave ratios are difficult to measure accurately, some of this theoretical accuracy is usually lost, although the short-circuit method of measuring attenuation is the only convenient means available for measurements of attenuation below 0.1 db. Contrary to the power-measuring and substitution methods, the short-circuit method is independent of the generator impedance, thereby eliminating any mismatch error. Also, input power monitoring becomes unnecessary because of the ease and speed with which measurements may be checked.

**13-4. Measurement of Very Small Attenuation Values.**—An alternative method for the measurement of very small values of attenuation utilizes the resonance characteristics of metallically bounded field spaces as expressed in the definition of  $Q$  by

$$\frac{1}{Q} = \frac{\Delta f}{f} = \frac{R}{\omega L}, \quad (9)$$

where  $f$  is the resonance frequency at which maximum power is absorbed, and where  $\Delta f$  is defined as the interval between the upper and lower frequencies near  $f$  at which the magnitude of the admittance has fallen to one-half its peak value. The  $\Delta f/f$  can also be taken as the ratio of dissipated to stored field energy analogous to the condition at lower frequencies.

*Direct Measurement of Attenuation Constant of Transmission Lines.*— Since the measurement of the  $Q$  of cavities is discussed in Chap. 5 only the modification of the method for measurement of conductive attenuation in transmission lines (coaxial or waveguide) will be given here. As shown in Slater,<sup>1</sup> the input admittance of a uniform, short-circuited, coaxial transmission line has periodic maxima and zeros. Near the maxima, it can be expressed in the first approximation as

$$|Y| = \frac{1}{Z_0} \frac{1}{\sqrt{(\alpha s)^2 + \delta^2}}. \quad (10)$$

In this form,  $Z_0$  is the characteristic impedance of the line, assumed as real in this simplified case,  $\alpha$  is the attenuation constant of the line,  $s$  is the length of the line to the short circuit, and  $\delta$  is defined by

$$\beta s = n\pi + \delta, \quad (11)$$

where  $\beta = 2\pi/\lambda = 2\pi f/v$  is the phase constant. Thus  $|Y|$  regarded as a function of  $\delta$  varies in the same way as a familiar resonance curve, as it should, since  $\beta$  is proportional to frequency. The spatial half-power points are indicated by the distances  $\delta'$  for which the square of the admittance is reduced to one-half the maximum value for  $\delta = 0$ , since small attenuation has been assumed. This leads to

$$\frac{1}{Z_0^2} \frac{1}{(\alpha s)^2 + (\delta')^2} = \frac{1}{2} \frac{1}{Z_0^2} \frac{1}{(\alpha s)^2},$$

from which

$$\delta' = \pm \alpha s. \quad (12)$$

The measurement of the distance  $\delta'$  gives directly, therefore, the total attenuation ( $\alpha s$ ) of length of the transmission line.

Because of the obvious symmetry, the interval between the two half-power points is  $2\delta'$ . Using Eqs. (9) and (12),

$$\frac{1}{Q} = \frac{\Delta f}{f} = \frac{2|\delta'|}{\beta s} = \frac{2\alpha}{\beta}. \quad (13)$$

Therefore the conventional methods of measuring  $Q$  will, if the phase constant is known, give the value of the attenuation constant of the transmission line.

A practical arrangement for this measurement is shown in Fig. 13-16. The slotted section  $G$  should preferably be of the same transmission-line size as the line to be measured in order to avoid spurious reflections. By means of the cutoff attenuator, the indication for maximum power in the probe is adjusted on the final detector (preferably a spectrum ana-

<sup>1</sup> J. C. Slater, *Microwave Transmission* McGraw-Hill, New York, 1942, p. 35.



lyzer) to a convenient magnitude; the distances  $\delta'$  through which the probe has to be moved in either direction from the maximum in order to obtain half-power indication, are then recorded.

Although the derivation of Eq. (12) was based on the theory of the coaxial transmission line with real characteristic impedance, it can be shown that for small values of attenuation, such as encountered in transmission systems and low-loss cables, the same result is obtained with a

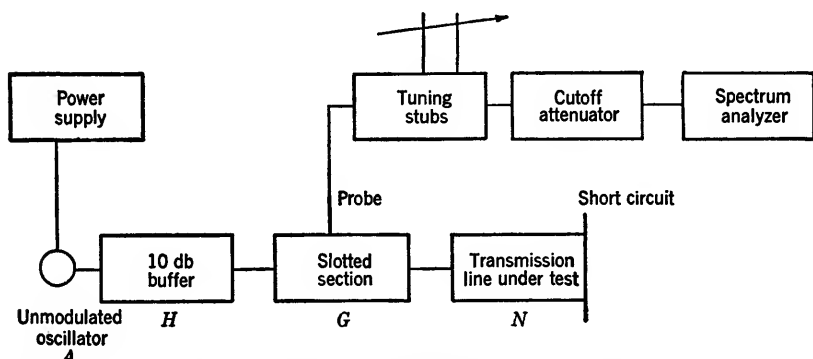


FIG. 13-16.—Schematic arrangement for measurement of attenuation constant of transmission lines.

complex characteristic impedance as is normally associated with a complex propagation constant. It is also irrelevant whether the losses are caused by series resistance, such as the losses in the conductors themselves, or whether they are caused by transverse conductance, such as the losses in dielectric materials filling the space between the conductors; the total attenuation  $\alpha$  becomes the sum of these two separate contributions. Finally, the same analysis is directly applicable to waveguide transmission systems in which only one mode is utilized for power transmission.

*Direct Measurement of Standing-wave Ratio.*—The previous method requires a precision measurement of a very small distance if the attenuation is very slight. In order to improve the accuracy, the same physical arrangement may be used as is shown in Fig. 13-16 to measure directly the large VSWR by means of the cutoff attenuator. The VSWR is defined in terms of maximum and minimum values of the voltage distribution on the line by

$$r = \frac{|V_{\max}|}{|V_{\min}|}, \quad (14)$$

and can, of course, be converted into decibels of power ratio by taking  $20 \log_{10} r$ ; this value is then directly read on the attenuator indicator.

Since the voltage distribution along a short-circuited transmission

line as referred to the short-circuit terminal is given by

$$V = V_0 \sinh \gamma x$$

with the absolute value

$$|V| = |V_0| (\sinh^2 \alpha x + \sin^2 \beta x)^{1/2}, \quad (15)$$

the maximum and minimum values may be easily found and the VSWR of Eq. (14) may be deduced for the approximation of slight attenuation,

$$r = \frac{\beta_0}{n\pi\alpha} = \frac{2Q}{n\pi}, \quad (16)$$

or also

$$\alpha = \frac{\beta_0}{n\pi r} = \left( n \frac{\lambda_0}{2} r \right)^{-1} \quad \text{neper/m}, \quad (17)$$

where  $n(\lambda_0/2)$  is the distance of the voltage minimum utilized in Eq. (14). It is irrelevant whether the VSWR is measured to the preceding or to the succeeding voltage maximum as long as the attenuation is small enough to justify the simplified derivation. This method is equally applicable to coaxial transmission lines and waveguides that utilize only one mode for the transmission of power. Of course,  $\alpha$  will refer to this particular mode only.

For the measurement of the large VSWR, other suitable detector arrangements may be substituted, such as a crystal detector with galvanometer. A calibrated d-c attenuator would be placed between the crystal detector and the galvanometer in order to operate the galvanometer at optimum accuracy.

**13-5. Common Sources of Error in Attenuation Measurements.**—The most prominent sources of error in almost all methods of attenuation measurement are directly related to the physical arrangements. The attenuation of a microwave component has been defined in Sec. 11-1 in terms of normalized terminal conditions in either direction from the unknown component. Seldom, however, will these conditions be met exactly in practical measurements. The deviations constitute some of the most important sources of error. Other important sources are: leakage at the junctions of the microwave transmission system, which becomes particularly important in the measurement of large values of attenuation; reaction of the input impedance of the unknown component upon the generator power level or frequency if this impedance deviates from the standardized line impedance; and finally, instability in the detector section which usually contains an amplifier or heterodyne receiver.

*Errors Caused by Reflection Interactions.*—For a consideration of the effects caused by mismatches in the generator and detector sections, it is

most convenient to replace the unknown microwave component by a general, passive, linear four-terminal network of matrix  $\begin{pmatrix} A & B \\ C & D \end{pmatrix}$ .

The general equivalent network arrangement of Fig. 13.1 then becomes that of Fig. 13.17. Performing the measurement according to the definition of attenuation, first, the power in load  $Z_L$  would be measured when it is directly connected to the generator section, then with the network inserted. The power ratio is given by conventional network theory as

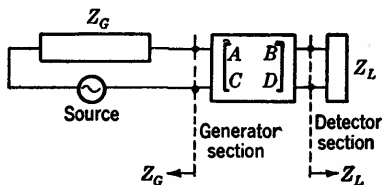


FIG. 13.17.—Equivalent network for attenuation measurement.

$$p = \left| \frac{(AZ_L + B) + (CZ_L + D)Z_G}{Z_L + Z_G} \right|^2. \quad (18)$$

Since attenuation is defined in terms of the power ratio with

$$Z_L = Z_G = Z_0,$$

the characteristic impedance of the transmission-line system,

$$p_0 = \left| \frac{(AZ_0 + B) + (CZ_0 + D)Z_0}{2Z_0} \right|^2 = \frac{1}{4} |A + \mathfrak{B} + \mathfrak{C} + D|^2, \quad (19)$$

if the convenient normalized parameters are used,

$$\mathfrak{B} = \frac{B}{Z_0}, \quad \mathfrak{C} = CZ_0. \quad (20)$$

The error of measurement can now be expressed in terms of Eqs. (18) and (19) as a correction factor,

$$\frac{p}{p_0} = \left| \frac{(Aq_L + \mathfrak{B}) + (\mathfrak{C}q_L + D)q_G}{A + \mathfrak{B} + \mathfrak{C} + D} \cdot \frac{2}{q_L + q_G} \right|^2, \quad (21)$$

where the further abbreviations have been introduced

$$q_L = \frac{Z_L}{Z_0}, \quad q_G = \frac{Z_G}{Z_0}. \quad (22)$$

It is most convenient to reduce all terms in Eq. (21) to directly measurable reflection factors, as for example:

$$R_G = \frac{1 - q_G}{1 + q_G}, \text{ reflection factor of generator section,}$$

$$R_L = \frac{1 - q_L}{1 + q_L}, \text{ reflection factor of detector section,}$$

$R' = \frac{1 - q'}{1 + q'}$  with  $q' = \frac{Aq_L + \mathfrak{B}}{\mathfrak{C}q_L + D}$ , reflection factor at the left terminals of a four-terminal network if its right terminals are connected to load impedance  $Z_L$ ,

$R'_0 = \frac{1 - q'_0}{1 + q'_0}$ , with  $q'_0 = \frac{A + \mathfrak{B}}{\mathfrak{C} + D}$ , reflection factor at the left terminals of a four-terminal network if its right terminals are connected to a matched load  $Z_L = Z_0$ ,

$R'' = \frac{1 - q''}{1 + q''}$  with  $q'' = \frac{Dq_G + \mathfrak{B}}{\mathfrak{C}q_G + A}$ , reflection factor at the right terminals of a four-terminal network if its left terminals are connected to generator impedance  $Z_G$ ,

$R''_0 = \frac{1 - q''_0}{1 + q''_0}$ , with  $q''_0 = \frac{D + \mathfrak{B}}{\mathfrak{C} + A}$ , reflection factor at the right terminals of a four-terminal network if its left terminals are connected to a matched impedance  $Z_G = Z_0$ .

With these designations, the correction factor in Eq. (21) can be shown to take the alternative forms

$$\frac{p}{p_0} = \left| \frac{(1 - R''_0 R_L)(1 - R' R_G)}{1 - R_L R_G} \right|^2 = \left| \frac{(1 - R'_0 R_G)(1 - R'' R_L)}{1 - R_G R_L} \right|^2. \quad (23)$$

From an exact knowledge of the  $R$ -values, which are in general complex, the deviation in any particular measurement may be computed as

$$\Delta A = 20 \log_{10} \left| \frac{(1 - R''_0 R_L)(1 - R' R_G)}{1 - R_L R_G} \right| \quad \text{db.} \quad (24)$$

In most practical cases, however, the exact determination of the  $R$ -values is too cumbersome, if at all feasible, whereas the values of the voltage standing-wave ratio can be readily obtained. It is then possible to deduce only maximum errors in values obtained by accepting the measured power ratio as indicative of the attenuation of the tested component. The voltage standing-wave ratio is directly related to the absolute value of the reflection coefficient  $|R|$  by the monotonic relations

$$r = \frac{1 + |R|}{1 - |R|}, \quad |R| = \frac{r - 1}{r + 1}. \quad (25)$$

By choosing the worst phase combinations for the reflection factors  $R$ , the maximum error, either positive or negative, follows from Eq. (24) as

$$(\Delta A)_{\max} = 20 [\log_{10} (1 \pm |R''_0| |R_L|) + \log_{10} (1 \pm |R'| |R_G|) - \log_{10} (1 \pm |R_L| |R_G|)]. \quad (26)$$

From given values of the various standing-wave ratios, the absolute

values of the corresponding reflection coefficients are first calculated from Eq. (25); these values are then inserted in Eq. (26). The upper signs lead to the maximum positive error, the lower signs to the maximum negative error. It is not obvious which maximum will usually be the

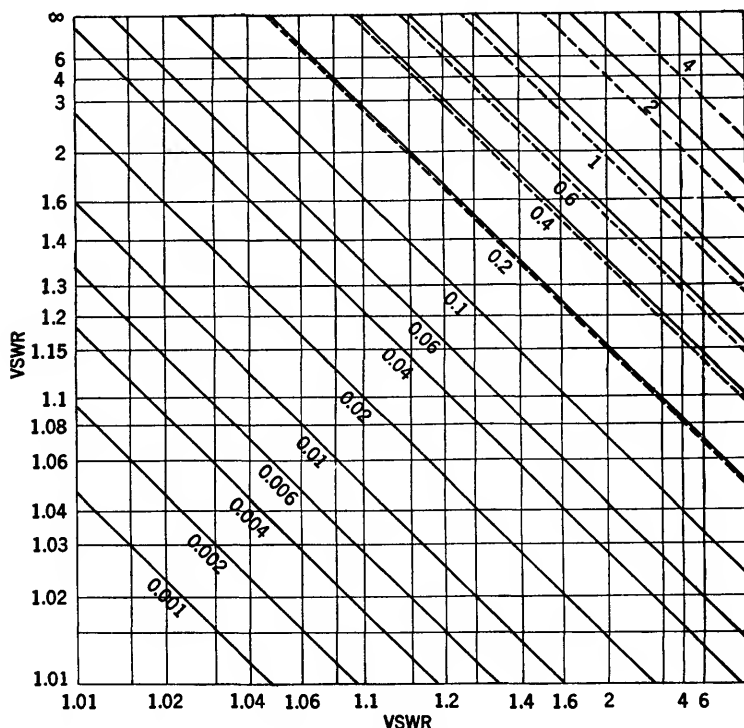


FIG. 13-18.—Values of  $\pm 20 \log_{10} \left( 1 \pm \frac{r_1 - 1}{r_1 + 1} \cdot \frac{r_2 - 1}{r_2 + 1} \right)$ . The solid lines refer to the plus sign, the dotted lines to the negative sign.

larger one. To aid in the application to practical cases a chart of the general function

$$\pm 20 \log_{10} (1 \pm |R_1||R_2|) = \pm 20 \log_{10} \left( 1 \pm \frac{r_1 - 1}{r_1 + 1} \cdot \frac{r_2 - 1}{r_2 + 1} \right)$$

is given in Fig. 13-18, whereby the solid diagonals refer to the upper sign and the dotted diagonals to the lower sign.

As a numerical example, assume that the VSWR values in the various combinations have been measured as

$$r' = 1.15, \quad r''_0 = 1.1, \quad r_G = 2, \quad r_L = 1.4.$$

From Fig. 13-18, the values are found

$$\begin{array}{r} +20 \log_{10} (1 \pm |R'_0||R_L|) = +0.20, -0.21 \\ +20 \log_{10} (1 \pm |R'||R_G|) = +0.07, -0.07 \\ -20 \log_{10} (1 \pm |R_L||R_G|) = +0.51, -0.48 \\ \hline (\Delta A)_{\max} = +0.78, -0.76 \quad \text{db.} \end{array}$$

The measured insertion loss can therefore be anywhere from 0.78 db higher to 0.76 db lower than the desired (matched) attenuation value.

From the general form of the correction factor in Eq. (21), it is obvious that reversal of the microwave component will lead to a different value of measured insertion loss, since, upon reversal, the parameters  $A$  and  $D$  interchange. If, on the other hand,  $Z_L = Z_G$ , but not matched, then reversal of the microwave component leaves the measured insertion loss unchanged because of the symmetrical form of Eq. (21).

A different and considerably simplified treatment<sup>1</sup> of the reflection effects on the input power level of attenuators is possible which permits the evaluation of deviations in the power level with fixed values, but varying phase relations, at any particular junction in a microwave system. It may be shown that the actual power level might differ in two separate measurements involving given VSWR values by a maximum amount of

$$\Delta P_{\max} = \pm 10 \left| \log_{10} \frac{q_1}{(1 - q_1)^2} - \log_{10} \frac{q_2}{(1 + q_2)^2} \right| \quad \text{db,} \quad (27)$$

where

$$\begin{array}{l} q_1 \text{ is the smaller of } r'/r_G \text{ or } r''/r_G, \\ q_2 \text{ is the larger of } r'/r_G \text{ or } r''/r_G, \end{array}$$

and where  $r_G$  is the VSWR at the junction towards the generator section, and  $r'$  and  $r''$  are the VSWR values at the same junction in two successive measurements towards the detector section. An alternative expression is

$$\Delta P_{\max} = \pm 10 \left| \log_{10} \frac{(1 + |R'||R_G|)^2}{(1 - |R''||R_G|)^2} \cdot \frac{1 - |R''|^2}{1 - |R'|^2} \right|, \quad (28)$$

in which the reflection factors correspond to the VSWR values defined above.

*Measurement of the VSWR of the Generator Section.*—The actual evaluation of the VSWR of the generator section with the oscillator in operation is generally rather difficult. A simple scheme, which avoids substantial reaction on the output voltage of the oscillator (if proper buffering is used), is the following. A sliding reactance, such as a deeply penetrating probe of a slotted section, is introduced and the

<sup>1</sup> E. Weber, "Errors in Attenuation Measurements Caused by Reflection Losses," NDRC 14-365, PIB-39, Mar 16, 1945.

maximum and minimum indications on the detector are observed. If  $R_L$  and  $R_G$  are the reflection factors already defined, and if the detector measures voltage, then the ratio of maximum to minimum indication is

$$\frac{V_{\max}}{V_{\min}} = r = \frac{1 + |R_L||R_G|}{1 - |R_L||R_G|}. \quad (29)$$

If the value  $|R_L|$  is known, it is easy to compute the value  $|R_G|$  or to find it from Fig. 13-19.

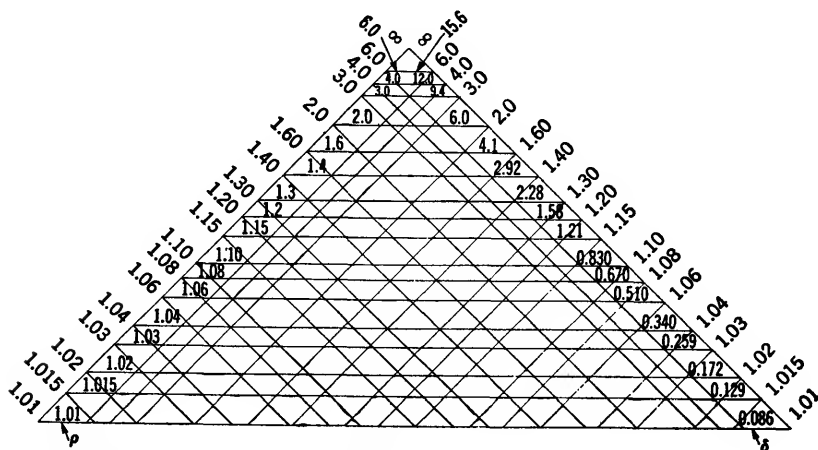


FIG. 13-19.—Values of  $\delta = 20 \log_{10} \rho$  and

$$\rho = \frac{1 + \left(\frac{r_1 - 1}{r_1 + 1}\right) \left(\frac{r_2 - 1}{r_2 + 1}\right)}{1 - \left(\frac{r_1 - 1}{r_1 + 1}\right) \left(\frac{r_2 - 1}{r_2 + 1}\right)}$$

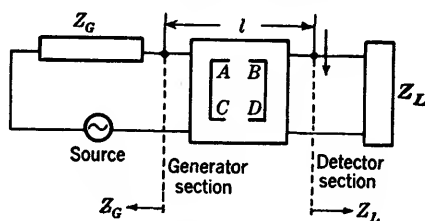


FIG. 13-20.—Schematic arrangement for the measurement of the VSWR of the generator section.

To demonstrate the validity of Eq. (29), assume as indicated in Fig. 13-20 that the probe forms part of the detector section, and that the transmission line of length  $l$  is a four-terminal network of variable insertion loss (caused by the phase of the probe reflection). The four-terminal-network parameters of the lossless transmission line of characteristic impedance  $Z_0$  and propagation constant  $\gamma = j\beta$  are

$$\begin{pmatrix} A & B \\ C & D \end{pmatrix} = \begin{pmatrix} \cos \beta l & jZ_0 \sin \beta l \\ j\frac{1}{Z_0} \sin \beta l & \cos \beta l \end{pmatrix}. \quad (30)$$

Using the previous definitions,

$$R' = R_L e^{-2j\beta l}, \quad R_0'' = 0,$$

and therefore the correction factor of the insertion loss from Eq. (23) is

$$\frac{p}{p_0} = \left| \frac{1 - R_L R_G e^{-2j\beta l}}{1 - R_L R_G} \right|. \quad (31)$$

The maximum and minimum values, respectively, can be found, and their ratio leads to

$$\frac{p_{\max}}{p_{\min}} = \left( \frac{1 + |R_L||R_G|}{1 - |R_L||R_G|} \right)^2,$$

from which Eq. (29) is obtained.

*Error Caused by Leakage.*—The second important source of error is leakage at junctions in the microwave transmission system. Suppose the microwave power level in a transmission line at a particular point is  $P_0$ , and there exists, at that point, a source of power  $P_L$  as leakage from the generator or from other parts of the line. The extreme values of the resulting power level must, however, be computed from the superposition of the signal voltage  $E_0$  and leakage voltage  $E_L$ . When attenuation is being measured, either by insertion of a microwave attenuator in the line or by changing a variable attenuator, the relative phase of the voltages  $E_0$  and  $E_L$  may take any value whatsoever, so that the error in the final power measurement becomes

$$\Delta P = 10 \log_{10} \left( \frac{E_0 \pm E_L}{E_0} \right)^2 = 20 \log_{10} \left( \frac{E_0 \pm E_L}{E_0} \right) \quad \text{db.} \quad (32)$$

Assume that in the measurement of large attenuation, the final power is 70 dbm, and that the leakage power radiating back into the transmission line is 90 dbm, then the relative leakage power is  $P_L = 0.01P_0$ , and, therefore, the relative voltage  $E_L = 0.1E_0$ . The error in power measurement thus becomes

$$\Delta P = 20 \log_{10} (1.1) \quad \text{or} \quad 20 \log_{10} (0.9) = \begin{Bmatrix} +0.827 \\ -0.915 \end{Bmatrix} \quad \text{db,}$$

a rather appreciable error affecting the accuracy of attenuation measurements. In order to make sure that the error is less than 0.1 db, the entering leakage power must be about 40 db below the main transmission-line power. Assuming a buffer attenuation of 10 db in the generator section, and another buffer of 10 db before the detector, then for the measurement of 75 db, the leakage path between generator and detector



must have at least 135 db attenuation. This indicates the seriousness of the problem. The following table gives the maximum errors in attenuation measurements with  $L = 10 \log_{10} (P_L/P_0)$ , a measure of the leakage power in decibels relative to  $P_0$ .

TABLE 13-1.—MAXIMUM ERROR IN ATTENUATION MEASUREMENT CAUSED BY LEAKAGE EFFECTS

<i>L</i> , db	Maximum error, in db	
	If leakage adds	If leakage subtracts
+ 6.0	.....	+9.6
+ 3.0	.....	+7.6
0.0	.....	+6.0
- 3.0	-10.7	+4.7
- 6.0	- 6.0	+3.5
-10.0	- 3.3	+2.4
-15.0	- 1.7	+1.4
-20.0	- 0.9	+0.8
-25.0	- 0.5	+0.4
-30.0	- 0.2	+0.2
-40.0	- 0.09	+0.09

Leakage may be detected by changing the relative phase and noting the variation of the signal. This may be done with a line stretcher or by moving a large sheet of metal in the vicinity of the transmission line. Leakage can usually be reduced sufficiently by putting the generator in a shield can, by using polyiron chokes on all d-c leads with access to the transmission line, by making all connections tight, and by covering joints with steel wool or conducting paint.

*Errors Caused by Instability of Power Level.*—Since most methods of attenuation measurement compare absolute power levels with and without the unknown microwave component, the measurements are very sensitive to variations in the power level of both the microwave power source and the local oscillator in the detector section, whether the detector is of microwave, intermediate, or audio frequency.

In order to minimize power-level fluctuations in the main oscillator, thermal stability, stability to supply-voltage variations, and stability of the cavity resonator are required. A number of schemes of automatic supply-voltage regulation, of cavity-resonator control, and of thermal compensations have been developed individually for the various types of oscillator tubes.

The importance of minimizing reflection interactions has already been stressed. The value and phase of the load impedance presented at the oscillator terminals greatly influences its output power, and

variations during attenuation measurement will cause errors of unpredictable magnitude. It is for this reason that the buffer  $H$  in Sec. 13-1 assumes considerable importance. Its value must be so chosen that variations of the impedance in its output plane are sufficiently reduced to cause only insignificant variations in its input plane. Usually about 10 db of attenuation proves sufficient. The allowable variations in the impedance of the input plane can best be gauged by the pertinent performance diagrams of the oscillator tube.

In a similar manner, power-level fluctuations of the local oscillator of the detector section will cause errors in attenuation measurements, and similar precautions must be taken. In addition, instability might occur in the amplifier, or in other associated circuits of the detector section with detrimental effects upon the accuracy of the indicator. Some of these effects will be treated more fully in connection with the calibration of attenuator standards, where they are, obviously, of greater concern.

**13-6. Calibration of Attenuation Standards.**—Even though absolute measurement of power ratios is possible, it is convenient to have available devices that may be calibrated for use as attenuation standards. The cutoff attenuator might be useful as a primary standard if freedom from higher modes could be assured. It seems safer, though, to verify by careful attenuation measurements or “absolute calibration,” that it is usable as a primary standard; reliance on the accuracy of mechanical construction alone is not advisable. For most purposes of laboratory or field measurements, secondary standards of the dissipative type are preferable and are satisfactory if they have been calibrated either by absolute power measurements or by comparison with a cutoff attenuator certified as a primary standard.

In general, the suitability of an attenuating device as a standard is characterized by the accuracy, permanency, and range of validity of its calibration. In turn, the accuracy of calibration relies upon the method of measuring attenuation; the permanency of the calibration is subject to the stability of the attenuating element as affected by aging, by atmospheric influences, and by the precision of the mechanical movement to ensure extreme reliability in setting; whereas the range of validity refers to the variation of calibration values with ambient temperature, with frequency, with air pressure, or with other influencing factors.

*Primary Standards.*—The waveguide-beyond-cutoff attenuator with only one mode of electromagnetic-field distribution could well be used as a primary standard since its attenuation rate (exclusive of conductor losses) is theoretically defined (see also Sec. 11-3) by

$$\alpha = \frac{2\pi}{\lambda_c} \sqrt{1 - \left(\frac{\lambda_c}{\lambda}\right)^2} \quad (33)$$

with

$$\lambda_c = \frac{2 \sqrt{k_e}}{\sqrt{\left(\frac{m}{a}\right)^2 + \left(\frac{n}{b}\right)^2}} \quad (34)$$

for rectangular waveguides of large inside dimension  $a$  and small inside dimension  $b$ ; or with

$$\lambda_c = \frac{2\pi \sqrt{k_e}}{k_{m,n}} a \quad (35)$$

for circular waveguide of inside radius  $a$ . In both cases  $k_e$  is the relative dielectric constant referred to that of free space. As discussed in Secs. 11.4 to 11.6 it is difficult to ensure the presence of only one mode of field distribution. In fact, the theoretical values of the rate of attenuation  $\alpha$  can be only approximately achieved by special selective microwave filter sections such as the iris coupling in the standard attenuators described in Secs. 11.10 and 11.11, or by special design of the coupling elements as described in Sec. 11.12, or, finally, by the most promising method of dielectric mode filters<sup>1</sup> as described briefly in Sec. 11.6. The most commonly encountered cutoff attenuators employ iris coupling, and only this type will be considered further.

Since the iris-coupled cutoff attenuator uses the dominant mode ( $TE_{11}$ ) in the circular waveguide with  $k_{11} = 1.841$ , the effect of the other modes, if present, upon linearity will necessarily be limited to the region of lower attenuation. It is advisable, in fact necessary, to check the beginning of the linear region in each individual cutoff attenuator with a fixed position of the receiving loop, since the absolute value of  $\alpha$  can be used only within the linear region. This requires a very accurate measurement of attenuation such as described in Sec. 13.7. Unfortunately, the large value of initial attenuation caused by the impedance-matching devices might cause the nonlinearity to extend as high as 40 or 50 db which makes it rather difficult in certain cases to verify the onset of the usable region.

Moreover, the accuracy of the value of  $\alpha$  used depends on the mechanical measurement of the diameter of the tube and of its true circular cylindrical shape. It is best, then, to verify the exact value of  $\alpha$  by accurate attenuation measurements, since according to Sec. 11.3.

$$\frac{d\alpha}{\alpha} = - \frac{da}{a} \quad (36)$$

for  $\lambda_c^2 \ll \lambda^2$ , the variations of the diameter have a directly proportional effect upon the attenuation rate  $\alpha$ .

<sup>1</sup> A. B. Giordano, "Microwave Attenuation Standards," NDRC 14-531, Oct. 31, 1945.

Permanency of calibration is dependent only on mechanical features, particularly the exact angular position of the receiving loop. As to the range of validity of the calibration, variation of the calibration value of  $\alpha$  is possible with frequency, temperature, humidity, and air pressure. From Eq. (35), assuming  $\lambda_c^2 \ll \lambda^2$ , one finds

$$\frac{d\alpha}{\alpha} = -\frac{1}{2} \frac{dk_e}{k_e}, \quad (37)$$

the effect of relative changes in the dielectric constant with temperature, humidity, or air pressure. Adequate corrections for these effects, however, can readily be made.

The variation of attenuation with wavelength can be obtained from Eq. (33) as

$$\frac{d\alpha}{\alpha} = 2 \left( \frac{\lambda_c}{\lambda} \right)^2 \frac{d\lambda}{\lambda}. \quad (38)$$

The variation is small for  $(\lambda_c/\lambda)^2 \ll 1$ , but has to be taken into account for wideband use of the cutoff attenuator (see Sec. 12-3). Equation (38) indicates a decreasing rate of change of  $\alpha$  with increasing wavelength so that the design wavelength should be chosen closer to the short-wavelength end of the band considered. Assuming that  $\lambda_1$  and  $\lambda_2$  are the shortest and longest wavelengths, respectively, in the design wavelength band, and that  $(\lambda_c/\lambda_1)^2 \ll 1$  to ensure minimum attenuation change over the band, then the design wavelength  $\lambda_d$  should be chosen in accordance with

$$\frac{1}{\lambda_d^2} = \frac{1}{2} \left( \frac{1}{\lambda_1^2} + \frac{1}{\lambda_2^2} \right), \quad (39)$$

in order to give symmetry with respect to attenuation variations. This total variation of attenuation is given by

$$\delta\alpha = \pm \frac{2\pi}{\lambda_c} \left[ \left( \frac{\lambda_c}{\lambda_1} \right)^2 - \left( \frac{\lambda_c}{\lambda_2} \right)^2 \right] \quad (40)$$

referred to the attenuation at the design wavelength. To illustrate, let  $\lambda_1 = 8$  cm,  $\lambda_2 = 12$  cm, and have  $\lambda_c = 2$  cm so that

$$\left( \frac{\lambda_c}{\lambda_1} \right)^2 = 0.0625 \ll 1,$$

then  $\lambda_d = 9.42$  cm, and  $\delta\alpha = \pm 0.027$  neper/cm =  $\pm 0.237$  db/cm, an appreciable value well above the accuracy of calibration.

Because of the exacting mechanical accuracies required, satisfactory primary standards have been developed principally for the longer wavelengths; none is available yet for wavelengths shorter than 3 cm. For accurate setting of a selected attenuation value or for recording

attenuation values in substitution measurements, the position of the receiver loop is read on a precision dial indicator with divisions of 0.001 in. In most measurements, only relative attenuation readings need be taken, namely, differences of indicator readings, which can be made very accurately. The knowledge of the theoretical attenuation rate makes the cutoff attenuator as accurate as the indicator reading can be made—makes it truly a primary standard for the linear range of attenuation.

*Secondary Standards.*—Any standard which requires calibration either by independent power measurement or by comparison with a primary standard is usually considered a secondary standard since its accuracy must be lower than that of a theoretically defined standard value. Thus, all cutoff attenuators in their nonlinear region are secondary standards. Because of their high minimum attenuation, these cutoff attenuators are not very useful as secondary standards, except that they can be built quite ruggedly and can be enclosed in a comparatively small space.

Dissipative attenuators have the advantage of practically vanishing minimum attenuation; the metalized-glass precision attenuators have, furthermore, the advantage of permanency and considerable range of validity of calibration, and, if variable, they can also be made very accurate by suitable precision drives. These metalized-glass attenuators have, therefore, gained considerable prominence as secondary standards in laboratories and for portable microwave test sets.

Fixed coaxial attenuators of the metalized-glass type in  $\frac{7}{8}$ -in. line size are particularly suitable as gauge blocks or fixed attenuation standards (see Sec. 12-13); they can also be used to extend the range of precise power measurements. The performance of these units has been extremely reliable. Similarly, broadband fixed waveguide attenuators with metalized-glass plates in the various standard sizes can be carefully calibrated for use as gauge blocks to verify linearity of cutoff attenuators, or for extending the range of precise power measurements (see Sec. 12-16). In order to ensure permanency of calibration, it is necessary to use metalized-glass plates with German-silver eyelets and to solder these to the supporting struts; the use of cements cannot be recommended because atmospheric conditions sooner or later cause deterioration with attendant drift of calibration.

Variable coaxial attenuators with metalized glass as power absorbing inserts have been used as secondary laboratory standards (see Sec. 12-14); the permanence of the calibration of well-made assemblies has been demonstrated, although moderate fragility prevents their use outside of laboratories. The internal mechanical structure makes the unit in the present form suitable only for narrow frequency bands that can be accommodated in the  $\frac{7}{8}$ -in. coaxial-line size.

Several very satisfactory designs of variable waveguide secondary attenuator standards have been developed using metalized-glass plates. One example suitable for the wavelength range from 3.1 to 3.6 cm is shown in Fig. 13-21. The waveguide casing of this precision attenuator is made of cast brass, accurately milled in two halves to attain a high degree of uniformity. The two halves are soldered together. The casing is pinned and screwed to a cast steel base. The struts supporting the

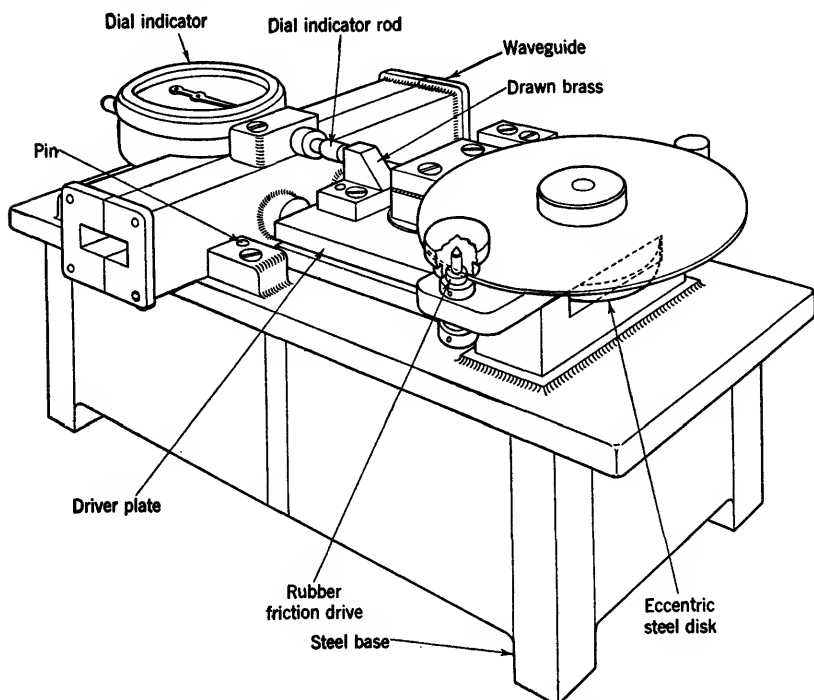


FIG. 13-21.—Waveguide metalized-glass attenuator standard.

glass plate are short and move freely through the side wall of the waveguide casing without contact bearing, the motion being supplied by a precision mechanical drive. This drive is kinematically designed and the carriage is supported on precision ball bearings. The movement of the plate in  $1/10,000$ -in. steps is recorded on a dial indicator fastened securely to the waveguide casing. The front plane of the boss driving the rod of the indicator dial is also the driving plane of the struts so that only the differential expansion of the rod and strut materials can cause uncompensated temperature effects on the mechanical alignment. A typical calibration curve is shown in Fig. 12-60 indicating an over-all spread of attenuation with frequency of the same order as would be

expected from a corresponding cutoff attenuator; the VSWR over most of the frequency range is less than 1.1 because of the short supporting struts for the metalized-glass plate.

In order to check temperature sensitivity, special tests were performed with one sample attenuator. At room temperature, with the plate in its minimum position close to the guide wall, the movable dial of the gauge was set so that the indicating hand pointed to the zero of the dial. This will be referred to as the zero setting. By attenuation measurements, the dial reading for a 30-db change in attenuation at 3.2 cm was determined at room temperature. The attenuator was heated by using incandescent light bulbs distributed around and above the unit. The temperature was observed at various parts of the attenuator, and when a temperature equilibrium was reached, measurements were repeated to ascertain the dial reading corresponding to 30 db at the new temperature and the zero setting. The results of these tests are shown in Table 13-2.

TABLE 13-2.—CHECK OF TEMPERATURE SENSITIVITY OF SECONDARY ATTENUATION STANDARD

Temp., °C	Average dial reading of 4 tests, mils	Zero setting, mils	Temp. change, °C	Dial reading minus zero setting, mils	Deviation with reference to dial reading of 108.59 mils, db
25	108.59	0	0	108.59	0
30	108.37	-0.22	5	108.59	0.00
35	108.25	-0.37	10	108.62	0.015
40	108.08	-0.53	15	108.61	0.01
45	107.92	-0.70	20	108.62	0.015
25	108.59	0	0	108.59	0

The negative value of the zero setting signifies that the indicating hand read less than the zero value of the dial when the metalized-glass plate was returned to its minimum position. The average dial reading of the 30-db value is with respect to the zero of the dial. However, if the change in the zero setting is taken into account, the dial reading of the 30-db value of the attenuator remains practically constant with temperature. This leads to the conclusion that the change of zero setting with temperature is caused only by the temperature coefficient of the gauge and that temperature changes do not affect the attenuation calibration of this precision attenuator if the minimum position of the indicating hand is made to correspond to the zero of the dial when the unit is being used.

Another example suitable for frequencies near 24,000 Mc/sec has been described in Sec. 12-17 by the calibration curve shown in Fig. 12-62.

The special drive mechanism for this guillotine attenuator is accurate enough to permit resetting to better than  $\pm 0.1$  db.

**13-7. Calibration with Absolute Power Measurement.**—For the calibration of secondary standards as well as for the verification of linearity of a primary standard, very accurate methods of attenuation measurement must be chosen. The most reliable method based on direct measurement of the power ratio is the Ballantine-voltmeter method. Although the common errors in attenuation measurements have been described in Sec. 13-5, a more extensive and quantitative discussion of the specific errors in this particular method will be given in order to demonstrate possible improvements in accuracy as needed for careful calibration.

The circuit arrangement of the method is as shown in Fig. 13-3. The effects of instability of the generator and of variable contacts in the connectors of the transmission-line equipment, can with care be kept to less than  $\pm 0.05$  db. Particular care must be taken to establish proper and repeatable contacts at all junctions. To realize this condition, all contact surfaces should be cleaned with alcohol. In the case of  $\frac{1}{8}$ -in. coaxial lines, all male pins should be sprung. Coaxial fittings with type N couplings should be fastened securely to the table, so that no relative motion can occur between the components; the type N fittings themselves should also be thoroughly cleaned with alcohol and mechanically adjusted to afford the best possible contact. The importance of cleanliness is emphasized by the fact that dirty contact faces on  $\frac{1}{8}$ -in. couplings can increase the above error to 0.15 or 0.2 db. If the components of the setup are loosely connected, additional errors may result. These errors depend on the location of the loose connections and are erratic; errors as large as 1 db have been observed when loose connections are present and components are out of line. They may be attributed to leakage as well as the large reflections created at the discontinuities. It is, therefore, necessary to make all connections reasonably tight.

Specifically associated with the Ballantine-voltmeter arrangement is the error produced by the nonlinearity of the Wollaston-wire bolometer, and the total residual error of the Ballantine voltmeter after all known corrections have been made.

*Nonlinearity of Bolometer Characteristic.*—The nonlinearity of the static (d-c) characteristic of the bolometer element can easily be demonstrated as in Sec. 3-24. For practical evaluation of the bolometer characteristics it is more convenient to use an approximate empirical relation

$$R - R_0 = KP^n, \quad (41)$$

where  $R$  is the bolometer resistance in ohms at a specific d-c power level  $P$  in milliwatts,  $R_0$  the bolometer resistance at  $P = 0$ ,  $n$  the exponent



to be determined experimentally, and  $K$  a proportionality factor. The unknown parameters  $n$  and  $K$  of this expression may be determined by means of the method of least squares from experimental data of  $P$  and  $R$  for any particular bolometer element. With the actual units typical values for Sperry barretters are  $n = 0.9$ ,  $K = 7.57$ .

Measuring attenuation, the bolometer will first carry the larger r-f power without the unknown attenuator inserted. Using symmetrical square-wave modulation the peak r-f power ( $P_2 - P_1$ ) superimposed on the bias d-c power  $P_1$  is twice the average r-f power which defines the average over-all resistance. Inserting the unknown attenuator, the r-f power in the bolometer element is reduced considerably so that the total resistance will be close to the value  $R_1$  corresponding to the power  $P_1$ . Since the audio amplifier utilizes only the a-c component of the voltage established across the bolometer resistance, the nonlinearity will cause an error in the power ratio. Figure 3-49 is a graph of the percentage deviation from square-law response as a function of the power increment  $P_2 - P_1$ .

*Accuracy of Ballantine Voltmeter and Preamplifier.*—In the analysis of the over-all error introduced by the Ballantine voltmeter and preamplifier, the problem can be divided into two parts: (1) the combined error caused by the nonlinearity of the preamplifier and voltmeter amplifier, by inaccurate meter graduations, by discrepancies introduced by the meter movement, and by personal error in the meter reading, and (2) the error introduced by the inaccuracy of the range switches on the Ballantine voltmeter.

The accuracy of the complete Ballantine-voltmeter circuit together with the preamplifier is best determined by measuring it with a well-calibrated Daven decade attenuator as a reference standard.

As an example, a Ballantine voltmeter Model No. 300 with a battery-operated preamplifier was selected. The combination has an over-all gain of 120 db. The preamplifier employs a highly selective feedback circuit such that only the modulation frequency is amplified; thus the noise level at the input terminals of the Ballantine voltmeter is reduced. The scale of the voltmeter is linear in decibels and is of such dimensions that it can be read accurately to 0.1 db. For its calibration a Daven decade attenuator box, Model T-692, with a range from 0 to 111 db was chosen.

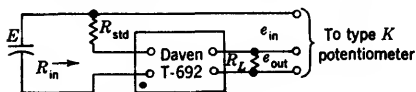
The calibration of the Daven attenuator box was carried through with a Leeds and Northrup type K precision potentiometer using the circuit arrangement shown in Fig. 13-22. The input voltage to the decade attenuator is given by

$$e_{in} = \frac{R_{in}}{R_{std}} e'_{in}; \quad (42)$$

the attenuation for each step is found by

$$a_{\text{step}} = 20 \log_{10} \frac{e_{\text{in}}}{e_{\text{out}}} \quad (43)$$

As indicated, the values of the resistor  $R_L$ ,  $R_{\text{in}}$ ,  $R_{\text{std}}$  were determined



$R_L = 500.000 \pm 0.1\%$  ohms  
 $R_{\text{std}} = 50.064 \pm 0.1\%$  ohms  
 $R_{\text{in}}$  measured at each step  $\pm 0.1\%$  ohms

FIG. 13-22.—Calibration of Daven decade attenuator box.

with good accuracy, the repeatability of the type K potentiometer for two successive runs being within  $\pm 0.01$  per cent on the 10-db and 1-db step dials, and  $\pm 0.1$  per cent on the 0.1-db step dial.

The calibration of the Ballantine voltmeter and preamplifier

was carried out with the calibrated Daven attenuator box connected to the unit under test, as shown in Fig. 13-23. With the 10-db step dial, the insertion loss of the decade attenuator was adjusted for 20 db, and the audio level set to full-scale reading on the Ballantine voltmeter. The decade attenuator was adjusted so that the voltmeter read the

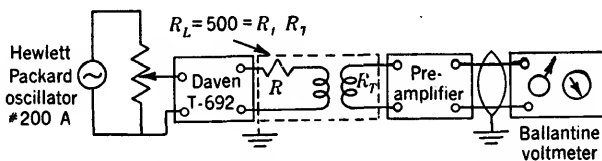


FIG. 13-23.—Calibration of the Ballantine voltmeter and preamplifier.

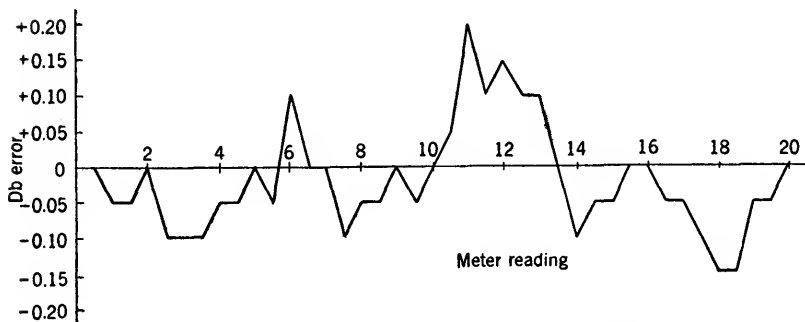


FIG. 13-24.—Correction curve for Ballantine voltmeter.

exact scale markings from 20 to 0 db in one-half-decibel steps. The corrected reading was taken at each scale graduation from the calibration data of the Daven attenuator box, T-692, and the correction plotted in Fig. 13-24.

The personal error was reduced to a minimum value, for each reading

was repeated by two different observers for three successive runs. From the figure, it can be seen that when this instrument is used with a square-law detector, the resulting error  $\Delta_v$  will be  $\pm 0.15$  db. Interpolation of the curve in Fig. 13-24 will reduce this error to  $\pm 0.05$  db.

The range switches on the Ballantine voltmeter can be checked by a procedure similar to that described for the amplifier-linearity test. In the same example, the range-switch error was not detectable for any one step. It was estimated that the sum of the four range positions would not introduce an error greater than  $\pm 0.05$  db.

**Total Accuracy of the Method.**—If all the precautions enumerated above are properly taken, the over-all error can at worst be the sum of all the individual contributions. The errors are summarized in Table 13-3.

TABLE 13-3.—ACCURACY OF BALLANTINE-VOLTMETER METHOD

Individual error	Without calibration correction, db	With calibration correction, db
Generator instability and contact effects	$\pm 0.05$	$\pm 0.05$
Nonlinearity of bolometers	$-0.07$	.....
Ballantine voltmeter and preamplifier	$\pm 0.15$	$\pm 0.05$
Range switches of Ballantine voltmeter	$\pm 0.05$	$\pm 0.05$
Total	$+0.25$ $-0.32$	$\pm 0.15$

The importance of the calibration of the individual components is therefore emphasized for precision calibrations. By exercising great care, it is possible to achieve an over-all accuracy of  $\pm 0.15$  db in individual measurements, whereas for repeated measurements the probable accuracy should be not worse than  $\pm 0.05 \sqrt{3} = \pm 0.087$  db if the individual errors given in the table are assumed to be independent. This indicates that the above method is a most suitable calibration method.

With the introduction of a gauge block or precision fixed attenuator as discussed in Sec. 13-6, and with sufficient power available in the oscillator, the over-all attenuation range can be extended; the accuracy of the range is however, influenced by the accuracy of the gauge block itself.

**13-8. Calibration of Secondary Standards by the Substitution Method.**—The calibration of secondary standards is most conveniently done by comparison with a primary standard by means of the substitution method described in Sec. 13-2. The accuracy that can be achieved will be discussed in detail here, together with the sources of error peculiar to this method, and not already covered in Sec. 13-5.

An important point to observe is that the substitution method normally gives only relative values of attenuation referred to the minimum attenuation of the unknown component. For small values, the minimum attenuation certainly cannot be accurately determined by removing the unknown component and compensating the removed attenuation with adjustment of the standard; rather, this minimum attenuation must be determined by absolute measurement of the power ratio with and without the unknown component. This measurement has to be made very carefully since its value is additive to the relative values of the entire calibration curve.

*Choice of the Buffer Sections.*—The general test arrangement for the substitution calibration is that shown in Fig. 13-5 which indicates a waveguide setup such as used at about 9000 Mc/sec. The same block diagram applies with possible slight modifications for other frequency ranges and transmission-line systems. Buffer *H*, in the generator section, prevents reaction of load impedance changes upon the frequency and output power of the oscillator. The value of attenuation needed to keep the VSWR at a desired value close to unity can be ascertained from Fig. 11-11. Thus, if the maximum VSWR expected from the unknown attenuator is 1.30, the buffer *H* must be chosen as 10.15 db in order to keep the VSWR at the oscillator side to 1.025. Usually, if a value of 10 db or 12 db is chosen, the input impedance to the load system at the oscillator terminals will remain substantially constant.

Through the matching-stub section *G*, buffer *I* presents a matched termination to the attenuator undergoing calibration. In Fig. 13-5, this buffer is set for 10 db so that the power reflected from the cutoff attenuator and adapter section is completely absorbed. The matching stubs are employed to create a matched termination of VSWR equal to 1.03 or less, since the calibration is reliable only if the attenuator is terminated by a matched load. The VSWR must remain substantially constant throughout the process of calibration; it has been observed that with a variation from 1.03 to 1.1, only a negligible error is introduced into the calibration. However, if the VSWR is above 1.1, an appreciable error may be produced depending on the phase change introduced by the matching stubs and on the wavelength. For the worst phases, the conditions are depicted for a particular wavelength by the experimental curve shown in Fig. 13-25 where  $r_1$  is the VSWR looking into the detector section, and  $r_2$  is the VSWR looking into the unknown attenuator at an attenuation setting of 30 db so that  $r_2$  is independent of  $r_1$ . As  $r_1$  increases beyond 1.1, the error in attenuation rises rapidly above 0.1 db so that the calibration becomes meaningless.

Buffer *M* prevents power feedback from the local oscillator of the spectrum analyzer into the calibration line. It also serves to terminate

the reference cutoff standard by the characteristic impedance of the line. Its value was chosen at 4 db and variation up to 15 db did not indicate any noticeable error. This is because the cutoff attenuator possesses an inherent termination that is highly reactive. The calibration of the cutoff attenuator is not, therefore, critically dependent on the setting of buffer  $M$ .

The total safe minimum insertion loss of the calibration system is, therefore,  $12 + 10 + 4 = 26$  db in the three buffers alone, whereas the cutoff-attenuator standard has a minimum attenuation value of about 15 db. A total power loss of 41 db occurs and calibration can be con-

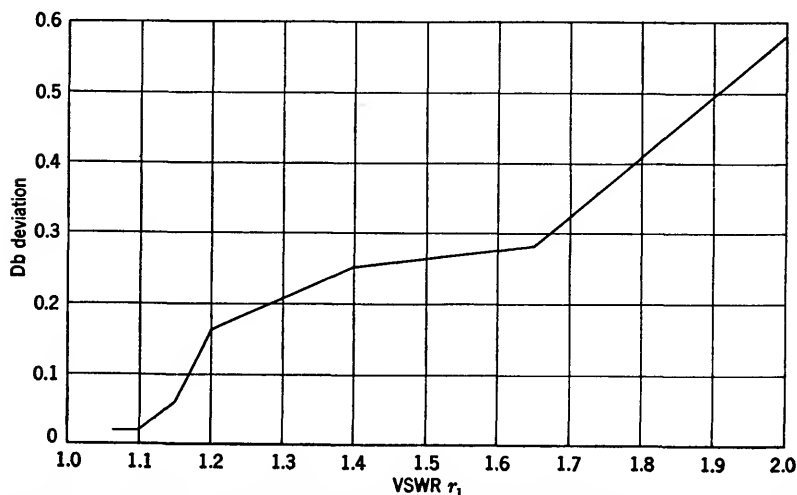


FIG. 13-25.—Influence of mismatch at input terminals of the detector upon measured attenuation. Attenuation level was 30 db and  $r_2 = 1.07$ .

ducted effectively only up to about a 90-db power-level difference between source and detector, hence a useful and accurate calibration range of 49 db remains.

The large minimum insertion loss with the cutoff-attenuator standard has led frequently to the use of a very well calibrated secondary dissipative standard as a reference standard. In this case, the arrangement of the detector section is shown in Fig. 13-6. Buffer  $H$  is chosen in the same manner as above, but buffer  $I$  need have a value of only 3 db since the input VSWR of the precision attenuator usually is less than 1.1 over the frequency range for which it is designed; otherwise it would be difficult to obtain an accurate calibration in accordance with the discussions of Sec. 13-5.

Buffer  $M$  terminates the dissipative-attenuator standard by a matched load. To ascertain the error caused by an improper termination, buffer

$H$  and buffer  $M$  were both set at 15 db and two precision attenuators were chosen as reference values. These attenuators were calibrated at 30 db, one against the other. The 30-db value of the first standard was recalibrated for different attenuation values of buffer  $M$  and the deviation in decibels determined. The procedure was repeated at several wavelengths. The results are given in Table 13-4. Table 13-5 shows the deviation in decibels when the experiment was repeated for the 2-db setting of the same standards. These data show that it is necessary to choose buffer  $M$  with a minimum value of 12 db of attenuation.

Following the same procedure as outlined above, the deviation in decibels can also be determined when both buffer  $H$  and buffer  $M$  are varied. This yields the effect of two sources of error. The resulting maximum errors were +0.03 db and -0.04 db with variations of each buffer between 15 db and 9 db. This clearly indicates that utmost attention must be paid to proper buffering in order to keep the calibration errors within tolerable limits.

TABLE 13-4.—INFLUENCE OF ATTENUATION VALUE OF BUFFER  $M$  UPON THE CALIBRATION WITH A DISSIPATIVE STANDARD AT THE 30-DB ATTENUATION LEVEL

Setting of buffer $M$ , db	$\lambda = 3.13$ cm db deviation	$\lambda = 3.20$ cm db deviation	$\lambda = 3.30$ cm db deviation	$\lambda = 3.53$ cm db deviation
15	0	0	0	0
9	+0.02	-0.01	+0.01	-0.01
0.4	+0.02	-0.01	+0.08	-0.01
0	+0.01	-0.00	+0.05	+0.02

TABLE 13-5.—INFLUENCE OF ATTENUATION VALUE OF BUFFER  $M$  UPON THE CALIBRATION WITH A DISSIPATIVE STANDARD AT THE 2-DB ATTENUATION LEVEL

Setting of buffer $M$ , db	$\lambda = 3.13$ cm db deviation	$\lambda = 3.20$ cm db deviation	$\lambda = 3.30$ cm db deviation	$\lambda = 3.53$ cm db deviation
15	0	0	0	0
9	-0.02	+0.03	-0.02	-0.03
0.2	-0.05	+0.03	-0.02	-0.00
0	-0.05	+0.01	-0.07	-0.04

The total safe minimum insertion loss of the calibration system is, in this case,  $12 + 3 + 12 = 27$  db, or 14 db less than when the cutoff-attenuator standard is used.

*Accuracy in Setting the Reference Standard.*—The mechanical accuracy in setting the cutoff-attenuator standard can be made as good as  $\pm 0.1$  mil, which corresponds at 9000 Mc/sec to  $\pm 0.01$  db, approximately. For the dissipative-attenuator standard at 9000 Mc/sec described in Sec. 13-6

the setting accuracy is  $\pm 0.01$  mil. Since the slope of the attenuation curve of this precision attenuator varies from 0.15 to 0.80 db/mil, the setting accuracy is from  $\pm 0.002$  to  $\pm 0.008$  db. It is, of course, desirable to make this mechanical adjustment as accurate as possible, since it can be most easily controlled.

Effects of temperature and humidity usually cause additional errors, which can be kept small with proper design particularly by utilizing inherent compensation features. The attenuation rate (db/cm) of the cutoff attenuator standard depends on the diameter of the cylindrical bore. Since the material is usually solid silver, the diameter change with temperature is about 0.00126 per cent/ $^{\circ}\text{C}$ . For ordinary laboratory uses, this change is entirely negligible. A diameter variation of  $\pm 0.063$  per cent causes an equal change in the attenuation rate  $\alpha$  according to Eq. (36). For values of 15 db/cm this change results in  $\delta\alpha = \pm 0.0095$  db/cm. Therefore, in 60 db, the total error is  $\pm 0.038$  db, an error comparable with some of the other errors to be considered. Humidity will affect the dielectric constant of air; this effect is negligible unless condensation of water vapor takes place.

The effect of temperature and humidity on metalized-glass-attenuator standards is negligible if the metalized-glass plate is soldered on to the struts as pointed out in Sec. 13-6.

*Effect of Detector Noise.*—In the calibration of higher values of attenuation, about 40 db with the cutoff-attenuator standard and about 55 db with the dissipative standard, the total attenuation between the oscillator and the spectrum analyzer is 90 db or more, and the gain of the receiver must be set high. The noise of the receiver is amplified to such an extent that the signal or "pip" appearing on the screen of the cathode-ray oscilloscope fluctuates widely. Inherently, this fluctuation tends to introduce a calibration error. In order to determine the magnitude of this error, a series of tests was performed at about 9400 Mc/sec in which the attenuation at a constant dial setting of a calibrated attenuator was recalibrated as a function of the amplitude of the fluctuation, the average height of the pip being kept constant. The results indicate that attenuation measured with a fluctuating pip is always higher than attenuation measured with a steady pip. The deviation in decibels as a function of the height of the fluctuation has been plotted in Fig. 13-26; the values represent the averages of three independent tests.

In these tests, the amplitude of the fluctuation was varied by decreasing the input power to the spectrum analyzer and increasing the gain. This power decrease was accomplished by increasing the attenuation in buffer *T* and rematching the termination. Within the fluctuation range of 0 to 0.05 in. as shown in Fig. 13-26, an approximate error of  $\pm 0.04$  db can be made in measuring high values of attenuation. Actu-

ally, the calibration should not be carried into ranges of larger amplitudes of fluctuations because of the larger inaccuracies obtained.

*Accuracy of Readings of the Unknown Component.*—Individual observations of the setting of the unknown component will vary because

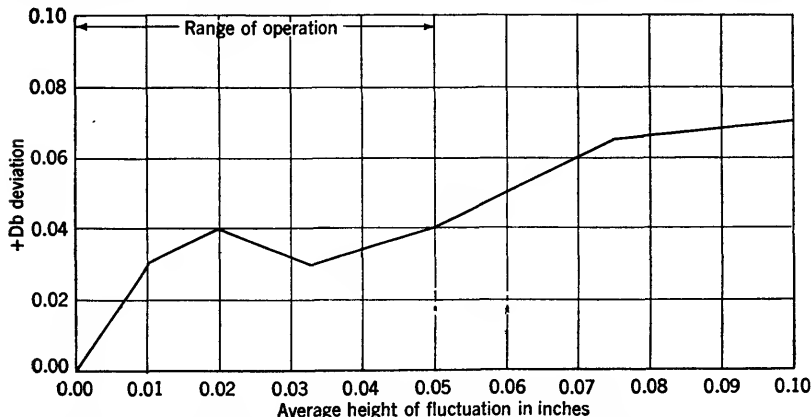


FIG. 13-26.—Calibration error contributed by signal fluctuation at high attenuation value.

of needed interpolation, parallax of indicator and scale, mechanical inaccuracies, and so forth. In order to minimize these influences, it is recommended to proceed as follows (refer to Figs. 13-5 or 13-6):

1. For the operating wavelength, match the buffer *I* (as termination of the unknown attenuator) to a VSWR of 1.03 or less by means of matching stubs *G*.
2. Set the reference standard for a value that is a few decibels higher than the attenuation to be measured.
3. By means of the receiver gain control, set the pip of the spectrum analyzer at a convenient level on the screen of the oscilloscope.
4. Reduce the attenuation of the reference standard by a known amount.
5. Insert attenuation of the unknown attenuator until the pip returns to the level set according to Step (3).
6. Return the dial setting of the reference standard to the value selected in Step (2).
7. Return the dial setting of the unknown attenuator to its original value.
8. View the pip level. If the pip returns to the same level as in Step (3), the dial reading obtained in Step (5) is accepted. If the level has changed, the dial reading is discarded.
9. This procedure is repeated for four acceptable dial readings and the average is taken to be the correct reading.



The dispersion of the four acceptable values will depend on all the factors enumerated above and particularly on the mechanical drive of the unknown attenuator. In the case of secondary standards of the metalized-glass type this accuracy can be made rather high. In the region of the maximum slope of this secondary standard at 9000 Mc/sec (see Sec. 14-6), the maximum spread has been found to be  $\pm 0.04$  db for careful calibration procedure.

TABLE 13-6.—COMPARISON OF MAXIMUM CALIBRATION ERRORS AT 9000 MC/SEC

Individual contributions	Calibration with cutoff standard, db	Calibration with metalized-glass standard, db
Combination of buffers <i>H</i> and <i>M</i>	+0.02 to -0.02	+0.03 to -0.04
Buffer <i>I</i>	+0.02 to -0.02	+0.02 to -0.02
Mechanical resettability of reference standard	+0.01 to -0.01	+0.008 to -0.008
Calibration error of reference standard	.....	+0.064 to -0.064
Effect of detector noise	+0.04	+0.04
Reading of the unknown component	+0.04 to -0.04	+0.04 to -0.04
Total	+0.13 to -0.09	+0.202 to -0.172

*Total Error of Calibration Method.*—The maximum total error incurred in the calibration of secondary standards is summarized in Table 13-6. With calibration against a cutoff standard, which has been certified to be truly linear, the error in the calibration can be anywhere between +0.13 and -0.09 db. However, the most probable measure of the reliability of the final result depends on the square root of the sum of the individual errors squared. This value is  $\pm 0.064$  db, approximately.

On the other hand, if the calibration is made against a secondary standard, the over-all calibration of this standard itself must be included and the maximum total error becomes +0.202 to -0.172 db. Again, the most probable error depends on the square root of the sum of the squares of the individual errors. This value, selecting the maximum deviations in each contribution, is  $\pm 0.10$  db, approximately.

These errors exist, of course, only under the conditions outlined, apply to the method of calibration, and presuppose good care in avoiding the more obvious general sources of error discussed in Sec. 13-5. The absolute values of attenuation may have still larger errors if the actual measurement of attenuation is not made under the proper conditions of termination. With the precautions indicated, however, and with the range of calibration restricted to the regions of small individual errors, the maximum deviation of absolute attenuation values should be small. As an illustration, take Eq. (26) and use the following values:

$r' = 1.10$ ,  $r''_0 = 1.10$ , assuming the maximum VSWR of a secondary standard,

$r_G = 1.03$ , because of careful match of input buffer  $H$ ,

$r_L = 1.03$ , because of careful match of the detector section.

Then  $(\Delta A)_{\max.} = \pm 0.014$  db, a very small value indeed. The most probable error of a careful calibration measurement also gives the error in the value of the absolute attenuation.

**13-9. Production Calibration.**—Microwave test equipment frequently contains among its components attenuators of fixed or variable attenuation values. The calibration of these attenuators in a rapid and accurate manner is an important production problem.

*Calibration of Fixed Attenuators.*—Fixed-value attenuator pads are usually used to extend the range of power meters or other instruments in a manner similar to the equivalent range selectors at lower frequencies. The attenuation values, therefore, must be calibrated, yet they need not be calibrated as accurately as secondary standards. Because of the special need for rapid measurement of similar pieces, convenient modifications can be made in the substitution method of calibration. Figure 13-27 indicates a particularly useful arrangement whereby the unknown attenuators are inserted between the generator and detector section at  $ab$ . The microwave oscillator is modulated at audio frequency, and the output voltage of the first detector  $I$  can be either directly connected to the final audio amplifier and detector at  $C$  or connected to it at  $D$  over a carefully calibrated audio-frequency attenuator. With the unknown attenuator connected between  $a$  and  $b$ , and the audio selector switch at  $C$ , a convenient indication is obtained on the final detector-indicator by adjusting the gain of the audio amplifier. Leaving this gain adjustment fixed, and moving the audio selector switch to neutral position  $0$ , the unknown component is removed and the detector section directly connected to the generator section. The audio selector switch is moved to  $D$ , and the a-f attenuator pad adjusted to restore the same indication on the final detector as previously selected. The dial reading of the audio pad gives directly the attenuation value of the unknown attenuator. For calibration of many attenuators of the same nominal value, this method is extremely rapid, since the audio pad can stay adjusted to the nominal value and only a fine adjustment is needed to the exact value of the particular unknown attenuator. If a tolerance range has been defined, this range can be marked on the fine-adjustment dial of the audio attenuator and any unknown attenuator outside this range can be rejected. Inasmuch as the first detector must carry the microwave power with and without the unknown attenuator inserted, the method is practically limited to about 20 to 30 db if good accuracy is desired.

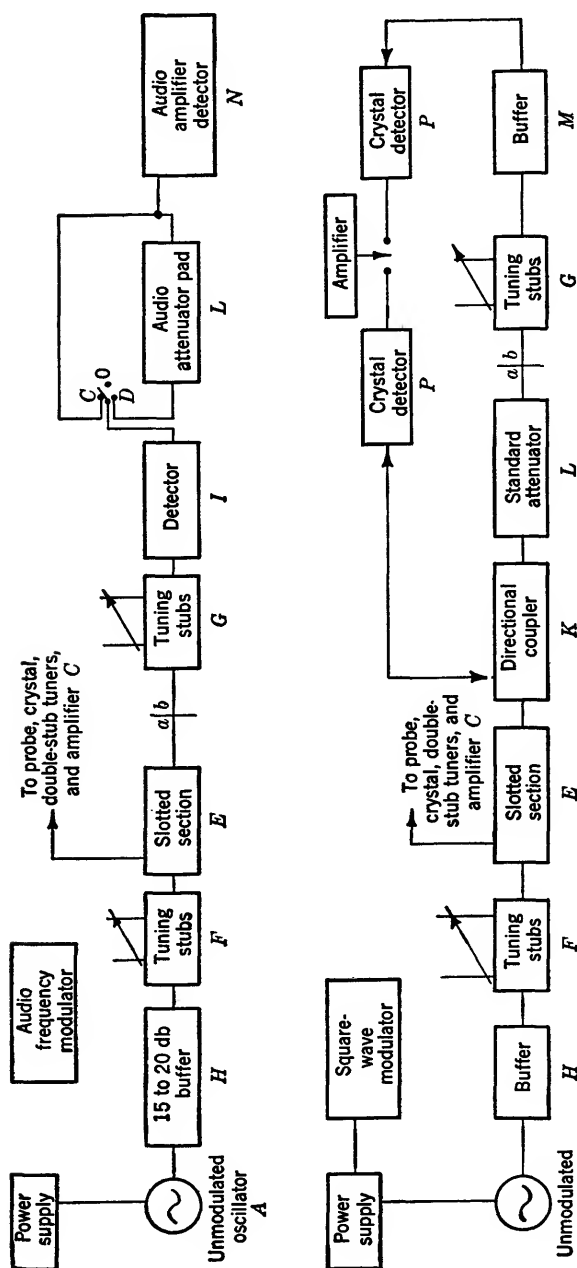


Fig. 13-27.—Top: Schematic arrangement for calibration of microwave fixed-value attenuators by means of a-f attenuator pad. Bottom: Schematic arrangement for setting of attenuator pads to selected value.

Rather careful buffering of the oscillator is required in order to maintain output power and frequency setting; from time to time it is necessary to check these settings. A power monitor can easily be added for this purpose. One of the principal advantages of this method is that the audio pad can be calibrated at direct current with a precision potentiometer. By exercising care with all the other factors, this method can be made as accurate as the Ballantine-voltmeter method of absolute calibration. With proper modifications of the first detector  $I$ , the method can also be used for any microwave frequency desired.

*Adjustment of Fixed Attenuators.*—In many instances, particularly in the case of fixed waveguide attenuators, it is desired to set the insertion loss of each of a large number of similar pieces at a single value. A very suitable arrangement is that shown<sup>1</sup> in Fig. 13-27 where the output power of the side arm of a directional coupler  $K$  in the generator section is compared with the final power from buffer  $M$ . With the detector section connected directly to the generator section at the output terminal of the standard attenuator as shown, conditions are adjusted so that the input signals to the amplifier are equal. A push-button switch may be installed to facilitate comparisons between the two signals. If the standard attenuator is reduced by the desired amount, and if the unknown attenuator is inserted between  $a$  and  $b$  in Fig. 13-27 and adjusted so that the signals become equal, the proper setting has been obtained. The advantage of the method is that small changes in amplifier gain or oscillator output power do not necessitate recalibration. Both signals go through the same amplifier channel, and changes in gain affect both signals equally. If both crystals follow approximately the same law, small changes in the output power of the oscillator affect both signals about equally.

Because there is a small amount of coupling between the two input terminals of the amplifier, it is desirable that both input signals be of the same order of magnitude. To accomplish this, it may be necessary to insert an additional attenuator between the side arm of the directional coupler  $K$  and the monitoring crystal detector  $P$ .

*Comparison of Directional Couplers.*—It is often desired to measure the coupling of a large number of directional couplers of the same type. This may be done conveniently by comparison with one of the directional couplers which previously has been carefully calibrated as a standard. This standard coupler may again be  $K$  in Fig. 13-27, and the coupler to be measured is inserted in the detector section as shown in Fig. 13-28. The difference between the powers out of the two side arms is measured by means of bolometers and amplifiers with an audio attenuator. The

<sup>1</sup> W. E. Waller, "Microwave Attenuation Measurements," RL Report No. 55.5—11/12/45, p. 14.

bolometers replace the crystal detectors to ensure the same dependence on power in both detectors and the audio attenuator is used to bring the signal in the amplifier without gain adjustment to the same level in both cases. The difference in the audio-attenuator reading gives the difference in coupling of the two directional couplers.

If the couplers sample anything but a negligible portion of the power in the main line, compensation must be made for the reduction in the amount of power that enters the coupler under test, which can be done best by means of the audio attenuator.

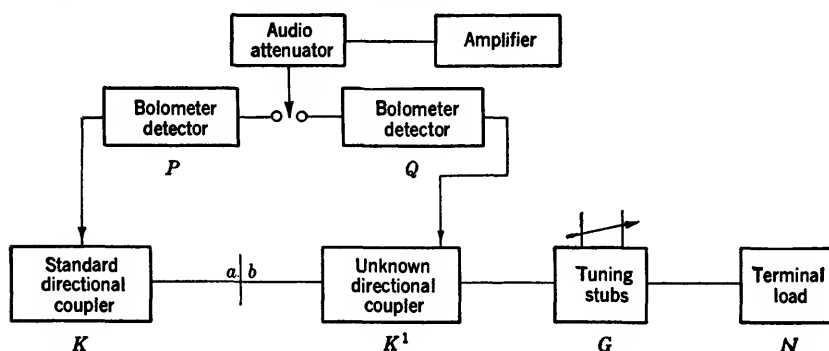


FIG. 13-28.—Modification of schematic arrangement in Fig. 13-27 (bottom) for comparison of directional couplers with standard.

*Calibration of Variable Attenuators for Signal Generators.*—Attenuators for signal generators for testing receivers and transmitters usually require wide ranges of adjustment, in most cases up to 75 or 85 db. As indicated in Sec. 13-2, such a range of attenuation calibration is difficult to achieve. It is not possible at present with a waveguide-beyond-cutoff primary standard because of its very high minimum insertion loss. The most common calibration procedure is, therefore, the substitution method with resistive precision attenuators as secondary standards, preferably of the metalized-glass type as described in Sec. 13-6. Calibration of these resistive standards over the entire range of 80 db must be done in pairs. One member of the pair is calibrated by a primary method, such as is described in Sec. 13-7, the other member of the pair is then calibrated by comparison with the first using the substitution procedure. As a detector, either a spectrum analyzer or a standard radar receiver with a frequency band of 2 Mc/sec and an intermediate frequency of 30 Mc/sec, may be used. The output signal of this receiver may be indicated either as a pip if the local oscillator is sawtooth-modulated, or as a deflection of a voltmeter connected to the second detector if the local oscillator is operated without modulation. Despite its wider pass band, such a receiver has at least as great a sensitivity and has more stability than

a spectrum analyzer. The high sensitivity expected from the narrow-band receiver in the analyzer is seldom realized, and a tendency for regeneration usually hampers stability. The optical advantage caused by the manner in which noise adds to the signal from the wider bandpass receiver when an oscilloscope is used, permits operation closer to noise. A signal that is equal to noise is about  $-125$  dbw, and this is therefore the final limit of sensitivity.

The accuracy of the upper range of secondary standards is considerably lower than the accuracy of the lower range (see Sec. 13-8). Consequently, the absolute accuracy of calibration of the signal-generator attenuators is still lower, probably not better than  $\pm 0.45$  db at about 70 db total attenuation, since the mechanical drive is also less accurate than that of the standards. In the comparison of attenuators, possible deviations of twice this value must be expected.

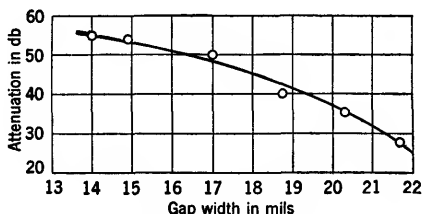


FIG. 13-29.—Shift of crossover of attenuation curves with variations in glass widths from  $\lambda = 3.13$  and 3.53 cm.

In view of the unavoidable inaccuracies of individual calibrations the possibility of eliminating the calibration by careful quality control of the production of attenuators should be considered. This cannot be done, at least in the case of waveguide attenuators, as has been demonstrated clearly in experiments on metalized-glass attenuators by studying the influence of mechanical tolerances upon the variation of attenuation with frequency. It has been shown in Sec. 12-18 that the capacitances produced by the electric field fringing between the metalized-glass plate and the waveguide walls exert a strong influence on the attenuation characteristics. The metalized-glass plate shown in Fig. 12-58 was used with slightly varying widths in the same specially selected waveguide casing of 0.399 in. small dimension and of exceptional uniformity. The attenuation curves for the wavelengths 3.13 and 3.53 cm intersect with normal tolerances in the neighborhood of 40 db total attenuation. For glass plates of widths varying between 0.356 and 0.371 in., Fig. 13-29 indicates how the crossing point of these two attenuation curves shifts from about 28 db to 55 db. As this crossover shifts, the spread between the attenuation curves at a fixed medium value

of 40 db varies according to Fig. 13-30. Thus only a very small variation in the gap is allowed if an over-all spread of attenuation of 1 db or less between the wavelengths chosen is desired.

In order to reduce variations from attenuator to attenuator in production, the tolerances on waveguide dimensions as well as on glass width and thickness must be set close. If the glass plate shown in Fig. 12-58 with a width of  $0.363 \pm 0.001$  in. is selected and if the inner dimension of the waveguide is set at  $0.400 \pm 0.002$  in., a total maximum variation

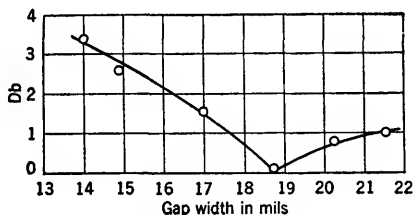


FIG. 13-30.—Total attenuation change at 40 db from  $\lambda = 3.13$  to 3.53 cm.

of  $\pm 0.0015$  in. in gap width will result centered about 18.5 mils as indicated in Fig. 13-29. This causes a variation of total attenuation change with frequency at 40 db from approximately 0.6 db at one tolerance extreme to 1.5 db at the other. A glass width of  $0.3635 \pm 0.001$  in. reduces this to about 1 db. Other mechanical factors are also important, such as slight bowing of the glass plate, curvature in the waveguide casing, nonparallelism of the struts supporting the glass plates, and many others. Consequently any attempt to produce waveguide signal-generator attenuators of identical attenuation curves that would obviate calibration procedures seems utterly hopeless with present-day means.

## CHAPTER 14

### DIRECTIONAL COUPLERS

By R. L. KYHL

**14.1. Introduction.**—In microwave systems it is often necessary to monitor the power which is being transferred through a transmission line, the line from a transmitter to an antenna, for example. Usually the monitoring must be accomplished by a simple device which does not add weight or complexity to the system. Such a device will employ a detector or detectors and some means of coupling power out of the transmission line in question. The simplest way of accomplishing the coupling is by means of a small probe such as that which is used in slotted-section measurements. Serious objections to this become evident at once. The voltage generated in such a probe is proportional to the electric intensity at the position of the probe; this intensity varies from point to point along the transmission line to give the familiar standing-wave pattern. The voltage generated in the probe is then by no means a unique measure of power transfer. The same objection may be made to a probe consisting of a small loop projecting into the line. In this case it is the magnetic intensity that is picked up; the standing-wave pattern, although displaced, will be of the same magnitude.

It is possible, of course, by means of a slotted section and sliding probe, or by means of a sufficient number of fixed probes, to determine completely the configuration of the electromagnetic waves in the transmission line, and in this way to determine, among other things, the net power transfer. This is far too complicated to be a satisfactory solution of the problem. What is desired is a type of coupling which will deliver, to a single detector, power which is proportional to the power transfer in the transmission line.

An attempt to answer this problem is the directional coupler, which measures the forward-going wave. Although this does not give exactly the power transfer, since there may be a reflected wave, it represents a much better approximation when the reflected power is small than does the simple probe. Equation (1) gives the dependence of power transfer on the amplitude of the forward wave,

$$P = \frac{|E|^2}{2Z_0} (1 - |\Gamma|^2), \quad (1)$$



where  $P$  is the power delivered to the load,  $E$  is the complex voltage amplitude of the wave in the forward direction,  $Z_0$  is the characteristic impedance of the transmission line, and  $\Gamma$  is the complex voltage reflection coefficient of the terminating load. Since the directional coupler is sensitive only to the forward wave, the power reaching a detector connected to the coupler is proportional to the power transfer in the line, independently of the value of  $\Gamma$ , except for second-order terms in  $\Gamma$ .

$$P_d \propto \frac{P}{1 - |\Gamma|^2} \approx P(1 + |\Gamma|^2), \quad (2)$$

where  $P_d$  is the power extracted by a directional coupler. A simple probe, on the other hand, is sensitive to the total field strength  $|E(1 + \Gamma)|$ , so that

$$P'_d \propto P \frac{|1 + \Gamma|^2}{1 - |\Gamma|^2}, \quad (3)$$

where  $P'_d$  is the power extracted by a simple probe. The probe power is then independent of  $\Gamma$  only if first-order terms in  $\Gamma$  are neglected. Since, in practical transmission lines, values of  $|\Gamma| = 0.2$  corresponding to a standing-wave ratio in voltage of 1.5 are common, these effects are by no means trivial.

It is often desired to monitor or to measure the available power of a matched generator which is driving a transmission line. In this case power carried by the forward wave is proportional to the available power, and the directional coupler gives the correct value independent of the standing-wave ratio in the line. If the generator is not matched, the forward wave will depend upon load and generator impedances, but in all cases the simple probe gives a coupling which is more dependent on load and generator impedances than does the directional coupler.

The above considerations also apply when the role of generator and detector are reversed, as can be seen from a consideration of reciprocity relations. This means that the directional coupler offers the same advantages when the problem is, for example, to put into a receiver a test signal which will be independent of the impedance of the antenna and of the other components in the transmission line. Then, too, there are many cases in which it is desirable to know the magnitude of a traveling wave for its own sake, as in the case of the reflectometer for measuring reflection coefficients. It has been assumed that the transmission line in question must remain operative. If it is possible to break the transmission line to insert detectors or generators, then the particular properties of the directional coupler are of no special value.

**14-2. Equivalent Circuit of a Directional Coupler.**—The problem of designing a device which is sensitive only to the wave in one direction

is equivalent to that of designing a device to excite a wave traveling in the reverse direction. From reciprocity considerations, a solution to one of the problems is automatically a solution of the other. This can be seen as follows: if a generator sends a wave down the transmission line in the rejected direction, that is, the direction in which the coupler is not sensitive, no power reaches the detector. Therefore, by reciprocity, if the detector and the generator are reversed and the probe generates, no power reaches the end of the transmission line containing the detector; therefore any wave generated must travel toward the other end of the transmission line. The same argument of course can also be applied in the opposite direction. This indicates that a simple probe cannot be used since it would radiate power into the line in both directions. It suggests the use of two or more probes driven in the appropriate phases to cancel the radiated waves in one direction in a manner analogous to that employed in certain directional antennas. Thus, since most directional couplers consist of a section of the main transmission line coupled to an auxiliary transmission line, the problem of sensitivity to power flowing in one direction in the main line is equivalent to the problem of exciting the transmission of power in a single direction in the auxiliary line.

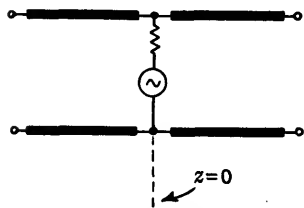


FIG. 14-1.—Electric probe coupling.

Consider, then, the generation of waves by a generator driving a probe or other device forming a weak coupling to the line. Such a generator can be represented in several equivalent ways. A single electric probe may be represented by a shunt generator, Fig. 14-1. The waves excited will be of the form

$$\left. \begin{aligned} e &= E_0 e^{j(\omega t - kz)} \\ i &= \left( \frac{E_0}{Z_0} \right) e^{j(\omega t - kz)} \end{aligned} \right\} \quad z > 0, \quad (4)$$

$$\left. \begin{aligned} e &= +E_0 e^{j(\omega t + kz)} \\ i &= - \left( \frac{E_0}{Z_0} \right) e^{j(\omega t + kz)} \end{aligned} \right\} \quad z < 0.$$

A probe may be generalized to include any device which couples to the transverse electric field of the waves in the transmission line. For this type of excitation the voltages at symmetrical points on the two sides of the probe have the *same phase*.

A simple loop may be represented by a series generator, Fig. 14-2. The waves excited will be of the form

$$\left. \begin{aligned} e' &= E'_0 e^{j(\omega t - kz)} \\ i' &= \frac{E'_0}{Z_0} e^{j(\omega t - kz)} \end{aligned} \right\} \quad z > 0, \quad (5)$$

$$\left. \begin{aligned} e' &= -E'_0 e^{j(\omega t + kz)} \\ i' &= +\frac{E'_0}{Z_0} e^{j(\omega t + kz)} \end{aligned} \right\} \quad z < 0.$$

A loop may be generalized to include any device which couples to the transverse magnetic field of the waves in the transmission line. For this type of excitation the voltages at symmetrical points on the two sides of the probe are *out of phase*.

Next consider the problem of a transmission line excited by two probes. Both probes must be driven by the same generator, of course, so that the waves will be coherent. The resulting waves will be linear combinations of the individual waves.

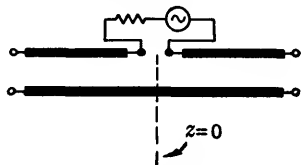


FIG. 14-2.—Magnetic loop coupling.

We shall consider two cases.

Case 1. A shunt and a series probe excite the line at the same point. Here,

$$\left. \begin{aligned} e &= (E_0 + E'_0) e^{j(\omega t - kz)} \\ i &= \frac{1}{Z_0} (E_0 + E'_0) e^{j(\omega t - kz)} \end{aligned} \right\} \quad z > 0, \quad (6)$$

$$\left. \begin{aligned} e &= +(E_0 - E'_0) e^{j(\omega t + kz)} \\ i &= -\frac{1}{Z_0} (E_0 - E'_0) e^{j(\omega t + kz)} \end{aligned} \right\} \quad z < 0.$$

If now the relative magnitudes and phases of the coupling are adjusted so that  $E_0 = E'_0$ , then  $e = 0$  for  $z < 0$ , and the wave excited to the left will vanish.

Conversely, from reciprocity considerations, a wave falling on the probe combination from the left would not be detected at the terminal pair which drives the two probes. In other words, the probe combination is sensitive only to an incident wave traveling from the right to the left, and has the properties

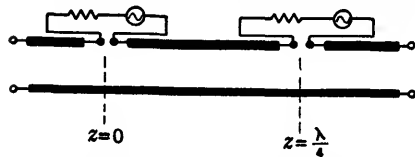


FIG. 14-3.—Probes spaced  $\lambda/4$  apart.

of a directional coupler. On the other hand, if we had made  $E_0 = -E'_0$ , the wave excited to the right would have vanished and the directional coupler would have been sensitive to waves traveling in the opposite direction.

Case 2. Two series probes drive the line at points separated by a quarter wavelength; Fig. 14.3. Here,

$$\left. \begin{aligned} e &= E_1 e^{j(\omega t - kz)} + E_2 e^{j\left[\omega t - k\left(z - \frac{\lambda}{4}\right)\right]} \\ i &= \frac{1}{Z_0} E_1 e^{j(\omega t - kz)} + \frac{1}{Z_0} E_2 e^{j\left[\omega t - k\left(z - \frac{\lambda}{4}\right)\right]} \end{aligned} \right\} \quad z > \frac{\lambda}{4},$$

$$\left. \begin{aligned} e &= -E_1 e^{j(\omega t + kz)} - E_2 e^{j\left[\omega t + k\left(z - \frac{\lambda}{4}\right)\right]} \\ i &= +\frac{1}{Z_0} E_1 e^{j(\omega t + kz)} + \frac{1}{Z_0} E_2 e^{j\left[\omega t + k\left(z - \frac{\lambda}{4}\right)\right]} \end{aligned} \right\} \quad z < 0,$$

giving

$$\left. \begin{aligned} e &= (E_1 + jE_2) e^{j(\omega t - kz)} \\ i &= \frac{1}{Z_0} (E_1 + jE_2) e^{j(\omega t - kz)} \end{aligned} \right\} \quad z > \frac{\lambda}{4},$$

$$\left. \begin{aligned} e &= -(E_1 - jE_2) e^{j(\omega t + kz)} \\ i &= +\frac{1}{Z_0} (E_1 - jE_2) e^{j(\omega t + kz)} \end{aligned} \right\} \quad z < 0.$$

If the relative magnitudes and phases of the couplings are adjusted so that  $E_1 = jE_2$ , the wave excited to the left will vanish, and by a similar argument, when a detector is used instead of a generator, the device is a directional coupler sensitive to a wave coming from the right. Notice that in this case the two probes must be connected so that there is a phase difference of  $90^\circ$  between them.

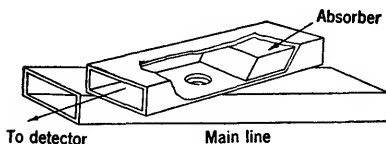


FIG. 14-4.—The Bethe-hole coupler.

These two examples will suffice to illustrate the general methods of obtaining directional properties. The various ways of obtaining the desired shunt and series excitation

will be described subsequently. Actually any microwave junction can be represented either as a series or as a shunt circuit; however, the corresponding reference planes will be displaced one-quarter wavelength from one case to the other. Usually one of the choices has greater physical significance.

**14-3. The Bethe-hole Coupler.**—We shall now consider a particular example of a directional coupler. A typical Bethe-hole coupler is the design shown in Fig. 14-4 for rectangular waveguide. It consists of two waveguides with their broad sides adjoining and a single hole furnishing coupling between them. The lower guide is the main transmission line. The upper guide is terminated at one end to absorb unwanted power, and the other end is connected to the detector.

To describe the characteristics of a directional coupler, use is made of the terms "coupling," "directivity," and also standing-wave ratio in the main transmission line. These are defined in terms of the quantities

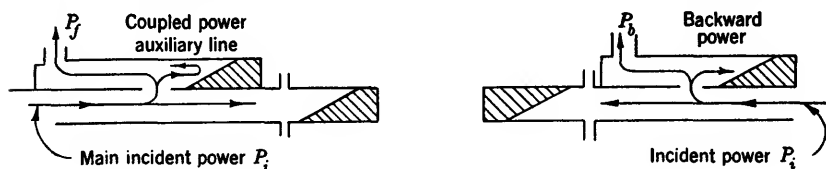


FIG. 14-5.—Definition of coupling and directivity.

shown schematically in Fig. 14-5. A coupler is designed so that ideally  $P_b = 0$ , but actually it may have some value which is small compared to  $P_f$ . Coupling is defined by

$$C = 10 \log_{10} \left( \frac{P_i}{P_f} \right). \quad (9)$$

Directivity is a measure of the quality of the coupler and is defined by

$$D = 10 \log_{10} \left( \frac{P_f}{P_b} \right). \quad (10)$$

The standing-wave ratio which is measured in the main line looking in the direction of the wave to which the coupler is sensitive, with the other end matched, is often used to specify one characteristic of a coupler. Usually the standing-wave ratio in the main line is the same looking in either direction with the main line terminated in a match.

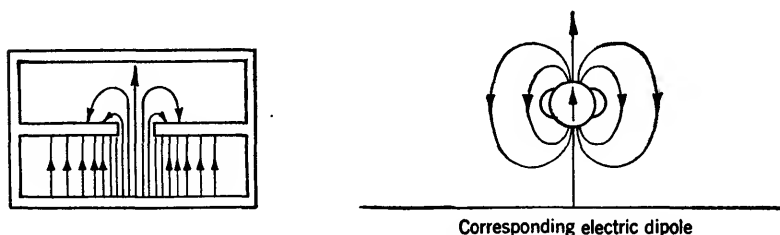


FIG. 14-6.—Electric coupling through a small hole.

In the Bethe-hole coupler, it can be seen that the hole provides coupling to both the electric and the transverse magnetic field components. This is illustrated in Figs. 14-6 and 14-7. The electric fields in the auxiliary guide in the neighborhood of the hole are similar to those generated by an oscillating electric dipole with its dipole moment parallel to the electric field of the incident wave in the main guide. Propagating waves will be set up in the auxiliary guide similar to those caused by such a dipole. In a like manner, the magnetic fields will behave as

though the hole contained a magnetic dipole moment which, however, is parallel to the transverse magnetic field in the main guide but in the direction opposite from it. In a pure traveling wave in the main line, the transverse electric and magnetic fields will be in phase. The electric dipole moment of the hole will also be in phase, while the magnetic dipole will be opposite in phase. Because of this reversal of sign of one type of coupling with respect to the other, the waves in the auxiliary line will cancel in the forward direction relative to the direction of propagation in the main line, and will reinforce in the backward direction. It is a general property of Bethe-hole couplers that the wave in the auxiliary line travels in the opposite direction from the wave in the main line.

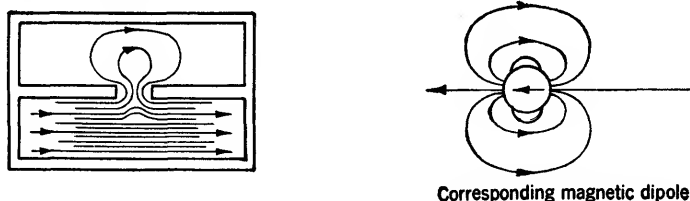


FIG. 14-7.—Magnetic coupling through a small hole.

As indicated in Sec. 14-2, the waves generated by the two types of coupling must be of equal amplitude in order to have complete cancellation and perfect directivity. The magnitude of the coupling through small holes has been calculated by Bethe,<sup>1</sup> and his results can be used for design purposes. Bethe assumes that the radius of the hole is small compared to a wavelength, and the hole is far from corners or other discontinuities in the plane containing the hole. The strength of the electric or magnetic dipole formed in the hole is proportional to the strength of the incident field and the polarizability of the hole. The polarizability depends on the shape of the hole and the direction of the incident field with respect to a line in the plane of the hole.

The voltage coupling is given by  $(\pi j / \lambda_0 S)(E_1 E_2 P)$ ;  $E_1$  and  $E_2$  are the electric-field intensities corresponding to waves of unit amplitude in the primary and secondary guides respectively, which would have existed at the position of the hole if the hole had been absent.  $P$  is the electric polarizability of the hole, and  $S$  is a normalizing factor. Similarly, the magnetic coupling is given by  $(\pi j / \lambda_0 S)(H_1 H_2 M)$ , where  $M$  is the magnetic polarizability of the hole. The polarizabilities for a small round hole are given by  $M = \frac{4}{3}r^3$  for the magnetic coupling, and  $P = \frac{2}{3}r^3$  for the electric coupling, where  $r$  is the radius of the hole. It is seen that the ratio of the two kinds of coupling is independent of the size of the hole.

<sup>1</sup> H. A. Bethe, "Lumped Constant for Small Holes," RL Report No. 194, Mar. 24, 1943; "Theory of Side Windows in Waveguide," RL Report No. 199, Apr. 4, 1943.

The voltage coupling varies as the cube of  $r$ , so the coupled power varies as the sixth power of the hole radius.

To equalize the couplings, the axis of one guide is rotated with respect to the other as illustrated in Fig. 14-4. The magnetic dipole in the hole must now be resolved into a transverse and a longitudinal component in the auxiliary guide. Since only the transverse components couple, the magnetic coupling is reduced by a factor equal to a cosine function. The electric coupling is unchanged. This scheme is effective only if the magnetic coupling is stronger than the electric coupling when the guides are parallel. Fortunately, this is often the case. When the couplings are equal, the phase relations of the two components are such as to produce a wave in the auxiliary guide traveling in only one direction from the hole.

The wall thickness of the hole has the effect of reducing the coupling by a considerable amount. Moreover, it attenuates the two types of coupling by different factors. The hole may be regarded as a very short section of circular waveguide beyond cutoff. The electric coupling fields correspond to the  $TM_{01}$ -mode, and the magnetic coupling corresponds to the  $TE_{11}$ -mode in the round guide. Since the  $TM_{01}$ -mode is farther from cutoff, it is attenuated more rapidly than the  $TE_{11}$ -mode. Thus the effect of the wall thickness is always to increase the proportion of magnetic coupling.

If we let  $A_{\text{inc}}$  refer to the voltage amplitude of the wave incident in the main line, and  $A_E$  refer to the wave coupled into the auxiliary guide, then for the electric case

$$\frac{A_E}{A_{\text{inc}}} = \frac{\pi j}{\lambda_0 S} (E_1 E_2) \frac{2r^3}{3} F_E(t), \quad (11)$$

where  $F_E(t)$  represents the attenuation in the hole of thickness  $t$ .

If the two guides are alike,  $E_1 = E_2$ , and if the hole is in the center of the broad side of the waveguide of dimensions  $a$  and  $b$ ,

$$S = \frac{\lambda_0 ab}{2\lambda_0} H_1^2 = \frac{\lambda_0 ab}{2\lambda_0} E_1^2 \left( \frac{\lambda_0}{\lambda_g} \right)^2, \quad (12)$$

giving

$$\frac{A_E}{A_{\text{inc}}} = \frac{4\pi j r^3}{3\lambda_0 ab} \left( \frac{\lambda_g}{\lambda_0} \right)^2 F_E(t). \quad (13)$$

Similarly, for the magnetic case,

$$\frac{A_H}{A_{\text{inc}}} = \frac{8\pi j r^3}{3\lambda_0 ab} \cos\theta F_H(t). \quad (14)$$

The total coupled wave is then

$$\frac{A_E + A_H}{A_{\text{inc}}} = \frac{8\pi j r^3}{3ab\lambda_0} \left[ \cos\theta F_H(t) + \frac{1}{2} \left( \frac{\lambda_g}{\lambda_0} \right)^2 F_E(t) \right]. \quad (15)$$

Coupling is then

$$C = 20 \log_{10} \left\{ \frac{\pi d^3}{3ab\lambda_g} \left[ \cos \theta + \frac{1}{2} \left( \frac{\lambda_g}{\lambda_0} \right)^2 \frac{F_E}{F_H} \right] F_H \right\}, \quad (16)$$

where  $d$  is the diameter of the hole. The condition for equality of couplings becomes

$$\cos \theta = \frac{1}{2} \left( \frac{\lambda_g}{\lambda_0} \right)^2 \frac{F_E}{F_H}. \quad (17)$$

For this adjustment of the angle the coupling reduces to

$$C = 20 \log_{10} \left\{ \frac{2\pi d^3}{3ab\lambda_g} \cos \theta F_H \right\}. \quad (18)$$

The directivity is given by

$$D = 20 \log_{10} \frac{\left| \cos \theta + \frac{1}{2} \left( \frac{\lambda_g}{\lambda_0} \right)^2 \frac{F_E}{F_H} \right|}{\left| \cos \theta - \frac{1}{2} \left( \frac{\lambda_g}{\lambda_0} \right)^2 \frac{F_E}{F_H} \right|}. \quad (19)$$

The attenuation factors for the effect of the thickness of the hole are

$$F_E = e^{-2\pi \left[ \left( \frac{1}{1.31d} \right)^2 - \frac{1}{\lambda^2} \right]^{1/2} t}, \quad (20)$$

and

$$F_H = e^{-2\pi \left[ \left( \frac{1}{1.71d} \right)^2 - \frac{1}{\lambda^2} \right]^{1/2} t}, \quad (21)$$

for a hole of thickness  $t$  and diameter  $d$ . If the thickness is very small, so that  $F_E/F_H$  can be set equal to unity, then

$$\cos \theta = \frac{1}{2} \left( \frac{\lambda_g}{\lambda} \right)^2; \quad (22)$$

$\cos \theta$  is unity and the two waveguides are parallel when  $(\lambda_g/\lambda)^2 = 2$  or when  $\lambda = \sqrt{2} a$ . This is very nearly the case for the standard 1-in. by  $\frac{1}{2}$ -in. waveguide at a wavelength of 3.2 cm.

The frequency sensitivity of the various properties of the directional coupler is usually of some concern. From the formula for directivity, it can be seen that frequency sensitivity appears in a term

$$\frac{1}{2} \left( \frac{\lambda_g}{\lambda_0} \right)^2 \left( \frac{F_E}{F_H} \right).$$

For thin walls the term  $F_E/F_H$  is relatively insensitive to frequency so that the frequency sensitivity is largely determined by the  $(\lambda_g/\lambda_0)^2$  term. The directivity falls off rapidly in both directions with frequency, from an infinite value at the design frequency. It is simple to calculate the



bandwidth for a minimum directivity of 20 db. If a coupler is assumed for which  $F_E/F_H = 1$ ,  $\cos \theta = 1$ , and  $\lambda_0/\lambda_0 = \sqrt{2}$ , the range of  $\lambda_0$  for which  $D > 20$  db is

$$\sqrt{\frac{13}{11}} > \frac{\lambda_0}{\lambda_{00}} > \sqrt{\frac{7}{9}} \quad (23)$$

where  $\lambda_{00}$  is the design wavelength. The total bandwidth is thus approximately 20 per cent.

A coupling factor of 20 db in a Bethe-hole coupler requires a hole so large that the approximations of Bethe's theory do not hold. Rotation

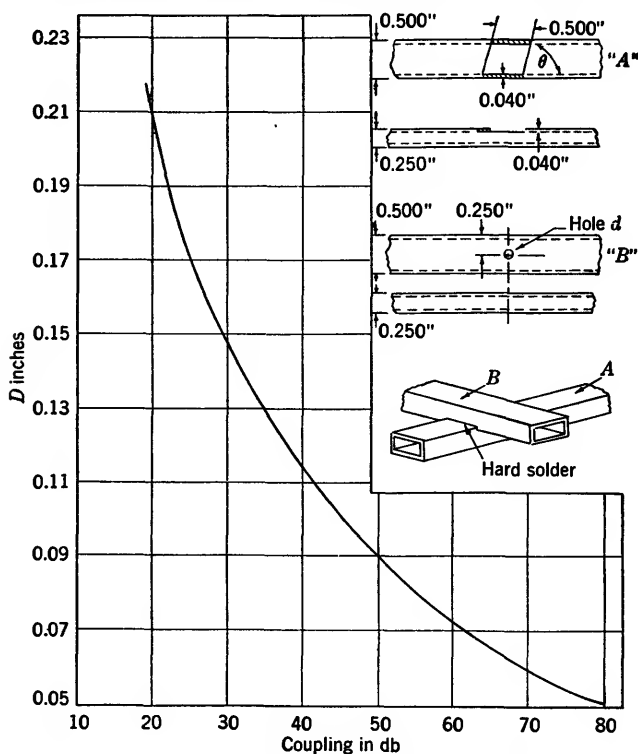


FIG. 14-8.—Design curve for Bethe-hole couplers in  $\frac{1}{2}$ - by  $\frac{1}{4}$ - by 0.040-in. wall waveguide,  $\lambda_0 = 1.25$  cm.

of the guides from the angle predicted by the theory is necessary to obtain good directivity. The large hole in the guide wall sets up a reflection in the main transmission line. This is commonly matched out with a suitable iris. This problem becomes of importance for extremely tight coupling, 10 db or less.

It is readily seen that the directivity of a practical coupler is a function

not only of the coupling mechanism but also of the reflection from the termination in the auxiliary line, since energy from the backward direction can reach the detector by being reflected from this termination. An analysis of the effect of termination standing-wave ratio upon directivity is given in Sec. 14-10. The directivity of the actual coupler can be either better or worse than the directivity of the coupler with a perfect termina-

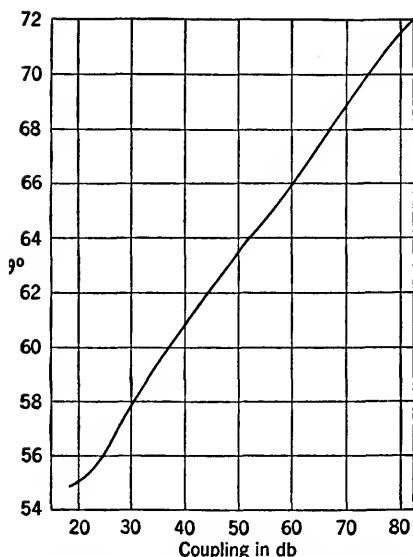


FIG. 14-9.—Design curve for Bethe-hole couplers in  $\frac{1}{2}$ - by  $\frac{1}{2}$ - by 0.040-in. wall waveguide,  $\lambda_0 = 1.25$  cm.

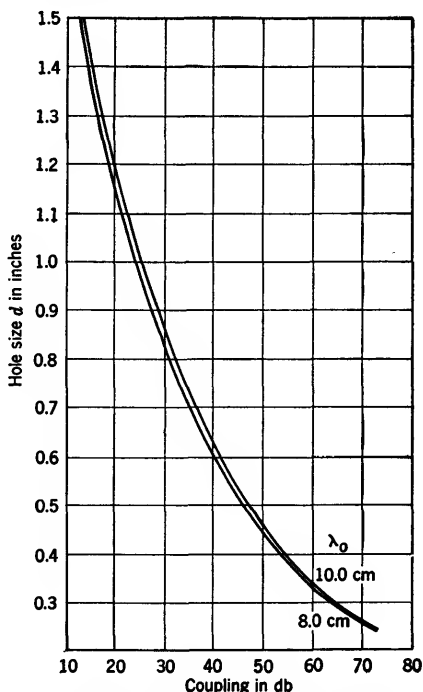


FIG. 14-10.—Design curves for Bethe-hole couplers in 3- by  $1\frac{1}{2}$ - by 0.081-in. wall waveguide.

tion. It is not practical to compensate for an imperfect directivity by using a mismatched termination. This would be a critical procedure at best and in any case a narrow-band solution. A coupler is designed to give as good directivity as possible and the termination is matched within the tolerances of the over-all directivity required.

Figures 14-8, 14-9, 14-10, 14-11 give pairs of curves for designing Bethe-hole couplers in several sizes of waveguide which have been investigated. The hole size is first determined to give the desired coupling, and then the angle of rotation of the second guide is chosen to peak the directivity. The curves were obtained from theoretical calculations.

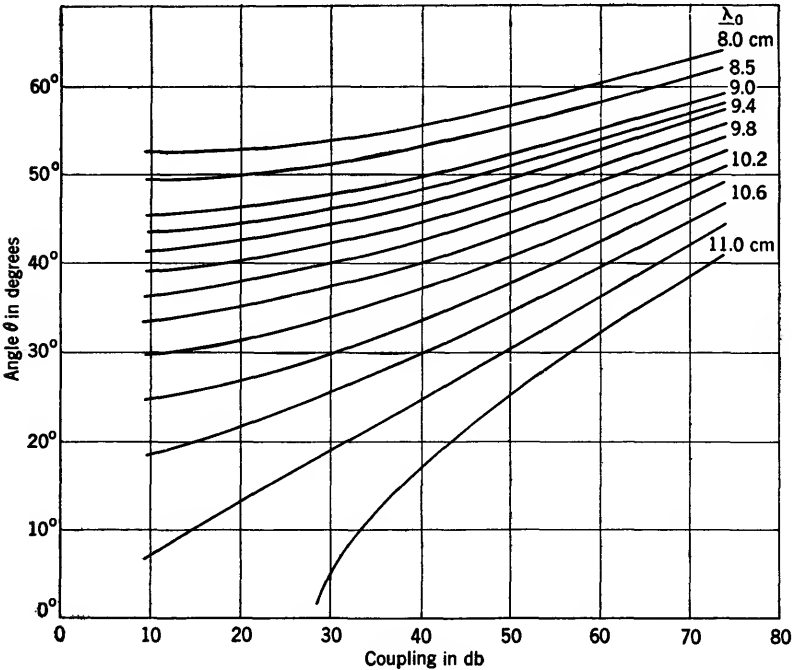


FIG. 14-11.—Design curves for Bethe-hole coupler in 3- by 1½- by 0.081-in. wall waveguide.

TABLE 14-1.—COUPLING AND DIRECTIVITY FOR BETHE-HOLE COUPLERS IN THE 10-CM BAND

Dimensions			Wave-length, cm	Coupling			Directivity, db	
Small hole, in.	Large hole, in.	Angle, deg.		Theory, db	Experiment, db	Theory minus experiment, db	Theory	Experiment,
0.740	1.375	52	8.5	34.13	35.7	-1.6	50.1	15
0.740	1.375	25	10.7	34.73	36.1	-1.4	50.9	24
0.740	1.5	38.5	10.0	34.6	35.7	-1.1		21
0.828	1.375	30	10.7	31.54	32.6	-1.1	30.2	23
1.105	1.5	30	10.7	22.84	24.4	-1.6	26.9	20
1.3	1.5	34.5	10.0	17.8	10.5	1.7		15
0.406	1.5	35	10.7	54.2	54.7	-0.5		19

For mechanical purposes, the hole for the 3- by 1½-in. waveguide is in a large recess in the second thickness of wall as is shown in Fig. 14-12. It is found empirically that it is necessary to design for a slightly larger value, by about 1 db, of coupling than is actually desired. Figure

14-12 shows the construction of this size of coupler. Table 14-1 gives a comparison of some of the experimental and theoretical values for the 3- by  $1\frac{1}{2}$ -in. guide.

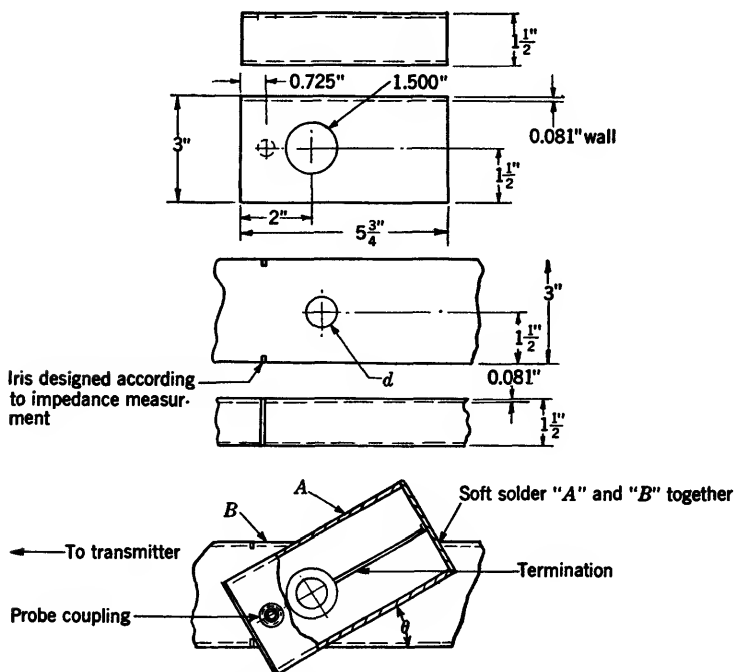


FIG. 14-12.—Bethe-hole couplers in 3- by  $1\frac{1}{2}$ - by 0.081-in. wall waveguide. Choose  $d$  and  $\theta$  according to design curves in Figs. 14-10 and 14-11.

**14-4. Branched-guide Couplers.**—The branched-guide coupler is a two-hole coupler which is particularly susceptible to exact analysis. Other types of two-hole couplers will be discussed in somewhat less detail in a later section. Figure 14-13 shows a branched-guide coupler in its usual form.

A qualitative idea of the operation of this coupler is obtained from the discussion of the two series probes in Sec. 14-2. If a pure traveling wave exists in one line, the relative phases of the waves in the small guides are exactly right to generate a pure traveling wave in the second guide in the *same* direction. In this respect, all two-hole couplers are different from the Bethe-hole coupler previously described.

In the following remarks the type of branched-guide coupler shown in Fig. 14-13 will be considered. The same analysis with only minor modifications can be applied as well to coaxial lines, or combinations of waveguide and coaxial lines; or indeed, to any type of transmission lines

arranged in this way. The representation of transmission lines as lumped circuits for purposes of analysis presents no difficulties. T-junctions present a more difficult problem, but it may be shown<sup>1</sup> that any symmetrical T-junction can be represented in the manner shown in Fig. 14-14. Four parameters are necessary to describe the symmetrical

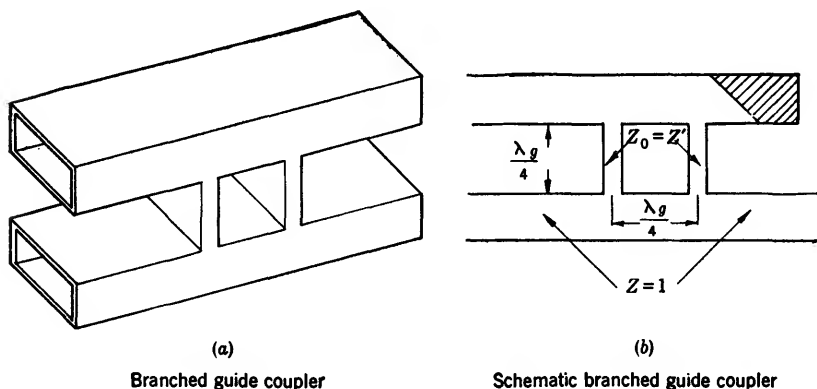


FIG. 14-13.—Branched-guide coupler.

junction: two to locate the three reference planes, and two to denote the values of the circuit elements. Similar circuits can be given for other types of T-junctions. The positions of these reference planes are not arbitrary. Only for certain positions is the simple equivalent circuit valid. For an *E*-plane T-junction, however, the change in the position

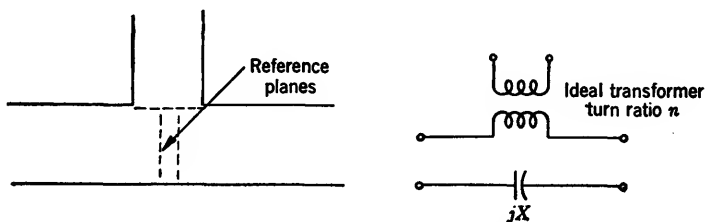


FIG. 14-14.—Equivalent circuit of T-junction.

of these reference planes with frequency is very small. As a first approximation, we shall assume that the positions of the reference planes at the junction are independent of frequency. In addition, we shall assume that  $jX = 0$  and that the turns ratio of the ideal transformer is independent of frequency. This turns ratio will, in practice, be of the order of unity.

With these assumptions, the branched-guide coupler has the equivalent circuit of Fig. 14-15, where the quarter-wave branches have a charac-

<sup>1</sup> *Principles of Microwave Circuits*, Vol. 8, Chap. 8, Radiation Laboratory Series.

teristic impedance  $Z'_0$  relative to that of the main transmission line. Since all the transformers are alike, they serve only to change the imped-

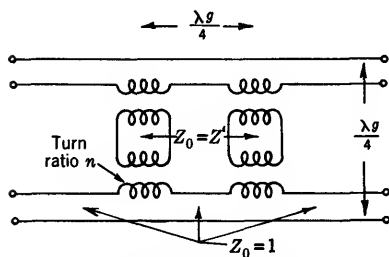


FIG. 14.15.—Equivalent circuit of branched-guide coupler.

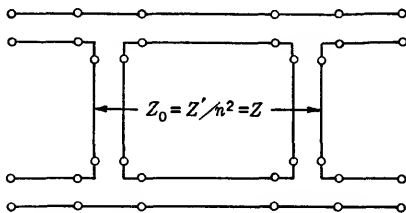


FIG. 14.16.—Modified equivalent circuit.

ance level of the stub lines so that we lose no generality in drawing the circuit as in Fig. 14.16, if we let

$$Z = \frac{Z'}{n^2}. \quad (24)$$

The equivalent circuit of a quarter-wavelength line of characteristic impedance  $Z_0$  may be chosen to be a T-network with the series elements equal to  $jZ_0$ , and the shunt element equal to  $-jZ_0$ . The equivalent circuit of the coupler is then reduced to that in Fig. 14.17. The impedance matrix may be written down immediately by inspection,

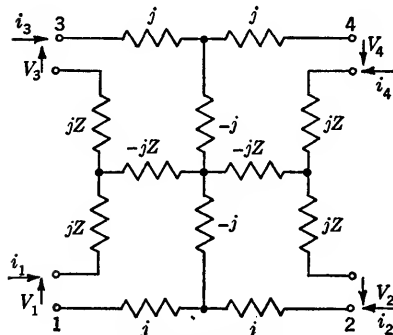


FIG. 14.17.—Equivalent circuit with lumped elements.

rememering that  $Z_{mn}$  is the voltage appearing at terminals  $m$  caused by a unit current at terminals  $n$  with all other terminals open-circuited.

$$\begin{pmatrix} V_1 \\ V_2 \\ V_3 \\ V_4 \end{pmatrix} = \begin{pmatrix} 0 & j & jZ & 0 \\ j & 0 & 0 & jZ \\ jZ & 0 & 0 & j \\ 0 & jZ & j & 0 \end{pmatrix} \begin{pmatrix} i_1 \\ i_2 \\ i_3 \\ i_4 \end{pmatrix}. \quad (25)$$

We now assume matched generators of voltages  $e_1, e_2, e_3, e_4$  connected to guides 1, 2, 3, 4 respectively. Then, since  $V_i = e_i - i_i$ ,

$$\begin{pmatrix} e_1 \\ e_2 \\ e_3 \\ e_4 \end{pmatrix} = \begin{pmatrix} 1 & j & jZ & 0 \\ j & 1 & 0 & jZ \\ jZ & 0 & 1 & j \\ 0 & jZ & j & 1 \end{pmatrix} \begin{pmatrix} i_1 \\ i_2 \\ i_3 \\ i_4 \end{pmatrix}. \quad (26)$$

If  $W$  is the determinant of the above matrix, and  $W^{ij}$  is the cofactor of the  $ij$ -element in the matrix, we may solve for  $i_j$  as

$$i_j = \sum_{k=1}^4 \frac{e_k W^{kj}}{W} \quad j = 1, 2, 3, 4. \quad (27)$$

We may now compute all the quantities of interest. It is sufficient to put

$$e_2 = e_3 = e_4 = 0 \quad (28)$$

to compute the effect of an incident wave at terminals 1. The currents produced by the other generators follow from symmetry considerations. We find the following expressions for the input impedance  $Z_{in}$ , the coupling  $C$ , and the directivity  $D$ :

$$Z_{in} = \frac{V_1}{i_1} = \frac{e_1}{i_1} - 1 = \frac{|W|}{W^{11}} - 1 = 1 - Z^2 \left( \frac{1 - \frac{Z^2}{2}}{1 + \frac{Z^2}{2}} \right), \quad (29)$$

$$\begin{aligned} C &= 10 \log_{10} \left( \frac{P_{incident}}{P_{coupled}} \right) = 10 \log_{10} \left| \frac{\frac{1}{2}(e_1)^2}{(i_4)^2} \right| \\ &= 10 \log_{10} \left[ \frac{\frac{1}{4}|e_1|^2(4 + Z^4)^2}{|-2Z|^2|e_1|^2} \right] \\ &= 20 \log_{10} \left( \frac{4 + Z^4}{4Z} \right) \\ &= 20 \log_{10} \left( \frac{1}{Z} + \frac{1}{4} Z^3 \right), \end{aligned} \quad (30)$$

$$\begin{aligned} D &= 10 \log_{10} \left( \frac{P_{coupled forward}}{P_{coupled backward}} \right) = 10 \log_{10} \left| \frac{(i_4)^2}{(i_3)^2} \right| \\ &= 10 \log_{10} \left( \frac{-2Z}{Z^3} \right)^2 = 20 \log_{10} \left( \frac{2}{Z^2} \right) \end{aligned} \quad (31)$$

It is seen that neither the voltage standing-wave ratio nor the directivity is perfect at the design frequency, but that both improve as the value of  $Z$  decreases.

The frequency sensitivity of the branched-guide couplers is the result of several factors of which only the change in the electrical length of the line sections can be readily analyzed. This is the principal cause of frequency sensitivity. Other causes are the change of the position of the reference planes of the junction with frequency (cf. Fig. 14-14) and the change in the turns ratio of the ideal transformer in the junction representation. Also, there is the reactive term  $jX$  shown in the equivalent circuit which has been ignored in the analysis. In practice this term is quite small.

To perform the analysis of change in line length we must replace the representation for a quarter-wave line by that of a line of length  $l$  shown in Fig. 14-18, where  $\beta = 2\pi/\lambda_g$ . The frequency sensitivity arises from the change in  $\beta$ . The same analysis can be used to predict effects caused by changes in line length  $l$  at a single frequency since these variables always occur as the product,  $\beta l$ . For  $l \approx \lambda_g/4$  we approximate

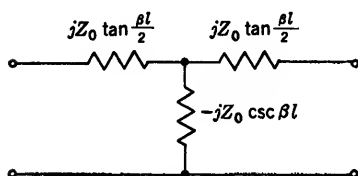


FIG. 14-18.—Equivalent circuit of a transmission line.

$$-jZ_0 \csc \beta l \approx -jZ_0$$

and

$$jZ_0 \tan \frac{\beta l}{2} \approx jZ_0(1 + \Delta\beta l), \quad (32)$$

where  $\Delta\beta l$  represents the deviation of  $\beta l$  from  $\pi/2$ , its value when  $l$  is a quarter wavelength. The impedance matrix becomes

$$\begin{pmatrix} K & j & jZ & 0 \\ j & K & 0 & jZ \\ jZ & 0 & K & j \\ 0 & jZ & j & K \end{pmatrix}, \quad (33)$$

where  $K = j(1 + Z)\Delta\beta l$ . Proceeding as before with matched generators we have

$$\begin{pmatrix} e_1 \\ \cdot \\ \cdot \\ \cdot \end{pmatrix} = \begin{pmatrix} 1 + K & j & jZ & 0 \\ j & 1 + K & 0 & jZ \\ jZ & 0 & 1 + K & j \\ 0 & jZ & j & 1 + K \end{pmatrix} \begin{pmatrix} i_1 \\ \cdot \\ \cdot \\ \cdot \end{pmatrix}, \quad (34)$$

the only changes being in the diagonal elements. We may, as before, put  $e_2 = e_3 = e_4 = 0$  corresponding to sending a wave into one arm of the coupler, and solve for the  $i$ 's. We neglect all terms with higher powers of  $K$  than the first. The parameters of the coupler are then

$$Z_{in} = \frac{V_1}{i_1} = \frac{e_1}{i_1} - 1 = \frac{W}{W_{11}} - 1 = 1 - Z^2 + \dots, \quad (35)$$

neglecting terms of order  $Z^4$ ,  $K^2$ ,  $KZ^2$  and higher orders. Thus  $Z_{in}$ , to this order of approximation, is independent of frequency. The expression, of course, agrees with the exact expression previously derived, to the same order of approximation. The coupling is

$$C = 10 \log_{10} \left( \frac{\frac{1}{4}|e_1|^2}{|i_4|^2} \right), \quad (36)$$

$$C = 10 \log_{10} \left( \frac{\frac{1}{4}|4 + 8K|^2}{-4Z^2|1 + K|^2} \right). \quad (37)$$



Remembering that  $K = -K^*$ ,

$$C = 10 \log_{10} \left[ \frac{1 - 4K^2}{Z^2(1 + K^2)} \right] = 10 \log_{10} \left( \frac{1}{Z^2(1 + 3K^2 + \dots)} \right), \quad (38)$$

so that the coupling also varies only with  $K^2$ , and is frequency-independent to the first order. Similarly, the directivity is

$$\begin{aligned} D &= 10 \log_{10} \left( \frac{|i_4|^2}{|i_3|^2} \right) \\ &= 10 \log_{10} \left[ \frac{4Z^2(1 - K^2)}{Z^2(Z^4 - 4K^2)} \right] \\ &= 10 \log_{10} \left( \frac{1}{\frac{Z^4}{4} - K^2} \right) = 20 \log_{10} \left[ \frac{2}{Z^2} \left( 1 - \frac{4K^2}{Z^4} \right)^{1/2} \right]. \end{aligned} \quad (39)$$

It should be pointed out that since  $K$  is imaginary,  $K^2$  is negative, so the directivity given by the above formula is never perfect. The other causes of frequency sensitivity—changes in the parameters and in the reference planes of the junction—are important only for tight coupling and large  $Z$ .

*Values of the Circuit Parameters.*—If the height of the branched guide is small compared with the height of the main guide, several good approximations may be made. First, as before, the series reactance  $jX$  may be neglected. Second, the spacing of the reference planes in the main waveguide may be taken as zero, (see Fig. 14-14). The approximate reference planes are shown in Fig. 14-19. The parameter  $d$  may not be neglected, however. Relative to the small branched waveguide, the main guide appears as an open circuit at a distance  $d$  beyond the plane of junction. At the junction plane, the open circuit appears as a shunt capacitance on the branched line. Third, the turns ratio of the transformer may be taken equal to unity, so that the branch-line impedance  $Z$  is the ratio of the height of the branched guide  $b'$  to the height of the main guide  $b$ .

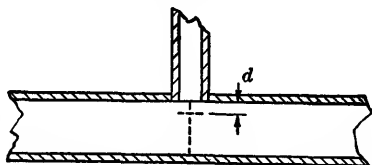


FIG. 14-19.—Approximate reference planes when  $b' \ll b$ .

The value of the shunt capacitive susceptance on the branched line is

$$B_c = \frac{2b'}{\lambda_g} \left( 1 + \ln \frac{b}{2b'} \right). \quad (40)$$

This corresponds to a value of  $d$  given by

$$d = \frac{b'}{\pi} \left( 1 + \ln \frac{b}{2b'} \right). \quad (41)$$

The design procedure in this simple case is straightforward. The height of the branched guide is chosen for the desired value of the coupling given by Eq. (30). To sufficient accuracy Eq. (30) reduces to

$$C = 20 \log_{10} \frac{b}{b'} \quad (42)$$

The two branched guides are spaced a quarter of a wavelength apart along the main transmission line. The lengths of the branched guides are chosen to be smaller than a quarter wavelength by the amount  $2d$ .

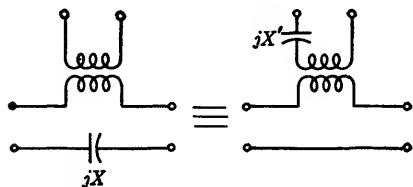


FIG. 14-20.—Alternative representation of T-junctions.

If a close coupling is desired, so that  $b'$  approaches  $b$ , the above approximations are no longer valid. The correct values of the circuit parameters,  $n$ ,  $d$ ,  $jX$ , and the separation of the reference

planes in the main waveguide may be found in the *Waveguide Handbook* for the *E*-plane T-junction.

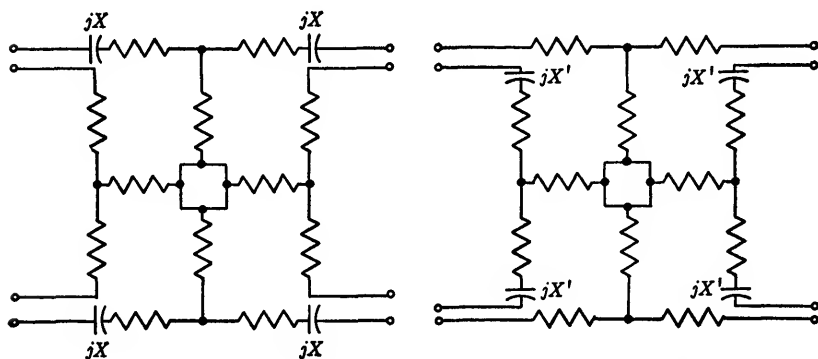


FIG. 14-21.—Lumped circuit for coupler with junction reactance.

**Effect of Junction Reactance.**—In addition to the method employed earlier in this section, the general representation of a T-junction can be made in another form as indicated in Fig. 14-20. If  $jX$  or  $jX'$  cannot be neglected, the lumped-circuit representation for the entire coupler can be of the form shown in Fig. 14-21. Since any lossless symmetrical T-network can be realized as a length of transmission line of real length and real characteristic impedance, correction for the effect of junction reactance can be accomplished by changing the length of one set of arms or even by changing both sets. There will be a corresponding change in coupling. If only the stub lines are changed, the coupler will still be of

the simple form treated above. The values of the parameter  $X$  are given in the *Waveguide Handbook*.

**Modified Branched-guide Coupler.**—It is useful at tight couplings to use a variation which has three different guide sizes instead of two. The ordinary type has a directivity of only 26 db at a coupling of 10 db, whereas the modification which is shown in Fig. 14.22 is perfect at the design wavelength. Unfortunately for the design of this type of coupler the parameters for unsymmetrical junctions have not been tabulated.

Branched-guide couplers can be designed which have perfect directivity although none of the lines are a quarter wavelength long and all the branches are of different characteristic impedances. The investigation of these possibilities is too involved<sup>1</sup> to present here, and has not yet produced any forms of practical value.

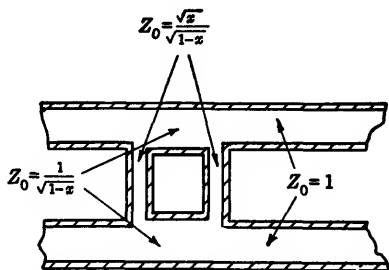


FIG. 14.22.—Modified branched-guide directional coupler.

**14.5. Two-hole Couplers.**—Two-hole couplers are included among those types which have a main transmission line, an auxiliary line, and two identical coupling devices spaced an odd number of quarter wavelengths apart. The branched-guide coupler treated in the previous section is one member of this class. Others are the two-hole coupler shown in Fig. 14.23 and the “inside-out” coaxial coupler shown in Fig. 14.24. The individual coupling devices should be nondirectional, or if directional, should favor the same direction as the complete coupler so that the directivity will be high. Two rectangular guides connected by holes in their broad sides would not operate satisfactorily since each hole is a Bethe-hole coupler transmitting primarily a backward wave and the cancellation of the backward waves would be imperfect. The frequency sensitivity of directivity is similar for all two-hole couplers. If the amplitude of the forward wave is unity, the amplitude of the wave in the backward direction is, to a first approximation,  $\frac{1}{2}(1 + e^{2j\beta l})$ , where  $l$  is the distance between the holes, assuming that the elements are non-directional. The power in the backward wave is

$$\left| \frac{1}{2}(1 + e^{2j\beta l}) \right|^2 = \cos^2 \beta l. \quad (43)$$

If we write

$$\beta l = (2n + 1) \left( \frac{\pi}{2} + \Delta \beta l \right), \quad (44)$$

<sup>1</sup> B. A. Lippmann, “Theory of Directional Couplers,” RL Report No. 860, Dec. 28, 1945; also Principles of Morewave Circuits, Vol. 8, Chap. 8, Radiation Laboratory Series.

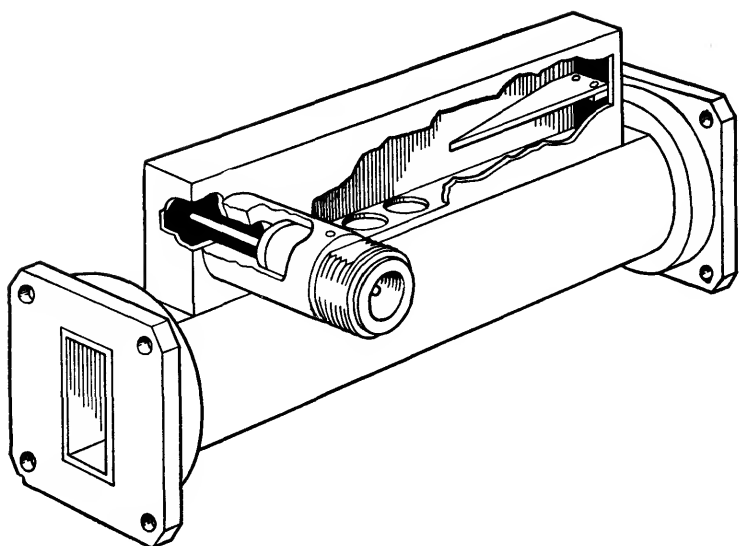


FIG. 14-23.—Two-hole directional coupler.

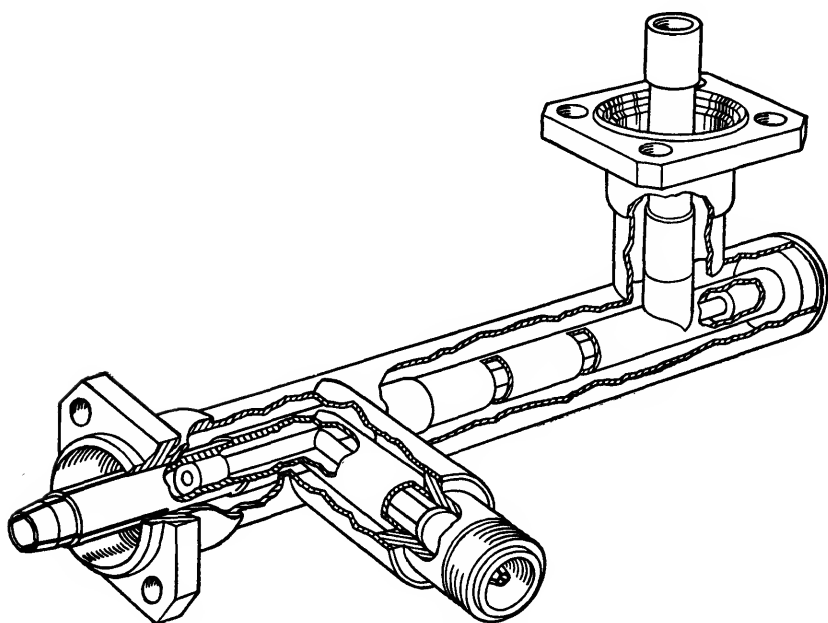


FIG. 14-24.—“Inside-out” coaxial coupler.

then the backward power is

$$\sin^2 [(\Delta\beta l)(2n + 1)], \quad (45)$$

where  $(\Delta\beta l)$  is the departure of the hole spacing from an integral number of quarter wavelengths. Making the approximation  $\sin \theta \approx \theta$ , we have

$$D = 10 \log_{10} \frac{1}{(\Delta\beta l)^2 (2n + 1)^2}. \quad (46)$$

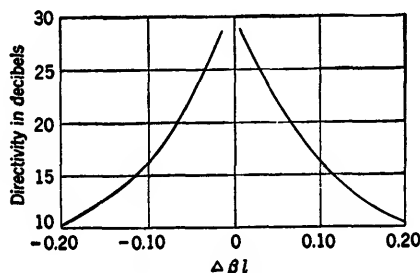


FIG. 14-25.—Frequency variation of directivity for two-hole couplers.

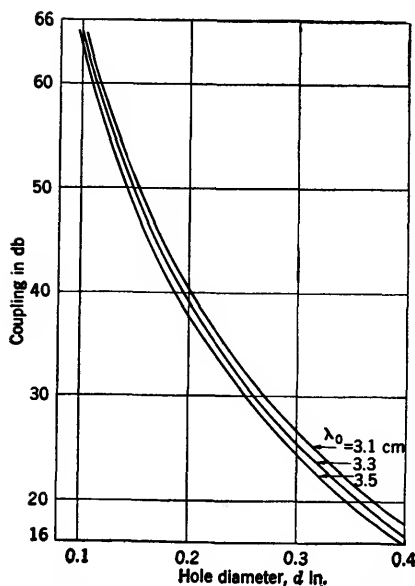


FIG. 14-26.—Design curves for two-hole couplers using round holes in the side of 1- by  $\frac{1}{2}$ -in. waveguide with 0.050-in. wall.

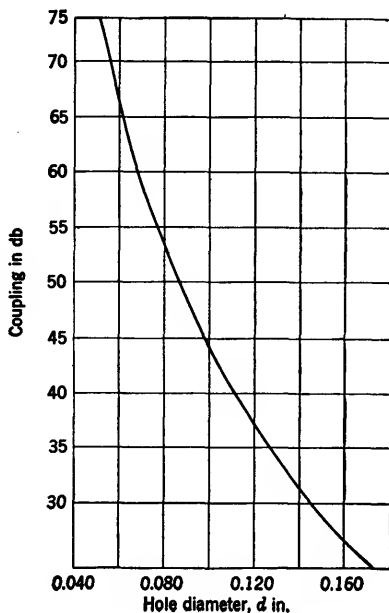


FIG. 14-27.—Design curve for two-hole couplers using round holes in the side of  $\frac{1}{2}$ - by  $\frac{1}{4}$ -in. waveguide with 0.040-in. wall, for  $\lambda_0 = 1.25$  cm.

This approximate formula gives an infinite directivity at the design wavelength which is generally not realized in practice because of reflections, inaccuracies, or interactions between coupling elements. Far from the design wavelength, where the directivity is determined primarily by the spacing of the coupling elements, this formula is a good approximation. A plot of  $D$  against  $\Delta\beta l$  is shown in Fig. 14-25 for  $n = 0$ .

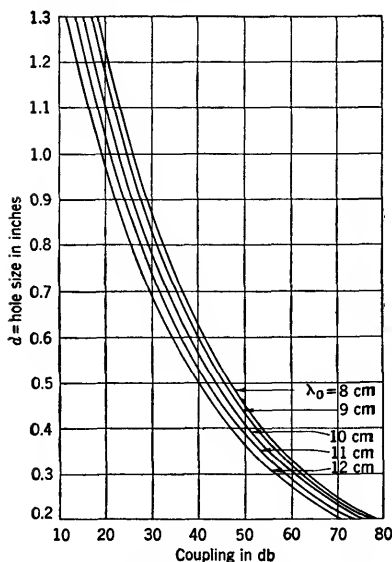


FIG. 14-28.—Design curves for two-hole couplers using round holes in the side of 3- by 1½-in. waveguide with 0.080-in. wall.

The frequency sensitivity of coupling is almost wholly dependent upon that of the individual coupling elements since the addition of waves in the forward direction depends only upon the equality of the two paths and thus does not depend upon frequency.

Design curves for an ordinary two-hole coupler such as that shown in Fig. 14-23 are given in Figs.

TABLE 14.2.—DIRECTIONAL COUPLERS USING TWO SLOTS  
Data to accompany Fig. 14.30

Waveguide size	Slot length $t$ , in.	Slot spacing $s$ , in.	Slot height $d$ , in.	Wall thickness $l$ , in.	Curve in Fig. 14-30	Coupling, db
1½ by ¾ by 0.064 in.	0.350	0.385	0.094	0.187	..	24.6 at $\lambda_0 = 3.1$ cm
	0.328	0.400	0.156	0.187	A	26.7 at $\lambda_0 = 3.5$ cm
	0.400	0.400	0.094	0.187	B	
1 by ½ by 0.050 in.	0.290	0.430	0.200	0.150	C	
	0.325	0.486	0.187	0.144	D	
	0.350	0.430	0.187	0.144	E	
	0.350	0.430	0.200	0.150	F	
¾ by ½ by 0.040 in.	0.070	0.152	0.062	0.080		34.3 at $\lambda_0 = 1.25$ cm
	0.100	0.152	0.062	0.080		29.0
	0.135	0.152	0.062	0.080		19.0
	0.166	0.152	0.062	0.080		8.5

14.26, 14.27, 14.28 for various sizes of waveguide. The curves show theoretical coupling from the formula given by Bethe,

$$C = 20 \log_{10} \left( \frac{\pi d^3 \lambda_g}{6a^3 b} \right) - 32.0 \left[ 1 - \left( \frac{1.71d}{\lambda_0} \right)^2 \right]^{\frac{1}{2}} \frac{t}{d}. \quad (47)$$

The coupling can be increased and at the same time broadbanded by using slots instead of holes. The slots, which are about a quarter wavelength long, are staggered in the side wall of the guide to prevent over-

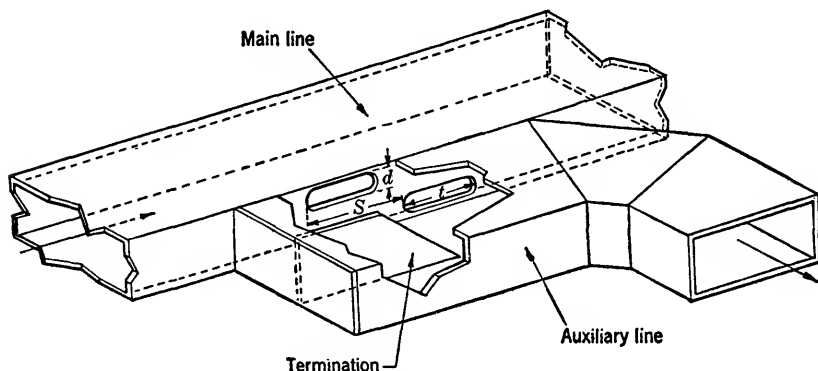
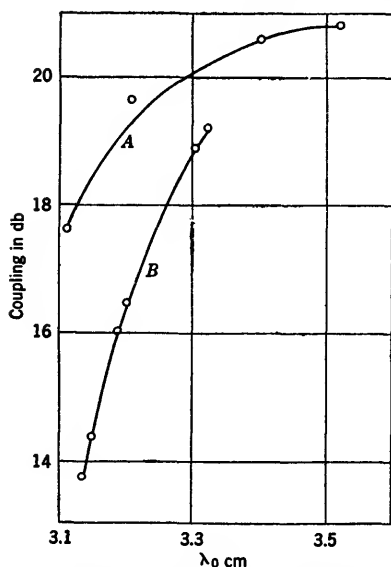
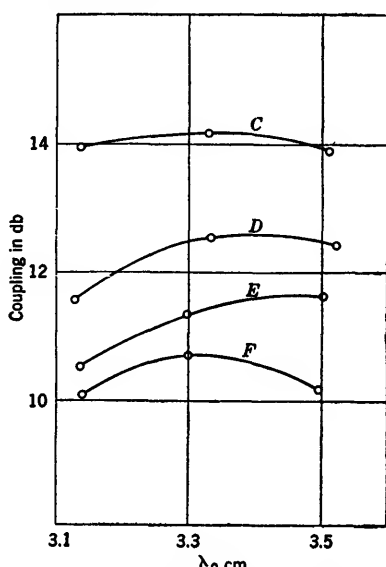


FIG. 14.29.—Coupler employing two slots.



1 1/4 in. by 5/8 in. by 0.064 in. wall waveguide



1 in. by 1/2 in. by 0.050 in. wall waveguide

FIG. 14.30.—Experimental results on two-element couplers using slots in the side of guide.

lapping. Such a coupler is shown in Fig. 14-29. Figure 14-30 characterizes some of the couplers which have been made with this type of construction. The results are empirical. The theory of coupling through slots of this type has not been worked out. Table 14-2 gives the dimensions of the couplers whose characteristics are shown in Fig. 14-30 together with some additional observations.

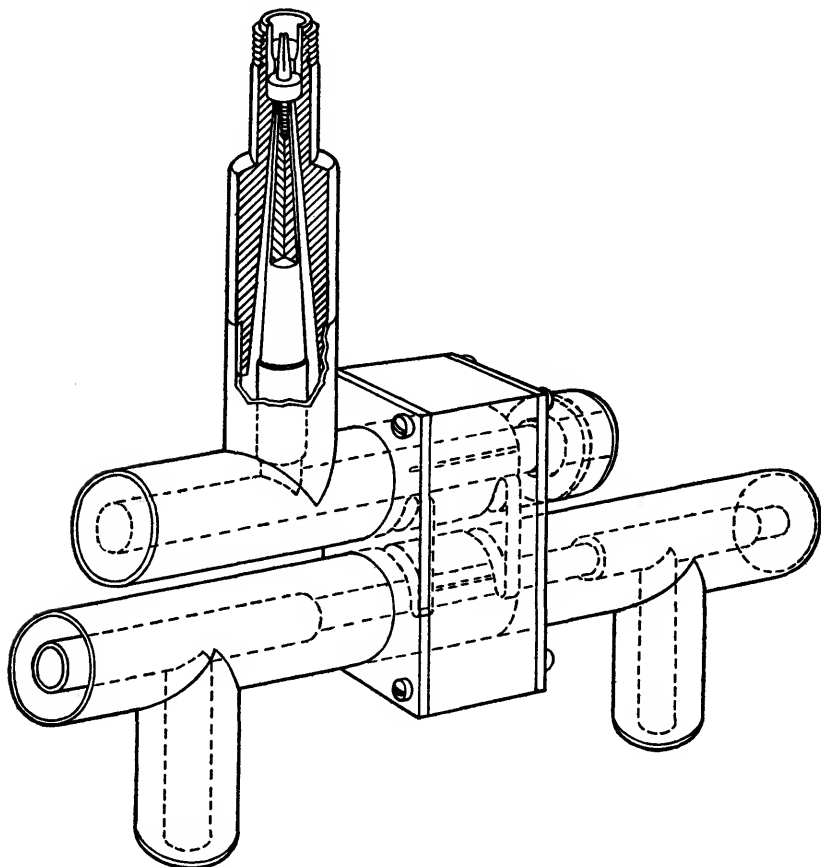


FIG. 14-31.—Slotted-block directional coupler for coaxial line.

Two-hole couplers have also been constructed in coaxial line. One method employs two coaxial lines side by side with slots joining them,<sup>1</sup> as shown in Fig. 14-31. It is difficult by this method to obtain sufficient coupling without introducing large reflections in the transmission lines.

<sup>1</sup> R. S. Julian, "Directional Transmission Line Taps," BTL MM-44-170-6, Jan. 26, 1944.



Experimental results for such a coupler are shown in Figs. 14-32 and 14-33.

A more satisfactory method is to place one coaxial line inside the center conductor of the second coaxial line. Coupling apertures are cut out between them. The inner line can be brought out to terminals through stub supports. Figure 14-24 shows an "inside-out" coaxial-line coupler of this type. In this way it is possible to obtain close couplings as is shown in the design curves of Figs. 14-34 and 14-35. In Fig. 14-35 the points represent experimental determinations; the curve is drawn on the assumption that the coupled power varies as  $\theta^6$ . An approximate formula has been derived for the coupling of inside-out couplers by making the assumption that the coupling aperture is an elliptical hole in a plane conducting wall. This gives

$$C \approx 20 \log_{10} \left[ \frac{5\pi r \theta^3}{2Z_0 \lambda \left( \ln \frac{4r\theta}{W} - 1 \right)} \right] + \frac{27t}{\theta r}, \quad (48)$$

where  $\theta$  is the angular aperture of the slot in radians;  $r$  is the radius of the cylindrical surface between the two transmission lines;  $Z_0$  is the line impedance;  $\lambda$  is the wavelength;  $t$  is the wall thickness; and  $W$  is the width of the aperture. The second term gives the attenuation through the aperture. The dashed line in Fig. 14-35 shows the results of applying this formula. The circled points are experimental.

Broadband coupling can be obtained by using a composite coupler composed of two units in cascade. If the frequency sensitivities of the two couplers are of opposite sign, it is possible to obtain an over-all coupling which is frequency-insensitive. For example, a coupler with two round holes and a slot coupler could be used together. This method is of course applicable only where weak coupling is desired.

**14-6. Multiple-path Couplers.**—An extension of the principle of the two-hole coupler is the multiple-path coupler. Waves add in the forward direction and cancel in the backward direction, but cancellation is obtained between waves excited by three or more coupling elements, usually spaced a quarter wavelength apart. A coupler of this type may

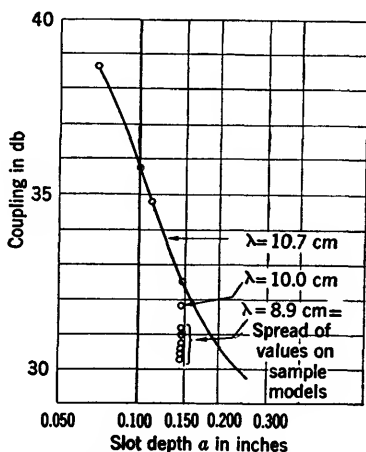


Fig. 14-32.—Design data on slotted-block coaxial couplers in  $\frac{1}{2}$ -in. line.

be used to increase the coupling in the forward direction or to improve the frequency sensitivity of the directivity. For this purpose a set of coupling elements for which the coupled voltages vary as the coefficients

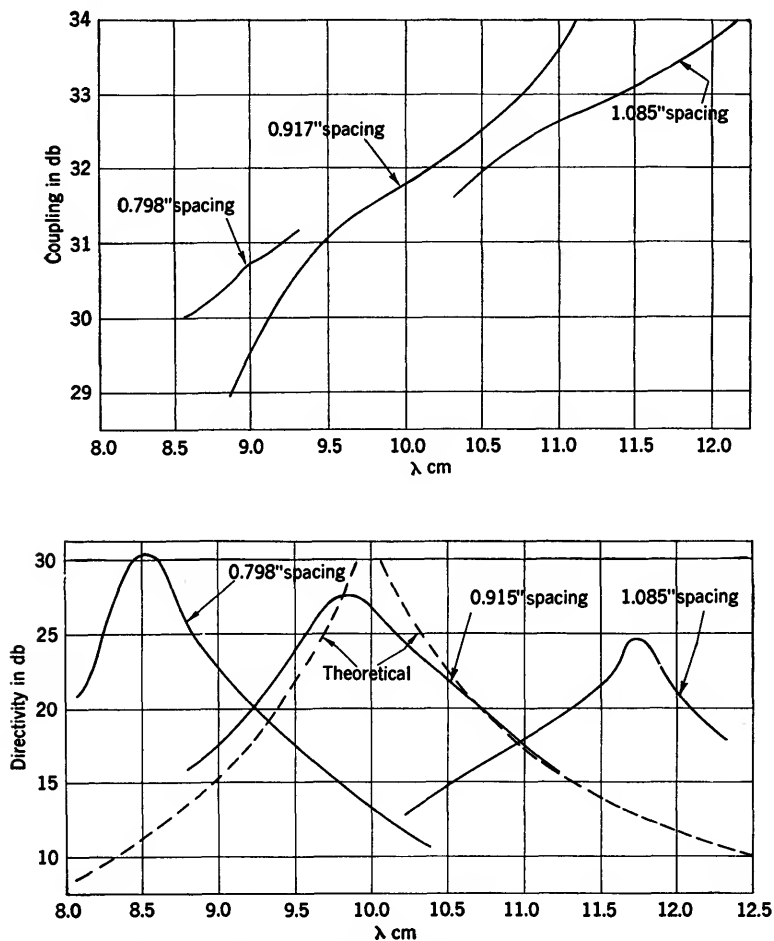


FIG. 14-33.—Experimental results on slotted-block directional coupler in  $\frac{1}{2}$ -in. coaxial line. Upper curves give the measured coupling for two-slot couplers with a nominal slot depth of 0.145 in. for different spacings between slots. The lower curves show the measured directivity.

in a binomial expansion may be used. This improves frequency sensitivity in much the same manner as the use of binomial tapers in impedance matching.<sup>1</sup>

<sup>1</sup> J. C. Slater, *Microwave Transmission*, McGraw-Hill, New York, 1942, p. 60.

Suppose we have two two-hole couplers spaced along a transmission line. If they do not have perfect directivity, each will produce a wave in the backward direction. If we space the couplers by an odd number of

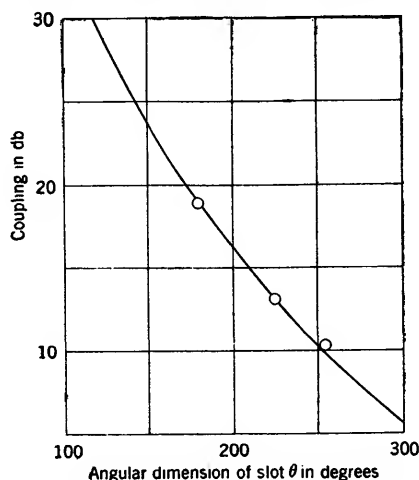


FIG. 14-34.—Design data for concentric coaxial coupler between  $\frac{1}{8}$ -in. OD and  $\frac{1}{4}$ -in. OD coaxial lines for  $\lambda_0 = 10$  cm.

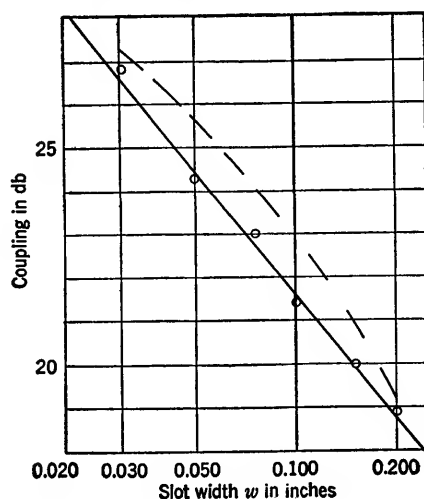


FIG. 14-35.—Design data for concentric coaxial coupler between  $\frac{1}{8}$ -in. OD and  $\frac{1}{4}$ -in. OD coaxial lines.

quarter wavelengths, the two backward waves will cancel. If we attempt to space them by one-quarter wavelength, the second hole of the first coupler will coincide with the first hole of the second coupler. We have a

three-hole coupler, with the center hole producing coupled waves of twice the amplitude of the waves produced by the outer holes. By repeating this process, we arrive at an  $(n + 1)$ -hole coupler with binomial coupling. We can calculate the relative couplings by this same argument as indicated schematically below.

$$\begin{array}{r}
 1 \quad 1 \\
 + \quad \frac{1 \quad 1}{1 \quad 2 \quad 1} \\
 + \quad \frac{1 \quad 2 \quad 1}{1 \quad 3 \quad 3 \quad 1} \\
 + \quad \frac{1 \quad 3 \quad 3 \quad 1}{1 \quad 4 \quad 6 \quad 4 \quad 1} \\
 + \dots\dots\dots
 \end{array}$$

Let  $(n + 1)$  be the number of such holes. Then let the voltage coupling through these holes be proportional to the coefficients of the binomial expansion

$$1, n, \frac{n(n-1)}{1 \cdot 2}, \frac{n(n-1)(n-2)}{1 \cdot 2 \cdot 3}, \dots, \frac{n(n-1) \dots (1)}{1 \cdot 2 \cdot 3 \dots n}.$$

In the forward direction these will add in phase to give a coupling proportional to  $2^n$ . This does not mean that the coupling can be increased indefinitely since it is limited by the maximum coupling possible for the largest hole, and in order to materially increase the coupling the number of holes must be enormous.

In the backward direction the waves add with alternating signs so that at the design frequency the backward wave vanishes

$$1 - n + \frac{n(n-1)}{2} - \dots (-1)^n \frac{n(n-1) \dots (1)}{1 \cdot 2 \cdot 3 \dots n} = (1-1)^n = 0. \quad (49)$$

To determine the frequency sensitivity of directivity we introduce a small deviation from quarter-wave spacing. The expression for the backward wave is then

$$\begin{aligned}
 1 - ne^{j\Delta} + \frac{n(n-1)}{1 \cdot 2} e^{2j\Delta} - \frac{n(n-1)(n-2)}{1 \cdot 2 \cdot 3} e^{3j\Delta} \\
 + (-1)^n \frac{n(n-1) \dots 1}{1 \cdot 2 \cdot 3 \dots n} e^{nj\Delta} = (1 - e^{j\Delta})^n. \quad (50)
 \end{aligned}$$

For small values of  $\Delta$ , the backward wave is  $(-j\Delta)^n$ , so that the backward wave vanishes to the  $n$ 'th order of the frequency deviation. Some improvements over this method of broadbanding might be expected if

the spacings were staggered slightly so as to get the broadest bandwidth. However, interactions have been neglected in the analysis, and a more laborious calculation would be necessary to predict the optimum design. In addition, the frequency sensitivities of the coupling elements would have to be taken into consideration. Branched-guide couplers with many branches are also possible and form a type of multiple-path coupler.

**14.7. Reverse-coupling Types.**—An important variation of the two-hole coupler is the reverse-coupling type. This differs from the ordinary two-hole coupler in having a reversal of phase in one coupling element as compared to the other. This is accomplished by using the symmetry properties of the coupling and can be done only in certain

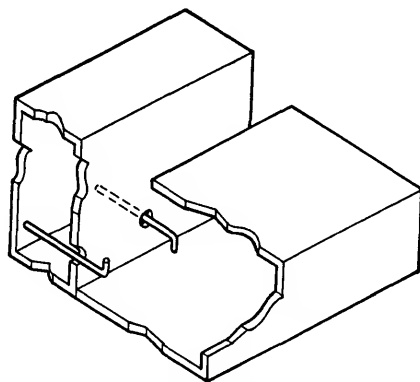


FIG. 14-36.—Reverse-coupling directional coupler.

cases. The advantage of a coupler of this kind is that the waves reinforce in the backward direction and cancel in the forward direction so that the cancellation is not so frequency-sensitive as in the simpler coupler. Because of the addition of the two waves in the backward direction, the coupling will have increased frequency sensitivity, but this is a slowly varying effect compared to the change in directivity of the usual variety of coupler. The individual coupling elements may have frequency sensitivity which can perhaps be used to balance out the other effect.

One method of obtaining the phase reversal is shown in Fig. 14-36.

The action of this coupler may be easily understood from the cross sections shown in Fig. 14-37. Here identical currents are produced in the secondary line by fields which are opposite in phase in the primary line for the two elements.

Another method is shown in Fig. 14-38. The direction of the current lines across the slot, and hence the phase of coupling, will depend upon the side of the slot into which the screw is inserted. The strength of the

current and therefore the coupling will depend on the depth of insertion. This scheme has often been employed in antenna arrays.<sup>1</sup>

A third method which has proved useful in practice is known as the Schwinger reversed-phase coupler. This coupler is shown in Fig. 14-39.

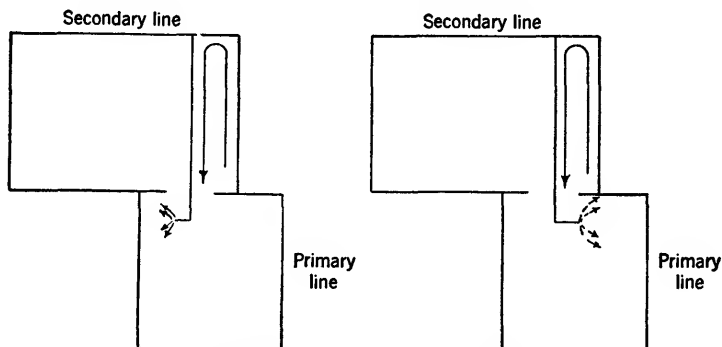


FIG. 14-37.—Action of RCA coupler.

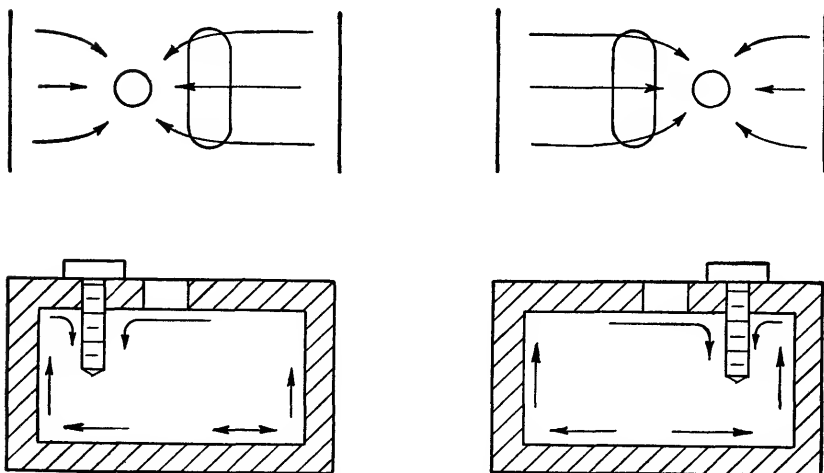


FIG. 14-38.—Second variety of reverse-phase coupling element.

The reversal of phase between the two elements is indicated in Fig. 14-40. The coupling is between the longitudinal magnetic field in one guide and the transverse magnetic field in the other. The use of a slot about a quarter-wavelength long results in broadband coupling (cf. Sec. 14-5). Experimental measurements on couplers of this type are shown in Fig. 14-41. Table 14-3 gives some results on a 10-cm-band model, built in 3- by 1½-in. waveguide.

<sup>1</sup> Microwave Antenna Theory and Design, Vol. 12 Radiation Laboratory Series.

TABLE 14-3.—10-CM-BAND SCHWINGER COUPLER

$\lambda$ , cm	Coupling, db	Directivity, db
8.9	+19.6	22
9.24	+20.8	24
10.0	+22.1	30
10.55	+22.7	30
11.1	+22.9	26
11.55	+22.7	22

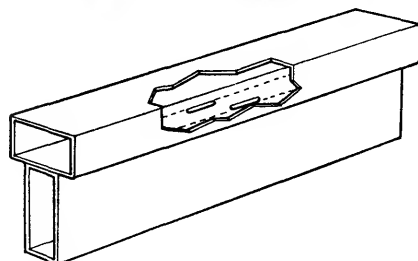


FIG. 14-39.—Schwinger directional coupler.

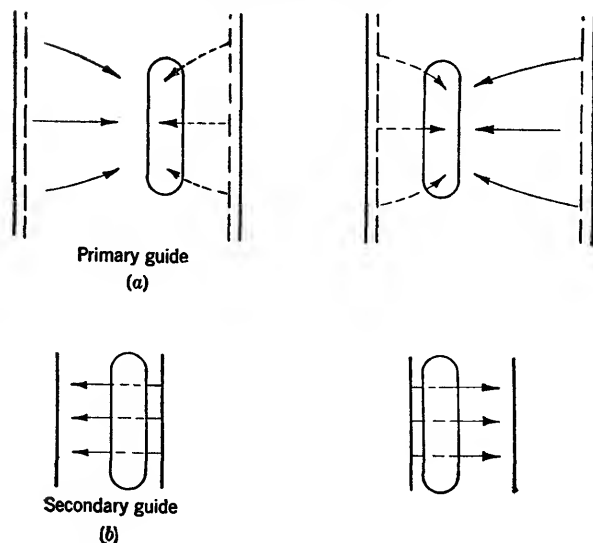


FIG. 14-40.—Reversal of phase in Schwinger coupler showing current lines.

Figure 14-42 shows the slot dimensions for the coupler whose characteristics are shown in the table.

**14-8. Long-slot Couplers.**—As the name implies, the long-slot coupler is formed of two transmission lines joined by a slot in the direction of

propagation. The slot is presumed to radiate or "leak" energy from one guide to the other at each point along its length. In the forward direction these incremental waves reinforce in phase. In the reverse

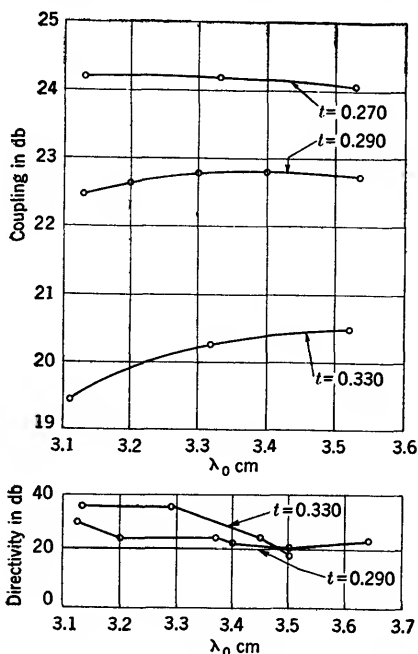


FIG. 14-41.—Schwinger directional coupler in 1- by  $\frac{1}{2}$ - by 0.050-in. wall waveguide.

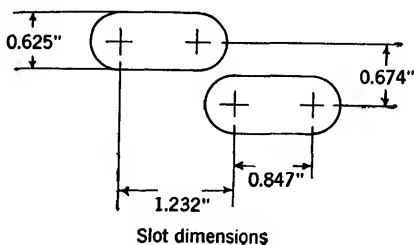


FIG. 14-42.—Slot dimensions of 10-cm-band Schwinger coupler.

direction the incremental waves are of all phases and tend to cancel. According to this simple picture, when the slot is an integral number of half wavelengths long, all phases are equally represented in the reverse direction so that there is no net wave and the directivity is perfect. In any case, the longer the slot, the greater the ratio of forward-to-backward coupling.

More sophisticated analysis shows that if the slot is carefully tapered



to prevent reflection from the ends, the directivity should be perfect even for very wide short slots. Further, it is possible to get all the energy into the auxiliary guide for any slot width by making the slot long enough. Making the slot still longer decreases the coupling. This limitation,

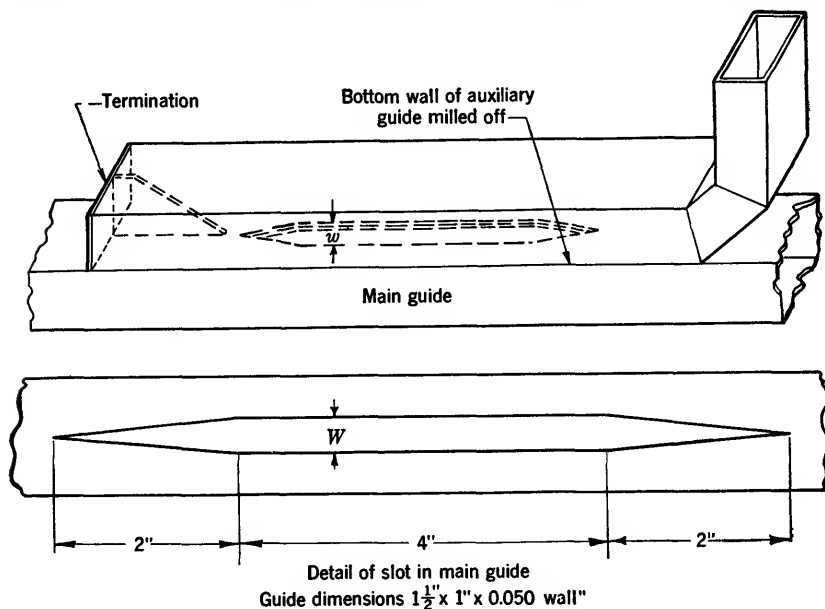


FIG. 14.43.—Construction of long-slot directional coupler.

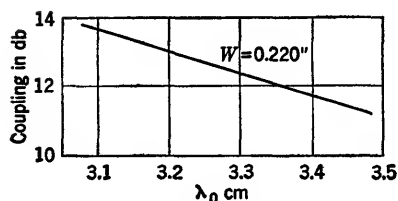


FIG. 14.44.—Frequency dependence of coupling for long-slot coupler in 1- by  $\frac{1}{2}$ - by 0.050-in. wall waveguide.

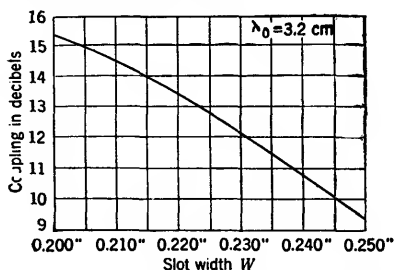


FIG. 14.45.—Design data for long-slot couplers in 1- by  $\frac{1}{2}$ - by 0.050-in. wall waveguide.

however, is never reached in practice. For small coupling, the coupled power is proportional to the square of the slot length and to the sixth power of the slot width. It is possible to obtain high directivities in practice with this type of coupler so that it is suitable for reflectometer purposes (cf. Sec. 14.12). Its length, however, makes it unsuitable for most applications. The construction of a long-slot directional coupler

is shown in Fig. 14-43. The frequency sensitivity of coupling is large as shown in Fig. 14-44. The coupling obtained as a function of slot width is plotted in Fig. 14-45.

In order to demonstrate some of the properties of the long-slot coupler it may prove instructive to consider the problem from two widely different approaches. First, we shall consider infinitesimal sections of the length of the slot as separate radiators. As was shown in Sec. 14-3,

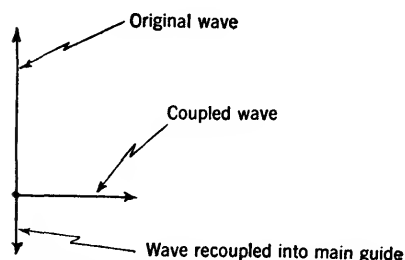


FIG. 14-46.—Operation of long-slot coupler.

fringing fields in the auxiliary guide will behave as if there were electric and magnetic dipoles in the slot in phase with the incident wave. These will radiate wavelets which will reinforce in the forward direction and tend to cancel in the reverse direction. We ignore any possible directional properties of the individual slot segments.

Once a wave is set up in the auxiliary guide it will, in turn, radiate into the primary guide. It might be supposed that once half the power had entered the auxiliary guide a sort of equilibrium would be set up and further lengthening of the slot would produce no change. This is not the case, however. If the expression for dipole radiation into free space is recalled, it will be noticed that there is a  $90^\circ$  phase difference between the radiated field and the exciting field. The same holds for waveguides. The imaginary factor  $j$  in Eq. (11) represents the same phenomenon. The wave traveling in the auxiliary guide will hence be  $90^\circ$  behind the exciting wave. This is shown in Fig. 14-46. Figure 14-46 also shows that the wave reradiated into the primary guide is of such phase as to decrease the total intensity in the primary guide. One might almost say that the wave in the auxiliary guide "sucks" power out of the main guide. This process continues until all of the power has been transferred to the auxiliary guide, at which point the process reverses and power is transferred from the auxiliary guide back into the main guide. This action is exactly analogous to the behavior of two loosely coupled tuned circuits.

For fairly short slot lengths, when the power transfer from the auxiliary guide to the main line can be neglected, the coupled voltage is proportional to slot length and hence coupled power varies as the square of slot length. As with coupling holes, the coupled power varies as the sixth power of the slot width (cf. Sec. 14-3). The directivity for short slot lengths is by this analysis

$$D = 10 \log_{10} \left( \frac{\beta l}{\sin \beta l} \right)^2, \quad (51)$$

if the possible directional effect of an incremental section of slot is ignored. Since, however, most long-slot couplers have tapered ends on the slots, this formula, as will be seen, is not particularly significant.

The second method of approach to these problems stems from a consideration of the two lines joined by the slot as a single transmission line of somewhat peculiar cross section. Figure 14-47 shows the types of modes which can be propagated in such a transmission line. Mode *C*

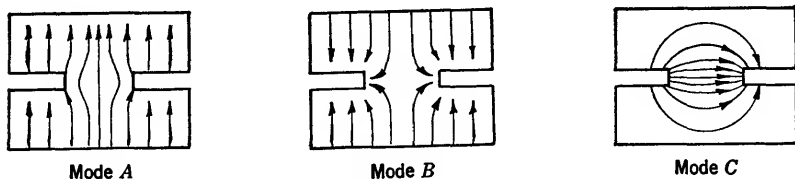


FIG. 14-47.—Normal modes in slotted guides.

cannot be excited except by irregularities, but it can cause the troublesome “slot resonance” in long-slot couplers, or in slotted sections, (cf. Sec. 8-3). It is totally reflected from the ends of the slot so that the slot behaves as a resonant section of line coupled to the rest of the system only by asymmetries. It is probably worth while to try to damp out this resonance, although this has not yet been investigated.

At the ends of the slots, modes *A* and *B* couple to the two guides only in certain symmetrical ways which we shall refer to as modes *A'* and *B'*,

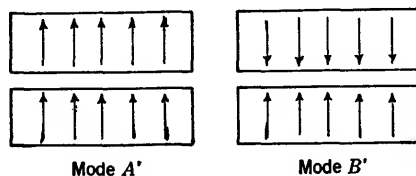


FIG. 14-48.—Normal modes in two guides.

respectively. These modes represent the two possible symmetries of the configuration and are shown in Fig. 14-48. There may also be reflections of these modes at the ends of the slot. We shall assume in this analysis that the ends of the slot have been carefully tapered to prevent reflections. Hence, if we simultaneously send waves down two guides to produce mode *A'*, there will be a smooth transition to mode *A* along the slot and back to mode *A'* at the other end of the slot, without any reflections. Similarly with modes *B* and *B'*. This is illustrated in Fig. 14-49.

It can be seen from the figure that sending a wave down the primary guide from terminal 1, is equivalent to sending mode  $(A' + B')$  in at terminals 1 and 3. The fields in arm 3 will cancel. Waves will come out at arms 2 and 4 only; and there will be no reflected waves. In other

words, the coupler will have perfect directivity and be perfectly matched, independently of everything except the quality of the tapering of the slot. The coupling comes about by virtue of the fact that modes  $A$  and  $B$  will have slightly different propagation velocities with the result that

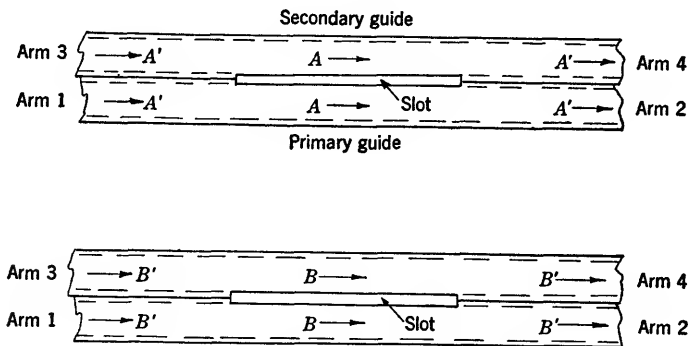


FIG. 14-49.—Modes in long-slot coupler.

modes  $A'$  and  $B'$  will no longer be in phase in arms 2 and 4. In arm 4 the amplitude will be

$$E_4 = e^{-j\beta_A l} - e^{-j\beta_B l} = e^{-j(\beta_B + \beta_A)\frac{l}{2}} [e^{j(\beta_B - \beta_A)\frac{l}{2}} - e^{-j(\beta_B - \beta_A)\frac{l}{2}}]$$

$$|E_4| = \left| 2 \sin (\beta_B - \beta_A) \frac{l}{2} \right|. \quad (52)$$

In arm 2 similarly

$$|E_2| = \left| 2 \cos (\beta_B - \beta_A) \frac{l}{2} \right|, \quad (53)$$

where  $\beta_A$  and  $\beta_B$  are the wave numbers of the corresponding modes and  $l$  is the length of the slot. The effect of slot width comes in by way of its effect on  $\beta_A - \beta_B$ .

Since  $\beta$  is dependent only on the cutoff wavelength, the behavior of such a long-slot coupler over a frequency range is given by two parameters in addition to length. Usually both cutoff wavelengths are near the cutoff wavelength for the unperturbed guide so that the only quantities necessary to specify the coupler are the length and the difference between the two cutoff wavelengths. Further analysis shows that care must be taken to ensure that the waves in the two guides have the same propagation velocity. Otherwise the running waves will get out of phase with each other, and it will not be possible to obtain maximum coupling. This is more critical for long slots than for short ones; the condition is that the difference in path lengths for the length of the slot should be negligible compared with a wavelength.

**14-9. Resistive-loop Couplers.**—It is well known that coupling loops have a tendency to couple to the electric as well as the magnetic field. This is exploited in the resistive-loop type of coupler shown in Fig. 14-50.<sup>1</sup>

Without the resistance the device could not have directive properties, since it would then be a three-terminal-pair *lossless* device, which can be rigorously represented as a pure shunt (or series) junction. This theorem is prove in Vol. 8, Chap. 9.

The relative strengths of magnetic and electric coupling can be adjusted by rotation of the loop. In addition, the value of resistance controls not only the relative magnitudes of the couplings but also their phases. This type of coupler can be inserted in either waveguide or coaxial transmission line.

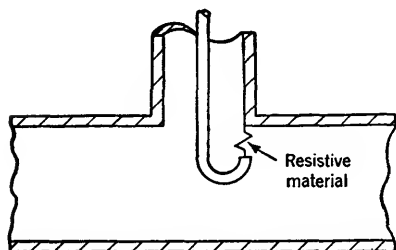


FIG. 14-50.—Resistive-loop coupler.

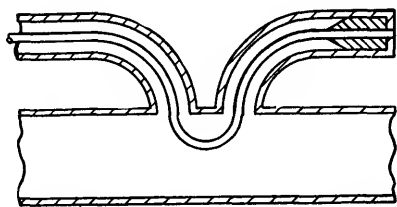


FIG. 14-51.—Resistive-loop coupler with fourth line brought out.

An unusual feature of the resistive-loop coupler is that the absorbing material is placed within the coupling region rather than in the end of a transmission line as is the case in the other couplers described. A variation which is more like the conventional design is shown in Fig. 14-51.

Little is known about the design of resistive-loop couplers. Since it is difficult to construct loops to close tolerances, it is probable that this design will find its most suitable applications at frequencies lower than 3000 Mc/sec.

**14-10. General Theoretical Considerations.**—For most purposes it is sufficient to describe a directional coupler in terms of directivity, coupling, and possibly its reflection coefficient in the main line. For some purposes, however, it may be necessary to describe the coupler more completely and exactly. It is sufficient to specify the impedance or admittance matrix of the coupler considered as a three-terminal-pair linear network containing loss. It will be more convenient to specify instead the scattering matrix, since the directional properties are more

<sup>1</sup> G. B. Myers and B. P. Charles, "The Reflectometer," Navy Report 521, Aug. 25, 1944.

evident in this form. Only the method of approach to the general problem will be indicated here.

The scattering matrix gives the relationship between the waves leaving the network and the waves entering the network. We write

$$\mathbf{b} = \mathbf{S}\mathbf{a},$$

$$\begin{pmatrix} b_1 \\ b_2 \\ b_3 \end{pmatrix} = \begin{pmatrix} S_{11} & S_{12} & S_{13} \\ S_{12} & S_{22} & S_{23} \\ S_{13} & S_{23} & S_{33} \end{pmatrix} \times \begin{pmatrix} a_1 \\ a_2 \\ a_3 \end{pmatrix}, \quad (54)$$

where the  $a$ 's are the complex voltage amplitudes of the incident waves and the  $b$ 's are the complex voltage amplitudes of the scattered waves. For a three-terminal-pair network, the scattering matrix (which is always symmetrical) has six complex parameters. The phases of the complex  $S_{ij}$  elements are functions of the positions of the arbitrarily selected reference planes.

The magnitudes of the scattering coefficients are immediately interpretable in terms of the previously defined quantities. If in Eq. (54), we call terminals 1 and 2 the terminals of the main transmission line with power going from 1 to 2 in the forward direction, and call 3 the probe terminal, then the various elements in the matrix have the following physical significance. The coefficients  $S_{11}$ ,  $S_{22}$ ,  $S_{33}$  represent reflection coefficients in the various arms, 1, 2, and 3, with the other arms matched, and in a good directional coupler they are all small. For the usual

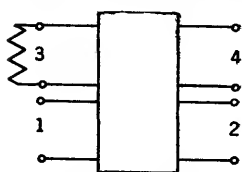


FIG. 14-52.—Four-terminal-pair representation.

symmetrical coupler construction  $S_{11} = S_{22}$ . Ordinarily, only  $S_{11}$  is specified. The coefficient  $S_{12}$  represents the transfer of power in the main line past the coupling mechanism. The value of  $|S_{12}|$  is slightly less than unity. The coefficient  $S_{13}$  represents the voltage coupled to the detector from a wave in the forward direction incident at terminal 1. It is a measure of the coupling  $C$ .

The voltage coupled in the backward direction is represented by  $S_{23}$ . If the directivity is perfect,  $S_{23} = 0$ . More exactly

$$C = -20 \log_{10} |S_{12}|,$$

$$D = 20 \log_{10} \left| \frac{S_{13}}{S_{23}} \right|. \quad (55)$$

A more fruitful method of general approach is to consider the directional coupler as a four-terminal-pair nondissipative network with an external load (see Fig. 14-52). This representation is permissible since usually the resistive material is actually placed in an external line. This does not hold for the resistive-loop type of coupler, but here the resistance may be considered a single lumped element to a good approxi-

mation and as such can always be represented in this manner. This approach is valuable since it allows use of the theorems concerning nondissipative networks. Besides, there are a few applications in which directional couplers are used without the terminating resistance and all four terminal pairs are connected to other networks or components.

In this representation an ideal directional coupler is represented by the scattering matrix

$$\begin{array}{l} \text{Main line} \\ \text{Auxiliary line} \end{array} \begin{array}{l} (1) \\ (2) \\ (3) \\ (4) \end{array} \left\{ \begin{array}{cccc} 0 & S_{12} & 0 & S_{14} \\ S_{12} & 0 & S_{23} & 0 \\ 0 & S_{23} & 0 & S_{34} \\ S_{14} & 0 & S_{34} & 0 \end{array} \right\}, \quad (56)$$

where

$$|S_{12}| = |S_{34}|, \quad \text{and} \quad |S_{23}| = |S_{14}|,$$

and

$$|S_{12}|^2 + |S_{23}|^2 = 1,$$

so that by a suitable choice of reference planes we may write the scattering matrix as

$$\left( \begin{array}{cccc} 0 & \sqrt{1-\gamma^2} & 0 & \gamma \\ \sqrt{1-\gamma^2} & 0 & \gamma & 0 \\ 0 & \gamma & 0 & \sqrt{1-\gamma^2} \\ \gamma & 0 & \sqrt{1-\gamma^2} & 0 \end{array} \right), \quad (57)$$

where  $\gamma$  is a real quantity. The ideal coupler then has these properties: it is matched in all directions; the directivity is perfect both ways; and the coupling coefficient is the same both ways. Such ideal couplers are realizable in practice only at a single frequency.

The influence of the built-in termination upon the directivity of the coupler considered as a three-terminal-pair network can be determined in the following manner. In Sec. 14-3 directivity was defined as

$$D = 10 \log_{10} \left( \frac{P_f}{P_b} \right), \quad (58)$$

where  $P_f$  is the power coupled through the guide in the preferred direction. Since the amount of power reaching the termination from a forward wave is much smaller than this, the voltage standing-wave ratio of the termination cannot appreciably affect  $P_f$ . For  $P_b$  the situation is much different. The directional element alone contributes an amount  $P_0$ , caused by a unit backward wave. At the same time the termination receives an amount of power which is approximately equal to  $P_f$  since the directional element is symmetrically constructed. The amount of power to the termination is, in the case of a backward wave, large com-

pared to  $P_0$ . Any reflection from the termination will go largely to the output terminals and will contribute to  $P_b$ , in which it may indeed be the primary factor. If  $\Gamma_t$  is the reflection coefficient of the termination, then the output voltage will be a vector sum of the voltages from these two sources or

$$P_b = |P_0^{1/2} + \Gamma_t P_f^{1/2} e^{i\phi}|^2, \quad (59)$$

where  $e^{i\phi}$  takes care of the possible phase relationship between the two waves. The extreme values of the directivity will be given by

$$\begin{aligned} D_{\text{extreme}} &= 10 \log_{10} \left( \frac{P_f}{|\sqrt{P_0} \pm \Gamma_t \sqrt{P_f}|^2} \right) \\ &= 10 \log_{10} \frac{P_f}{P_0} \left( \frac{1}{\left| 1 \pm \Gamma_t \frac{\sqrt{P_f}}{\sqrt{P_0}} \right|^2} \right) \\ &= 10 \log_{10} \frac{P_f}{P_0} - 20 \log_{10} \left| 1 \pm \Gamma_t \frac{\sqrt{P_f}}{\sqrt{P_0}} \right|. \end{aligned} \quad (60)$$

Letting  $D_0 = 10 \log_{10} (P_f/P_0)$ , we obtain

$$D = D_0 - 20 \log_{10} \left| 1 \pm \Gamma_t \left( \frac{\sqrt{P_f}}{\sqrt{P_0}} \right) \right|. \quad (61)$$

The second term may be larger than the first. The magnitude and phase of  $\Gamma_t$  may always be chosen so as to make the directivity infinite. This is not feasible in practice. It is usually more convenient to design couplers with a satisfactory value of  $D_0$  and to keep the effect of  $\Gamma_t$  small. This means in effect keeping

$$\Gamma_t \sqrt{\frac{P_f}{P_0}} \ll 1. \quad (62)$$

It is often convenient, instead of speaking of directivities, to define unbalance reflection coefficients as

$$\begin{aligned} \Gamma_D &= \sqrt{\frac{P_b}{P_f}} \\ \Gamma_0 &= \sqrt{\frac{P_0}{P_f}}. \end{aligned} \quad (63)$$

Equation (59) then becomes

$$\Gamma_D = |\Gamma_0 + \Gamma_t e^{i\phi}|. \quad (64)$$

Also

$$D = -20 \log_{10} \Gamma_D. \quad (65)$$

**14-11. Measurements of the Properties of Directional Couplers.**—The measurement of the various properties of directional couplers is not



appreciably different from other r-f attenuation and impedance measurements. Certain techniques, are, however, especially applicable. Distinction can be made between the measurement of a completed coupler including termination and adapters to particular types of fittings or line connections, and the measurement of the coupling element itself; that is, the hole, or slots, or other means of providing the directional property. Measurement of the coupling element would be, of course, primarily for purposes of research or design of new coupler types. This discussion will confine itself to the measurement of directivity, coupling, and VSWR.

Measurement of  $S_{11}$  does not need to be mentioned further. Obviously, in measuring VSWR in the main line, a termination should be used that is better than the desired accuracy of the measurement. The technique of a sliding termination described in Sec. 8-7 is useful here.

The measurement of coupling is a standard attenuation measurement. Since most couplers are designed to couple more closely than 40 db, no great difficulty should be met. Often the coupling must be measured between two different types of transmission lines which fact introduces a slight complication. Methods of making such measurements are described in detail in Chap. 13. Incidentally it should be pointed out that a directional coupler with well-matched terminations on two arms forms an excellent fixed-attenuation standard, especially for the higher attenuation ranges. Since the absorbing material appears only in the form of terminations, the device is completely stable and independent of power level, temperature, or humidity.

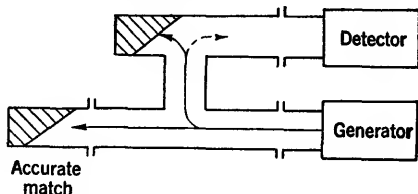


FIG. 14-53.—Measurement of directivity.

Directivity is somewhat more difficult to measure. In the first place, the attenuation is greater. If a 40-db coupler has a directivity of 30 db, to take an extreme case, the total attenuation from the main line is 70 db in the backward direction. This offers serious problems. In addition, for measuring completed couplers the termination which is connected to the far end of the main line must be very accurately matched. The effect on measured directivity is the same as that of the matched termination incorporated in the coupler. The experimental arrangement for measuring directivity is shown in Fig. 14-53.

The voltage reaching the output load from the forward wave as a result of the imperfect directivity of the coupler is

$$\sqrt{P_b} = \sqrt{\frac{P_b}{P_f}} \sqrt{P_f} = \Gamma_D \sqrt{P_f} \quad (66)$$

If the termination used in the measurement has a reflection coefficient

$\Gamma$ , then a portion of the reflected wave given approximately by  $\Gamma \sqrt{P_I}$  in voltage will reach the output terminals. The resulting wave  $\sqrt{P_b}$  will be the vector sum of the two. If we define the measured unbalance reflection coefficient

$$\Gamma_M = \sqrt{\frac{P_b}{P_I}} = \frac{1}{\sqrt{P_I}} (\Gamma_D \sqrt{P_I} + e^{i\theta} \Gamma \sqrt{P_I}), \quad (67)$$

then

$$\Gamma_M = |\Gamma_D + \Gamma e^{i\theta}|, \quad (68)$$

but this has exactly the same form as Eq. (64) describing the effect of the built-in termination on directivity. Another method of determining directivity is to use a tunable impedance to terminate the main line. This can now be tuned until no power reaches the detector. The reflection coefficient  $\Gamma$  of the variable impedance is now equal to the unbalance reflection coefficient  $\Gamma_D$  and can be measured with an ordinary slotted section. This method has the advantages of being a null method and of being independent of generator and detector impedances. It is suitable for the ordinary range of directivities. A directivity of 40 db corresponds to an unbalance voltage standing-wave ratio of 1.02, which is about as low a value of voltage standing-wave ratio as can be conveniently measured with a slotted section. Care must be taken to measure the tunable load at exactly the same frequency as was used in balancing the coupler.

**14-12. The Reflectometer.**—The application of directional couplers to the measurement of reflection coefficients of transmission-line components by measuring the magnitude of the reflected wave is an obvious one;<sup>1</sup> but the accuracy needed and the techniques used are sufficiently different from those used in measuring power transfer that a separate discussion is advisable. Directional couplers used for the measurement of reflected waves have commonly been called "reflectometers." Normally, two directional couplers are needed, one to measure the incident power, and the other the reflected power. A single directional coupler with a second detector substituted for the termination can perform both functions, but this places very stringent requirements on the match of both detectors so that it is usually more convenient to use two couplers.

The most critical requirement of a reflectometer is good directivity of the coupler used to measure reflected power. As was pointed out in Sec. 14-11 there is a relation between directivity and  $\Gamma$ . We interpret  $P_b$  as being caused by the reflected wave from the unknown impedance. Actually, however, there is a contribution from the imperfect directivity.

<sup>1</sup> R. S. Julian, "A Precision Impedance Comparator," BTL MM-44-170-18, Mar. 10, 1944.

By a method analogous to that used in the previous section we can obtain the result

$$\Gamma'_x = \Gamma_x \pm \Gamma_D e^{i\alpha}, \quad (69)$$

where  $\Gamma'_x$  is the observed reflection coefficient,  $\Gamma_x$  is the true unknown reflection coefficient, and  $\alpha$  takes care of possible phase differences between the waves. An ordinary good coupler will have a directivity of 20 db which corresponds to a VSWR of 1.22, which is an intolerable error for a laboratory VSWR measurement. One might set up the requirement that the error caused by imperfect directivity should be of the order of 1.01 in VSWR which means a directivity of 46 db. The error caused by an imperfect termination in the coupler is given by the  $\Gamma_t$  of the termination itself, so that the termination would be required to have a VSWR of less than 1.01. For many field uses, these accuracy requirements can be relaxed to more reasonable values.

The long-slot type of coupler is preferred for reflectometers because of the high directivity obtainable, although the length is a disadvantage. The techniques used in conjunction with reflectometers are similar to those described in Chap. 9 for use with magic-T impedance bridges. Rather than to rely on calibrations of detector sensitivity to determine the reflected-wave amplitude with the reflectometer, it is convenient to have some "gauge blocks" in the form of standard mismatches which can be used to check the readings.

Since directivities of reflectometers must be high, the problem of directivity measurement becomes more difficult. Here again methods for measuring "balance" described in Chap. 9 will be found effective.

## CHAPTER 15

### R-F PHASE AND PATTERN MEASUREMENTS

BY HARVEY R. WORTHINGTON

The measurement of r-f phase and intensity in free space requires experimental procedures and circuits different from those used for analogous measurements in transmission lines. In order for the measurements to provide accurate and useful information it is necessary to observe certain optical requirements. The first purpose of this chapter is to show how the ideal optical conditions may be approximated in the experimental setup and to discuss the effect of these approximations on the various measurements. The second purpose is to describe the general procedures and circuits used for r-f intensity, gain, and phase measurements. The specialized applications of these techniques to such problems as antenna design will not be discussed.<sup>1</sup>

**15-1. Terminology and Definitions.**—In this chapter it will be necessary to use some new terms and to treat antenna properties not previously defined in this book. These are described briefly below to facilitate the subsequent discussion.

*Near and Far Fields.*—These fields are, respectively, the regions of Fresnel and Fraunhofer diffraction. The two regions are distinguished by the manner in which contributions from elements of the aperture surface add together at a distant point on the normal axis of the aperture. The Fraunhofer region is characterized by the condition that such contributions to the intensity at the distant point on the axis arrive with effectively their initial phase relationships. Since the transition between regions is gradual an arbitrary limit is defined. The limit between regions is given in terms of aperture diameter and wavelength by the equation

$$R = \frac{D^2}{\lambda}.$$

*Pattern Parameters.*—The principal parameters affecting the characteristics of the radiation pattern are the dimensions of the aperture and the functions that describe the distribution of illumination and phase over the aperture. For an aperture uniformly illuminated by a plane

<sup>1</sup> Volume 12 of this series discusses microwave antenna design and contains a chapter on antenna measurements.

wave the amplitude pattern in the far field is of the form

$$g(x) = g_0 \frac{\sin x}{x},$$

where  $x$  is a function of the aperture size, wavelength, and the angle of orientation with respect to the normal axis,

$$x = \frac{\pi D \sin \theta}{\lambda}.$$

When the illumination function is "tapered," the pattern is described by a different function having similar qualitative characteristics.

*Gain.*—The gain of an antenna expresses its effectiveness in concentrating power in a given direction. It is the ratio of the peak intensity of the pattern to the intensity of an isotropic radiator emitting the same amount of power. The maximum gain for an aperture of given area is obtained by uniform illumination with a plane wave,

$$G_0 = \frac{4\pi A}{\lambda^2}.$$

In practical antennas the gain is usually lower than this.

*Efficiency* can, therefore, be expressed conveniently as a ratio of the actual gain to the gain of a uniformly illuminated aperture of the same area. This ratio is called the "gain factor"

$$f = \frac{G}{G_0}.$$

*Absorption Cross Section* is a useful term describing an effective aperture area such that the gain calculated on the basis of uniform illumination of this area is equal to the actual gain of the full aperture,

$$G = \frac{4\pi(fA)}{\lambda^2}.$$

*Scattering by an Antenna.*—When radiation is intercepted by an antenna aperture only a part is absorbed. The remainder is reradiated or scattered. The fraction so scattered cannot be stated concisely in terms of simple antenna parameters, nor is it practical to undertake an accurate calculation. Roughly speaking it will be of the order of  $(1 - f)$ , where  $f$  is again the gain factor. The pattern of such scattered radiation is not capable of even a rough evaluation for general purposes. Therefore in anticipating the effect of scattering on intensity measurements it may be advisable to assume the unlikely possibility that the scattering gain factor is as large as  $(1 - f)$ .

*Center of Phase.*—For sources emitting spherical or cylindrical waves there is a geometric center point or line from which the rays appear to emanate. This is called the center of phase. Its location within the radiating element is of particular interest when this element is to be placed at the focus of some optical system.

**15-2. Pattern Intensity Measurements.**—To determine the intensity pattern of an antenna, the relative power received by a second antenna in the field is measured at the various positions of interest. The second antenna is maintained at a fixed range and is directed toward the center of the test antenna so as to subtend a constant solid angle at all orientations. The relative power received is then directly proportional to the intensity. A polar plot of the pattern in any given plane can be obtained by rotating either antenna about the proper axis through the center of the aperture of the test antenna. For short-range measurements in the laboratory it is usually most convenient to move the r-f pickup probe in a circular path while the test antenna remains fixed at the center. In the case of large antennas where long ranges are required it is necessary to rotate the test antenna about its own center keeping the second antenna stationary. Usually the fixed antenna is used as a transmitter so that the moving element need carry only the relatively small detecting apparatus.

The range of separation required for a given pair of antennas is an important factor in determining the physical features of the apparatus as well as the requirements of power and receiver sensitivity. Therefore it will be necessary, before proceeding, to establish some relationships between the range and the antenna diameters on the basis of optical requirements.

In most intensity measurements it is the far-field pattern that is of interest. This must be measured under far-field conditions because proper correction of the near-field pattern would require more information than is obtained by a single pattern measurement. On the other hand, the long ranges required for large antennas frequently make it necessary to work at the minimum range that will yield a satisfactory approximation of the far-field pattern. A convenient rule for determining the minimum range  $R$  for a given pair of antennas is

$$R = \frac{(D_1 + D_2)^2}{\lambda}, \quad (1)$$

where  $D_1$  and  $D_2$  are the aperture diameters and  $\lambda$  is the wavelength. This rule represents an approximation suitable for most developmental antenna measurements and for pattern testing of operational antennas. The basis for the relationship and the approximations involved in it may be shown by a brief analysis of the optical problem.

Since there is no single criterion on which to base a minimum range, several reasonable requirements may be satisfied. (1) The measured gain should not be more than 5 per cent lower than that which would be obtained under true far-field conditions. With the possibility of a calculated correction this is tolerable in most cases. (2) Relative intensity values should be maintained within 5 per cent. (3) The probe antenna must subtend a small enough angle to render good resolution of the pattern. (4) Errors in phase should not exceed  $\pi/4$ , in order to approximate Fraunhofer conditions. To facilitate the discussion it will be assumed that the antennas involved are circular and that they have the characteristics of uniformly illuminated apertures.

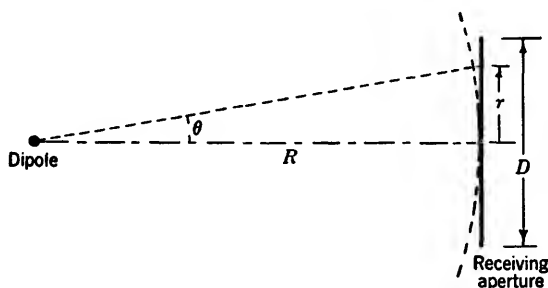


FIG. 15.1.—Dimensions for determining minimum range for pattern measurement.

A simple case in which only phase errors are significant is shown in Fig. 15.1. A small transmitter, such as a dipole, is shown illuminating the large circular aperture of a receiving antenna. The curved dashed line represents a spherical phase contour of the transmitted wave. Construction lines are also included to indicate the magnitude of the resultant phase errors in terms of the system parameters. The phase error  $\phi$  will be a function of the angle off axis,  $\theta$ ,

$$\phi = \frac{2\pi R}{\lambda} (1 - \sec \theta). \quad (2)$$

For small values of  $\theta$ ,

$$\phi \approx \frac{2\pi R}{\lambda} \left[ 1 - 1 + \frac{1}{2} \left( \frac{r}{R} \right)^2 \cdots \right] = \frac{\pi r^2}{\lambda R}. \quad (3)$$

The phase error at the edge of the aperture is

$$\phi_D = \frac{\pi D^2}{4\lambda R}. \quad (4)$$

One effect of a spherical wave front can be seen from the ratio of the power received to that expected in the absence of phase errors,

$$\frac{P_r}{P_e} = \frac{\left| \int r \cos \phi \, dr \right|^2 + \left| \int r \sin \phi \, dr \right|^2}{\left| \int r \, dr \right|^2} \quad (5)$$

$$\frac{P_r}{P_e} \approx 1 - \frac{1}{12} \left( \frac{\pi D_2^2}{4\lambda R} \right)^2. \quad (6)$$

The relationship can be interpreted more easily if the range is expressed in terms of a multiple  $n$  of the Fresnel-Fraunhofer boundary range,

$$R = n \left( \frac{D_2^2}{\lambda} \right).$$

If this value is substituted in Eq. (6),

$$\begin{aligned} \frac{P_r}{P_e} &= 1 - \frac{\pi^2}{12 \cdot 16} \left( \frac{1}{n} \right)^2 \\ &= 1 - 0.05 \left( \frac{1}{n} \right)^2, \\ \frac{P_r}{P_e} &= 0.95, \quad \text{for } n = 1. \end{aligned} \quad (7)$$

This reduction in received power is just within the arbitrary 5 per cent tolerance so that the minimum range for this case may be taken as

$$R = \frac{D^2}{\lambda}. \quad (8)$$

The corresponding phase error at the edge of the aperture is found to be

$$\phi_D = \frac{\pi D^2}{4\lambda R} = \frac{\pi}{4}, \quad (9)$$

which corresponds to a distance of  $\lambda/8$ . This degree of deviation from a plane phase front is the maximum which can safely be neglected.

The expression for the reduction in received power can be interpreted reciprocally to mean that the intensity at a point on the axis of a transmitter of aperture  $D_2$  at a range  $D_2^2/\lambda$  would be down 5 per cent as a result of phase errors caused by the varying path length between different elements of the transmitter aperture and the point on the axis.

Where antennas of comparable size are used at inadequate range, errors would be expected from nonuniform intensity of illumination as well as phase. An expression for the power reduction in such a case is given below, neglecting higher-order terms,

$$\frac{P_r}{P_e} \approx 1 - 0.05 \left( \frac{1}{\lambda R} \right)^2 (D_1^4 + 6D_1^2 D_2^2 + D_2^4), \quad (10)$$

where  $D_1$  and  $D_2$  are the aperture diameters. This is an approximate



relationship which applies only where  $P_r/P_e > 0.9$ . If the ratio  $P_r/P_e$  is set equal to 0.95, corresponding to a 5 per cent reduction in received power,

$$R^2 = \frac{1}{\lambda^2} (D_1^4 + 6D_1^2D_2^2 + D_2^4). \quad (11)$$

For the case of equal antenna diameters,

$$\begin{aligned} D_1 &= D_2 = D, \\ R^2 &= \frac{8D^4}{\lambda^2}, \\ R &= 2.83 \left( \frac{D^2}{\lambda} \right). \end{aligned} \quad (12)$$

This value for  $R$  indicates that the sum of the minimum ranges ( $D^2/\lambda$ ) for the two separate antennas is not great enough for the combination, as might have been supposed. In fact even this range is not adequate to satisfy the other requirements that were initially stated. The full angular width  $\beta_1$  of the main lobe for a uniformly illuminated aperture is  $2\lambda/D$ , whereas the angle  $\beta_2$  subtended by the probe antenna is approximately  $D/R$ . From Eq. (12)

$$\frac{\beta_1}{\beta_2} = 5.66.$$

Such a ratio of angles results in an additional reduction in peak intensity of about 3 per cent whereas side lobes are reduced about 9 per cent. Moreover, at this range a phase difference of approximately  $\pi/3$  can exist between components of the signal from different portions of the transmitter aperture because of path-length differences.

Accordingly, a longer range is necessary and the range given by Eq. (1) is a satisfactory minimum value. The limitations of this rule in two special cases are the following:

Case I. When the maximum antenna diameter for a given range is to be used, the second antenna must be very small and the expression reduces to Eq. (8),  $R = D^2/\lambda$ . This condition represents a maximum phase error of  $\pi/4$  or  $\lambda/8$  and a loss of 5 per cent in received power. The effect of the loss can be compensated to some extent by a calculated correction. The same relationship applies for noncircular apertures if  $D$  is the greatest linear dimension of the aperture. Although the errors arising from the reduction in power are less, the phase error is the same and determines the limit.

Case II. When  $D_1 = D_2 = D$  the minimum range has its greatest value for a given  $D$ ,

$$R = 4 \frac{D^2}{\lambda}.$$

This range results in a reduction of about 2.5 per cent in received power caused by near-field effects. The angle subtended by the probe antenna is about  $\frac{1}{8}$  of the full width of the main lobe. Discrepancies in phase among the various contributions from the transmitter aperture do not exceed  $\pi/4$ .

These approximations based upon uniformly illuminated circular apertures are not greatly changed when practical antennas with tapered illumination patterns are used. The reduction in received power is not so large because the contributions from the extreme edges of the aperture are less important. However, the loss is decreased only by a factor roughly equal to the gain factor. It may be repeated, also, that the expressions derived for power reduction caused by near-field effects are only approximations. They do not apply for reductions exceeding 10 per cent and do not hold where both antennas are small compared to the wavelength.

Having established the requirements upon range it is possible to determine the power and receiver-sensitivity requirements. For a pair of antennas having gains  $G_1$  and  $G_2$  the ratio of power received to power transmitted is given by the expression

$$\frac{P_r}{P_0} = \frac{G_1 G_2 \lambda^2}{(4\pi R)^2}.$$

This expression in terms of antenna area involves the gain factor  $f$  since for each antenna

$$G = \frac{4\pi f A}{\lambda^2}.$$

Therefore

$$\frac{P_r}{P_0} = \frac{(f_1 A_1)(f_2 A_2)}{\lambda^2 R^2}.$$

Again, for the purposes of illustration, assume that the antennas are of equal diameter  $D$  with an average value of  $f$  equal to  $\frac{2}{3}$  and apply Eq. (1) for the minimum range,

$$\begin{aligned} f_1 A_1 &= f_2 A_2 = \frac{\pi D^2}{6} \\ R &= \frac{4D^2}{\lambda}, \\ \frac{P_r}{P_0} &= \frac{\pi^2}{36.16} = 0.0172. \end{aligned}$$

In decibels this is

$$\left( \frac{P_r}{P_0} \right) = -17.6.$$

It is of interest to note that this expression is independent of  $D$  and  $\lambda$  under the minimum-range conditions. In practice, however, having

chosen the range for a certain measurement path on the basis of the maximum antenna diameter, it is likely that this range will be used with antennas of smaller area as well. For example, a line source with a length equal to the maximum permissible diameter, but with a width equal only to  $\frac{1}{100}$  of the length would have an area equal to  $\frac{1}{100}$  of the circular-aperture area. This would cause an additional power drop of -19 db. Since these figures apply to the peak sensitivity of the antennas, an additional 30 db would be required to render proper side-lobe detail. Thus a system for general use in testing antenna patterns should have power and receiver sensitivity enough for a 20-db drop in power plus a working range of 50 db, a total of 70 db.

The probe antennas may be of any design suited to the optical requirements. Where small apertures are desired, microwave horns are frequently used. These have the advantage that they are simple in construction and that their characteristics can be calculated without difficulty from their shape. Accurate formulas for such calculations are available. In cases where the length of the tapered section of the horn is made large with respect to the aperture dimensions, a simplified formula may be used for the gain,<sup>1</sup>

$$G = 4\pi \frac{fA}{\lambda^2},$$

where  $fA$  is the effective area of the aperture. The quantity  $f$  may be treated as a constant fraction of the actual aperture area  $A$  for long horns

$$f = \frac{8}{\pi^2}.$$

When coaxial line is used, a dipole or a coaxial probe may be employed as a small probe. A gain of about 3 db is obtained with such probes.

The characteristics of r-f power sources and detectors have been discussed elsewhere in this volume, so that it is possible to choose a suitable combination knowing the length of the transmitter-receiver path and the range of antenna gains to be used. Account must be taken of the additional power reduction which will be caused by padding attenuators. It is apparent that, in general, the sensitivity requirements are great enough to necessitate the use of a modulated source and an a-c receiver amplifier. A bolometer is indicated as the detecting element best suited for general application because of its linear behavior over a wide range of power levels. The response of a bolometer to pulsed power makes the use of an a-c amplifier simpler, whereas a crystal is easily saturated and great care must be taken. Superheterodyne receivers with calibrated attenuators in the r-f circuit are also suitable for these measurements.

<sup>1</sup> S. A. Schelkunoff, *Electromagnetic Waves*, McGraw-Hill, New York, 1943, p. 365.

The mechanical details of antenna mounts for pattern measurements will not be discussed here since this is a special problem depending upon the particular type of measurements to be made. Information about mounts as well as automatic pattern-recording equipment is presented in Vol. 12 dealing with antenna design. The problem of siting an antenna-measurement course is also treated.

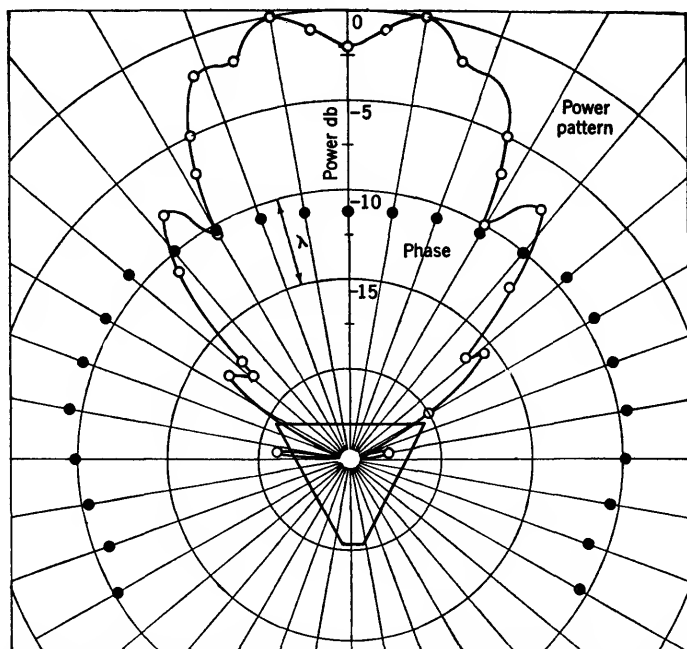


FIG. 15-2.—Radiation pattern of *E*-plane horn showing power pattern, phase front, and center of phase.

The general problem of interference from surrounding objects is met in practice by removing such objects as far as possible and by avoiding illumination of them. The use of poorly reflecting materials in the vicinity of antennas is necessary in some cases and this is best determined by experiment. The need for care in this matter is readily seen. When a receiving antenna is rotated during a pattern measurement, the main lobe may at times be pointed directly at some reflecting object. If the power received is from a  $-20$ -db side lobe of the transmitter and is reduced by another 20 db by scattering from the obstacle, it could still produce a serious effect on the measurements, because the directly received power would also be small. If a  $-20$ -db side lobe of the receiver were being measured under these conditions the ratio of amplitudes of the direct signal and the scattered signal would be 10.

This would produce a power variation of from  $(1.0 + 0.1)^2$  to  $(1.0 - 0.1)^2$  or  $\pm 20$  per cent. It is apparent, therefore, that particular care must be taken to avoid reflecting obstacles in the plane of rotation of the main lobe.

An example of a pattern measurement is shown in Fig. 15-2. The observations refer to a horn flared in the E-plane with aperture dimensions of 2.49 by 16.42 cm. The horn had a half angle of  $30^\circ$  and was used with waveguide  $1\frac{1}{2}$  by 3 inches OD. The observations were made at a wavelength of 10 cm. The pattern is plotted in decibels down from the power at  $0^\circ$ . The oscillations in the pattern arise from the fact that the phase is not uniform over the mouth of the horn. The phase pattern is also shown on the figure, and the center of phase is indicated by the shape of the horn sketched in. The manner of observing the phase is described in Sec. 15-8.

**15-3. The Measurement of Antenna Gain.**—The gain of an antenna is a quantity of great practical interest. It is determined by methods

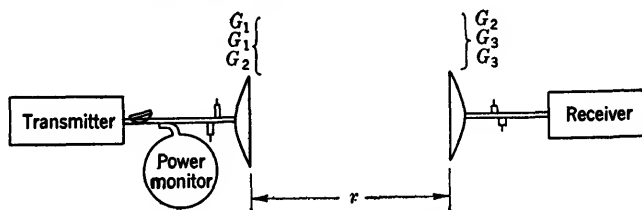


FIG. 15-3.—Measurement of gain by the three-antenna method.

which are essentially applications of power-measuring techniques, but these methods are sufficiently specialized as to merit some discussion. In practice, gain is usually measured with reference to a standard horn or to a parabolic antenna. A simple measurement of the ratio of the power received by the experimental antenna to that received by the standard gives the ratio of their respective gains. It is in the calibration of such gain standards and the measurement of other special antennas that the following techniques are employed.

The gain of an antenna may be measured by determining the fraction of power it receives from a transmitter at a known distance, provided the gain of the transmitting antenna is taken into account. In effect this is done by substituting a third antenna for each of the original pair in turn. Repetition of the experiment for each combination yields three expressions from which the three unknown gains can be evaluated.

The experimental setup is illustrated in Fig. 15-3. The transmitter consists of a stable c-w source, square-wave-modulated at an audio frequency. This source is loosely coupled to the line through a padding attenuator. In the waveguide line is a coupling for a power monitor and

for a matching device, if one is needed to match the particular antenna in use. Behind the receiving antenna is another matching device and the receiver consisting of a bolometer and an a-f amplifier. Three combinations of horns are represented according to their gains:  $G_1 - G_2$ ,  $G_1 - G_3$ , and  $G_2 - G_3$ . Conditions governing the range of separation  $r$  have already been discussed.

The measurements of transmitted and received power are most conveniently made with the same bolometer. The transmitter power may be measured by attaching the bolometer to the transmitter line in place of the antenna. Sufficient padding attenuation must be used to prevent reaction on the oscillator because of the change of load.

In examining the optics of the system it will be convenient to refer to an effective absorbing cross section  $A'$  of the antenna, which is the area of a uniformly illuminated aperture having the same gain. Thus

$$G = \frac{4\pi A'}{\lambda^2}. \quad (13)$$

If the transmitted power is  $P_0$ , the power received with the first combination of horns is  $P_{12}$ ,

$$P_{12} = P_0 G_1 \left( \frac{A'_2}{4\pi r^2} \right). \quad (14)$$

But

$$A'_2 = \frac{G_2 \lambda^2}{4\pi},$$

and hence

$$P_{12} = P_0 G_1 G_2 \left( \frac{\lambda}{4\pi r} \right)^2. \quad (15)$$

Accordingly, for the three combinations,

$$\left. \begin{aligned} G_1 G_2 &= \left( \frac{4\pi r}{\lambda} \right)^2 \frac{P_{12}}{P_0} \\ G_1 G_3 &= \left( \frac{4\pi r}{\lambda} \right)^2 \frac{P_{13}}{P_0} \\ G_2 G_3 &= \left( \frac{4\pi r}{\lambda} \right)^2 \frac{P_{23}}{P_0} \end{aligned} \right\}. \quad (16)$$

From these equations the value of gain for each antenna can be found, as for example,

$$G_1 = \frac{4\pi r}{\lambda} \sqrt{\frac{P_{12} P_{13}}{P_{23} P_0}}. \quad (17)$$

It has been assumed above that the value of  $P_0$  was the same throughout the experiment.

For some purposes adequate results can be obtained by a simplified form of the three-antenna method. If two horns or parabolic antennas of identical mechanical construction are used, it may be assumed that their gains are equal,

$$G_1 = G_2 = G.$$

In this case the expression for received power is given by the expression

$$P_r = P_0 \left( \frac{G\lambda}{4\pi r} \right)^2,$$

whence,

$$G = \left( \frac{4\pi r}{\lambda} \right) \sqrt{\frac{P_r}{P_0}}.$$

If the two antennas are checked for equal gain by the use of a third transmitting antenna, the experiment becomes practically the same as the three-antenna method.

**15-4. Effect of Antenna Scattering in Gain Measurements.**—Thus far the effect of antenna scattering has not been considered. The amount of scattered power reaching the receiver in the above experiments is, in fact, almost negligible at a reasonable distance of separation. This might be expected since the radiation involved has been scattered twice, transversing the course  $r$  three times before reaching the receiver. An approximate evaluation of the effect is easily made.

To aid in the analysis it will be convenient to assign to the antenna an effective scattering cross section  $A''$ . This area is a fraction of the total area  $A$  corresponding to that fraction of the intercepted power that is scattered. Considering that the gain factor of an average antenna is approximately  $\frac{2}{3}$ , or  $A'/A = G/G_0 = \frac{2}{3}$ , it is reasonable to assume

$$A'' = \frac{A'}{2}.$$

This value has been experimentally corroborated by measurements using the mirror method to be described in the next section. With this scattered radiation, a certain pattern and a certain gain must be associated. No definite relationship between receiving gain and scattering gain can be stated, but for purposes of illustration a value of

$$G'' = \frac{G}{2}$$

will be assumed. Accordingly, the power initially scattered is

$$P_s = P_0 G \frac{A''}{4\pi r^2}.$$

Some of this radiation reaches the transmitter to be scattered a second time.

$$P'_s = P_s G'' \frac{A''}{4\pi r^2}.$$

Finally a portion of the power reaches the receiver,

$$P''_s = P'_s G'' \frac{A'}{4\pi r^2}.$$

The ratio of scattered power received to direct power received may be expressed in terms of  $G$ ,

$$P''_s = P_0 G \left( \frac{A''}{4\pi r^2} \right) G'' \left( \frac{A''}{4\pi r^2} \right) G'' \left( \frac{A'}{4\pi r^2} \right),$$

$$P''_s = P_0 \left( \frac{G'' \lambda}{4\pi r} \right)^4 \left( \frac{G \lambda}{4\pi r} \right)^2,$$

$$P''_s = \frac{1}{16} P_0 \left( \frac{G \lambda}{4\pi r} \right)^6.$$

But

$$P_r = P_0 \left( \frac{G \lambda}{4\pi r} \right)^2;$$

therefore,

$$P''_s = \frac{1}{16} \frac{P_r^3}{P_0^2},$$

or

$$\frac{P''_s}{P_r} = \left( \frac{1}{4} \frac{P_r}{P_0} \right)^2.$$

To reduce this expression to definite terms another condition may be assumed. If a fixed relationship between the antenna diameter  $D$  and the separation  $r$  be maintained, it can be seen that the above ratio depends principally upon this relationship for a given type of antenna. For example let us try

$$r = \frac{nD^2}{\lambda}.$$

The received power is

$$P_r = P_0 G \frac{A'}{4\pi r^2},$$

or

$$\frac{P_r}{P_0} = \left( \frac{A'}{\lambda r} \right)^2.$$

Since

$$A' = \frac{2}{3} A = \frac{2}{3} \left( \frac{\pi D^2}{4} \right),$$

$$\frac{P_r}{P_0} = \left( \frac{\pi D^2}{6 \lambda r} \right)^2 = \left( \frac{\pi}{6n} \right)^2,$$



and

$$\frac{P'_s}{P_r} = \left( \frac{1}{4} \frac{P_r}{P_0} \right)^2 = \left( \frac{\pi}{12n} \right)^4.$$

In terms of the corresponding signal amplitudes,

$$\frac{E''_s}{E_r} = \left( \frac{\pi}{12n} \right)^2.$$

For  $n = 4$ ,

$$\frac{E''_s}{E_r} = 0.004.$$

This corresponds to a negligible error of  $\pm 0.04$  db in the gain determination. With some antenna designs, however, the scattering may be appreciable. Moreover this error can be eliminated if necessary by measuring the maximum value of power, as  $r$  is varied. Since scattered power travels a distance  $2r$  farther than the directly received power, the in-phase and out-of-phase conditions of  $E''_s$  and  $E_r$  will occur at quarter-wavelength intervals of  $r$ .

**15-5. The Mirror Method of Gain Determination.**—A technique for gain determination involving more convenient measurements is the mirror method.<sup>1</sup> By reflecting the transmitted power from a large, plane mirror it is possible to use a single antenna as transmitter and receiver. The ratio of transmitted to received power can then be determined by means of standing-wave measurements in the waveguide. The antenna and its image in the mirror form a system analogous to that in the two-antenna method.

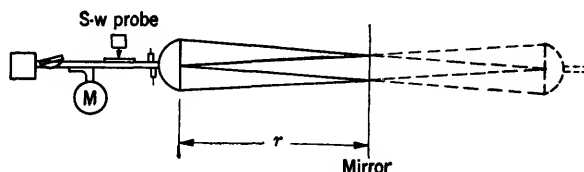


FIG. 15-4.—Mirror method for gain determination.

Figure 15-4 illustrates the apparatus required. The oscillator may provide either straight c-w power or square-wave-modulated power depending upon the power level available. A padding attenuator providing considerable decoupling (15 db) is used to prevent reaction of the reflected wave upon the oscillator. Included in the line also are a coupling for a wavemeter, a standing-wave probe, and a matching device for the antenna. The mirror is a first-surface reflector, flat in terms of the wavelength involved and placed normal to the axis of the disk or

<sup>1</sup> E. M. Purcell, "A Method for Measuring the Absolute Gain of Microwave Antennas," RL Report 168, No. Jan. 3, 1943.

horn. The size of the mirror should be sufficient to subtend an angle at the antenna which will include all side lobes of appreciable magnitude. Ideally the mirror need only include the main lobe, but to avoid appreciable currents at the boundary of the surface and to permit diversified use of the system it is preferable to have a mirror about ten times the antenna diameter. The requirement of flatness is of importance only in the region of the main lobe. The use of separations beyond the minimum value is limited by the sensitivity of standing-wave measurements.

The expression for power received by direct reflection is of familiar form,

$$P_1 = P_0 G \frac{A'}{4\pi(2r)^2},$$

$$P_1 = P_0 \left( \frac{G\lambda}{8\pi r} \right)^2.$$

If it is assumed again that

$$A' = \frac{2}{3} A = \frac{2}{3} \frac{\pi D^2}{4}$$

and

$$r = \frac{nD^2}{\lambda},$$

the power ratio may be written

$$\frac{P_1}{P_0} = \left( \frac{\pi}{12n} \right)^2.$$

For  $n = 2$ ,

$$\frac{P_1}{P_0} = \left( \frac{\pi}{24} \right)^2.$$

The corresponding amplitude ratio is

$$\frac{E_1}{E_0} = \left( \frac{\pi}{24} \right) = 0.13.$$

The voltage standing-wave ratio is

$$\frac{E_0 + E_1}{E_0 - E_1} = 1.3,$$

which is easily measured accurately.

Scattered power in this experiment is much more serious than in the previous ones. In this case the scattering takes place only once, returning to the mirror and back again into the receiver. With the same assumptions as before, this effect may be examined. The power scattered after the first reflection is given by the expression

$$P_2 = P_0 G \frac{A''}{4\pi(2r)^2}.$$

The portion of this radiation reaching the receiver is

$$\begin{aligned} P_3 &= P_2 G'' \frac{A'}{4\pi(2r)^2} \\ &= \frac{1}{4} G P_1 \frac{A'}{4\pi(2r)^2} \\ &= \frac{1}{4} \frac{P_1^2}{P_0} \end{aligned}$$

Thus

$$\begin{aligned} \frac{P_3}{P_1} &= \frac{1}{4} \frac{P_1}{P_0}, \\ \frac{E_3}{E_1} &= \frac{1}{2} \frac{E_1}{E_0} = \frac{\pi}{24n} \end{aligned}$$

or, if  $r = 2D^2/\lambda$ ,

$$\frac{E_3}{E_1} = 0.065.$$

Since this amount of scattered radiation is not negligible, it is necessary to eliminate its effect by suitable experimental procedure. It is desirable to match the antenna into space as well as possible.

Since the path traversed by  $E_3$  is greater than that traversed by  $E_1$  by a distance of  $2r$ , it is possible to change the relative phase of the two signals by varying  $r$ . Therefore a position is sought which produces an in-phase relationship between  $E_1$  and  $E_3$ , corresponding to a maximum VSWR.

$$R_1 = \frac{1 + E_1 + E_3}{1 - E_1 - E_3},$$

where the transmitter amplitude is taken as unity. A change of  $\lambda/4$  in the length of  $r$  will give an out-of-phase condition of  $E_1$  and  $E_3$  and a minimum VSWR,

$$R_2 = \frac{1 + E_1 - E_3}{1 - E_1 + E_3}.$$

The value of  $E_1$  can then be found in terms of  $R_1$  and  $R_2$ ,

$$E_1 = \frac{1}{2} \left( \frac{R_1 - 1}{R_1 + 1} \right) + \frac{1}{2} \left( \frac{R_2 - 1}{R_2 + 1} \right).$$

But

$$G = \frac{8\pi r}{\lambda} E_1,$$

therefore

$$G = \frac{4\pi r}{\lambda} \left( \frac{R_1 - 1}{R_1 + 1} + \frac{R_2 - 1}{R_2 + 1} \right).$$

This is the expression for the gain in terms of measured quantities under the condition that antenna mismatch is negligibly small. If for any reason the mismatch is not tuned out to a sufficient degree, it will be

necessary to make use of the information given by the minimum positions of each of the above standing-wave ratios,  $R_1$  and  $R_2$ , to eliminate the mismatch amplitude from the calculations.

**15-6. Gain Determination by Pattern Integration.**—For practical purposes the definition of gain is somewhat loosely interpreted. Optically it is the ratio of the peak intensity of the pattern to the average or isotropic intensity of all the power radiated. In an actual antenna it is usually taken as the ratio of the peak intensity to the intensity that would exist if all power incident in the transmission line to the antenna were isotropically distributed. This effective gain is the quantity of practical interest in calculations of system performance and is the quantity determined in any method of direct measurement.

To determine the gain in the optical sense it is necessary to resort to integration of the radiation pattern. The accuracy of integration methods is not particularly high because of the inadequacy of detailed information concerning the pattern and the inaccuracy of techniques for graphical integration. For a rectangular aperture illuminated by a line source, reasonably good results can be obtained from only two patterns, one in the E-plane and the other in the H-plane, through the peak of the main lobe. This requires that it be possible to express the complete pattern as a product of two independent functions involving the two spherical angular coordinates.

$$I(\theta, \phi) = g(\theta) \cdot f(\phi).$$

For each plane the unidimensional gain of the pattern can be determined

$$\left[ G_\theta = \frac{I_{\max} \int_{-\pi}^{\pi} d\theta}{\int_{-\pi}^{\pi} g(\theta) f(\phi) d\theta} \right]_{\phi=0},$$

or

$$G_\theta = \frac{2\pi I_{\max}}{f(\phi = 0) \int_{-\pi}^{\pi} g(\theta) d\theta},$$

and

$$G_\phi = \frac{2\pi I_{\max}}{g\left(\theta = \frac{\pi}{2}\right) \int_{-\pi}^{\pi} f(\phi) d\phi}.$$

The value of the integrals may be obtained by graphical integration of the pattern plotted in rectangular coordinates as intensity vs. angle. The combination of these values to give the two-dimensional gain requires that the pattern be narrow in one plane so that all the power is concentrated within an angular range such that

$$\sin \theta \approx 1.$$

In this case the gain becomes

$$G_{\theta,\phi} = \frac{G_{\theta}G_{\phi}}{\pi}.$$

The usefulness of a gain value of this kind is limited. It is of some interest in studies of the optical characteristics of various types of aperture illumination. It also affords a means of evaluating losses in the antenna system caused by dissipation and leakage. The ratio of the measured gain to the integrated gain would ideally show the degree of attenuation of power.

**15-7. R-f Phase Measurements.**—The measurement of phase in microwave radiation fields is of principal importance in the development of microwave antenna components. Since certain phase conditions must be maintained for efficient performance, it is desirable in many cases to determine directly that the various elements of an antenna system have the proper characteristics. The measurements are, therefore, chiefly concerned with the determination of contours of constant phase, the location of centers of phase, and the examination of effects due to objects in the field.

In the several methods to be discussed the basic principle is the same. A sample of radiation picked up in the antenna field is compared in phase with a reference signal which comes directly from the source. Some means is provided for varying the phase of one signal with respect to the other so as to produce a recognizable interference condition between them, such as a minimum or maximum. The various types of apparatus differ in the means employed for this purpose, in their applicability to particular problems, and in ease of operation. A simple, versatile form of phase apparatus is one in which the pickup probe is connected by means of a coaxial cable to a mixer wherein the reference signal from the source is also present. The flexible cable permits the probe to be moved freely about in the antenna field, and allows the tracing of contours and the adjustment of the relative phase of the two signals to the reference condition.

Such an apparatus is shown in Fig. 15-5. Power from a square-wave-modulated oscillator is introduced into a waveguide section and radiated from the experimental antenna, shown as a horn. A sample of this radiation picked up by the probe is led back by cable to the mixer guide. In this same guide is a signal which is tapped off by a directional coupler from the transmitter line. The two signals interfere at the crystal detector terminating the section. The crystal output signal is amplified and indicated on a meter. By moving the probe back and forth along the line of propagation it is possible to find the position of an interference minimum.

The pickup probe is represented as a dipole terminating the coaxial line. It is supported by a mount attached well back from the dipole and made of a poorly reflecting material. To the base of the mount a marker may be attached directly below the dipole to permit direct plotting of the minimum position. A series of such points made by following a chosen minimum will give a detailed plot of the constant-phase contour. The location of the center of phase with respect to the horn aperture can then be found from the plot. The dipole is mounted so as to permit orientation about the longitudinal axis according to the polarization employed.

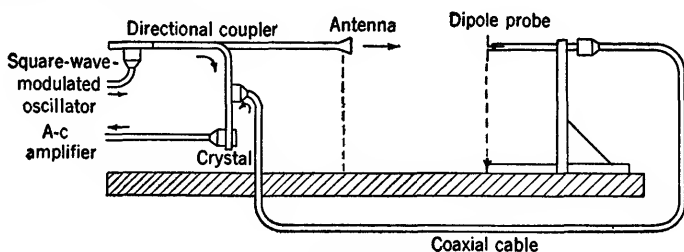


FIG. 15-5.—Simple phase apparatus.

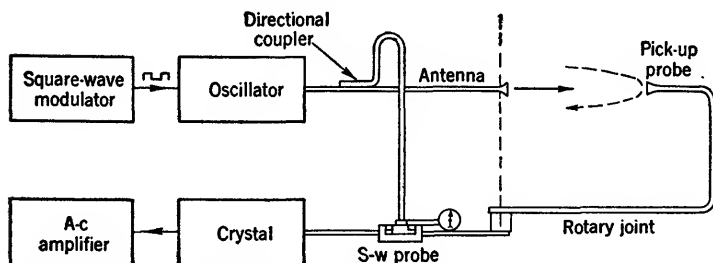


FIG. 15-6.—Phase apparatus in a waveguide system for circular phase contours.

**15-8. Phase Apparatus for Point Sources.**—If waveguide is used instead of coaxial cable, a different system is preferred in which it is not necessary to move the pickup itself in order to establish the reference condition of interference between the two signals. Instead, provision is made for adjusting the phase of the reference signal. This is conveniently done by using a standing-wave probe to introduce the reference signal into the mixer line. An arrangement of this type for studying circular phase contours is shown in Fig. 15-6. The pickup probe in this case is a small waveguide horn attached to a rotary joint so that it can be moved freely in a circular path. It is centered so that the experimental horn is approximately on the axis of rotation and the circular path corresponds fairly well with the circular contours to be studied.

In this apparatus the source is shown as a c-w oscillator modulated

by a square wave of audio frequency. Sufficient padding attenuation is used to eliminate the need for careful matching of experimental antennas. The reference signal is tapped off by means of a directional coupler with good directivity in order to prevent reflections from the antenna line from entering the reference line to disturb the phase and amplitude of that signal. A loop of waveguide leads from the coupler to the sliding probe. Its length and design are chosen to permit uninhibited movement of the probe through a distance of  $\lambda_g$ , or greater. With the sliding probe the reference signal is introduced into the mixer line. The coupling is nondirective with the ordinary probe and power is sent toward the field probe as well as toward the mixer. Consequently, it is necessary that the pickup probe and the rotary joint be well matched. The mixer itself may be either a crystal or bolometer connected to an a-c amplifier.

The matching required in the mixer line is not difficult to achieve and can be readily checked in the following way. With only the reference signal present in the mixer line, any reflected power from the pickup probe or rotary joint will produce an interference with the portion of the signal reaching the mixer directly. The interference will pass through a cycle with a displacement of the sliding probe equal to  $\frac{1}{2}\lambda_g$ . To avoid such mismatches, a properly designed horn and rotary joint should be used or a tuner should be incorporated in the line. The rotary joint in addition to being well matched should have a phase length that is independent of rotational angle. A well-designed joint employing a circularly symmetrical mode affords this characteristic.

In operation, the procedure with this apparatus is to measure the deviations of the minimum from the fixed circle described by the probe. At the initial point the position of the sliding probe is indicated on a scale or dial indicator. Variations in the phase  $\phi$  of the probe signal are compensated by a measured displacement  $S$  of the sliding probe. In terms of the shift the phase change is

$$\Delta\phi = \frac{2\pi}{\lambda_g} \Delta S.$$

The results of these measurements may be plotted to give a constant-phase contour for the antenna. An example of such measurements is illustrated in Fig. 15-2 of Sec. 15-2.

**15-9. Frequency Sensitivity of Phase.**—Frequency sensitivity affecting phase is a problem to be dealt with in all two-channel systems of this type. It is desirable that the change in phase with frequency be identical in the two paths between their common points regardless of the variety of conductors making up the circuit. Usually the reference path will be corrected to suit the length of the probe signal path. The wavelength

in the air-gap is  $\lambda_0$ ; the wavelength in the coaxial cable is  $\lambda_0/\sqrt{k_e}$ , where  $k_e$  is the relative dielectric constant of the cable. Thus if the two lines have lengths of waveguide, coaxial cable, and air gap corresponding to  $l_g$ ,  $l_c$ , and  $l_0$  and  $l'_g$ ,  $l'_c$ ,  $l'_0$ , respectively, it is desired to choose the value of  $l_g$  to satisfy the condition of equal phase shift with a change in frequency. The required length is given by the expression

$$l_g = l'_g + \frac{\lambda_0}{\lambda_g} (l'_c \sqrt{k_e} + l'_0 - l_c \sqrt{k_e} - l_0)$$

where  $\lambda_0$  and  $\lambda_g$  are respectively the free-space wavelength and guide wavelength for the design frequency.

The compensating length of waveguide may conveniently be used as the flexible loop leading to the sliding probe. The accuracy of the correction can, of course, be checked directly by changing the frequency and noting whether a corresponding shift in the minimum position occurs.

**15-10. Phase Apparatus for Line Sources.**—The type of phase apparatus used for line sources may be the same in principle as that used for point sources. When waveguide is used, it is merely necessary to provide an additional rotary joint to permit straight-line motion of the probe. Two rotary joints suffice if the field probe is of a coaxial type with circular

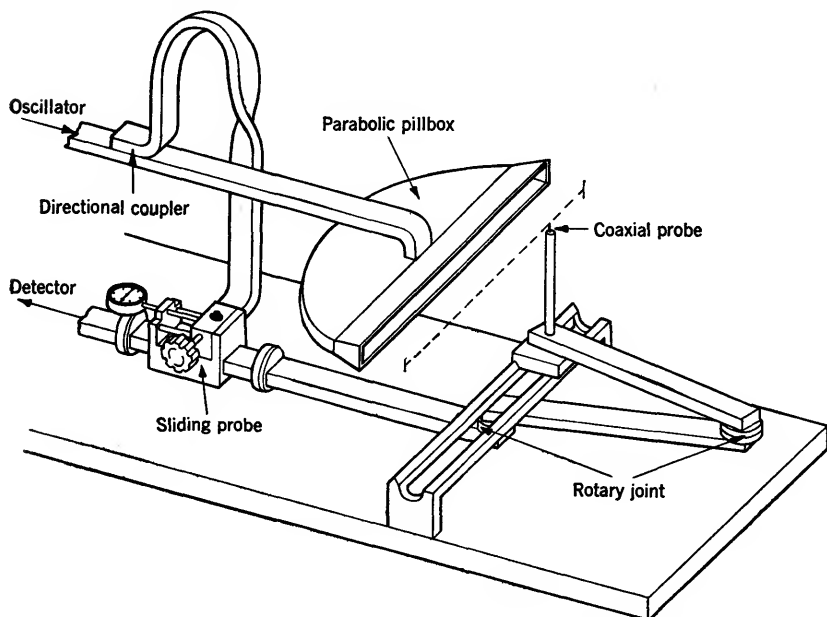


FIG. 15-7.—Phase apparatus suitable for linear phase contours.



phase symmetry. If a waveguide horn is used as a probe, a third rotary joint is required to permit orientation of the probe with respect to the wavefront.

An arrangement of components for use with the coaxial probe is shown in Fig. 15-7. The antenna is shown as a parabolic pillbox which is used as a line source for a reflector. The probe is located a short distance from the mouth of the pillbox and is articulated so as to move in a straight line parallel with it. To facilitate manipulation of the apparatus the probe is mounted on a track such as an optical bench. The track itself is well below the plane of the pillbox to minimize the disturbance of the field. The phase-measuring part of the system is identical with the previous model and is subject to the same conditions.

The plotting of wavefronts is also done in a similar manner, except that the variations in phase are measured with respect to the straight line. It should be remarked that for a center-fed parabola the phase contours will not be straight lines. The diffraction pattern due to the presence of the antenna feed, the superimposed pattern of the back wave from the feed and the fact that the probe is in the near field of the parabola combine to cause a wavy contour. The irregularities may be of the order of  $\pm \frac{1}{8}\lambda$  and are largest at the center. With other types of line sources more nearly linear phase fronts would be observed.

**15-11. Phase-modulation Method.**—By employing phase modulation<sup>1</sup> of the reference signal it is possible to provide direct indication of phase on an oscilloscope. Either the position of a sinusoidal trace on the screen or the shape of a Lissajous figure serves to show instantaneously the phase of the field-probe signal at any point in the field. To determine the existence of a geometrically regular contour of constant phase it is simply necessary to traverse the desired curve with the probe. Deviations of the phase front from this line are indicated at once by a shift in the oscilloscope figure and without the need of detailed measurements. The centering of the antenna may readily be adjusted until the phase contour corresponds with the probe path.

In this method continuous phase modulation of the reference signal replaces the manual phase shift employed in the previous methods described. Instead of being adjusted to give an interference minimum or maximum, the phase is swept through the full cycle of interference, producing a sinusoidal interference signal of audio frequency. The position at which the minimum occurs within the modulation cycle indicates the relative phases of the two signals.

Linear modulation of phase at a suitable frequency for a-c amplification is the essential requirement of this method and it may be produced

<sup>1</sup> H. R. Worthington, "Measurements of Phase in Microwave Antenna Fields by Phase Modulation Methods," RL Report, No. 966, Mar. 14, 1946.

by many different means. The means thus far used has been the one requiring no special components. It involves frequency modulation in conjunction with a very long waveguide line in the reference-signal channel. A small change of frequency with a correspondingly small change in  $\lambda_g$  becomes sufficient to produce a full cycle of phase change when one line is many hundreds of wavelengths longer than the other.

To illustrate the principle, the simplest form of this apparatus is shown in bare outline in Fig. 15-8. Practical features such as rotary

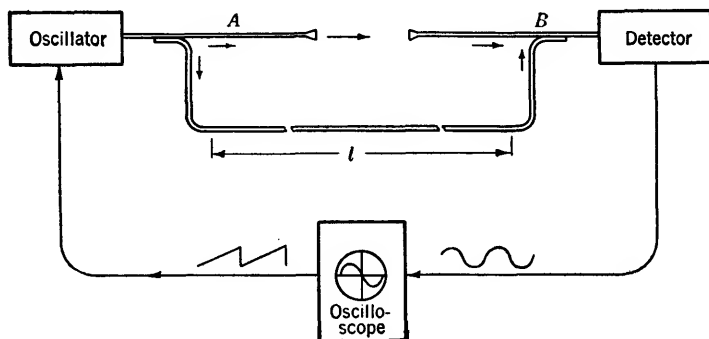


FIG. 15-8.—Phase-modulation system for phase determination.

joints have been omitted. The oscillator tube on the left is modulated by a sawtooth voltage from the oscilloscope sweep. The output power is frequency-modulated but of effectively constant amplitude. The power is divided into two channels at point A. One of these paths contains the antenna and pickup probe, the other the long waveguide line. The two channels rejoin at point B delivering both signals to the mixer. From the mixer an a-c voltage is obtained which is amplified and applied to the vertical plates of the cathode-ray tube.

The relative phase shift of the two signals is determined by the difference in length of the two paths. In previous systems the requirements for zero relative phase shift with frequency have been discussed. By taking the derivative of the phase change through the long line with respect to frequency a relationship is obtained for the change in phase for a given fractional change in frequency,

$$\Delta\phi = 2\pi l \left( \frac{\lambda_g}{\lambda_0^2} \right) \frac{\Delta f}{f},$$

where  $\lambda_g$  and  $\lambda_0$  are the guide wavelength and free-space wavelength of the nominal frequency. The ratio is treated as a constant for standard guide within a particular frequency band.

Thus for a phase shift of  $2\pi$  and a frequency change of 0.1 per cent

at 1.25 cm, the required length becomes

$$l = 1000 \left( \frac{\lambda_0}{\lambda_g} \right)^2 \lambda_g,$$

$$= 660 \lambda_g.$$

This is a considerable length but at 1.25 cm it is practical. The range of frequency modulation is easily obtained without causing appreciable amplitude modulation of the signal. It is important to avoid amplitude modulation since all alternating current at the crystal should be caused by interference only.

With an effectively continuous phase modulation taking place, the two signals arriving at the detector vary constantly and linearly in relative phase. The resultant power level is of the form

$$p = e_s^2 + e_r^2 + 2e_s e_r \cos \phi,$$

where  $e_s$  and  $e_r$  are the probe-signal and reference-signal amplitudes, respectively. Thus with a square-law detector the a-c component of output voltage is sinusoidal,

$$v \approx \cos \phi.$$

The phase angle is a function of the initial phase at the start of the modulation cycle and of  $\Delta\phi$  as previously defined,

$$\begin{aligned}\phi &= \phi_0 + \Delta\phi \\ &= \phi_0 + 2\pi f t.\end{aligned}$$

The choice of the modulation frequency  $f$  is governed by the requirements of sawtooth modulation and a-c amplification.

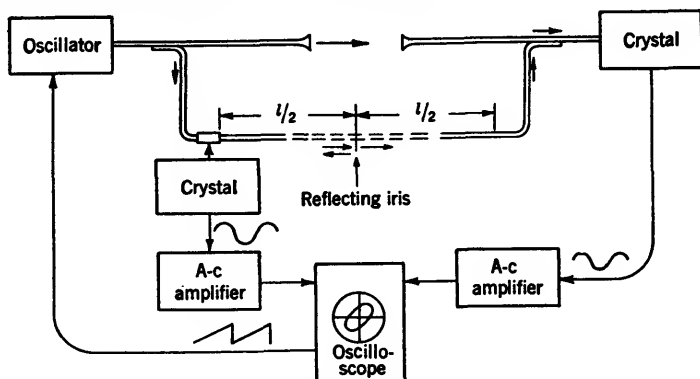


Fig. 15-9.—Phase-modulation system with frequency-drift compensation.

It will be noted that the system as it stands is sensitive to frequency drift. This can be taken into account in the measuring procedure by monitoring with a wavemeter. If the power passing through a high- $Q$

transmission wavemeter is applied to the vertical CRT plates through a second pair of input terminals to the amplifier, a sharp pip is obtained which can be used as a reference point on the sweep. The position of the phase signal with respect to this pip does not depend upon frequency.

A refinement of the above system can be made whereby inherent insensitivity to frequency is obtained and a Lissajous figure is provided as a very sensitive indicator of the "in-phase" condition for the two signals. Figure 15-9 shows the modifications involved. A standing-wave probe is inserted at the beginning of the long line and a diaphragm producing a partial reflection of power is introduced half-way down the line, a distance of  $l/2$  beyond the probe. This arrangement gives rise to two signals at the probe which have the same path difference as the original interfering signals. Their frequency behavior will be identical with that of the other pair so that an a-c reference signal is obtained. The relative phase of the two signals is independent of frequency and varies directly as the phase of the r-f field signal. By moving the standing-wave probe it is possible to compensate for a shift in the field-signal phase quickly and accurately. The phase shift so compensated is measured in terms of the probe displacement.

$$\Delta\phi_0 = \frac{\pi\Delta s}{\lambda_g},$$

where  $\Delta s$  is the probe displacement.

This type of oscilloscope figure does not indicate directly the magnitude of phase shift as does the sine-wave figure, but it is extremely sensitive when a straight line is used for the reference condition. Accuracy of about  $\pm 1.5^\circ$  is provided in the measurement of phase over several cycles. Small deviations can be measured even more accurately. The sensitive, instantaneous indication is particularly useful in examining the effects of objects placed in the antenna field, for example, in locating flanges or baffles to take care of the back lobe from a feed horn.

For greater convenience in operation and electrical alignment of the apparatus itself a mechanical phase-modulating device can profitably be used to replace the frequency modulation and long-line system. At microwave frequencies lower than 24,000 Mc/sec this is particularly true.

## APPENDIX A

### MANUFACTURERS OF MICROWAVE EQUIPMENT

The sources of supply of most of the microwave equipment that was developed and used during the war are not well known to the public at large; nearly all of the equipment was made under military security regulations. In an effort to facilitate the procurement of measuring equipment the following list of manufacturers is presented. No attempt has been made to make the listing complete, and the omission of a company or item is not intended to imply anything concerning the nature of the product. The listing comprises some of the companies who supplied microwave equipment to the Radiation Laboratory during the war. It is not known whether this equipment will be manufactured or can be obtained from these sources in the future. The numbers in the right-hand column refer to the manufacturers' names listed on pages 925, 926, and 927.

<i>1. R-f Cables and Connectors</i>		Manufacturer
RG-5/U	Nonlossy, small-diameter cable	18 to 24
RG-9/U	Nonlossy, large-diameter cable	18 to 22, 24
RG-21/U	Lossy cable	18 to 20, 24
UG-18/U	Type N plug for RG-5/U and RG-21/U	34 to 38
UG-19/U	Type N jack for RG-5/U and RG-21/U	34 to 38
UG-24/U	Type N plug for RG-9/U	34 to 38
UG-25/U	Type N jack for RG-9/U	34 to 38
 <i>2. Waveguide and Rigid Coaxial Line and Connectors</i>		
RG-44/U	10-cm-band stub-supported $\frac{1}{8}$ " OD coaxial line	36
RG-48/U	$1\frac{1}{2}$ - by 3- by 0.080-in. 10-cm-band waveguide	31 to 33
RG-52/U	$\frac{3}{4}$ - by 1- by 0.050-in. 3-cm-band waveguide	31 to 33
RG-53/U	$\frac{1}{2}$ - by $\frac{1}{4}$ - by 0.040-in. 1-cm-band waveguide	31 to 33

CG-163/U	1-cm-band flexible waveguide	17
CG-164/U	3-cm-band flexible waveguide	17
CG-170/U	10-cm-band flexible waveguide	17
UG-45/U male } UG-46/U female }	Connectors for RG-44/U	28, 29
UG-53/U cover } UG-54/U choke }	Connectors for RG-48/U	41
UG-39/U cover } UG-40/U choke }	Connectors for RG-52/U	41
UG-116/U cover } UG-117/U choke }	Pressurized connectors for RG-53/U	41
Nonpressurized connectors for RG-53/U		30
Electroformed bends for 1-cm-band waveguide		46
Electroformed bends for 3-cm-band waveguide		46
Adaptor from waveguide coaxial line		45
<b>3. Amplifiers and Power Supplies</b>		
Audio-frequency, narrow band		1, 5
20 and 40 Mc/sec, narrow band		9
30 Mc/sec, 2 to 3 Mc/sec wide		11
Power supplies with square-wave modulators for low power oscillators		4
Klystron power supplies		27
Signal generators		14
<b>4. Crystal Rectifiers</b>		
1N21	10-cm band	9, 25
1N23	3-cm band	9, 25
1N26	1-cm band	9, 25
<b>5. Oscillator Tubes</b>		
2K25 (type 723)	3-cm band	25, 26
2K28 (type 707)	10-cm band	9, 25, 26
2K33	1-cm band	26
419B	3-cm band	27
411	10-cm band	27
410R	10-cm band	27
417 and 2K41	10-cm band	27
<b>6. Power Measurements</b>		
Thermistor bridges		9, 16
Bead Thermistors		
D-168527	3-cm band	25
D-163903	10-cm band	25

D-170575	1-cm band	25
Thermistor Mounts		
1-cm band		4
3-cm band		8, 15
10-cm band		16
7. Attenuators		
1-cm band		1, 2
3-cm band		2, 10, 6
10-cm band		2, 3
8. Spectrum Analyzers		9, 47
9. R-f Components		
1-cm components		
Crystal holder		1
Directional coupler		1
Termination		46
Slotted section		1
Squeeze section		1
Supports for waveguide		40
3-cm components		
Slotted section		8, 10, 13
Crystal mount		10
Tuner		10
2K25 tube mount		10
Termination		10
Plunger		10
Impedance bridges		14
10-cm components*		
Slotted section and probe		3, 7, 8, 43*
Wavemeter coupler		3, 7
Termination		2, 3, 28*, 42*
Mixer		44
2K28 oscillator-tube cavity		3
10. Wavemeters		
1-cm band		1, 15, 43
3-cm band		12, 6, 39
10-cm band		6

## MANUFACTURERS

1. Humble Oil and Refining Co., Houston 5, Tex.
2. PIB Products Inc., 66 Court St., Brooklyn 2, N. Y.

\* The items marked with an asterisk are in waveguide, the other 10-cm components are in coaxial line.

3. Diamond Instrument Co., Wakefield, Mass.
4. Browning Laboratories, Winchester, Mass.
5. Electronics Corp. of America, 45 West 18th St., N. Y. C., N. Y.
6. Maguire Industries, 342 W. Putnam Ave., Greenwich, Conn.
7. Nat'l. Silver Deposit Ware Co., 44 W. 18th St., N. Y. C., N. Y.
8. F-R Machine Works, 44-26 Purvis St., Long Island City, N. Y.
9. Sylvania Electric Co., 1221 W. 3rd St., P.O. Box 750, Williamsport, Pa.
10. Graham Mfg. Co., East Greenwich, R. I.
11. Harvey Radio, Cambridge, Mass.
12. Electric Corp., 150 Middle St., Pawtucket, R. I.
13. Yale and Towne Mfg. Co., Stamford Div., Stamford, Conn.
14. Boonton Radio Corp., Boonton, N. J.
15. Kannenstine Laboratories, 1922 W. Grey St., Houston, Tex.
16. Cover Dual Signal Systems, Inc., Div. of Electra Voice Corp., 5215 N. Ravenswood Ave., Chicago, Ill.
17. American Hose Branch of American Brass Co., Waterbury, Conn.
18. American Phenolic Corp., 1830 South 54th Ave., Chicago, Ill.
19. Anaconda Wire and Cable Co., 49 Federal St., Boston, Mass.
20. Federal Tel. and Radio Corp., 320 Orange St., Newark, N. J.
21. General Electric Co., 1 River Rd., Schenectady, N. Y.
22. Okonite Co., 1100 Statler Office Bldg., Boston, Mass.
23. Phelps Dodge Co., 143 Sidney St., Cambridge, Mass.
24. Simplex Wire and Cable Co., 79 Sidney St., Cambridge, Mass.
25. Western Electric Co., 120 Broadway, N. Y. C., N. Y.
26. Raytheon Mfg. Co., Foundry Ave., Waltham, Mass.
27. Sperry Gyroscope Co., Garden City, L. I., N. Y.
28. Lambert Meter Co., 715 W. Front St., Plainfield, N. J.
29. J. C. Rhodes Co., New Bedford, Mass.
30. Henry L. Crowley Co., 1 Central Ave., West Orange, N. J.
31. Chase Brass Co., Waterbury, Conn.
32. American Brass Co., Waterbury, Conn.
33. Revere Brass and Copper Co., 140 Federal St., Boston, Mass.
34. Mendelsohn Speedgun Co., 457-461 Bloomfield Ave., Bloomfield, N. J.
35. Astatic Co., 830 Market St., Youngstown, Ohio.
36. Selectar Mfg. Co., 21-10 49th Ave, Long Island, N. Y.
37. Ucinite Corp., 458 Watertown St., Newtonville, Mass.
38. M. Joseph Sewing Co., 5287 Washington St., West Roxbury, Mass.
39. Texas Co., Houston, Tex.
40. Central Scientific Co., 79 Amherst St., Cambridge, Mass.
41. Walworth Co., 60 E. 42nd St., N. Y. C., N. Y.



42. Gerstein and Copper, 1 West Third St., South Boston, Mass.
43. Chauncy Wing Co., 78 Pierce St., Greenfield, Mass.
44. Cundy-Bettoney, 96 Bradlee St., Hyde Park, Mass.
45. Wm S. Haynes Co., 108 Mass. Ave., Boston, Mass.
46. Bernard Rice's Sons, Inc., 325 Fifth Ave., N. Y. C. 16, N. Y.
47. Westinghouse Electric Manufacturing Co., East Pittsburgh, Pa.

# Index

(This comprehensive index covers both volumes of the work. Volume I contains pages 1 through 470; Volume II, pages 471 through 927.)

## A

Admittance, 476  
AFC, 58  
Alpert, D., 307  
Altar, W., 674  
Amplifier, 924  
  i-f, W-5, 555  
  pulse, 550  
  for standing wave measurements, 496-503  
  twin-T, 501  
Amplitude transmission measurement, 577-584  
Angular frequency, 3  
ANRFCCC, 9  
Antenna, gain of, 899  
  scattering by, 899  
Apker, L., 675  
Attenuation, 680  
  angular dependency of, 690  
  cable, 701  
  definitions of, 679-682  
  dissipative, 681  
  frequency sensitivity of, 683  
  as function of wavelength in coaxial-line attenuators, 764, 766  
  in line, change in standing-wave voltage ratio resulting from, 702  
  measurement of, 804-853  
  of microwave cables, 744  
  reflective, 681  
  very small, measurement of, 821-824  
  and voltage standing-wave ratio, 820  
Attenuation calibration with absolute power measurement, 838-841  
Attenuation constant, 3, 682, 686  
  measurement of, 822  
Attenuation measurement, with Ballantine voltmeter, 806  
  with i-f standard attenuator, 812  
  sources of error in, 824-832  
  by standing waves, 816-821

Attenuation measurement, substitution method of, 808-816  
  with thermistor bridge, 813  
  with two slotted sections, 805  
Attenuation standards, calibration of, 832-838  
  secondary, calibration of, 841-848  
Attenuator, coaxial, cable as, 743-745  
  carbon-coated, 745-747  
  variable metalized-glass, 769-774  
  coaxial-line,  $\frac{1}{8}$ -in., 762  
   $\frac{1}{4}$ -in., 762  
  cutoff, 685-719  
  equivalent circuit of, 700  
  input impedance of, 696-700  
  mode purity of, 687-689  
  principles of, 685-687  
  3-cm-band  $TE_{11}$ -mode, 715  
  with  $TM_{01}$ -mode, 719  
  design considerations for, 682-685  
  dissipative, 720  
  double-vane, 785  
  fixed, adjustment of, 850  
  TMX-81 PB, 782  
  flap, 748  
  helical-spring r-f contacts for, 714  
  impedance matching in, 700-707  
  iris coupling in, 709  
  loop-coupled  $TE_{11}$ -mode, 689  
  metalized-glass, precision, 751-799  
  microwave, 679-803  
  model O, 709  
  model S, 710  
  model T, 709  
  1-cm-band, 925  
  power dividers as, 799-803  
  production calibration of, 848-853  
  for reflection reduction, 573  
  resistive, 720-799  
  general laboratory, 743-751  
  separation of undesirable modes in, 689-693  
  standard coaxial, 763

- Attenuator, 3-cm-band, 925  
 10-cm-band, 925  
 TPK 35/PB/40, 786  
 TPS-15, 707  
 for 24,000 Mc/sec, 716-718  
 vane, 749  
 variable, calibration of, for signal generators, 851  
   cam drive for, 784  
   1-cm-band, 786  
    $\frac{1}{8}$ -in.-line, 770  
    $\frac{1}{4}$ -in.-line, 771  
 variable coaxial-line, matching of, 772  
 waveguide, fixed, 747  
   for 3000 Mc/sec, 707-715  
   for 9000 Mc/sec, 715  
   variable, 748-751  
     construction of, 784-790  
     performance of, 790-799
- Attenuator inserts, evaporation chamber for, 760
- Attenuator pads (*see* Pads)
- Attenuator standard, waveguide metalized glass, 836
- Automatic frequency control (*see* AFC)
- B**
- Bandwidth of cavity (*see* Cavity, bandwidth of)
- Barretter, 81 156-171  
   direct-reading bridges for, 169-171  
   theory of operation of, 161-169  
   type 821, 160
- Barretter-amplifier combinations, 171-175
- Barretter demodulation, 166
- Barretter mount, 175-179  
   type 82X, 178
- Barrow, W. L., 297, 303, 307, 329
- Beads, dielectric, 11
- Becker, J. A., 141, 188
- Beers, Y., 273
- Beggs, H. E., 180
- Bell Telephone Laboratories, 188, 201, 212, 512, 735
- Beringer, R., 273
- Bessel functions, roots of, 299
- Bethe, H. A., 860
- Bethe-hole coupler, 858-866
- Bibliography of dielectric constant measurements, 673-676
- Birks, J. B., 676
- Bleaney, B., 168
- Bode, H. W., 61
- Bodtman, W. F., 198, 212
- Bolometer, 81  
   a-f response of, 100-103  
   metalized-glass, 184-187
- Bolometer bridges, temperature compensation of, 103-105
- Boonton Radio Corporation, 552
- Borgnis, F., 294, 297, 303, 307, 673
- Breazeale, W. M., 273
- Breckenridge, R., 674, 675
- Bridge, self-balancing, 127-130  
   (*See also* type of bridge, Impedance; W-; etc.)
- Bridge circuit, 84-89  
   operation of thermistor in, 97-100  
   (*See also* type of bridge)
- Bridge sensitivity, 86
- Brownlow, J. M., 675
- Bunching, 24, 25
- Burrows, C. R., 675
- C**
- Cable attenuation, 701
- Cables, 9  
   flexible, 8, 244
- Calbick, C. J., 195, 202, 673
- Calorimeter for measuring loss, 582
- Cavity, bandwidth of, 291  
   beacon-reference, 377  
   as circuit element, 286-293  
   containing dielectric materials, 307  
   filter, 377  
   normal-mode fields in, 293-308  
   partial-coaxial, 377-379  
   resonant, 285-342, 375-384  
   standard, external temperature compensation for, 386-390  
     humidity effects for, 384, 390-392  
     temperature-compensated, 384  
     temperature effects, for, 384-390  
     for 24,000 Mc/sec, 383  
   standard measurement conditions for, 393  
   TE<sub>011</sub>-mode, 325, 379-382  
   hybrid, 382-384
- Cavity comparator, 403-407, 446  
   TFU-1RL, 406
- Cavity-coupling system, 286, 330-342  
   single-line, equivalent circuit of, 286  
   two-line, equivalent circuit of, 289  
   transmission through, 289

Cavity oscillator, 707B, 250  
 Cavity Q-meter, 396-403, 447  
 Cavity systems, very-high-Q, 340  
     very-low-Q, 339  
 Chaloff, R. S., 175  
 Charles, B. P., 891  
 Chesley, F. G., 675  
 Clamping circuit, diode, 238  
 Coaxial resonator, 303  
 Coaxial T's, 527  
 Coaxial wavemeter, 320-322  
 Cole, P. A., 193  
 Collie, C. H., 673  
 Columbia Radiation Laboratory, 511  
 Condon, E. U., 294  
 Connector, 923  
     for coaxial line, 13  
     type N, 9  
     UHF, 10  
 Coupler, Bethe-hole, 858-866  
     branched-guide, 866-873  
         equivalent circuit of, 868  
     coaxial, inside-out, 874  
     directional (*see* Directional Coupler)  
     long-slot, 885-890  
     multiple-path, 879-883  
     resistive-loop, 891  
     two-hole, 873-879  
 Coupling, definition of, 859  
     measurement of, 895  
     (*See also* Line, coaxial; Waveguide; etc.)  
 Coupling coefficient, 487  
 Coupling loop, resistive-stripe, for cutoff attenuator, 703  
     for  $TE_{11}$ -mode cutoff attenuator, 703  
 Coupling parameters, 288  
 Crossover phenomenon, 693  
 Cross section, absorption, 899  
 Crystal, r-f impedance of, 498  
     silicon, rectification of, 498  
 Crystal barrier, equivalent circuit of, 279  
 Crystal boundary layer, 279  
 Crystal holder, 7, 925  
 Crystal oscillator (*see* Oscillator, crystal)  
 Crystal rectifier, 4, 924  
     harmonic generation by, 373  
 Crystal units, cartridge, properties of, 7  
 Cutoff attenuator (*see* Attenuator, cutoff)  
 Cutoff parameter, 686  
 Cutoff wavelength, 685

## D

Dakin, T. W., 675  
 Davidson, C. F., 675  
 De Bretteville, A. P., Jr., 675  
 Decrement measurements, 340-342  
 Detector, coherent-signal, 546  
     for standing-wave measurements, 496-503  
 Detector nonlinearity, effects of, 635  
 Dicke, R. H., 271, 273  
 Dielectric constant, 3, 561  
     complex, 561  
     relations for analysis of data, 562-568  
     relative (*see* Specific inductive capacity)  
 Dielectric constant measurement, 561-676  
     bibliography of, 673-676  
     choice of method for, 568-570  
     comparison of, with optical methods, 604  
     comparison of methods for, 671  
     consistency of results in, 666  
     corrections for clearance of, 576  
     details of computation for, 584  
     by phase shift in guide, 571  
     by reflection, 606-625  
     by resonant-cavity methods, 657-665  
     by short-circuited-line method, 621, 625-656  
     gap between sample and short circuit, 631  
     measurement procedure, 633-640  
     method of, 646  
     modifications for low power, 644-654  
     sample thickness for, 630  
     sources of error in, 640-644  
     theory of, 625-633  
     uses of, 654-657  
     summary of methods for, 666-672  
     by transmission in free space, 591-606  
     by transmission in guide, 570-591  
 Diffraction, 898  
 Diode rectifiers, 193  
 Direct-reading bridge, 84  
     for barretter, 169-171  
 Directional coupler, 522, 800, 854-897, 925  
     branched-guide, modified, 873  
     comparison of types of, 850  
     equivalent circuit of, 855-858

- Directional coupler, properties of, measurements of, 894  
 reverse-coupling, 883  
 Schwinger, 885  
 slotted block, for coaxial line, 878  
 theoretical considerations for, 891-894  
 two-hole, 873-879  
 with two slots, 876  
 (*See also* Coupler)
- Directivity, definition of, 859  
 measurement of, 895
- Discriminator, microwave, 63-67  
 employing two magic T's, 66
- Double-probe coupling, 213
- Dowker, Y., 488, 673-675
- Du Mont K1017 oscilloscope, 469
- Du Mont Laboratories, Allen B., 469
- Dunsmuir, R., 675
- Frequency measuring equipment and techniques, 392-407
- Frequency multiplication, 33
- Frequency multiplier, push-pull, 368  
 push-push, 368  
 vacuum-tube, 365-373  
 velocity-modulated, 373
- Frequency-pulling, 291-293
- Frequency stabilization (*see* Stabilization, frequency)
- Frequency stabilizer, 67
- Frequency standard, accuracy of, 375  
 microwave, 344  
 design considerations of, 345-347  
 Radiation Laboratory, 347-375  
 primary, 343-347  
 secondary, 375-384
- Friis, H. T., 223

## E

- E*-plane horn, center of phase of, 906  
 phase front of, 906  
 power pattern of, 906  
 radiation pattern of, 906
- E*-plane T, wavemeter on, 314-316
- Ebert, J., 816
- Echo boxes, 192, 303, 325  
 OBU-3, 327  
 TS-218A, 447
- Ehlers, F. E., 743
- Electric field, 3
- Electroforming, 524
- Electronic-tuning hysteresis, 30
- Englund, C. R., 674
- Equivalence relations for free space and waveguide, 565
- Equivalent circuit of lossless devices, 513
- Everhart, E. M., 675, 676

## F

- Feenberg, E., 166, 374, 675, 725
- Ferguson, J. F., 749
- Fisher, H. J., 749
- Frank, N. H., 718
- Frequency, 3  
 standard, broadcasts of, 353
- Frequency-difference measurements, 453
- Frequency dividers, 354-357  
 regenerative-modulator, 356
- Frequency measurements, 343-407, 453  
 spectrum-analyzer for, 393-395

## G

- Gain, antenna, 899  
 measurement of, 907-909
- Gain determination, mirror method of, 911-914  
 by pattern integration, 914
- Gain factor, 899
- Gain measurements, scattering in, effect of 909-911
- Gainsborough, G. F., 136, 812
- Galvanometer-amplifier, 499
- General Electric Company, 180, 193, 443
- Gent, A. W., 674
- Ginzton, E., 374
- Giordano, A. B., 833
- GL-559, 193
- GL-582 diode, 193
- Grant, A. S., 674
- Green, E. I., 749
- Guillemin, E. A., 341
- Guillotine attenuator, 787
- Guthrie, G. B., 175, 807

## H

- Hansen, W. W., 272, 294, 307, 674
- Harmonic generation, by crystal rectifiers, 373  
 frequency range covered by, 374
- Harrison A., 374

Harrison, R. J., 175  
 Hatch, R., 374  
 Haugen, M., 673  
 Hegarty, M., 675  
 Helical-spring r-f contact for attenuator, 714  
 Hersberger, W. D., 214  
 Hollman, H. E., 468  
 Horner, F., 674-676  
 Hower, P. A., 350  
 Hughes, Rita, 212  
 Humidity-effect nomograph for cavities, 391  
 Hunt, L. E., 676  
 Hybrid coil, 546  
 Hysteresis, electronic-tuning, 30

## I

Image, higher-order, 416  
 Imaginary unit, 3  
 Impedance, 476  
   of polyiron, in coaxial line, 724  
   in waveguide, 727  
 Impedance bridge, 446, 515-560  
   basic measuring techniques with, 530-537  
   built-in calibrator for, 558  
   calibration of, 556-559  
   error for, 560  
   with f-m discrimination, 543-548  
   line components for, 540-545, 549, 554  
   multifrequency, 537-543  
     with panoramic receiver, 539  
     with panoramic receiver, 552-556  
   pulse-modulated, 538, 548-552  
   single-frequency, 530  
   sources of error for, 559  
 Impedance-bridge elements, 516-530  
 Impedance-circle diagrams, 476, 697  
 Incidence, angle of, measurement of, 602  
   arbitrary, measurements at, 599-604  
   far from normal, 613  
   normal, measurements at, 593-599  
 Inductive capacity, specific, 561  
 Insertion loss, 680  
 Interface reflection, 600  
 Iris-coupling in attenuators, 709

## J

Jackson, W., 674-676  
 Jamieson, H. W., 180  
 Jelatis, D., 673, 674

Johnson, M. H., 216  
 Johnson, S. A., 184, 816  
 Johnson meter, 216  
 Julian, R. S., 801, 878, 896

## K

Kallman, H. E., 512  
 Katz, S., 228  
 King, R. W. P., 754  
 Kinzer, J. P., 294, 297, 302, 303  
 Kircher, R. J., 198  
 Klystron, double-cavity, 374  
   reflex, 21  
     characteristics of, 35  
     1-cm, 47-51  
     oscillator, 23-33  
     power supplies, 51-58  
     tube types, 34-51  
     2K28, 41  
     723A/B, 31  
     2K25, 37  
     type 417, 43  
 Klystron power supplies, 924  
 Konig, H., 308  
 Korman, N. I., 509  
 Krock, R., 109  
 Kuper, J. B. H., 193, 274  
 Kyhl, R. L., 273

## L

L4PD load lamp, 180  
 Lane, J. A., 673  
 Leakage, r-f, 240-243  
   techniques to minimize, 242  
 Lee, Gordon M., 468  
 Leiter, H. A., 673  
 Letter symbols, 3  
 Lighthouse diode, 2B22, 461  
 Lighthouse tube, 2C40, 22  
 Lighthouse-tube cavity, 256  
 Line, bifurcated, 801  
   coaxial, 11-13  
     connector for, 13  
     rigid, 923  
 Lippmann, B. A., 873  
 Littelfuse mount, tunable, 176  
 Llewellyn, F. B., 813  
 Load, coaxial-line, high-power, 732-735  
   gas, for power measurement, 214  
   high-power, 721

- Load, high-power, dissipative-wall, 739
    - 1.25-cm-band, 742
    - 3-cm-band, 738
  - hot transmission-line, 271
  - IRC resistance, for rectangular waveguide, 729
  - low-power, 721
  - matched, 503-505
  - water, 194-213
    - closed-flow system for, 209
    - for coaxial line, 195-199
    - flow systems for, 204-211
    - for 1-cm-band, 203
    - for 3-cm-band, 202
    - thermopiles for, 211
    - for waveguide, 199-204
  - waveguide, high-power, 735-743
  - Load lamps, 180-183
  - Loaded  $Q$ , 289
  - Loss tangent, 561
    - calculation of, 629
    - for distilled water, 195
    - of water, 587
  - Loughlin, R., 675
- M
- Magic T, 63, 237, 331, 517, 525, 546
  - Magic-T alignment, 535
  - Magnetic field, 3
  - Magnetic permeability, 3
  - Mann, L., 127
  - Manufacturers of microwave equipment, 923-927
  - Match, sliding, 534
  - Matching techniques for T's, 525
  - Mathison, W. W., 175
  - Meahl, H. R., 676
  - Measurement (*see* quantity to be measured)
  - Merchant, R., 675
  - Metalization of glass plates, 775
  - Metalized glass, coaxial-line termination of, 724
    - use of, with low-power terminations, 731
  - Metalized-glass plates, matching of, 778
  - Microwave attenuator (*see* Attenuator, microwave)
  - Microwave current, heating effects of, 166
  - Microwave equipment, manufacturers of, 923-927
  - Microwave oscilloscopes, 468
  - Microwave region, 1
  - Microwave wavemeters, 319-330
  - Microwaves, detection of, 4-8
  - Mie, G., 307
  - Mieher, W. W., 297, 303, 307, 329
  - Mismatches, adjustable reference, 557
  - Mode chart, 298
    - for coaxial cylinder, 304
    - for right circular cylinder, 298
    - for TFX-30 wavemeter, 324
  - Mode filtering, 693-696
  - Mode patterns, reflector, 26
  - Mode shapes, universal, 28
  - Model O attenuator, 709
  - Model S attenuator, 710
  - Model T attenuator, 709
  - Modes, in circular waveguide, 690
    - normal, of cavity, 285, 293
      - in coaxial resonator, 303-307
      - in rectangular parallelepiped cavity, 294-296
    - of right-circular cylinder, 297-303
    - in slotted guides, 889
  - Modulation, amplitude, 24
    - frequency, 24
    - velocity, 24
  - Modulator, single-sideband, 331
  - Moore, A. A. S., 776
  - More, K. R., 193
  - Moreno, T., 177
  - Morgan, S. O., 735
  - Mueller, G. E., 512
  - Multivibrator, pulse, 239
  - Myers, G. B., 891
- N
- National Bureau of Standards, 344, 347, 355, 393
  - National Physical Laboratory, 813
  - Neon tubes as power indicators, 218
  - Networks, ring, 527
  - Niemann, F. L., 149
  - Noise figure, receiver, 222-226
  - Noise-figure measurement, 224
    - with microwave noise source, 225
  - Noise generators, 222
  - Noise klystron, 274
  - Noise source, crystal, 278-281
    - microwave, 270-281
    - 723A/B Klystron, 277
    - shot, 273-278

Noise source, Sperry 419, 277

sun as, 272

thermal, 271-273

Noise temperature, 225

of Sperry 417-A Klystron, 276

Nordsieck, A., 511

Normal incidence, 612

## O

OBU-3 Echo Box, 327

Optical methods, comparison of, with other dielectric constant measurement, 604

Oscillator, audio interpolation, 359-361

crystal, for frequency standard, 352

crystal-controlled, for frequency standard, 350-353

frequency-marker, 437

microwave, 21-58

pulse modulation of, 237-240

stabilized, 331

tunable, 357-359

Oscillator tubes, 924

Oscilloscope, comparison, 361-365

Oscilloscope, Du Mont K1017, 469

r-f (*see* R-f oscilloscope)

Oster, G., 675

## P

Pad inserts, coaxial, electrical design of, 752-757

Pads, coaxial, fixed, 745-747

construction of, 757-763

performance characteristics of, 763-769

polyiron waveguide, 747

waveguide, fixed, 781-784

Painter, N., 109

Pattern, radiation, of *E*-plane horn, 906

Pattern integration, gain determination by, 914

Pattern intensity measurements, 900-907

Pattern measurement, 898-915  
minimum range for, 901

Pattern parameters, 898

Payne-Scott, Ruby, 272

Penrose, R. P., 673, 676

Permeability, complex, 561  
magnetic, 3

Peskin, E., 161

Peterson, L. C., 813

Pfister, 674

Phase, center of, 900

of *E*-plane horn, 906

frequency sensitivity of, 917

Phase apparatus, for line sources, 918

for point sources, 916

Phase constant, 3

Phase front, of *E*-plane horn, 906

Phase measurement, in free space, 592

by phase-modulation method, 919-922

of *Q*, 336-340

Phase-shift measurement, 570-577

Phase shifter, 570

Plunger, 925

short-circuiting, 504

Polyiron, impedance of, in coaxial line, 724

in waveguide, 727

low-power waveguide termination with, 726-728

Polytechnic Institute of Brooklyn, 184

Pound, R. V., 331

Power, 3

average, 80

pulse, 80

Power divider, 799-803

adjustable, 214

for high-power measurements, 213-215

Power measurements, 924

at high level, 194-220

at low and medium levels, 84-194

microwave, 79-220

Power pattern, of *E*-plane horn, 906

Power ratio, measurement of, 805-808

Power supply for klystron, 51-58

Mark SX-12, 55

Probe, calibrated pickup, 799

design of, 488-496

distortion of standing-wave pattern by, 485

electric, 479

magnetic, 479

shielded, 489

10-cm, 495

traveling, 478-480, 483-488

Propagation constant, 3, 569

Pulse-forming circuits, 237

Pulse response, of receiver, 227

Pulsed modulation of oscillator, 237-240

Pulses, synchronization of, 239

Purcell, E. M., 911



## Q

- Q, loaded, 289
  - phase measurements of, 336-340
  - unloaded, 289
- Q-factors, 288, 293
- Q-meter, cavity, 396-403, 447

## R

- R6271 diode, 464
- Radiation Q, 289
- Radio Corporation of America, 214, 464
- Radio Research Laboratory, 198
- Rambo, W. R., 198
- Receiver, comparison, 353
  - pulse, measurements on, 226-234
    - response of, to frequency-modulated signals, 230
  - testing of, 222-234
  - ultimate sensitivity of, 222
- Recovery time of receiving system, 233
- Rectifiers for power indication, 191-194
- Reddish, W., 676
- Redheffer, R. M., 488, 673-675
- Reflection, interface, 565, 606-612
  - large, measurement of, 536
  - probe, 607-609
- Reflection coefficient, 3, 475
  - complex, 565
- Reflection measurement in free space, 612-616
- Reflectometer, 896
- Reflector-mode pattern (*see* Mode pattern, reflector)
- Resistive disk, 705
- Resistivity, d-c, of common metals and alloys, 296
- Resonant cavities, 285-342, 5-384
- R-f cables, 8, 923
- R-f envelope viewer, 193, 408, 455-468
  - crystal, 458
  - detector for, 459
  - diode detectors for, 461
- R-f oscilloscope, 408, 455, 467-469
- R-f phase measurements, 898-900, 915-922
- R-f source, modulation of, 500
- Richtmeyer, R. D., 307
- Rieke diagram, 31
- Roberts, S., 223, 674
- Robertson, S. D., 676

Roth, 674

RP-347 spectrum analyzer, 443

RP-392-K spectrum analyzer, 443

## S

- Saxton, J. A., 673, 676
- Scaling theorems, 308
- Scattering matrix, 517, 892
- Schelkunoff, S. A., 905
- Schneeberger, R. J., 203, 220
- Seaman, E. C. H., 675
- 707B cavity oscillator, 250
- 707B characteristics, 35
- 723A/B characteristics, 35
- 723A/B klystron, 31
- Shaw, R. C., 198, 212
- Shive, J. N., 188
- Short-circuited-line method, dielectric constant measurement by (*see* Dielectric constant measurement, by short-circuited-line method)
- Shot noise, 270
- Shot-noise sources, 273-278
- Side-outlet T, 516-522
- Signal generator, 221-281
  - with magic T, 236
  - microwave, design of, 234-270
  - pulsed, 228
  - pulsed-lighthouse-tube, 253-259
  - pulsed-off, 229
  - simple, 235
  - TGS-5BL, 247-253
  - for 3000-Mc/sec region, 247-253
  - TS-147, 259-264
  - for 24,000-Mc/sec region, 265-270
- Signal generator calibration, 245
- Similitude, principle of, 308
- Simmonds, J. C., 675
- Skin depth, 296
- Slater, J. C., 822, 880
- Slot waves, 482
- Slotted guide, wavelength in, 481
- Slotted line, characteristic impedance of, 480
- Slotted section, 478-483, 925
  - design of, 488-496
- Smith, P. H., 478
- Southworth, G. C., 273
- Specific inductive capacity, 3

- Spectrum, interpretation of, 448
    - power, 412
    - of pulse, 409
      - examples of, 449
  - Spectrum analyzer, 408, 925
    - beat-frequency indications of, 395
    - design considerations of, 416-423
    - for frequency measurement, 393-395
    - low-frequency, using microwave oscillators, 441-446
    - measurements with, 448-455
    - operation of, theory of, 411-416
    - principles and design of, 409-423
    - representative, 423-448
    - RP-347, 443
    - RP-347-K, 443
    - sensitivity of, 420
    - stability of, 422
    - TS-148/UP, 409, 429-434
    - TSK-2SE, 435, 440
    - TSK-3RL, 411, 423-429
    - TSS-4SE, 434-439
    - TSS-4SF, 411
    - TSX-4SE, 416, 429, 435, 439
  - Spectrum-analyzer principle, other instruments using, 446
  - Spectrum image, 415, 419
  - Sperry Gyroscope Company, 157, 162, 169, 177, 182, 307, 675, 788
  - Squeeze section, 507-510, 925
  - Stabilization, frequency, of microwave oscillator, 58-78
  - Stabilization factor, 62
  - Stabilization, frequency, i-f system, 69-75
    - results and limitations of, 75-78
  - Stabilizer, electronic frequency, 67
    - frequency, 67
  - Standing-wave detector, coaxial, 496
    - continuously indicating, 511
    - high-power, 510
    - for 1.25 cm, 490
    - for 3.2-cm wavelength, 492, 494
  - Standing-wave measurement, on cavities, 333-336
    - apparatus for, 503
    - detector for, 496-503
    - at high power, 510
    - on lossless devices, 512-514
  - Standing-wave minimum, shift in, 338
  - Standing-wave pattern, 475
  - Standing-wave ratio, direct measurement of, 634
  - Standing-wave ratio, high, measurement of, 505-507
    - voltage, VSWR, 3
  - Standing-wave voltage ratio, 3, 476
    - and attenuation, 820
    - of cavity, 335
    - change in, with line attenuation, 702
    - of TFX-30EC cavity, 335
  - Standing waves, fundamental relations of, 475-478
    - measurements of, 473-514
  - Strachey, C., 676
  - Stratton, J. A., 674
  - Strickland, A. C., 391
  - Strong, J., 776
  - Stub support, broadband, 13
  - Sturtevant, J. M., 218
  - Suen, T. J., 675
  - Sun, as noise source, 272
  - Superheating, 195
  - Sylvania Electric Products Co., 430, 434
  - Symbols, letter, 3
  - Synchroscope, 457
- T
- T (*see* type of T, e.g. Magic; Waveguide; etc.)
  - T-asymmetry, 532
  - T-junction, equivalent circuit of, 867
    - monitoring, 257
  - Tangential signal, 228
  - Taylor, T. A., 674, 676
  - TBX-1BR microwave impedance bridge, 446, 552
  - $TE_{11}$ -mode in circular waveguide, 690
  - Telecommunications Research Establishment, 200, 218, 512
  - Temperature compensation, of bolometer bridges, 103-105
    - with two thermistor disks, 108-118
  - Terminations, 720, 925
    - coaxial-line, low-power, 722-726
      - of metalized glass, 724
    - coaxial polyiron, 723
    - low-power, with metalized glass, 731
    - transmission-line, matched, 720-743
    - waveguide, low-power, 726-731
      - with polyiron, 726-728
  - TFK-2 wavemeter, 327
  - TFS-5 coaxial wavemeter, 320
  - TFS-10, 377

- TFU-1RL cavity comparator, 406  
 TFX-30 wavemeter, 323  
 TGS-5BL signal generator, 247-253  
 Thermistor, 81  
   bead, 89, 924  
   d-c characteristics of, 96  
   disk, 90  
   equivalent circuit for, 149  
   operation of, in bridge circuit, 97-100  
   V-519, 90  
 Thermistor bridge, 924  
   self-balancing, 128  
   two-disk, 117  
 Thermistor mount, 130-155, 925  
   broadband coaxial-line, 136  
   coaxial-line, 132  
   double, 136  
   fishtail, 150  
   impedance variations of, 147  
   1-cm-band, 151  
   O-O, 140  
   S-S, 140  
   tri-tuner, 146  
   waveguide, 139  
 Thermistor parameters, 89-97  
 Thermistor power monitors, 155  
 Thermocouple dipole, 190  
 Thermocouple power detectors, 187-191  
   sensitivity of, 187  
 Tisza, L., 675  
 TM<sub>01</sub>-mode in circular waveguide, 690  
 TMX-81 PB fixed attenuator, 782  
 Tonks, L., 675  
 TPK 35/PB/40 attenuator, 786  
 TPS-15 attenuator, 707  
 Transmission, measurement of, 577  
 Transmission coefficient, complex, 565  
 Transmission loss, 333  
 Transmission measurement, 332  
   in free space, 592  
 TRE, (*see* Telecommunications Research Establishment)  
 Trigger pulses, 239  
 TS-218A echo box, 447  
 TS-148/UP spectrum analyzer, 409, 429-434  
 TS-155, 253-259  
 TS-270, 325-327  
 TSK-2SE spectrum analyzer, 435, 440  
 TSK-3RL spectrum analyzer, 411, 423-429  
 TSS-4SE spectrum analyzer, 411, 434-439  
 TSX-4SE spectrum analyzer, 416, 429, 435, 439  
 2B22 lighthouse diode, 193, 461  
 2C40 lighthouse tube, 22  
 2K25 klystron, 35, 37  
 2K25 mount, 39  
 2K28 reflex klystron, 35, 41  
 2K33, 47  
   characteristics of, 36  
 2K45, 45  
 2K50, 47  
 Tung-Sol Lamp Works, 165  
 Tuning, electronic, 23, 29  
   hysteresis, 30  
   thermal, 46  
 Turner, L. B., 673  
 TVN-7BL, 52
- U
- Unitary matrix, 518  
 Units, system of, 2  
 Unloaded Q, 289
- V
- Van Vleck, J. H., 273  
 Vane, A. B., 273  
 V-bridge, 105-108  
 V-519 thermistor, 90  
 von Hippel, A. R., 590, 621, 673-675  
 VSWR (*see* Standing-wave voltage ratio)
- W
- Walker, R. M., 203  
 Waller, W. E., 515, 850  
 Waltz, M. C., 274  
 Water load (*see* Load, water)  
 Wattmeter, coaxial, for field use, 215  
 Wave number, 3  
 Waveguide, 923  
   flexible, 244  
   standard rectangular, 15  
   wall losses in, 590  
 Waveguide coupling, 15  
   choke-flange, 14  
 Waveguide T's, manufacture of, 524  
 Waveguide transmission lines, 13-16  
 Wavelength, 3  
   measurement of, 285-342  
   in waveguide, 3

- Wavemeter, 925  
  cavity, transmission, 309-311  
  coaxial, TFS-5, 320  
  on coaxial stub, 318  
  on *E*-plane T, 314-316  
  microwave, 319-330  
  mode,  $TE_{011}$ , 322-325, 328-330  
     $TE_{11n}$ , 327  
  reaction, 311-314  
  TFK-2, 327  
  TFX-30, 323  
  on top of waveguide, 316-318  
  for 24,000-Mc/sec region, 327  
Wavemeter circuits, practical, 308-319  
Wax, N., 202  
W-bridge, 118-123  
Webber, H. E., 166  
Weber, E., 828  
Wesson, L. G., 675  
Westinghouse Electric Corporation, 176,  
  202, 220  
Westinghouse Electric and Mfg. Co.,  
  430  
Westphal, W., 673-675  
Whitcher, S. L., 675  
Wiesner, J. B., 100  
Winkler, E. D., 673, 675  
Wollaston wire, 157  
Wood, R. F., 676  
Worthington, H. R., 919  
WWV, Radio Station, 344, 353  
  
X  
X-bridge, 123-127  
  
Y  
Yunker, E. L., 589, 673

## CATALOGUE OF DOVER BOOKS

## CATALOGUE OF DOVER BOOKS

### BOOKS EXPLAINING SCIENCE AND MATHEMATICS

#### General

**WHAT IS SCIENCE?**, Norman Campbell. This excellent introduction explains scientific method, role of mathematics, types of scientific laws. Contents: 2 aspects of science, science & nature, laws of science, discovery of laws, explanation of laws, measurement & numerical laws, applications of science. 192pp. 5½ x 8. S43 Paperbound **\$1.25**

**THE COMMON SENSE OF THE EXACT SCIENCES**, W. K. Clifford. Introduction by James Newman, edited by Karl Pearson. For 70 years this has been a guide to classical scientific and mathematical thought. Explains with unusual clarity basic concepts, such as extension of meaning of symbols, characteristics of surface boundaries, properties of plane figures, vectors, Cartesian method of determining position, etc. Long preface by Bertrand Russell. Bibliography of Clifford. Corrected, 130 diagrams redrawn. 249pp. 5½ x 8. T61 Paperbound **\$1.60**

**SCIENCE THEORY AND MAN**, Erwin Schrödinger. This is a complete and unabridged reissue of **SCIENCE AND THE HUMAN TEMPERAMENT** plus an additional essay: "What is an Elementary Particle?" Nobel laureate Schrödinger discusses such topics as nature of scientific method, the nature of science, chance and determinism, science and society, conceptual models for physical entities, elementary particles and wave mechanics. Presentation is popular and may be followed by most people with little or no scientific training. "Fine practical preparation for a time when laws of nature, human institutions . . . are undergoing a critical examination without parallel," Waldemar Kaempffert, N. Y. TIMES. 192pp. 5½ x 8. T428 Paperbound **\$1.35**

**FADS AND FALLACIES IN THE NAME OF SCIENCE**, Martin Gardner. Examines various cults, quack systems, frauds, delusions which at various times have masqueraded as science. Accounts of hollow-earth fanatics like Symmes; Velikovsky and wandering planets; Hoerbiger; Bellamy and the theory of multiple moons; Charles Fort; dowsing, pseudoscientific methods for finding water, ores, oil. Sections on naturopathy, iridagnosis, zone therapy, food fads, etc. Analytical accounts of Wilhelm Reich and orgone sex energy; L. Ron Hubbard and Dianetics; A. Korzybski and General Semantics; many others. Brought up to date to include Bridey Murphy, others. Not just a collection of anecdotes, but a fair, reasoned appraisal of eccentric theory. Formerly titled **IN THE NAME OF SCIENCE**. Preface. Index. x + 384pp. 5½ x 8. T394 Paperbound **\$1.50**

**A DOVER SCIENCE SAMPLER**, edited by George Barkin. 64-page book, sturdily bound, containing excerpts from over 20 Dover books, explaining science. Edwin Hubble, George Sarton, Ernst Mach, A. d'Abro, Galileo, Newton, others, discussing island universes, scientific truth, biological phenomena, stability in bridges, etc. Copies limited; no more than 1 to a customer, FREE

**POPULAR SCIENTIFIC LECTURES**, Hermann von Helmholtz. Helmholtz was a superb expositor as well as a scientist of genius in many areas. The seven essays in this volume are models of clarity, and even today they rank among the best general descriptions of their subjects ever written. "The Physiological Causes of Harmony in Music" was the first significant physiological explanation of musical consonance and dissonance. Two essays, "On the Interaction of Natural Forces" and "On the Conservation of Force," were of great importance in the history of science, for they firmly established the principle of the conservation of energy. Other lectures include "On the Relation of Optics to Painting," "On Recent Progress in the Theory of Vision," "On Goethe's Scientific Researches," and "On the Origin and Significance of Geometrical Axioms." Selected and edited with an introduction by Professor Morris Kline. xii + 286pp. 5½ x 8½. T799 Paperbound **\$1.45**

### BOOKS EXPLAINING SCIENCE AND MATHEMATICS

#### Physics

**CONCERNING THE NATURE OF THINGS**, Sir William Bragg. Christmas lectures delivered at the Royal Society by Nobel laureate. Why a spinning ball travels in a curved track; how uranium is transmuted to lead, etc. Partial contents: atoms, gases, liquids, crystals, metals, etc. No scientific background needed; wonderful for intelligent child. 32pp. of photos, 57 figures. xii + 232pp. 5½ x 8. T31 Paperbound **\$1.50**

**THE RESTLESS UNIVERSE**, Max Born. New enlarged version of this remarkably readable account by a Nobel laureate. Moving from sub-atomic particles to universe, the author explains in very simple terms the latest theories of wave mechanics. Partial contents: air and its relatives, electrons & ions, waves & particles, electronic structure of the atom, nuclear physics. Nearly 1000 illustrations, including 7 animated sequences. 325pp. 6 x 9. T412 Paperbound **\$2.00**

## CATALOGUE OF DOVER BOOKS

**FROM EUCLID TO EDDINGTON: A STUDY OF THE CONCEPTIONS OF THE EXTERNAL WORLD,** Sir Edmund Whittaker. A foremost British scientist traces the development of theories of natural philosophy from the western rediscovery of Euclid to Eddington, Einstein, Dirac, etc. The inadequacy of classical physics is contrasted with present day attempts to understand the physical world through relativity, non-Euclidean geometry, space curvature, wave mechanics, etc. 5 major divisions of examination: Space; Time and Movement; the Concepts of Classical Physics; the Concepts of Quantum Mechanics; the Eddington Universe. 212pp. 5½ x 8. T491 Paperbound \$1.35

**PHYSICS, THE PIONEER SCIENCE, L. W. Taylor.** First thorough text to place all important physical phenomena in cultural-historical framework; remains best work of its kind. Exposition of physical laws, theories developed chronologically, with great historical, illustrative experiments diagrammed, described, worked out mathematically. Excellent physics text for self-study as well as class work. Vol. 1: Heat, Sound; motion, acceleration, gravitation, conservation of energy, heat engines, rotation, heat, mechanical energy, etc. 211 illus. 407pp. 5½ x 8. Vol. 2: Light, Electricity: images, lenses, prisms, magnetism, Ohm's law, dynamos, telegraph, quantum theory, decline of mechanical view of nature, etc. Bibliography. 13 table appendix. Index. 551 illus. 2 color plates. 508pp. 5½ x 8.

Vol. 1 S565 Paperbound \$2.00

Vol. 2 S566 Paperbound \$2.00

The set \$4.00

**A SURVEY OF PHYSICAL THEORY, Max Planck.** One of the greatest scientists of all time, creator of the quantum revolution in physics, writes in non-technical terms of his own discoveries and those of other outstanding creators of modern physics. Planck wrote this book when science had just crossed the threshold of the new physics, and he communicates the excitement felt then as he discusses electromagnetic theories, statistical methods, evolution of the concept of light, a step-by-step description of how he developed his own momentous theory, and many more of the basic ideas behind modern physics. Formerly "A Survey of Physics." Bibliography. Index. 128pp. 5½ x 8. S650 Paperbound \$1.15

**THE ATOMIC NUCLEUS, M. Korsunsky.** The only non-technical comprehensive account of the atomic nucleus in English. For college physics students, etc. Chapters cover: Radioactivity, the Nuclear Model of the Atom, the Mass of Atomic Nuclei, the Disintegration of Atomic Nuclei, the Discovery of the Positron, the Artificial Transformation of Atomic Nuclei, Artificial Radioactivity, Mesons, the Neutrino, the Structure of Atomic Nuclei and Forces Acting Between Nuclear Particles, Nuclear Fission, Chain Reaction, Peaceful Uses, Thermocuclear Reactions. Slightly abridged edition. Translated by G. Yankovsky. 65 figures. Appendix includes 45 photographic illustrations. 413 pp. 5½ x 8. S1052 Paperbound \$2.00

**PRINCIPLES OF MECHANICS SIMPLY EXPLAINED, Morton Mott-Smith.** Excellent, highly readable introduction to the theories and discoveries of classical physics. Ideal for the layman who desires a foundation which will enable him to understand and appreciate contemporary developments in the physical sciences. Discusses: Density, The Law of Gravitation, Mass and Weight, Action and Reaction, Kinetic and Potential Energy, The Law of Inertia, Effects of Acceleration, The Independence of Motions, Galileo and the New Science of Dynamics, Newton and the New Cosmos, The Conservation of Momentum, and other topics. Revised edition of "This Mechanical World." Illustrated by E. Kosa, Jr. Bibliography and Chronology. Index. xiv + 171pp. 5½ x 8½. T1067 Paperbound \$1.00

**THE CONCEPT OF ENERGY SIMPLY EXPLAINED, Morton Mott-Smith.** Elementary, non-technical exposition which traces the story of man's conquest of energy, with particular emphasis on the developments during the nineteenth century and the first three decades of our own century. Discusses man's earlier efforts to harness energy, more recent experiments and discoveries relating to the steam engine, the engine indicator, the motive power of heat, the principle of excluded perpetual motion, the bases of the conservation of energy, the concept of entropy, the internal combustion engine, mechanical refrigeration, and many other related topics. Also much biographical material. Index. Bibliography. 33 illustrations. ix + 215pp. 5½ x 8½. T1071 Paperbound \$1.25

**HEAT AND ITS WORKINGS, Morton Mott-Smith.** One of the best elementary introductions to the theory and attributes of heat, covering such matters as the laws governing the effect of heat on solids, liquids and gases, the methods by which heat is measured, the conversion of a substance from one form to another through heating and cooling, evaporation, the effects of pressure on boiling and freezing points, and the three ways in which heat is transmitted (conduction, convection, radiation). Also brief notes on major experiments and discoveries. Concise, but complete, it presents all the essential facts about the subject in readable style. Will give the layman and beginning student a first-rate background in this major topic in physics. Index. Bibliography. 50 illustrations. x + 165pp. 5½ x 8½. T978 Paperbound \$1.00

**THE STORY OF ATOMIC THEORY AND ATOMIC ENERGY, J. G. Feinberg.** Wider range of facts on physical theory, cultural implications, than any other similar source. Completely non-technical. Begins with first atomic theory, 600 B.C., goes through A-bomb, developments to 1959. Avogadro, Rutherford, Bohr, Einstein, radioactive decay, binding energy, radiation danger, future benefits of nuclear power, dozens of other topics, told in lively, related, informal manner. Particular stress on European atomic research. "Deserves special mention . . . authoritative," Saturday Review. Formerly "The Atom Story." New chapter to 1959. Index. 34 illustrations. 251pp. 5½ x 8. T625 Paperbound \$1.60

## CATALOGUE OF DOVER BOOKS

**THE STRANGE STORY OF THE QUANTUM, AN ACCOUNT FOR THE GENERAL READER OF THE GROWTH OF IDEAS UNDERLYING OUR PRESENT ATOMIC KNOWLEDGE, B. Hoffmann.** Presents lucidly and expertly, with barest amount of mathematics, the problems and theories which led to modern quantum physics. Dr. Hoffmann begins with the closing years of the 19th century, when certain trifling discrepancies were noticed, and with illuminating analogies and examples takes you through the brilliant concepts of Planck, Einstein, Pauli, de Broglie, Bohr, Schroedinger, Heisenberg, Dirac, Sommerfeld, Feynman, etc. This edition includes a new, long postscript carrying the story through 1958. "Of the books attempting an account of the history and contents of our modern atomic physics which have come to my attention, this is the best," H. Margenau, Yale University, in "American Journal of Physics." 32 tables and line illustrations. Index. 275pp. 5% x 8. T518 Paperbound \$1.50

**THE EVOLUTION OF SCIENTIFIC THOUGHT FROM NEWTON TO EINSTEIN, A. d'Abro.** Einstein's special and general theories of relativity, with their historical implications, are analyzed in non-technical terms. Excellent accounts of the contributions of Newton, Riemann, Weyl, Planck, Eddington, Maxwell, Lorentz and others are treated in terms of space and time, equations of electromagnetics, finiteness of the universe, methodology of science. 21 diagrams. 482pp. 5% x 8. T2 Paperbound \$2.25

**THE RISE OF THE NEW PHYSICS, A. d'Abro.** A half-million word exposition, formerly titled **THE DECLINE OF MECHANISM**, for readers not versed in higher mathematics. The only thorough explanation, in everyday language, of the central core of modern mathematical physical theory, treating both classical and modern theoretical physics, and presenting in terms almost anyone can understand the equivalent of 5 years of study of mathematical physics. Scientifically impeccable coverage of mathematical-physical thought from the Newtonian system up through the electronic theories of Dirac and Heisenberg and Fermi's statistics. Combines both history and exposition; provides a broad yet unified and detailed view, with constant comparison of classical and modern views on phenomena and theories. "A must for anyone doing serious study in the physical sciences," JOURNAL OF THE FRANKLIN INSTITUTE. "Extraordinary faculty . . . to explain ideas and theories of theoretical physics in the language of daily life." ISIS. First part of set covers philosophy of science, drawing upon the practice of Newton, Maxwell, Poincaré, Einstein, others, discussing modes of thought, experiment, interpretations of causality, etc. In the second part, 100 pages explain grammar and vocabulary of mathematics, with discussions of functions, groups, series, Fourier series, etc. The remainder is devoted to concrete, detailed coverage of both classical and quantum physics, explaining such topics as analytic mechanics, Hamilton's principle, wave theory of light, electromagnetic waves, groups of transformations, thermodynamics, phase rule, Brownian movement, kinetics, special relativity, Planck's original quantum theory, Bohr's atom, Zeeman effect, Broglie's wave mechanics, Heisenberg's uncertainty, Eigen-values, matrices, scores of other important topics. Discoveries and theories are covered for such men as Alembert, Born, Cantor, Debye, Euler, Foucault, Galois, Gauss, Hadamard, Kelvin, Kepler, Laplace, Maxwell, Pauli, Rayleigh, Volterra, Weyl, Young, more than 180 others. Indexed. 97 illustrations. ix + 982pp. 5% x 8. T3 Volume 1, Paperbound \$2.00  
T4 Volume 2, Paperbound \$2.00

**SPINNING TOPS AND GYROSCOPIC MOTION, John Perry.** Well-known classic of science still unsurpassed for lucid, accurate, delightful exposition. How quasi-rigidity is induced in flexible and fluid bodies by rapid motions; why gyrostaf falls, top rises; nature and effect on climatic conditions of earth's precessional movement; effect of internal fluidity on rotating bodies, etc. Appendixes describe practical uses to which gyroscopes have been put in ships, compasses, monorail transportation. 62 figures. 128pp. 5% x 8. T416 Paperbound \$1.00

**THE UNIVERSE OF LIGHT, Sir William Bragg.** No scientific training needed to read Nobel Prize winner's expansion of his Royal Institute Christmas Lectures. Insight into nature of light, methods and philosophy of science. Explains lenses, reflection, color, resonance, polarization, x-rays, the spectrum, Newton's work with prisms, Huygens' with polarization, Crookes' with cathode ray, etc. Leads into clear statement of 2 major historical theories of light, corpuscle and wave. Dozens of experiments you can do. 199 illus., including 2 full-page color plates. 293pp. 5% x 8. S538 Paperbound \$1.85

**THE STORY OF X-RAYS FROM RÖNTGEN TO ISOTOPES, A. R. Bleich.** Non-technical history of x-rays, their scientific explanation, their applications in medicine, industry, research, and art, and their effect on the individual and his descendants. Includes amusing early reactions to Röntgen's discovery, cancer therapy, detections of art and stamp forgeries, potential risks to patient and operator, etc. Illustrations show x-rays of flower structure, the gall bladder, gears with hidden defects, etc. Original Dover publication. Glossary. Bibliography. Index. 55 photos and figures. xiv + 186pp. 5% x 8. T662 Paperbound \$1.35

**ELECTRONS, ATOMS, METALS AND ALLOYS, Wm. Hume-Rothery.** An introductory-level explanation of the application of the electronic theory to the structure and properties of metals and alloys, taking into account the new theoretical work done by mathematical physicists. Material presented in dialogue-form between an "Old Metallurgist" and a "Young Scientist." Their discussion falls into 4 main parts: the nature of an atom, the nature of a metal, the nature of an alloy, and the structure of the nucleus. They cover such topics as the hydrogen atom, electron waves, wave mechanics, Brillouin zones, co-valent bonds, radioactivity and natural disintegration, fundamental particles, structure and fission of the nucleus, etc. Revised, enlarged edition. 177 illustrations. Subject and name indexes. 407pp. 5% x 8 1/2. S1046 Paperbound \$2.25



## CATALOGUE OF DOVER BOOKS

**OUT OF THE SKY, H. H. Nininger.** A non-technical but comprehensive introduction to "meteoritics", the young science concerned with all aspects of the arrival of matter from outer space. Written by one of the world's experts on meteorites, this work shows how, despite difficulties of observation and sparseness of data, a considerable body of knowledge has arisen. It defines meteors and meteorites; studies fireball clusters and processions, meteorite composition, size, distribution, showers, explosions, origins, craters, and much more. A true connecting link between astronomy and geology. More than 175 photos, 22 other illustrations. References. Bibliography of author's publications on meteorites. Index. viii + 336pp. 5½ x 8. 1519 Paperbound \$1.85

**SATELLITES AND SCIENTIFIC RESEARCH, D. King-Hele.** Non-technical account of the manmade satellites and the discoveries they have yielded up to the autumn of 1961. Brings together information hitherto published only in hard-to-get scientific journals. Includes the life history of a typical satellite, methods of tracking, new information on the shape of the earth, zones of radiation, etc. Over 60 diagrams and 6 photographs. Mathematical appendix. Bibliography of over 100 items. Index. xii + 180pp. 5½ x 8½. 1703 Paperbound \$2.00

## BOOKS EXPLAINING SCIENCE AND MATHEMATICS

### Mathematics

**CHANCE, LUCK AND STATISTICS: THE SCIENCE OF CHANCE, Horace C. Levinson.** Theory of probability and science of statistics in simple, non-technical language. Part I deals with theory of probability, covering odd superstitions in regard to "luck," the meaning of betting odds, the law of mathematical expectation, gambling, and applications in poker, roulette, lotteries, dice, bridge, and other games of chance. Part II discusses the misuse of statistics, the concept of statistical probabilities, normal and skew frequency distributions, and statistics applied to various fields—birth rates, stock speculation, insurance rates, advertising, etc. "Presented in an easy humorous style which I consider the best kind of expository writing," Prof. A. C. Cohen, Industry Quality Control. Enlarged revised edition. Formerly titled "The Science of Chance." Preface and two new appendices by the author. Index. xiv + 365pp. 5½ x 8. 11007 Paperbound \$1.85

**PROBABILITIES AND LIFE, Emile Borel.** Translated by M. Baudin. Non-technical, highly readable introduction to the results of probability as applied to everyday situations. Partial contents: Fallacies About Probabilities Concerning Life After Death; Negligible Probabilities and the Probabilities of Everyday Life; Events of Small Probability; Application of Probabilities to Certain Problems of Heredity; Probabilities of Deaths, Diseases, and Accidents; On Poisson's Formula. Index. 3 Appendices of statistical studies and tables. vi + 87pp. 5½ x 8½. 1121 Paperbound \$1.00

**GREAT IDEAS OF MODERN MATHEMATICS: THEIR NATURE AND USE, Jagjit Singh.** Reader with only high school math will understand main mathematical ideas of modern physics, astronomy, genetics, psychology, evolution, etc., better than many who use them as tools, but comprehend little of their basic structure. Author uses his wide knowledge of non-mathematical fields in brilliant exposition of differential equations, matrices, group theory, logic, statistics, problems of mathematical foundations, imaginary numbers, vectors, etc. Original publication. 2 appendices. 2 indexes. 65 illustr. 322pp. 5½ x 8. 5587 Paperbound \$1.75

**MATHEMATICS IN ACTION, O. G. Sutton.** Everyone with a command of high school algebra will find this book one of the finest possible introductions to the application of mathematics to physical theory. Ballistics, numerical analysis, waves and wavelike phenomena, Fourier series, group concepts, fluid flow and aerodynamics, statistical measures, and meteorology are discussed with unusual clarity. Some calculus and differential equations theory is developed by the author for the reader's help in the more difficult sections. 88 figures. Index. viii + 236pp. 5½ x 8. 1440 Clothbound \$3.50

**THE FOURTH DIMENSION SIMPLY EXPLAINED, edited by H. P. Manning.** 22 essays, originally Scientific American contest entries, that use a minimum of mathematics to explain aspects of 4-dimensional geometry: analogues to 3-dimensional space, 4-dimensional absurdities and curiosities (such as removing the contents of an egg without puncturing its shell), possible measurements and forms, etc. Introduction by the editor. Only book of its sort on a truly elementary level, excellent introduction to advanced works. 82 figures. 251pp. 5½ x 8. 1711 Paperbound \$1.35

## MATHEMATICS—INTERMEDIATE TO ADVANCED

## General

**INTRODUCTION TO APPLIED MATHEMATICS**, Francis D. Murnaghan. A practical and thoroughly sound introduction to a number of advanced branches of higher mathematics. Among the selected topics covered in detail are: vector and matrix analysis, partial and differential equations, integral equations, calculus of variations, Laplace transform theory, the vector triple product, linear vector functions, quadratic and bilinear forms, Fourier series, spherical harmonics, Bessel functions, the Heaviside expansion formula, and many others. Extremely useful book for graduate students in physics, engineering, chemistry, and mathematics. Index. 111 study exercises with answers. 41 illustrations. ix + 389pp. 5% x 8½.

S1042 Paperbound \$2.00

**OPERATIONAL METHODS IN APPLIED MATHEMATICS**, H. S. Carslaw and J. C. Jaeger. Explanation of the application of the Laplace Transformation to differential equations, a simple and effective substitute for more difficult and obscure operational methods. Of great practical value to engineers and to all workers in applied mathematics. Chapters on: Ordinary Linear Differential Equations with Constant Coefficients; Electric Circuit Theory; Dynamical Applications; The Inversion Theorem for the Laplace Transformation; Conduction of Heat; Vibrations of Continuous Mechanical Systems; Hydrodynamics; Impulsive Functions; Chains of Differential Equations; and other related matters. 3 appendices. 153 problems, many with answers. 22 figures. xvi + 359pp. 5% x 8½.

S1011 Paperbound \$2.25

**APPLIED MATHEMATICS FOR RADIO AND COMMUNICATIONS ENGINEERS**, C. E. Smith. No extraneous material here!—only the theories, equations, and operations essential and immediately useful for radio work. Can be used as refresher, as handbook of applications and tables, or as full home-study course. Ranges from simplest arithmetic through calculus, series, and wave forms, hyperbolic trigonometry, simultaneous equations in mesh circuits, etc. Supplies applications right along with each math topic discussed. 22 useful tables of functions, formulas, logs, etc. Index. 166 exercises, 140 examples, all with answers. 95 diagrams. Bibliography. x + 336pp. 5% x 8.

S141 Paperbound \$1.75

## Algebra, group theory, determinants, sets, matrix theory

**ALGEBRAS AND THEIR ARITHMETICS**, L. E. Dickson. Provides the foundation and background necessary to any advanced undergraduate or graduate student studying abstract algebra. Begins with elementary introduction to linear transformations, matrices, field of complex numbers; proceeds to order, basal units, modulus, quaternions, etc.; develops calculus of linear sets, describes various examples of algebras including invariant, difference, nilpotent, semi-simple. "Makes the reader marvel at his genius for clear and profound analysis," Amer. Mathematical Monthly. Index. xii + 241pp. 5% x 8.

S616 Paperbound \$1.50

**THE THEORY OF EQUATIONS WITH AN INTRODUCTION TO THE THEORY OF BINARY ALGEBRAIC FORMS**, W. S. Burnside and A. W. Panton. Extremely thorough and concrete discussion of the theory of equations, with extensive detailed treatment of many topics curtailed in later texts. Covers theory of algebraic equations, properties of polynomials, symmetric functions, derived functions, Horner's process, complex numbers and the complex variable, determinants and methods of elimination, invariant theory (nearly 100 pages), transformations, introduction to Galois theory, Abelian equations, and much more. Invaluable supplementary work for modern students and teachers. 759 examples and exercises. Index in each volume. Two volume set. Total of xxiv + 604pp. 5% x 8.

S714 Vol I Paperbound \$1.85

S715 Vol II Paperbound \$1.85

The set \$3.70

**COMPUTATIONAL METHODS OF LINEAR ALGEBRA**, V. N. Faddeeva, translated by C. D. Benster. First English translation of a unique and valuable work, the only work in English presenting a systematic exposition of the most important methods of linear algebra—classical and contemporary. Shows in detail how to derive numerical solutions of problems in mathematical physics which are frequently connected with those of linear algebra. Theory as well as individual practice. Part I surveys the mathematical background that is indispensable to what follows. Parts II and III, the conclusion, set forth the most important methods of solution, for both exact and iterative groups. One of the most outstanding and valuable features of this work is the 23 tables, double and triple checked for accuracy. These tables will not be found elsewhere. Author's preface. Translator's note. New bibliography and index. x + 252pp. 5% x 8.

S424 Paperbound \$1.95

**ALGEBRAIC EQUATIONS**, E. Dehn. Careful and complete presentation of Galois' theory of algebraic equations; theories of Lagrange and Galois developed in logical rather than historical form, with a more thorough exposition than in most modern books. Many concrete applications and fully-worked-out examples. Discusses basic theory (very clear exposition of the symmetric group); isomorphic, transitive, and Abelian groups; applications of Lagrange's and Galois' theories; and much more. Newly revised by the author. Index. List of Theorems. xi + 208pp. 5% x 8.

S697 Paperbound \$1.45

## CATALOGUE OF DOVER BOOKS

### Differential equations, ordinary and partial; integral equations

**INTRODUCTION TO THE DIFFERENTIAL EQUATIONS OF PHYSICS, L. Hopf.** Especially valuable to the engineer with no math beyond elementary calculus. Emphasizing intuitive rather than formal aspects of concepts, the author covers an extensive territory. Partial contents: Law of causality, energy theorem, damped oscillations, coupling by friction, cylindrical and spherical coordinates, heat source, etc. Index. 48 figures. 160pp. 5½ x 8.

\$120 Paperbound **\$1.25**

**INTRODUCTION TO THE THEORY OF LINEAR DIFFERENTIAL EQUATIONS, E. G. Poole.** Authoritative discussions of important topics, with methods of solution more detailed than usual, for students with background of elementary course in differential equations. Studies existence theorems, linearly independent solutions; equations with constant coefficients; with uniform analytic coefficients; regular singularities; the hypergeometric equation; conformal representation; etc. Exercises. Index. 210pp. 5½ x 8.

\$629 Paperbound **\$1.65**

**DIFFERENTIAL EQUATIONS FOR ENGINEERS, P. Franklin.** Outgrowth of a course given 10 years at M. I. T. Makes most useful branch of pure math accessible for practical work. Theoretical basis of D.E.'s; solution of ordinary D.E.'s and partial derivatives arising from heat flow, steady-state temperature of a plate, wave equations; analytic functions; convergence of Fourier Series. 400 problems on electricity, vibratory systems, other topics. Formerly "Differential Equations for Electrical Engineers." Index 41 illus. 307pp. 5½ x 8.

\$601 Paperbound **\$1.65**

**DIFFERENTIAL EQUATIONS, F. R. Moulton.** A detailed, rigorous exposition of all the non-elementary processes of solving ordinary differential equations. Several chapters devoted to the treatment of practical problems, especially those of a physical nature, which are far more advanced than problems usually given as illustrations. Includes analytic differential equations; variations of a parameter; integrals of differential equations; analytic implicit functions; problems of elliptic motion; sine-amplitude functions; deviation of formal bodies; Cauchy-Lipschitz process; linear differential equations with periodic coefficients; differential equations in infinitely many variations; much more. Historical notes. 10 figures. 222 problems. Index. xv + 395pp. 5½ x 8.

\$451 Paperbound **\$2.00**

**DIFFERENTIAL AND INTEGRAL EQUATIONS OF MECHANICS AND PHYSICS (DIE DIFFERENTIAL- UND INTEGRALGLEICHUNGEN DER MECHANIK UND PHYSIK),** edited by P. Frank and R. von Mises. Most comprehensive and authoritative work on the mathematics of mathematical physics available today in the United States: the standard, definitive reference for teachers, physicists, engineers, and mathematicians—now published (in the original German) at a relatively inexpensive price for the first time! Every chapter in this 2,000-page set is by an expert in his field: Carathéodory, Courant, Frank, Mises, and a dozen others. Vol. I, on mathematics, gives concise but complete coverages of advanced calculus, differential equations, integral equations, and potential, and partial differential equations. Index. xxiii + 916pp. Vol. II (physics): classical mechanics, optics, continuous mechanics, heat conduction and diffusion, the stationary and quasi-stationary electromagnetic field, electromagnetic oscillations, and wave mechanics. Index. xxiv + 1106pp. Two volume set. Each volume available separately. 5½ x 8¾.

\$787 Vol I Clothbound **\$7.50**

\$788 Vol II Clothbound **\$7.50**

The set **\$15.00**

**LECTURES ON CAUCHY'S PROBLEM, J. Hadamard.** Based on lectures given at Columbia, Rome, this discusses work of Riemann, Kirchhoff, Volterra, and the author's own research on the hyperbolic case in linear partial differential equations. It extends spherical and cylindrical waves to apply to all (normal) hyperbolic equations. Partial contents: Cauchy's problem, fundamental formula, equations with odd number, with even number of independent variables; method of descent. 32 figures. Index. iii + 316pp. 5½ x 8.

\$105 Paperbound **\$1.75**

**THEORY OF DIFFERENTIAL EQUATIONS, A. R. Forsyth.** Out of print for over a decade, the complete 6 volumes (now bound as 3) of this monumental work represent the most comprehensive treatment of differential equations ever written. Historical presentation includes in 2500 pages every substantial development. Vol. 1, 2: EXACT EQUATIONS, PFAFF'S PROBLEM; ORDINARY EQUATIONS, NOT LINEAR: methods of Grassmann, Clebsch, Lie, Darboux; Cauchy's theorem; branch points; etc. Vol. 3, 4: ORDINARY EQUATIONS, NOT LINEAR; ORDINARY LINEAR EQUATIONS: Zeta Fuchsian functions, general theorems on algebraic integrals, Brun's theorem, equations with uniform periodic coefficients, etc. Vol. 4, 5: PARTIAL DIFFERENTIAL EQUATIONS: 2 existence-theorems, equations of theoretical dynamics, Laplace transformations, general transformation of equations of the 2nd order, much more. Indexes. Total of 2766pp. 5½ x 8.

\$576-7-8 Clothbound: the set **\$15.00**

**PARTIAL DIFFERENTIAL EQUATIONS OF MATHEMATICAL PHYSICS, A. G. Webster.** A keystone work in the library of every mature physicist, engineer, researcher. Valuable sections on elasticity, compression theory, potential theory, theory of sound, heat conduction, wave propagation, vibration theory. Contents include: deduction of differential equations, vibrations, normal functions, Fourier's series, Cauchy's method, boundary problems, method of Riemann-Volterra. Spherical, cylindrical, ellipsoidal harmonics, applications, etc. 97 figures. vii + 440pp. 5½ x 8.

\$263 Paperbound **\$2.00**

## CATALOGUE OF DOVER BOOKS

**ELEMENTARY CONCEPTS OF TOPOLOGY, P. Alexandroff.** First English translation of the famous brief introduction to topology for the beginner or for the mathematician not undertaking extensive study. This unusually useful intuitive approach deals primarily with the concepts of complex, cycle, and homology, and is wholly consistent with current investigations. Ranges from basic concepts of set-theoretic topology to the concept of Betti groups. "Glowing example of harmony between intuition and thought," David Hilbert. Translated by A. E. Farley. Introduction by D. Hilbert. Index. 25 figures. 73pp. 5% x 8. S747 Paperbound **\$1.00**

### Number theory

**INTRODUCTION TO THE THEORY OF NUMBERS, L. E. Dickson.** Thorough, comprehensive approach with adequate coverage of classical literature, an introductory volume beginners can follow. Chapters on divisibility, congruences, quadratic residues & reciprocity, Diophantine equations, etc. Full treatment of binary quadratic forms without usual restriction to integral coefficients. Covers infinitude of primes, least residues, Fermat's theorem, Euler's phi function, Legendre's symbol, Gauss's lemma, automorphs, reduced forms, recent theorems of Thue & Siegel, many more. Much material not readily available elsewhere. 239 problems. Index. 1 figure. viii + 183pp. 5% x 8. S342 Paperbound **\$1.65**

**ELEMENTS OF NUMBER THEORY, I. M. Vinogradov.** Detailed 1st course for persons without advanced mathematics; 95% of this book can be understood by readers who have gone no farther than high school algebra. Partial contents: divisibility theory, important number theoretical functions, congruences, primitive roots and indices, etc. Solutions to both problems and exercises. Tables of primes, indices, etc. Covers almost every essential formula in elementary number theory! Translated from Russian. 233 problems, 104 exercises. viii + 227pp. 5% x 8. S259 Paperbound **\$1.60**

**THEORY OF NUMBERS AND DIOPHANTINE ANALYSIS, R. D. Carmichael.** These two complete works in one volume form one of the most lucid introductions to number theory, requiring only a firm foundation in high school mathematics. "Theory of Numbers," partial contents: Eratosthenes' sieve, Euclid's fundamental theorem, G.C.F. and L.C.M. of two or more integers, linear congruences, etc. "Diophantine Analysis": rational triangles, Pythagorean triangles, equations of third, fourth, higher degrees, method of functional equations, much more. "Theory of Numbers": 76 problems. Index. 94pp. "Diophantine Analysis": 222 problems. Index. 118pp. 5% x 8. S529 Paperbound **\$1.35**

### Numerical analysis, tables

**MATHEMATICAL TABLES AND FORMULAE, Compiled by Robert D. Carmichael and Edwin R. Smith.** Valuable collection for students, etc. Contains all tables necessary in college algebra and trigonometry, such as five-place common logarithms, logarithmic sines and tangents of small angles, logarithmic trigonometric functions, natural trigonometric functions, four-place antilogarithms, tables for changing from sexagesimal to circular and from circular to sexagesimal measure of angles, etc. Also many tables and formulae not ordinarily accessible, including powers, roots, and reciprocals, exponential and hyperbolic functions, ten-place logarithms of prime numbers, and formulae and theorems from analytical and elementary geometry and from calculus. Explanatory introduction. viii + 269pp. 5% x 8 1/2. S111 Paperbound **\$1.00**

**MATHEMATICAL TABLES, H. B. Dwight.** Unique for its coverage in one volume of almost every function of importance in applied mathematics, engineering, and the physical sciences. Three extremely fine tables of the three trig functions and their inverse functions to thousandths of radians; natural and common logarithms; squares, cubes; hyperbolic functions and the inverse hyperbolic functions;  $(a^2 + b^2) \exp. \frac{1}{2} \alpha$ ; complete elliptic integrals of the 1st and 2nd kind; sine and cosine integrals; exponential integrals  $Ei(x)$  and  $Ei(-x)$ ; binomial coefficients; factorials to 250; surface zonal harmonics and first derivatives; Bernoulli and Euler numbers and their logs to base of 10; Gamma function; normal probability integral; over 60 pages of Bessel functions; the Riemann Zeta function. Each table with formulae generally used, sources of more extensive tables, interpolation data, etc. Over half have columns of differences, to facilitate interpolation. Introduction. Index. viii + 231pp. 5% x 8. S445 Paperbound **\$1.75**

**TABLES OF FUNCTIONS WITH FORMULAE AND CURVES, E. Jahnke & F. Emde.** The world's most comprehensive 1-volume English-text collection of tables, formulae, curves of transcendent functions. 4th corrected edition, new 76-page section giving tables, formulae for elementary functions—not in other English editions. Partial contents: sine, cosine, logarithmic integral; factorial function; error integral; theta functions; elliptic integrals, functions; Legendre, Bessel, Riemann, Mathieu, hypergeometric functions, etc. Supplementary books. Bibliography. Indexed. "Out of the way functions for which we know no other source." SCIENTIFIC COMPUTING SERVICE, Ltd. 212 figures. 400pp. 5% x 8. S133 Paperbound **\$2.00**

# CATALOGUE OF DOVER BOOKS

## CHEMISTRY AND PHYSICAL CHEMISTRY

**ORGANIC CHEMISTRY, F. C. Whitmore.** The entire subject of organic chemistry for the practicing chemist and the advanced student. Storehouse of facts, theories, processes found elsewhere only in specialized journals. Covers aliphatic compounds (500 pages on the properties and synthetic preparation of hydrocarbons, halides, proteins, ketones, etc.), alicyclic compounds, aromatic compounds, heterocyclic compounds, organophosphorus and organometallic compounds. Methods of synthetic preparation analyzed critically throughout. Includes much of biochemical interest. "The scope of this volume is astonishing." **INDUSTRIAL AND ENGINEERING CHEMISTRY.** 12,000-reference index. 2387-item bibliography. Total of x + 1005pp. 5% x 8. S700 Vol I Paperbound **\$2.25**  
S701 Vol II Paperbound **\$2.25**  
The set **\$4.50**

**THE MODERN THEORY OF MOLECULAR STRUCTURE, Bernard Pullman.** A reasonably popular account of recent developments in atomic and molecular theory. Contents: The Wave Function and Wave Equations (history and bases of present theories of molecular structure); The Electronic Structure of Atoms (Description and classification of atomic wave functions, etc.); Diatomic Molecules; Non-Conjugated Polyatomic Molecules; Conjugated Polyatomic Molecules; The Structure of Complexes. Minimum of mathematical background needed. New translation by David Antin of "La Structure Moléculaire." Index. Bibliography. vii + 87pp. 5% x 8 1/2. S987 Paperbound **\$1.00**

**CATALYSIS AND CATALYSTS, Marcel Prettre, Director, Research Institute on Catalysis.** This brief book, translated into English for the first time, is the finest summary of the principal modern concepts, methods, and results of catalysis. Ideal introduction for beginning chemistry and physics students. Chapters: Basic Definitions of Catalysis (true catalysis and generalization of the concept of catalysis); The Scientific Bases of Catalysis (Catalysis and chemical thermodynamics, catalysis and chemical kinetics); Homogeneous Catalysis (acid-base catalysis, etc.); Chain Reactions; Contact Masses; Heterogeneous Catalysis (Mechanisms of contact catalyses, etc.); and Industrial Applications (acids and fertilizers, petroleum and petroleum chemistry, rubber, plastics, synthetic resins, and fibers). Translated by David Antin. Index. vi + 88pp. 5% x 8 1/2. S998 Paperbound **\$1.00**

**POLAR MOLECULES, Pieter Debye.** This work by Nobel laureate Debye offers a complete guide to fundamental electrostatic field relations, polarizability, molecular structure. Partial contents: electric intensity, displacement and force, polarization by orientation, molar polarization and molar refraction, halogen-hydrides, polar liquids, ionic saturation, dielectric constant, etc. Special chapter considers quantum theory. Indexed. 172pp. 5% x 8. S64 Paperbound **\$1.50**

**THE ELECTRONIC THEORY OF ACIDS AND BASES, W. F. Luder and Saverio Zuffanti.** The first full systematic presentation of the electronic theory of acids and bases—treating the theory and its ramifications in an uncomplicated manner. Chapters: Historical Background; Atomic Orbitals and Valence; The Electronic Theory of Acids and Bases; Electrophilic and Electrodotic Reagents; Acidic and Basic Radicals; Neutralization; Titrations with Indicators; Displacement; Catalysis; Acid Catalysis; Base Catalysis; Alkoxides and Catalysts; Conclusion. Required reading for all chemists. Second revised (1961) edition, with additional examples and references. 3 figures. 9 tables. Index. Bibliography xii + 165pp. 5% x 8. S201 Paperbound **\$1.50**

**KINETIC THEORY OF LIQUIDS, J. Frenkel.** Regarding the kinetic theory of liquids as a generalization and extension of the theory of solid bodies, this volume covers all types of arrangements of solids, thermal displacements of atoms, interstitial atoms and ions, orientational and rotational motion of molecules, and transition between states of matter. Mathematical theory is developed close to the physical subject matter. 216 bibliographical footnotes. 55 figures. xi + 485pp. 5% x 8. S95 Paperbound **\$2.55**

**THE PRINCIPLES OF ELECTROCHEMISTRY, D. A. MacInnes.** Basic equations for almost every subfield of electrochemistry from first principles, referring at all times to the soundest and most recent theories and results; unusually useful as text or as reference. Covers coulometers and Faraday's Law, electrolytic conductance, the Debye-Hueckel method for the theoretical calculation of activity coefficients, concentration cells, standard electrode potentials, thermodynamic ionization constants, pH, potentiometric titrations, irreversible phenomena, Planck's equation, and much more. "Excellent treatise." **AMERICAN CHEMICAL SOCIETY JOURNAL.** "Highly recommended." **CHEMICAL AND METALLURGICAL ENGINEERING.** 2 Indices. Appendix. 585-item bibliography. 137 figures. 94 tables. ii + 478pp. 5% x 8 3/4. S52 Paperbound **\$2.45**

**THE PHASE RULE AND ITS APPLICATION, Alexander Findlay.** Covering chemical phenomena of 1, 2, 3, 4, and multiple component systems, this "standard work on the subject" (*NATURE*, London), has been completely revised and brought up to date by A. N. Campbell and N. O. Smith. Brand new material has been added on such matters as binary, tertiary liquid equilibria, solid solutions in ternary systems, quinary systems of salts and water. Completely revised to triangular coordinates in ternary systems, clarified graphic representation, solid models, etc. 9th revised edition. Author, subject indexes. 236 figures. 505 footnotes, mostly bibliographic. xii + 494pp. 5% x 8. S91 Paperbound **\$2.50**

# CATALOGUE OF DOVER BOOKS

## PHYSICS

### General physics

**FOUNDATIONS OF PHYSICS, R. B. Lindsay & H. Margenau.** Excellent bridge between semi-popular works & technical treatises. A discussion of methods of physical description, construction of theory; valuable for physicist with elementary calculus who is interested in ideas that give meaning to data, tools of modern physics. Contents include symbolism, mathematical equations; space & time foundations of mechanics; probability; physics & continua; electron theory; special & general relativity; quantum mechanics; causality. "Thorough and yet not overdetalled. Unreservedly recommended," NATURE (London). Unabridged, corrected edition. List of recommended readings. 35 illustrations. xi + 537pp. 5½ x 8. S377 Paperbound **\$2.75**

**FUNDAMENTAL FORMULAS OF PHYSICS, ed. by D. H. Menzel.** Highly useful, fully inexpensive reference and study text, ranging from simple to highly sophisticated operations. Mathematics integrated into text—each chapter stands as short textbook of field represented. Vol. 1: Statistics, Physical Constants, Special Theory of Relativity, Hydrodynamics, Aerodynamics, Boundary Value Problems in Math. Physics; Viscosity, Electromagnetic Theory, etc. Vol. 2: Sound, Acoustics, Geometrical Optics, Electron Optics, High-Energy Phenomena, Magnetism, Biophysics, much more. Index. Total of 800pp. 5½ x 8. Vol. 1 S595 Paperbound **\$2.00**  
Vol. 2 S596 Paperbound **\$2.00**

**MATHEMATICAL PHYSICS, D. H. Menzel.** Thorough one-volume treatment of the mathematical techniques vital for classic mechanics, electromagnetic theory, quantum theory, and relativity. Written by the Harvard Professor of Astrophysics for junior, senior, and graduate courses, it gives clear explanations of all those aspects of function theory, vectors, matrices, dyadics, tensors, partial differential equations, etc., necessary for the understanding of the various physical theories. Electron theory, relativity, and other topics seldom presented appear here in considerable detail. Scores of definitions, conversion factors, dimensional constants, etc. "More detailed than normal for an advanced text . . . excellent set of sections on Dyadics, Matrices, and Tensors," JOURNAL OF THE FRANKLIN INSTITUTE. Index. 193 problems, with answers. x + 412pp. 5½ x 8. S56 Paperbound **\$2.00**

**THE SCIENTIFIC PAPERS OF J. WILLARD GIBBS.** All the published papers of America's outstanding theoretical scientist (except for "Statistical Mechanics" and "Vector Analysis"). Vol. I (thermodynamics) contains one of the most brilliant of all 19th-century scientific papers—the 300-page "On the Equilibrium of Heterogeneous Substances," which founded the science of physical chemistry, and clearly stated a number of highly important natural laws for the first time; 8 other papers complete the first volume. Vol. II includes 2 papers on dynamics, 8 on vector analysis and multiple algebra, 5 on the electromagnetic theory of light, and 6 miscellaneous papers. Biographical sketch by H. A. Bumstead. Total of xxxvi + 718pp. 5½ x 8¾. S721 Vol I Paperbound **\$2.50**  
S722 Vol II Paperbound **\$2.00**  
The set **\$4.50**

**BASIC THEORIES OF PHYSICS, Peter Gabriel Bergmann.** Two-volume set which presents a critical examination of important topics in the major subdivisions of classical and modern physics. The first volume is concerned with classical mechanics and electrodynamics; mechanics of mass points, analytical mechanics, matter in bulk, electrostatics and magnetostatics, electromagnetic interaction, the field waves, special relativity, and waves. The second volume (Heat and Quanta) contains discussions of the kinetic hypothesis, physics and statistics, stationary ensembles, laws of thermodynamics, early quantum theories, atomic spectra, probability waves, quantization in wave mechanics, approximation methods, and abstract quantum theory. A valuable supplement to any thorough course or text. Heat and Quanta: Index. 8 figures. x + 300pp. 5½ x 8½. S968 Paperbound **\$1.75**  
Mechanics and Electrodynamics: Index. 14 figures. vii + 280pp. 5½ x 8½. S969 Paperbound **\$1.75**

**THEORETICAL PHYSICS, A. S. Kompaneys.** One of the very few thorough studies of the subject in this price range. Provides advanced students with a comprehensive theoretical background. Especially strong on recent experimentation and developments in quantum theory. Contents: Mechanics (Generalized Coordinates, Lagrange's Equation, Collision of Particles, etc.), Electrodynamics (Vector Analysis, Maxwell's equations, Transmission of Signals, Theory of Relativity, etc.), Quantum Mechanics (the Inadequacy of Classical Mechanics, the Wave Equation, Motion in a Central Field, Quantum Theory of Radiation, Quantum Theories of Dispersion and Scattering, etc.), and Statistical Physics (Equilibrium Distribution of Molecules in an Ideal Gas, Boltzmann statistics, Bose and Fermi Distribution, Thermodynamic Quantities, etc.). Revised to 1961. Translated by George Yankovsky, authorized by Kompaneys. 137 exercises. 56 figures. 529pp. 5½ x 8½. S972 Paperbound **\$2.50**

**ANALYTICAL AND CANONICAL FORMALISM IN PHYSICS, André Mercier.** A survey, in one volume, of the variational principles (the key principles—in mathematical form—from which the basic laws of any one branch of physics can be derived) of the several branches of physical theory, together with an examination of the relationships among them. Contents: the Lagrangian Formalism, Lagrangian Densities, Canonical Formalism, Canonical Form of Electrodynamics, Hamiltonian Densities, Transformations, and Canonical Form with Vanishing Jacobian Determinant. Numerous examples and exercises. For advanced students, teachers, etc. 6 figures. Index. viii + 222pp. 5½ x 8½. S1077 Paperbound **\$1.75**

# CATALOGUE OF DOVER BOOKS

## MATHEMATICAL PUZZLES AND RECREATIONS

**AMUSEMENTS IN MATHEMATICS**, Henry Ernest Dudeney. The foremost British originator of mathematical puzzles is always intriguing, witty, and paradoxical in this classic, one of the largest collections of mathematical amusements. More than 430 puzzles, problems, and paradoxes. Mazes and games, problems on number manipulation, unicursal and other route problems, puzzles on measuring, weighing, packing, age, kinship, chessboards, joining, crossing river, plane figure dissection, and many others. Solutions. More than 450 illustrations. vii + 258pp. 5½ x 8. T473 Paperbound \$1.25

**SYMBOLIC LOGIC AND THE GAME OF LOGIC**, Lewis Carroll. "Symbolic Logic" is not concerned with modern symbolic logic, but is instead a collection of over 380 problems posed with charm and imagination, using the syllogism, and a fascinating diagrammatic method of drawing conclusions. In "The Game of Logic," Carroll's whimsical imagination devises a logical game played with 2 diagrams and counters (included) to manipulate hundreds of tricky syllogisms. The final section, "Hit or Miss" is a lagniappe of 101 additional puzzles in the delightful Carroll manner. Until this reprint edition, both of these books were rarities costing up to \$15 each. Symbolic Logic: Index, xxxi + 199pp. The Game of Logic: 96pp. 2 vols. bound as one. 5½ x 8. T492 Paperbound \$1.50

**MAZES AND LABYRINTHS: A BOOK OF PUZZLES**, W. Shepherd. Mazes, formerly associated with mystery and ritual, are still among the most intriguing of intellectual puzzles. This is a novel and different collection of 50 amusements that embody the principle of the maze: mazes in the classical tradition; 3-dimensional, ribbon, and Möbius-strip mazes; hidden messages; spatial arrangements; etc.—almost all built on amusing story situations. 84 illustrations. Essay on maze psychology. Solutions. xv + 122pp. 5½ x 8. T731 Paperbound \$1.00

**MATHEMATICAL RECREATIONS**, M. Kraitchik. Some 250 puzzles, problems, demonstrations of recreational mathematics for beginners & advanced mathematicians. Unusual historical problems from Greek, Medieval, Arabic, Hindu sources: modern problems based on "mathematics without numbers," geometry, topology, arithmetic, etc. Pastimes derived from figurative numbers, Mersenne numbers, Fermat numbers; fairy chess, latruncles, reversi, many topics. Full solutions. Excellent for insights into special fields of math. 181 illustrations. 330pp. 5½ x 8. T163 Paperbound \$1.75

**MATHEMATICAL PUZZLES OF SAM LOYD, Vol. I**, selected and edited by M. Gardner. Puzzles by the greatest puzzle creator and innovator. Selected from his famous "Cyclopaedia of Puzzles," they retain the unique style and historical flavor of the originals. There are posers based on arithmetic, algebra, probability, game theory, route tracing, topology, counter, sliding block, operations research, geometrical dissection. Includes his famous "14-15" puzzle which was a national craze, and his "Horse of a Different Color" which sold millions of copies. 117 of his most ingenious puzzles in all, 120 line drawings and diagrams. Solutions. Selected references. xx + 167pp. 5½ x 8. T498 Paperbound \$1.00

**MY BEST PUZZLES IN MATHEMATICS**, Hubert Phillips ("Caliban"). Caliban is generally considered the best of the modern problemists. Here are 100 of his best and wittiest puzzles, selected by the author himself from such publications as the London Daily Telegraph, and each puzzle is guaranteed to put even the sharpest puzzle detective through his paces. Perfect for the development of clear thinking and a logical mind. Complete solutions are provided for every puzzle. x + 107pp. 5½ x 8½. T91 Paperbound \$1.00

**MY BEST PUZZLES IN LOGIC AND REASONING**, H. Phillips ("Caliban"). 100 choice, hitherto unavailable puzzles by England's best-known problemist. No special knowledge needed to solve these logical or inferential problems, just an unclouded mind, nerves of steel, and fast reflexes. Data presented are both necessary and just sufficient to allow one unambiguous answer. More than 30 different types of puzzles, all ingenious and varied, many one of a kind, that will challenge the expert, please the beginner. Original publication. 100 puzzles, full solutions. x + 107pp. 5½ x 8½. T119 Paperbound \$1.00

**MATHEMATICAL PUZZLES FOR BEGINNERS AND ENTHUSIASTS**, G. Mott-Smith. 188 mathematical puzzles to test mental agility. Inference, interpretation, algebra, dissection of plane figures, geometry, properties of numbers, decimation, permutations, probability, all enter these delightful problems. Puzzles like the Odic Force, How to Draw an Ellipse, Spider's Cousin, more than 180 others. Detailed solutions. Appendix with square roots, triangular numbers, primes, etc. 135 illustrations. 2nd revised edition. 248pp. 5½ x 8. T198 Paperbound \$1.00

**MATHEMATICS, MAGIC AND MYSTERY**, Martin Gardner. Card tricks, feats of mental mathematics, stage mind-reading, other "magic" explained as applications of probability, sets, theory of numbers, topology, various branches of mathematics. Creative examination of laws and their applications with scores of new tricks and insights. 115 sections discuss tricks with cards, dice, coins; geometrical vanishing tricks, dozens of others. No sleight of hand needed; mathematics guarantees success. 115 illustrations. xii + 174pp. 5½ x 8. T335 Paperbound \$1.00

## CATALOGUE OF DOVER BOOKS

**RECREATIONS IN THE THEORY OF NUMBERS: THE QUEEN OF MATHEMATICS ENTERTAINS**, Albert H. Beller. The theory of numbers is often referred to as the "Queen of Mathematics." In this book Mr. Beller has compiled the first English volume to deal exclusively with the recreational aspects of number theory, an inherently recreational branch of mathematics. The author's clear style makes for enjoyable reading as he deals with such topics as: perfect numbers, amicable numbers, Fermat's theorem, Wilson's theorem, interesting properties of digits, methods of factoring, primitive roots, Euler's function, polygonal and figurate numbers, Mersenne numbers, congruence, repeating decimals, etc. Countless puzzle problems, with full answers and explanations. For mathematicians and mathematically-inclined laymen, etc. New publication. 28 figures, 9 illustrations. 103 tables. Bibliography at chapter ends. vi + 247pp. 5½ x 8½. T1096 Paperbound \$1.85

**PAPER FOLDING FOR BEGINNERS**, W. D. Murray and F. J. Rigney. A delightful introduction to the varied and entertaining Japanese art of origami (paper folding), with a full crystal-clear text that anticipates every difficulty; over 275 clearly labeled diagrams of all important stages in creation. You get results at each stage, since complex figures are logically developed from simpler ones. 43 different pieces are explained: place mats, drinking cups, bonbon boxes, sailboats, frogs, roosters, etc. 6 photographic plates. 279 diagrams. 95pp. 5½ x 8½. T713 Paperbound \$1.00

**1800 RIDDLES, ENIGMAS AND CONUNDRUMS**, Darwin A. Hindman. Entertaining collection ranging from hilarious gags to outrageous puns to sheer nonsense—a welcome respite from sophisticated humor. Children, toastmasters, and practically anyone with a funny bone will find these zany riddles tickling and eminently repeatable. Sample: "Why does Santa Claus always go down the chimney?" "Because it soots him." Some old, some new—covering a wide variety of subjects. New publication. iii + 154pp. 5½ x 8½. T1059 Paperbound \$1.00

**EASY-TO-DO ENTERTAINMENTS AND DIVERSIONS WITH CARDS, STRING, COINS, PAPER AND MATCHES**, R. M. Abraham. Over 300 entertaining games, tricks, puzzles, and pastimes for children and adults. Invaluable to anyone in charge of groups of youngsters; for party givers, etc. Contains sections on card tricks and games, making things by paperfolding—toys, decorations, and the like; tricks with coins, matches, and pieces of string; descriptions of games; toys that can be made from common household objects; mathematical recreations; word games; and 50 miscellaneous entertainments. Formerly "Winter Nights Entertainments." Introduction by Lord Baden Powell. 329 illustrations. v + 186pp. 5½ x 8. T921 Paperbound \$1.00

**DIVERSIONS AND PASTIMES WITH CARDS, STRING, PAPER AND MATCHES**, R. M. Abraham. Another collection of amusements and diversion for game and puzzle fans of all ages. Many new paperfolding ideas and tricks, an extensive section on amusements with knots and splices, two chapters of easy and not-so-easy problems, coin and match tricks, and lots of other parlor pastimes from the agile mind of the late British problemist and gamester. Corrected and revised version. Illustrations. 160pp. 5½ x 8½. T1127 Paperbound \$1.00

**STRING FIGURES AND HOW TO MAKE THEM: A STUDY OF CAT'S-CRADLE IN MANY LANOS**, Caroline Furness Jayne. In a simple and easy-to-follow manner, this book describes how to make 107 different string figures. Not only is looping and crossing string between the fingers a common youthful diversion, but it is an ancient form of amusement practiced in all parts of the globe, especially popular among primitive tribes. These games are fun for all ages and offer an excellent means for developing manual dexterity and coordination. Much insight also for the anthropological observer on games and diversions in many different cultures. Index. Bibliography. Introduction by A. C. Haddon, Cambridge University. 17 full-page plates. 950 illustrations. xxiii + 407pp. 5½ x 8½. T152 Paperbound \$2.00

**CRYPTANALYSIS**, Helen F. Gaines. (Formerly ELEMENTARY CRYPTANALYSIS.) A standard elementary and intermediate text for serious students. It does not confine itself to old material, but contains much that is not generally known, except to experts. Concealment, Transposition, Substitution ciphers; Vigenere, Kasiski, Playfair, multifid, dozens of other techniques. Appendix with sequence charts, letter frequencies in English, 5 other languages, English word frequencies. Bibliography. 167 codes. New to this edition: solution to codes. vi + 230pp. 5½ x 8. T97 Paperbound \$2.00

**MAGIC SQUARES AND CUBES**, W. S. Andrews. Only book-length treatment in English, a thorough non-technical description and analysis. Here are nasik, overlapping, pandiagonal, serrated squares; magic circles, cubes, spheres, rhombuses. Try your hand at 4-dimensional magical figures! Much unusual folklore and tradition included. High school algebra is sufficient. 754 diagrams and illustrations. viii + 419pp. 5½ x 8. T658 Paperbound \$1.85

**CALIBAN'S PROBLEM BOOK: MATHEMATICAL, INFERENCE, AND CRYPTOGRAPHIC PUZZLES**, H. Phillips ("Caliban"), S. T. Shovelton, G. S. Marshall. 105 ingenious problems by the greatest living creator of puzzles based on logic and inference. Rigorous, modern, piquant, and reflecting their author's unusual personality, these intermediate and advanced puzzles all involve the ability to reason clearly through complex situations; some call for mathematical knowledge, ranging from algebra to number theory. Solutions. xi + 180pp. 5½ x 8. T736 Paperbound \$1.25



# CATALOGUE OF DOVER BOOKS

## FICTION

**THE LAND THAT TIME FORGOT and THE MOON MAID, Edgar Rice Burroughs.** In the opinion of many, Burroughs' best work. The first concerns a strange island where evolution is individual rather than phylogenetic. Speechless anthropoids develop into intelligent human beings within a single generation. The second projects the reader far into the future and describes the first voyage to the Moon (in the year 2025), the conquest of the Earth by the Moon, and years of violence and adventure as the enslaved Earthmen try to regain possession of their planet. "An imaginative tour de force that keeps the reader keyed up and expectant," *NEW YORK TIMES*. Complete, unabridged text of the original two novels (three parts in each). 5 illustrations by J. Allen St. John. vi + 552pp. 5% x 8 1/2.

T1020 Clothbound **\$3.75**  
T358 Paperbound **\$2.00**

**AT THE EARTH'S CORE, PELLUCIOAR, TANAR OF PELLUCIOAR: THREE SCIENCE FICTION NOVELS BY EDGAR RICE BURROUGHS.** Complete, unabridged texts of the first three Pellucidar novels. Tales of derring-do by the famous master of science fiction. The locale for these three related stories is the inner surface of the hollow Earth where we discover the world of Pellucidar, complete with all types of bizarre, menacing creatures, strange peoples, and alluring maidens—guaranteed to delight all Burroughs fans and a wide circle of adventure lovers. Illustrated by J. Allen St. John and P. F. Berdanier. vi + 433pp. 5% x 8 1/2.

T1051 Paperbound **\$2.00**

**THE PIRATES OF VENUS and LOST ON VENUS: TWO VENUS NOVELS BY EDGAR RICE BURROUGHS.** Two related novels, complete and unabridged. Exciting adventure on the planet Venus with Earthman Carson Napier broken-field running through one dangerous episode after another. All lovers of swashbuckling science fiction will enjoy these two stories set in a world of fascinating societies, fierce beasts, 5000-ft. trees, lush vegetation, and wide seas. Illustrations by Fortunino Matania. Total of vi + 340pp. 5% x 8 1/2.

T1053 Paperbound **\$1.75**

**A PRINCESS OF MARS and A FIGHTING MAN OF MARS: TWO MARTIAN NOVELS BY EDGAR RICE BURROUGHS.** "Princess of Mars" is the very first of the great Martian novels written by Burroughs, and it is probably the best of them all; it set the pattern for all of his later fantasy novels and contains a thrilling cast of strange peoples and creatures and the formula of Olympian heroism amidst ever-fluctuating fortunes which Burroughs carries off so successfully. "Fighting Man" returns to the same scenes and cities—many years later. A mad scientist, a degenerate dictator, and an indomitable defender of the right clash—with the fate of the Red Planet at stake! Complete, unabridged reprinting of original editions. Illustrations by F. E. Schoonover and Hugh Hutton. v + 356pp. 5% x 8 1/2.

T1140 Paperbound **\$1.75**

**THREE MARTIAN NOVELS, Edgar Rice Burroughs.** Contains: Thuvia, Maid of Mars; The Chessmen of Mars; and The Master Mind of Mars. High adventure set in an imaginative and intricate conception of the Red Planet. Mars is peopled with an intelligent, heroic human race which lives in densely populated cities and with fierce barbarians who inhabit dead sea bottoms. Other exciting creatures abound amidst an inventive framework of Martian history and geography. Complete unabridged reprintings of the first edition. 16 illustrations by J. Allen St. John. vi + 499pp. 5% x 8 1/2.

T39 Paperbound **\$1.85**

**THREE PROPHETIC NOVELS BY H. G. WELLS, edited by E. F. Bleiler.** Complete texts of "When the Sleeper Wakes" (1st book printing in 50 years), "A Story of the Days to Come," "The Time Machine" (1st complete printing in book form). Exciting adventures in the future are as enjoyable today as 50 years ago when first printed. Predict TV, movies, intercontinental airplanes, prefabricated houses, air-conditioned cities, etc. First important author to foresee problems of mind control, technological dictatorships. "Absolute best of imaginative fiction," *N. Y. Times*. Introduction. 335pp. 5% x 8.

T605 Paperbound **\$1.50**

**28 SCIENCE FICTION STORIES OF H. G. WELLS.** Two full unabridged novels, *MEN LIKE GODS* and *STAR BEGOTTEN*, plus 26 short stories by the master science-fiction writer of all time. Stories of space, time, invention, exploration, future adventure—an indispensable part of the library of everyone interested in science and adventure. **PARTIAL CONTENTS:** Men Like Gods, The Country of the Blind, In the Abyss, The Crystal Egg, The Man Who Could Work Miracles, A Story of the Days to Come, The Valley of Spiders, and 21 more! 928pp. 5% x 8.

T265 Clothbound **\$4.50**

**THE WAR IN THE AIR, IN THE DAYS OF THE COMET, THE FOOD OF THE GODS: THREE SCIENCE FICTION NOVELS BY H. G. WELLS.** Three exciting Wells offerings bearing on vital social and philosophical issues of his and our own day. Here are tales of air power, strategic bombing, East vs. West, the potential miracles of science, the potential disasters from outer space, the relationship between scientific advancement and moral progress, etc. First reprinting of "War in the Air" in almost 50 years. An excellent sampling of Wells at his storytelling best. Complete, unabridged reprintings. 16 illustrations. 645pp. 5% x 8 1/2.

T1135 Paperbound **\$2.00**

## CATALOGUE OF DOVER BOOKS

**SEVEN SCIENCE FICTION NOVELS, H. G. Wells.** Full unabridged texts of 7 science-fiction novels of the master. Ranging from biology, physics, chemistry, astronomy to sociology and other studies, Mr. Wells extrapolates whole worlds of strange and intriguing character. "One will have to go far to match this for entertainment, excitement, and sheer pleasure . . ." *NEW YORK TIMES*. Contents: *The Time Machine*, *The Island of Dr. Moreau*, *First Men in the Moon*, *The Invisible Man*, *The War of the Worlds*, *The Food of the Gods*, *In the Days of the Comet*. 1015pp. 5½ x 8. T264 Clothbound \$4.50

**BEST GHOST STORIES OF J. S. LE FANU**, Selected and introduced by E. F. Bleiler. LeFanu is deemed the greatest name in Victorian supernatural fiction. Here are 16 of his best horror stories, including 2 nouvelles: "Carmilla," a classic vampire tale couched in a perverse eroticism, and "The Haunted Baronet." Also: "Sir Toby's Will," "Green Tea," "Schalken the Painter," "Ultor de Lacy," "The Familiar," etc. The first American publication of about half of this material: a long-overdue opportunity to get a choice sampling of LeFanu's work. New selection (1964). 8 illustrations. 5¾ x 8¾. T415 Paperbound \$1.85

**THE WONDERFUL WIZARD OF OZ, L. F. Baum.** Only edition in print with all the original W. W. Denslow illustrations in full color—as much a part of "The Wizard" as Tenniel's drawings are for "Alice in Wonderland." "The Wizard" is still America's best-loved fairy tale, in which, as the author expresses it, "The wonderment and joy are retained and the heartaches and nightmares left out." Now today's young readers can enjoy every word and wonderful picture of the original book. New introduction by Martin Gardner. A Baum bibliography. 23 full-page color plates. viii + 268pp. 5¾ x 8. T691 Paperbound \$1.50

**GHOST AND HORROR STORIES OF AMBROSE BIERCE**, Selected and introduced by E. F. Bleiler. 24 morbid, eerie tales—the cream of Bierce's fiction output. Contains such memorable pieces as "The Moonlit Road," "The Damned Thing," "An Inhabitant of Carcosa," "The Eyes of the Panther," "The Famous Gilson Bequest," "The Middle Toe of the Right Foot," and other chilling stories, plus the essay, "Visions of the Night" in which Bierce gives us a kind of rationale for his aesthetic of horror. New collection (1964). xxii + 199pp. 5¾ x 8¾. T767 Paperbound \$1.00

## HUMOR

**MR. DOOLEY ON IVRYTHING AND IVRYBODY, Finley Peter Dunne.** Since the time of his appearance in 1893, "Mr. Dooley," the fictitious Chicago bartender, has been recognized as America's most humorous social and political commentator. Collected in this volume are 102 of the best Dooley pieces—all written around the turn of the century, the height of his popularity. Mr. Dooley's Irish brogue is employed wittily and penetratingly on subjects which are just as fresh and relevant today as they were then: corruption and hypocrisy of politicians, war preparations and chauvinism, automation, Latin American affairs, superbombs, etc. Other articles range from Rudyard Kipling to football. Selected with an introduction by Robert Hutchinson. xii + 244pp. 5¾ x 8¾. T626 Paperbound \$1.00

**RUTHLESS RHYMES FOR HEARTLESS HOMES and MORE RUTHLESS RHYMES FOR HEARTLESS HOMES, Harry Graham ("Col. D. Streamer").** A collection of Little Willy and 48 other poetic "disasters." Graham's funniest and most disrespectful verse, accompanied by original illustrations. Nonsensical, wry humor which employs stern parents, careless nurses, uninhibited children, practical jokers, single-minded golfers, Scottish lairds, etc. in the leading roles. A precursor of the "sick joke" school of today. This volume contains, bound together for the first time, two of the most perennially popular books of humor in England and America. Index. vi + 69pp. 5¾ x 8. T930 Paperbound 75¢

**A WHIMSEY ANTHOLOGY, Collected by Carolyn Wells.** 250 of the most amusing rhymes ever written. Acrostics, anagrams, palindromes, alphabetical jingles, tongue twisters, echo verses, alliterative verses, riddles, mnemonic rhymes, interior rhymes, over 40 limericks, etc. by Lewis Carroll, Edward Lear, Joseph Addison, W. S. Gilbert, Christina Rossetti, Chas. Lamb, James Boswell, Hood, Dickens, Swinburne, Leigh Hunt, Harry Graham, Poe, Eugene Field, and many others. xiv + 221pp. 5¾ x 8¾. T195 Paperbound \$1.25

**MY PIOUS FRIENDS AND DRUNKEN COMPANIONS and MORE PIOUS FRIENDS AND DRUNKEN COMPANIONS, Songs and ballads of Conviviality Collected by Frank Shay.** Magnificently illuminated by John Held, Jr. 132 ballads, blues, vaudeville numbers, drinking songs, cowboy songs, sea chanties, comedy songs, etc. of the Naughty Nineties and early 20th century. Over a third are reprinted with music. Many perennial favorites such as: *The Band Played On*, *Frankie and Johnnie*, *The Old Grey Mare*, *The Face on the Bar-room Floor*, etc. Many others unlocatable elsewhere: *The Dog-Catcher's Child*, *The Cannibal Maiden*, *Don't Go in the Lion's Cage Tonight*, *Mother*, etc. Complete verses and introductions to songs. Unabridged republication of first editions, 2 indexes (song titles and first lines and choruses). Introduction by Frank Shay. 2 volumes bound as 1. Total of xvi + 235pp. 5¾ x 8¾. T946 Paperbound \$1.25

## CATALOGUE OF DOVER BOOKS

**MAX AND MORITZ, Wilhelm Busch.** Edited and annotated by H. Arthur Klein. Translated by H. Arthur Klein, M. C. Klein, and others. The mischievous high jinks of Max and Moritz, Peter and Paul, Ker and Plunk, etc. are delightfully captured in sketch and rhyme. (Companion volume to "Hypocritical Helena.") In addition to the title piece, it contains: Ker and Plunk; Two Dogs and Two Boys; The Egghead and the Two Cut-ups of Corinth; Deceitful Henry; The Boys and the Pipe; Cat and Mouse; and others. (Original German text with accompanying English translations.) Afterword by H. A. Klein. vi + 216pp. 5 3/8 x 8 1/2.

T181 Paperbound \$1.15

**THROUGH THE ALIMENTARY CANAL WITH GUN AND CAMERA: A FASCINATING TRIP TO THE INTERIOR.** Personally Conducted by George S. Chappell. In mock-travelogue style, the amusing account of an imaginative journey down the alimentary canal. The "explorers" enter the esophagus, round the Adam's Apple, narrowly escape from a fierce Amoeba, struggle through the impenetrable Nerve Forests of the Lumbar Region, etc. Illustrated by the famous cartoonist, Otto Soglow, the book is as much a brilliant satire of academic pomposity and professional travel literature as it is a clever use of the facts of physiology for supremely comic purposes. Preface by Robert Benchley. Author's Foreword. 1 Photograph. 17 illustrations by O. Soglow. xii + 114pp. 5 3/8 x 8 1/2.

T376 Paperbound \$1.00

**THE BAD CHILD'S BOOK OF BEASTS, MORE BEASTS FOR WORSE CHILDREN, AND A MORAL ALPHABET.** H. Belloc. Hardly an anthology of humorous verse has appeared in the last 50 years without at least a couple of these famous nonsense verses. But one must see the entire volumes—with all the delightful original illustrations by Sir Basil Blackwood—to appreciate fully Belloc's charming and witty verses that play so subacutely on the platitudes of life and morals that beset his day—and ours. A great humor classic. Three books in one. Total of 157pp. 5 3/8 x 8.

T749 Paperbound \$1.00

**THE DEVIL'S DICTIONARY.** Ambrose Bierce. Sardonic and irreverent barbs puncturing the pomposities and absurdities of American politics, business, religion, literature, and arts, by the country's greatest satirist in the classic tradition. Epigrammatic as Shaw, piercing as Swift, American as Mark Twain, Will Rogers, and Fred Allen. Bierce will always remain the favorite of a small coterie of enthusiasts, and of writers and speakers whom he supplies with "some of the most gorgeous witticisms of the English language." (H. L. Mencken) Over 1000 entries in alphabetical order. 144pp. 5 3/8 x 8.

T487 Paperbound \$1.00

**THE COMPLETE NONSENSE OF EDWARD LEAR.** This is the only complete edition of this master of gentle madness available at a popular price. A BOOK OF NONSENSE, NONSENSE SONGS, MORE NONSENSE SONGS AND STORIES in their entirety with all the old favorites that have delighted children and adults for years. The Dong With A Luminous Nose, The Jumbies, The Owl and the Pussycat, and hundreds of other bits of wonderful nonsense. 214 limericks, 3 sets of Nonsense Botany, 5 Nonsense Alphabets. 546 drawings by Lear himself, and much more. 320pp. 5 3/8 x 8.

T167 Paperbound \$1.00

**SINGULAR TRAVELS, CAMPAIGNS, AND ADVENTURES OF BARON MUNCHAUSEN.** R. E. Raspe, with 90 illustrations by Gustave Doré. The first edition in over 150 years to reestablish the deeds of the Prince of Liars exactly as Raspe first recorded them in 1785—the genuine Baron Munchausen, one of the most popular personalities in English literature. Included also are the best of the many sequels, written by other hands. Introduction on Raspe by J. Carswell. Bibliography of early editions. xiv + 192pp. 5 3/8 x 8.

T698 Paperbound \$1.00

**HOW TO TELL THE BIRDS FROM THE FLOWERS.** R. W. Wood. How not to confuse a carrot with a parrot, a grape with an ape, a puffin with nuffin. Delightful drawings, clever puns, absurd little poems point out farfetched resemblances in nature. The author was a leading physicist. Introduction by Margaret Wood White. 106 illus. 60pp. 5 3/8 x 8.

T523 Paperbound 75¢

**JOE MILLER'S JESTS OR, THE WITS VADE-MECUM.** The original Joe Miller jest book. Gives a keen and pungent impression of life in 18th-century England. Many are somewhat on the bawdy side and they are still capable of provoking amusement and good fun. This volume is a facsimile of the original "Joe Miller" first published in 1739. It remains the most popular and influential humor book of all time. New introduction by Robert Hutchinson. xxi + 70pp. 5 3/8 x 8 1/2.

T423 Paperbound \$1.00

*Prices subject to change without notice.*

*Dover publishes books on art, music, philosophy, literature, languages, history, social sciences, psychology, handicrafts, orientalia, puzzles and entertainments, chess, pets and gardens, books explaining science, intermediate and higher mathematics, mathematical physics, engineering, biological sciences, earth sciences, classics of science, etc. Write to:*

*Dept. catrr.*

*Dover Publications, Inc.*

*180 Varick Street, N.Y. 14, N.Y.*

(continued from front flap)

- Mathematical Tables of Elementary and Some Higher Mathematical Functions, Herbert B. Dwight. \$1.75
- The Theory and Operation of the Slide Rule, John P. Ellis. \$1.50
- Differential Equations for Engineers, Philip Franklin. \$1.65
- Hydraulics and Its Applications, A. H. Gibson. Clothbound \$8.00
- A Treatise on Gyrostatics and Rotational Motion, Andrew Gray. \$2.75
- Inductance Calculations: Working Formulas and Tables, Frederick W. Grover. \$1.85
- The Principles of Electromagnetism Applied to Electrical Machines, Bernard Hague. \$2.25
- Elasticity, Plasticity and Structure of Matter, Roelof Houwink. \$2.45
- Applied Mechanics for Engineers, Sir Charles Inglis. \$2.00
- Tables of Functions with Formulae and Curves, Eugene Jahnke and Fritz Emde. \$2.00
- Photoelasticity: Principles and Methods, H. T. Jessop and F. C. Harris. \$2.00
- Optics and Optical Instruments, B. K. Johnson. \$1.65
- Mathematics of Modern Engineering, Ernest G. Keller and Robert E. Doherty. Two volume set \$3.70
- Fundamental Electromagnetic Theory, Ronald P. King. \$2.75
- Calculus Refresher for Technical Men, A. Albert Klaf. \$2.00
- Trigonometry Refresher for Technical Men, A. Albert Klaf. \$2.00
- Stress Waves in Solids, H. Kolsky. \$1.55
- Tensors for Circuits, Gabriel Kron. \$2.00
- The Dynamical Theory of Sound, Horace Lamb. \$1.50
- Hydrodynamics, Horace Lamb. \$3.75
- Selected Papers on New Techniques for Energy Conversion, edited by Sumner N. Levine. \$3.00
- Selected Papers on Semiconductor Microwave Electronics, edited by Sumner N. Levine and Richard M. Kurzrok. \$2.25
- Fundamentals of Electricity and Magnetism, Leonard B. Loeb. \$2.75
- The Principles of Electrochemistry, Duncan A. MacInnes. \$2.45
- Loud Speakers: Theory, Performance, Testing, and Design, Norman W. McLachlan. \$2.25

Paperbound unless otherwise indicated. Prices subject to change without notice. Available at your book dealer or write for free catalogues to Dept. Eng., Dover Publications, Inc., 180 Varick St., N. Y., N. Y. 10014. Please indicate field of interest. Dover publishes over 125 new books and records each year on such fields as mathematics, physics, explaining science, art, languages, philosophy, classical records, and others.

MONTGOMERY

TECHNIQUE OF  
MICROWAVE MEASUREMENTS

VOLUME II

DOVER

S1596

TECHNIQUE OF  
MICROWAVE  
MEASUREMENTSEDITED BY  
CAROL G. MONTGOMERY

IN TWO VOLUMES

VOLUME II

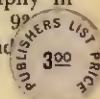
Highly intensified research activities carried on at government laboratories during World War II resulted in major developments in the radio electronics and high-frequency fields. Classified during the war, much of this information was held to be so valuable that it was written up afterwards by a staff of prominent physicists, mathematicians, and engineers at the Radiation Laboratory of M.I.T. The resulting "Radiation Laboratory Series" is recognized as the most distinguished and comprehensive series on radio engineering ever published.

This still timely book is extremely useful for its detailed discussions of methods and devices for measuring various quantities pertinent in microwave technology. The methods described, for the most part, are based on the wave character of high-frequency currents rather than on the low-frequency techniques of direct determination of current or voltage.

After a brief introduction, the authors proceed to a discussion of the low-power sources that are useful for microwave measurements, with a full description of the characteristics and operating principles of the reflex klystron. Chapter 3 takes up the methods of measuring power at low, medium, and high levels. Next follows a chapter on microwave signal generators and their use in testing receivers. Sources of noise are also described. Chapters 5-7 treat the measurement of wavelength and frequency, particularly in cavities, including those measurements peculiar to radiation from pulsed generators. The remainder of the book is devoted to measurements that combine power measurements and determinations of wavelength. Specific topics covered here include: measurements of standing waves, impedance bridges, the measurement of dielectric constants, cutoff attenuators, resistive attenuators, the measurement of attenuation, directional couplers, r-f phase and pattern measurements.

Unabridged and unaltered republication of 1st (1947) edition. Foreword by L. A. DuBridge. Preface by editor. 628 figures. 55 tables. Bibliography in notes and at end of chapter 10. Appendix. Index. Total of xix + 990 pages. 5 3/8 x 8 1/2.

2 vol. set, S1595-6 Paperbound



A DOVER EDITION DESIGNED FOR YEARS OF USE!

We have made every effort to make this the best book possible. Our paper is opaque, with minimal show-through; it will not discolor or become brittle with age. Pages are sewn in signatures, in the method traditionally used for the best books, and will not drop out, as often happens with paperbacks held together with glue. Books open flat for easy reference. The binding will not crack or split. This is a permanent book.